GAS ENGINES FOR DOMESTIC ENGINE-DRIVEN HEAT PUMPS

by

Michael John Boswell

A thesis submitted to the Council for National Academic Awards in partial fulfilment of the degree of Doctor of Philosophy

School of Engineering
Oxford Polytechnic
in collaboration with
British Gas plc

June 1992

ACKNOWLEDGEMENTS

I should like to take this opportunity to gratefully acknowledge contributions made to this work by many individuals and organisations and in particular:

The continual support of Dr. G. R. Bremble as Head of the School of Engineering.

Tony Hern for valued and consistent supervision, encouragement and guidance throughout the duration of the work.

The supervision and expertise of Dr. M. C. Patterson, Manager of The Built Environment Division, British Gas plc and other members of the Research Station at Watson House.

The technicians in the School of Engineering especially Paul Allen for technical support in the drafting and experimental work.

My family especially Diana for enduring patience, support and encouragement and the final proof reading of the manuscript.

British Gas plc, The Science and Engineering Research Council and The School of Engineering, Oxford Polytechnic for providing financial support for the study. In recent years British Gas plc has supported a number of projects associated with engine-driven heat pumps.

CONTENTS

		page no
ABSTRACT		i
NOMENCLATURE		ii
CHAPTER 1	INTRODUCTION	1
	Summary	1
1.1	Introduction	1
1.2	Primary energy reserves	2
1.3	Comparative performance of the heat pump	2
1.4	Natural gas as an engine fuel	3
1.5	Engine-driven heat pump developments	4
1.6	Project background	8
1.7	Heat pump simulation	9
1.8	Engine thermal efficiency	10
1.9	Emission control	13
1.10	Conclusions	16
1.11	Objectives of the study	17
	Figures	20
	References	25
CHAPTER 2	TEST FACILITY	31
	Summary	31
2.1	Modifications	31
2.2	Instrumentation	32
2.3	Range of experimental observation	36
2.4	Experimental procedure	38
2.5	Performance analysis	41
	Figures and plates	45
	References	51
CHAPTER 3	PROTOTYPE DEVELOPMENT	52
	Summary	52
3.1	General modifications	52
3.2	Cylinder head	53
	Figures and plates	57

		page no
CHAPTER 4	COMPUTER SIMULATION	65
	Summary	65
4.1	The combustion process	65
4.2	Combustion modelling	67
4.3	Details of the engine model	76
	Figures	92
	References	94
CHAPTER 5	COMBUSTION ANALYSIS	99
	Summary	99
5.1	Introduction	99
5.2	Range of experimental observation	101
5.3	Combustion model	102
5.4	Flame development model	102
5.5	Laminar flame speed correlation	103
5.6	Analysis of pressure-crankangle data	104
5.7	Experimental results and discussion	108
	Figures and tables	130
	References	177
CHAPTER 6	EVALUATION OF THE ENGINE MODEL	179
	Summary	179
6.1	Evaluation of the Weibe function	179
6.2	The influence of experimental error or theoretical assumptions	181
	Figures and tables	182
CHAPTER 7	ENERGY FLOWS	188
	Summary	188
7.1	Introduction	188
7.2	Indicated thermal efficiencies	191
7.3	Engine heat transfer	192
7.4	Exhaust heat transfer	196
7.5	Crankcase blowby	200
7.6	Ambient loss	203
7.7	Unburned hydrocarbons	205

page no

7.8 Losses at the gas analyser 205
7.9 Oil heat transfer 206
7.10 Frictional losses 206
7.11 Miscellaneous observations 219
Figures and tables 221
References 245

CHAPTER 8 EMISSIONS 247
Summary 247
8.1 Formation of pollutants 247
8.2 Discussion of experimental results 251
8.3 Conclusions 260
Figures and tables 264
References 276

CHAPTER 9 FLOW 277
Summary 277
Figures 281
References 283

CHAPTER 10 CONCLUSIONS 284
10.1 Parametric tests 284
10.2 Engine modelling 286
10.3 Lean burn strategy 287

CHAPTER 11 FUTURE WORK 288
11.1 Engine design 288
11.2 Operating strategy 289
11.3 Engine model 290

APPENDICES

APPENDIX I COMBUSTION ANALYSIS AND ENGINE MODEL OUTPUT I.1
Figures I.2 - I.57 I.2

		page no
APPENDIX II	PERFORMANCE DATA AND ENERGY TRANSFERS	II.1
	Figures II.2 - II.19	II.2
APPENDIX III	COMPUTER PROGRAMMES	III.1
	Performance analysis	III.2
	Thermodynamic engine model	III.24
	Single cycle pressure-crankangle analysis	III.55
APPENDIX IV	CALIBRATION PROCEDURES	IV.1
	Figures IV.5 - IV.9	IV.5
APPENDIX V	GAS CHROMATOGRAPH ANALYSIS OF EXHAUST HYDROCARBONS	V.1
	Figures V.2 - V.3	V.2

Gas engines for domestic engine-driven heat pumps

by Michael John Boswell

ABSTRACT

An experimental and theoretical investigation has been undertaken into the performance of a small prototype, water-cooled, gas-fuelled engine designed for use as a domestic heat pump prime mover. In light of the application, fuel type and capacity, both experimental and theoretical study of similar engines is at best poorly documented in the literature.

A comprehensive engine test facility has been set up, incorporating extensive calorimetry, a separate lubrication system, emissions monitoring and high speed data acquisition for in-cylinder pressure measurement and analysis. Two new experimental cylinder heads have been designed together with new induction and exhaust systems, both to improve performance and to enable further investigation of the combustion process.

A preliminary parametric study of the combustion process established that the thermal efficiency and emission levels are strongly dependent on operational and design variables and that a lean, fast-burning combustion process in a slow speed engine coupled with careful control of other operating variables had the potential for improving efficiency, reducing emissions, and lowering frictional losses and noise levels with enhanced durability.

Accordingly, new information has been obtained relating to rates of heat release, energy flows and emission levels over a wide range of design and operating conditions with utility for and consistent with an envelope of conditions appropriate to such a lean burn strategy.

Modelling techniques have been developed and used as diagnostic tools in conjunction with the experimental data to investigate the influence of operating and design variables on rates of heat release and energy flows. The models have been validated using the experimental data over a wide range of operating conditions and incorporated into a thermodynamic engine model for use as a sub-model in an overall heat pump model.

The experimental and theoretical programme has provided a valuable insight into the lean burn strategy and realised a considerable improvement in the performance of the prototype engine. The theoretical study benefits from a new approach to small gas engine design and development.

NOMENCLATURE

The following list defines general symbols, subscripts, notation and abbreviations; specific nomenclature is defined in the appropriate text.

A	Area
a	Weibe function duration parameter
B, b	Bore
C	Blowby coefficient
C_s	Swirl number
c_P	Specific heat at constant pressure
d	Diameter
H	Enthalpy
h	Specific enthalpy
$\mathbf{h}$	Heat transfer coefficient
h_s	Chamber height at start of combustion
k	Thermal conductivity
L	Valve lift
m	Mass
N	Engine speed
n	Index of compression or expansion
Nu	Nusselt number
P	Cylinder pressure
Q	Heat transfer
R	Universal gas constant
r, cr	Compression ratio
Re	Reynolds number
S	Stroke
$\bar{S}_p$	Mean piston speed
S_t	Turbulent flame propagation speed - relative to the unburned charge
S_l	Laminar flame speed
s	Specific entropy
T	Temperature
Tq	Torque
t	Time
U	Internal energy

u_t	Turbulence intensity
u	Specific internal energy
V	Volume
Vis	Isentropic velocity
Vo	Volume at tdc
Vs	Swept volume
v	Specific volume
W	Work transfer
x	Fractional mass consumed, position
z	Weibe function shape parameter
ϵ	Stoichiometric molar fuel-to-air ratio, half stroke to rod length ratio
η_{vol}	Volumetric efficiency
θ	Crankangle
θ_b	Combustion interval, 0 to 100% mass consumed
θ_d	Flame development interval, 0 to 1% mass consumed
θ_s	Crankangle at which combustion starts
ν	Kinematic viscosity, molar coefficient
ρ	Density
σ	Stefan-Boltzmann constant
ϕ	Fuel-to-air equivalence ratio, valve seat angle
ω	Angular velocity

Subscripts

b	Burned
e	Entrained, equilibrium
f	Enflamed, flow
i	ith component, ignition
l	Loss
u	Unburned
v	Valve
w	Wall
I	Start of combustion
F	End of combustion

Notation

[ ]	Concentration
∧	Maximum value
·	Time rate of change
-	Average

Abbreviations

bdc	Bottom dead centre
bmep	Brake mean effective pressure
CHP	Combined heat and power
COP	Coefficient of performance
ca	Crankangle
Eoc	End of combustion
EVC	Exhaust valve closes
EVO	Exhaust valve opens
FSR	Flame speed ratio (S_t/S_l)
fmep	Friction mean effective pressure
HHV	Fuel higher heating value
IGN	Ignition
IVC	Inlet valve closes
IVO	Inlet valve opens
imep	Indicated mean effective pressure
LHV	Fuel lower heating value
LML	Lean mixture limit
MMEP	Motoring mean effective pressure
PER	Performance effectiveness ratio
Pmax	Maximum in-cylinder pressure
ppm	Parts per million
SD	Standard deviation
Soc	Start of combustion
Tex	Mean exhaust temperature
tdc	Top dead centre
UHC	Unburned hydrocarbons
wot	Wide open throttle

PRESENTATION OF FIGURES AND TABULATED DATA

Figures and tabulated data are presented at the end of each chapter in the order in which they are referred to in the text. Figures included in the Appendices are referred to by page number.

CHAPTER 1 - INTRODUCTION

Summary

In this chapter the incentive for heat pump development is discussed within the context of environmental impact. An overview is presented of the development of the engine-driven heat pump, including the previous work conducted on gas-fuelled units with reference to the extensive research programmes in America and Japan and academic institutions in the United Kingdom. Engine modelling techniques in heat pump simulations are discussed. High engine thermal efficiency and low exhaust emissions are identified as fundamental criteria in determining the success of such units. A review of the literature, relating mostly to petrol-fuelled engines, is undertaken to investigate and evaluate the methods commonly used to improve efficiency and reduce emissions. A summary of the main points established from the literature survey in this and succeeding chapters is presented from which the scope and objectives of the study are derived.

1.1 Introduction

In recent years the incentives for developing technology with low environmental impact have become increasingly urgent because of growing demand on finite natural reserves and widespread apprehension about the effects of earlier technology on the environment. Whilst organised inquiry into such effects has not yet developed into a mature science the initial prognosis is far from encouraging. It is unlikely that harmonious solutions will be achieved without global co-operation on both consumption and pollution or without some form of integrated policy embracing all methods of energy conversion, consumption and conservation with particular reference to local resources and needs. As a tentative first step it seems desirable that technological products be assessed by some form of environmental audit initiated at the point of extraction of the various materials used in manufacture and with due regard to the scarcity of the resource. Subsequent transportation, manufacturing, distribution and use all accrue a penalty commensurate with environmental impact. With such an audit product longevity and re-use are also attractive features.

1.2 Primary energy reserves

Whilst proved world reserves of oil have increased threefold and those of natural gas fourfold over the past 25 years the projected lifespan of reserves has risen only slightly due to increased consumption, that of oil from 30 to 45 years and that of gas from 40 to 60 years. World reserves of coal currently stand at around 240 years, (1.1). (Proved reserves are resources which geological and engineering data indicate with reasonable certainty can be recovered in the future from known reservoirs under existing economic and operating conditions.)

In the United Kingdom the projected lifespan of proved natural gas reserves has reduced from around 50 years in 1987 to a current level of around 23 years as gas production has risen markedly, (1.2). It has been estimated however, that only 25 to 30% of potential gas-bearing geological formations throughout the world have been explored, particularly in offshore locations, (1.3), and as economic conditions change, extraction from less profitable sources and other methods of production such as coal gasification and biomass or collection from waste may prove attractive.

1.3 Comparative performance of the heat pump

In comparison with conventional methods of producing heat, heat pumps utilise primary energy more effectively. Whilst electrically-driven units convert electricity efficiently, potentially greater savings of natural reserves with proportionally lower emission levels can be achieved with engine-driven units since there are no electrical generation or transmission losses. Figure 1.1 illustrates the potential of the heat pump for primary energy conservation when compared with conventional methods of producing heat.

The following heat pump performance criteria are adopted:

Coefficient of performance

$$COP = \frac{\text{heat delivered to high temperature sink}}{\text{work input}}$$

Performance effectiveness ratio

$$PER = \frac{\text{useful heat output from complete installation}}{\text{energy input to complete installation}}$$

1.4 Natural gas as an engine fuel

Natural gas is transported from source to point of use more efficiently than any other form of fossil fuel. It has been reported that with increased pipeline diameters characteristic of contemporary practice, around 10% of the primary energy transmitted is required to deliver the gas through a distance of 6000 km, (1.3, 1.4). Unlike conventional fuels for spark-ignited engines or for power generation there is no demand on transportation systems or environmental penalty to consider from the pollutants associated with transportation; it has been estimated that cross-border movements of oil throughout the world amounted to around 3 billion tonnes in 1990, (1.1). In comparison with oil processing, penalties are negligible. For stationary engines the fuel supply, control and distribution systems are in most cases well established.

Natural gas is in many ways an ideal engine fuel. It readily forms a mixture with air and burns cleanly and progressively; as the hydrogen-to-carbon ratio of a fuel increases, levels of CO_2, unburned hydrocarbons and NO_x diminish at equal equivalence ratios, all other factors being equal, (1.5). Laminar flame speeds exceed those of petrol fuels at the weaker mixture strengths, suggesting improved lean mixture operation and the potential for output control by quality governing, (1.6, 1.7). High compression ratios can be utilised since natural gas is inherently resistant to detonation. Improved lean mixture operation, quality governing and high compression ratios offer the potential for improved thermal efficiency. Engine output is however lower for the gas-fuelled engine in comparison with the petrol-fuelled counterpart since the breathing capacity is inhibited by the lower density of the fuel.

Natural gas offers an alternative to dependence on imported oil which is of particular concern following the recent events in the Gulf and

the effect that instability in the region in the past 20 years has had on the world economy.

1.5 Engine-driven heat pump developments

The theory of heat engines was first proposed by Carnot in 'Reflections on the Motive Power of Fire' in 1824, (1.8) and practical demonstrations of these principles applied to heat upgrading were later made by Lord Kelvin, (1.9), in the mid nineteenth century. Whilst the cooling application of heat pumps has since developed into a mature technology, the heating potential has not been fully exploited due to a perceived abundance of natural reserves of primary energy and simpler alternative methods of converting these to heat.

The provision of summer cooling is attractive for most industrialised countries outside of Northern Europe, and in those countries also requiring some form of winter heating the development of a reversible heat pump is of particular interest since a net reduction in capital cost can be achieved from the replacement of separate appliances. The economic success of the Northern European heat pump, however, is determined solely on its cost effectiveness in satisfying a heating requirement and until the increases in the price of oil in the early 1970's its development has been mainly restricted to fairly large applications where significant reductions in energy consumption could offset the capital expenditure on the plant.

The increased cost of energy during the 1970's stimulated heat pump development in Europe, America and Japan as a means of reducing dependence on imported oil. In Europe the number of residential and commercial installations had risen to around 100,000 by 1980, (1.10). Annual sales in 1982 for the United States, Japan, the former West Germany and France were running at 400, 1000, 40 and 50 (thousands) respectively, (1.11). Virtually all units were electrically driven due to the availability of supply and the simplicity, reliability and low noise of the electric motor.

Reciprocating spark-ignition engines fuelled with natural gas have aroused considerable interest in recent years, both for combined

heating and in-house power schemes, see for example References 1.12 and 1.13, and as prime movers for heat pumps. In comparison with the electrically-driven heat pump, high overall performance together with high outlet temperatures can be achieved with engine-driven units by recovering the heat rejected by the engine and using it in the heating system. More efficient use of primary energy is made since around three units are required to produce a unit of electrical energy due to losses in generation and transmission. The heat output can be matched more readily to the heating load using a variable-speed engine drive than the on/off control of the conventional electric motor.

Most of the engine-driven installations in Europe in the past decade have been packaged units installed in commercial buildings under sponsorship from the gas utilities or the Government. Only in the former West Germany had significant development of the market occurred by 1984 with 600 units operational. In Holland, Switzerland, and the United Kingdom growth has been much slower with 50, 12, and 33 installations respectively, (1.11).

In the United Kingdom some typical applications reported in recent years are for providing heat in malting kilns and swimming pools and cooling of administrative buildings, (1.14 - 1.17). Steam raising from a high temperature liquid effluent source is reported in References 1.18 and 1.19. Capacities range from 100 to 2,700 kW and the units are typically based on modified petrol or diesel engines used together with conventional heat pump or refrigeration components.

In comparison with larger units the requirements for a domestic engine-driven heat pump are more demanding and if progress is to be made it is likely that a different approach will be required. Before such a unit is introduced into the domestic environment further study is required in a number of important areas. Amongst the most significant of these are associated with achieving a clean, quiet, low cost, reliable, durable and efficient small engine. In the United Kingdom research in this field has been restricted by the lack of a suitable small water-cooled engine. Most of the world's expertise on small engines lies in America and Japan. In both these countries large research projects are concentrating on domestic engine-driven heat pump development.

In Japan, a strong dependence on imported oil together with a growing home market for reversible electrically-driven heat pumps has encouraged intensive research into the reversible gas-fuelled engine-driven counterpart. A research association including three major gas related companies, six engine manufacturers and seven system manufacturers has been formed under funding from the Government to investigate domestic and small commercial heat pump systems resulting in the commercial availability of several units.

As part of this programme, Kawamoto et al., (1.20, 1.21), of Osaka Gas have investigated a number of different reversible heat pump cycles with capacities varying from 6 to 8 kW for heating and 3.5 to 6 kW for cooling. Two and four-stroke engines with various compressor configurations have been developed. Performance effectiveness ratios of 1.2 and 0.8 for heating and cooling respectively and 1.4 for hot water supply were reported for a specimen configuration. Engine thermal efficiencies from 25 to 28% were achieved based on the higher heating value (HHV) and emissions of CO/CO_2 were maintained at 0.01 with NO_x below 150 ppm using a ternary catalyst.

At Tokyo Gas, Yamagishi et al., (1.22), have developed a reversible heat pump system utilising a single-cylinder, 2-stroke, water-cooled engine and a rotary compressor with R12 as the working fluid. At the rated speed the capacities reported for heating, cooling and hot water were 5.9, 3.2 and 6.16 kW respectively with corresponding performance effectiveness ratios of 1.15, 0.57 and 0.97. The noise level was recorded at 50 dB (A) at one metre distance from the unit at the rated speed. An engine thermal efficiency of 21% (HHV) was achieved and emission levels reduced to 50 ppm for CH_4 and CO and 145 ppm for NO_x using a platinum catalyst. A service life of 20,000 hours was considered a desirable feature for the engine and endurance tests were successfully conducted for 3,000 hours.

A number of other systems have also been developed at Tokyo Gas. Kaizaki, (1.23), reports on the construction of five water-cooled, single-cylinder, 4-stroke engines together with various compressor configurations using R22 as the working fluid. Field tests have been conducted on five heat pump systems with capacities ranging from 5.8 to

10.5 kW for heating and hot water and 3.5 to 5.8 kW for cooling. Sample performance characteristics are presented for a single heat pump configuration: at the design point a heating capacity of 5.7 kW with a PER of 1.58 and for cooling a capacity of 3.8 kW with a PER of 1.08. Noise levels were measured at 51 dB (A). An engine thermal efficiency of 28% based on the lower heating value (LHV) was achieved with NO_x reduced to 125 ppm by exhaust gas recirculation (EGR) and a 3-way catalyst. The engines have undertaken 11,000 hours of endurance testing.

In the United States an intensive research programme has been undertaken with the collaboration of The Gas Research Institute and two major manufacturers; Briggs and Stratton Corporation and Battelle Columbus Division, (1.24, 1.25). A prototype, packaged unit has been designed, the main features including a 4-stroke, single-cylinder, water-cooled engine together with a reciprocating compressor and gas fired auxiliary heating. R22 is used for the working fluid. The design criteria specify a capacity of 10.6 kW, a PER of 1.0 at 35 degrees C ambient for cooling and a PER of 1.7 at 8.3 degrees C ambient for heating. To meet these performance targets considerable engine development work has been undertaken. A lean burn strategy coupled with careful control of design and operating variables has increased efficiency levels to 31%, (HHV), with NO_x levels below 150 ppm. The engine incorporates numerous features to meet a durability target of 30,000 to 40,000 hours service before opening the engine.

A number of research programmes have also been undertaken within academic institutions in the United Kingdom. Of particular interest are the collaborative 2-stroke engine and compressor design and development project undertaken by The Queens University of Belfast and the University of Leeds under funding from British Gas, (1.26) and the gas engine-driven heat pump designed and tested by Phillips of the Open University in collaboration with Lucas Aerospace and the Department of Energy, (1.27). The main features of the system studied by the latter group include a single-cylinder, 4-stroke, water-cooled Brit Imp marine engine coupled to a Hall Thermotank compressor with R12 as the working fluid. Extensive testing of the unit was undertaken which was reported to work well but suffer from poor engine performance. At the rated

speed over a 50 degrees C temperature lift the heat output was measured at 14 kW with a PER of 1.1. The engine thermal efficiency at this point was 17% (HHV). At 1 metre distance from the heat pump a noise level of 65 dB (A) was noted.

1.6 Project background

For several years The School of Engineering at Oxford Polytechnic has collaborated with Task Power and Control on engine-driven heat pump development. The initial work involved a feasibility study on a 200 kW gas fired Rankine/vapour compression cycle for which a computer simulation was prepared to optimise the working fluids in both the power and heat pump parts of the cycle. In 1980, Task, in collaboration with Grundy Morgan Ltd., initiated the development of a 10 kW heat pump for the domestic market. A survey of engine-driven heat pump projects undertaken at that time indicated that they had not fulfilled their promise because the components utilised had not been specifically designed for this type of application. Recognising this and to keep capital costs to a minimum and obtain a better balanced machine, Task proposed a heat pump design based on a novel reciprocating integrated engine/compressor unit, fuelled by natural gas, specifically designed for the application to take full advantage of the potential energy savings available with this type of heat pump.

Design studies commenced in 1981 and at the same time the existing heat pump simulation model was modified to include a reciprocating engine instead of the original Rankine power cycle. This was used for optimisation studies and performance predictions, both on and off design, for various heat pump cycle arrangements and with different working fluids. A two stage compression and expansion cycle with two throttle valves and a flash chamber was eventually chosen using R114 as the working fluid.

In parallel with the above, a 10 kW heat pump was constructed at Oxford Polytechnic using standard refrigeration components and a modified Honda engine. Valuable operating experience was gained with this heat pump and the mathematical model was considerably improved. A new engine model was added together with models of the evaporator and condenser.

Manufacture of the first engine/compressor unit was completed in 1983. It was a reciprocating machine having four in-line cylinders. The gas engine occupied cylinder 1 with its crankshaft coupled to the crankshaft of a two stage compressor running in the remaining three cylinders. Cylinders 3 and 4 formed the low pressure stage and cylinder 2 the high pressure stage. Separate cylinder heads were used for the engine and compressor with the crankcase divided into two parts incorporating a bellows-type face seal between them to prevent refrigerant loss. Figures 1.2 and 1.3 illustrate the heat pump system and proposed package.

The gas engine was subsequently assembled using a dummy crankshaft and flywheel in place of the compressor rotating assembly and testing of the engine took place later in the year. During 1984 the compressor section was assembled and a limited test and development programme undertaken using the engine/compressor unit in a heat pump cycle with both R114 and R11 as working fluids. The results of this programme were very promising with a heating capacity around 8 kW, a PER of 1.2 and temperature lifts of up to 85 degrees C reported, (1.28).

In 1985 a similar engine only version of the Task unit, with a dummy shaft in place of the compressor crankshaft was prepared for engine testing at Oxford Polytechnic. The performance of this engine is described in References 1.29 and 1.30. Details of the engine are given in Figures 1.4 and 1.5.

1.7 Heat pump simulation

A heat pump simulation model is of value because it can provide detailed information on the complex interaction of individual components, the performance of a working fluid and allow evaluation of a control strategy. This information can be used to optimise heat pump performance without recourse to a costly and time consuming empirical approach.

Whilst the development of an overall heat pump model is beyond the scope of this work, a survey of the literature has been conducted, (1.29, 1.31 - 1.37), which has revealed no evidence of the application

of gas engine cycle simulation to heat pump models. In general the models are related to electrically-driven units with the various system components modelled to a greater or lesser sophistication depending on the objectives of the study. Van Rij, (1.37), Patani and Bonne, (1.35) and Tam, (1.29), modelled engine characteristics using simple correlations obtained from empirical data.

The development of a gas engine cycle simulation to be used in conjunction with a heat pump model is of value since new information relating to emission levels from engine-driven units can be predicted as the heat pump operating conditions vary. There is also opportunity for a new approach to small gas engine design and development since the optimisation and evaluation of the design, operating variables and control strategy can be investigated based on the requirements of a heat pump.

1.8 Engine thermal efficiency

High engine thermal efficiency is of fundamental importance for heat pump applications since this governs the amount of primary energy multiplied by the heat pump cycle. Assuming a coefficient of performance for the heat pump cycle at around 3 and unrecoverable energy losses from the engine at about 15% - approximate figures which vary with operating conditions - an engine thermal efficiency of 28% (HHV) is required to produce a performance effectiveness ratio of 1.4. This value is considerably higher than that of the Task engine in its original configuration or other off-the-shelf engines of similar output where a range of 18 - 22% applies. New engines under development, however, as part of the Japanese and American programmes have reported efficiencies in the range 22 - 32% as noted earlier, (1.20 - 1.25).

A number of different approaches to improving engine thermal efficiency have been reported in the literature, mostly with reference to petrol-fuelled engines. The most significant of these in this application are likely to be increased compression ratio and lean mixture operation.

It is known that higher compression ratios yield higher efficiencies but in practice the onset of detonation limits the useful compression

ratio that can be used. Methane has good detonation resistance in comparison with other fuels and thus higher compression ratios can be utilised. Although operating variables and engine-specific characteristics such as combustion chamber geometry and spatial arrangements of components within the chamber influence the onset of detonation, useful compression ratios of 15 to 16:1 over the complete range of mixture strength have been reported for a number of different natural gas-fuelled engines in References 1.38 - 1.40. It is thought that a further limitation is imposed by higher frictional losses which ensue through increased gas loads; Kawamoto, (1.20), reports only marginal increases in efficiency for compression ratios greater than 12:1, and other workers, for example Swain et al., (1.25), have considered these small gains unjustified in light of adverse consequences for durability. Typically compression ratios in common use for gas engine applications range from 8 to 12:1.

Theoretically, improved efficiency results from the combustion of weaker mixtures but these in practice produce lower flame speeds, extended burn duration, increased cyclic variability and eventually prevent complete combustion of the charge as the lean flammability limits are approached. The shorter the burn duration, the more closely combustion approaches the ideal constant volume heat addition, heat losses are reduced and increases in efficiency can be expected.

Two methods are commonly used to reduce the burn duration. The first involves generation of turbulent charge motion by a directed, tangentially-oriented outflow from the valve or by pre-swirl generated in the port upstream from the valve. Further motion amplification can be promoted by squish regions within the combustion chamber (radially-directed flow achieved through piston movement). Disadvantages associated with the generation of turbulent charge motion are increased heat transfer to the cylinder walls and higher frictional losses.

Reductions of up to 60% of the 0 - 90% burn time, and reduced cyclic dispersion were obtained by Endo et al., (1.41), by offsetting the inlet tract from both cylinder and valve centre lines. This induces mixture motion directed tangentially along the cylinder wall and promotes a swirl within the cylinder. Masked inlet valves have also

been used by other workers, (1.42 - 1.45), to investigate the effects of directed mixture motion. These have been found to promote enhanced burn rates, but are disadvantaged by high pumping losses and additional mechanical complexity to control valve rotation.

Nested delta wings have been used by Lucas et al., (1.46), to generate vortices within the port upstream of the valve, increasing the flame speed and extending the lean mixture limit. Again high pumping losses are to be expected. A more practical approach to pre-swirl generation is the helical pre-chamber situated above the valve seat. Helical ports are compact and are capable of producing high swirl at low valve lifts, whereas directed ports require lengthy, straight sections and may impose spatial limitations on other cylinder head components. Directed ports produce most swirl at higher valve lifts. Current high swirl ports often combine features of both directional and helical ports.

The second method of decreasing the burn duration is to increase the frontal area of the flame front as it propagates into the unburned charge. The combustion chamber is designed for minimal contact between flame front and cylinder walls; a compact, small surface area-to-volume arrangement results with particular attention given to spark plug location. In comparison to turbulent charge generation, pumping and heat transfer losses are smaller.

Using cycle simulation, Poulus and Heywood, (1.47), examined the performance of four combustion chamber shapes representative of current design: open, disc, hemispherical and bowl in piston. It was concluded that burn duration is significantly affected by both chamber geometry and turbulence. Furthermore, a positive influence on burn duration from chamber shape is preferable to that of turbulence since higher efficiency is achieved through lower heat loss. Additionally, modification of the flame shape by spatial location of the spark plug may be more important in governing burn duration than combustion chamber shape alone. The model predicts the shortest burn duration for an open chamber with a centrally located plug.

The extensive experimental work of Lucas and Brunt, (1.48), suggests that the influence of squish on flame speed is small and that reduced

burn duration results from the degree of compactness of combustion chambers with squish features. Bowl in piston and bathtub configurations with around 48% squish reduced the burn angle (2 - 90% charge consumed) by 10 and 12% respectively when compared with a disc chamber of zero squish, whilst a May Fireball with dual ignition reduced the burn angle by 45%. A complementary simulation predicted that a hemispherical chamber with dual ignition was most likely to yield the smallest burn duration and be most suited to lean burn. Conversely, other workers, (1.49), ascribe reduced burn durations with changing chamber shape to both differences in turbulence intensity and flame area development. Bowl in piston chambers with 60 and 75% squish were found effective in reducing the 10 - 90% burn durations by 40 and 60% respectively when compared with a disc of zero squish.

Recent gas engine research programmes have reported some results of experimental investigations into combustion chamber geometry. Kawamoto, (1.20), reports on three configurations, of which the optimum design selected for further development appears similar to the May Fireball with a recess volume below the exhaust valve seat. This work suggests that the ratio of recess volume to the total chamber volume is an important design variable with the highest thermal efficiencies of 31% (LHV) obtained with ratios greater than 0.8. The GRI/Battelle project, (1.24, 1.25), has published results from a preliminary comparative study of three types of combustion chamber: 20 degree wedge, high ratio compact chamber and a twin plug open system. Peak efficiencies of 31, 28 and 27.5% (HHV) respectively, have been reported with air-to-fuel ratios and ignition timing optimised for NO_x levels below 150 ppm. This work concluded that squish was more effective than swirl in reducing burn durations and implied that some form of compact chamber was required. Yanmar, in Reference 1.50, reports an increase in thermal efficiency from 20 - 28% on a 1.2 kW engine as a result of changing the combustion chamber to the May Fireball.

1.9 Emission control

Although there is no current legislation in the United Kingdom to cover emissions from small stationary engines of this type it is unlikely that an engine-driven heat pump will gain public acceptance unless its

exhaust can be demonstrated to be clean. Both the American and Japanese, (1.20 - 1.25), development programmes are aimed at meeting stringent emissions levels. Pollutants which cause most concern are oxides of carbon and nitrogen and unburned hydrocarbons.

Methods currently used or under investigation for the control of emissions include: optimisation of operating variables, design of the combustion process, exhaust gas recirculation, after-treatment devices in the exhaust system and water induction to the inlet manifold.

As a baseline for comparison, naturally-aspirated, single-cylinder, natural gas-fuelled engines lacking any form of emission control and operating at near stoichiometric mixtures have been reported to produce levels of NO_x, CO, and unburned hydrocarbons (UHC) around 3000, 500, and 2000 ppm respectively, (1.51 - 1.53).

With the introduction of emission control by operating variables the above workers report significant reductions in pollutant levels. For example, increasing the excess air ratio from the stoichiometric to 1.4 was found in References 1.52 and 1.53 to reduce NO_x to around 300 ppm and CO to less than 500 ppm with UHC falling slightly and then rising back to the stoichiometric level. Fleming and Alsup, (1.52), achieved up to a 70% reduction in peak NO_x levels and an 80% reduction in UHC levels (g/BHp basis) over the weak mixture range by retarding the ignition timing by 20 degrees. A similar strong dependence of NO_x formation on ignition timing is reported by the GRI/Battelle project, (1.24, 1.25), for example, retarding by 5 degrees at an excess air ratio of 1.65 reduced NO_x from 200 to 100 ppm. With particular reference to petrol-fuelled engines other workers have reported strong dependence of NO_x formation on operating variables such as ignition timing, coolant temperature, chamber deposits, excess air ratio, compression ratio and engine speed, (1.54 - 1.56).

The quantity of residual gas in the cylinder at the start of compression influences NO_x formation and by artificially increasing the residuals by exhaust gas recirculation emission levels can be controlled, (1.57). Cycle simulation suggests that NO_x formation is inhibited by lower burned gas temperatures which ensue as residuals

absorb a portion of the chemical energy released during combustion, (1.58). Exhaust gas recirculation has been found effective in reducing NO_x emissions from a single cylinder natural gas-fuelled engine. With exhaust gas recirculation ratios ranging from 0 to 7%, Kawamoto, (1.20), reports NO_x levels reducing from 3000 to 2000 ppm at stoichiometric mixtures and from 300 to 100 ppm at excess air ratios of 1.4.

Water induction to the manifold reduces burned gas temperatures and consequently NO_x emissions. With reference to petrol-fuelled engines, decreases from 3000 to 2000 ppm at weak mixtures have been noted, (1.59), and substantial reductions predicted by cycle simulation, (1.58).

Three-way catalytic converters have been employed for a number of years in some areas of the world to lower emission levels in the exhaust by simultaneously promoting oxidation of CO and unburned hydrocarbons and reduction of NO through contact with an active catalytic material, typically a noble metal mix of platinum and rhodium. Whilst a welcome development in emission control they are disadvantaged on a number of grounds when compared with a lean burn strategy. The materials used in manufacture are costly and the units have a finite life, effectiveness diminishing with age. Only for exhaust gas temperatures exceeding around 300 degrees C is the catalytic converter effective in reducing pollutants, and as a result emission control is severely limited during engine warm-up. Primary fuel conversion is less efficient since effective pollutant control is achieved only in a narrow window of excess air around the stoichiometric air-to-fuel ratio whereas higher engine thermal efficiencies are at weaker mixture strengths. Furthermore, quality governing of the output is precluded hence pumping losses are more significant. At stoichiometric operation CO_2 levels are highest and these are compounded by additional CO_2 production from the converter. The restriction of near stoichiometric operation with attendant deleterious effect on efficiency could be remedied by exact control of exhaust gas recirculation, which, diluting the charge, improves the engine efficiency without impairing the function of the catalyst. In addition to the feedback system required to control the air-to-fuel ratio within precise limits some form of exhaust gas

admission control is also necessary adding greatly to the complexity of the system.

1.10 Conclusions

It is convenient at this juncture to outline the scope and establish the context of this work. The following points summarise the main findings of a survey of the previous work reported in the literature and discussed in this and following chapters, together with those findings established from a survey of the previous work undertaken by Task Power and Control and Oxford Polytechnic.

(i) Engine design and performance are key factors in producing a commercially viable domestic engine-driven heat pump.

(ii) Thermal efficiencies based on gross calorific values in excess of 28% are desirable compared with the more usual 18 - 20% for off-the-shelf engines of this capacity.

(iii) A clean exhaust is required with NO_x levels not exceeding 150 to 200 ppm, and CO and UHC less than 500 ppm.

(iv) In comparison with after-treatment devices in the exhaust, combustion system design coupled with optimisation of operational variables offers the possibility of both improving engine efficiency and reducing emission levels with a further potential for developing an effective engine control strategy.

(v) A reduction in unrecoverable energy losses is particularly important in this application since heat recovery is a significant factor in the performance of both heat pump and combined heat and power units and other losses, for example, the power to drive ancillaries have a greater significance with engines of low power output.

(vi) Reduction in frictional losses is desirable as these have been found to be significant in engines of this type, and remaining sensibly constant at a given speed, they become substantially more significant as the output reduces.

(vii) Although a quiet engine is attractive it should be possible to achieve acceptable noise levels with a low speed engine and acoustic enclosure.

(viii) Some modification to the original Task concept is necessary to produce an engine with these performance characteristics: a more compact, high compression ratio combustion chamber, incorporating turbulence enhancement features to promote a fast burn allowing efficient lean mixture operation with reduced emission levels; a lower design speed to improve durability and reduce frictional losses and noise levels in conjunction with careful control of other operating variables.

(ix) The prototypical nature of the unit under investigation precludes availability of experimental data or theoretical study in the literature, a lacuna compounded by the limited number of similar engines of this capacity, the proposed application and the type of fuel used. Detailed analysis of combustion, the energy transfers within the engine including the magnitude and distribution of heat transfer, frictional losses, the significance of blowby, unburned fuel and ambient losses are of particular interest but are poorly documented.

(x) No evidence has been found of the application of cycle simulation to small gas engine design and development or to engine-driven heat pump models. This approach has considerable potential for establishing and evaluating design criteria and operational methods for increasing efficiency and reducing emissions in engines for this application based on the requirements of a heat pump.

1.11 Objectives of the study

Following this appraisal it was felt that priority should be given to the study of emissions, combustion and energy transfer processes to determine how the required performance characteristics could be achieved at minimum cost.

(i) To modify the original Task engine according to the conceptual design outlined above.

(ii) To obtain original benchmark data relating to rates of heat release, heat transfer, emission levels and frictional losses over a wide range of design and operating conditions consistent with an envelope of conditions appropriate to a lean burn strategy, with the objectives of supporting this study and contributing information to the lacuna, and hence to complement any subsequent investigation where such data is required for further analysis or development of an engine model utilising natural gas as a fuel.

(iii) To investigate the effects of such changes on the rates of heat release, heat transfer and emissions.

(iv) To establish the distribution and magnitude of frictional losses within the engine.

(v) To conduct overall energy balances, with particular reference to small quantities thought to be significant in low output engines, and hence assess the distribution and magnitude of energy transfers within the engine and to use such audits to support experimental measuring techniques.

(vi) To use the data to develop a combustion model incorporating flame development with utility for the analysis of combustion in natural gas-fuelled engines and to evaluate a suitable friction model.

(vii) To develop a thermodynamic engine model suitable for use as a sub-model in an overall heat pump simulation.

(viii) To validate the model over a wide range of operating conditions.

(ix) To use the model, in conjunction with the data from parametric testing, as a diagnostic tool for a comparative study of the effects of operating and design variables, with the objectives of evaluating and improving the conceptual design and to further understanding of the combustion process, heat transfer, emissions and performance.

(x) To investigate and evaluate a lean burn strategy.

Additionally, in order to satisfy the above objectives, it was necessary to set up a comprehensive engine test facility and make revisions to the design of the prototype engine. This work is detailed in the following two chapters.

PAGE/PAGES EXCLUDED UNDER INSTRUCTION FROM THE UNIVERSITY

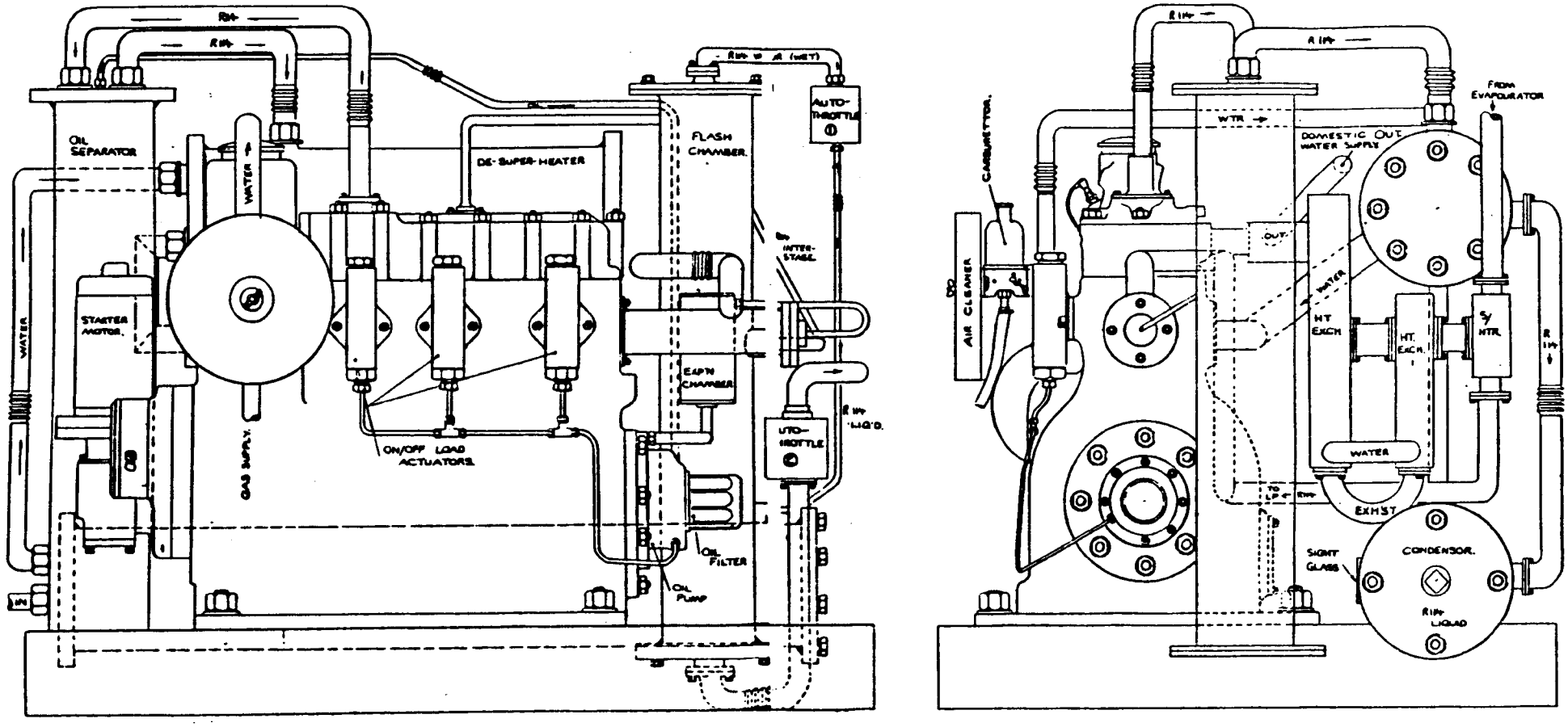

Figure 1.3 Heat pump proposed package.

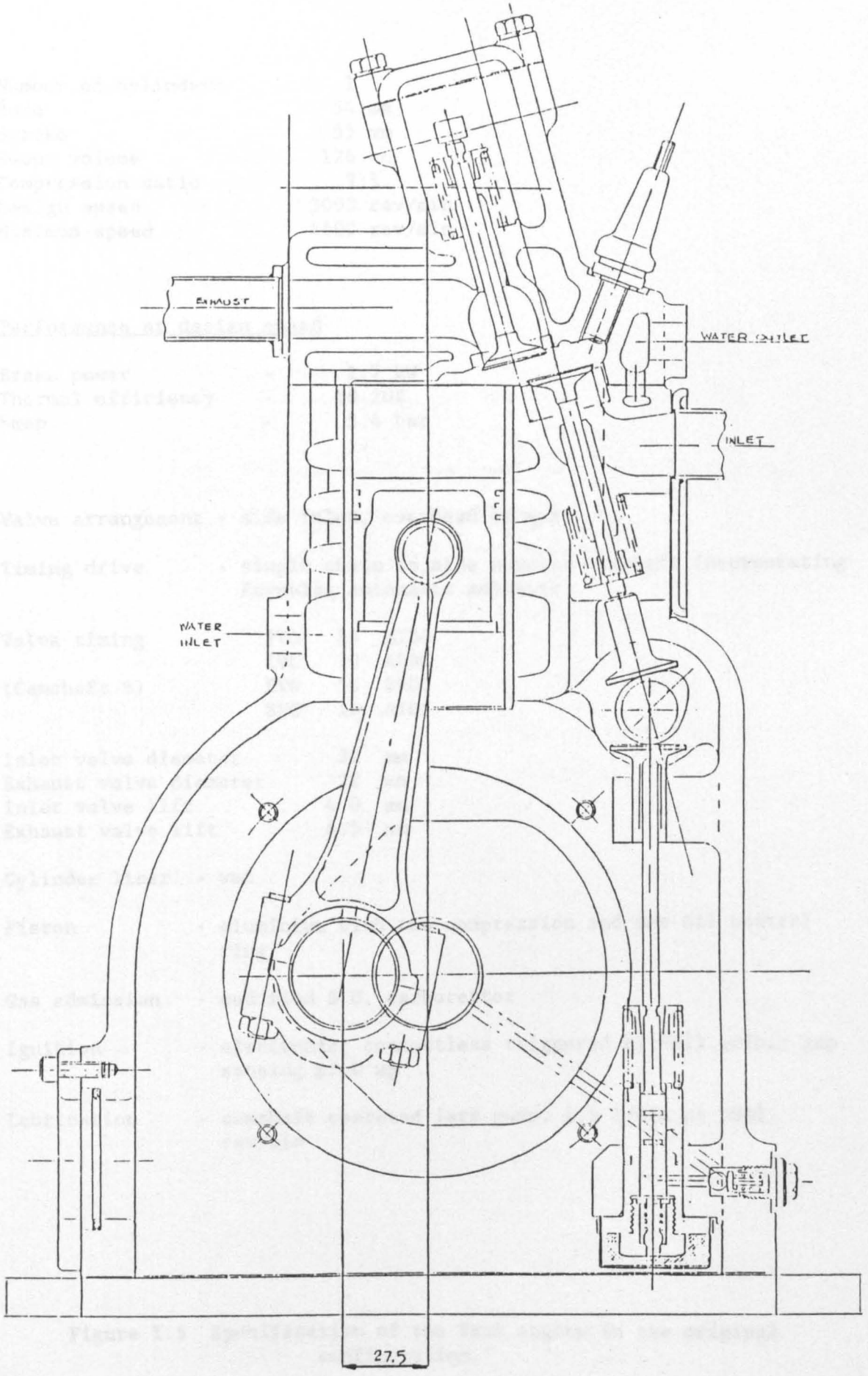

Figure 1.4 Section through the Task engine.

Number of cylinders	1
Bore	54 mm
Stroke	55 mm
Swept volume	126 cc
Compression ratio	9:1
Design speed	3000 rev/min
Maximum speed	4500 rev/min

Performance at design speed

Brake power	-	1.7 kW
Thermal efficiency	-	18-20%
bmep	-	5.4 bar

Valve arrangement - side inlet, overhead exhaust

Timing drive - single chain to side mounted camshaft incorporating Reynolds automatic adjuster

Valve timing	IVO	15	BTDC
	IVC	10	ABDC
(Camshaft B)	EVO	50	BBDC
	EVC	15	ATDC

Inlet valve diameter	22	mm
Exhaust valve diameter	22	mm
Inlet valve lift	4.0	mm
Exhaust valve lift	4.5	mm

Cylinder liner - wet

Piston - aluminium with two compression and one oil control ring

Gas admission - modified S.U. carburettor

Ignition - electronic, contactless triggered by Hall effect gap sensing pick up

Lubrication - camshaft operated jerk pump, 1.5 l/min at 3000 rev/min

Figure 1.5 Specification of the Task engine in the original configuration.

References

1.1 The British Petroleum Company plc
Bp statistical review of world energy.
The British Petroleum Company plc, 1991.

1.2 British Gas plc
Financial and operating statistics.
British Gas plc, 1991.

1.3 Brecht, C.
The need for gas research.
International Gas Research Conference, London, June 1983.

1.4 Brecht, C.
Gas - energy of the future, some thoughts on Western European gas supplies.
International Gas Research Conference, Chicago, June 1980.

1.5 Harrington, J.A., Shishu, R.C.
A single-cylinder engine study of the effects of fuel type, fuel stoichiometry and hydrogen-to-carbon ratio on CO, NO and HC exhaust emissions.
SAE paper 730476, 1973.

1.6 Metghalchi, M., Keck, J.C.
Laminar burning velocity of propane-air mixtures at high temperature and pressure.
Combust. Flame, Vol. 38, pp. 143-154, 1980.

1.7 Metghalchi, M., Keck, J.C.
Burning velocities of mixtures of air with methanol, iso-octane and indolene at high pressure and temperature.
Combust. Flame, Vol. 48, pp. 191-210, 1982.

1.8 Mendoza, E. (Ed.)
Reflections on the motive power of fire by Sadi Carnot and other papers on The Second Law of Thermodynamics by E. Clapeyron and R. Clausius.
Dover, 1960.

1.9 Thomson, W.
On the economy of the heating or cooling of buildings by means of currents of air.
Proc. Glasgow Phil. Soc., December 1852.

1.10 Tassou, S.A., Marquand, C.J., Wilson, D.R.
Development and potential growth in Western Europe.
Energy World Heat Pumps Supplement, October 1981.

1.11 Miriam, J.M., Green, M.B.
The potential for gas-fired heat pumps in domestic heating.
British Gas Corporation, Communication 1248, 1985.

1.12 Koplow, M.D., Sakhuja, R.K., Raymond, R.
Development of a 60 kW cogeneration module for the commercial/ light industrial sector.
International Gas Research Conference, 1984.

1.13 Anon.
Total energy systems - universal module uses car engine.
International Power Generation, June/July 1978.

1.14 Hoggarth, M.L.
Gas engine-driven heat pumps for industrial and commercial applications.
Energy World Heat Pump Supplement, October 1981.

1.15 Pearson, J.
Gas engines for heat pump installations and small CHP units.
Pap. Technol. Ind., Vol. 25, pp. 28-32, March 1984.

1.16 Metcalf, J.H.
Heating with a gas engine-driven heat pump.
The Heating and Ventilation Engineer, February 1981.

1.17 Masters, J., Pearson, J.
Automotive engines power air conditioning system, heat pump installations and heat and power units.
Joint Meeting of the South Western and Wales Sections of the Institution of Gas Engineers, Bristol, January 1981. British Gas Publication, MRS E 381.

1.18 Kew, P.A.
Design, construction and testing of a gas, engine-driven high temperature industrial heat pump.
IRD Research Report 81/ 29.

1.19 Macmichael, D.B.A., Reay, D.A.
Feasibility and design study of a gas engine-driven high temperature industrial heat pump.
IRD Research Report 78/ 19.

1.20 Kawamoto, H.
Development of gas engine heat pumps for domestic use.
International Conference on Directly Fired Heat Pumps, Bristol, September 1984.

1.21 Kawamoto, H., Takata, Y., Shibuya, K.
Development of a gas engine heat pump for domestic and commercial use.
International Conference on Directly Fired Heat Pumps, Bristol, September 1984.

1.22 Yamagishi, T., Ogura, M., Yokoyama, T., Omata, T.
Research and development of a suitable gas engine driven heat pump for residential use.
International Conference Directly Fired Heat Pumps, Bristol, September 1984.

1.23 Kaizaki, M.
Small gas engine heat pump systems.
Tokyo Gas Company (internal communication 1247), 1984.

1.24 Anon.
Reciprocating gas engine heat pump development.
GRI/Battelle (internal report), May 1986.

1.25 Swain, J.C., Klausing, T.A., Lambert, J.E., Trayser, D.A.
Design and test of an internal combustion gas engine for residential heat pumps.
International Gas Research Conference, Toronto, September 1986.

1.26 Anon.
The design and development of a small two-stroke gas engine.
The Queen's University of Belfast (internal report), May 1987.

1.27 Phillips, C.A.
Evaluation of the design, construction and operation of a gas fuelled engine-driven heat pump.
Energy Research Group, The Open University, Report ERG 034, 1981.

1.28 Anon.
Heat pump development.
Task Power and Control Ltd. (final internal report), January 1985.

1.29 Tam, S.
The characteristics of a small gas engine and a simulation study of its effect on the performance of a domestic engine driven heat pump.
M. Phil. Thesis, Oxford Polytechnic, 1987.

1.30 Hern, A., Boswell, M.J.
Gas engine-driven heat pump.
Oxford Polytechnic (internal report), November 1987.

1.31 Hiller, C.C., Glicksman, L.R.
Heat pump improvement using compressor flow modulation.
ASHRAE Trans., 1977.

1.32 Hodgett, D.L., Lincoln, P.
A mathematical model of a dehumidifying evaporator for high temperature heat pumps.
Electricity Council Research Centre, Report ECRC/ M1147, June 1978.

1.33 Blundell, C.J.
Experimental confirmation of a mathematical model of an air to air heat pump.
Electricity Council Research Centre, Report ECRC/ M1302, December, 1979.

1.34 Bildstein, P., Hamam, Y., Ehrhart, J.
Heat pump models for microprocessor based control systems.
Proc. Int. Sem. organised by the Commission of the European Communities, Brussels, 1979.

1.35 Patani, A., Bonne, U.
Modelling the performance of gas-fired heat pump systems.
14th IECE Conference, paper 799360, Boston, August 1979.

1.36 Lloyd, S.
The heat pump.
Building Services Research and Information Association, Bibliography LB 103/ 81, 1981.

1.37 Van Rij, M.L.D.
A detailed calculation model of a compression heat pump.
International Gas Research Conference, London, June 1983.

1.38 Karim, G.A., Klat, S.A.
The knock and autoignition characteristics of some gaseous fuels and their mixtures.
Journal of The Institute of Fuels, pp. 109-117, March 1966.

1.39 Moore, N.P.W., Roy, B.N.
Comparative studies of methane and propane as engine fuels.
Proc. Instn. Mech. Engrs., Vol. 170, pp. 1157-1172, 1956.

1.40 Karim, G.A., Wierzbal, I.
Comparative studies of methane and propane as fuels for spark ignition and compression ignition engines.
SAE Paper 831196, 1983.

1.41 Endo, Y., Yamashita, R., Matsumoto, H.
Improvement of combustion in spark ignition engines with YICS.
J.SAE Review No. 6, pp. 27-33, November 1981.

1.42 Mitchell, G.P., Whitehouse, N.D.
The effect of the method of gas admission on performance of a spark ignition gas engine.
Proc. Instn. Mech. Engrs., Vol. 185, pp. 571-582, 1970-1971.

1.43 Annand, W.J.D., Sulaiman, S.J.
Knock limits and performance of some gaseous fuels in a supercharged spark ignition engine.
Proc. Instn. Mech. Engrs., Vol. 185, pp. 857-867, 1970-1971.

1.44 Nakajima, Y., Sugihara, K., Takagi, Y., Muranaka, S.
Effects of exhaust gas recirculation on fuel consumption.
Proc. Instn. Mech. Engrs., Vol. 195, pp. 369-376, 1981.

1.45 Gatowski, J.A., Heywood, J.B.
Effects of valve-shrouding and squish on combustion in a spark-ignition engine.
SAE paper 852093, 1985.

1.46 Lucas, G.G., Brunt, M., Petrovic, S.
Lean mixture running of the spark ignition engine by the generation of a vortex system within the intake.
SAE paper 780964, 1978.

1.47 Poulos, S.G., Heywood, J.B.
The effect of chamber geometry on spark ignition engine combustion.
SAE paper 830334, 1983.

1.48 Lucas, G.G., Brunt, M.F.J.
The effect of combustion chamber shape on the rate of combustion in a spark ignition engine.
SAE paper 820165, 1982.

1.49 Belaire, R.C., Davis, G.C., Kent, J.C., Tabaczynski, R.J.
Combustion chamber effects on burn rates in a high swirl spark ignition engine.
SAE paper 830335, 1983.

1.50 Kamo, R., Kamo, L.
Formation of a natural gas engine data base.
Report prepared by Adiabatics, Inc. for GRI, Contract No. 5084-233-0969, October 1985.

1.51 Karim, G.A., Ali, I.A.
Combustion, knock and emission characteristics of a natural gas fuelled spark ignition engine with particular reference to low intake temperature conditions.
Proc. Instn. Mech. Engrs., Vol. 189, pp. 139-147, 1975.

1.52 Fleming, R.D., Allsup, J.R.
Emission characteristics of natural gas as an automotive fuel.
SAE paper 710833, 1971.

1.53 Nagalingham, B., Duebel, F., Schmillen, K.
Performance study using natural gas, hydrogen-supplemented natural gas and hydrogen in AVL research engine.
Int. J. Hydrogen Energy, Vol. 8, No. 9, pp. 715-720, 1983.

1.54 Huls, T.A., Nickol, H.A.
Influence of engine variables on exhaust oxides of nitrogen concentrations from a multi-cylinder engine.
SAE paper 670482, 1967.

1.55 Komiyama, K., Heywood, J.B.
Predicting NOx emissions and effects of exhaust gas recirculation in spark-ignition engines.
SAE paper 730475, 1973.

1.56 Nebel, G.J., Jackson, M.W.
Some factors affecting the concentration of oxides of nitrogen in exhaust gases from spark ignition engines.
J. APCA, Vol. 8, No. 3, pp. 213-218, November 1958.

1.57 Tadahide Toda, Hidetaka Nohira, Kiyoshi Kobashi.
Evaluation of burned gas ratio (BGR) as a predominant factor to NOx.
SAE paper 760765, 1976.

1.58 Lucas, G.G., James, E.H.
A computer simulation of a spark ignition engine.
SAE paper 730053, 1973.

1.59 Robison, J.A.
Humidity effects on engine nitric oxide emissions at steady-state conditions.
SAE paper 700467, 1970.

CHAPTER 2 - TEST FACILITY

Summary

The major modifications made to the test facility necessary to fulfil the programme of work are discussed in this chapter. A description of the instrumentation and data acquisition systems is presented. The range of experimental observation, experimental methodology and subsequent processing of data are outlined. Plate 2.1 illustrates the engine and modified test facility.

2.1 Modifications

Since operation at higher temperatures is an important factor in reducing heat and frictional losses, a pressurised cooling system was installed including extensive calorimetry, an ancillary flow calibration circuit and a thermostatically controlled heating facility.

A thermal enclosure was manufactured and mounted on the test bed with the objectives of reducing the radiative heat loss from the engine to the environment and allowing measurement of ambient losses. The enclosure incorporated aluminium panels backed with high density Rockwool fibres, located on an aluminium frame with quick release fasteners.

To reduce exhaust back pressure, the exhaust heat exchanger was re-designed to a shell and tube counterflow type incorporating 30 tubes of length 570 mm and bore 5 mm with the exhaust gas flowing through the tubes. External surfaces were lagged.

To conduct motoring tests with the engine in progressive stages of disassembly and under simulated firing conditions, the wet sump and camshaft-operated oil pump were replaced by a remote lubrication system with an externally-driven pump and heating option together with pressure and temperature control.

Accurate and simple control of the spark timing was considered of value in the early stages of the work since it was observed to significantly

influence the concentration of NO_x. The original manual adjustment was replaced by a stepper motor drive interfaced with a BBC microcomputer. A resolution of one degree was provided with the timing displayed on the terminal.

The resolution of the stepper motor-controlled gas flow valve was adjusted by revising the dimensions of the internal slot to improve control over the air-to-fuel ratio setting in keeping with the lean burn and quality governing strategy (see Figure 2.1).

The above modifications were accompanied by extensions to the instrumentation. A full exhaust gas analysis system was added and comprehensive revisions made to the air, gas and coolant flow, temperature and pressure measuring systems. All measuring systems were interfaced with an IBM XT microcomputer for data logging.

To conduct in-cylinder pressure analysis, a software-driven data acquisition system was installed based on the IBM XT microcomputer interfaced with two analogue to digital converters with on-board memory, a time base module, together with an in-cylinder pressure transducer and an optical encoder driven from the engine crankshaft. To improve the accuracy of pressure-crankangle referencing, an enlarged timing disc of diameter 0.3 m with graduations at 1 degree intervals was produced and mounted on the crankshaft at the rear of the engine.

2.2 Instrumentation

In addition to the measurements of cylinder pressure and crankshaft position numerous other (around thirty) quantities required measurement at each operating point. These included temperatures, gas analysis, flows, pressures, engine speed and load, gas power input and ignition timing. These values were displayed continuously throughout the tests together with calculated quantities such as air-to-fuel ratio, thermal efficiency etc. A full instrumentation schematic is shown in Figure 2.2. Calibration procedures are discussed in Appendix IV.

Engine test bed

Engine tests were conducted on a Cussons Automotive 12, type P8060, test bed. The unit incorporates a swinging field regenerative d.c. dynamometer rated at 9 kW at a maximum speed of 4000 rpm together with a thyristor speed control unit. The casing of the dynamometer is rigidly fixed to a strain gauge load cell capable of measuring force accurately in both directions.

Engine speed

The engine speed was monitored with a tachogenerator attached to the free end of the dynamometer. A CP electro-magnetic transducer activated by a slotted disc attached to the engine crankshaft together with a CP digital display was also installed to measure engine speed.

Gas analysis

The concentrations of NO_x, UHC, CO, CO_2 and O_2 in the exhaust were measured continually using an Analysis Automation emissions monitoring system. The sample was delivered from the exhaust manifold through an external heated line to an oven maintained at constant temperature within the system. An internal heated line subsequently conveyed a portion of the sample to a chemiluminescent NO_x analyser, the remainder passing through filters and a cooler to non-dispersive infra-red CO and CO_2 analysers, a flame ionisation detector for UHC and a micro-fuel cell O_2 analyser. Measuring NO_x using the chemiluminescence principle is desirable since dry samples are required with alternative techniques such as NDIR. Condensing the water vapour within the sample 'washes out' NO_x and hence lower concentrations are measured with such instruments.

Combustion pressure

A Kistler 6123A1 miniature quartz transducer in conjunction with a Kistler 5007 charge amplifier was used to measure cylinder pressure. This particular transducer was selected to conform with the spatial arrangement of cylinder head components and the constraints imposed by

the small volume of the combustion chamber without compromising its performance. The transducer is of rugged design able to operate without coolant in arduous conditions close to knocking and is relatively insensitive to coking. A passageway was used to connect the transducer to the combustion chamber and a housing produced to allow mounting. It has been reported in the literature that such arrangements can produce errors in the pressure data due to pressure oscillations in the connecting passageway, (2.1, 2.2). To establish the significance of such effects, comparative testing was undertaken with a flush mounted transducer. This investigation together with the results is detailed in Appendix IV and shows that the arrangements are comparable.

Pressures

Furness FC004, FC012 and FC060 micromanometers were used to measure gas pressure, air flow and inlet manifold pressures respectively. Where necessary the exhaust manifold pressure was obtained with an Airflow U-tube oil manometer.

Crankshaft angular position

A Hohner 3202 incremental optical shaft encoder of robust construction was installed on the engine test bed, driven from the crankshaft by a stub shaft and anti-backlash coupling. The encoder produced a square wave pulse at 1 and 360 degree increments. The latter pulse was used to mark bdc.

Gas flow

A microprocessor-based gas meter (Gemini) interfaced through an optical sensor to a Wright DM3F saturator and wet meter were kindly supplied by British Gas plc. The Gemini displays updated values of gas flow rate, total volume of gas and energy consumed, input power and the run time every one tenth of a revolution of the wet meter. The instrument takes into account gas temperature, pressure, calorific value, the saturated vapour pressure in the gas and atmospheric pressure.

Air flow

An Alcock, Type S, viscous flow meter was used in conjunction with a Furness FC012 micromanometer. This type of flow meter is relatively insensitive to the pulsating flow encountered in single-cylinder engines.

Coolant flow

A Litre Metre LM45 SS turbine type impulse flow meter was used to measure the flow rate of the engine coolant. The fluid is passed through a jet within the meter and directed onto a Pelton Wheel. Ferrites located in the rotor tips are detected as they pass a sensing coil producing a pulsed output linear to flow rate which is indicated on a moving coil meter.

The flow rate in the coolant temperature control circuit was measured manually by timing a measured volume of flow. This procedure was favoured since the flow rates were very small and consequently difficult to measure accurately with conventional instruments.

Temperatures

These measurements were needed to evaluate the energy transfers from the engine, to establish the thermodynamic state of the charge at the inlet and exhaust manifolds and for monitoring and control of oil and emissions sampling temperatures etc. TC Chromel/Alumel, type K thermocouples and type 16 platinum resistance thermometers in a three wire configuration were used in conjunction with Comark 6110 and 6800 microprocessor thermometers respectively. All cables were screened.

Data acquisition

To allow for the stochastic nature of engine combustion it is usual to average the pressure traces over a large number of consecutive cycles; the less stable the combustion process the more cycles are required to produce a representative result. The sampling rate is determined by the event under investigation within the engine cycle; finer resolution is

necessary for the study of the ignition process, for example, where conditions change rapidly.

A Biodata, Microlink modular waveform capture system was installed for fast data acquisition. The main features included a Microlink mainframe with IEEE-488 interface, power supply and slots for modules, two single channel 12 bit analogue to digital converters with on-board memory for 64K samples and accepting a maximum sample rate of 125 kHz. A timebase unit provided all the sample timing, stop and start facilities and controlled the sample rate. The system was software-driven from an IBM XT microcomputer which together with the Polytechnic's Prime 750 mainframe was used for data processing and analysis.

Sampling interval

A sampling interval of 1 degree of crankshaft rotation was selected as a compromise between the requirements for greater resolution during the combustion interval, the need for producing a representative ensemble-averaged cycle with the finite on-board memory capacity of the data acquisition system and simplicity of data collection. Such a choice allowed sampling of around 90 consecutive cycles.

Additional instrumentation and experimental facilities installed and commissioned for the blowby, ambient loss, friction and flow tests are discussed in Chapters 7 and 9.

2.3 Range of experimental observation

Engines

Two similar prototype engines were available for engine testing: an engine only unit produced specifically for engine testing and an engine/compressor unit originally incorporated in a heat pump. Whilst preliminary parametric investigations were undertaken on the engine only unit, mechanical problems were encountered which eventually dictated that the engine/compressor unit be prepared and commissioned for subsequent testing. The experimental programme reported on in this thesis was conducted largely on the latter unit although some reference

is made to the results of the preliminary programme which are detailed further in References 1.29 and 1.30. Limited testing was also undertaken on a Ricardo E6 engine.

Combustion chambers

Three distinct combustion systems: the original Task hybrid arrangement, a bathtub chamber and a high ratio compact chamber were investigated at wide open throttle over a range of engine speeds, air-to-fuel ratios, ignition timings and compression ratios. The layout of these chambers is described in greater detail in Chapter 3.

Excess air ratio

The excess air ratio was increased from around the stoichiometric to the point at which rough running was observed at the lean mixture limit, arbitrarily defined as that point at which unburned hydrocarbon emissions were noted to increase by more than 10% of the steady value and the load reading to vary by +/- 0.5 N. Mixtures richer than stoichiometric were not investigated due to the lean burn strategy favoured in this work.

Engine speed

The engine speed was varied from 1500 to 2100 rpm. Whilst a design speed of 3000 rpm and a maximum speed of 4500 rpm was specified by Task for this engine, slower speeds were considered of greater interest since low frictional losses, noise levels and enhanced durability are important features of engines for this application. References 1.29 and 1.30 discuss the performance of the engine only unit at speeds up to 3000 rpm.

Ignition timing

The ignition timing was usually set at the minimum advance required for maximum efficiency although ignition timing scans were also conducted.

Compression ratio

The effect of changes in compression ratio was studied on the bathtub chamber over the range 9 to 14:1.

Gas admission

A limited investigation was undertaken into the effects of changes in the gas admission and mixing system as part of the preliminary programme, (1.30). The optimum configuration established as part of that study was used throughout the work conducted on the engine/ compressor unit and is illustrated in Figures 2.1 and 2.3.

Camshaft

Three camshafts (camshafts A, B and C) were supplied by Task Power and Control Ltd. In response to wear noted on the lobes, a camshaft manufacturing procedure was established in the Polytechnic workshop and a replacement camshaft (camshaft D) produced. Figure 2.4 illustrates the camshaft design and Figure 2.5 the various camshaft profiles. Replacing camshaft A with camshaft B, Tam, (1.29), noted improvements in volumetric efficiency of 6% over the complete range of speed which he attributed to the later exhaust valve closing. The early parametric tests with the engine only unit were conducted with camshafts B, C, and D and the later tests on the engine/compressor unit with camshaft D.

Ricardo E6 variable compression ratio engine

The effect of compression ratio on the rate of combustion was studied on a Ricardo E6 variable compression engine. These tests were conducted at a single speed of 1800 rpm with the ignition timing at minimum advance for maximum efficiency, the weakest mixture for maximum power and a range of compression ratios from 8 to 16:1.

2.4 Experimental procedure

In addition to the calibration procedures described in Appendix IV, the following procedures were adhered to during the experimental work.

Engine configuration

The settings of the valve timing, valve lift, tappet clearances, compression ratio and spark plug gap were checked with each change in chamber arrangement or compression ratio. The camshaft profile and valve timing were measured both after manufacture using a dividing head and dial test indicator (DTI) and with the camshaft in situ using crankshaft markings together with a DTI located on the valve retainer. Compression ratios were estimated by introducing methylated spirits into the combustion chamber from a burette. A perspex plate together with silicon grease was used to seal the block/cylinder head interface and the fluid fed through a hole in the plate. This procedure also indicated the presence of any sealing problems at the valve/valve seat face. The tappet clearances were maintained at 0.005 and 0.013 inches at the inlet and exhaust valves respectively. The spark plug gap was set to 0.014 inches or 0.02 inches in the case of the original Task chamber. The oil pressure was maintained at around 30 psi. Testing was initiated with clean combustion chambers and since natural gas burns cleanly this condition was preserved for the duration of the programme.

In-cylinder pressure measurement

Calibration of the in-cylinder pressure measuring system was also undertaken with each change in combustion chamber or compression ratio setting. This rigorous technique is detailed in Reference 2.3. Additionally the system was checked for leaks at the transducer housing, electrical connections were cleaned with tri-chloroethane and the high tension shielding on the ignition circuit inspected. The condition of the encoder anti-backlash coupling was inspected statically and its dynamic operation observed using a stroboscope. Both the pressure traces and encoder output were displayed continually on a cathode ray oscilloscope during the tests allowing early indication of malfunction.

Ignition timing

Since the pressure-crankangle calibration procedure requires the angular displacement of the engine crankshaft to be referenced

precisely to bdc, the setting and function of the stepper motor-controlled spark ignition system was conveniently inspected following each calibration.

Other procedures

Prior to each test the gas analysers, other instrumentation, lubricating oil and engine coolant were allowed to warm-up for several hours with the oil and coolant circulating around the engine. During this period the satisfactory function of the various control mechanisms and the condition of instrument connections and seals were checked where necessary. The gas analysers were subsequently calibrated using zero and span gases and the load cell using the procedure recommended by Cussons. Other instruments were zeroed. Temperature measuring systems monitoring the coolant circuit were checked for equal output with circulating coolant at constant temperature. With the engine firing, the temperatures within the thermal enclosure and around the oil and coolant circuits were allowed to stabilise before testing was conducted. The necessary data were input to the Gemini gas flow meter.

During the tests the engine was allowed to stabilise for several minutes following each change in operating condition. The temperature of exhaust gas in the sample line was maintained at the recommended level by varying the amount of lagging on the exhaust manifold connection. In-cylinder pressure correlated with crankshaft position was displayed continually on a storage oscilloscope. The values of the numerous other variables of interest were logged at a sampling rate of 0.17 Hz and displayed continually on the IBM XT microcomputer, together with calculated values of performance parameters such as thermal efficiency and operating conditions such as air-to-fuel ratio. The setting of the air-to-fuel ratio or optimum ignition timing was achieved using the displayed variables in conjunction with the control systems. High speed sampling of in-cylinder pressure at 1 degree intervals and for around 90 consecutive cycles, together with sampling of the other variables, was undertaken at operating points of interest. Following capture, the pressure data were down-loaded to the IBM XT microcomputer with individual cycles displayed sequentially on the screen for inspection. These, together with the other variables, were

subsequently down-loaded to the Prime 750 mainframe computer at the Polytechnic for processing and analysis. Processing and analysis of the data is detailed in Sections 2.5 and 5.6.

Immediately following each series of tests, with the engine still at operating temperature, motoring tests were conducted at the relevant speeds. The gas analysers and load cell were recalibrated to account for drift.

The experimental procedures followed for the blowby, ambient loss, friction and flow tests are described in Chapters 7 and 9.

2.5 Performance analysis

It was necessary to develop a computer programme (see Appendix III) to process the wealth of data generated during the experimental work. This produced a tabulated output of performance parameters, an energy balance, operating and design conditions, frictional losses, together with the raw data. Graphical presentation was subsequently undertaken using the Quattro spreadsheet, these data are included in Appendix II. The following text outlines the main features of the analysis and the methods used in calculating the various performance parameters. Analysis of pressure data is described later in Chapter 5.

Frictional losses

The engine friction and component contributions were calculated from correlations determined from friction tests together with the correlations of Bishop, (2.4) and the SAE J816b standard, (2.5), for comparative purposes.

Gas quality

Gas quality data applicable to the local area on the dates of testing were kindly supplied by R.J. Wadsworth of British Gas. A sample analysis is presented in Appendix IV and includes gas composition, density and calorific values.

Excess air ratio

The mixture strength was evaluated both from the measured exhaust gas analysis according to the method of Spindt, (2.6), together with gas quality data applicable to the test date, and from the observed gas and wet air flows.

Brake power

Where appropriate, the brake power was corrected to reference conditions according to the SAE J1349 standard, (2.7), to account for differences in the pressure, temperature and humidity of the incoming air between test conditions.

Sensible enthalpy of exhaust gas

The composition and properties of low temperature combustion products were determined according to a method described in Reference 2.8. For the lean or stoichiometric case four product species are considered, the combustion reaction is:

$$\epsilon\phi C_\alpha H_\beta O_\gamma N_\delta + 0.21O_2 + 0.79N_2 \rightarrow \nu_1 CO_2 + \nu_2 H_2O + \nu_3 N_2 + \nu_4 O_2$$

Atom balancing is sufficient to yield the product coefficients. The fuel-to-air equivalence ratio is known from exhaust analysis and the fuel composition (α, β, γ, δ) from gas quality data.

Specific heats and enthalpies of component species are curve fitted to polynomials in temperature according to Gordon and McBride (cited in 2.8). The appropriate temperatures are measured and atmospheric pressure is assumed.

Energy loss through incomplete combustion

A gas chromatograph analysis of various samples of exhaust gas kindly undertaken by British Gas research station at Watson House showed the unburned hydrocarbon concentration to be composed of almost entirely methane at around 90% by volume (see sample analysis Appendix V). A relationship was subsequently developed to express the measured

concentration of unburned hydrocarbons in the exhaust, assumed on the above basis at 100% methane, as a fraction of the incoming fuel energy.

Energy loss at the gas analyser

The energy loss at the analyser was calculated from the measured sample flow rate and temperature together with the thermodynamic properties of exhaust gas.

Energy loss to blowby

Mass loss to blowby during the experimental programme was estimated at each operating point based on a speed correlation determined from blowby measurements (see Section 7.5). In the absence of experimental data the proportion of reactants to products within the blowby was set to a nominal value of 0.6 consistent with previous studies, (2.9). The energy loss then comprised the chemical energy of the unburned fuel together with the enthalpies of air, gas and products referred to standard conditions.

Oil heat transfer

The oil heat transfer was determined from measurements of the flow rate through the remote gear type oil pump in conjunction with the measured oil temperatures at engine inlet and outlet and appropriate thermodynamic properties. Inspection of the early test data showed that this quantity was small and remained substantially unchanged as operating conditions were varied; accordingly, subsequent heat transfers were based on representative values from the earlier work. The oil temperatures were however continuously monitored.

Volumetric efficiency

The following definition was used:

$$\eta_{vol} = \frac{\text{actual mass of dry air and gas inducted}}{\text{max. mass of wet air and gas inducted at manifold conditions}}$$

Specific emissions

Calculations were included to normalise emissions to a g/h basis according to SAE J1088, (2.10), and Spindt, (2.6). Indicators were then developed (g/kWh basis) to relate mass emission rates to the sum of power output and reclaimed heat for CHP assessment and to the heat output from a heat pump assuming a COP of 3.

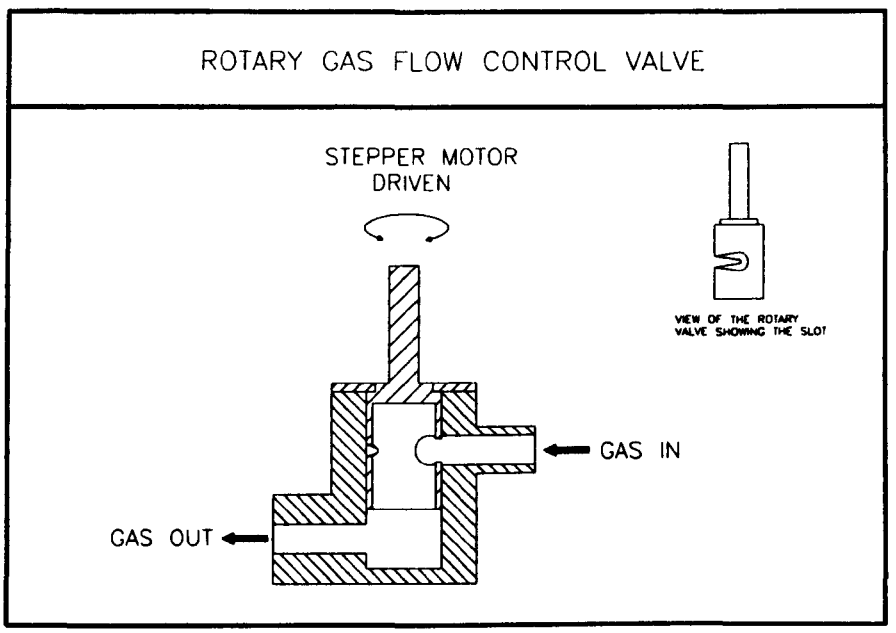

Figure 2.1 Rotary gas flow control valve.

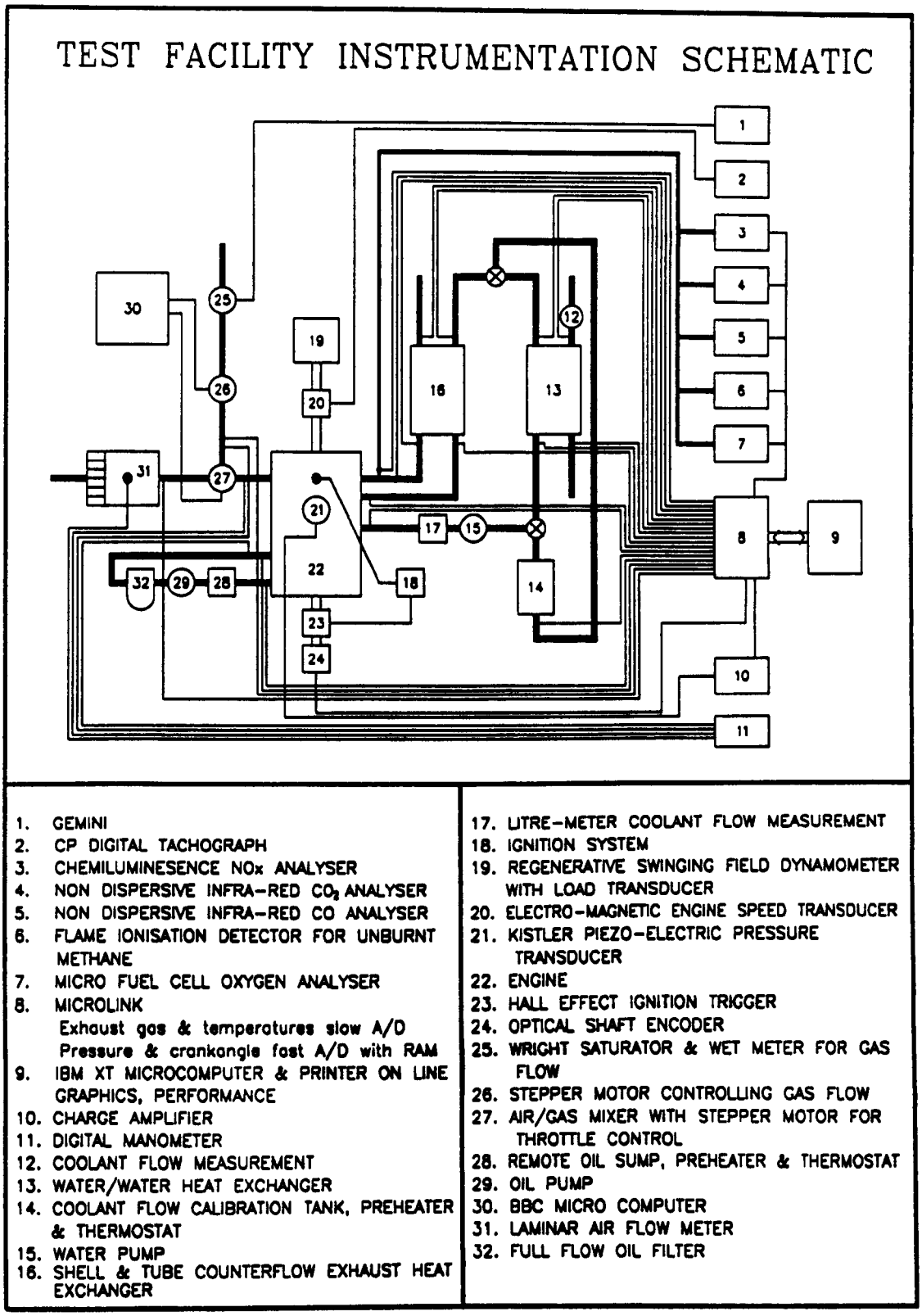

Figure 2.2 Test facility instrumentation schematic.

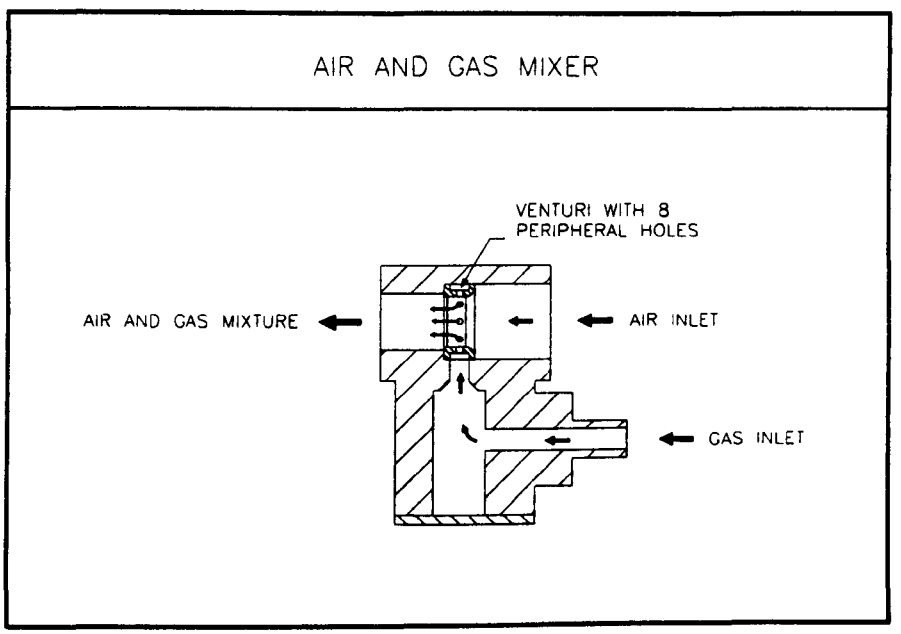

Figure 2.3 Air and gas mixer.

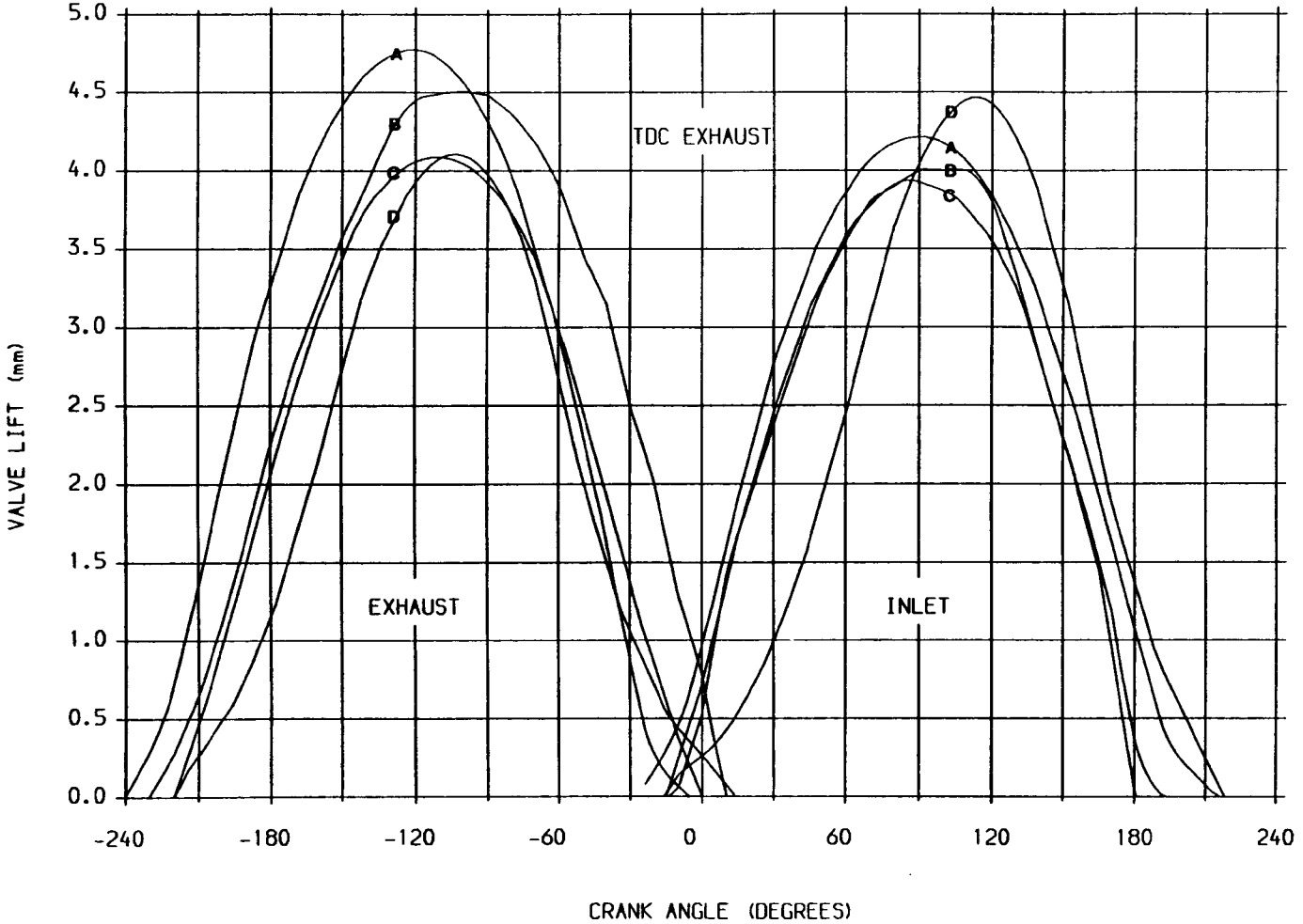

Figure 2.5 Profiles of camshafts A, B, C and D.

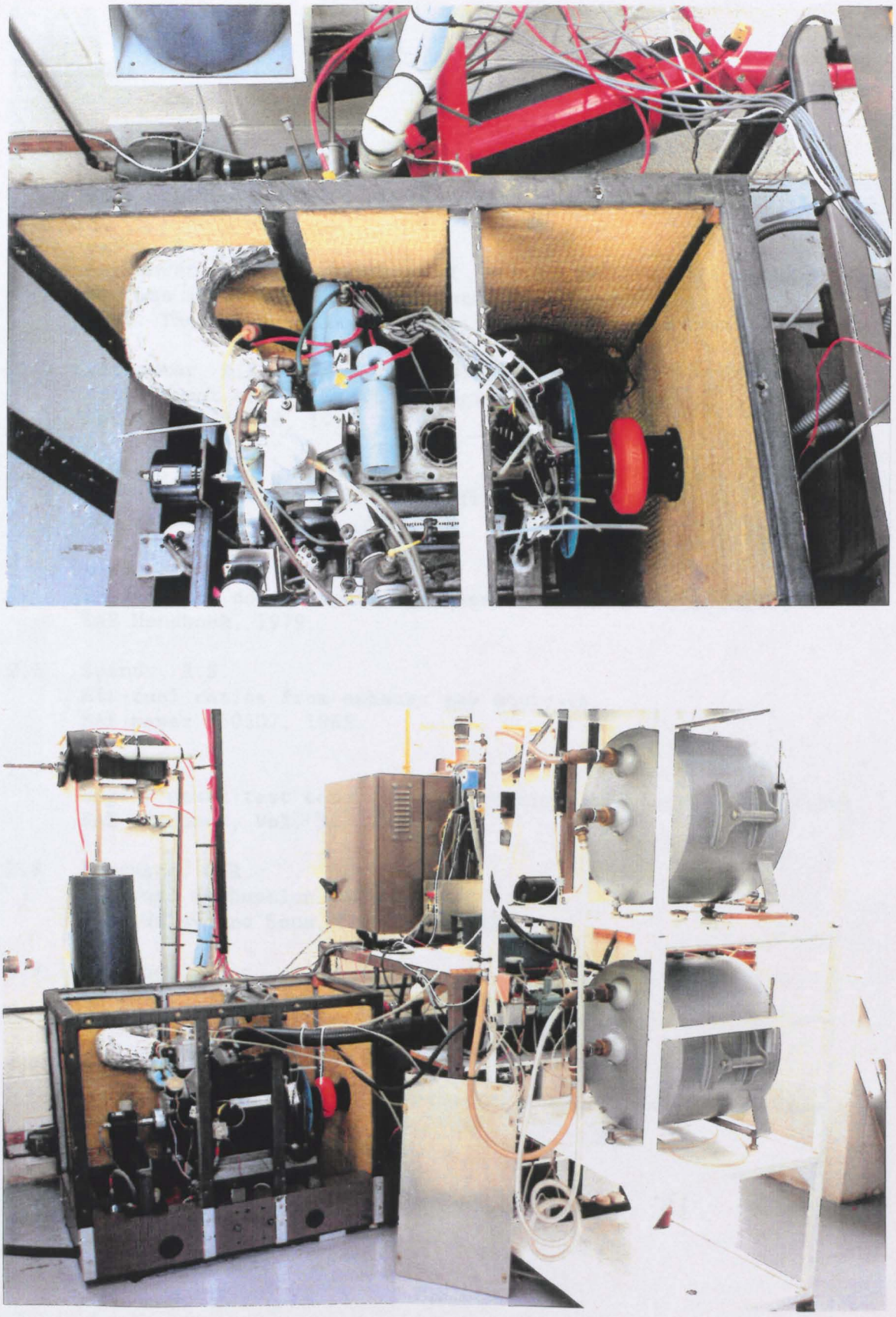

Plate 2.1 Engine and test facility.

References

2.1 Van Aken, C.
Adaptor errors in indicator diagrams of combustion engines.
Proc. Instn. Mech. Engrs., Vol. 191, No. 8, pp. 125-134, 1977.

2.2 Agnew, B.
A theoretical and experimental investigation of the combustion process in a spark ignition internal combustion engine.
Ph.D. Thesis, The City University London, April 1981.

2.3 Lancaster, D.R., Krieger, R.B., Lienesch, J.H.
Measurement and analysis of engine pressure data.
SAE paper 750026, 1975.

2.4 Bishop, I.N.
Effect of design variables on friction and economy.
SAE paper 812A, 1964.

2.5 Anon.
Engine test code - spark ignition and diesel - SAE J816b.
SAE Handbook, 1979.

2.6 Spindt, R.S.
Air-fuel ratios from exhaust gas analysis.
SAE paper 650507, 1965.

2.7 Anon.
Engine power test code - spark ignition and diesel - SAE J1349.
SAE Handbook, Vol. 3, 1988.

2.8 Ferguson, C.R.
Internal combustion engines.
John Wiley and Sons, New York, 1986.

2.9 Heywood, J.B.
Internal combustion engine fundamentals.
McGraw-Hill, New York, 1988.

2.10 Anon.
Test procedure for the measurement of exhaust emissions from small utility engines - SAE J1088.
SAE Handbook, Vol. 3, 1988.

CHAPTER 3 - PROTOTYPE DEVELOPMENT

Summary

This chapter details some necessary modifications made to the engine arising from problems encountered during the proving procedure. The design and production of two new cylinder heads is discussed together with the geometry of the combustion chambers investigated in the study.

3.1 General modifications

A number of changes and modifications were made to the engine in addition to those originally anticipated to be necessary to fulfil this programme of work. These arose through the normal proving procedure associated with prototype engines as around 180 hours of operating experience accrued. Whilst the engine design evolved accordingly, such work added greatly to the complications of running an experimental programme.

Gas sealing problems were encountered due to the proximity of the coolant passageways with the cylinder bore. The design of the original Corruseal-type steel cylinder head gasket was modified and a number of alternative materials including copper-asbestos sandwich and solid copper were investigated. The solid copper gasket was found the most suitable, with the additional advantages of a simple production technique and the potential to vary the compression ratio easily by changes in gasket thickness. The required dimensions were achieved through a cold rolling and annealing process.

Excessive mechanical noise in the bottom end of the engine was traced to a misalignment in the connecting rod, excessive end float on the crankshaft and wear in the dummy shaft coupling. Remedial work to both components was undertaken; the end float was reduced with a thrust washer and the journals reground. Should further development of the engine occur a more robust shaft coupling, possibly incorporating a conventional splined fitting, would be desirable to enhance reliability. The arrangement of the present coupling is detailed in Figure 3.1. Solely on the grounds of logistics further modifications

are required to the connecting rod since the current big end bearings are now obsolete without a suitable replacement evident in the manufacturing literature. Some progress has been made on the manufacture of a prototype connecting rod using a replacement bearing set of the appropriate dimensions (part no. GS 2529 SA). The state of production is illustrated in Plate 3.1.

In response to wear noted on the original camshaft lobes and to allow flexibility in specifying valve timings and profiles, a camshaft manufacturing procedure was established in the Polytechnic workshop and a replacement camshaft (camshaft D) produced. Whilst the finer detail of such procedures and the effects of valve timing on engine performance are outside the scope of this work, the camshaft was manufactured from EN24 through hardening steel using a Bridgeport CNC vertical milling machine with a T cutter. Co-ordinates for the 3 arc cam profile were generated from a knowledge of the desired lift, flank and ramp angles together with the base radius and ramp velocity. Figure 2.4 details the camshaft design and Figure 2.5 the camshaft profiles.

Other minor modifications were made to the exhaust silencing system, to the lubrication system - incorporating full flow filtering and a crankcase breather was found necessary to reduce crankcase pressure.

3.2 Cylinder head

The most significant engine modifications undertaken were the design of alternative cylinder heads. Two additional units and a perspex prototype were manufactured. Plate 3.2 illustrates the original cylinder head and Plate 3.3 the revised design. Dimensional detail is included in Figures 3.2 and 3.3.

The original cylinder head is a hybrid configuration with side inlet and overhead exhaust valves and a compression ratio setting of around 9:1. The revised designs incorporate an overhead valve arrangement, compact combustion configurations based on the bathtub and high ratio compact chamber (Hrcc) layouts, and a nominal compression ratio of around 13:1. The original camshaft position was retained and used with push rods and offset rockers.

The main considerations in the design of the new cylinder heads were:

(i) Meeting the spatial arrangement of components on the existing block.

(ii) Producing a compact combustion chamber with low surface area-to-volume ratio to reduce heat loss, the flame travel path and to promote squish.

(iii) An inlet system design which would allow the incorporation of various amounts of swirl and turbulence to promote a fast burn without too great a loss in volumetric efficiency.

(iv) Space in the combustion chamber for instrumentation.

(v) A design which allows different combustion geometries to be examined.

Initially the perspex prototype was produced which allowed both quantitative and qualitative assessment of the design and established a production procedure including tooling, jigs etc.

Where possible, commercially available components were used in the design and these included Honda valves, springs and guides with Well Tight valve seats. Inlet valves were 22 mm in diameter giving an inlet Mach index of around 0.35 at 35 rev/sec. Valve seat material comprised a nickel/chrome alloy (40% nickel, 12% chrome) especially developed for natural gas burning applications. Other components such as push rods, cam followers, rocker shaft and rockers required manufacture and subsequent heat treatment. A small, 10 mm diameter, Champion G61 spark plug was selected to conform with the spatial arrangement of other cylinder head components. Honda valve stem oil seals were subsequently included in the design to reduce the high levels of unburned hydrocarbons occurring through oil leakage at the valve guides.

Whilst the necessary chamber layouts could have been achieved with a single cylinder head using insert and spacer arrangements it was considered prudent to manufacture a spare cylinder head. Furthermore,

this reduced engine down time when modifying combustion configurations and allowed a more flexible approach to design. The Honda valves were unsuitable for use in the Hrcc configuration since the inlet and exhaust valve stem lengths vary with the change in combustion chamber depth. The valves used were machined from forging blanks to replicate the head geometry of the Honda valves referred to above. The forgings were a silicon and chromium based steel alloy normally used in exhaust applications and were kindly supplied by Mantro Engineering.

The cylinder heads were machined from Fortal STS cast tooling plate high strength aluminium alloy for ease of manufacture and good resistance to thermal and mechanical stresses. Coolant enters the head from the original passage in the block and is supplied through drillings to areas of high temperature.

Combustion chamber geometries

The three geometries are illustrated in Figures 3.4 - 3.6. The arrangement of the original configuration (code TaskII) is characterised by a long flame travel path and high surface area-to-volume ratio which tend to increase heat loss and burn duration. The squish area is high however, corresponding to the sectional area of the bore. Additionally its design does not allow a high enough compression ratio, at 9:1, to take full advantage of the detonation characteristics of natural gas.

Compared to the original arrangement, the bathtub configuration (code 3-2) is considerably more compact although the squish area is diminished. The flame travel path is reduced both from chamber compactness and the centrally located side ignition. A nominal compression ratio of 13:1 was adjusted by the use of gaskets of differing thickness.

The high ratio compact chamber was considered worthy of investigation since it has been reported to be suited to higher compression ratios and lean mixture operation. With this type of arrangement, the inlet and exhaust valves are seated at different depths producing a stepped combustion chamber with the majority of the volume situated under the

exhaust valve. This particular configuration incorporates a high degree of squish/compactness.

In both the new cylinder heads the inlet valves are offset from the bore centre line, potentially generating swirl by a directed outflow from the valves. In the Hrcc arrangement the inlet tract is offset from both the valve and cylinder centre lines forming a helical pre-chamber above the valve seat. A rotating, internally-tapered sleeve is incorporated within the port which allows the amount of swirl to be varied. This latter configuration consequently combines the features of both directed and helical ports. In the configurations applicable to data reported in this work however, the level of swirl is slight for all the chambers (see Chapter 9).

When comparing the effects of chamber arrangement it is essential to keep the volumetric efficiency constant at a given operating condition. Accordingly, the valve timing, geometry and lift remained unchanged throughout the test programme. Whilst some differences in port geometry were unavoidable, particularly when replacing the hybrid valve layout of the original configuration or including directed and helical port features in the Hrcc arrangement, the effect of these on the volumetric efficiency was anticipated to be moderate, in light of measurements made on the steady state flow rig (see Chapter 9) and the early parametric investigations. Such assumptions were subsequently justified as the experimental evidence accrued. Volumetric efficiencies are presented in Appendix II.

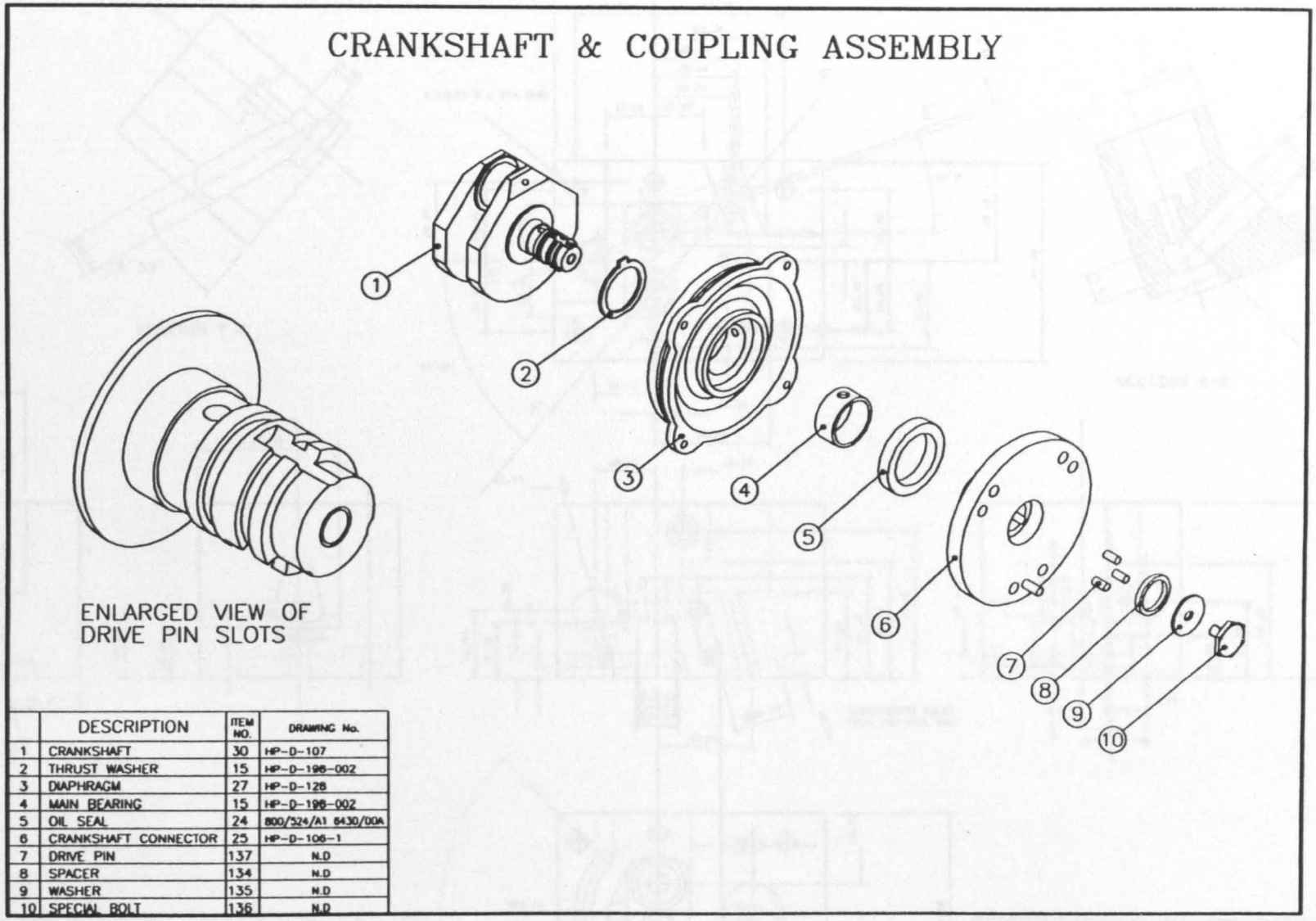

	DESCRIPTION	ITEM NO.	DRAWING No.
1	CRANKSHAFT	30	HP-D-107
2	THRUST WASHER	15	HP-D-198-002
3	DIAPHRAGM	27	HP-D-128
4	MAIN BEARING	15	HP-D-198-002
5	OIL SEAL	24	800/324/A1 8430/00A
6	CRANKSHAFT CONNECTOR	25	HP-D-106-1
7	DRIVE PIN	137	N.D
8	SPACER	134	N.D
9	WASHER	135	N.D
10	SPECIAL BOLT	136	N.D

Figure 3.1 Crankshaft and coupling assembly.

Figure 3.4 Combustion chamber geometry: TaskII.

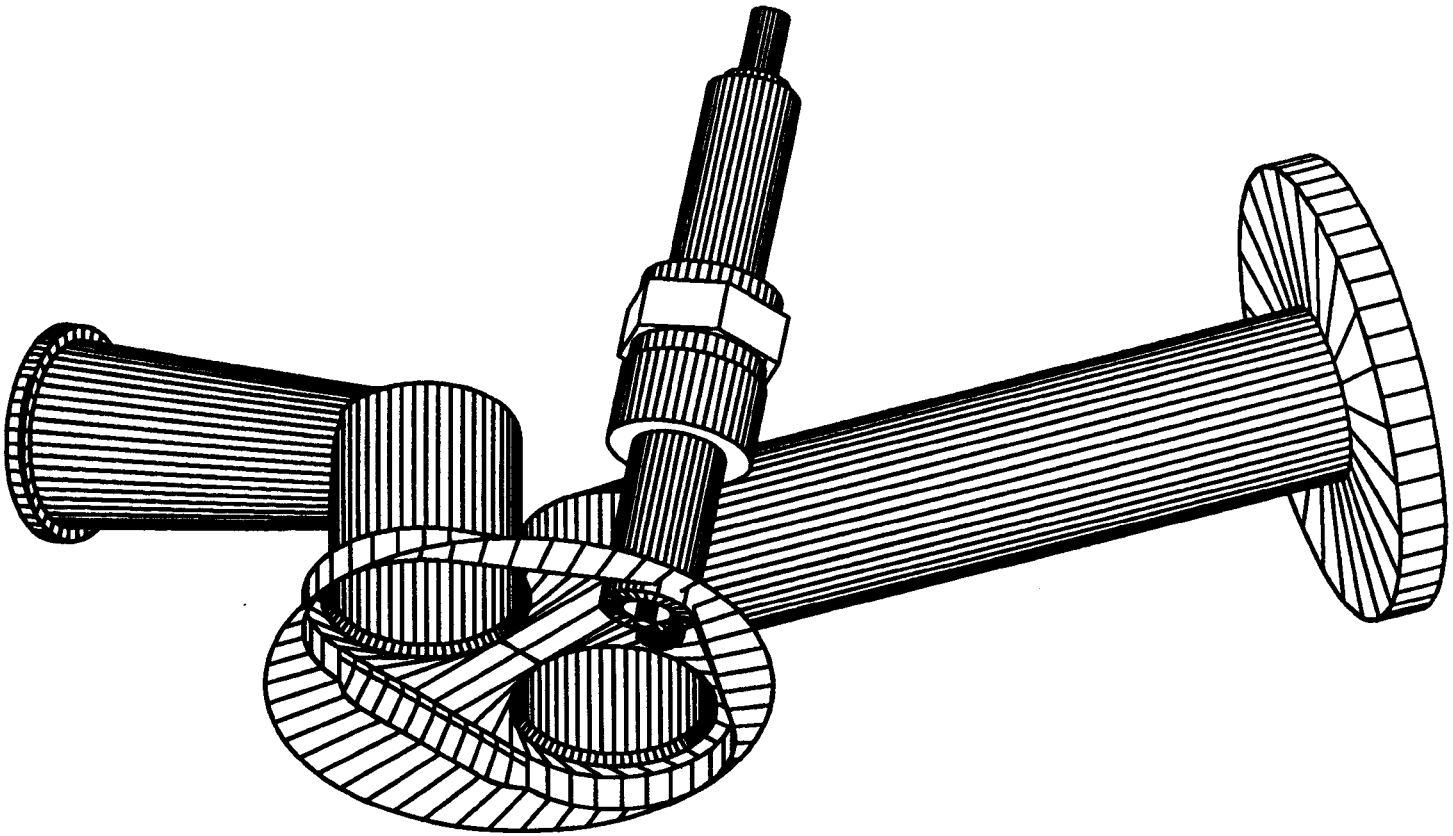

Figure 3.5 Combustion chamber geometry: 3-2.

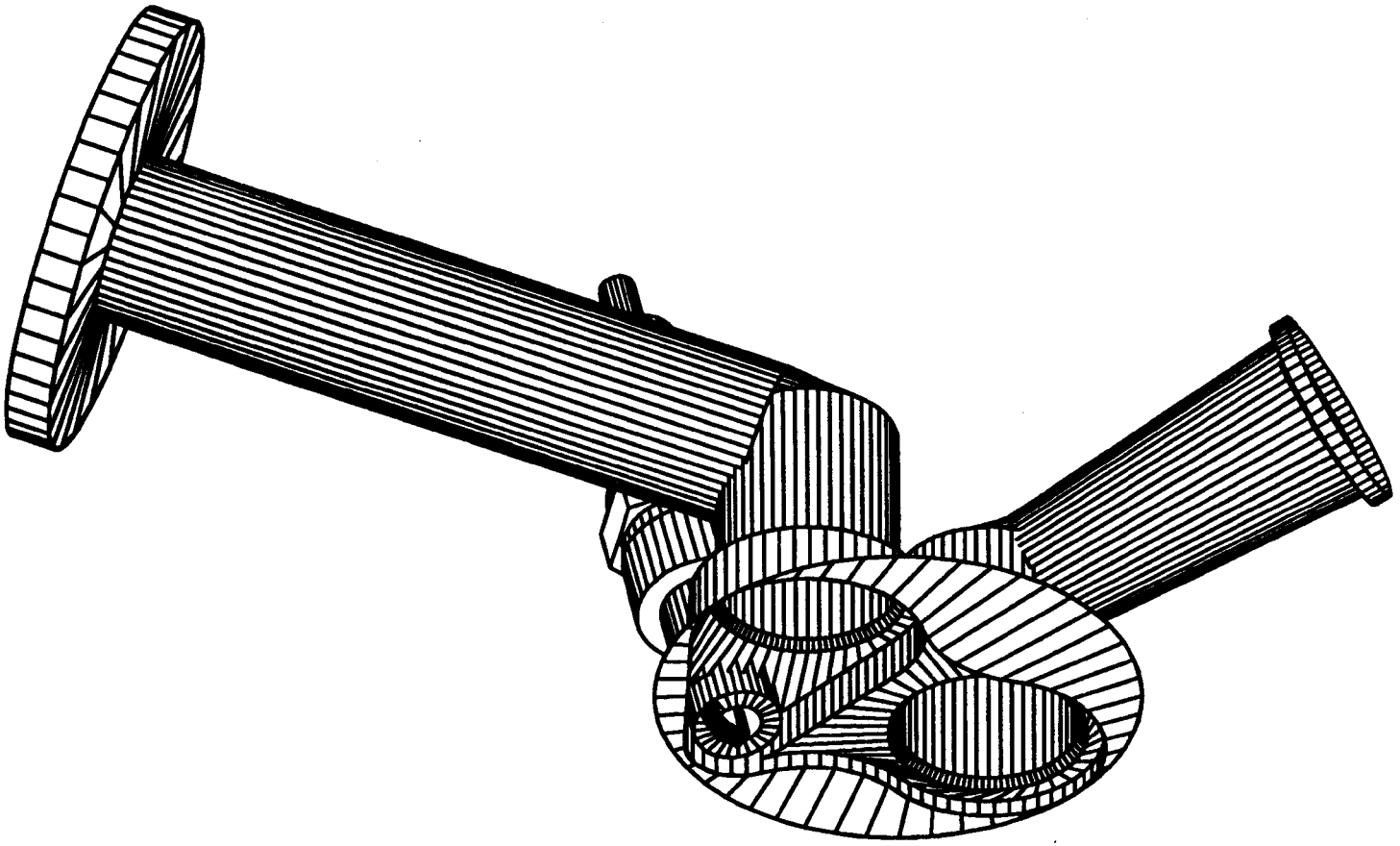

Figure 3.6 Combustion chamber geometry: Hrcc.

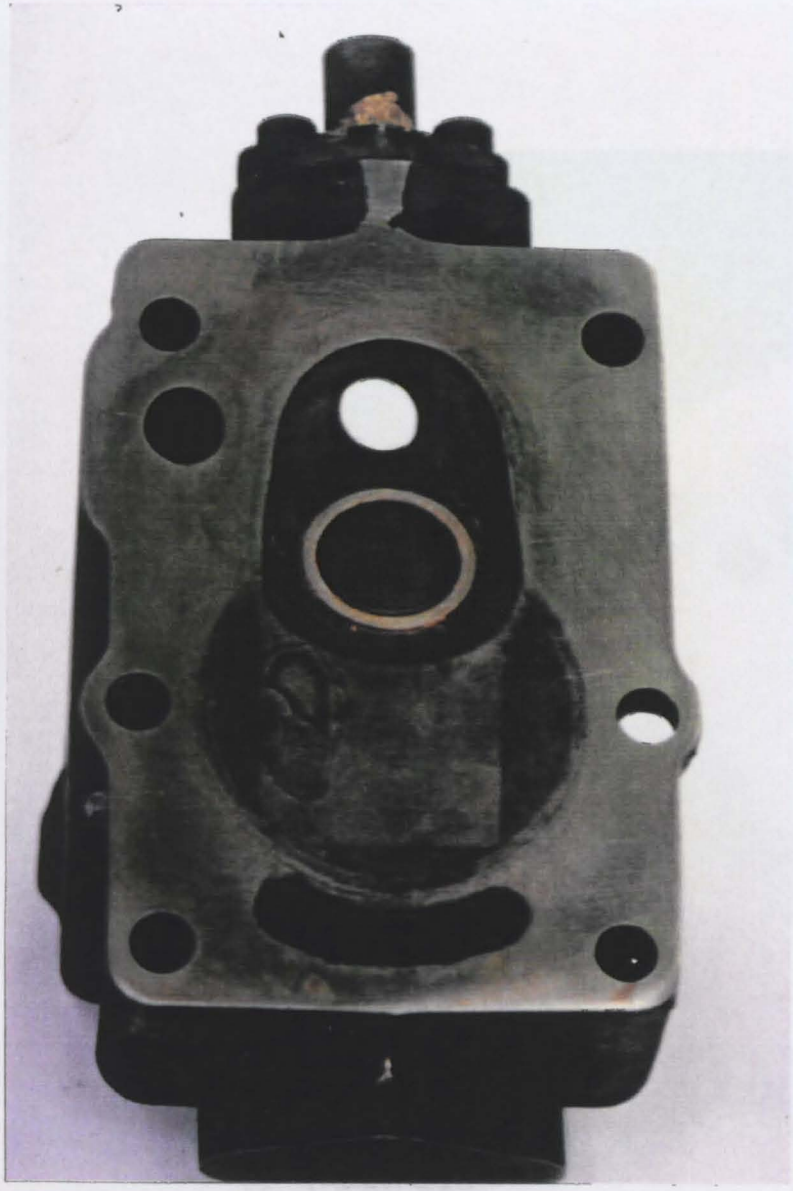

Plate 3.2 The original Task cylinder head.

Plate 3.1 Replacement connecting rod.

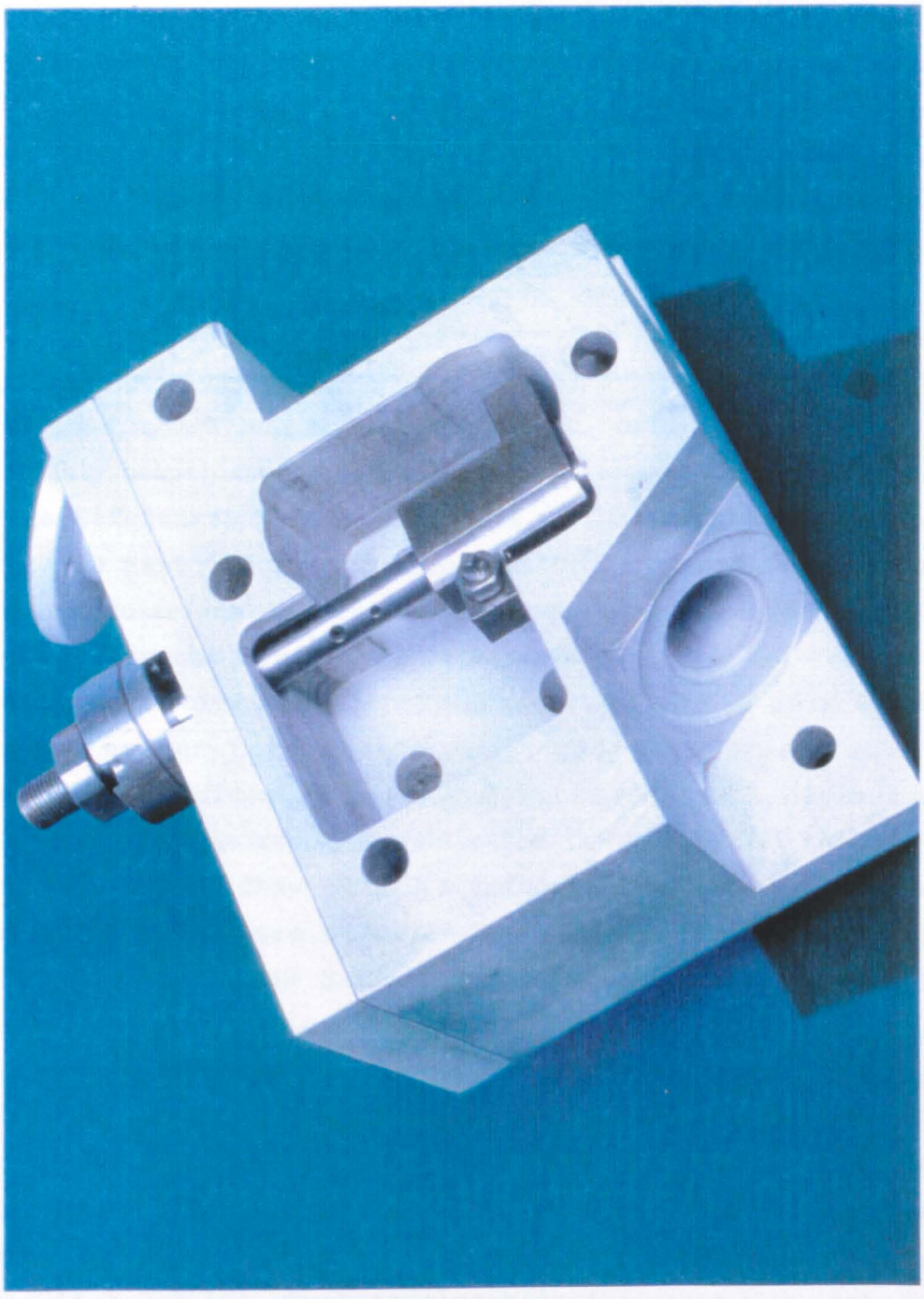

Plate 3.3 The revised cylinder head design.

CHAPTER 4 - COMPUTER SIMULATION

Summary

Previous studies of combustion and engine heat transfer processes together with modelling techniques of relevance to this work are reviewed in the following pages. The chapter concludes with a description of the structure of a closed cycle thermodynamic engine model and phenomenological sub-models synthesised as part of this study.

4.1 The combustion process

This highly complicated phenomenon is extensively documented in reviews such as References 2.8, 2.9 and 4.1 and currently retains a high profile in many research programmes. It is illuminating, however, at the outset to relate briefly some relevant aspects of the process and hence clarify the contextual framework for this and the following chapter. Qualitative analysis of the shape and growth of the reaction zone has arisen through the application of direct high speed photographic techniques to the combustion chamber with optical access achieved through quartz windows located in the cylinder head or piston crown, (4.2 - 4.4). These studies indicate that a highly convoluted flame front propagates outwards from the spark plug approximately spherical in shape until truncated by the cylinder wall. Due to the appreciable density ratio between the unburned and burned gases (around 4) significant unburned charge remains when the combustion space is almost completely enflamed; typically 50% remaining at 75% enflamed, (4.2). More sophisticated photographic methods sensitive to density variations in the charge such as schlieren or laser shadowgraph have provided additional information on the structure of the propagating flame, (4.5 - 4.10). Such studies have indicated that combustion is initiated with a small approximately spherical developing flame kernel of smooth surface containing high temperature gases. As the developing kernel expands away from the spark plug however, the turbulent nature of the flow within the chamber distorts the surface producing irregularities and also influences bodily movement through convective processes which can vary substantially between cycles, (4.5 and 4.11).

The evidence suggests that the growing flame is a wrinkled thin reaction sheet with thickness of the order of 0.1 mm separating burned and unburned gases, which moves through the chamber becoming increasingly wrinkled and convoluted but with diminishing scale, forming a turbulent 'brush' with thickness of the order of 5 to 10 mm, (4.5, 4.8, 4.12). Additionally, the evidence suggests that the scale of these wrinkles is dependent on a turbulent Reynolds number, (4.9, 4.10).

Flame development

A previous study, (4.13), concluded that the development of the flame follows four distinct stages; ignition and kernel growth, flame development, fully developed propagation and flame termination.

Johns, (4.14), following Chomiak, (4.15), refers to other features within the ignition and kernel growth period; a heat transfer period succeeding the spark where a cylindrical column of gas between the spark plug electrodes is heated to the self-ignition temperature and instantaneous self ignition of the gas, followed by a period during which the flame kernel is consolidated leading to the establishment of a self-propagating turbulent flame.

Numerous studies cited in Reference 4.16 and Reference 4.15 describe the very early stage of the ignition and kernel growth period as highly repeatable, possibly corresponding to a laminar flame growth. Chomiak, (4.15), found no dependence on turbulence, flow velocity, or mixture strength, Hirao and Kim (cited in Reference 4.16), no dependence on spark location or timing. Conversely, the subsequent period of kernel growth has been found to be highly irregular and to have a marked effect on burn rates in the fully developed period; it is thought to be responsible for the stochastic nature of the combustion process. The rate of flame propagation in the fully developed period has been found to be dependent on the duration of the ignition and kernel growth period; rapid rates of combustion associated with shorter ignition and kernel growth stages, (4.14, 4.17).

4.2 Combustion modelling

Despite the considerable effort directed towards a theoretical understanding of the combustion process, particularly stimulated in recent years by the desire for clean and thermally efficient engines, the extreme complexity of the mechanisms and processes described above and the difficulty associated with obtaining reliable and detailed measurements in the hostile environment of the combustion chamber has precluded a complete and fundamental insight and hence predictive capability is presently limited.

Whilst the underlying fundamental concepts are the goal of continuing and extensive research, a substantial body of information, mostly with reference to petrol-fuelled engines, has been generated over the years which has been used to develop simplified theoretical models incorporating empirically derived relationships or ad hoc approximations.

Contemporary modelling techniques fall into two main categories: the zero-dimensional models whose analytical structure emphasises an energy conservation approach where time is the single independent variable and the multi-dimensional models which emphasise the influence of a three-dimensional turbulent flow field on the combustion process. The zero-dimensional approach is currently applied to petrol-fuelled engines, where parametric studies of the combustion process are undertaken, and to engine design and development. Since the flow field is only partially represented such models require calibration to establish engine-specific constants. They are therefore of limited value for the study of changes in combustion chamber shape or inlet geometry, although Reference 4.18, for example, details an extensive investigation into the effects of the former. The multi-dimensional approach is currently the subject of ongoing and extensive research and attempts to provide both spatial and temporal resolution of thermodynamic properties, gas velocities and chemical species. The approach is presently restricted by limited knowledge of the fundamental concepts of combustion, lack of quality benchmark data - particularly related to the simultaneous measurements of flame speed and flow properties, (4.23), and computer storage facilities.

The zero-dimensional technique requires further detail in the form of sub-models to simulate such processes as the burn rate, turbulence, heat transfer, emissions and the geometry and interaction of the propagating flame with the confining walls of the combustion chamber.

4.2.1 Turbulence intensity

Ensemble averaging is commonly used to quantify the periodic flow encountered in internal combustion engines. The ensemble-averaged velocity, $\bar{u}_i$, is defined as the mean velocity of a component of the flow, u_i, at a given spatial and crankshaft position over a number of engine cycles, N:

$$\bar{u}_i(x,\theta) = \frac{1}{N}\sum_{j=1}^{N} u_i(x,\theta,j)$$

An instantaneous turbulent fluctuation, u_i', within a given cycle is then defined associated with that spatial and crankshaft position:

$$u_i(x,\theta,j) = \bar{u}_i(x,\theta) + u_i'(x,\theta,j)$$

The magnitude of the turbulent fluctuation is quantified by the turbulence intensity, u_i^t :

$$u_i^t(x,\theta) = \left[\frac{1}{N}\sum_{j=1}^{N} u_i'^2(x,\theta,j)\right]^{1/2}$$

Measurements of turbulence intensity

Induction-generated turbulence is known to decay following the closure of the inlet valve and in simple combustion arrangements incorporating disc chambers and flat topped pistons this condition persists throughout the compression stroke, (4.19). From the perspective of combustion modelling the turbulence intensity close to tdc on the compression stroke is of particular interest. A linear relationship for quiescent configurations with mean piston speed has been reported by numerous studies cited in References 4.19 - 4.23, the constant of proportionality varying from 0.3 to 0.5, viz.:

$$u_t = a\bar{S}_p$$

with turbulence nearly homogeneous and isotropic, (4.19).

The promotion of swirl - vortices with axes parallel to that of the cylinder - through induction arrangement has been found however, to both enhance and reduce the turbulence intensity close to tdc, (4.24, 4.25) and a positive effect has been achieved through reduced valve lift, (4.26). Whilst it might be expected that rapid compression of the unburned charge during combustion may effect enhanced turbulence intensity in the unconsumed mixture, Gosman, (4.23), cites conflicting evidence for such a mechanism.

4.2.2 Burn rate

Gosman, (4.23), classified the main approaches to simulating the burn rate as follows:

(i) The mass consumed varies as a prescribed function of crankangle.

(ii) Assuming the process is chemical-kinetically controlled and the volumetric fuel consumption rate varies according to a classical Arrhenius type relation.

(iii) Correlating the turbulent flame propagation speed to the laminar flame speed and turbulence intensity using empirical data.

(iv) Using a theoretically based turbulent combustion model.

In the first category are those relationships of Weibe, (4.27), and the cosine function, respectively:

$$x = 1 - \exp\left\{-a\left[(\theta - \theta_s)/\theta_b\right]^{(z+1)}\right\} \quad , \qquad x = \frac{1}{2}\left\{1 - \cos\left[(\theta - \theta_s)/\theta_b\pi\right)\right]\right\}$$

The predictive capability of such a technique is limited since the burn rate is dependent on operating and design variables. It is therefore, only appropriate where the objectives of the study are not critically dependent on the rate of heat release or are satisfied by a range of assumed profiles. Extended application has been achieved by correlating the shape parameter, z, with operating variables allowing interpolation between measurement points for a given combustion chamber, (4.14).

A commonly used approach is to correlate the turbulent flame propagation speed with properties of the flow field and the laminar flame speed, a relationship typically of the form:

$$\frac{S_t}{S_l} = a + bu_t$$

known as the flame speed ratio, FSR, where a and b are engine-specific constants and the turbulence intensity is taken to be proportional to engine speed, consistent with observation. Typical values of the constants for various engines are detailed in References 4.18, 4.28 and 1.58 and are of a similar order ($a \simeq 1$, $b \simeq 0.002$).

Alternative formulations, for example Reference 4.29, relate the turbulence intensity to an engine Reynolds number based on the mean jet velocity through the induction valve:

$$u_t = f\{Re\}$$

Observation has shown that the FSR varies throughout the combustion process, (4.13), and hence a consequence of such correlations is that they inadequately represent the flame development and flame termination stages where the flame speed ratio varies markedly. Theoretically or empirically based or ad hoc corrections have been applied to the FSR in these stages of flame propagation, (4.13, 4.18, 4.29). Further refinements to the FSR incorporate the scale of turbulence, (4.28, 4.30).

Turbulent entrainment models are distinguished from the previous approaches in that they attempt to simulate features of a turbulent combustion process from purely fundamental theoretical considerations. Tabaczynski, (4.20), describes their utility as 'a compromise between the global nature of the thermodynamic model and the specificity of the multi-dimensional models'.

Such a model was first proposed by Blizard and Keck, (4.31), and later refined in Reference 4.32. The original formulation was extended by Tabaczynski, (4.20), incorporating a more detailed eddy structure and refinements to the entrainment velocity assumptions.

An idealised spatially homogeneous, isotropic and coherent turbulent structure is assumed to exist in the combustion space. Figure 4.1 illustrates the coherent structure of a single turbulent eddy and the three length scales used to define the turbulence structure.

The integral length scale, L, defines the characteristic size of the large scale turbulent structure.

The Kolmogorov scale, η, defines the scale of the vortex tubes. Highly dissipative regions or vortex tubes of Kolmogorov thickness are assumed to be associated with the luminous reaction zone in a turbulent flame in which chemical reactions are assumed instantaneous. Ignition sites are assumed to propagate along the vortex tubes at a rate governed by convective and diffusive processes - the turbulence intensity and laminar flame speed respectively.

The Taylor microscale, λ, is defined as the spacing of the spaghetti-like vortex tubes and describes the internal structure of an eddy; at this scale laminar combustion predominates.

A characteristic reaction time, τ_c, is defined for the microscale as the time required to burn a cell of size, λ, at the laminar flame speed:

$$\tau_c = \frac{\lambda}{S_l}$$

The Taylor microscale is related to the macroscale and a turbulent Reynolds number, Re_t, through the relationship for isotropic turbulence:

$$\frac{\lambda}{L} = \left(\frac{15}{A}\right)^{1/2} (Re_t)^{-1/2} \quad \text{where} \quad Re_t = \frac{u_t L}{\nu}$$

and A is a constant equal to 1.

The eddy geometry is assumed approximately spherical with ignition occurring centrally and ignition sites propagating radially outwards along the vortex tubes.

A simplified relationship based on a numerical correlation is presented for the eddy burnup time, τ_b :

$$\tau_b = \left(\frac{L}{u_t}\right)^{1/3} 1.8 \left(\frac{\lambda}{S_l}\right)^{2/3}$$

An entrainment front is described as the surface which separates a region of burned, burning and unburned gas from a region of unburned gas. Propagation of the flame through the chamber is governed by two processes: (i) Entrainment of unburned charge by the flame according to:

$$\dot{m}_e = \sqrt{\rho_u \rho_b} u_e A_e$$

where u_e is an entrainment velocity and A_e the area of the entrainment front. (ii) Burning of the entrained charge at a rate proportional to the mass of unburned charge within the entrainment front according to:

$$\dot{m}_b = (m_e - m_b)/\tau_b$$

In a later work, (4.33), the model is extended to improve the transition from flame development to fully developed flame propagation. Unburned charge is entrained into the flame front at a velocity comprising a convective component, the turbulence intensity, and a diffusive component, the laminar flame speed according to:

$$\dot{m}_e = \rho_u A_e (u_t + S_l)$$

Subsequent inward burning of discrete cellular volumes of entrained charge occurs within the front from peripheral ignition sites at the laminar flame speed according to:

$$\dot{m}_b = \frac{m_e - m_b}{\tau_c}$$

Application of the model is simplified by a number of assumptions. The entrainment velocity is taken to be proportional to the turbulence intensity. At the time of the spark the turbulence intensity is assumed proportional to the mean piston speed and the integral scale proportional to the chamber height. Both variables are subsequently governed by the conservation of angular momentum. In Reference 4.20

this applies to the charge following 1% mass consumed and in Reference 4.33 after the passing of the spark, viz.:

$$u_t = u_{t,i}\left(\frac{\rho_u}{\rho_i}\right)^{1/3}, \quad L = L_i\left(\frac{\rho_i}{\rho_u}\right)^{1/3}$$

where subscript i refers to quantities evaluated at either ignition or 1% mass consumed.

Extensive validation of the Blizard and Keck model is detailed in Reference 4.34 and that of Tabaczynski et al. in Reference 4.30.

4.2.3 Geometry of the expanding flame front

In the zero-dimensional approach the flame front is assumed to propagate spherically, truncated by the chamber walls with the centre based at the source of ignition. With the radius of the expanding flame front specified and for chambers with simple geometries, relationships have been derived from purely geometrical considerations to describe the surface area of the expanding flame front and burned gas areas in contact with the cylinder head, walls and piston crown (4.18).

4.2.4 Heat transfer

The heat transferred from the working fluid to the engine cylinder varies appreciably with time and position according to the spatial and temporal variations in temperature, pressure, chemical species and gas velocities, together with large changes in surface area due to piston motion. The controlling mechanisms are those of convection and radiation and the rapid time rate of change in the gas temperature. The variance is such that both measurement and modelling prove extremely difficult. Notwithstanding, progress in engine development and cycle simulation benefits from the assumption of spatially averaged temporal values.

In the study of convective heat transfer under steady flow conditions a heat transfer coefficient is defined as:

$$\mathrm{h} = \frac{\dot{Q}}{A(T - T_w)}$$

and through the dimensionless groups for the forced convective condition according to:

$$Nu = a(Re)^b$$

With the assumption of quasi-steady flow, this concept is extended to an instantaneous heat transfer rate based on momentary values of both temperature difference and areas for the study of convective heat transfer in the engine cylinder. In a review of previous work, however, experimental evidence was cited to raise a fundamental objection to this approach. Due to the heat capacity of the fluid a time lag exists between the driving temperature difference and the heat transfer rate - implying an infinite value for the heat transfer coefficient at instants of zero temperature difference, (4.35).

Since the radiative component of the heat transfer in the spark-ignition engine is small, at around 5 to 10% of the convective, (2.8, 2.9), it is usually considered in lumped form or alternatively as a separate term based on a simplified approach, (4.35), according to:

$$\dot{Q} = Ac(T^4 - T_w^4)$$

where c is a constant.

In an extensive review of previous work, Annand, (4.35), concluded that the available formulae for predicting engine heat transfer were limited empirical relationships, defective both theoretically and dimensionally. Maintaining the quasi-steady state assumption on the grounds that heat transfer is small when the apparent heat transfer coefficient varies dramatically, he proposed an empirical relationship intended to account separately for both convective and radiative forms of heat transfer whose terms included the constants a and b to be evaluated for a given engine:

$$\frac{\dot{Q}}{A} = \frac{ak}{B}(Re)^{0.7}(T - T_w) + b(T^4 - T_w^4)$$

where T is the bulk gas temperature and $\mathbf{h}$ is evaluated through:

$$Nu = a(Re)^b$$

$$0.35 < a < 0.8, \quad b = 0.7$$

Woschni, (4.37), pointed out in a later review that for a given engine operating condition previous formulae, including that of Annand, gave widely varying results for closed cycle engine heat transfer. This he attributed largely to the erroneous application of a relationship derived from tests using a spherical bomb, where free convective conditions prevail. This relationship had been used by earlier workers together with lumped parameters or terms to describe the influence of piston motion and radiative effects, a typical example being that of Eichelberg, (4.38), which is still commonly used. Woschni proposed that the conditions within the chamber are more accurately described by an expression which considers forced convection in turbulent fluid flow, introducing a further term to account for convection induced by combustion. Radiative heat transfer is considered to be minimal and accounted for as a lumped parameter. The expression takes the following form:

$$Nu = 0.035(Re)^{0.8}$$

where the bore is the characteristic length and the average gas velocity is based on the mean piston speed together with an additional term to account for the effects of combustion.

The review of Woschni was succeeded by that of Hassan, (4.39), who also indicated inconsistency in previous formulae through a process of dimensional analysis. Using instantaneous measurements of gas and wall temperatures, gas velocity and gas pressure over the engine cycle in a series of motoring tests, correlations were produced however which supported the use of the Nusselt, Reynolds number relationship used in steady state forced convective heat transfer over flat plates or through pipes, confirming the functional form of the convective terms used for example by Woschni, (4.37).

Rao and Bardon, (4.40), attributed the inconsistency between the relationships to the unrealistic attempt to ascribe single representative values to the velocity and scale of turbulent fluid flow within the engine cylinder and proposed that the heat transfer coefficient be related to a more readily defined characteristic of flow such as the turbulence intensity, according to:

$$\mathrm{h} = 0.058\rho c_p u_t$$

A recent study on a motored compression ignition engine, (4.41), has reported significant heat transfer when the bulk gas and wall temperatures are of equal values. Also, during expansion, heat transfer from the wall to the gas was noted when the bulk gas temperature greatly exceeded that of the former. This was attributed to non-steady heat transfer and the interaction of temperature gradients within the bulk gas and the boundary layer where temperatures in the former are controlled by gas compression and in the latter by a diffusive mechanism. A simple modification to the expression of Annand was proposed to allow for these effects:

$$\frac{\dot{Q}}{A} = \frac{k}{B}\left\{a(Re)^b(T_g - T_w) - 2.75LT_w\right\} + c\sigma(T_g^4 - T_w^4)$$

where a, b and c are constants, T_g is the bulk gas temperature and L is a compressibility number.

4.3 Details of the engine model

4.3.1 Introduction

The closed cycle simulation synthesised as part of this study is based on a thermodynamic or zero-dimensional approach, incorporating a two-zone combustion model with the heat release specified as a prescribed function of crankangle based on experimental data correlated to the Weibe function, (4.27) and a flame development period specified according to the turbulent entrainment model of Hires et al., (4.30). The heat loss is calculated using a spatially-averaged instantaneous heat transfer coefficient based on both the Woschni, (4.37) and Eichelberg, (4.38), correlations. Compositions of equilibrium combustion products are determined using the method of Olikara and Borman, (4.42). Estimates of frictional loss are achieved through a synthesis of the correlations of Bishop, (2.4), Taylor, (4.43) and Millington, (4.44), or through correlations obtained from motoring tests with the engine in various stages of disassembly. Mass loss varies with engine speed and piston position according to a simple functional relationship calibrated from data obtained from blowby measurements. During compression the working fluid comprises a mixture of fuel, air and residual gas. Simultaneous integration of the set of

ordinary differential equations describing the rate of change of cylinder pressure, temperatures of burned and unburned zones, work, heat transfer and enthalpy loss with respect to crankangle is through the NAG library of numerical routines.

Major assumptions

During compression and combustion the unburned charge is regarded as a homogeneous mixture of air, fuel and residual gas at uniform pressure and temperature which behaves as a perfect gas with variable specific heats.

Combustion products are governed by chemical equilibria and are regarded as a homogeneous mixture at uniform pressure and temperature. The pressures of the burned and unburned zones are equal.

4.3.2 Formulation of equations

Application of the First Law of Thermodynamics to the control volume enclosing the cylinder contents with consideration to mass loss:

$$m\frac{du}{d\theta} + u\frac{dm}{d\theta} = \frac{dQ}{d\theta} - P\frac{dV}{d\theta} - \frac{\dot{m}_l h_l}{\omega}$$

Treating the unburned gas as an open system losing mass via leakage and combustion:

$$-\dot{Q}_u = \omega m(1-x)T_u\frac{ds_u}{d\theta}$$

Using the instantaneous mass leakage rate, $\dot{m}_l$ and defining a blowby constant, C,:

$$\frac{dm}{d\theta} = \frac{-\dot{m}_l}{\omega} = \frac{-Cm}{\omega}$$

Defining the mass fraction of cylinder contents that have been burned:

$$x = \frac{m_b}{m_b + m_u} = 1 - \exp\left\{-a\left[(\theta - \theta_s)/\theta_b\right]^{(z+1)}\right\}$$

Assuming the enthalpy loss is related to the burned fractional mass according to:

$$h_l = (1 - x^2)h_u + x^2 h_b$$

The specific internal energy of the system is :

$$u = \frac{U}{m} = xu_b + (1 - x)u_u$$

and

$$\frac{du}{d\theta} = x\frac{du_b}{d\theta} + (1 - x)\frac{du_u}{d\theta} + (u_b - u_u)\frac{dx}{d\theta}$$

The specific volume is given by:

$$v = \frac{V}{m} = xv_b + (1 - x)v_u$$

and

$$\frac{dv}{d\theta} = x\frac{dv_b}{d\theta} + (1 - x)\frac{dv_u}{d\theta} + (v_b - v_u)\frac{dx}{d\theta}$$

Writing the functional relationships between the specific volume, specific internal energy and specific entropy of the gas with the cylinder pressure and temperature as:

$$v_b = v_b(P, T_b)$$

$$v_u = v_u(P, T_u)$$

$$u_b = u_b(P, T_b)$$

$$u_u = u_u(P, T_u)$$

$$s_u = s_u(P, T_u)$$

Differentiating with respect to crankangle and introducing logarithmic derivatives:

$$\frac{dv_b}{d\theta} = \frac{v_b}{T_b}\frac{\partial \ln v_b}{\partial \ln T_b}\frac{dT_b}{d\theta} + \frac{v_b}{P}\frac{\partial \ln v_b}{\partial \ln P}\frac{dP}{d\theta}$$

$$\frac{dv_u}{d\theta} = \frac{v_u}{T_u}\frac{\partial \ln v_u}{\partial \ln T_u}\frac{dT_u}{d\theta} + \frac{v_u}{P}\frac{\partial \ln v_u}{\partial \ln P}\frac{dP}{d\theta}$$

$$\frac{du_b}{d\theta} = \left(c_{Pb} - \frac{Pv_b}{T_b}\frac{\partial \ln v_b}{\partial \ln T_b}\right)\frac{dT_b}{d\theta} - v_b\left(\frac{\partial \ln v_b}{\partial \ln T_b} + \frac{\partial \ln v_b}{\partial \ln P}\right)\frac{dP}{d\theta}$$

$$\frac{du_u}{d\theta} = \left(c_{Pu} - \frac{Pv_u}{T_u}\frac{\partial \ln v_u}{\partial \ln T_u}\right)\frac{dT_u}{d\theta} - v_u\left(\frac{\partial \ln v_u}{\partial \ln T_u} + \frac{\partial \ln v_u}{\partial \ln P}\right)\frac{dP}{d\theta}$$

$$\frac{ds_u}{d\theta} = \left(\frac{c_{Pu}}{T_u}\right)\frac{dT_u}{d\theta} - \frac{v_u}{T_u}\frac{\partial \ln v_u}{\partial \ln T_u}\frac{dP}{d\theta}$$

Assigning equal values for the heat transfer coefficient in the burned and unburned zones and neglecting heat transfer between the zones:

$$\frac{dQ}{d\theta} = \frac{-\dot{Q}_l}{\omega} = \frac{-\dot{Q}_b - \dot{Q}_u}{\omega} = \mathbf{h}\left[A_b(T_b - T_w) - A_u(T_u - T_w)\right]/\omega$$

where the areas of burned and unburned zones are assumed to be:

$$A_b = \left(\frac{\pi b^2}{2} + \frac{4V}{b}\right)x^{1/2} \quad , \quad A_u = \left(\frac{\pi b^2}{2} + \frac{4V}{b}\right)1 - x^{1/2}$$

From geometric considerations the cylinder volume at any crankangle is given by:

$$V = V_0\left[1 + \frac{r-1}{2}\left\{1 - \cos\theta + \frac{1}{\epsilon}\left[1 - (1 - \epsilon^2\sin^2\theta)^{1/2}\right]\right\}\right]$$

The above relationships can be manipulated into standard form for simultaneous numerical integration, viz.:

$$\mathbf{A} = \frac{1}{m}\left(\frac{dV}{d\theta} + \frac{VC}{\omega}\right)$$

$$B = \mathrm{h}\frac{\left(\frac{\pi b^2}{2} + \frac{4V}{b}\right)}{\omega m}\left[\frac{v_b}{c_{Pb}}\frac{\partial \ln v_b}{\partial \ln T_b}x^{1/2}\frac{T_b - T_w}{T_b} + \frac{v_u}{c_{Pu}}\frac{\partial \ln v_u}{\partial \ln T_u}(1 - x^{1/2})\frac{T_u - T_w}{T_w}\right]$$

$$\mathbf{C} = -(v_b - v_u)\frac{dx}{d\theta} - v_b\frac{\partial \ln v_b}{\partial \ln T_b}\frac{h_u - h_b}{c_{Pb}T_b}\left[\frac{dx}{d\theta} - \frac{(x - x^2)C}{\omega}\right]$$

$$D = x\left[\frac{v_b^2}{c_{Pb}T_b}\left(\frac{\partial \ln v_b}{\partial \ln T_b}\right)^2 + \frac{v_b}{P}\frac{\partial \ln v_b}{\partial \ln P}\right]$$

$$E = (1 - x)\left[\frac{v_u^2}{c_{Pu}T_u}\left(\frac{\partial \ln v_u}{\partial \ln T_u}\right)^2 + \frac{v_u}{P}\frac{\partial \ln v_u}{\partial \ln P}\right]$$

$$\frac{dP}{d\theta} = \frac{\mathbf{A} + B + \mathbf{C}}{D + E}$$

$$\frac{dT_b}{d\theta} = \frac{-\mathrm{h}\left(\frac{\pi b^2}{2} + \frac{4V}{b}\right)x^{1/2}(T_b - T_w)}{\omega m c_{Pb}x} + \frac{v_b}{c_{Pb}}\frac{\partial \ln v_b}{\partial \ln T_b}\left(\frac{\mathbf{A} + B + \mathbf{C}}{D + E}\right)$$

$$+\frac{h_u - h_b}{x c_{Pb}}\left[\frac{dx}{d\theta} - (x - x^2)\frac{C}{\omega}\right]$$

$$\frac{dT_u}{d\theta} = \frac{-\mathrm{h}\left(\frac{\pi b^2}{2} + \frac{4V}{b}\right)(1 - x^{1/2})(T_u - T_w)}{\omega m c_{Pu}(1 - x)} + \frac{v_u}{c_{Pu}}\frac{\partial \ln v_u}{\partial \ln T_u}\left(\frac{\mathbf{A} + B + \mathbf{C}}{D + E}\right)$$

$$\frac{dW}{d\theta} = P\frac{dV}{d\theta}$$

$$\frac{dQ_l}{d\theta} = \frac{\mathrm{h}}{\omega}\left(\frac{\pi}{2}b^2 + \frac{4V}{b}\right)\left[x^{1/2}(T_b - T_u) + (1 - x^{1/2})(T_u - T_w)\right]$$

$$\frac{dH_l}{d\theta} = \frac{Cm}{\omega}\left[(1 - x^2)h_u + x^2 h_b\right]$$

Specification of the outstanding thermodynamic and transport properties, logarithmic derivatives together with the heat transfer coefficient and initial conditions required for the solution of the above equations is described in the following sections.

Further details of the method including a programme listing are described in Reference 2.8.

4.3.3 Burn rate

The heat-release profile was specified according to the Weibe, (4.27), function:

$$x = 1 - \exp\left\{-a\left[(\theta - \theta_s)/\theta_b\right]^{(z+1)}\right\}$$

In the calculation of heat-release profiles from experimental pressure data a number of previous studies, (4.14, 4.18, 4.45), have reported maximum fractional mass burned within the range 70 to 90%. This has been attributed to cyclic dispersion, flame quenching and inaccuracies in measurement or assumptions within the heat release calculations. Addressing the effects of such experimental errors and theoretical assumptions, Peters and Borman, (4.46), concluded that the maximum fractional mass consumed is most sensitive to errors in the inducted mass and absolute pressure reference, with weak dependence on residual fraction assumptions, the pressure-crankangle phasing, the heat transfer correlation, burned gas dissociation and the assignment of uniform burned gas temperature. The effects of significant errors in

this work are discussed in Chapter 6. A normalised fractional mass burned curve was defined:

$$\frac{x}{\hat{x}} = 1 - \exp\left\{-a\left[(\theta - \theta_s)/\theta_b\right]^{(z+1)}\right\}$$

The normalised function was achieved using the measured values of hydrocarbon emissions, an estimation for blowby based on experimental data together with an assumption of the magnitude of post-combustion hydrocarbon oxidation levels:

$$\frac{x}{\hat{x}} = 1 - \text{uhc} - \text{oxidation} - \text{blowby}$$

Using rapid gas sampling techniques, post-combustion hydrocarbons within engine cylinders have been measured at one and a half to twice the level of average exhaust concentrations, (4.47, 4.48). Based on these observations and the experimental hydrocarbon analysis, the magnitude of post-combustion oxidation was set to a representative value of 0.06.

4.3.4 Flame development

The incorporation of a flame development model coupled with that of main stage combustion is of particular interest in combustion analysis and has utility for an overall heat pump simulation. Providing the main stage combustion can be modelled adequately from empirically derived correlations describing the change in the shape and duration factors with operating conditions, greater flexibility in specifying heat release timing is provided. Clearly predictive capability is limited to the envelope between measurements or operating points, however, there is potential to describe engine performance in a form analogous to, but extended from, the nomograph or engine map. Furthermore, such models assist the understanding of the mechanisms involved in flame development and close agreement between generalised relationships and experimental data support the quality of the latter.

The flame development period was modelled according to the turbulent entrainment approach detailed in References 4.20 and 4.30 and reviewed in Section 4.2.2.

Formulation of equations

The solution of a second order differential equation describing the burning process of a single turbulent eddy produces the following correlation for two dimensionless parameters:

$$\tau^* = 1.8\epsilon^{2/3}$$

where:

$$\tau^* = \frac{\tau_b}{\tau_e} \quad \text{and} \quad \epsilon = \frac{\tau_c}{\tau_e}$$

τ_b is the characteristic reaction time to burn the mass of an eddy of characteristic size L, the integral scale.

τ_e is the eddy half life, $\tau_e = \dfrac{L}{u_t}$

τ_c is the characteristic chemical reaction time, $\tau_c = \dfrac{\lambda}{S_l}$

Substitution of the above relationships for the dimensionless parameters, τ^* and ϵ gives the characteristic reaction time to burn a turbulent eddy of characteristic size L:

$$\tau_b = \left(\frac{L}{u_t}\right)^{1/3} 1.8 \left(\frac{\lambda}{S_l}\right)^{2/3}$$

Assuming that the flame development stage is completed at 1% mass consumed and that this is proportional to the characteristic reaction time:

$$\theta_d = C_1 \tau_b$$

Using the relationship for isotropic turbulence:

$$\frac{\lambda}{L} = \left(\frac{15}{A}\right)^{1/2} (Re_t)^{-1/2}$$

where the value of the constant A is 1 and Re_t is the turbulent Reynolds number:

$$Re_t = \frac{u_t L}{\nu}$$

Assuming that the integral scale and turbulence intensity are proportional to the instantaneous chamber height, h, and mean piston speed respectively:

$$L = C_2 h \quad \text{and} \quad u_t = C_3 \bar{S}_p$$

The flame development period can be written as:

$$\theta_d = C(\bar{S}_p \nu)^{1/3} \left(\frac{h}{S_l}\right)^{2/3}$$

where C is an engine-specific constant to be evaluated, stated to be independent of operating conditions, and:

h	- instantaneous chamber height	(m)
S_l	- laminar flame speed	(m/s)
$\bar{S}_p$	- mean piston speed	(m/s)
θ_d	- flame development period	(degrees)
ν	- kinematic viscosity	(m^2/s)

Whilst such turbulent entrainment models have been validated over a wide range of operating conditions with petrol-fuelled engines, (4.30), there is no evidence of a similar study with a natural gas-fuelled engine. Such study is of value not only with respect to the difference in fuel type but also in the light of the higher compression ratios and very weak mixture strengths utilised, since these variables influence the characteristic reaction time through the laminar flame speed and integral scale dependency.

4.3.5 Heat transfer

Heat transfer was modelled using the instantaneous, spatially-averaged correlation of Woschni, (4.37), based on the empirical relationship appropriate to forced convection in turbulent flow in pipes or over flat plates:

$$Nu = 0.035(Re)^{0.8}$$

where the bore is taken to be the characteristic length and the velocity taken as the local average gas velocity within the cylinder. Since the latter is unknown both in magnitude or with variation in

crankangle, Woschni determined empirical formulations relating the gas velocity, w, to mean piston speed.

During induction and exhaust: $w = 6.18\,\bar{S}_p$

During compression: $w = 2.28\,\bar{S}_p$

During combustion and expansion Woschni considered gas velocity from piston motion augmented by that induced by combustion, wc:

$$w = 2.28\,\bar{S}_p + wc$$

An empirical correlation was developed for wc:

$$w = 2.28\,\bar{S}_p + 3.24.10^{-3}\,Vs\,T_1(P - Po)/P_1V_1$$

where:

P	- instantaneous gas pressure	(bar)
P_1	- gas pressure at inlet valve closure	(bar)
Po	- gas pressure in the cylinder corresponding to the motored engine	(bar)
$\bar{S}_p$	- mean piston speed	(m/s)
T_1	- gas temperature at inlet valve closure	(K)
V_1	- cylinder volume at inlet valve closure	(cm^3)
V_S	- swept volume	(cm^3)
w	- local average gas velocity	(m/s)

Radiative effects are considered as a lumped parameter.

A limited comparative study was undertaken using the Eichelberg, (4.38), relationship where convective heat transfer within the engine is based on experimental data obtained from tests on a spherical bomb and corrected for the effects of piston motion and radiation according to:

$$\mathrm{h} = 0.523.10^{-6}\left(\frac{SN}{300}\right)^{1/3}(P.T)^{1/2}$$

where:

h -	heat transfer coefficient	(W/mm^{2}K)
N -	engine speed	(rpm)
P -	gas pressure	(bar)
S -	stroke	(mm)
T -	gas temperature	(K)

4.3.6 Equilibrium analysis

The composition of equilibrium combustion products, specific heats, thermodynamic properties and logarithmic derivatives are calculated according to the method of Olikara and Borman, (4.42). Specific heat data are curve fitted to polynomials in temperature according to Gordon and McBride (cited in Reference 2.8).

The pressure, temperature, fuel composition and equivalence ratio of a hydrocarbon fuel are specified and the combustion reaction proceeds according to:

$$\epsilon\phi C_\alpha H_\beta O_\gamma N_\delta + 0.21O_2 + 0.79N_2 \rightarrow \nu_1 CO_2 + \nu_2 H_2O + \nu_3 N_2$$
$$+\nu_4 O_2 + \nu_5 CO + \nu_6 H_2 + \nu_7 H$$
$$+\nu_8 O + \nu_9 OH + \nu_{10} NO$$

where ϵ is the stoichiometric molar fuel-to-air ratio, ϕ is the fuel-to-air equivalence ratio and ν_i the molar coefficients of the product species.

Atom balancing produces four equations:

$$\begin{array}{lll} C & \epsilon\phi\alpha & = (y_1 + y_5)N \\ H & \epsilon\phi\beta & = (2y_2 + 2y_6 + y_7 + y_9)N \\ O & \epsilon\phi\gamma + 0.42 & = (2y_1 + y_2 + 2y_4 + y_5 + y_8 + y_9 + y_{10})N \\ N & \epsilon\phi\delta + 1.58 & = (2y_3 + y_{10})N \end{array}$$

where y_i is the molar fraction of the product species and N the total number of moles of products.

Also by definition a further relationship:

$$\sum_{i=1}^{10} y_i - 1 = 0$$

Introducing equilibrium constants produces a total of eleven equations for the ten unknown mole fractions, y_i, and the number of moles, N:

$$\frac{1}{2}H_2 \rightleftharpoons H \qquad K_1 = \frac{y_7 P^{1/2}}{y_6^{1/2}}$$

$$\frac{1}{2}O_2 \rightleftharpoons O \qquad K_2 = \frac{y_8 P^{1/2}}{y_4^{1/2}}$$

$$\frac{1}{2}H_2 + \frac{1}{2}O_2 \rightleftharpoons OH \qquad K_3 = \frac{y_9}{y_4^{1/2} y_6^{1/2}}$$

$$\frac{1}{2}O_2 + \frac{1}{2}N_2 \rightleftharpoons NO \qquad K_4 = \frac{y_{10}}{y_4^{1/2} y_3^{1/2}}$$

$$H_2 + \frac{1}{2}O_2 \rightleftharpoons H_2O \qquad K_5 = \frac{y_2}{y_4^{1/2} y_6 P^{1/2}}$$

$$CO + \frac{1}{2}O_2 \rightleftharpoons CO_2 \qquad K_6 = \frac{y_1}{y_5 y_4^{1/2} P^{1/2}}$$

where P is the pressure in atmospheres.

Equilibrium constants, K_p, are curve fitted to data from JANAF tables according to the following functional form:

$$\log K_p = A\,ln(T/1000) + B/T + C + DT + ET^2$$

where T is the temperature in Kelvin.

Manipulation of the above relationships yields four non-linear equations in four unknowns, y_3, y_4, y_5, y_6:

$$f_j\{y_3, y_4, y_5, y_6\} = 0 \quad j = 1,2,3,4$$

As a first approximation the molar fractions are assigned the known values of the molar coefficients for low temperature combustion products, yielding the vector:

$$\left[y_3^{(1)}, y_4^{(1)}, y_5^{(1)}, y_6^{(1)}\right]$$

which is close to the solution vector:

$$[y_3^*, y_4^*, y_5^*, y_6^*]$$

Let $\Delta y_i = y_i^* - y_i^{(1)}$

Neglecting second order and higher derivatives, the four non-linear equations, $f_j\{y_3, y_4, y_5, y_6\} = 0$ are expanded round the known vector as a Taylor's series to produce a set of four linear equations that yield approximations to Δy_i, i = 3, 4, 5, 6:

$$f_j + \frac{\partial f_j}{\partial y_3}\Delta y_3 + \frac{\partial f_j}{\partial y_4}\Delta y_4 + \frac{\partial f_j}{\partial y_5}\Delta y_5 + \frac{\partial f_j}{\partial y_6}\Delta y_6 \approx 0 \quad j = 1,2,3,4$$

where f_j and their partial derivatives are evaluated at the known vector. A Gaussian elimination method is employed to solve for Δy_i, i = 3, 4, 5, 6.

Further details of the method together with that used to calculate transport properties, including programme listings, are described in References 2.8 and 4.42.

4.3.7 Friction model

A detailed investigation into the distribution of frictional losses within the engine was undertaken as part of this programme of work (see Section 7.10). Correlations were produced from experimental data obtained by motoring the engine in various stages of disassembly. These describe the mechanical losses associated with the main engine components and the overall mechanical loss with simulated combustion pressures. Pumping correlations were also obtained with the engine both firing and motoring at wot. A comparative study of these results with the correlations presented by other workers suggested a synthesis of previous work, (2.4, 4.43, 4.44), most closely fit the experimental data with the advantage of geometric generality. The correlation is as follows:

$$fmep = 370.10^3\frac{S}{B^2}n + 756.10^3\frac{M}{BS}\bar{S}_p + 2083imep + 414\frac{B}{S}NK$$

$$+393.10^3[30-0.24N]\frac{GH^{1.75}}{B^2S} + 600\bar{S}_p^2$$

where the terms describe respectively: piston ring wall tension, piston viscous friction, a gas pressure term, journal bearing viscous friction, the valve train, and the pumping loss.

K is defined as:

$$K = \frac{6}{B^3}[a^2c + b^2d/m + e^2f]$$

where:

a	-	main bearing diameter	(mm)
B	-	bore	(mm)
b	-	rod bearing diameter	(mm)
c	-	total length of all main bearings/ number of cylinders	(mm/cylinder)
d	-	rod bearing length	(mm)
e	-	accessory shaft bearing diameter	(mm)
f	-	total length of all accessory shaft bearings/ number of cylinders	(mm/cylinder)
$fmep$	-	friction mean effective pressure	(N/m^2)
G	-	number of intake valves per cylinder	
H	-	intake valve head diameter	(mm)
$imep$	-	indicated mean effective pressure	(bar)
M	-	projected area of piston skirt/ cylinder bore diameter	(mm)
m	-	number of pistons per rod bearing	
N	-	engine speed	(rev/sec)
n	-	total number of piston rings per cylinder	
S	-	stroke	(mm)
$\bar{S}_p$	-	mean piston speed	(m/s)

Heat/mass loss or ancillaries are not included.

The engine-specific correlations obtained from the experimental data were incorporated into the engine model for validation purposes and energy flow analysis. The overall correlation synthesised above is included as a more generalised tool in prototype development.

4.3.8 General specifications

Conditions at inlet valve closure

At inlet valve closure the temperature of the charge is specified by the inducted mass and cylinder pressure which are known from experimental measurement together with an assumed value for the residual mass.

Residual mass

The residual fraction is known to vary with changes in operating and design conditions such as engine speed, mixture strength, compression ratio, throttle position and valve timing, (1.57). A residual fraction of 7% was assumed based on values reported in the literature commensurate with the range of design and operating conditions under investigation, (1.57, 1.58, 4.18, 4.30, 4.45).

Blowby allowance

Based on experimental observation (see Section 7.5) mass loss is specified according to:

$$m_l = -0.3N + 14.26$$

where m_l is the mass loss to blowby (percentage of incoming charge) and N is the engine speed in rev/sec.

The experimental blowby measurements were correlated to the following function:

$$\frac{m}{\tilde{m}} = \exp\left[\frac{-C(\theta+\pi)}{\omega}\right]$$

Before the calculations commence at inlet valve closure a simple iterative technique is employed to evaluate the constant, C, so that experimental and theoretical mass loss are equal at exhaust valve opening.

Wall temperature assignment

In the absence of experimental data a survey of the literature, (1.47, 1.58, 4.1, 4.14, 4.18, 4.28, 4.49, 4.50), suggested that a typical wall temperature of the order of 400 K was appropriate.

4.3.9 Data input and output

All data required by the engine model is read in from file and includes a calibrated set of ensemble-averaged pressure-crankangle data, the appropriate operating and design variables, gas quality and emissions analysis together with statistical parameters, performance and heat release criteria, heat transfer data and the variables required to set initial conditions and mass loss.

Results from the cycle simulation are written to file and a graphical routine employed to compare the theoretical and experimental pressure-crankangle diagram.

Using the above data files, a detailed comparison of experimental and theoretical criteria, including fractional mass burned, heat transfer, gas analysis and performance data, is presented in graphical and tabulated form. Typical output is detailed in Figure 4.2. All other operating points are included in Appendix I.

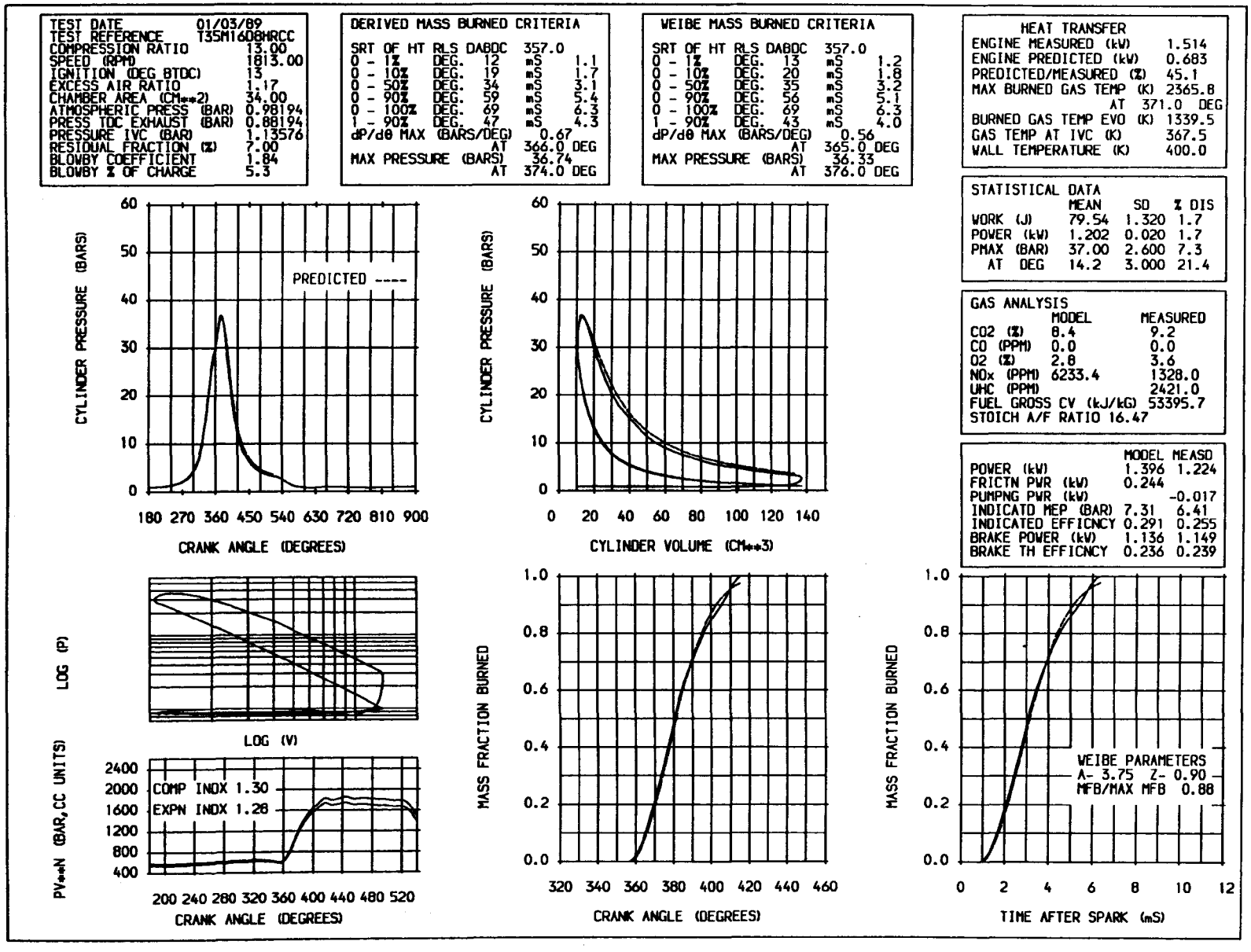

Figure 4.2 Comparison between measured data and model output.

References

4.1 Fenton, J. (Ed.)
Gasoline engine analysis.
University Press, Cambridge, 1986.

4.2 Rassweiler, G.M., Withrow, L.
Motion pictures of engine flames correlated with pressure cards.
SAE Transactions, Vol. 42, No. 5, pp. 185-204, 1938.

4.3 Nakanishi, K., Hirano, T., Inoue, T., Ohigashi, S.
The effects of charge dilution on combustion and its improvement - flame photograph study.
SAE paper 750054, 1975.

4.4 Nakamura, H., Ohinouye, T., Hori, K., Kiyota, Y., Nakagami, T., Akishino, K., Tsukamoto, Y.
Development of a new combustion system (MCA-JET) in gasoline engine.
SAE paper 780007, 1978.

4.5 Gatowski, J.A., Heywood, J.B., Deleplace, C.
Flame photographs in a spark-ignition engine.
Combust. Flame, Vol. 56, pp. 71-81, 1984.

4.6 Witze, P.O.
The effect of spark location on combustion in a variable-swirl engine.
SAE paper 820044, 1982.

4.7 Witze, P.O., Vilchis, F.R.
Stroboscopic laser shadowgraph study of the effect of swirl on homogeneous combustion in a spark-ignition engine.
SAE paper 810226, 1981.

4.8 Heywood, J.B., Vilchis, F.R.
Comparison of flame development in a spark-ignition engine fuelled with propane and hydrogen.
Combust. Sci. Technol., Vol. 38, pp 313-324, 1984.

4.9 Uzkan, T. (Ed.)
Flows in internal combustion engines: article by Smith, J.R., The influence of turbulence on flame structure in an engine.
ASME, New York, 1982.

4.10 Smith, J.R.
Turbulent flame structure in a homogeneous-charge engine.
SAE paper 820043, 1982.

4.11 Beretta, G.P., Rashidi, M., Keck, J.C.
Turbulent flame propagation and combustion in spark ignition engines.
Combust. Flame, Vol. 52, No. 3, pp. 217-245, 1983.

4.12 Keck, J.C.
Turbulent flame structure and speed in spark-ignition engines.
Proceedings of the Nineteenth International Symposium on Combustion, The Combustion Institute, pp. 1451-1466, 1982.

4.13 Lancaster, D.R., Krieger, R.B., Sorenson, S.C., Hull, W.L.
Effects of turbulence on spark-ignition engine combustion.
SAE paper 760160, 1976.

4.14 Johns, R.A.
The analysis of the combustion of methanol in lean-burning, high-compression engines using an engine combustion model.
Ph.D. Thesis, University of Surrey, 1985.

4.15 Chomiak, J.
Flame development from an ignition kernel in laminar and turbulent homogeneous mixtures.
Seventeenth Symposium on Combustion, pp. 255-263, 1978.

4.16 Young, M.B.
Cyclic dispersion in the homogeneous-charge spark-ignition engine - a literature survey.
SAE paper 810020, 1981.

4.17 Young, M.B.
Cyclic dispersion - some quantitive cause-and-effect relationships.
SAE paper 800459, 1980.

4.18 Brunt, M.F.J.
The effect of combustion chamber design on the combustion rate in an S.I. engine.
Ph.D. Thesis, Loughborough University of Technology, 1980.

4.19 Arcoumanis, C., Whitelaw, J.H.
Fluid mechanics of internal combustion engines - a review.
Proc. Instn. Mech. Engrs., Vol. 201, No. C1, pp. 57-74, 1987.

4.20 Tabaczynski, R.J., Ferguson, C.R., Radhakrishnan, K.
A turbulent entrainment model for spark-ignition engine combustion.
SAE paper 770647, 1977.

4.21 Tabaczynski. R.J.
Turbulence measurements and modelling in reciprocating engines - an overview.
Proceedings of International Conference on Combustion in Engineering, Vol. 1, 1983, paper C51/83 (Mechanical Engineering Publications, London).

4.22 Davis, G.C., Tabaczynski, R.J., Belaire, R.C.
The effect of intake valve lift on turbulence intensity and burn rate in S.I. engines - model versus experiment.
SAE paper 840030, 1984.

4.23 Gosman, A.D.
Aspects of the simulation of combustion in reciprocating engines. Proceedings of Symposium on Numerical Simulation of Combustion Phenomena, France, 1985. Lecture Notes in Physics, Vol. 241 (Springer-Verlag, Berlin).

4.24 Liou, T.M., Hall, M., Santavicca, D.A., Bracco, F.V.
Laser doppler velocimetry measurements in valved and ported engines.
SAE paper 840375, 1984.

4.25 Bopp, S., Vafidis, C., Whitelaw, J.H.
The effect of engine speed on the tdc flowfield in a motored reciprocating engine.
SAE paper 860023, 1986.

4.26 Stivender, D.L.
Intake valve throttling (IVT) - a sonic throttling intake valve engine.
SAE paper 680399, 1968.

4.27 Weibe, J.J.
Das Weibe-Brenngesitz, ein Fortschnitt in der Thermodynamik der Kreigspozesses von Verbrennungsmotoren.
Trans. by Prof. A. Joute and T.H. Dresen, Kraftfahrzeugtechnik, Vol. 9, Berlin, 1960.

4.28 Newlyn, H.A.
The effects of changes in engine geometry on the breathing and combustion in a spark ignition engine.
Ph.D. Thesis, Leicester Polytechnic, 1982.

4.29 Samaga, B.S., Murthy, B.S.
On the problem of predicting burning rates in a spark ignition engine.
SAE paper 750688, 1975.

4.30 Hires, S.D., Tabaczynski, R.J., Novak, J.M.
The prediction of ignition delay and combustion intervals for a homogeneous charge, spark ignition engine.
SAE paper 780232, 1978.

4.31 Blizard, N.C., Keck., J.C.
Experimental and theoretical investigation of turbulent burning model for internal combustion engines.
SAE paper 740191, 1974.

4.32 Keck, J.C., Heywood, J.B., Noske, G.
Early flame development and burning rates in spark ignition engines and their cyclic variability.
SAE paper 870164, 1987.

4.33 Tabaczynski, R.J., Trinker, F.H., Shannon, B.A.S.
Further refinement and validation of a turbulent flame propagation model for spark-ignition engines.
Combust. Flame, Vol. 39, pp. 111-121, 1980.

4.34 McCuiston, F.D., Lavoie, G.A., Kauffman, C.W.
Validation of a turbulent flame propagation model for a spark ignition engine.
SAE paper 770045, 1977.

4.35 Annand, W.J.D.
Heat transfer in the cylinders of reciprocating internal combustion engines.
Proc. Instn. Mech. Engrs., Vol. 177, No. 36, pp. 973-996, 1963.

4.36 Nusselt, W.
Die Warmeubergang in den Verbrennungskraftmaschinen.
Z. Ver. Dtsch. Ing., Vol. 67, pp. 692 and 708, 1923.

4.37 Woschni, G.
A universally applicable equation for the instantaneous heat transfer coefficient in the internal combustion engine.
SAE paper 670931, 1967.

4.38 Eichelberg, G.
Some new investigations on old combustion engine problems.
Engineering, Vol. 148, pp. 463 and 547, 1939.

4.39 Hassan, H.
Unsteady heat transfer in a motored internal combustion engine cylinder.
Proc. Instn. Mech. Engrs., Vol. 185, No. 80, pp. 1139-1148, 1970-1971.

4.40 Rao, V.K., Bardon, M.F.
Convective heat transfer in reciprocating engines.
Proc. Instn. Mech. Engrs., Vol. 199, No. D3, pp. 221-225, 1985.

4.41 Lawton, B.
Effect of compression and expansion on instantaneous heat transfer in reciprocating internal combustion engines.
Proc. Instn. Mech. Engrs., Vol. 201, No. A3, pp. 175-186, 1987.

4.42 Olikara, C., Borman, G.L.
A computer program for calculating properties of equilibrium combustion products with some applications to I.C. engines.
SAE paper 750468, 1975.

4.43 Taylor, M.P.
The effect of gas pressure on piston friction.
SAE Trans., Vol. 38, No. 5, pp. 200-205, 1936.

4.44 Millington, B.W., Hartles, E.R.
Frictional losses in diesel engines.
SAE paper 680590, 1968.

4.45 Peters, B.D.
Mass burning rates in a spark ignition engine operating in the partial-burn regime.
Instn. Mech. Engrs. Conference on Fuel Economy and Emissions of Lean-Burning Engines, paper C92/79, London, 1979.

4.46 Peters, B.D., Borman, G.L.
Cyclic variations and average burning rates in a S.I. engine.
SAE paper 700064, 1970.

4.47 LoRusso, J.A., Lavoie, G.A., Kaiser, E.W.
An electrohydraulic gas sampling valve with application to hydrocarbon emissions studies.
SAE paper 800045, 1980.

4.48 Weiss P., Keck, J.C.
Fast sampling valve measurements of hydrocarbons in the cylinder of a CFR engine.
SAE paper 810149, 1981.

4.49 Zeleznik, F.J., McBride, B.J.
Modeling the complete Otto cycle - preliminary version.
SAE paper 770223, 1977.

4.50 Finlay, I.C., Harris, D., Boam, D.J., Parks, B.I.
Factors influencing combustion chamber wall temperatures in a liquid-cooled, automotive, spark-ignition engine.
Proc. Instn. Mech. Engrs., Vol. 199, No. D3, pp. 207-214, 1985.

CHAPTER 5 - COMBUSTION ANALYSIS

Summary

In this chapter the utility of fractional mass consumed curves is discussed together with the parameters used to characterise the combustion process. Combustion, flame development and laminar flame speed models developed for combustion analysis and as sub-models in an overall closed cycle thermodynamic model are described. A method of producing heat-release curves from experimental pressure-crankangle data is evaluated within the context of the objectives of the study and the method subsequently employed for capture and analysis of such data is described. The effect of a wide range of operating and design variables on rates of heat release is discussed and evaluated using the experimental data in conjunction with the diagnostic combustion model. A turbulent entrainment flame development model is validated over a similar range in design and operating conditions. The relationship between the durations of the flame development and rapid burn stages of the combustion process is considered.

5.1 Introduction

A survey of the literature has revealed only limited information from the analysis of pressure data or combustion rates in natural gas-fuelled engines, (4.45, 5.1 - 5.4), and no evidence of studies made on units of similar capacity to the Task engine. A number of workers have reported more general performance criteria relating to output and emission levels which were discussed in Chapter 1.

Mass fraction burned curves derived from experimental pressure-crankangle data provide information on rates of combustion and the various stages of flame propagation. Although somewhat arbitrary in nature, or to some extent based on convenience, parameters of interest are chosen to characterise reference states near which the salient features of flame growth and propagation occur. Figure 5.1 shows a typical curve illustrating the parameters used to characterise the combustion process. The flame development period is usually taken as 1 or 10% of the mass consumed although other fractions of 5 and 2% have

been used, (4.18, 4.34, 5.5). This stage is considered to represent the duration of the ignition and kernel growth period and is the point on the pressure-crankangle diagram where the pressure deviates significantly from that due to motoring only.

To gain greater insight into this period of flame propagation it proved convenient in some cases to consider two further stages: that from the initiation of the spark to the point at which PV^n deviates from the value associated with compression only and the succeeding portion to 1% mass consumed. The former stage has been described as the ignition delay or lag, (5.4, 5.6), at the end of which flame kernel initiation has been considered to commence, (5.4).

It is of interest to note that pressure analysis techniques based on the two-zone model, employed with the objective of quantifying the early stages of flame growth through expansion velocities of the developing flame kernel, (4.14), suggest that such definitions conform closely at stoichiometric and near stoichiometric conditions with the heat transfer and kernel consolidation and growth stages referred to in fundamental studies, (4.15) and discussed earlier in Section 4.1. Poor correlation has been observed however at weak mixture strengths due to less robust kernel growth. In keeping with these studies the two stages of flame development are referred to in this work as the heat transfer and kernel growth periods.

The heat transfer stage is that period in which the pressure rise due to combustion is too small to be detected. Calculations for the cumulative mass fraction burned commence at the end of this period. The 1% mass consumed consequently corresponds to the kernel consolidation and growth stage and as such is indicative of the quality of kernel development.

The rapid burn stage reflects the portion from the end of flame development to the end of flame propagation during which a fully developed turbulent flame front has traversed the chamber and most of the mass is burned, typically 90% of the charge consumed. The burn duration is the duration of the combustion process and the sum of the previous periods. Scatter in experimental data and/or the difficulty

involved with locating precisely the start and end of combustion favour the choice of the 0 to 10% and the 10 to 90% parameters, (4.18, 4.30). Although some difficulty was encountered locating the end of combustion, by comparison the start of heat release proved relatively straightforward to identify and the 1% and the 1 - 90% definitions were consequently adopted in this work.

5.2 Range of experimental observation

Pressure-crankangle data were obtained at the stoichiometric air-to-fuel ratio and the lean mixture limit for all the configurations, engine speeds and compression ratio settings investigated. Data were also taken at 30 rev/sec at the excess air ratio for peak efficiency with optimum, retarded and advanced ignition settings.

It was recognised before conducting this work that significant changes in chamber geometry might occur from increasing the compression ratio. However, the effects on performance were unclear and consequently parallel compression ratio tests were undertaken on a Ricardo E6 variable compression engine through a range from 8 to 16:1. The tests were conducted at 30 rev/sec with the weakest mixture for maximum power and minimum spark advance for maximum torque.

In practice the restrictions on lean mixture operation are most likely those of tolerable hydrocarbon emission levels and load fluctuation. Accordingly, the definition of lean mixture limit in this work (see Section 2.3) encompasses these considerations although other more rigorous definitions have been used (see Reference 4.45 for example). Due to the wide range of combustion characteristics associated with each of the configurations investigated, particularly the tolerance to weakening mixture strength, comparisons between chambers at the lean mixture limit are often at a dissimilar excess air ratio. To some extent this restriction results from the conflicting objectives of producing and analysing original data and investigating a lean burn strategy. It may be argued, and rightly, that the former precedes the latter but both objectives are compromised ultimately by the time available for the study.

5.3 Combustion model

Experimental mass fraction burned data were correlated to the Weibe function, (4.27), using an interactive graphical technique. The function takes the following form:

$$\frac{x}{\hat{x}} = 1 - \exp\left\{-a[(\theta - \theta_s)/\theta_b]^{(z+1)}\right\}$$

The shape and duration parameters, z and a respectively, allow great flexibility in specifying the heat-release profile; the former controlling the points of inflexion and hence representing the early stages of combustion, the latter controlling the slope of the function and hence representing the rapid burn stage of the heat-release process. High values for the duration parameter indicate a diminished rapid burn stage whilst reduced flame development is associated with low values for the shape parameter.

5.4 Flame development model

A preliminary investigation suggested that the turbulent entrainment model proposed by Blizard and Keck, (4.31), later refined by Tabaczynski, (4.20), and extensively validated with petrol-fuelled engines by Hires et al., (4.30), gave good predictive capability when compared with experimental results. The model benefits from relative ease of use providing a suitable relationship for the laminar flame speed can be established. The expression for flame development, 0 to 1% mass burned, takes the following form:

$$\theta_d = C(\bar{S}_p \nu)^{1/3} \left(\frac{h}{S_l}\right)^{2/3}$$

The constant, C, was evaluated at a single operating condition for each engine. The other terms were defined in Section 4.3.4. Some flexibility in the assignment of the magnitude of the integral scale arises through the geometry of the combustion chamber, particularly with the Hrcc configuration which utilises a stepped cross-section and the TaskII chamber which incorporates a sloping roof. Chamber depths of 7.5, 4.25 and 3.4 mm were found satisfactory for the TaskII, 3-2 and Hrcc arrangements respectively. In the case of the Ricardo the choice is

straightforward since the combustion chamber is a disc of diameter equal to the bore. A shortcoming of such turbulent entrainment models arises through the difficulty in specifying the variation in the entrainment velocity and scale of turbulence throughout the engine cycle, (4.34), and single values ascribed to these variables is usual. Hence weaker correlation between predicted and experimental flame development periods are to be expected when durations are lengthy and/or piston movement appreciable. Time-averaged values over the flame development period have been used to overcome this problem, (4.30). In this work the quantities are evaluated at the start of combustion (i.e. PV^n deviates from linearity).

5.5 Laminar flame speed correlation

A previous study of spark-ignited engines utilising gaseous fuels concluded that empirically derived relationships, incorporating pressure and temperature dependence over the range of these variables usually found in the engine, most closely matched experimental data, (5.1). For the particular case of methane it was found that experimental data due to Babkin and Kosachenko, (5.7), evaluated over such conditions and correlated to an expression of functional form attributed to Kuehl, (5.8), had good predictive capability and suggested a similar approach for this work. References 5.9 - 5.10 detail other applications of the correlation of Kuehl. The expression is of the following form:

$$S_l = \frac{10^4}{[(10^4/T_b) + (900/T_u)]^{2.64}} P^{(0.00055T_u - 0.622)}$$

where:

P	- cylinder pressure	(atmospheres)
S_l	- laminar flame speed	(cm/sec)
T_b	- burned gas temperature	(K)
T_u	- unburned gas temperature	(K)

5.6 Analysis of pressure-crankangle data

Analysis of pressure-crankangle data was undertaken using the well established method of Rassweiler and Withrow, (4.2), in which the total pressure rise over a sampling interval is attributed to the pressure rise resulting from the change in volume due to the motion of the piston and that resulting from combustion. The method accounts for pressure rise due to piston motion by reducing the total incremental pressure rise over a sampling interval by the incremental pressure rise that would occur from polytropic compression or expansion over the interval. The combustion pressure rise over the volume of the interval is then referred to an equivalent pressure rise at the volume in the chamber at ignition. The summation of the preceding constant volume pressure increments at any crankangle to the total of such constant volume pressure rise increments was found to correlate with the fractional mass burned at that crankangle determined using high-speed photography. A simplified treatment presents the result:

$$x(\theta) = \frac{(Pv^n)_\theta - (Pv^n)_I}{(Pv^n)_F - (Pv^n)_I}$$

A similar relationship follows from a First Law analysis in References 4.34 and 5.5.

Although the method is widely used for analysis of experimental pressure-crankangle data, including commercially available packages such as Epicas, the technique does have certain limitations. In particular, a single value for the polytropic exponent is not consistent with observation. At lean mixture strengths partial burning may occur and fractional mass is unlikely to reach unity; lengthy combustion implies greater deviation from constant volume assumptions.

Comparison with two-zone, zero-dimensional combustion models, in which cumulative fractional mass consumed curves are produced from experimental pressure-crankangle data, have however, been markedly favourable around stoichiometric air-to-fuel ratios, (4.14, 4.18, 5.11). A less favourable comparison at weaker mixture strengths is reported by Johns, (4.14), attributed to partial burning cycles in which the pressure rise method over-predicts burn rates.

It is unlikely that this latter consideration is of undue concern in this work since measured levels of hydrocarbon emissions were of the same order of magnitude at both the stoichiometric air-to-fuel ratio and at the lean mixture limit and furthermore, with the comparative analysis undertaken in this work any error applies equally to all configurations. Additionally, all mean cycle data sets satisfy the criteria of complete combustion reported by Peters, (4.45), viz.: 20% mass burned by 25 degrees atdc, although individual cycle analysis was not undertaken.

Start and end of combustion

Following Rassweiler and Withrow, (4.2), the end of combustion can be ascertained by noting the crankangle at which the pressure rise due to combustion only is equal to or less than zero. Similarly, a combustion pressure rise greater than zero indicates the start of combustion on compression.

A second proposition utilises the fact that PV^n is sensibly constant prior to and after combustion. Numerical searching routines could easily be envisaged, based on either method, to identify when the appropriate conditions occurred for large numbers of cycles.

A problem associated with these methods is that scatter exists in the data towards the end of combustion. PV^n may fluctuate and pressure increments due to combustion alone may assume both positive and negative values, (4.14). Moreover, the slope of PV^n after combustion, and hence the apparent end of combustion, is strongly influenced by any error in the value of the polytropic exponent of expansion, (4.18).

The latter approach was used by Brunt, (4.18), but difficulty was encountered in selecting an appropriate value for the expansion index. It was concluded that a clearly defined end of combustion was evident only when a value for the expansion index was used which was equal to or lower than the true value. Consistent results were obtained using a value based on the compression index less an arbitrary constant.

Value of the polytropic index

Following the original derivation of Rassweiler and Withrow, (4.2), and the theoretical analysis by Harrington, (5.5), an average value of the measured polytropic indices of compression and expansion was assumed. Other methods have based calculations on the measured compression index prior to the initiation of the spark, (4.18, 5.11).

Evaluating the rate and quality of combustion

A number of parameters were used to evaluate the rate and quality of the combustion process. These included the timing and magnitude of the peak pressure and maximum rate of pressure rise together with parameters derived from the cumulative mass fraction burned curve which were taken to represent the various stages of flame growth or propagation. Ensemble averaging was undertaken due to the stochastic nature of the combustion process and statistical analysis was applied to the magnitude and timing of peak pressures of the individual cycles comprising the average: the percentage dispersion and standard deviation. When considering the implications of these parameters in comparative studies it is essential also to consider the influence of volume change due to piston motion on the pressure-time history.

Production of fractional mass burned curves

Pressure-crankangle data were down-loaded from the Biodata Microlink on-line data acquisition system to an IBM XT microcomputer and then to the Prime 750 mainframe computer at the Polytechnic. Analysis was conducted using interactive graphics software which was developed in Fortran 77 using the Ghost-80 library of graphical sub-routines. The output from the mean cycle analysis is correlated in graphical and tabular form in the figures of Appendix I. Each figure corresponds to a single operating point. Also presented in the figures is a comparison between the experimental and predicted values returned by the model, which will be referred to later in the text.

The initial stage involved calibration of the pressure data and evaluation of the pressure to crankangle assignment. Each cycle was

displayed for inspection on a log P/log V plot. Single cycle analysis was undertaken including statistical methods applied to the work, power and to the timing and magnitude of peak pressure, also average values for the polytropic index were obtained over 15 degree intervals at two positions along the compression line; prior to ignition and 40 to 55 degrees after bdc. Specimen output is included in Figure III.55 (Appendix III).

The ensemble-averaged cycle was produced from such calibrated pressure-crankangle data and displayed for inspection on a log P/log V plot. Average values of the polytropic indices of compression and expansion were evaluated over 15 degree intervals; prior to ignition, 40 to 55 degrees after bdc and 55 to 40 degrees before bdc. The timing and magnitude of the peak pressure and the work and power for the mean cycle were also calculated. Operational and mean cycle pressure-crankangle data together with the polytropic indices were written to file.

In order to overcome the difficulty of accurately specifying the completion of combustion (discussed previously in Section 5.6) an interactive graphical method was devised which has application to mean cycle analysis or to a limited number of consecutive cycles. The technique is based on the fact that PV^n is sensibly constant prior to and after combustion. PV^n was plotted to an enlarged scale using a nominal value for the polytropic index during the compression or expansion process. An updated value for the index was requested until PV^n appeared constant either prior to combustion or during expansion. The crankangle for the start or end of combustion was then identified. The value of the mean compression index could then be calculated from bdc to the start of combustion and that of the mean expansion index calculated from the end of combustion to near exhaust valve opening.

Using the mean cycle pressure-crankangle data, the crankangles at which combustion was initiated and completed together with the mean indices of expansion and compression evaluated previously, the mass fraction burned was evaluated according to the method of Rassweiler and Withrow, (4.2) and Harrington, (5.5). Graphical output presented pressure/crankangle, pressure/volume, PV^n/crankangle and mass fraction burned to

an angular and time base. Fractional mass burned criteria, together with operational and performance data were written to the graph and to file in tabulated form.

The previous method was extended to include calculations of the mass fraction burned based on the Weibe function, (4.27). An interactive graphical technique was used to adjust the shape and duration parameters until the theoretical function conformed closely to the experimental data.

5.7 Experimental results and discussion

The experimental results are discussed in the following format: the influence of operating variables on the rate of combustion is identified with particular reference to the measured and theoretical flame development period together with the rapid burn stage. The combustion rates are related to other pressure-derived parameters such as the maximum rate of pressure rise and peak pressures, with due consideration given to the phasing of heat release - which recognises the influence of piston-induced pressure and volume change. The salient points are outlined in a summary preceding each section. The tabulated and graphical output included in this chapter is derived from the detailed Figures I.2 - I.57 (Appendix I).

5.7.1 Values of the polytropic indices

Consistent with other studies, (2.3, 2.9, 4.2, 4.18), the polytropic indices of compression and expansion were found to be within the range 1.30 +/- 0.07 for the Ricardo E6 engine and the Task engine in all configurations. In contrast to the measurements made on the Ricardo engine and values reported by other workers, (4.2, 4.18), the index of expansion on the Task unit at 1.30 +/- 0.07, was noted to be marginally higher than that for compression at 1.28 +/- 0.05, most probably reflecting the level of mass loss measured in this engine (see Section 7.5).

5.7.2 The effect of compression ratio

Summary

The influence of increasing compression ratio on combustion rates in the Task engine compared with the effect in the Ricardo E6 unit at stoichiometric conditions is characterised by greater changes in geometry which are thought to be unfavourable. The flame development period shows a lesser dependence and is of shorter duration, the burn duration increases rather than decreases and is lengthier. Peak pressure dispersion is lower. The optimum compression ratio setting for maximum indicated efficiency occurs at a markedly lower value of 10:1 compared with a setting of 13:1 noted for the Ricardo. At compression ratios above 14:1, the influence of knock-limited timing is thought to promote extended burn durations in the Ricardo E6 engine.

A lengthening flame development stage in the Task engine, arising largely from an increasing heat transfer period, results from weakening mixtures and is significantly ameliorated by an increase in compression ratio. It is thought that an unfavourable influence from chamber geometry with increasing compression ratio restricted a similar but less marked effect on the rapid burn duration up to a setting of 12:1. Weaker mixtures favour a higher compression ratio for improved efficiency and enhanced combustion stability.

With the exception of very lean mixtures at high compression ratio settings where durations are lengthy, the measured and predicted flame development periods are remarkably consistent. Poor correlation, where observed, is thought most likely to arise as a consequence of representing the flow field by variables evaluated at a single point in the cycle.

The influence of compression ratio: Ricardo E6 engine

Experimental and theoretical data are presented in Table 5.2 and Figure 5.2. Theoretical and experimental flame development stages are compared in Figure 5.22.

A moderate reduction in the burn duration (0 to 90%) from 5.1 to 4.7 ms is evident from increasing compression ratio until a value of 14:1 is exceeded. This is noted to result through a reducing flame development period since the rapid burn stage remains unchanged at around 3.4 ms. The reducing flame development evidently occurs through shorter heat transfer, as reported by Johns, (4.14) and kernel growth stages with the greatest proportional reduction associated with the latter. Flame development relationships such as that of Hires et al., (4.30), imply a reduced flame development period with increasing compression ratio at constant speed, since it is assumed that the turbulence intensity scales with mean piston speed, the integral scale is proportional to chamber height and higher temperatures and pressures follow reduced volumes influencing the laminar flame speed. Note that the changing integral scale is the dominant variable influencing the development period. (Laminar flame speed dependency is complicated by the inverse pressure relationship and excess air varies moderately between settings.)

A further implication is that since only small changes in mass burned-to-crankangle phasing were observed, changes in performance parameters - indicated power and efficiency, arise largely from changes in the combustion-volume phasing resulting from increasing compression ratio. It is however evident from the literature that this is clearly not the general case since burn rates have been found to reduce, (5.12), moderately increase, (4.28, 4.34), and remain substantially unchanged, (Mayo, cited in 4.28), with increasing compression ratio.

Marked increases in peak cylinder pressure from around 40 to 70 bar together with significant increases in the maximum rate of pressure rise from around 1.25 to 2.0 bars/degree are noted, the timing of both parameters closing to tdc as the compression ratio increases. Note also that this suggests that the timing of peak pressure is not necessarily indicative of the proportion of mass burned - an observation consistent with the findings of some other workers, (5.12).

No discernible dependence on compression ratio can be identified for the dispersion of the magnitude of peak pressures, at typically 11%; the deviation of the timing of peak pressure reduces steadily however

with increasing compression ratio from 3 to 1.2. Other workers (Soltau, Winsor and Patterson, cited in 4.16) suggest only a weak steadying dependence of these parameters with increases in compression ratio from 6 to 12:1, attributed to higher temperatures and lower residuals. The latter work reports a constant peak pressure dispersion at 12.5% for compression ratios above 8:1.

Increasing the compression ratio above 14:1 markedly increases the rapid burn period without further change in the flame development. Note that although the latter is inconsistent with the reducing ratio of integral scale to laminar flame speed, the magnitude of the discrepancy is within the limits to be anticipated from measurement and subsequent analytical techniques. Ignition is knock-limited at 15:1, hence compared with the lower setting, heat release is initiated later in the stroke. Combustion-crankangle phasing reduces chamber compactness, despite volume change due to compression ratio increase and favours lower cylinder pressures and temperatures together with reducing laminar flame speed. Increased duration appears to be present in all stages of fully developed flame propagation suggesting that under the conditions investigated, combustion-volume phasing through knock-limited timing is the dominant factor in increased burn duration. Flame quenching at higher compression ratios reported by Curry, (5.13), in the latter stage of the combustion process does not seem to be the only factor. Later and longer combustion duration is reflected in later and reduced peak pressures together with reduced rates of pressure rise, the timing of the latter now associated with the early stage of the rapid burn period prior to tdc in contrast to the early expansion stroke at the lower compression ratios. The dispersion remains substantially unchanged.

<u>The influence of compression ratio: Task engine at stoichiometric conditions</u>

Experimental and theoretical data are presented in Table 5.3 and Figure 5.3. Theoretical and experimental flame development stages are compared in Figure 5.22.

Extended burn duration (4.7 to around 6.0 ms) and rapid burn period (3.5 to 4.7 ms) arise as the compression ratio increases from 9 to 13:1; a lesser dependency is noted between the settings of 12 and 13:1. The flame development period shows a weak tendency to diminish in duration from 1.19 to 1.09 ms over the range, consistent with the changing ratio of integral scale to laminar flame speed, and evidently without commensurate effect on the rapid burn stage. The intervals associated with the heat transfer and kernel growth stages show no discernable trend. (Limited testing at 25 and 35 rev/sec at settings of 12 and 13:1 indicates that the durations of the flame development and rapid burn stages at these speeds are similarly dependent on compression ratio. Further detail is given in Figures I.14, I.15, I.31 and I.32 - Appendix I.) A 9 degree spark retard over the range, together with increasing burn duration imply notable changes in combustion-crankangle phasing. From 9 to 10:1, the detrimental effect on performance from later and longer burn duration is evidently offset by reduced volume as the compression ratio increases, since the maximum indicated efficiency occurs at this setting (see Table 7.3).

Compared with the Ricardo the duration of the flame development stage is shorter most notably at lower compression ratios; by around 26% at 9:1. Whilst some difference in laminar flame speeds is apparent the most significant parameter affecting the duration of flame development between the engines at a given compression ratio is the variation in the integral scale.

In keeping with the Ricardo no clear trend-wise dependence on compression ratio can be discerned for the dispersion of peak pressures, whilst in contrast, the timing and magnitude of peak cylinder pressures, the maximum rate of pressure rise and the dispersion of the peak pressure indicate a transitional feature between settings of 10 and 12:1.

It is illustrative in this respect to consider the changing geometry of the chamber as the compression ratio increases over the range in the cases of the Task engine and the Ricardo. For the former engine, the nominal chamber depth is 4.25 mm which requires a change in gasket thickness from 3.25 to 0.621 mm to increase the compression ratio from

9 to 14:1. Consequently at the low compression ratios most of the volume of the chamber, 60%, is situated in the disc space between the piston and the bathtub while at the higher ratios around 60% is contained in the bathtub. The surface area-to-volume ratio at tdc varies from 2.25 to 3.19. The Ricardo disc chamber reduces in depth from 13.9 to 8.6 mm whilst the surface area-to-volume ratio at tdc varies from 1.24 to 1.69.

It may be concluded that in the case of the Task engine, a marked geometrical influence is likely to affect combustion, gas velocity and heat transfer characteristics, which implies that the choice of compression ratio is intimately related to the geometry of the chamber. The work of Thring et al., (5.14), and Kawamoto et al., (1.20 - 1.21), whilst relating to the effects of aspect ratio (chamber length to depth) and recess volume ratios respectively within Hrcc configurations, is instructive for future development.

The transitional feature referred to above coincides with the change in the majority volume from the disc space above the piston to the bathtub. The expected improvement in efficiency with increasing compression ratio appears to have been offset by the detrimental effect of changes in combustion geometry.

The influence of compression ratio: Task engine at the lean mixture limit

Experimental and theoretical data are presented in Table 5.4 and Figure 5.4. Theoretical and experimental flame development stages are compared in Figure 5.22.

As with the stoichiometric condition, longer burn durations (6.6 to 7.2 ms) rapid burn periods (4.4 to 5.8 ms) and shorter flame development stages (2.1 to 1.4 ms) are also evident at the lean mixture limit as the compression ratio increases from 9 to 13:1. The durations of the heat transfer and kernel growth stages show no clear trend with increasing compression ratio. Reducing peak pressure dispersion (12.2 to 9.8%) and deviation of peak pressure timing (1.9 to 1.2) indicate enhanced combustion stability with increasing compression ratio.

The influence of compression ratio with weakening mixture strength

Whilst all stages of flame propagation lengthen to some extent at a given compression ratio with weakening mixture strengths according to the laminar flame speed dependency, the influence on flame development is markedly ameliorated with increasing compression ratio; a 77% increase at 9:1 reduced to 25% at 13:1; the dominance of the heat transfer period is noted with kernel growth remaining relatively unchanged with respect to the stoichiometric.

A similar but diminished influence on the duration of the rapid burn stage is also apparent between the settings of 9 and 12:1; a 26% increase in duration reduced to 19%. At the higher setting of 13:1 the effect is not so marked registering a 23% increase, possibly reflecting the adverse geometrical changes referred to earlier.

Only a limited, but nonetheless useful, comparison of data obtained at 10:1 is possible since the excess air ratio at this setting is richer at 1.33. The most significant conclusion is that greater efficiency can be achieved at weaker mixture strengths utilising a compression ratio setting of 12:1. Thermal efficiencies are discussed in Section 7.2 and indicated efficiencies are detailed in Table 7.3.

Comparison with the model of flame development

The measured and predicted flame development periods are in general remarkably consistent. At near stoichiometric conditions a slightly weaker correlation of the order of 1 to 2 degrees of crank rotation is noted at the higher compression ratios for the Ricardo engine and a weaker correlation, around +/- 5 degrees or +/- 30%, evident at lean mixtures for the Task engine at higher settings. Whilst the former could be anticipated through experimental error: setting of the ignition timing, resolution of the encoder or subsequent analysis (discussed later in Chapter 6) the latter is more marked and may result from the poorer predictive capabilities of the model at weak mixture strengths as this has been reported by other workers, e.g. Pundir et al., (5.15). As a consequence of evaluating variables at a single position in the cycle, it is also possible that the model inadequately

represents changes in the flow field, producing errors where the duration of flame development is lengthy. (This subject is discussed in greater detail in Sections 5.4 and 5.7.7.) Furthermore, no consideration has been given to the residual fraction, apart from its influence on the laminar flame speed through the pressure and temperature dependence, which is known to reduce with increasing compression ratio, (1.57), and affect the duration of flame development, (4.17), or to variations in turbulence intensity which arise from changes in compression ratio, (4.20).

5.7.3 The effect of ignition timing

Summary

Earlier spark initiation promotes extended flame development consistent with increasing integral scale, although flame development may be influenced appreciably by unfavourable geometric or spatial configuration producing a contrary trend. Advanced combustion phasing promotes markedly higher cylinder pressures and temperatures as main stage combustion closes progressively towards tdc where the volume is smaller. In such conditions higher laminar flame speeds and improved chamber compactness are also thought to positively influence mass burning rates.

Rates of flame propagation, cylinder pressures and temperatures and combustion stability are less dependent on spark timing with the rapid burning Hrcc arrangement.

The predicted and measured flame development periods compare favourably - within 1 to 2 degrees in most cases.

The influence of ignition timing: 3-2 chamber

Experimental and theoretical data are presented in Table 5.5 and Figure 5.5. The flame development model is compared with measured data in Figure 5.23.

Notably reduced burn duration (6.3 to 4.2 ms) rapid burn stage (5.0 to 3.2 ms) and flame development period (1.3 to 0.9 ms) result from advancing the ignition through 15 degrees at a mixture strength corresponding to that for peak efficiency. These represent reductions of some 33, 36 and 31% respectively. Reducing flame development was surprising since the laminar flame speed would be expected to reduce with advancing ignition through lower temperatures and the integral scale increase with chamber height, effecting increasing flame development period as reported by other workers, (4.30, 4.34). Calculations for the laminar flame speed at these conditions do in fact show a moderate increase with advancing ignition. Such characteristics are supported by calculations undertaken with two further correlations, although associated with propane: those due to Kuehl, (5.8), and to Metghalchi et al., (1.6 - 1.7). Subsequent inspection of the laminar flame speed relationship used in this work together with the appropriate temperatures and pressures returned by the engine model at the start of heat release, suggests that the increase in the flame speed with advancing ignition occurs almost entirely as a consequence of the variation in the unburned gas temperature term in the pressure exponent and reducing pressures (the correlation is detailed in Section 5.5). The order of such increases is small however in relation to changes in the integral scale.

In the absence of additional experimental data and without recourse to further experimental work a number of possibilities are tentatively proposed to explain such conflicting trends.

(i) Considering that dimensions of flame kernels exceeding a radius of 5mm have been reported in the literature for propane-fuelled engines, (4.13), and noting the dimensions of the chamber height in the flame development period it seems possible that with retarded ignition timing flame growth is restricted in the vertical plane by both chamber roof and piston crown. The separating distance changes from 5.4 to 7.6 mm with advancing ignition at the start of heat release and from 5.2 to 7.2 mm at the end of the 1% burned stage. Figure 5.27 details the variation of chamber depth and volume with crankangle. Lancaster, (4.13), concluded that such a mechanism was responsible for reducing FSR during the early stage of flame propagation.

(ii) Interaction of the flame kernel with the vortex produced by the piston rolling-up the cylinder wall boundary layer, as discussed by Chomiak and Heywood in Reference 4.15, is a condition thought to prevail in chambers where the spark plug is situated near the cylinder wall since the dimensions of the vortex are of the order of the clearance height.

(iii) Piston-induced turbulence has been reported by Mayo, (cited in 4.28), to unfavourably influence the flame development period, and theoretical squish velocities are known to increase with proximity to tdc, (5.16). A diminishing flame development stage with advancing ignition was attributed to such a mechanism in Reference 1.49.

Advanced combustion phasing promotes markedly increased pressures and temperatures through main stage combustion closing progressively to tdc where the volume is smaller; 50% charge consumed at 33 degrees atdc in the most retarded case compared with 1 degree btdc for the most advanced. Higher laminar flame speeds and enhanced chamber compactness follow early heat-release timing. Peak pressures increase by around 1.75 bar/degree advance and predicted peak cycle temperatures by around 20 K/degree advance. Despite increasing burn duration, peak pressure dispersion reduces significantly from 10.4 to 3.3% with ignition retard since peak pressures approach those due to piston motion only; the deviation of the timing reduces from 3.1 to 1.9.

The influence of ignition timing: Hrcc arrangement

Experimental and theoretical data are presented in Table 5.6 and Figure 5.6. Theoretical and experimental flame development stages are compared in Figure 5.23.

In contrast to the 3-2 chamber, the Hrcc arrangement is characterised by a lengthening flame development period with advancing ignition timing: 1.1 to 1.3 ms or by 18%. The laminar flame speed relationship implies a constant flame speed over the range, hence flame development extends with increasing integral scale. Here it is of interest to note that ignition is initiated in the deeper recess of the chamber where the minimum depth is around 8 mm. The rapid burn stage reduces notably

from 4.3 to 3.3 ms (by 23%) with advancing ignition and is some 40% shorter than that in the 3-2 chamber at about 20 degrees advance; peak pressures and maximum rates of pressure rise are correspondingly higher. Peak pressures change by around 1.5 bar/degree advance and predicted peak temperatures by around 11 K/degree advance. Compared with the 3-2 chamber, peak pressure dispersion is reduced and is also of contrary trend-wise dependence on the ignition timing; reducing from 7.3 to 4.9% with spark advance despite significantly higher combustion generated pressures - both in relation to the 3-2 chamber and the retarded condition. It is possible that such a positive effect results from the enhanced rates of heat release centered more closely around tdc where volume change is reduced and pressure variations are least influenced by piston motion. For both configurations a minimum in the standard deviation of the timing of peak pressures occurs at the mbt timing, 22 and 25 degrees advance for the Hrcc and the 3-2 chamber respectively. Note however that this is not associated with a minimum in the dispersion of peak pressure - an observation consistent with the findings of Al-Alousi et al., (5.4).

The predicted and measured flame development periods are consistent - within 1 to 2 degrees in most cases. Whilst the trend-wise dependence of the model on spark timing appears satisfactory for the Hrcc arrangement, this is not the case for the 3-2 configuration for reasons which have been discussed earlier and which appear unlikely to be a shortcoming of the model.

5.7.4 Effect of engine speed

Summary

The experimental and theoretical data illustrating the influence of engine speed on the various chambers at the stoichiometric air-to-fuel ratio and at the lean mixture limit are included in Tables 5.7 - 5.12 and Figures 5.7 - 5.12. Measured and theoretical flame development periods are compared in Figures 5.24 - 5.25.

Increasing the engine speed from 25 to 35 rev/sec at stoichiometric conditions effects both reducing flame development (by 20 - 30%) and

rapid burn stages (by 16 - 40%) for all chambers. This is thought to be mainly through increased turbulence, change in combustion phasing is also thought to be significant. The duration of the flame development is least dependent on speed in the TaskII configuration with a similar dependence noted for the other chambers. The duration of the rapid burn period is most dependent in the 3-2 chamber and least dependent in the Hrcc arrangement. With the latter configuration the increase in burn rate is sufficient to maintain similar combustion phasing over the range of speed; the timing and magnitude of peak pressures and rates of pressure rise remain largely unchanged, illustrating the enhanced stability of the combustion process in this chamber.

At very weak mixture strengths, changes in both burn rates and the limit of stable lean mixture operation result from changes in speed. Extended lean mixture operation is strongly dependent on increasing speed up to the mid-range setting with the TaskII arrangement (excess air increasing from 1.23 to 1.50) whilst the lean mixture limit is moderately attenuated at the higher speed for both the TaskII and Hrcc configurations (excess air diminishing from 1.50 to 1.42 and 1.61 to 1.54 respectively). The TaskII chamber exhibits the least tolerance to weakening mixtures whilst the Hrcc exhibits the greatest. For all chambers, the duration of the flame development and rapid burn stages diminish as the speed increases; a greater dependency shown by the Hrcc configuration (the flame development period reducing by 43% and the rapid burn stage by 29%) but a similar dependency shown by the remaining arrangements (both stages reducing by around 15 - 30%). The observed dependency is, however, complicated by variations in operating points; it is reduced by extended lean mixture operation at high speed for the TaskII chamber and is emphasised by attenuated lean mixture operation at high speed in the case of the Hrcc.

At both stoichiometric and weak conditions, combustion stability is moderately enhanced with the Hrcc arrangement but reduced with the 3-2 chamber as the speed increases. The TaskII configuration is most stable at the mid-range speed.

At the stoichiometric condition, a good measure of agreement is evident between the measured and theoretical flame development stage, to within

a degree in most cases, with only two observations exceeding a percentage error of 10% - registering about 20%. At the lean mixture limit however, the quality of correlation diminishes with the duration of the stage.

The influence of engine speed at the lean mixture limit

In keeping with the lean burn strategy, the influence of engine speed will be considered in detail at the lean mixture limit. The main findings from a similar treatment at the stoichiometric condition are outlined in the summary. Experimental and theoretical data are included in Tables 5.10 - 5.12 and Figures 5.10 - 5.12. Measured and theoretical flame development stages are compared in Figure 5.25.

A linear relationship between turbulence intensity near tdc on the compression stroke in quiescent configurations and mean piston speed has been reported by the numerous studies cited earlier in Chapter 4, the constant of proportionality varying from 0.3 to 0.5, viz.:

$$u_t = a\bar{S}_p$$

Piston- and induction-generated turbulence are also known to vary with position on the compression stroke, see References 4.13, 4.20, 4.22 and 5.16 for example.

A consequence of the assumptions in turbulent combustion models such as that of Hires et al., (4.30), is that the mass entrainment velocity increases while the characteristic eddy burn time reduces with increases in turbulence intensity. Reductions in rapid burn and flame development periods follow, the latter according to:

$$\theta_d = c\nu^{1/3}\left[\frac{h_s}{S_l\bar{S}_p}\right]^{2/3}$$

h_s - chamber height at the start of combustion (m)
S_l - laminar flame speed (m/s)
$\bar{S}_p$ - mean piston speed (m/s)
θ_d - flame development period (ms)
ν - kinematic viscosity (m^2/s)
c - an engine-specific constant

The TaskII chamber shows a marked extension of stable lean mixture operation with increasing engine speed. This suggests the importance of promoting turbulence to maintain a sustainable flame across the relatively long flame travel path associated with this configuration. Despite the excess air ratio increasing from 1.23 to 1.42 over the range of speed, the flame development and rapid burn stages reduce from 2.8 to 2.0 ms (by 29%) and from 6.3 to 5.3 ms (by 16%) respectively. The heat-release phasing at the highest speed is advanced compared to the lowest until around 50% mass consumed and is retarded thereafter. The timing and magnitude of peak pressures and maximum rates of pressure rise vary accordingly. As the speed increases to the mid-range value, the influence of weakening mixture strength appears to predominate over the influence of turbulence and whilst stable combustion is sustained at considerably leaner mixtures, diminished rates of heat release and lower in-cylinder pressures are evident. The dispersion of the maximum pressure and the deviation of the timing are least at the mid-range speed (at 6.7% and 3.5 respectively). Although this is consistent with the observations at the stoichiometric condition, combustion-generated pressures are relatively small at this speed.

Compared with the previous configuration, the 3-2 chamber is less dependent on the engine speed for stable lean mixture operation, possibly through improved chamber compactness. As the speed increases, flame development is noted to reduce from 1.8 to 1.4 ms (by 22%) but remains unchanged between the mid-range and highest speeds. The fact that the kernel growth stage is completed before the chamber height reduces to around 7.5 mm at the mid-range setting whereas it is only initiated at a height of 7 mm in the case of the highest speed, suggests that the unfavourable geometrical effects referred to in Section 5.7.3 are influencing this stage of flame growth. (Figure 5.27 details the change in chamber height with crankshaft position.) Exceeding around 10% mass consumed however, burn rates are seen to diminish in the order of increasing speed; the rapid burn reducing from 6.2 to 5.2 ms (by 16%). A moderate increase in the maximum rate of pressure rise and magnitude of peak pressure is apparent at the mid-range speed where combustion phasing is advanced. As in the stoichiometric case, combustion stability diminishes weakly with

increasing speed: 8.8 to 9.8% and 1.5 for the dispersion of the maximum pressure and deviation of the timing respectively.

With the Hrcc arrangement, increasing engine speed reduces the flame development stage from 2.1 to 1.2 ms (by 43%) and the rapid burn duration from 7.2 to 5.1 ms (by 29%) but note that the higher speed is at moderately richer mixture strength. At the start of combustion, the ratio of the integral scale to the laminar flame speed remains substantially unchanged by speed, suggesting that the turbulence intensity is largely responsible for changes in flame development. Although the heat-release timing is advanced at the lowest speed when compared with the mid-range setting, moderately higher peak pressures and comparable maximum rates of pressure rise apply to the latter, suggesting in this case the relative importance of reduced mass loss and heat transfer over this portion of the cycle as the speed increases. The maximum peak pressure and rate of pressure rise are both consistent with the most advanced combustion phasing at the highest speed. In keeping with the stoichiometric case, combustion stability is moderately enhanced with increasing speed: 9.2 to 7.2% and 1.7 to 1.5 for the dispersion of the maximum pressure and deviation of the timing respectively.

5.7.5 Effect of chamber

Summary

The experimental and theoretical data illustrating the influence of chamber arrangement at various speeds at the stoichiometric air-to-fuel ratio and at the lean mixture limit are included in Tables 5.13 - 5.18 and Figures 5.13 - 5.18. Measured and theoretical flame development periods are compared in Figures 5.24 - 5.25.

When compared with the TaskII chamber at stoichiometric mixture strengths over the range of speed considered, the Hrcc arrangement promoted enhanced combustion stability (a reduction of 2 - 3 percentage points in peak pressure dispersion) and was found effective in reducing the duration of the flame development period by around 20 - 30%, effective in reducing the succeeding 1 - 50% mass consumed stage whilst

maintaining a comparable duration for the 50 - 90% burned interval. As a result, the rapid burn periods were some 20 - 30% shorter. Although the 3-2 configuration promoted shorter flame development in comparison with the TaskII chamber, the influence was comparable to the Hrcc arrangement only at low and high speeds. When compared with the TaskII configuration, and with the exception of a positive influence at the higher speed thought to result from enhanced turbulence, the 3-2 chamber had negligible effect on the duration of the 1 - 50% burned interval and adversely influenced the 50 - 90% and 1 - 90% stages; only at the slow speed was the combustion stability enhanced.

At all speeds the Hrcc promoted extended stable operation into the lean regime. The TaskII arrangement was the least tolerant of weakening mixtures, excluding the mid-range speed where the operating point was comparable with the 3-2 chamber. At the highest speed, chamber configuration was found less effective in extending the limits of stable lean mixture operation; the relative tolerance to weakening mixtures between the chambers diminishing (excess air varying from 1.4 to 1.5 between the chambers) and in the cases of the TaskII and Hrcc arrangements, the limit of stable operation was notably attenuated. (At the slowest speed the excess air ratio ranged from 1.23 to 1.63 between the chambers.)

At the lean mixture limit, irrespective of speed and despite considerably weakened mixture strength, the Hrcc arrangement promoted the fastest early stage combustion rates (0 - 50% mass consumed) but the slowest 50 - 90% burning rates. The extended duration of the later interval unfavourably influenced the rapid burn duration in comparison with other chambers except at the higher speed where mixture strengths were more comparable. At the lower speeds, the shortest rapid burn durations were achieved with the 3-2 chamber. In general, and in contrast to the Hrcc configuration, albeit at richer mixture strengths, the TaskII chamber promoted the slowest early stage combustion rates (0 - 50% mass consumed) but the fastest 50 - 90% combustion rates at all speeds. Although the Hrcc configuration operated at weaker mixture strengths, the combustion stability was comparable with other arrangements and moderately enhanced at high speed.

The influence of chamber arrangement at stoichiometric conditions

The influence of chamber arrangement at stoichiometric conditions will be considered in detail at the slow speed as representative and in keeping with the conceptual design. Although the relative performance of the chambers is influenced to some extent by engine speed this is significant only with the 3-2 arrangement and is thought to result from unfavourable geometry. The main findings from a detailed study of the influence of chamber arrangement at higher speeds is outlined in the summary. Experimental and theoretical data are included in Table 5.13 and Figure 5.13. Measured and theoretical flame development stages are compared in Figure 5.24.

Variations in flame travel paths through spark plug position and/or chamber compactness together with variations in piston- or port-induced turbulence are some of those significant influences which are expected to produce differences in combustion characteristics between the arrangements. (The salient features of each chamber were referred to in Section 3.2.) However, quantifying the levels of turbulence is extremely complex and involves sophisticated experimental techniques extending beyond the scope of this work. The variation in large scale mixture motion (swirl) between the configurations was found to be slight using steady state flow apparatus (see Chapter 9 for a more detailed discussion) and other parameters known to influence turbulence, such as volumetric efficiency, valve head/seat geometry and camshaft timing and profile were kept constant, although the TaskII chamber utilises a lower compression ratio. Furthermore, since combustion chambers with increased squish are usually compact and a positive influence on combustion rates has been attributed to both configurations, the relative importance of either feature within such chambers is difficult to establish and does not yet seem to have been resolved in the literature. This subject was discussed in greater detail in Sections 1.8 and 5.7.3.

At the slower speed, a reduction of 27% in the flame development period from 1.5 ms for the TaskII chamber to 1.1 ms for the 3-2 and Hrcc configurations is consistent with the reducing ratio of integral scale to laminar flame speed. Comparable burn rates between 1 and 50% mass

consumed together with similar combustion-crankangle phasing are noted for the TaskII and 3-2 chambers until the later stages of combustion (50 to 90% consumed) when the burn rate of the former is noted to exceed the latter and combustion crankangle-phasing advances. Initially retarded combustion-crankangle phasing rapidly advances with respect to the other configurations in the case of the Hrcc, with almost 90% mass consumed at the crankangle corresponding to 50% burned for the other chambers. The rapid burn duration is lengthiest for the 3-2 chamber at 5.5 ms reducing by some 42% to 3.2 ms for the Hrcc. Late stage combustion durations (50 to 90%) are comparable between the TaskII and Hrcc arrangements but extended with the 3-2 chamber, suggesting the detrimental geometrical effects discussed in Section 5.7.2. The highest peak pressures and maximum rates of pressure rise are associated with early combustion in the Hrcc. Enhanced combustion stability: dispersion of peak pressure and the deviation of the timing at 7.4% and 1.8 respectively, is noted for the quicker burning Hrcc.

The influence of chamber arrangement at the lean mixture limit

The influence of chamber arrangement on combustion rates at weak mixture strengths is clearly complicated by engine speed influencing stable lean mixture operation. It is illustrative to consider the higher speed in some detail where the range in mixture strengths is more comparable and the effect of chamber arrangement on burn rates more readily discernible. The main conclusions drawn from a detailed study at lower speeds are outlined in the summary. The experimental and theoretical data are presented in Table 5.18 and Figure 5.18 and a comparison between the theoretical and experimental flame development periods in Figure 5.25.

At the higher speed, stable lean mixture operation is notably attenuated in the case of the Hrcc when compared with the performance at slower speeds (significantly higher levels of unburned hydrocarbon emissions were measured during the tests). At this speed, lean mixture limits at excess air ratios of 1.42, 1.50 and 1.54 are noted for the TaskII, 3-2 and Hrcc arrangements respectively. Despite the expected influence of mixture strength on burn rates through the laminar flame speed dependency, such a tendency is evidently ameliorated through

combustion configuration and it is only in the latter stages of flame propagation (50 to 90% mass consumed) that slower burn rates correspond with weaker mixtures. The Hrcc configuration evidently promotes a marked reduction in the duration of flame development when compared with the TaskII chamber. This reduces from 2.0 to 1.2 ms (some 40%) consistent with diminishing integral scale through changes in ignition timing and compression ratio. A significant reduction in the duration of the succeeding stage (to 50% mass consumed) is also apparent, the Hrcc maintaining a relatively rapid rate of heat release around tdc - a reduction of some 31% from 2.9 to 2.0 ms with respect to the TaskII arrangement. In the latter stages of combustion (from 50 to 90% consumed) chamber arrangement is insufficient to prevent burn rates reducing as the excess air ratio increases. During this stage the rate of volume change with respect to crankangle increases more rapidly; chamber compactness suffers and the laminar flame speed reduces as temperatures and pressures diminish. Intake-generated turbulence also decays with time, (4.13). A 29% increase in the duration of this stage is noted for the Hrcc at 3.1 ms compared with the TaskII configuration at 2.4 ms. Enhanced combustion stability is noted for the Hrcc at 7.2% and 1.5 for the dispersion of the peak pressure and deviation of the timing of the peak pressure respectively.

5.7.6 Effect of excess air

Summary

The performance of the three chambers is considered at the mid-range speed with mixture strengths corresponding to the stoichiometric, the peak efficiency and the lean mixture limit. The experimental and theoretical data are detailed in Tables 5.19 - 5.21 and Figures 5.19 - 5.21. The experimental and theoretical flame development periods are compared in Figure 5.26.

The durations of the flame development and rapid burn stages in the TaskII chamber show significantly greater dependence on changes in mixture strength, even over the small range from the stoichiometric to the excess air ratio for maximum efficiency. These extend by around 30% compared with the 0 - 10% increase evident in the other arrangements.

Comparison with the Hrcc at weaker mixture strengths is complicated by extended stable lean mixture operation. However, as the excess air ratio increases from that at peak efficiency to that at the lean mixture limit, further increases in the flame development and rapid burn durations of 81 and 47% respectively, are markedly extended in the TaskII chamber in contrast to the 20 - 30% increases sustained in the 3-2 arrangement. The influence of mixture strength on the Hrcc is considered in more detail below.

Enhanced combustion stability occurs at the excess air ratio for maximum efficiency in both the Hrcc and 3-2 arrangements (dispersion of peak pressures of 5.2 and 8.9% respectively) and combustion is most stable at all mixture strengths in the Hrcc configuration.

The duration of experimental and theoretical flame development periods correlate well at stoichiometric air-to-fuel ratios and mixture strengths corresponding to peak efficiency. Poor agreement is noted at the lean mixture limit where this stage of flame propagation is extended.

The influence of mixture strength: Hrcc arrangement

Although the laminar flame speed is a significant factor in controlling the turbulent flame speed, a further influence on combustion rates is to be expected through unfavourable changes in chamber compactness and piston-induced pressures as the duration of heat release extends with weakening mixtures. Lengthening flame development with weakening mixtures is also to be anticipated, both as a consequence of reducing laminar flame speed and increasing integral scale as optimum ignition settings advance.

The flame development stage increases from 1.0 ms at the stoichiometric air-to-fuel ratio to 1.1 ms at the mixture strength for peak efficiency and by a further 63% to 1.8 ms at the lean mixture limit, a total increase of 80% as the excess air ratio changes from 1.03 to 1.61. The duration of the rapid burn stage remains unchanged at 3.1 ms between the stoichiometric air-to-fuel ratio and the mixture strength for peak efficiency, and increases by 116% to 6.7 ms at the lean mixture limit.

Combustion phasing is most advanced at the mixture strength for maximum efficiency and least advanced at the lean mixture limit. Maximum peak pressure and rates of pressure rise are associated with advanced combustion phasing at the mixture strength for peak efficiency. Peak pressure dispersion is reduced at the excess air ratio for maximum efficiency at 5.2%.

5.7.7 General observations

Flame development accounted for 17 to 33% of the burn duration over all conditions investigated. The lengthiest proportions were associated with the Ricardo engine at low compression ratios, the 3-2 configuration running weak at low compression ratios and the TaskII chamber at weak mixture strengths. The shortest proportions were associated with high compression ratios, retarded spark timings (excluding the 3-2 chamber where adverse geometric effects were suspected), the 3-2 configuration and the lean running Hrcc.

Only with variations in excess air and engine speed did diminishing rapid burn consistently follow reducing flame development. A contrary trend was evident for changes in ignition timing. In general, combustion chambers with the shortest flame development stages were also associated with shorter rapid burn stages, although unfavourable geometry is thought to influence the dependence.

The experimental and theoretical flame development periods correlated remarkably well over the range of conditions investigated with the exception of those operating points where extended durations (exceeding around 1.5 ms) were evident. Hence predictive capability is particularly limited in the very weak regime at the low speeds and with the slower burning configuration. This is considered to be a consequence of evaluating the laminar flame speed, the characteristic entrainment velocity and the scale of turbulence at a single point in the engine cycle, when in fact they are known to vary throughout the flame development period. Allowing the integral scale and turbulence intensity to vary according to conservation of angular momentum principles applied to the values at the start of combustion, may improve the correlation without further undue complexity.

Detailed attention to the flame development and 50 - 90% mass consumed periods is suggested in light of the diminished heat release and extended duration of these stages of flame propagation.

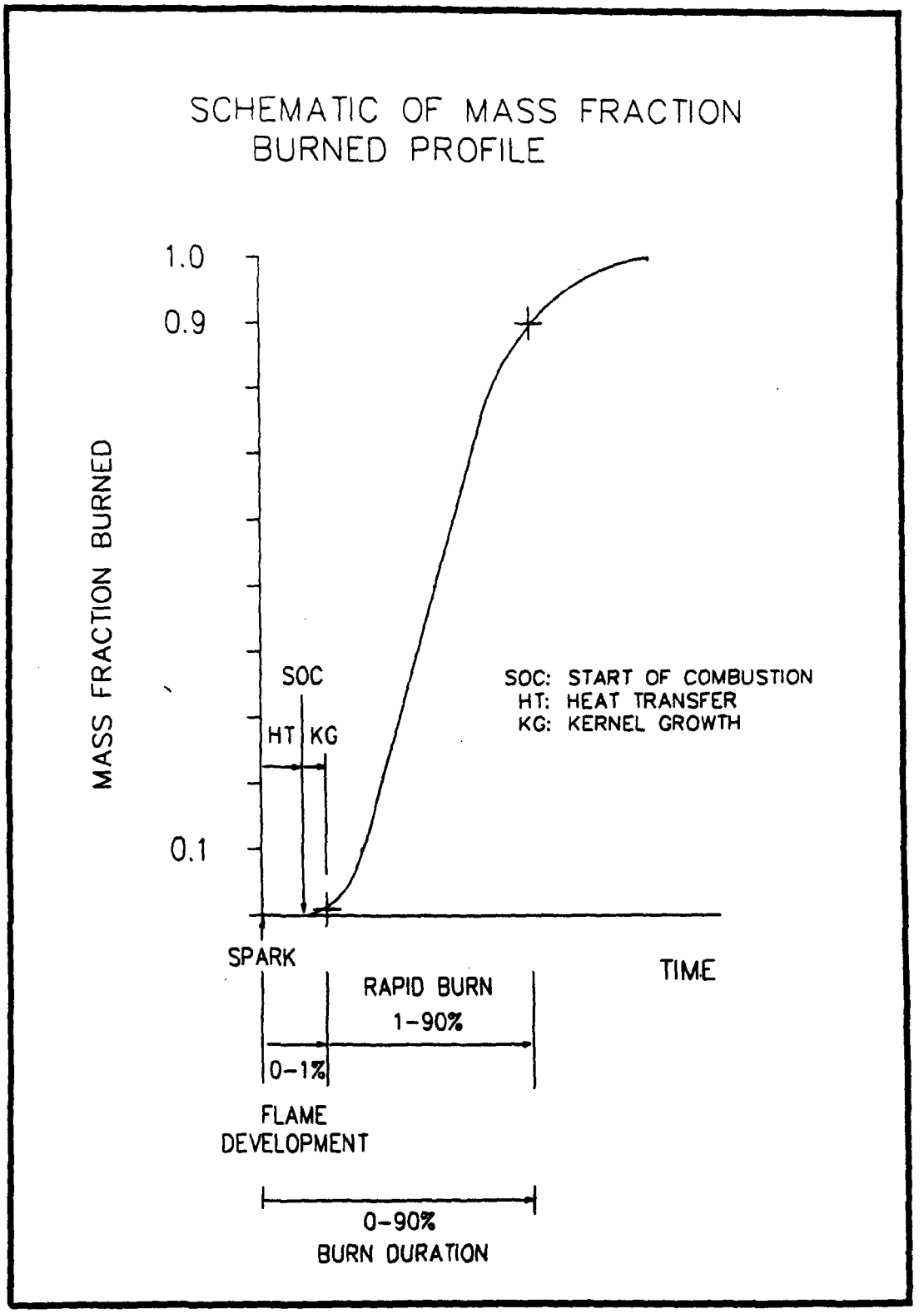

Figure 5.1 Typical fractional mass consumed curve illustrating the parameters used to characterise the combustion process.

Table 5.2 The effect of compression ratio: the Ricardo E6 at stoichiometric conditions, 1800 rpm.

Cr	Spark (deg btdc)	Soc at ca	0 to 1% ms/at ca	Spark to soc (ms)	Soc to 1% (ms)	0 to 50% ms/at ca	0 to 90% ms/at ca
8	30	-19	1.7/-12	1.02	0.65	3.9/12	5.1/25
9	28	-18	1.6/-11	0.93	0.65	3.7/12	4.9/25
10	28	-18	1.5/-12	0.93	0.55	3.6/11	5.0/26
11	27	-17	1.4/-12	0.93	0.46	3.4/10	4.8/25
12	27	-17	1.3/-13	0.93	0.37	3.3/ 9	4.7/24
13	27	-18	1.3/-13	0.83	0.46	3.3/ 9	4.7/24
14	27	-18	1.2/-14	0.83	0.37	3.4/10	4.7/24
15	22	-13	1.2/- 9	0.83	0.37	3.6/17	5.3/35
16	21	-12	1.2/- 8	0.83	0.37	3.5/17	5.3/36

Cr	1 to 50% (ms)	50 to 90% (ms)	1 to 90% (ms)	Vol at 1% (cc)	Vol at 50% (cc)	Vol at 90% (cc)	Pmax (bar) /at ca	% disp Pmax/ sd of timing
8	2.2	1.2	3.4				39.0/18	9.1/3.0
9	2.1	1.2	3.3				43.0/18	10.9/3.0
10	2.1	1.4	3.5				47.5/16	12.7/3.2
11	2.0	1.4	3.4				53.0/15	11.2/2.4
12	2.0	1.4	3.4				58.5/13	12.7/2.5
13	2.0	1.4	3.4				63.4/13	12.9/2.2
14	2.2	1.3	3.5	47.7	43.3	65.0	67.7/12	11.7/2.0
15	2.4	1.7	4.1	39.6	49.2	90.6	58.0/15	14.2/1.6
16	2.3	1.8	4.1	36.4	46.9	91.3	61.0/14	10.8/1.3

Engine model:

Cr	0 to 1% (ms)	Lam flm speed at soc (ms)	Integral scale at soc (mm)	T_b max (K)	Engine heat transfer (kW)	(% HHV)	Laminar flame speed (m/s) at ca (deg atdc) 0	10	20	30
8	1.67	0.522	19.00	2543	3.776	16.0				
9	1.64	0.462	16.69	2538	3.720	16.4				
10	1.51	0.473	14.83	2537	3.604	16.2				
11	1.51	0.454	13.93	2418	3.072	16.2				
12	1.28	0.526	12.6	2576	3.794	16.7				
13	1.19	0.573	12.11	2610	3.914	17.6				
14	1.14	0.579	11.40	2619	3.937	16.9	.84	.92	.79	.60
15	1.04	0.550	9.33	2534	3.479	15.0	.66	.71	.65	.54
16	1.01	0.528	8.57	2549	3.513	14.9	.69	.74	.66	.54

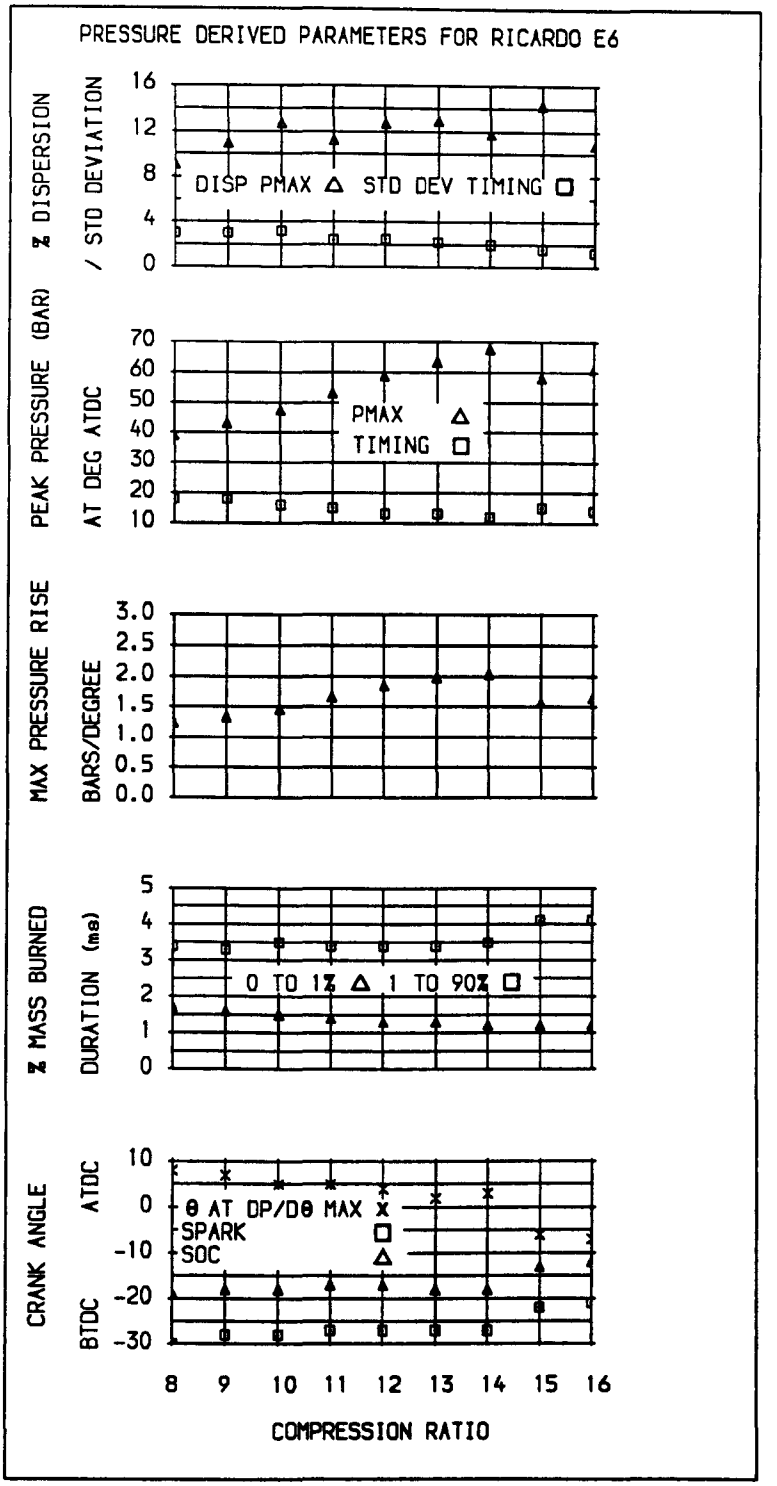

Figure 5.2 The effect of compression ratio – the Ricardo E6 at stoichiometric conditions, 1800 rpm.

Table 5.3 The effect of compression ratio: chamber 3-2 at stoichiometric conditions including some comparison with the Ricardo E6, 1800 rpm.

Reference	23	36	3	39
Chamber type	3-2	3-2	3-2	3-2
Excess air ratio	1.00	1.07	1.05	1.02
Engine speed (rpm)	1814	1829	1845	1825
Ignition (deg btdc)	30	24	21	22
Compression Ratio	9	10	12	13
0 to 1% (ms/deg)	1.19/13	1.18/13	1.26/14	1.09/12
at (deg btdc)	17	11	7	10
Spark to soc (ms)	0.83	0.91	0.99	0.73
Soc to 1% (ms)	0.36	0.27	0.27	0.36
0 to 50% (ms/deg)	3.1/34	3.6/40	4.0/44	3.5/38
at (deg atdc)	4	16	23	16
0 to 90% (ms/deg)	4.7/51	5.1/56	6.0/66	5.8/63
at (deg atdc)	21	32	45	41
1 to 50% (ms/deg)	1.9/21	2.4/27	2.7/30	2.4/26
50 to 90% (ms/deg)	1.6/17	1.5/16	2.0/22	2.3/25
1 to 90% (ms/deg)	3.5/38	3.9/43	4.7/52	4.7/51
Soc (deg btdc)	21	14	10	14
Eoc (deg atdc)	30	43	58	59
Max pressure (bar)	40.4	35.5	34.2	46.7
at (deg atdc)	12	16	13	12
Std deviation:				
Pmax	3.3	3.8	3.4	4.4
Ricardo	4.7	6.1	7.4	8.2
Timing Pmax	2.4	2.2	3.1	2.6
Ricardo	3.0	3.2	2.5	2.2
% Dispersion:				
Pmax	7.9	10.6	9.8	9.3
Ricardo	10.9	12.7	12.7	12.9
<u>Flame development model:</u>				
0 to 1% (ms/deg)	1.47/	1.33/	1.14/	1.04/
Integral scale at soc (mm)	9.50	7.60	6.05	6.07
Laminar flame speed at soc (m/s)	0.559	0.522	0.521	0.620
Max burned gas temperature (K)	2594	2475	2441	2539

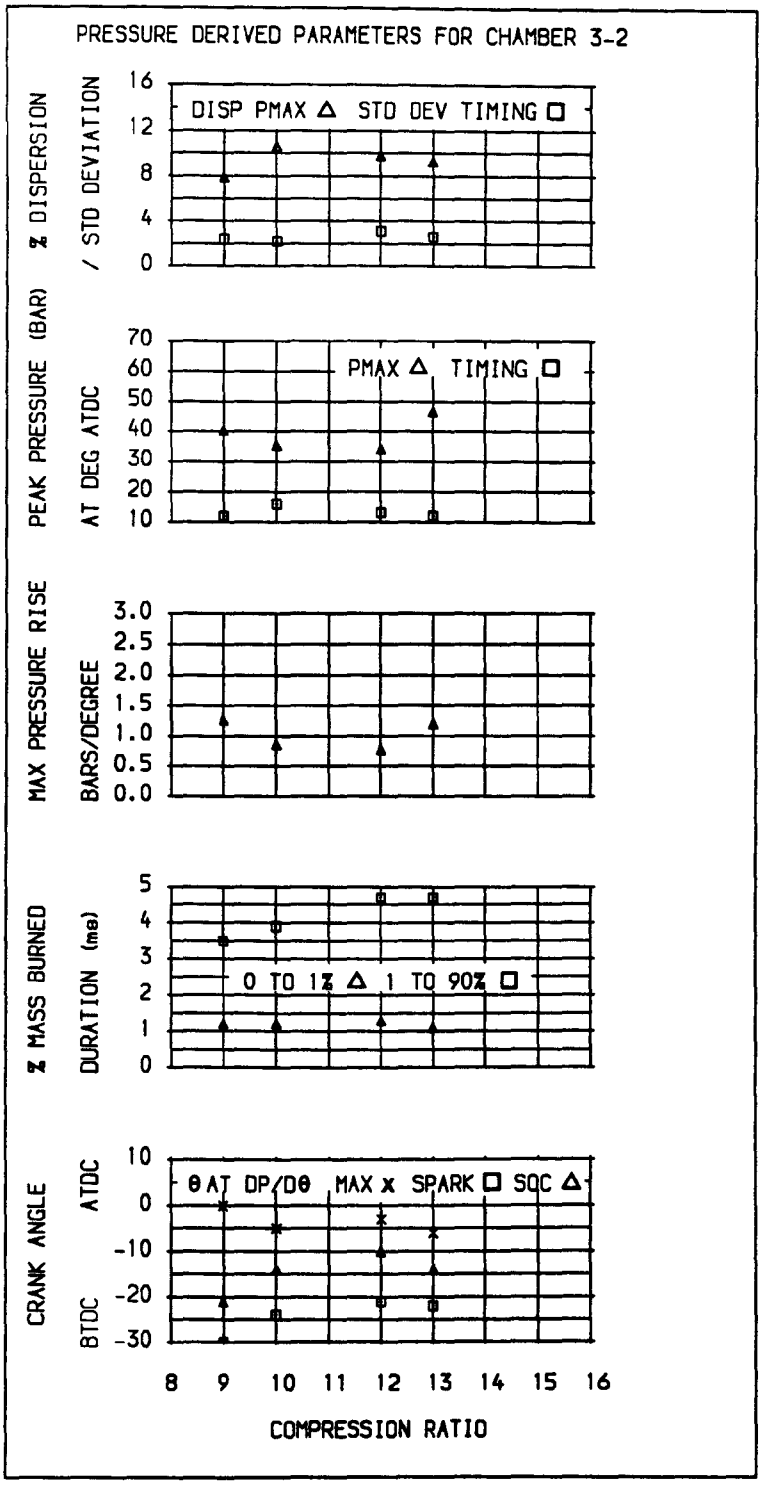

Figure 5.3 The effect of compression ratio — chamber 3-2, stoichiometric conditions, 1800 rpm.

Table 5.4 The effect of compression ratio: chamber 3-2 at the lean mixture limit including some comparison with the stoichiometric case, 1800 rpm.

Reference	24	7	40
Chamber type	3-2	3-2	3-2
Excess air ratio	1.50	1.50	1.49
Engine speed (rpm)	1805	1808	1807
Ignition (deg btdc)	43	37	37
Compression Ratio	9	12	13
0 to 1% (ms/deg)	2.12/23	2.12/23	1.38/15
at (deg btdc)	20	14	22
% change wrt stoich	77	68	25
Spark to soc (ms)	1.75	1.93	1.01
% change wrt stoich	110	95	38
Soc to 1% (ms)	0.37	0.18	0.37
% change wrt stoich	3	50	3
0 to 50% (ms/deg)	4.7/51	5.1/55	4.3/47
at (deg atdc)	8	18	10
0 to 90% (ms/deg)	6.6/71	7.7/84	7.2/78
at (deg atdc)	28	47	41
% change wrt stoich	40	28	24
1 to 50% (ms/deg)	2.6/28	3.0/32	2.9/27
50 to 90% (ms/deg)	1.9/20	2.6/29	2.9/31
1 to 90% (ms/deg)	4.4/48	5.6/61	5.8/63
% change wrt stoich	26	19	23
Soc (deg btdc)	24	16	26
Eoc (deg atdc)	39	58	58
Max pressure (bar)	31.4	38.4	49.5
at (deg atdc)	10	9	6
Std deviation:			
Pmax	3.8	4.3	4.8
Timing Pmax	1.9	1.9	1.2
% Dispersion:			
Pmax	12.2	11.3	9.8
<u>Flame development model:</u>			
0 to 1% (ms/deg)	2.12/23	1.58/17	1.83/20
Integral scale at soc (mm)	10.13	6.76	8.29
Laminar flame speed at soc (m/s)	0.340	0.363	0.354
Max burned gas temperature (K)	2134	2111	2193

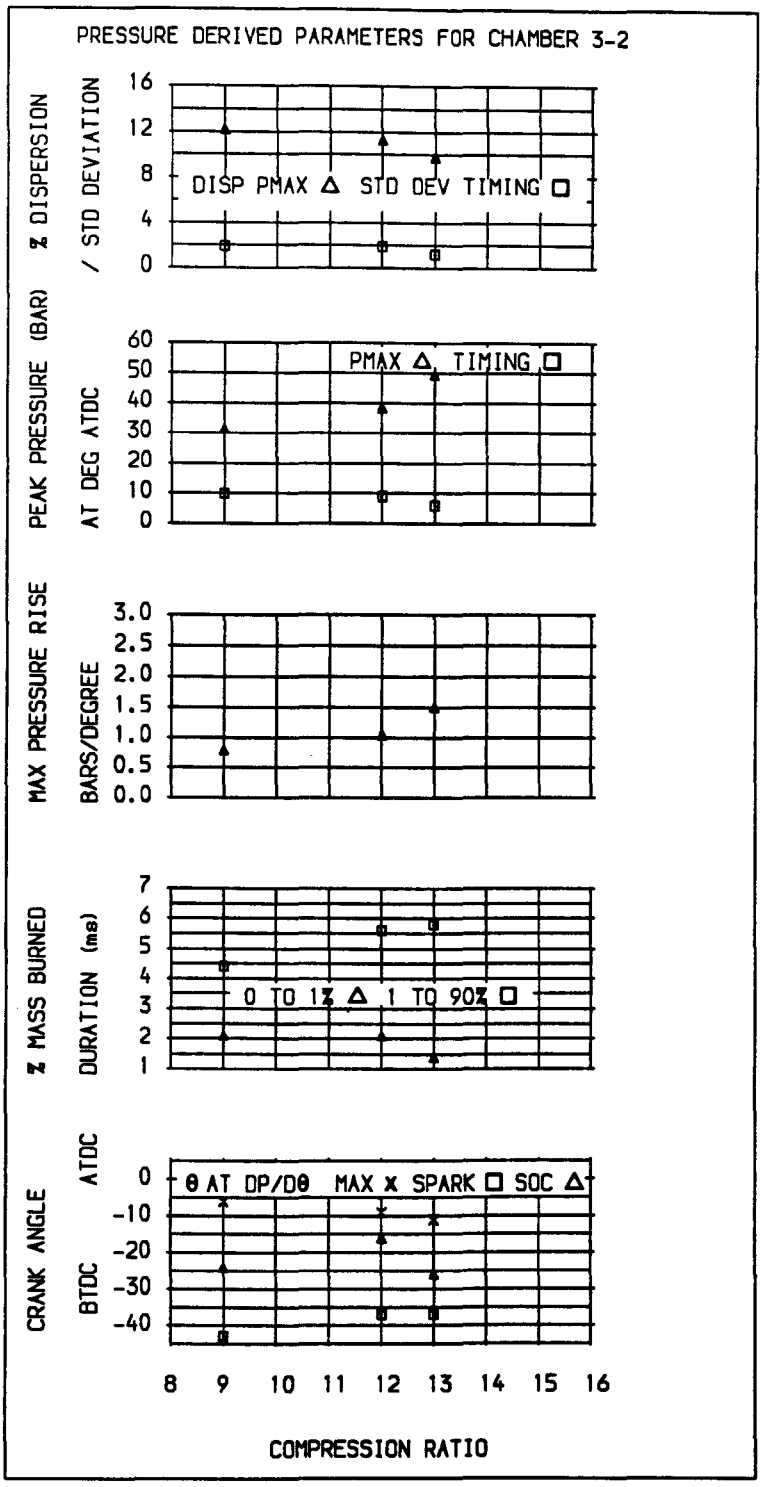

Figure 5.4 The effect of compression ratio — chamber 3-2 at the LML. Excess air 1.5, 1800 rpm.

Table 5.5 The effect of ignition timing: chamber 3-2 at the mixture strength for maximum efficiency.

Reference	44	43	41	42
Chamber type	3-2	3-2	3-2	3-2
Excess air ratio	1.19	1.19	1.17	1.16
Engine speed (rpm)	1807	1807	1806	1806
Ignition (deg btdc)	15	20	25	30
Compression Ratio	13	13	13	13
0 to 1% (ms/deg)	1.3/14	1.1/12	1.1/12	0.9/10
at (deg btdc)	1	8	13	20
Spark to soc (deg)	9	8	9	7
Soc to 1% (deg)	5	4	3	3
0 to 50% (ms/deg)	4.4/48	4.2/45	3.6/39	2.7/29
at (deg atdc)	33	25	14	-1
0 to 90% (ms/deg)	6.3/68	6.2/67	5.9/64	4.2/45
at (deg atdc)	53	47	39	15
1 to 50% (ms/deg)	3.1/34	3.1/33	2.5/27	1.8/19
50 to 90% (ms/deg)	1.9/20	2.0/22	2.3/25	1.5/16
1 to 90% (ms/deg)	5.0/54	5.1/55	4.8/52	3.2/35
Soc (deg btdc)	6	12	16	23
Eoc (deg atdc)	66	60	54	25
Max pressure (bar)	32.9	38.2	46.4	59.0
at (deg atdc)	5	8	10	6
Std deviation:				
Pmax	1.1	3.0	4.1	6.4
Timing Pmax	1.9	2.4	1.9	3.1
% Dispersion:				
Pmax	3.3	7.9	8.9	10.4
<u>Flame development model:</u>				
0 to 1% (ms/deg)	1.15/12.5	1.20/13.0	1.22/13.2	1.32/14.3
Integral scale at soc (mm)	5.35	5.83	6.34	7.61
Laminar flame speed at soc (m/s)	0.472	0.478	0.514	0.539
T_u at soc (K)	773	758	764	758
T_b at soc (K)	2305	2293	2315	2318
Pressure soc (bar)	29.5	26.0	23.0	18.0
Max burned gas temperature (K)	2267	2324	2421	2562
Predicted engine heat transfer (kW)	0.61	0.67	0.77	0.97

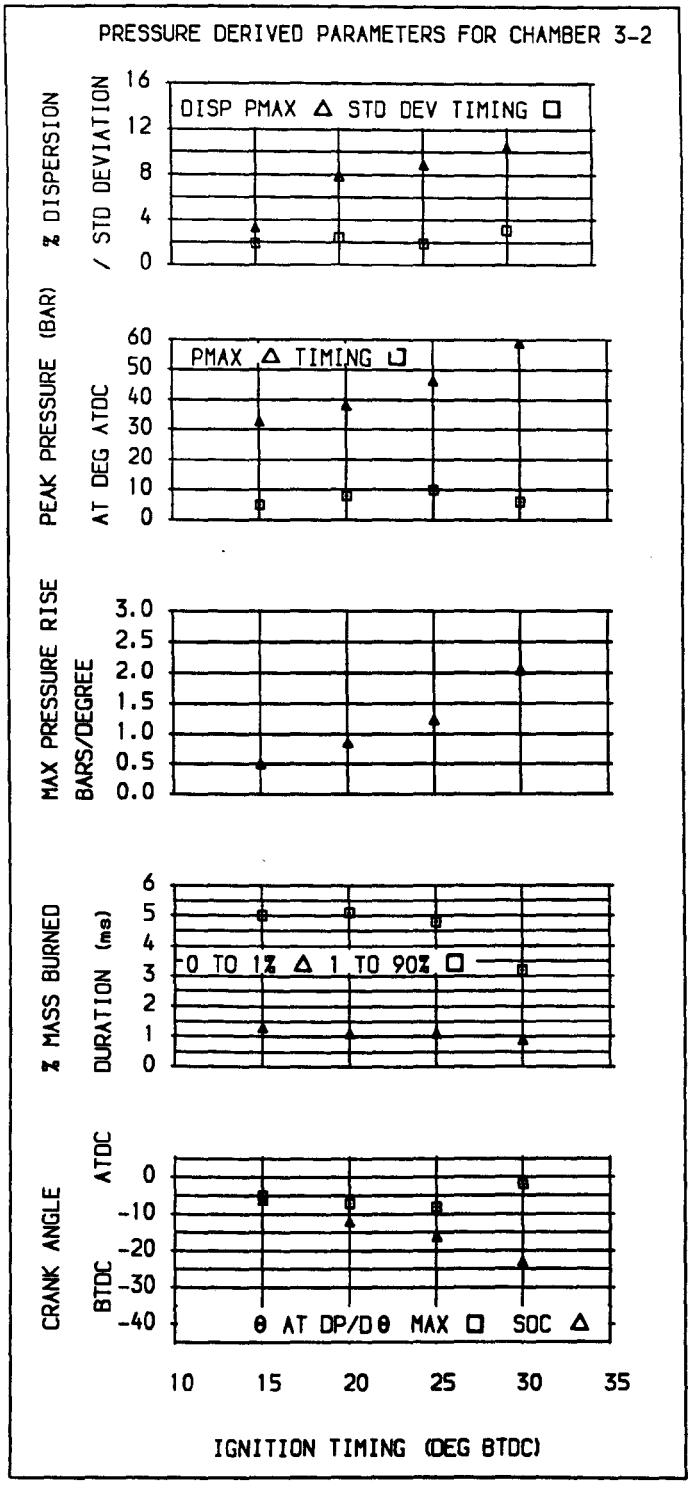

Figure 5.5 The effect of ignition timing – chamber 3-2 at the mixture strength for maximum efficiency. Excess air 1.2, 1800 rpm.

Table 5.6 The effect of ignition timing: Hrcc at the mixture strength for maximum efficiency.

Reference	16	15	18
Chamber type	Hrcc	Hrcc	Hrcc
Excess air ratio	1.17	1.18	1.15
Engine speed (rpm)	1813	1813	1815
Ignition (deg btdc)	13	22	26
Compression Ratio	13	13	13
0 to 1% (ms/deg)	1.1/12	1.1/12	1.3/14
at (deg btdc)	1	10	12
Spark to soc (deg)	10	10	12
Soc to 1% (deg)	2	2	2
0 to 50% (ms/deg)	3.1/34	2.5/27	2.8/31
at (deg atdc)	21	5	5
0 to 90% (ms/deg)	5.4/59	4.2/46	4.6/50
at (deg atdc)	46	24	24
1 to 50% (ms/deg)	2.0/22	1.4/15	1.5/17
50 to 90% (ms/deg)	2.3/25	1.7/19	1.8/19
1 to 90% (ms/deg)	4.3/47	3.1/34	3.3/36
Soc (deg btdc)	3	12	14
Eoc (deg atdc)	56	32	32
Max pressure (bar)	36.8	51.6	56.7
at (deg atdc)	14	8	8
Std deviation:			
Pmax	2.6	2.7	2.8
Timing Pmax	3.0	1.4	2.1
% Dispersion:			
Pmax	7.3	5.2	4.9

Flame development model:

0 to 1% (ms/deg)	0.94/10.2	1.02/11.1	1.03/11.3
Integral scale at soc (mm)	4.79	5.37	5.61
Laminar flame speed at soc (m/s)	0.584	0.575	0.585
T_u at soc (K)	822	804	794
T_b at soc (K)	2359	2335	2354
Pressure soc (bar)	29.0	25.0	23.0
Max burned gas temperature (K)	2365	2461	2506

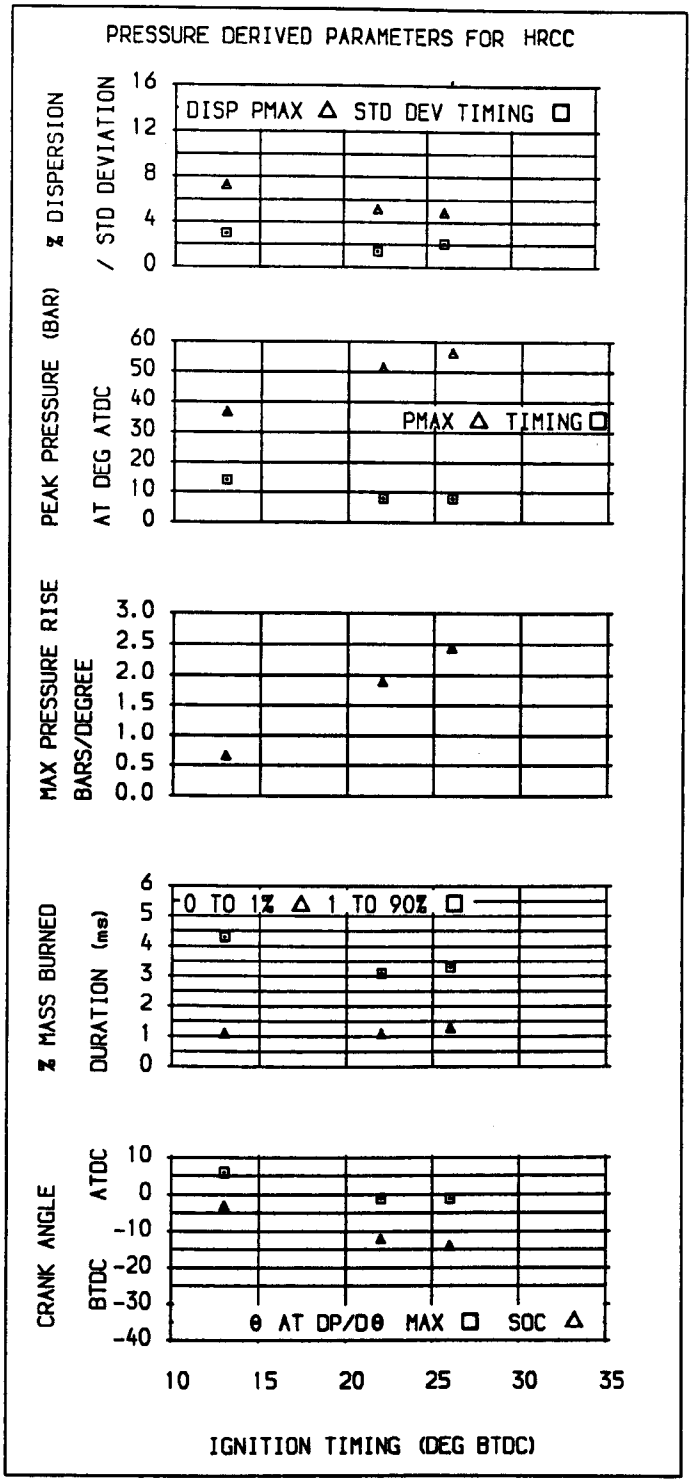

Figure 5.6 The effect of ignition timing – Hrcc at the mixture strength for maximum efficiency. Excess air at 1.2, 1800 rpm.

Table 5.7 The effect of speed: TaskII at the stoichiometric.

Reference	28	25	30
Chamber type	TaskII	TaskII	TaskII
Excess air ratio	1.01	1.04	1.06
Engine speed (rpm)	1515	1814	2105
Ignition (deg btdc)	21	26	28
Compression Ratio	9	9	9
0 to 1% (ms/deg)	1.5/14	1.2/13	1.2/15
at (deg btdc)	7	13	13
0 to 50% (ms/deg)	4.5/41	3.5/38	3.5/44
at (deg atdc)	20	12	16
0 to 90% (ms/deg)	6.2/56	5.1/55	4.9/62
at (deg atdc)	34	29	34
1 to 50% (ms/deg)	3.0/27	2.3/25	2.3/29
50 to 90% (ms/deg)	1.7/15	1.6/17	1.4/18
1 to 90% (ms/deg)	4.6/42	3.9/42	3.7/47
Soc (deg btdc)	10	16	18
Eoc (deg atdc)	44	42	46
Max pressure (bar)	28.0	34.0	31.0
at (deg atdc)	21	15	18
Std deviation:			
Pmax	2.8	2.7	3.1
Timing Pmax	3.7	1.8	3.3
% Dispersion:			
Pmax	9.9	7.9	9.7
<u>Flame development model:</u>			
0 to 1% (ms/deg)	1.52/13.80	1.45/15.83	1.31/16.57
Integral scale at soc (mm)	8.30	9.01	9.32
Laminar flame speed at soc (m/s)	0.565	0.544	0.572
$(h_s/S_l)^{2/3}$	0.060	0.065	0.064

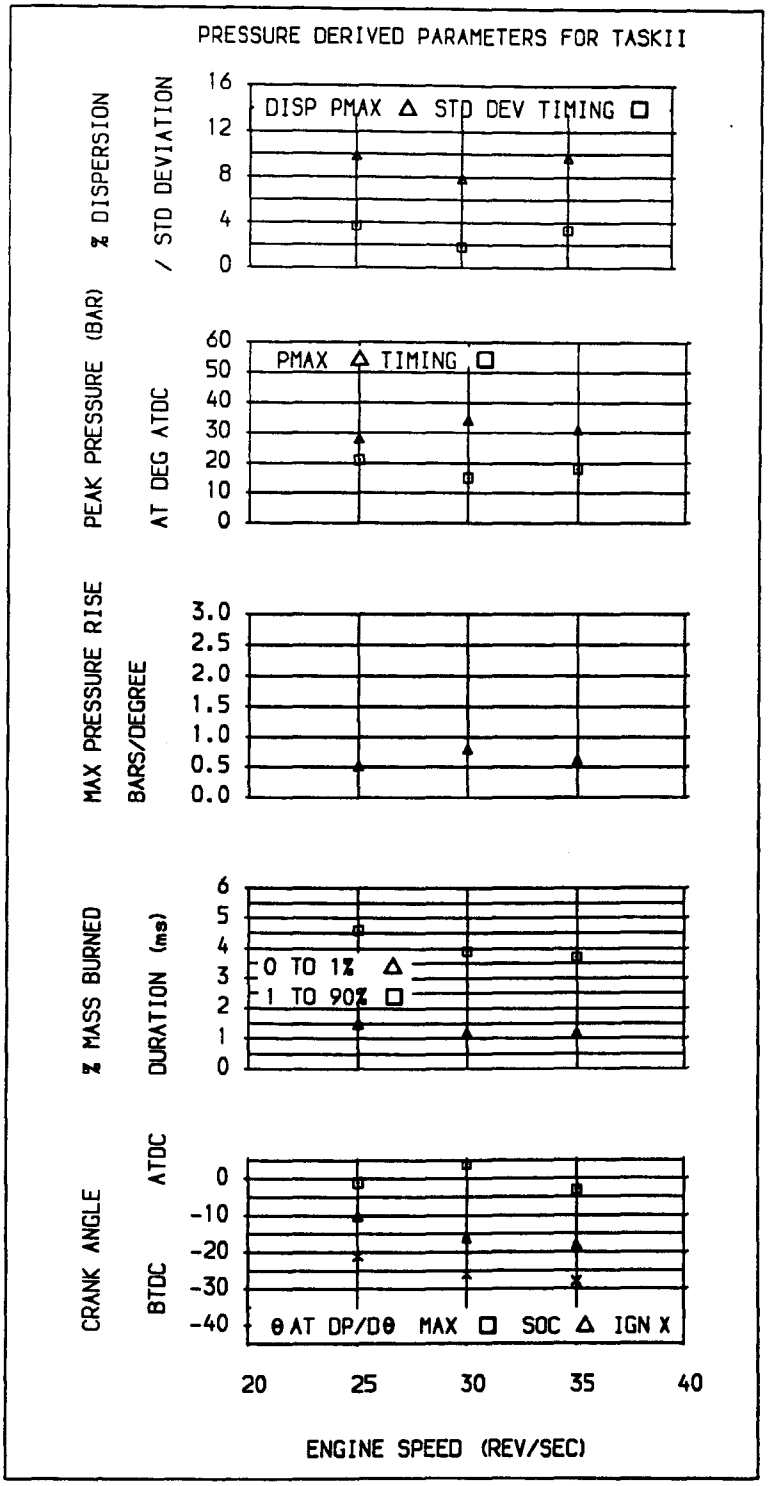

Figure 5.7 The effect of speed – TaskII at the stoichiometric mixture strength.

Table 5.8 The effect of speed: chamber 3-2 at the stoichiometric.

Reference	45	39	48
Chamber type	3-2	3-2	3-2
Excess air ratio	1.04	1.02	1.03
Engine speed (rpm)	1525	1825	2105
Ignition (deg btdc)	16	22	19
Compression Ratio	13	13	13
0 to 1% (ms/deg)	1.1/10	1.1/12	0.8/10
at (deg btdc)	6	10	9
0 to 50% (ms/deg)	4.2/38	3.5/38	2.8/35
at (deg atdc)	22	16	16
0 to 90% (ms/deg)	6.6/60	5.8/63	4.0/51
at (deg atdc)	44	41	32
1 to 50% (ms/deg)	3.1/28	2.4/26	2.0/25
50 to 90% (ms/deg)	2.4/22	2.3/25	1.2/16
1 to 90% (ms/deg)	5.5/50	4.7/51	3.2/41
Soc (deg btdc)	9	14	11
Eoc (deg atdc)	56	59	42
Max pressure (bar)	38.4	46.7	44.9
at (deg atdc)	11	12	11
Std deviation:			
Pmax	2.9	4.4	4.6
Timing Pmax	3.0	2.6	2.5
% Dispersion:			
Pmax	7.6	9.3	10.2
<u>Flame development model:</u>			
0 to 1% (ms/deg)	1.14/10.44	1.04/11.41	0.95/12.04
Integral scale at soc (mm)	5.55	6.07	5.73
Laminar flame speed at soc (m/s)	0.592	0.620	0.577

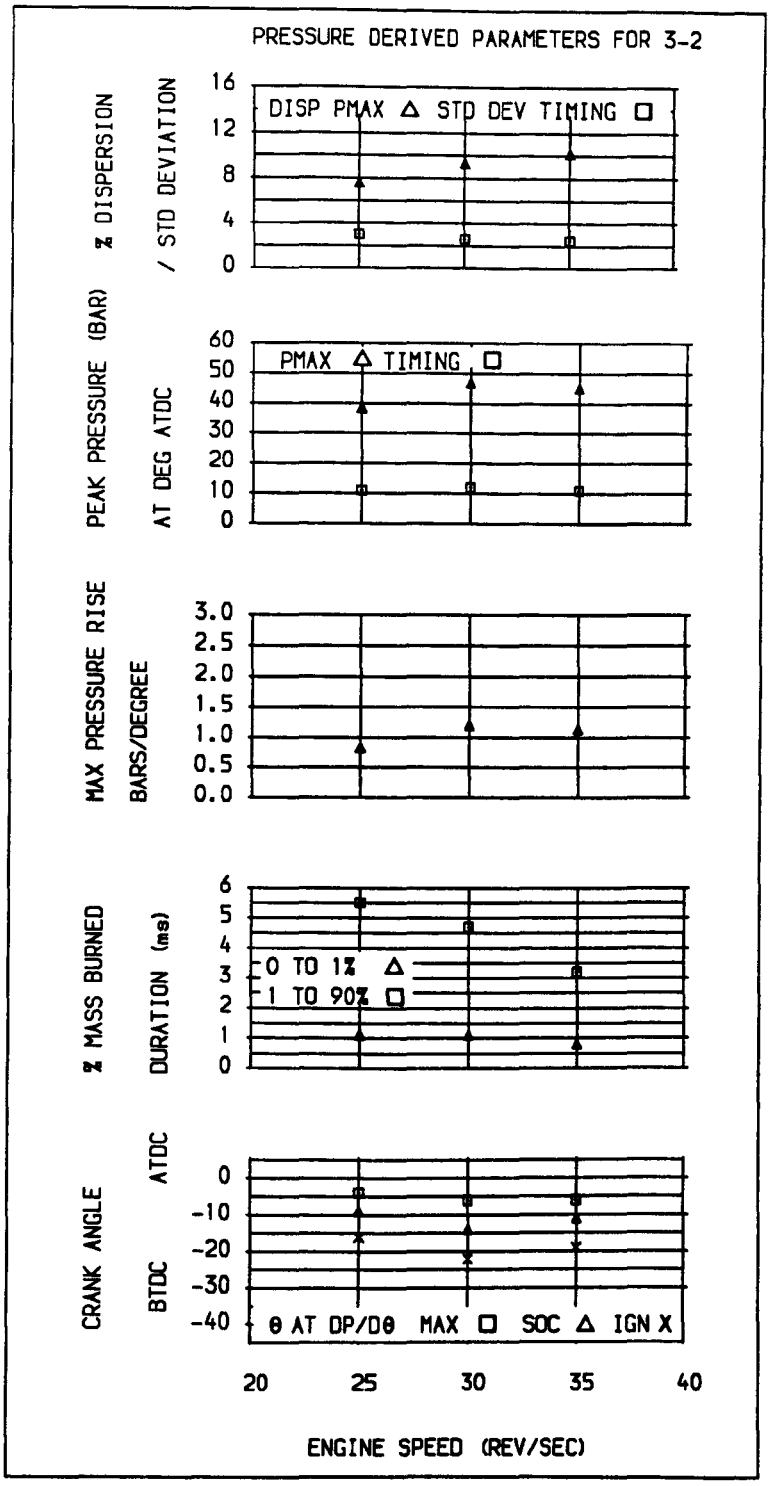

Figure 5.8 The effect of speed – chamber 3-2 at the stoichiometric mixture strength.

Table 5.9 The effect of speed: Hrcc at the stoichiometric.

Reference	11	9	20
Chamber type	Hrcc	Hrcc	Hrcc
Excess air ratio	1.03	1.03	1.02
Engine speed (rpm)	1516	1815	2116
Ignition (deg btdc)	14	16	15
Compression Ratio	13	13	13
0 to 1% (ms/deg)	1.1/10	1.0/11	0.8/10
at (deg btdc)	4	5	5
0 to 50% (ms/deg)	2.7/25	2.6/28	2.1/27
at (deg atdc)	11	12	12
0 to 90% (ms/deg)	4.3/39	4.1/45	3.5/44
at (deg atdc)	25	29	29
1 to 50% (ms/deg)	1.6/15	1.6/17	1.3/17
50 to 90% (ms/deg)	1.6/14	1.5/17	1.4/17
1 to 90% (ms/deg)	3.2/29	3.1/34	2.7/34
Soc (deg btdc)	6	7	7
Eoc (deg atdc)	34	40	38
Max pressure (bar)	45.1	46.1	47.9
at (deg atdc)	13	12	12
Std deviation:			
Pmax	3.3	2.9	3.2
Timing Pmax	1.8	1.4	1.5
% Dispersion:			
Pmax	7.4	6.4	6.8
<u>Flame development model:</u>			
0 to 1% (ms/deg)	1.01/9.16	0.92/10.06	0.79/10.08
Integral scale at soc (mm)	4.89	4.95	4.95
Laminar flame speed at soc (m/s)	0.639	0.609	0.663

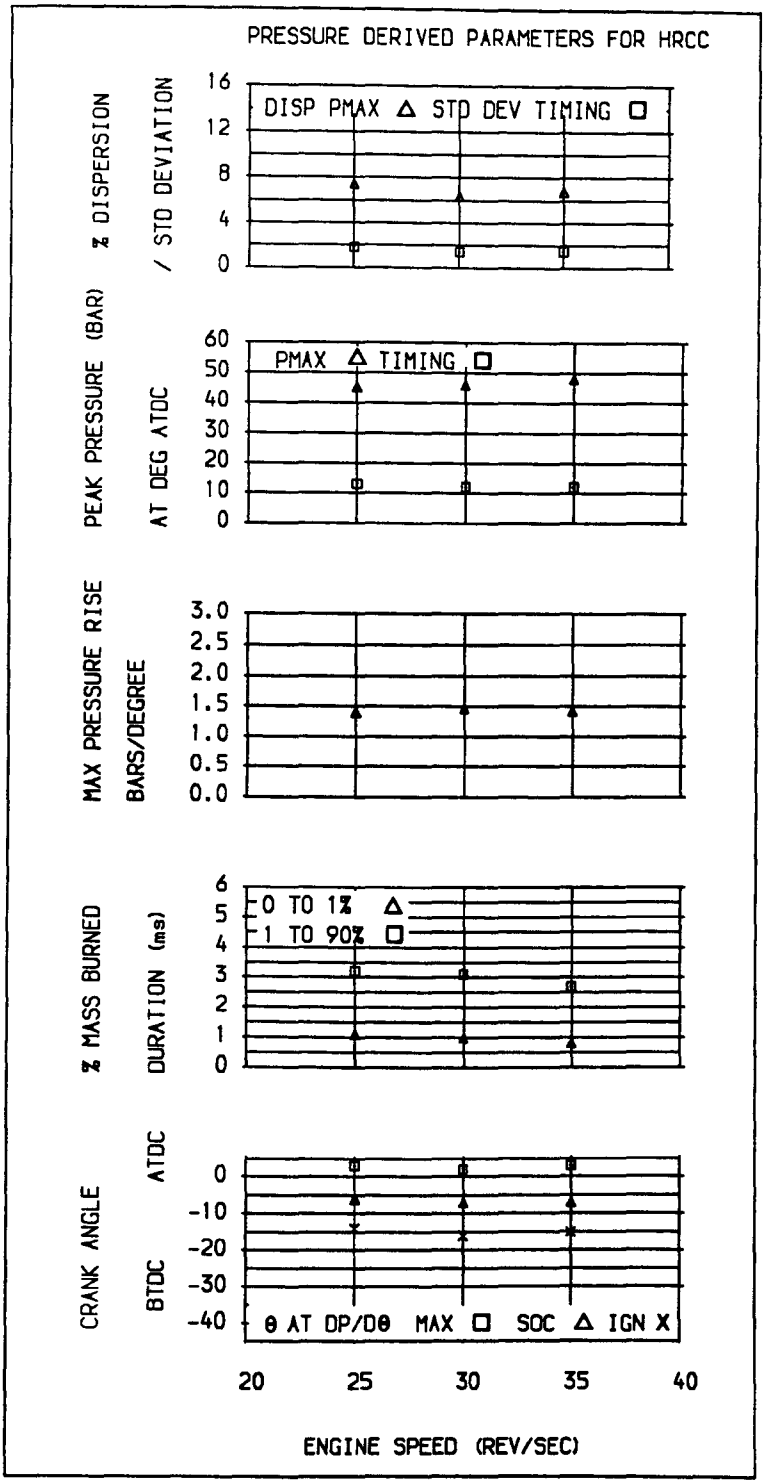

Figure 5.9 The effect of speed – Hrcc at the stoichiometric mixture strength.

Table 5.10 The effect of speed: TaskII at the lean mixture limit.

Reference	29	27	33
Chamber type	TaskII	TaskII	TaskII
Excess air ratio	1.23	1.50	1.42
Engine speed (rpm)	1513	1806	2116
Ignition (deg btdc)	33	33	38
Compression Ratio	9	9	9
0 to 1% (ms/deg)	2.8/25	2.9/31	2.0/26
at (deg btdc)	8	2	12
0 to 50% (ms/deg)	6.3/57	7.1/77	4.9/62
at (deg atdc)	24	44	24
0 to 90% (ms/deg)	9.0/82	10.3/112	7.3/93
at (deg atdc)	49	79	55
1 to 50% (ms/deg)	3.5/32	4.2/46	2.9/36
50 to 90% (ms/deg)	2.7/25	3.2/35	2.4/31
1 to 90% (ms/deg)	6.3/57	7.5/81	5.3/67
Soc (deg btdc)	12	6	16
Eoc (deg atdc)	60	98	72
Max pressure (bar)	25.2	20.7	27.2
at (deg atdc)	18	6	14
Std deviation:			
Pmax	3.3	1.4	3.4
Timing Pmax	6.7	3.5	4.5
% Dispersion:			
Pmax	12.8	6.7	13.3
<u>Flame development model:</u>			
0 to 1% (ms/deg)	1.75/15.87	1.85/20.01	1.67/21.15
Integral scale at soc (mm)	8.49	8.02	9.01
Laminar flame speed at soc (m/s)	0.469	0.337	0.377

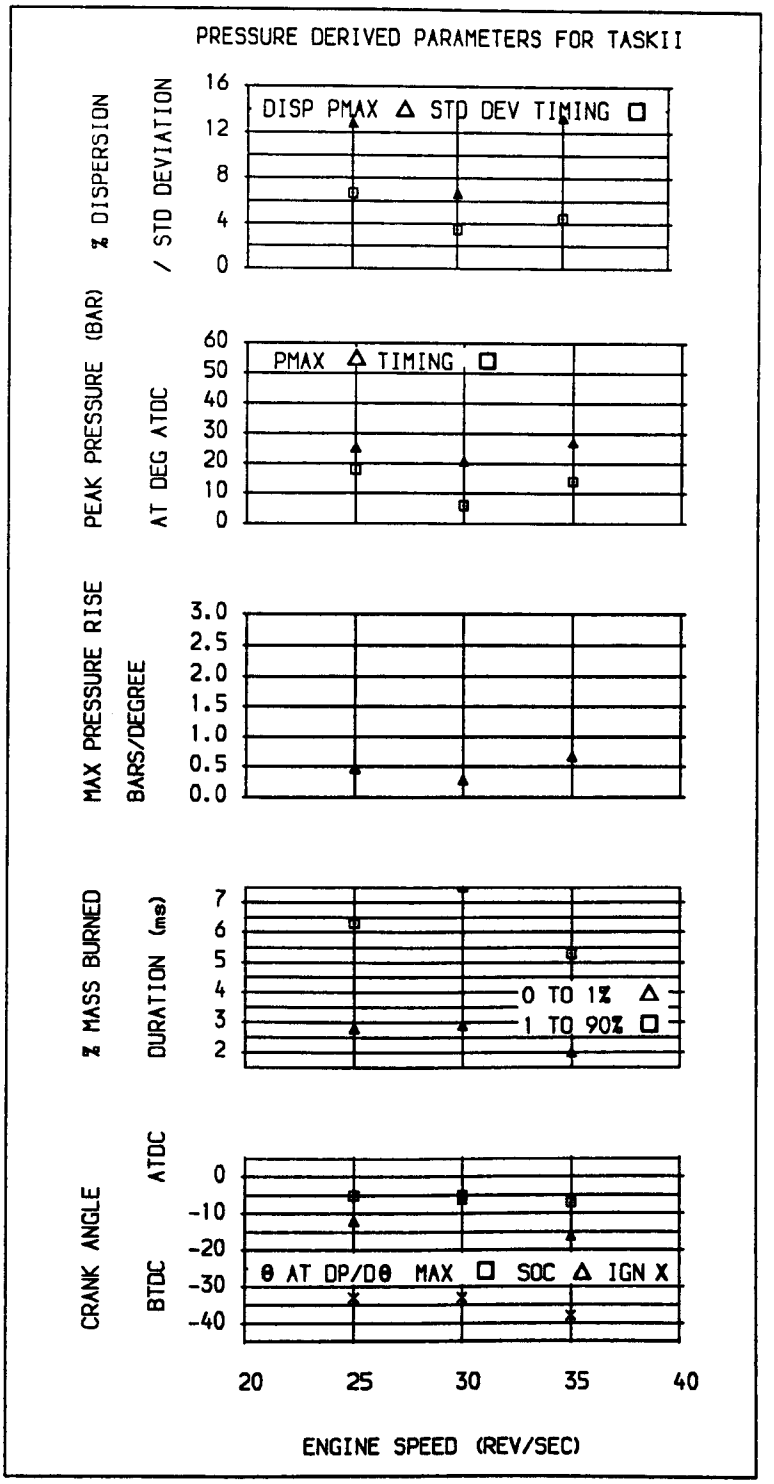

Figure 5.10 The effect of speed – TaskII at the lean mixture limit.

Table 5.11 The effect of speed: chamber 3-2 at the lean mixture limit.

Reference	47	40	1
Chamber type	3-2	3-2	3-2
Excess air ratio	1.48	1.49	1.50
Engine speed (rpm)	1500	1807	2105
Ignition (deg btdc)	29	37	33
Compression Ratio	13	13	13
0 to 1% (ms/deg)	1.8/16	1.4/15	1.4/18
at (deg btdc)	13	22	15
0 to 10% (ms/deg)	2.7/	2.3/	2.1/
at (deg atdc)			
0 to 50% (ms/deg)	4.9/44	4.3/47	4.0/51
at (deg atdc)	15	10	18
0 to 90% (ms/deg)	8.0/72	7.2/78	6.7/84
at (deg atdc)	43	41	51
1 to 50% (ms/deg)	3.1/28	2.9/27	2.6/33
50 to 90% (ms/deg)	3.1/28	2.9/31	2.7/33
1 to 90% (ms/deg)	6.2/56	5.8/63	5.2/66
Soc (deg btdc)	16	26	18
Eoc (deg atdc)	54	58	62
Max pressure (bar)	42.8	49.5	46.4
at (deg atdc)	6	6	7
Std deviation:			
Pmax	3.7	4.8	4.5
Timing Pmax	1.5	1.2	1.5
% Dispersion:			
Pmax	8.8	9.8	9.8
<u>Flame development model:</u>			
0 to 1% (ms/deg)	1.61/14.46	1.83/19.79	1.43/18.02
Integral scale at soc (mm)	6.34	8.29	6.66
Laminar flame speed at soc (m/s)	0.408	0.353	0.358

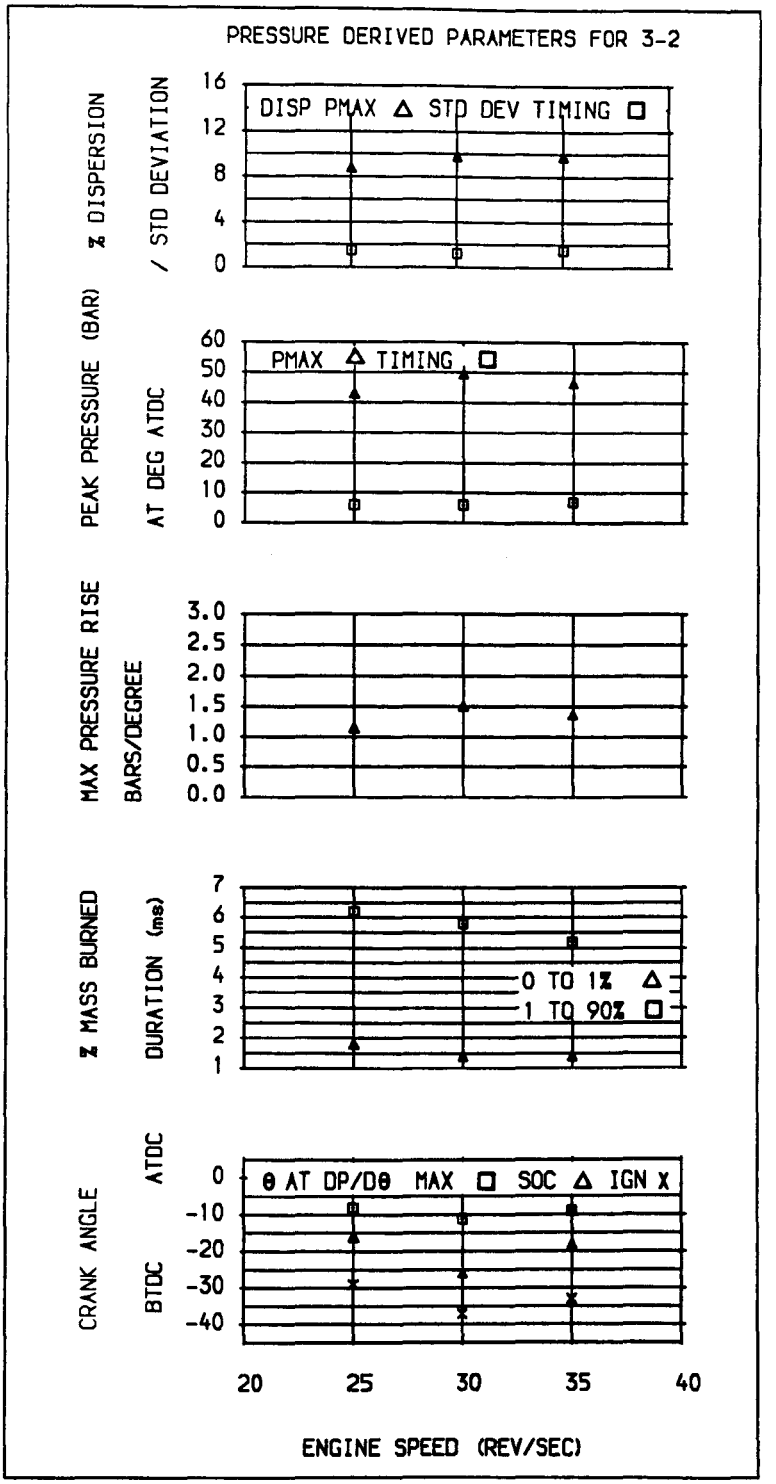

Figure 5.11 The effect of speed — chamber 3-2 at the lean mixture limit.

Table 5.12 The effect of speed: Hrcc at the lean mixture limit.

Reference	14	10	21
Chamber type	Hrcc	Hrcc	Hrcc
Excess air ratio	1.63	1.61	1.54
Engine speed (rpm)	1512	1810	2100
Ignition (deg btdc)	24	25	26
Compression Ratio	13	13	13
0 to 1% (ms/deg)	2.1/19	1.8/20	1.2/15
at (deg btdc)	5	5	11
0 to 10% (ms/deg)	2.8/25	2.5/27	1.7/22
at (deg atdc)	1	2	-4
0 to 50% (ms/deg)	4.5/41	4.2/46	3.2/40
at (deg atdc)	17	21	14
0 to 90% (ms/deg)	9.3/84	8.6/93	6.3/79
at (deg atdc)	60	68	53
1 to 50% (ms/deg)	2.4/22	2.4/26	2.0/25
50 to 90% (ms/deg)	4.8/43	4.4/47	3.1/39
1 to 90% (ms/deg)	7.2/65	6.7/73	5.1/64
Soc (deg btdc)	8	8	14
Eoc (deg atdc)	72	82	68
Max pressure (bar)	37.9	39.0	47.3
at (deg atdc)	10	9	9
Std deviation:			
Pmax	3.4	2.8	3.4
Timing Pmax	1.7	1.2	1.5
% Dispersion:			
Pmax	9.2	7.2	7.2
Flame development model:			
0 to 1% (ms/deg)	1.41/12.79	1.24/13.46	1.18/14.92
Integral scale at soc (mm)	5.01	5.01	5.61
Laminar flame speed at soc (m/s)	0.395	0.399	0.410
h_s/S_l	0.0127	0.0126	0.0137
x at pmax (%)	0.361	0.283	0.431
mass at ivc (g)	0.128	0.127	0.126

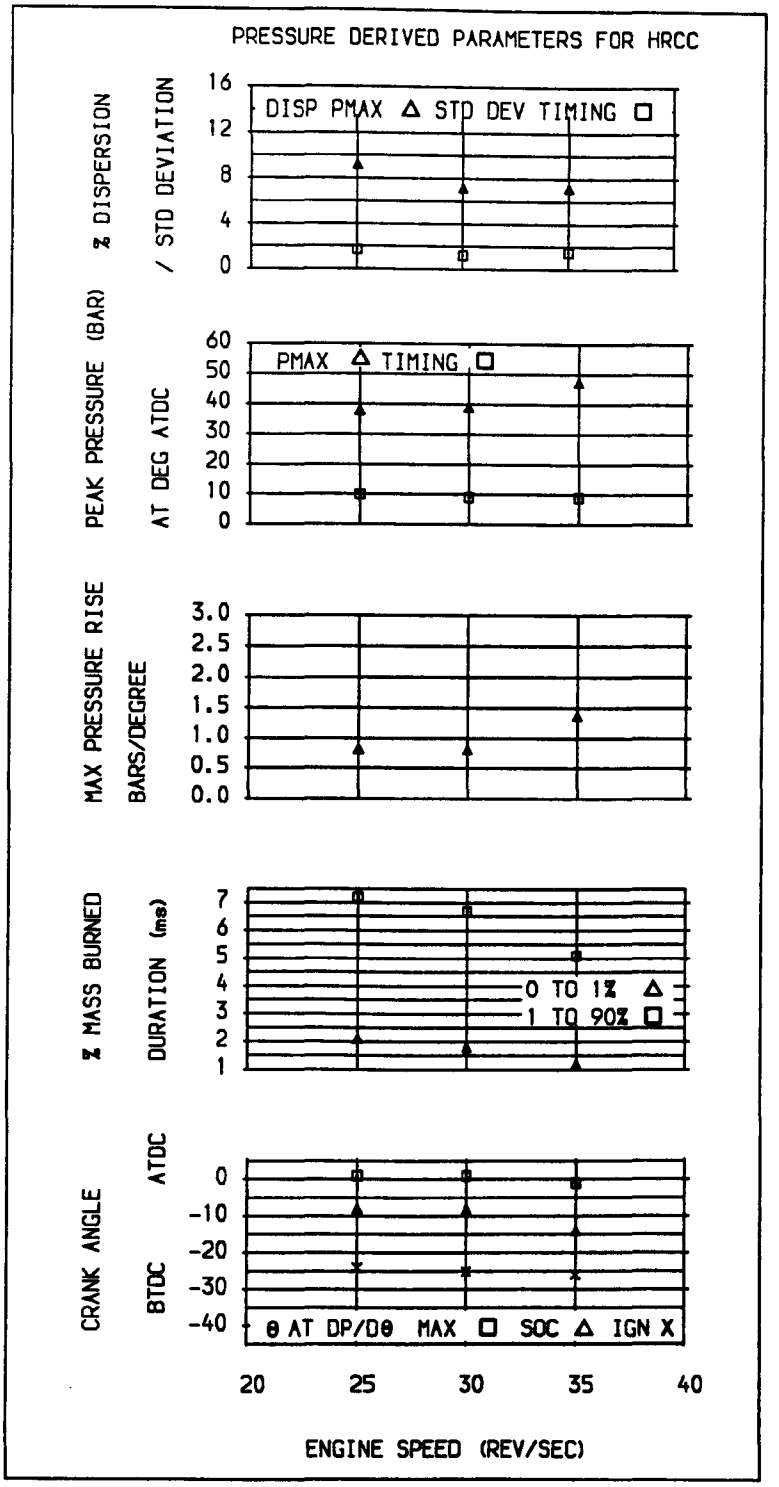

Figure 5.12 The effect of speed – Hrcc at the lean mixture limit.

Table 5.13 The effect of chamber at the stoichiometric, 25 revs/sec.

Reference	28	45	11
Chamber type	TaskII	3-2	Hrcc
Excess air ratio	1.01	1.04	1.03
Engine speed (rpm)	1515	1525	1516
Ignition (deg btdc)	21	16	14
Compression Ratio	9	13	13
0 to 1% (ms/deg)	1.50/14	1.09/10	1.10/10
at (deg btdc)	7	6	4
0 to 50% (ms/deg)	4.5/41	4.2/38	2.7/25
at (deg atdc)	20	22	11
0 to 90% (ms/deg)	6.2/56	6.6/60	4.3/39
at (deg atdc)	35	44	25
1 to 50% (ms/deg)	3.1/	3.1/	1.6/
50 to 90% (ms/deg)	1.7/	2.4/	1.6/
1 to 90% (ms/deg)	4.6/	5.5/	3.2/
Soc (deg btdc)	10	9	6
Eoc (deg atdc)	47	56	34
Max pressure (bar)	28.0	38.4	45.1
at (deg atdc)	21	11	13
$dp/d\theta$ max (bar/deg)	0.52	0.82	1.40
at (deg atdc)			
Std deviation:			
Pmax	2.8	2.9	3.3
Timing Pmax	3.7	3.0	1.8
% Dispersion:			
Pmax	9.9	7.6	7.4
<u>Flame development model:</u>			
0 to 1% (ms/deg)	1.52/13.80	1.14/10.44	1.01/9.16
Integral scale at soc (mm)	8.30	5.55	4.89
Laminar flame speed at soc (m/s)	0.565	0.592	0.639
$(h_s/S_l)^{2/3}$	0.060	0.045	0.039

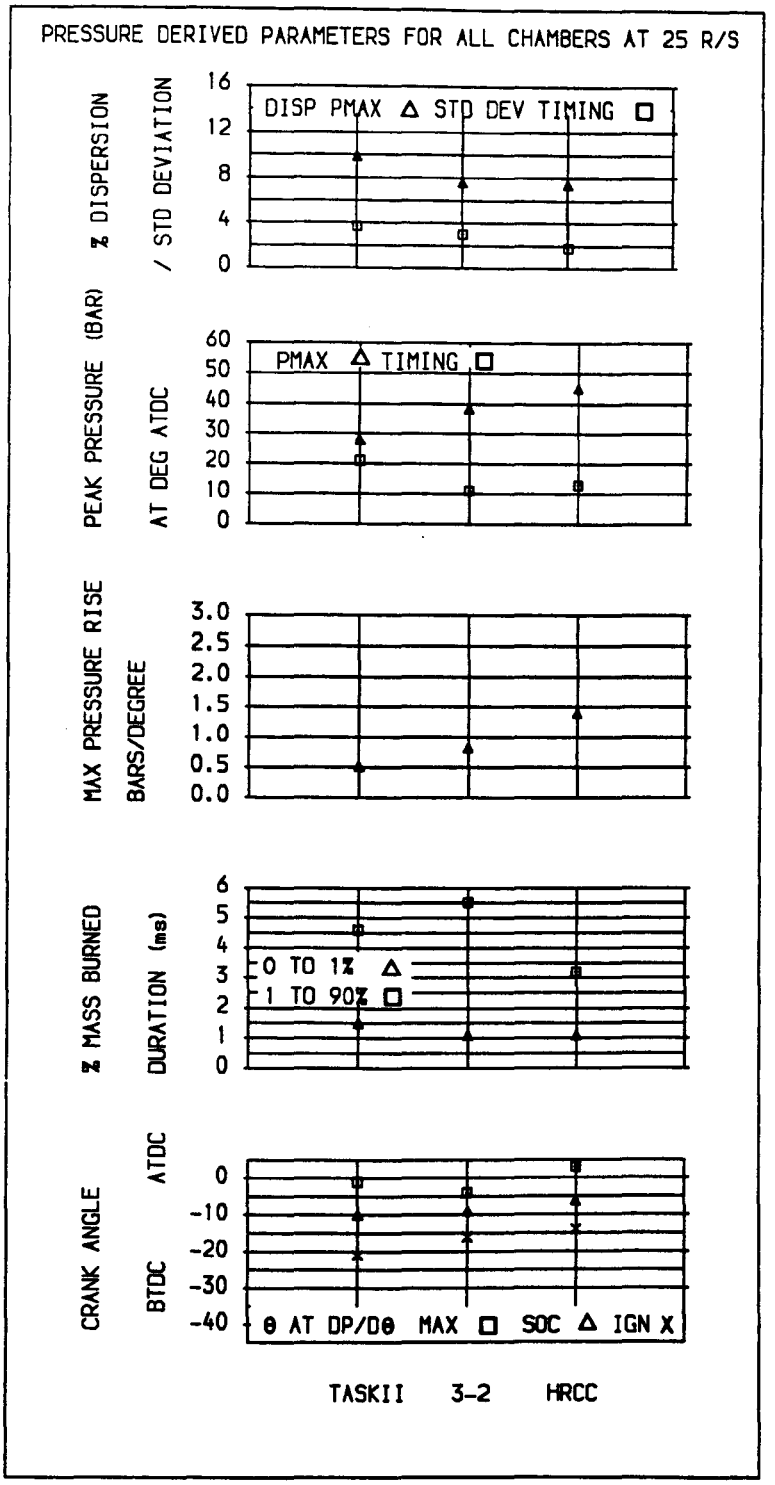

Figure 5.13 The effect of chamber at the stoichiometric mixture strength, 25 revs/sec.

Table 5.14 The effect of chamber at the stoichiometric, 30 revs/sec.

Reference	25	39	9
Chamber type	TaskII	3-2	Hrcc
Excess air ratio	1.04	1.02	1.03
Engine speed (rpm)	1814	1825	1815
Ignition (deg btdc)	26	22	16
Compression Ratio	9	13	13
0 to 1% (ms/deg)	1.20/13	1.10/12	1.00/11
at (deg btdc)	13	10	5
0 to 50% (ms/deg)	3.5/38	3.5/38	2.6/28
at (deg atdc)	12	16	12
0 to 90% (ms/deg)	5.1/55	5.8/63	4.1/45
at (deg atdc)	29	41	29
1 to 50% (ms/deg)	2.3/	2.4/	1.6/
50 to 90% (ms/deg)	1.6/	2.3/	1.5/
1 to 90% (ms/deg)	3.9/	4.7/	3.1/
Soc (deg btdc)	16	14	7
Eoc (deg atdc)	42	59	40
Max pressure (bar)	34.0	46.7	46.1
at (deg atdc)	15	12	12
$dp/d\theta$ max (bar/deg)	0.80	1.20	1.47
at (deg atdc)	4	-6	2
Std deviation:			
Pmax	2.7	4.4	2.9
Timing Pmax	1.8	2.6	1.4
% Dispersion:			
Pmax	7.9	9.3	6.4
Flame development model:			
0 to 1% (ms/deg)	1.45/15.83	1.04/11.41	0.92/10.06
Integral scale at soc (mm)	9.01	6.07	4.95
Laminar flame speed at soc (m/s)	0.544	0.620	0.609
$(h_s/S_l)^{2/3}$	0.065	0.046	0.041

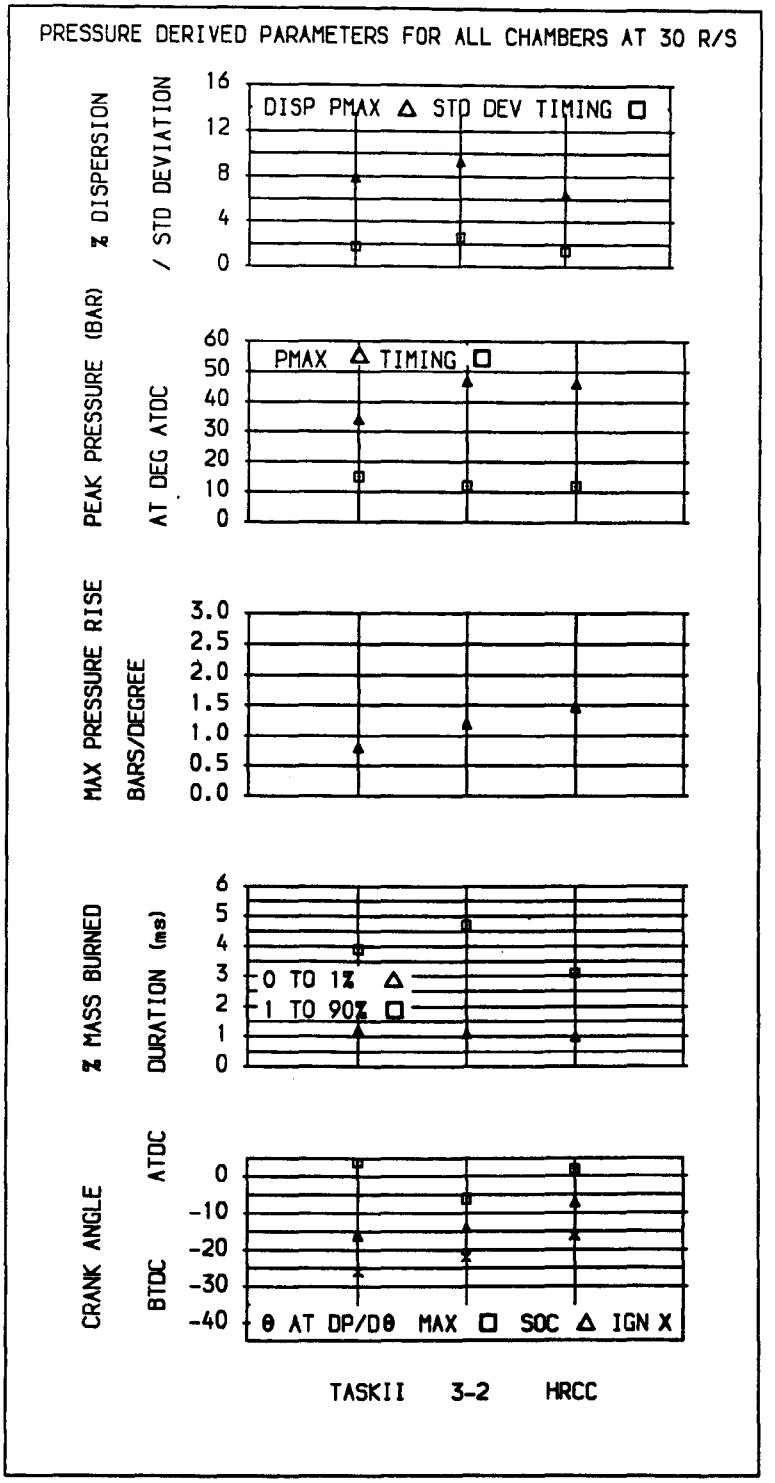

Figure 5.14 The effect of chamber at the stoichiometric mixture strength, 30 revs/sec.

Table 5.15 The effect of chamber at the stoichiometric, 35 revs/sec.

Reference	30	48	20
Chamber type	TaskII	3-2	Hrcc
Excess air ratio	1.06	1.03	1.02
Engine speed (rpm)	2105	2105	2116
Ignition (deg btdc)	28	19	15
Compression Ratio	9	13	13
0 to 1% (ms/deg)	1.20/15	0.80/10	0.80/10
at (deg btdc)	13	9	5
0 to 50% (ms/deg)	3.5/44	2.8/35	2.1/27
at (deg atdc)	16	16	12
0 to 90% (ms/deg)	4.9/62	4.0/51	3.5/44
at (deg atdc)	34	32	29
1 to 50% (ms/deg)	2.3/	2.0/	1.3/
50 to 90% (ms/deg)	1.4/	1.2/	1.4/
1 to 90% (ms/deg)	3.7/	3.2/	2.7/
Soc (deg btdc)	18	11	7
Eoc (deg atdc)	46	42	38
Max pressure (bar)	31.0	44.9	47.9
at (deg atdc)	18	11	12
$dp/d\theta$ max (bar/deg)	0.62	1.13	1.42
at (deg atdc)	-3	-6	3
Std deviation:			
Pmax	3.1	4.6	3.2
Timing Pmax	3.3	2.5	1.5
% Dispersion:			
Pmax	9.7	10.2	6.8

Flame development model:

0 to 1% (ms/deg)	1.31/16.57	0.95/12.04	0.79/10.08
Integral scale at soc (mm)	9.32	5.73	4.95
Laminar flame speed at soc (m/s)	0.572	0.577	0.663
$(h_s/S_l)^{2/3}$	0.064	0.046	0.038

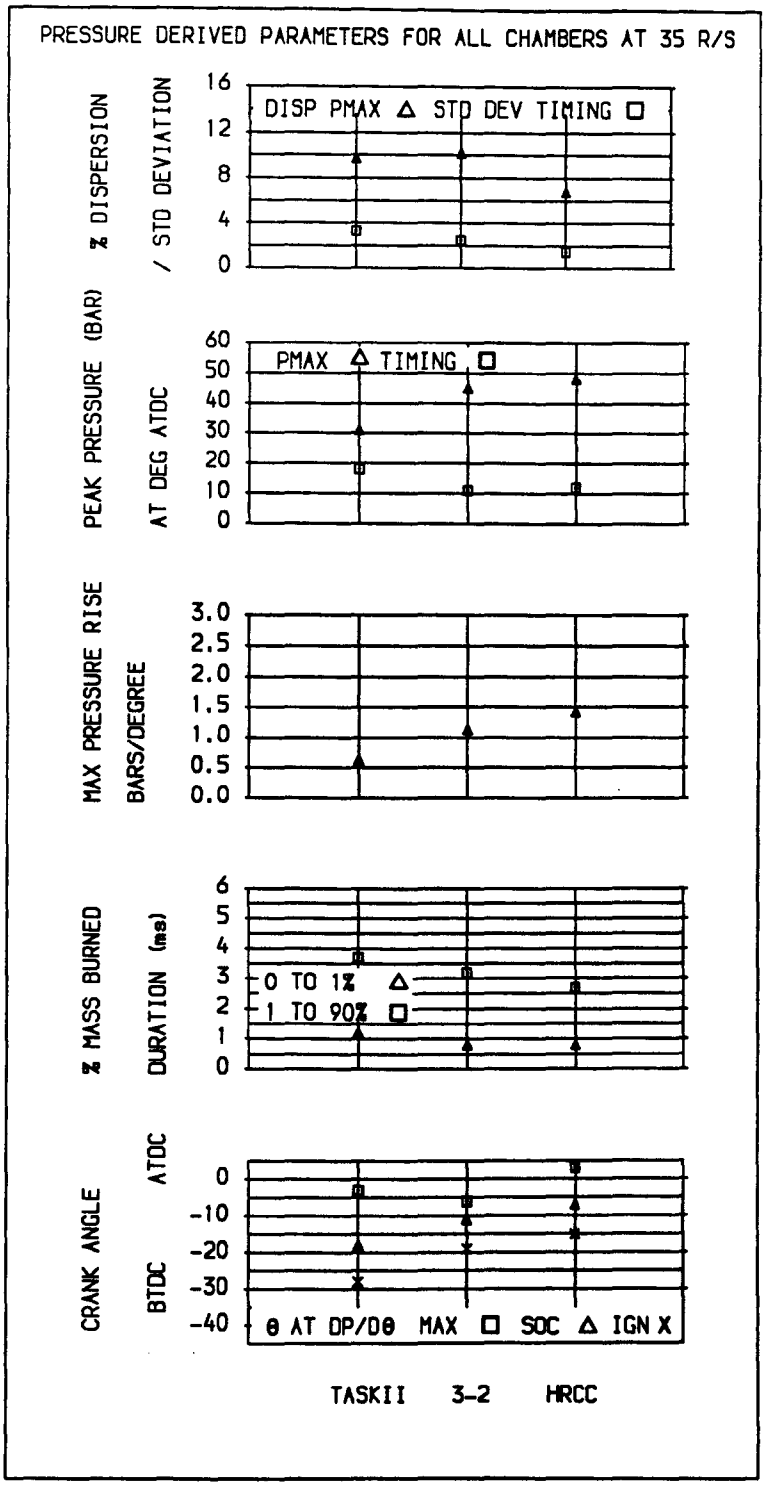

Figure 5.15 The effect of chamber at the stoichiometric mixture strength, 35 revs/sec.

Table 5.16 The effect of chamber at the lean mixture limit, 25 revs/sec.

Reference	29	47	14
Chamber type	TaskII	3-2	Hrcc
Excess air ratio	1.23	1.48	1.63
Engine speed (rpm)	1513	1500	1512
Ignition (deg btdc)	33	29	24
Compression Ratio	9	13	13
0 to 1% (ms/deg)	2.80/25	1.80/16	2.10/19
at (deg btdc)	8	13	5
0 to 10% (ms/deg)	4.00/	2.70/	2.80/
at (deg btdc)	-3	5	-1
0 to 50% (ms/deg)	6.3/57	4.9/44	4.5/41
at (deg atdc)	24	15	17
0 to 90% (ms/deg)	9.0/82	8.0/72	9.3/84
at (deg atdc)	49	43	60
1 to 50% (ms/deg)	3.5/32	3.1/28	2.4/22
50 to 90% (ms/deg)	2.7/	3.1/	4.8/
1 to 90% (ms/deg)	6.3/57	6.2/56	7.2/65
Soc (deg btdc)	12	16	8
Eoc (deg atdc)	60	54	72
Max pressure (bar)	25.2	42.8	37.9
at (deg atdc)	18	6	10
Std deviation:			
Pmax	3.3	3.7	3.4
Timing Pmax	6.7	1.5	1.7
% Dispersion:			
Pmax	12.8	8.8	9.2
<u>Flame development model:</u>			
0 to 1% (ms/deg)	1.75/	1.61/	1.41/12.79
Integral scale at soc (mm)	8.49	6.34	5.01
Laminar flame speed at soc (m/s)	0.469	0.408	0.395

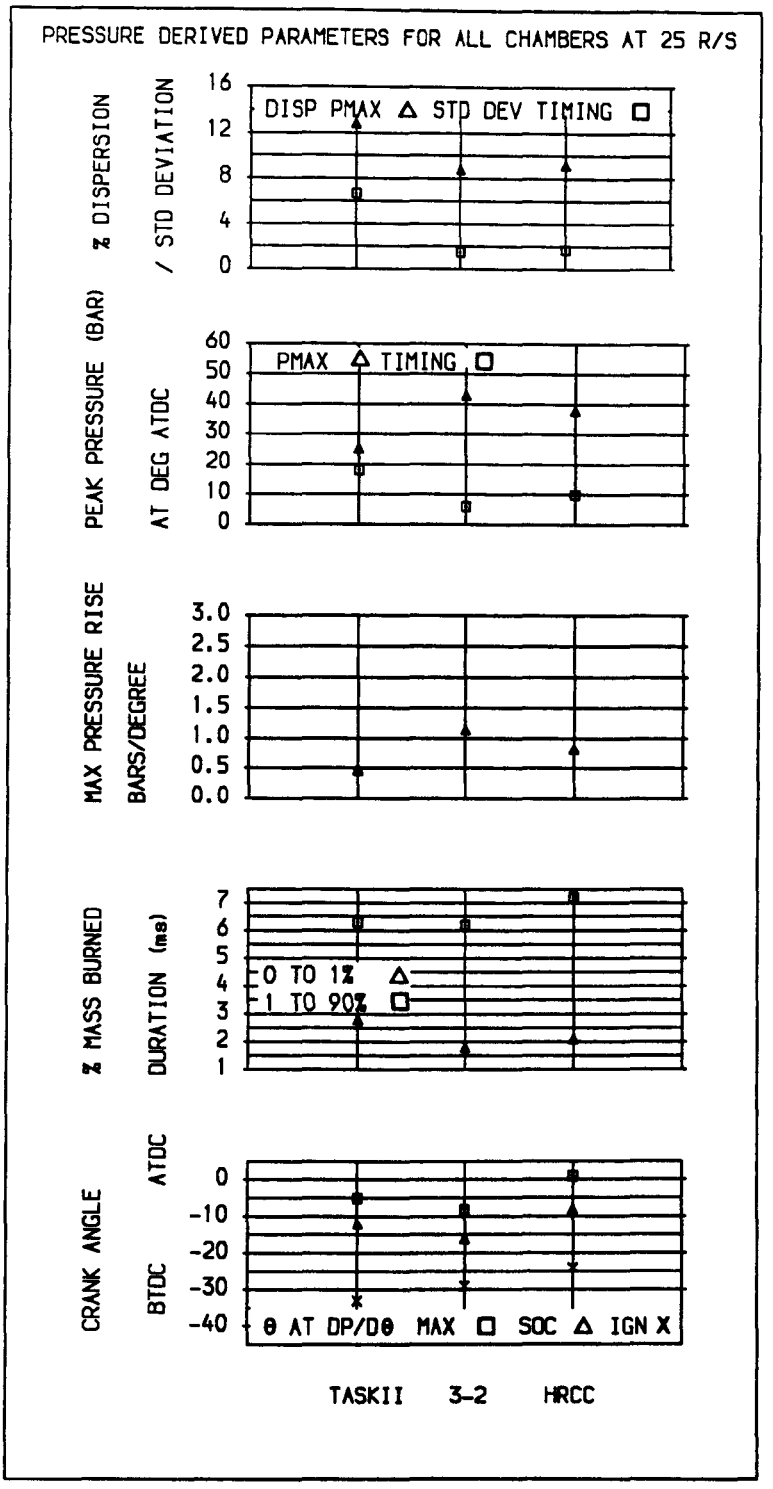

Figure 5.16 The effect of chamber at the lean mixture limit, 25 revs/sec.

Table 5.17 The effect of chamber at the lean mixture limit, 30 revs/sec.

Reference	27	40	10
Chamber type	TaskII	3-2	Hrcc
Excess air ratio	1.50	1.49	1.61
Engine speed (rpm)	1806	1807	1810
Ignition (deg btdc)	33	37	25
Compression Ratio	9	13	13
0 to 1% (ms/deg)	2.90/31	1.40/15	1.80/20
at (deg btdc)	2	22	5
0 to 50% (ms/deg)	7.1/77	4.3/47	4.2/46
at (deg atdc)	44	10	21
0 to 90% (ms/deg)	10.3/112	7.2/78	8.6/93
at (deg atdc)	79	41	68
1 to 50% (ms/deg)	4.2/46	2.9/27	2.4/26
50 to 90% (ms/deg)	3.2/35	2.9/31	4.4/47
1 to 90% (ms/deg)	7.5/81	5.8/63	6.7/73
Soc (deg btdc)	6	26	8
Eoc (deg atdc)	98	58	82
Max pressure (bar)	20.7	49.5	39.0
at (deg atdc)	6	6	9
Std deviation:			
Pmax	1.4	4.8	2.8
Timing Pmax	3.5	1.2	1.2
% Dispersion:			
Pmax	6.7	9.8	7.2
<u>Flame development model:</u>			
0 to 1% (ms/deg)	1.85/	1.83/	1.24/
Integral scale at soc (mm)	8.02	8.29	5.01
Laminar flame speed at soc (m/s)	0.337	0.353	0.399

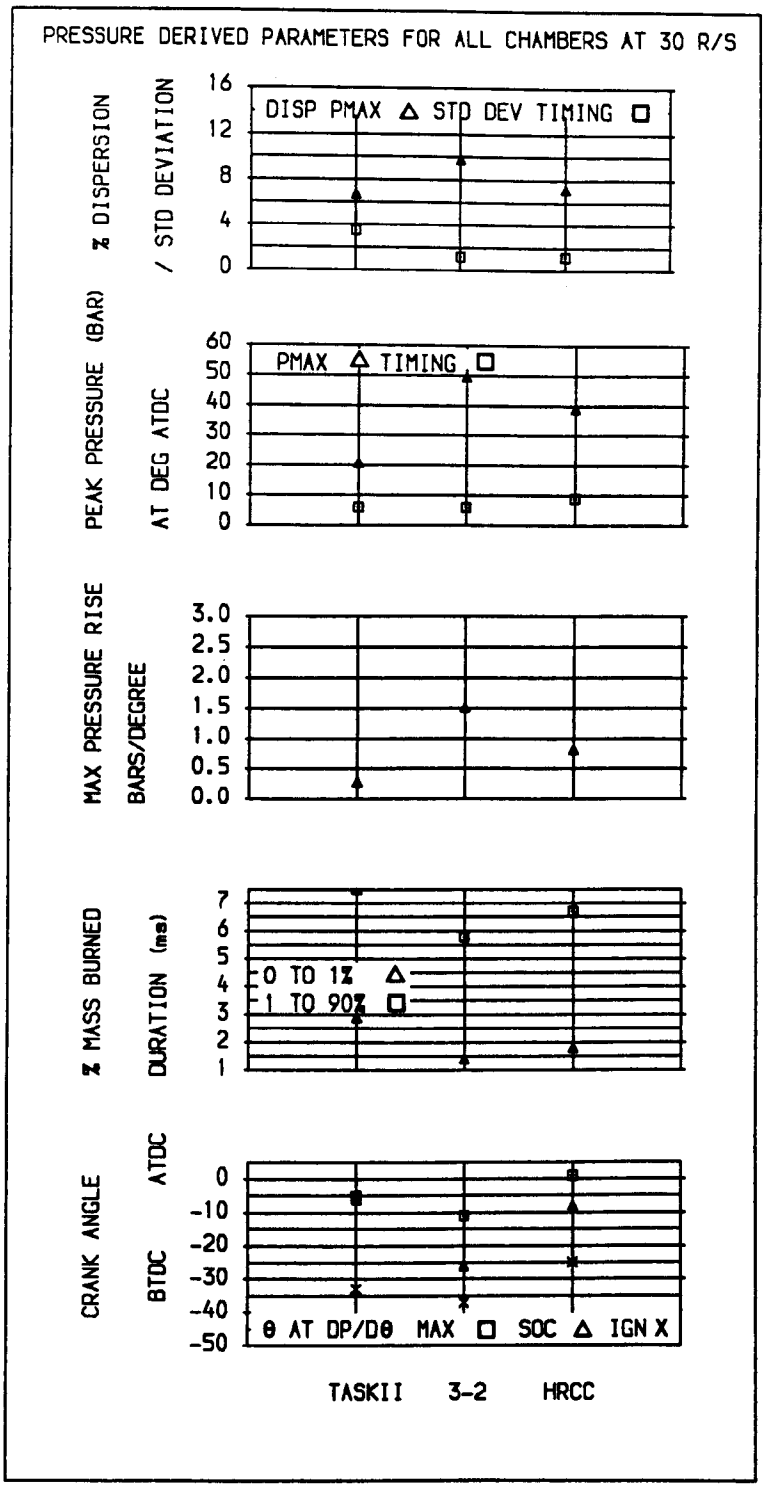

Figure 5.17 The effect of chamber at the lean mixture limit, 30 revs/sec.

Table 5.18 The effect of chamber at the lean mixture limit, 35 revs/sec.

Reference	33	1	21
Chamber type	TaskII	3-2	Hrcc
Excess air ratio	1.42	1.50	1.54
Engine speed (rpm)	2116	2105	2100
Ignition (deg btdc)	38	33	26
Compression Ratio	9	13	13
0 to 1% (ms/deg)	2.00/26	1.40/18	1.20/15
at (deg btdc)	12	15	11
0 to 50% (ms/deg)	4.9/62	4.0/51	3.2/40
at (deg atdc)	24	18	14
0 to 90% (ms/deg)	7.3/93	6.7/84	6.3/79
at (deg atdc)	55	51	53
1 to 50% (ms/deg)	2.9/	2.6/	2.0/
50 to 90% (ms/deg)	2.4/	2.7/	3.1/
1 to 90% (ms/deg)	5.3/67	5.2/66	5.1/64
Soc (deg btdc)	16	18	14
Eoc (deg atdc)	72	62	68
Max pressure (bar)	27.2	46.4	47.3
at (deg atdc)	14	7	9
Std deviation:			
Pmax	3.4	4.5	3.4
Timing Pmax	4.5	1.5	1.5
% Dispersion:			
Pmax	13.3	9.8	7.2
<u>Flame development model:</u>			
0 to 1% (ms/deg)	1.67/	1.43/	1.18/
Integral scale at soc (mm)	9.01	8.29	5.61
Laminar flame speed at soc (m/s)	0.377	0.353	0.410

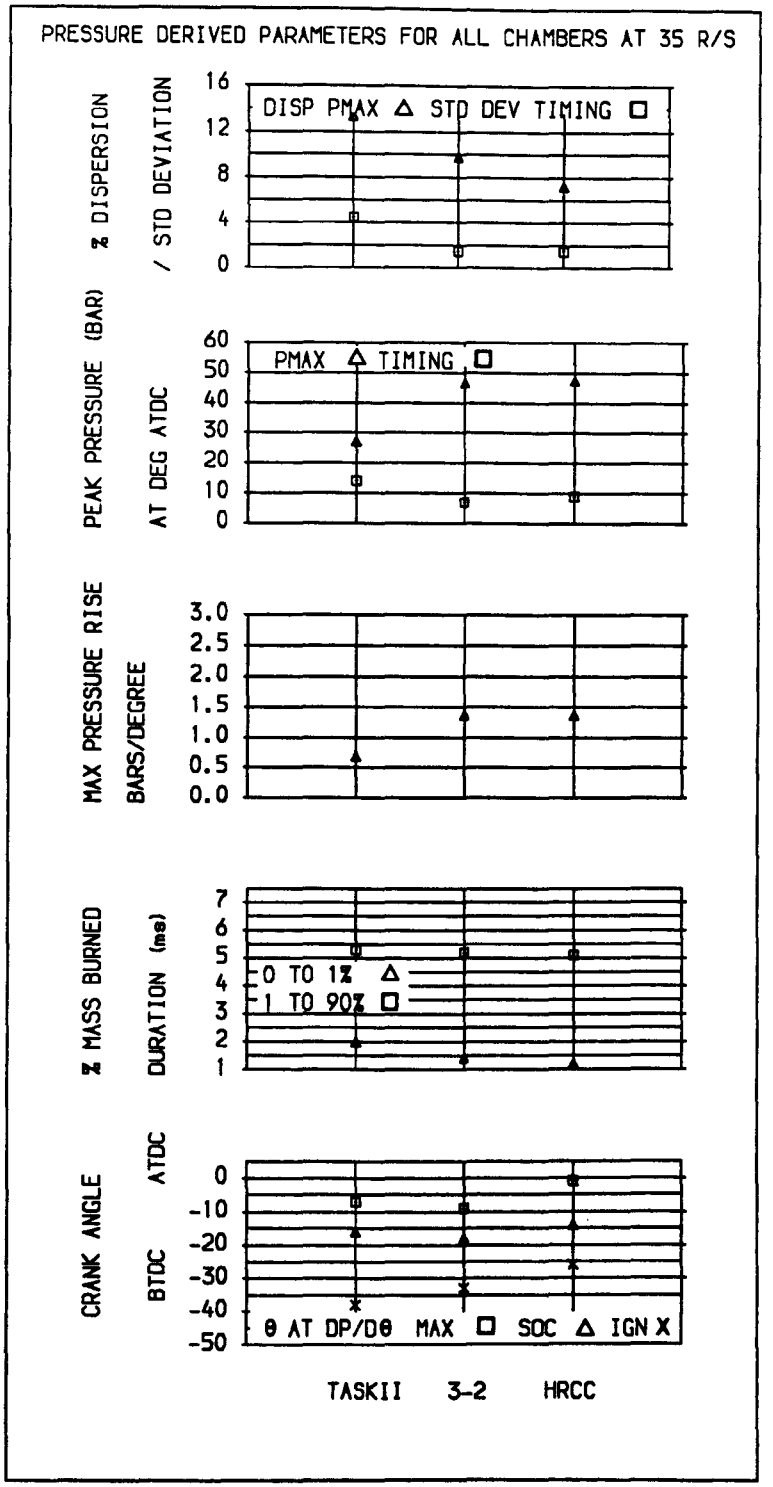

Figure 5.18 The effect of chamber at the lean mixture limit, 35 revs/sec.

Table 5.19 The effect of excess air: TaskII, 30 revs/sec.

Reference	25	26	27
Chamber type	TaskII	TaskII	TaskII
Excess air ratio	1.04	1.18	1.50
Engine speed (rpm)	1814	1807	1806
Ignition (deg btdc)	26	25	33
Compression Ratio	9	9	9
0 to 1% (ms/deg)	1.20/13	1.60/17	2.90/31
at (deg btdc)	13	8	2
0 to 50% (ms/deg)	3.5/38	4.1/44	7.1/77
at (deg atdc)	12	27	44
0 to 90% (ms/deg)	5.1/55	6.6/72	10.3/112
at (deg atdc)	29	47	79
1 to 50% (ms/deg)	2.3/25	2.5/27	4.2/46
50 to 90% (ms/deg)	1.6/17	2.5/28	3.2/35
1 to 90% (ms/deg)	3.9/42	5.1/55	7.5/81
Soc (deg btdc)	16	12	6
Eoc (deg atdc)	42	64	98
Max pressure (bar)	34.0	28.8	20.7
at (deg atdc)	15	19	6
Std deviation:			
Pmax	2.7	2.9	1.4
Timing Pmax	1.8	3.0	3.5
% Dispersion:			
Pmax	7.9	9.9	6.7
Flame development model:			
0 to 1% (ms/deg)	1.45/15.8	1.52/16.5	1.85/20.0
Integral scale at soc (mm)	9.01	8.49	8.02
Laminar flame speed at soc (m/s)	0.544	0.481	0.337

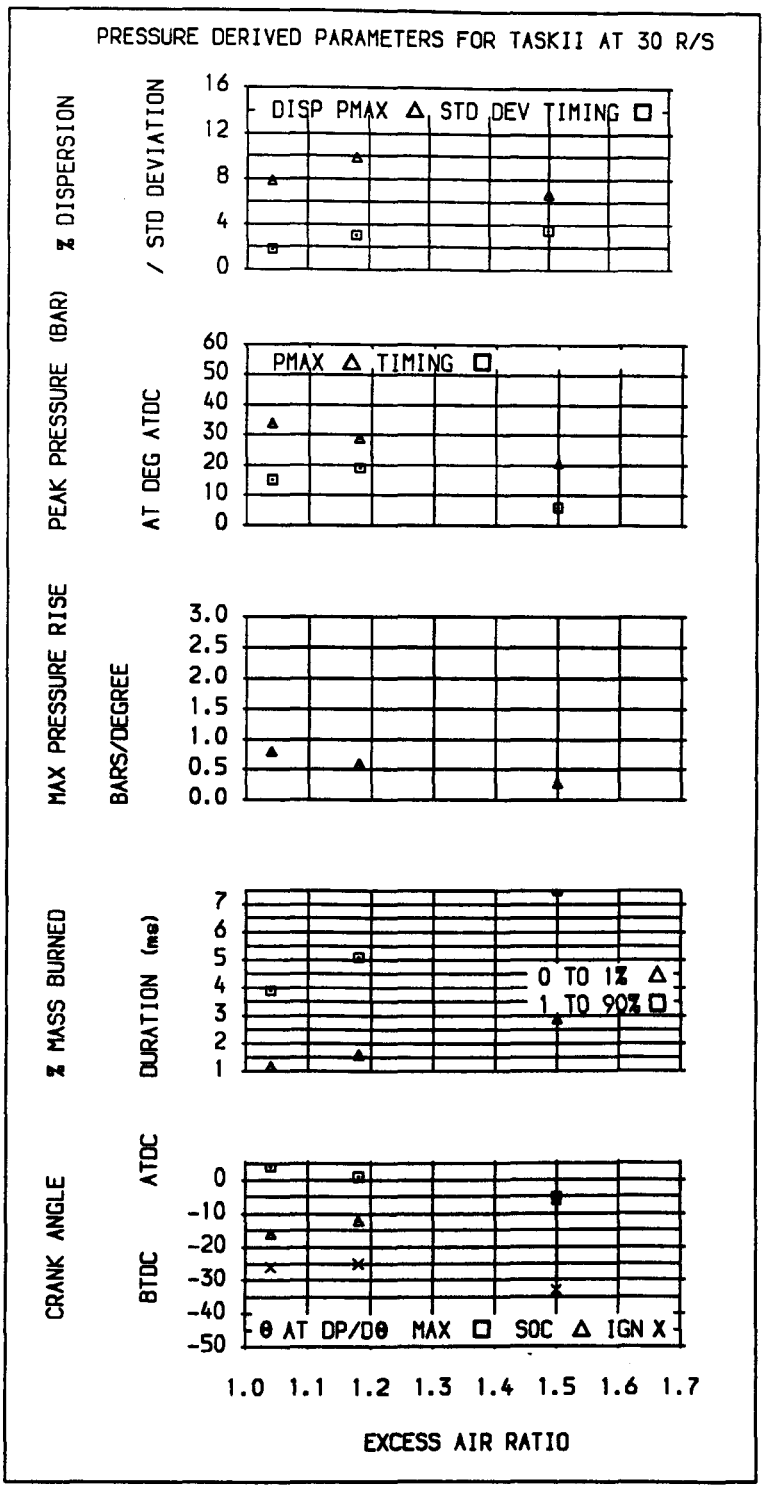

Figure 5.19 The effect of excess air – TaskII at 30 revs/sec.

Table 5.20 The effect of excess air: chamber 3-2, 30 revs/sec.

Reference	39	41	40
Chamber type	3-2	3-2	3-2
Excess air ratio	1.02	1.17	1.49
Engine speed (rpm)	1825	1806	1807
Ignition (deg btdc)	22	25	37
Compression Ratio	13	13	13
0 to 1% (ms/deg)	1.10/12	1.10/12	1.40/15
at (deg btdc)	10	13	22
0 to 50% (ms/deg)	3.5/38	3.6/39	4.3/47
at (deg atdc)	16	14	10
0 to 90% (ms/deg)	5.8/63	5.9/64	7.2/78
at (deg atdc)	41	39	41
1 to 50% (ms/deg)	2.4/26	2.5/27	2.9/27
50 to 90% (ms/deg)	2.3/25	2.3/25	2.9/31
1 to 90% (ms/deg)	4.7/51	4.8/	5.8/63
Soc (deg btdc)	14	16	26
Eoc (deg atdc)	59	54	58
Max pressure (bar)	46.7	46.4	49.5
at (deg atdc)	12	12	6
Std deviation:			
Pmax	4.4	4.1	4.8
Timing Pmax	2.6	1.9	1.2
% Dispersion:			
Pmax	9.3	8.9	9.8
<u>Flame development model:</u>			
0 to 1% (ms/deg)	1.04/	1.22/	1.83/
Integral scale at soc (mm)	6.07	6.34	8.29
Laminar flame speed at soc (m/s)	0.620	0.514	0.353

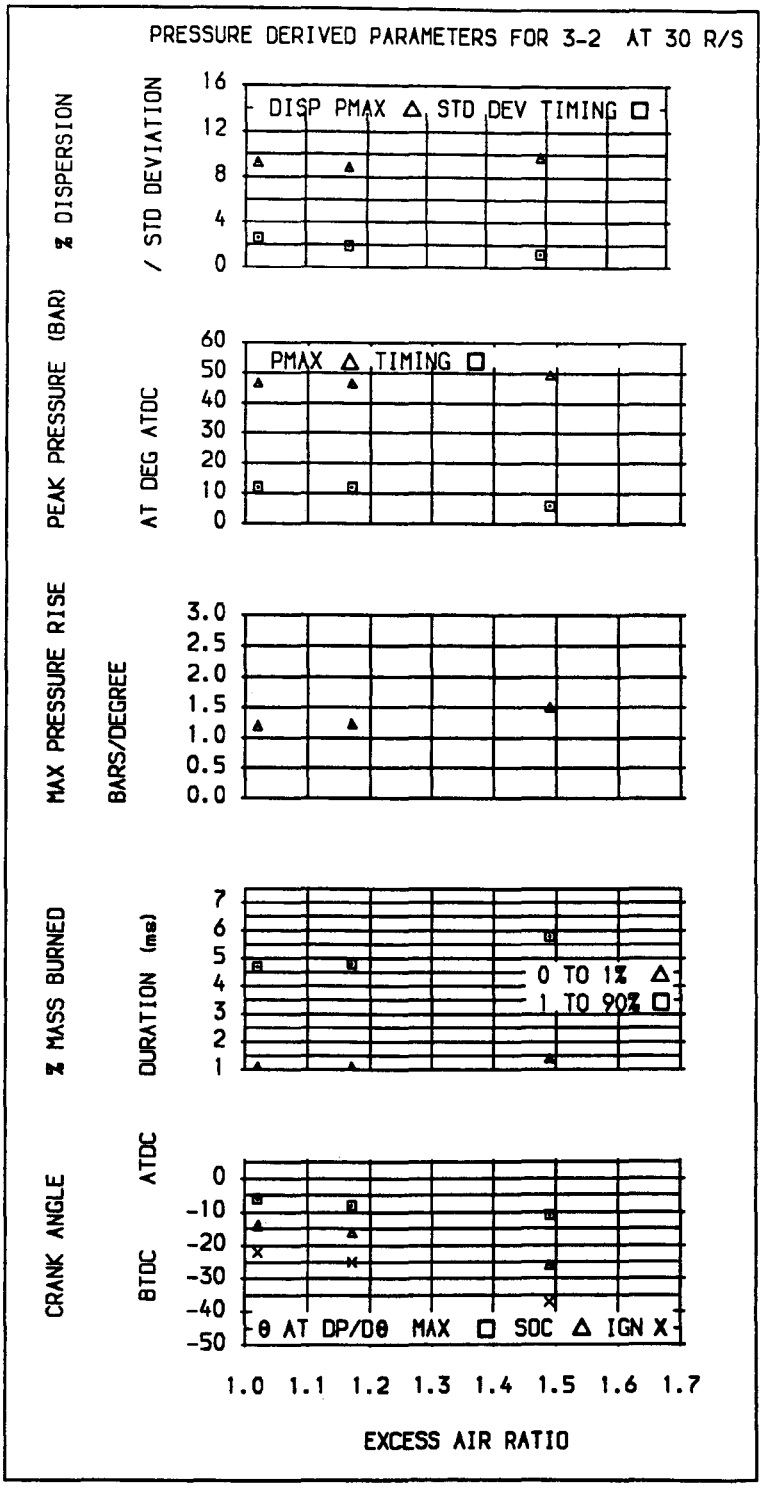

Figure 5.20 The effect of excess air – chamber 3-2 at 30 revs/sec.

Table 5.21 The effect of excess air: Hrcc, 30 revs/sec.

Reference	9	15	10
Chamber type	Hrcc	Hrcc	Hrcc
Excess air ratio	1.03	1.18	1.61
Engine speed (rpm)	1815	1813	1810
Ignition (deg btdc)	16	22	25
Compression Ratio	13	13	13
0 to 1% (ms/deg)	1.00/11	1.10/12	1.80/20
at (deg btdc)	5	10	5
0 to 50% (ms/deg)	2.6/28	2.5/27	4.2/46
at (deg atdc)	12	5	21
0 to 90% (ms/deg)	4.1/45	4.2/46	8.6/93
at (deg atdc)	29	24	68
1 to 50% (ms/deg)	1.6/17	1.4/15	2.4/26
50 to 90% (ms/deg)	1.5/17	1.7/19	4.4/47
1 to 90% (ms/deg)	3.1/34	3.1/34	6.7/73
Soc (deg btdc)	7	12	8
Eoc (deg atdc)	40	32	82
Max pressure (bar)	46.1	51.6	39.0
at (deg atdc)	12	8	9
Std deviation:			
Pmax	2.9	2.7	2.8
Timing Pmax	1.4	1.4	1.2
% Dispersion:			
Pmax	6.4	5.2	7.2
<u>Flame development model:</u>			
0 to 1% (ms/deg)	0.92/	1.02/	1.24/
Integral scale at soc (mm)	4.95	5.37	5.01
Laminar flame speed at soc (m/s)	0.609	0.575	0.399

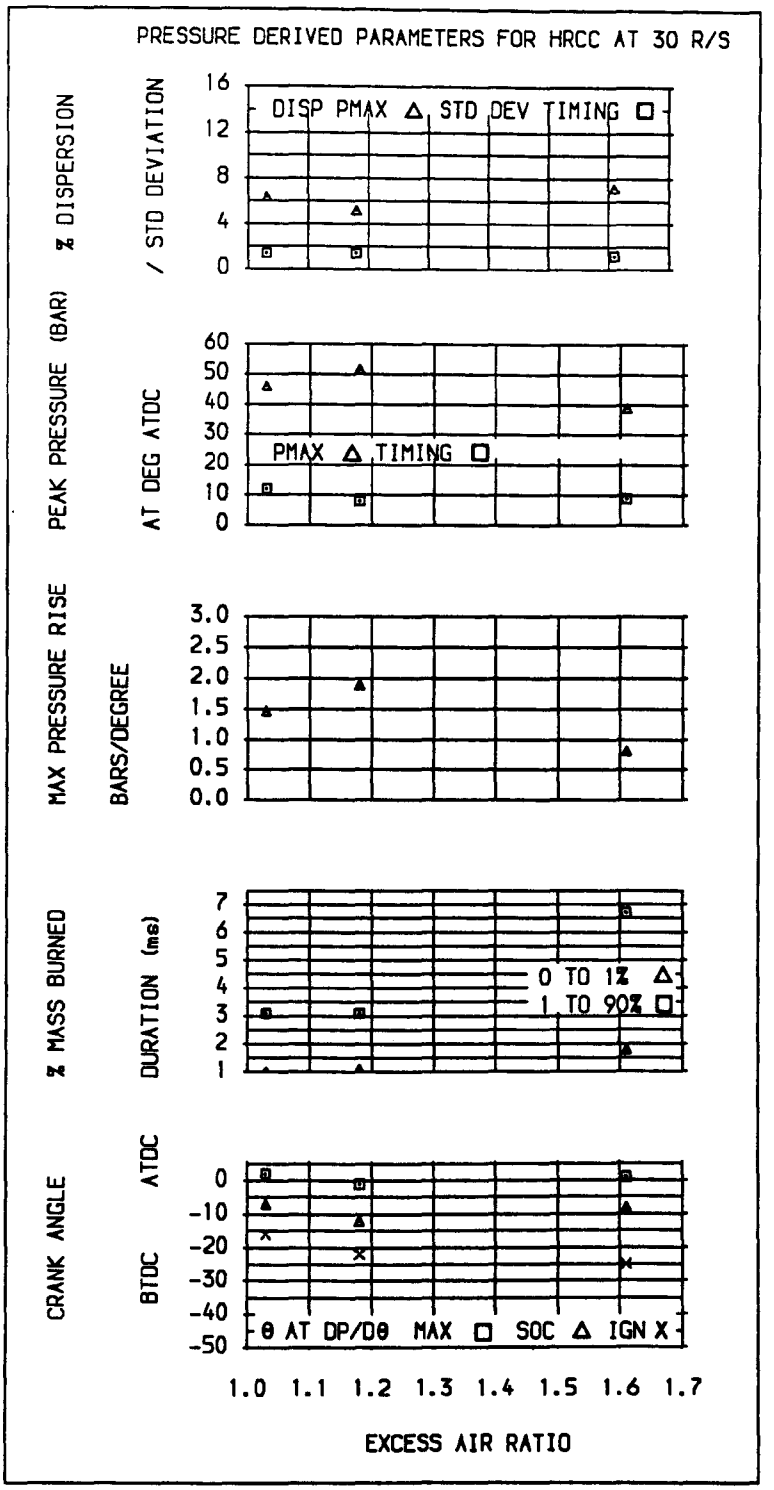

Figure 5.21 The effect of excess air ratio at Hrcc at 30 revs/sec.

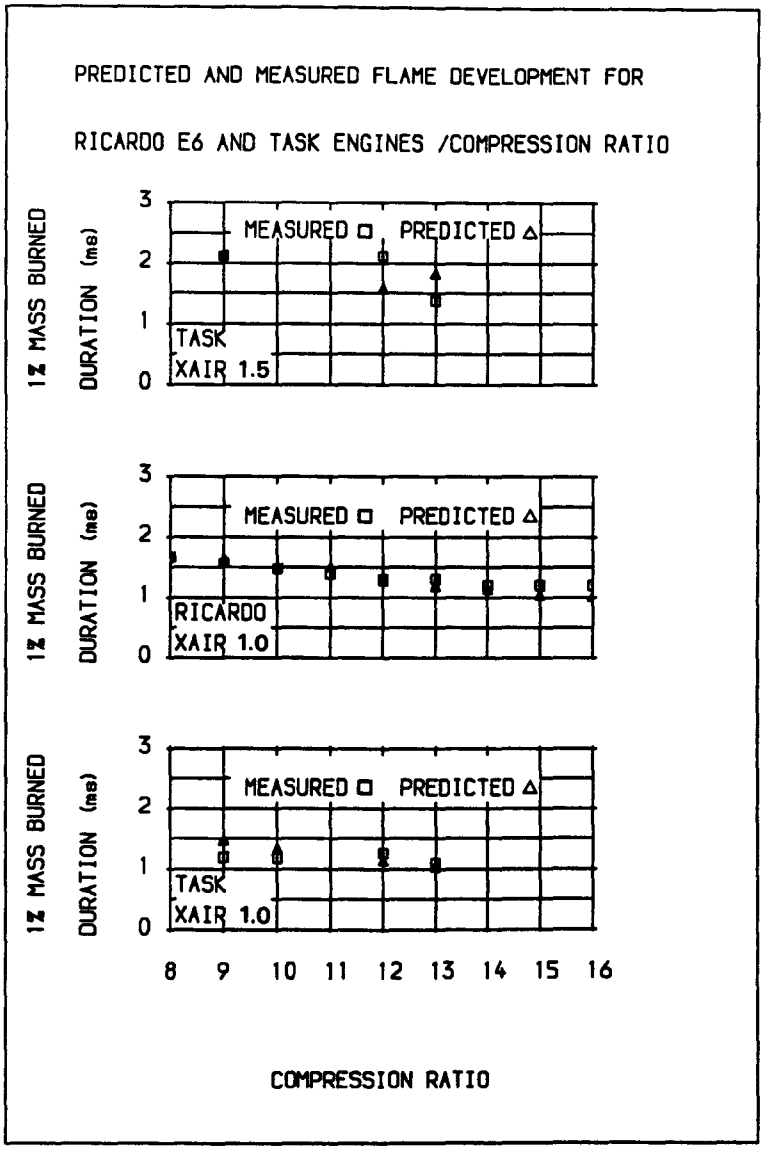

Figure 5.22 Comparison of predicted and measured flame development with changes in compression ratio. Task, (3-2 chamber) and Ricardo E6 engines.

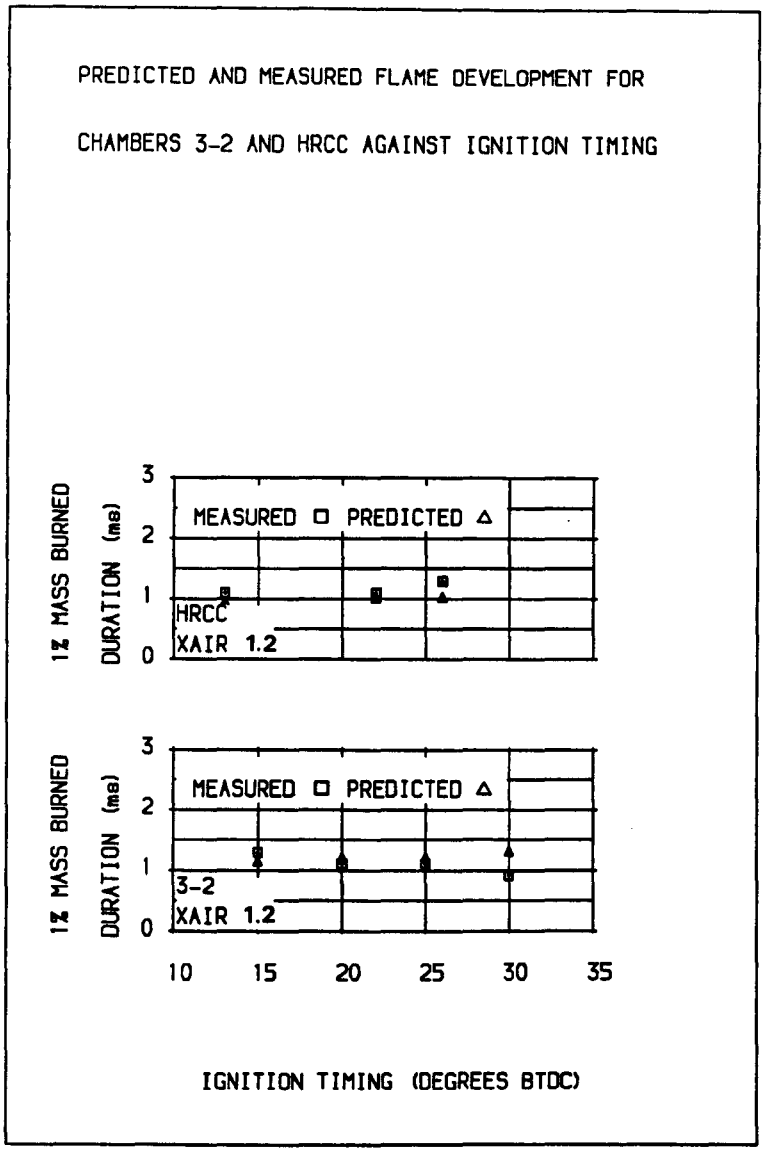

Figure 5.23 Comparison of predicted and measured flame development with changes in ignition timing.

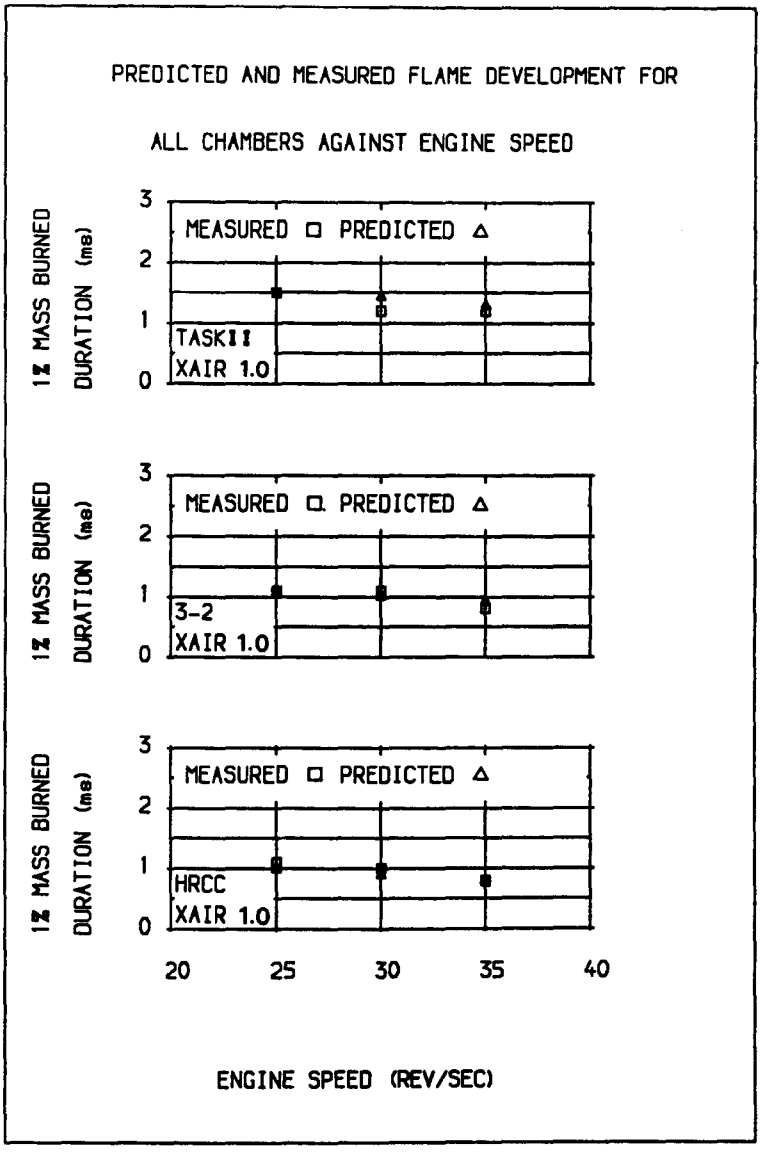

Figure 5.24 Comparison of predicted and measured flame development with changes in engine speed at the stoichiometric mixture strength.

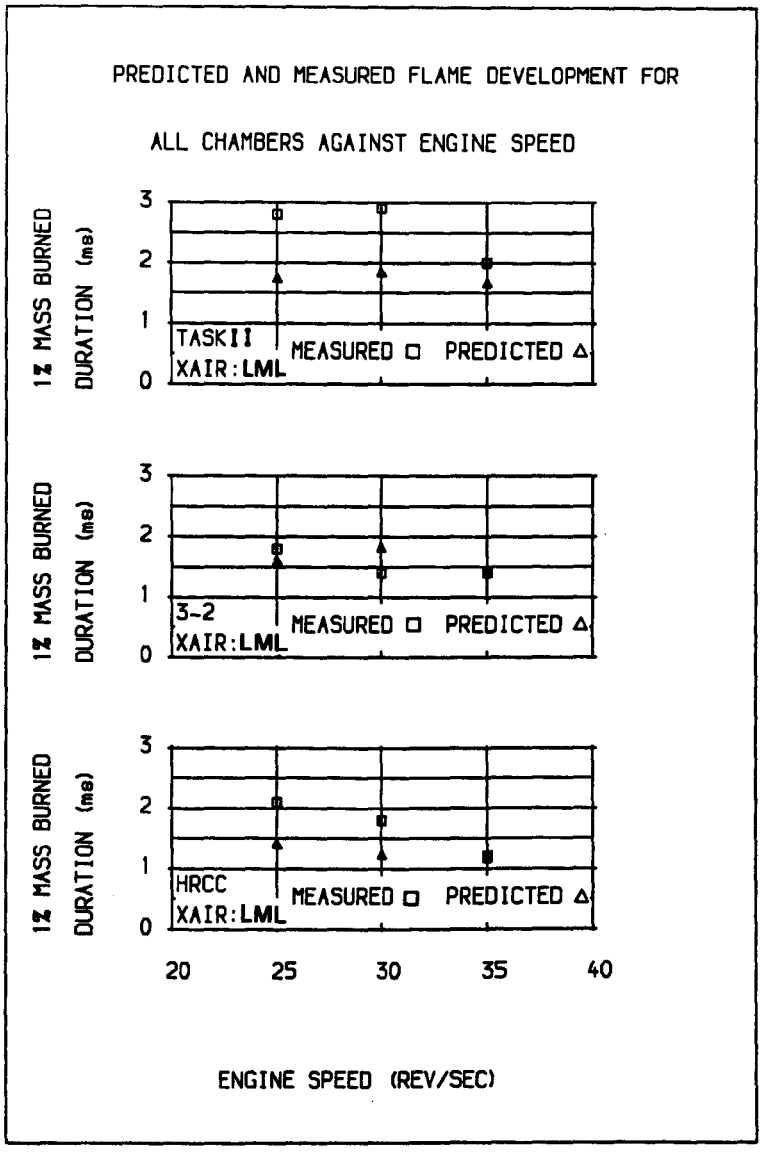

Figure 5.25 Comparison of predicted and measured flame development with changes in engine speed at the lean mixture limit.

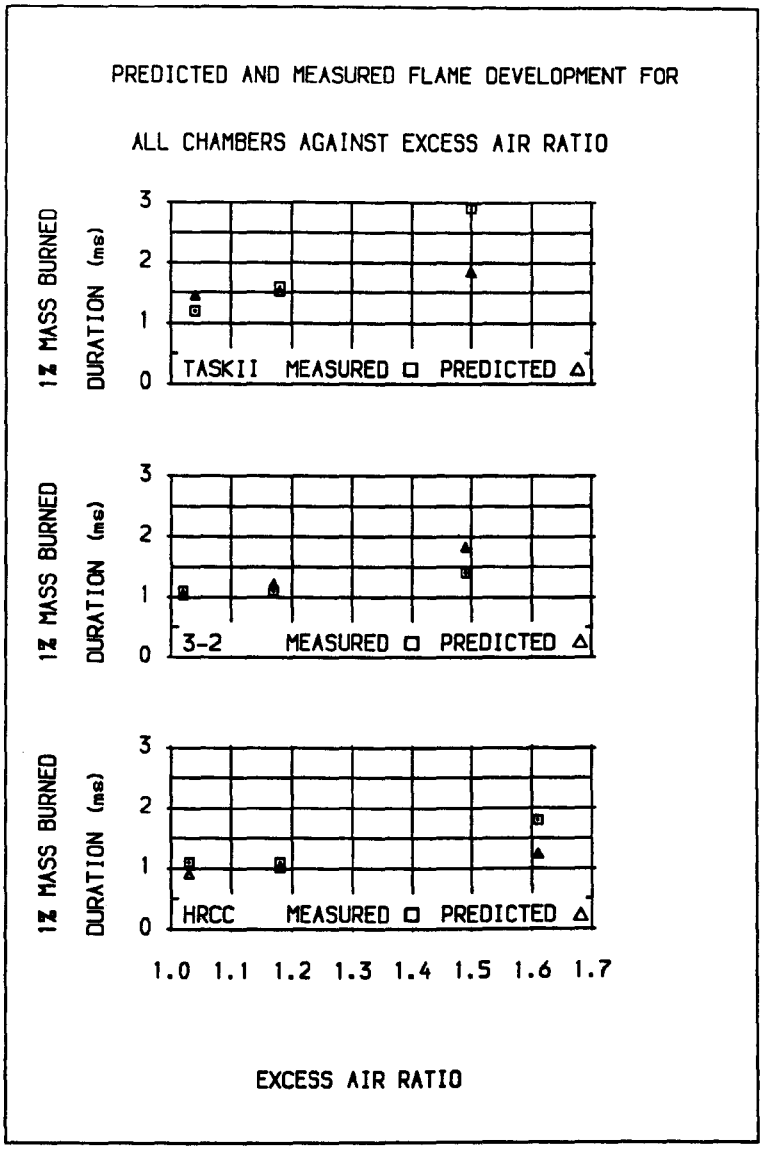

Figure 5.26 Comparison of predicted and measured flame development with changes in mixture strength.

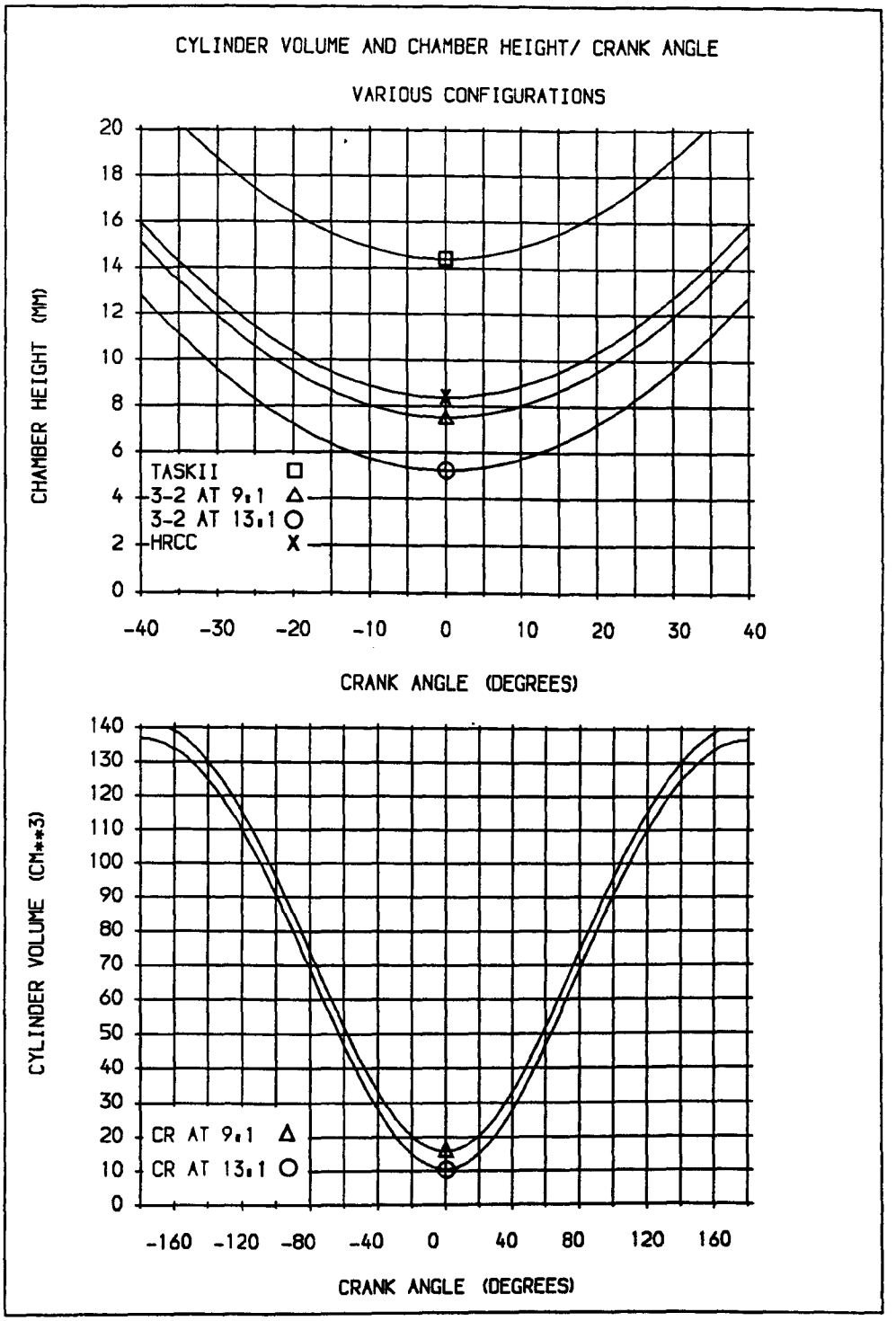

Figure 5.27 The change in cylinder volume and chamber height with crankshaft position.

References

5.1 Bailey, A.C.
Combustion limitations of gaseous fuels for reciprocating engines.
Ph.D. Thesis, University of Manchester, 1971.

5.2 Klimstra, J.
The application of combustion phasing analysis for gas engine process classification.
International Gas Research Conference, 1984.

5.3 Klimstra, J.
Inspection and tuning of reciprocating engines.
International Gas Research Conference, London, 1983.

5.4 Al-Alousi, Y.H., Karim, G.A.
Some considerations of cyclic variations in spark ignition engines fuelled with gaseous fuels.
SAE paper 840232, 1984.

5.5 Harrington, J.A.
Application of a new combustion analysis method in the study of alternative fuel combustion and emission characteristics.
Symposium on Future Automotive Fuels, General Motors, Research Lab., Warren, MI., pp. 177-213, October 1975.

5.6 Heywood, J.B., Higgins, J.M., Watts, P.A., Tabaczynski, R.J.
Development and use of a cycle simulation to predict SI engine efficiency and NOx emissions.
SAE paper 790291, 1979.

5.7 Babkin, B.C., Kosachenko, C.
Laminar velocity of methane-air flames at high pressure.
Fizika Goreniya i Vzryva, pp. 77-86, 1966.

5.8 Kuehl, D.K.
Laminar burning velocities of propane-air mixtures.
Eighth Symposium (International) on Combustion, pp. 510-520, 1962.

5.9 Benson, R.S., Baruah, P.C.
Performance and emission predictions for a multi-cylinder spark ignition engine.
Proc. Instn. Mech. Engrs., Vol. 191, No. 32, pp. 339-354, 1977.

5.10 Benson, R.S., Annand, W.J.D., Baruah, P.C.
A simulation model including intake and exhaust systems for a single cylinder four-stroke cycle spark ignition engine.
Int. J. Mech. Sci., Vol. 17, pp. 97-124, 1975.

5.11 Stone, C.R., Green-Armytage, D.I.
Comparison of methods for the calculation of mass fraction burnt from engine pressure-time diagrams.
Proc. Instn. Mech. Engrs., Vol. 201, No. D1, pp. 61-67, 1987.

5.12 Krieger, R.B., Borman, G.L.
The computation of apparent heat release for internal combustion engines.
ASME paper 66- WA/DGP-4, 1966.

5.13 Curry, S.
A three-dimensional study of flame propagation in a spark ignition engine.
SAE Trans., Vol. 71, pp. 628-650, 1963.

5.14 Thring, R.H., Overington, M.T.
Gasoline engine combustion - the high ratio compact chamber.
SAE paper 820166, 1982.

5.15 Pundir, B.P., Zvonow, V.A.
Nitric oxide formation in spark-ignition engines with in-cylinder charge non-homogeneity of a random nature.
Proc. Instn. Mech. Engrs., Vol. 199, No. D3, pp. 227-235, 1985.

5.16 Lichty, L.C.
Combustion engine processes.
McGraw-Hill, New York, Sixth Edition, 1967.

5.17 Lucas, G., Brunt, M., Anton, R.
The effect of squish on charge turbulence and flame propagation in an S.I. engine.
Auto. Div. Instn. Mech. Engrs. Conference on Fuel Economy and Emissions of Lean Burn Engines, paper C87/79, June 1979.

CHAPTER 6 - EVALUATION OF THE ENGINE MODEL

Summary

A comparison is made between the experimentally derived fractional mass consumed curves and the corresponding curves of the Weibe function. The utility of the latter is noted to improve significantly with the most rapid burning chamber since the rate of combustion is less dependent on operating variables and hence a single function can be used over a wide range of conditions. Experimental and theoretical pressure-crankangle diagrams are compared and the influence of significant experimental errors on the model output is evaluated. The effect of two heat transfer correlations on engine model output is considered. The flame development, heat transfer and friction sub-models are assessed in Chapters 5 and 7.

6.1 Evaluation of the Weibe function

The interactive graphical technique devised to correlate the derived fractional mass burned curves to the Weibe function produced closely coincident curves for virtually all the data sets. A detailed comparison of the experimental and correlated curves and mass burned criteria together with the corresponding shape (z) and duration (a) parameters is presented in Figures I.2 - I.57 (Appendix I). The agreement between curves is noted to deteriorate moderately towards the end of the combustion process, typically exceeding 80% mass fraction consumed. Such deviation is tolerable in light of the modest contribution to global variables from this portion of the process and the slight effect on fractional mass burned criteria. Poor correlation is noted for the Hrcc at very weak mixture strengths where the pressure-derived curve indicates a marked reduction in the burn rate during the latter stages of combustion. In these cases the function conforms closely up to a fractional mass consumed of around 60%, and thereafter deviates widely. Despite the advanced heat-release schedule this implies with respect to the conditions in the actual engine, the cycle simulation returns a pressure-crankangle diagram and other global parameters which vary in the same order of magnitude with respect to the measured as other data sets where the function is more

discriminating. Initial investigations into the effects of changes in the Weibe parameters suggested that the model was most sensitive to changes in the shape factor which influences the form of the curve in the early stages of flame propagation.

Improved versatility could be achieved through correlating the shape and duration parameters to changes in operating conditions, allowing interpolation between measurement points as suggested by a previous study, (4.14). However, the experimental results suggest a weaker dependence on changes in operating conditions with rapid burning chambers, and hence the shape and duration parameters vary only slightly. Over the range of operating conditions, neglecting the very weak mixture strengths for the Hrcc, values for the duration parameter varied from 3.75 +/- 0.95, 3.6 +/- 0.85, 3.5 +/- 0.25 for the TaskII, 3-2 and Hrcc arrangements respectively whilst the corresponding changes in the shape parameter were 1.2 +/- 0.3, 1.1 +/-0.3 and 0.95 +/- 0.15. Tables 6.1 - 6.2 illustrate the change in the values of the salient variables returned by the model for the slowest and most rapid burning heat-release profile - determined by the range in the shape and duration parameters appropriate to the Hrcc. The effect of such changes is noted to be modest. A more detailed comparison is included in Figures I.40 - I.42 (Appendix I).

Pressure-crankangle diagrams

Representative output is presented in Figures 6.1 - 6.3 and all operating points are included in Appendix I (Figures I.2 - I.57). Whilst experimental and theoretical pressures show close agreement during compression, the latter are consistently higher once combustion is initiated and remain so throughout the expansion stroke, with commensurate effect on the indicated power. It is probable that this results from error in the assignment of the maximum fractional mass consumed since the range in the value of this parameter over the operating conditions investigated (83 to 90%) is greater than the 70 to 90% reported by other workers, (4.14, 4.18, 4.45). The significant variables influencing the maximum fractional mass consumed were discussed in Section 4.3.3 and the effect of errors in some of these variables is considered in the following section.

6.2 The influence of experimental error or theoretical assumptions

Comparison of heat transfer correlations

A limited investigation was undertaken to compare the correlation of Woschni, (4.37), with that of Eichelberg, (4.38). The variation in the salient parameters returned by the engine model is detailed in Table 6.3. With the Eichelberg relationship the heat transfer to the coolant is seen to exceed that of the Woschni correlation by around 400 W or 62%. A considerably smaller change is noted in the values of the other variables, suggesting the relative insensitivity of these parameters to errors in the heat transfer coefficient or area assignment.

Effect of error in the crankangle-pressure phasing

The effect of errors in the crankangle-pressure phasing was investigated by assuming a phase shift of 2 degrees in the nominal ensemble-averaged cycle. Table 6.4 illustrates the influence on the derived fractional mass consumed curve and Table 6.5 the influence on the corresponding Weibe function. Only a slight change is evident in the profile of the former curve from the change in pressure-crankangle phasing; the early stages of combustion are lengthier whilst the latter are shorter. Appreciable effect is evident however in the value of the indicated power obtained from the experimental data. The theoretical fractional mass consumed curves are of very similar profile, although retarded by the magnitude of the phase shift. Retarded combustion phasing is reflected in the values of the variables output from the cycle simulation: marginally attenuated peak pressure, peak temperature, heat and work transfer (see Table 6.6). A more detailed comparison is included in Figures I.35 and I.36 of Appendix I.

Effect of error in the inducted mass

The value of the inducted mass was increased by 7% assuming that all other variables remained unchanged. The results are detailed in Table 6.7 and show a marked effect on the indicated power and pressure parameters, with only moderate effect on the other variables.

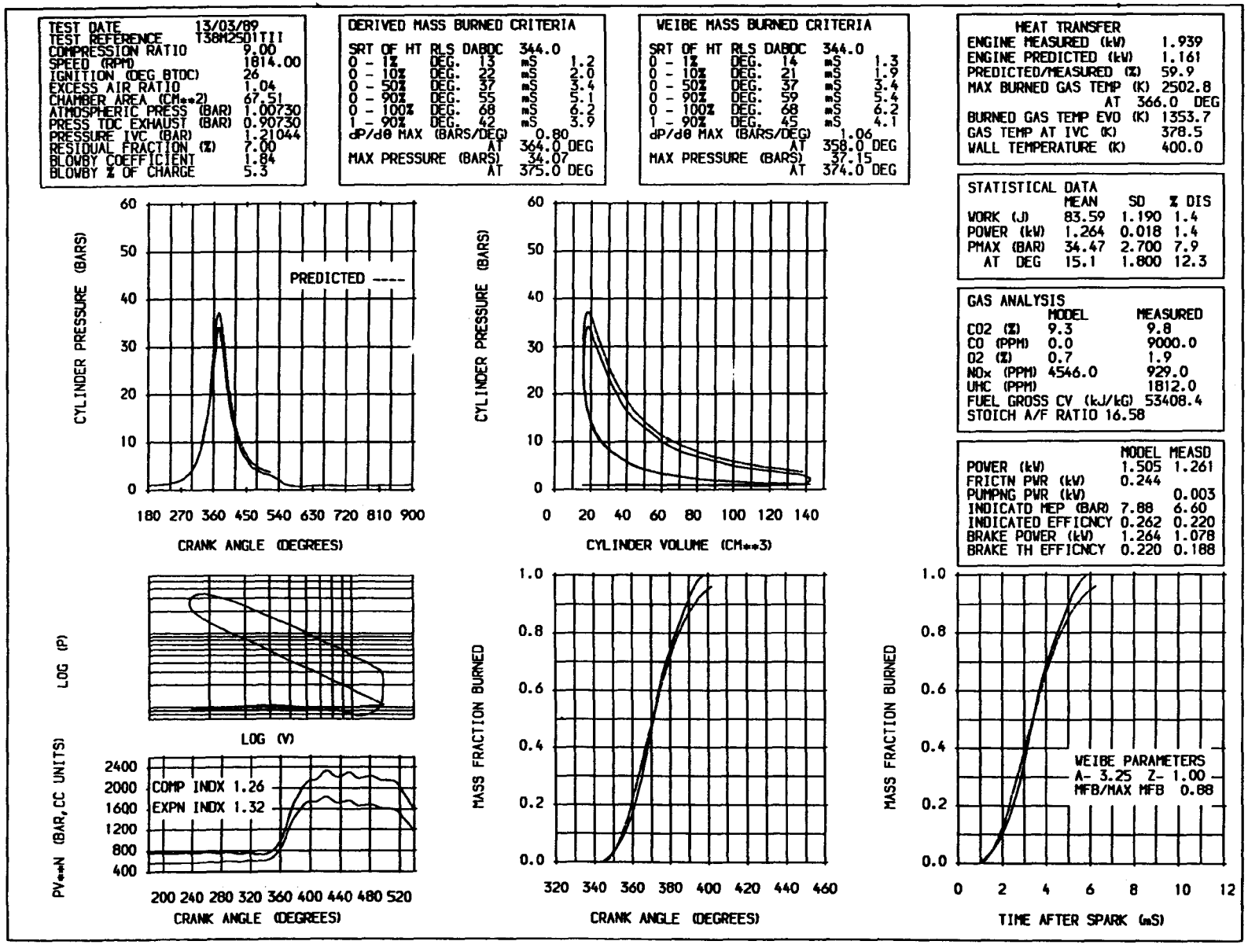

Figure 6.1 Comparison of measured and theoretical parameters for the TaskII arrangement.

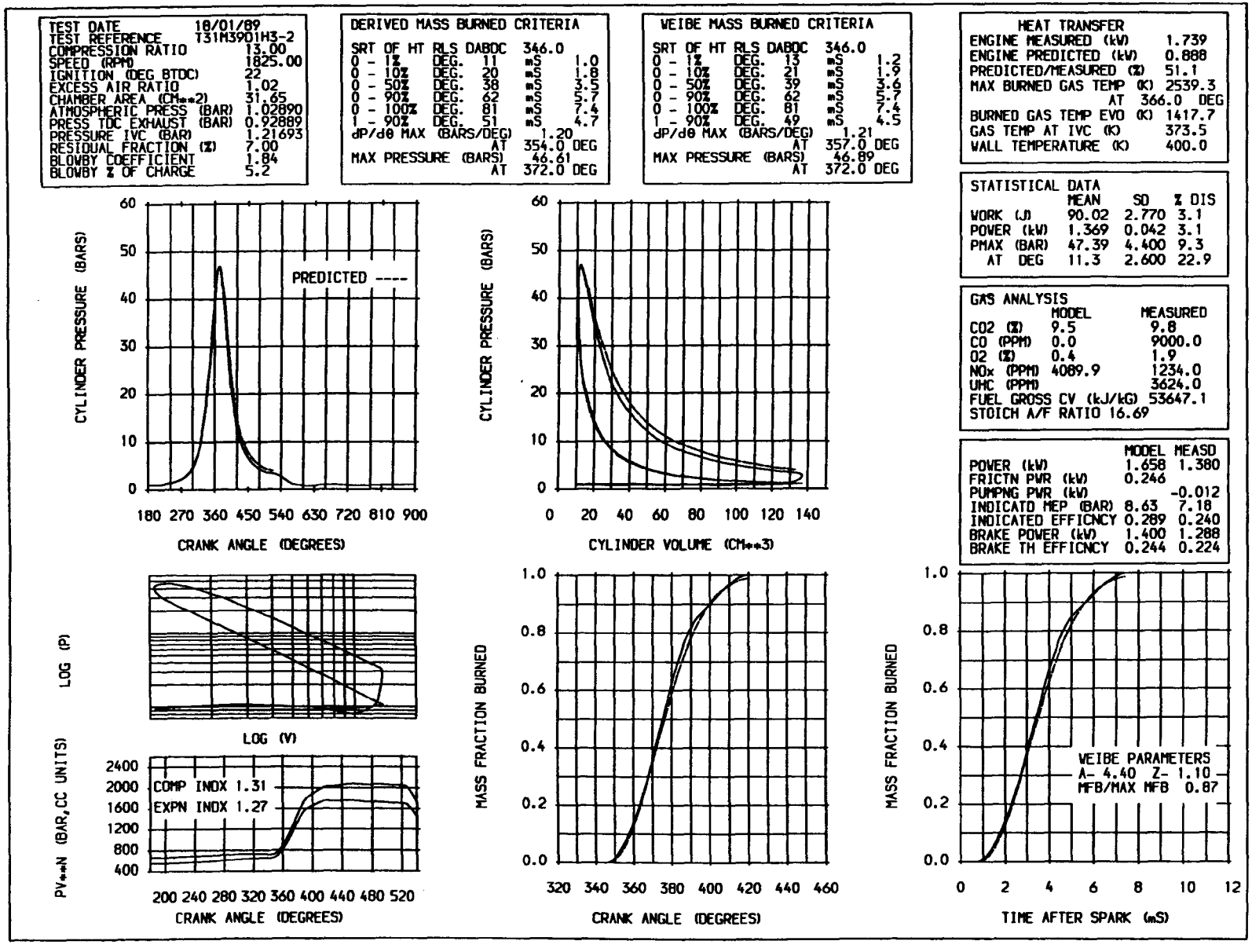

Figure 6.2 Comparison of measured and theoretical parameters for the 3-2 arrangement.

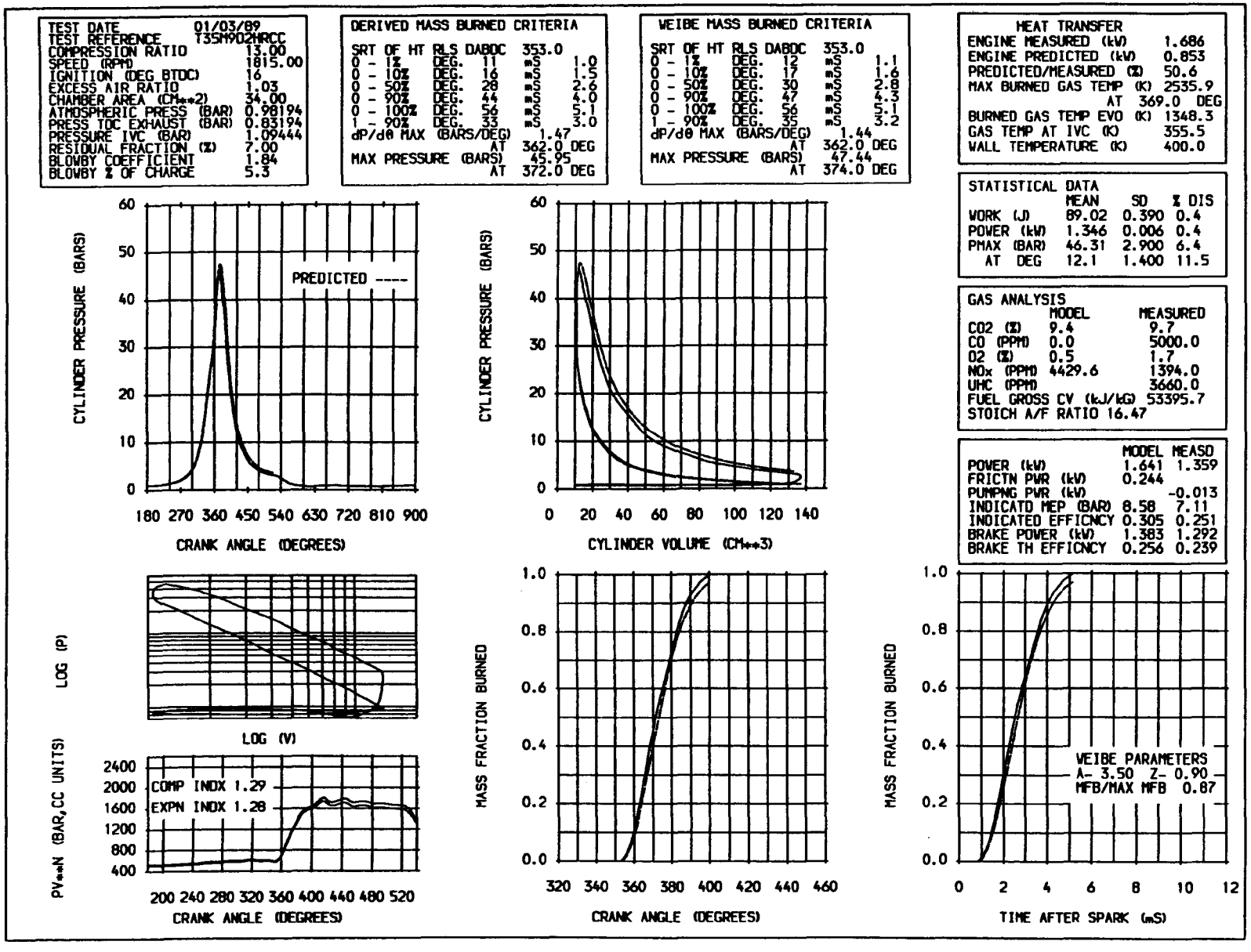

Figure 6.3 Comparison of measured and theoretical parameters for the Hrcc arrangement.

Table 6.1 Comparison of fractional mass burned from the Weibe function assuming the shape and duration parameters are adjusted to promote the slowest and most rapid rate of heat release.

		Slowest burn	Nominal burn	Fastest burn
Soc	(at ca)	353	353	353
Eoc	(at ca)	400	400	400
Duration factor	(a)	3.25	3.50	3.75
Shape factor	(z)	1.10	0.90	0.80
0 to 1%	(Deg)	12	12	11
0 to 10%	(Deg)	19	17	16
0 to 50%	(Deg)	32	30	28
0 to 90%	(Deg)	49	47	45
1 to 90%	(Deg)	37	35	34

Table 6.2 Comparison of model predictions, assuming the shape and duration parameters are adjusted to promote the slowest and most rapid rate of heat release.

		Slowest burn	Nominal burn	Fastest burn
Duration factor (a)		3.25	3.50	3.75
Shape factor (z)		1.10	0.90	0.80
Indicated power	(kW)	1.622	1.641	1.653
Eng heat transfer	(kW)	0.827	0.853	0.873
Peak pressure	(Bar)	43.9	47.4	49.9
Peak burned gas temp	(K)	2516	2536	2549
Gas temp at evo	(K)	1369	1348	1334

Chamber : Hrcc
Speed : 1815 rpm
Excess air: 1.03
Cr : 13:1

Table 6.3 Comparison of heat transfer correlations; Eichelberg, (4.38) and Woschni, (4.37).

		Eichelberg	Woschni	% Error
Indicated power	(kW)	1.112	1.247	11.0
Eng heat transfer	(kW)	0.999	0.615	62.0
Predicted/measured	(%)	89.0	54.7	62.0
Peak pressure	(Bar)	49.1	50.4	2.5
Peak burned gas temp	(K)	2114	2193	3.6
Peak unburned gas temp	(K)	890	896	0.7
Gas temp at evo	(K)	947	1100	14.0
Pressure at evo	(Bar)	2.8	3.2	14.0

Chamber : 3-2 (13:1)
Speed : 1800 rpm
A/F ratio: LML

Table 6.4 Comparison of derived fractional mass burned criteria, pressure retarded 2 degrees with respect to crankangle.

Soc	(at ca)	342	344
Eoc	(at ca)	422	424
0 to 1%	(Deg)	18	20
0 to 10%	(Deg)	26	28
0 to 50%	(Deg)	50	49
0 to 90%	(Deg)	84	83
1 to 90%	(Deg)	66	63
I Power	(W)	1268	1445

Chamber : 3-2 (13:1)
Speed : 2105 rpm
A/F ratio : LML
Soc : 342 deg

Table 6.5 Comparison of fractional mass burned from the Weibe function, pressure retarded 2 degrees with respect to crankangle.

Soc	(at ca)	342	344
Eoc	(at ca)	422	424
0 to 1%	(Deg)	19	21
0 to 10%	(Deg)	28	29
0 to 50%	(Deg)	48	49
0 to 90%	(Deg)	77	79
1 to 90%	(Deg)	58	58
Shape factor	(z)	0.90	0.83
Duration factor	(a)	3.75	3.75

Chamber : 3-2 (13:1)
Speed : 2105 rpm
A/F ratio : LML
Soc : 342 deg

Table 6.6 Comparison of model output, pressure retarded 2 degrees with respect to crankangle.

Soc	(at ca)	342	344
Indicated power	(kW)	1.489	1.481
Eng heat transfer	(kW)	0.632	0.622
Peak pressure	(Bar)	45.5	44.7
Peak burned gas temp	(K)	2132	2125
Gas temp at evo	(K)	1125	1130

Chamber : 3-2
Speed : 2105 rpm
A/F ratio : LML
Cr : 13:1
Soc : 342 deg

Table 6.7 Comparison of the effect of a 7% increase in the inducted mass.

				% change
Indicated power	(kW)	1.260	1.376	9.2
Eng heat transfer	(kW)	0.723	0.745	3.0
Peak pressure	(Bar)	40.2	42.4	5.5
Peak burned gas temp	(K)	2517	2498	-0.8
Gas temp at evo	(K)	1388	1379	-0.6
Pressure at evo	(Bar)	3.6	3.9	6.9

Chamber : 3-2
Speed : 1516 rpm
Excess air : 1.04
Cr : 12:1

CHAPTER 7 - ENERGY FLOWS

Summary

The utility of energy flow data is discussed within the context of this work and a lack of such data is identified in the literature. It is concluded that particular consideration to small energy transfers and to accurate measurement techniques is implied in light of the small capacity of the engine under study. Procedures are described to ensure the reliability of data. The observed influence of operating and design variables on the magnitude and distribution of heat and work transfers and frictional losses together with the significance of small terms including oil heat transfer, blowby, ambient, unburned fuel and measurement losses is discussed in detail. Where appropriate, the output from the engine model is compared with the experimental data. The chapter concludes with general comments on ignition timing and noise levels.

7.1 Introduction

The study of energy flows in small engines is poorly documented in the literature. The relevance of any previous study is also unclear in light of the novel construction, fuel type and proposed application of the unit under investigation. A study of the influence of changes in design and operating variables on the magnitude and relative proportions of the energy transfers is of value since benchmark data is accrued, contributing to the understanding of the processes involved and allowing potential areas for improvement to be identified. The data obtained can also be used in the form of an energy balance to confirm the reliability of measurement, to validate the engine model or to complement the combustion analysis.

Since heat recovery is an important factor in the performance of both heat pump and combined heat and power units, detailed heat transfer data is necessary to assess the performance of such units and the likely performance based on the potential for further development and improvement. Admitting geometric similarity between engines of different size, smaller engines have greater surface area-to-volume

ratios than larger counterparts and hence engine heat transfer can be expected to be higher, (2.8, 7.1, 7.2). Furthermore, energy flows reasonably neglected in the case of larger engines may well be of greater significance as size reduces, these could include ancillaries, blowby, unburned fuel or measurement techniques such as gas analysis. Implicit in such considerations is the requirement for accurate measurement. (Instrument calibration and other procedures undertaken to support the validity of measurements are discussed in Appendix IV.)

Frictional losses have also been found to be significant in engines of this type, (1.29, 7.1), whether this is due to low cylinder wall temperatures as suggested by Taylor, (7.1), or lack of incentive for detailed design is unclear.

Following these considerations and those relating to work transfer discussed in Chapter 1, investigations were undertaken to establish the effect of operating and design variables on energy transfers. The magnitude and distribution of heat and work transfer, frictional losses and the significance of small terms including oil heat transfer, blowby, unburned fuel, exhaust gas analyser and ambient losses were considered.

7.1.1 Energy balance

To complement instrument calibration (see Appendix IV) and validate experimental measurement, an energy balance was undertaken at all operating points where pressure-crankangle data were obtained. The energy balances were based on gas quality data applicable to the local area on the dates of testing which were kindly supplied by R.J. Wadsworth of British Gas. A sample analysis is presented in Appendix IV and includes gas composition, density and calorific values.

Where appropriate, the thermodynamic properties of low temperature combustion products were determined using a method detailed in Reference 2.8 and described in Section 2.5. The exhaust mass flow rate was evaluated from the calculated air-to-fuel ratio determined from exhaust gas analysis and the measured gas flow rate, with due consideration to mass loss through blowby and emissions sampling.

The significant terms in the energy balances are presented in Figures II.2 - II.19 (Appendix II). Further details of the experimental and theoretical techniques applied to evaluate the components of the energy balances are described in Section 2.5 and later sections of this chapter. The following quantities were considered:

Exhaust heat transfer

This term comprised losses at the exhaust manifold (despite extensive lagging with high temperature Kaowool ceramic fibres), the reclaimed heat at the exhaust heat exchanger and the losses associated with the removal of exhaust gas for analysis and referencing of exhaust products to standard conditions. This latter quantity comprised two components: that represented by the enthalpy change of gaseous products from exhaust exit temperature to the reference temperature and that represented by condensing vapour.

Engine heat transfer

The engine coolant included the contribution from the piston friction.

Unburned hydrocarbons

The energy loss from fuel surviving the combustion process was evaluated from the measured exhaust concentrations of unburned hydrocarbons.

Work transfer

The work transfer was determined by integrating the pressure-volume diagram.

Crankcase blowby

This term was based on a mass loss-to-speed correlation determined from blowby measurements.

Ambient loss

The ambient loss was assigned the value of the outstanding term in the energy audit. Comparisons were also made with the value determined using the heat transfer characteristics of the thermal enclosure surrounding the engine and the appropriate temperatures.

Frictional losses and oil heat transfer are included in the form of heat energy in the various quantities previously described. The change in magnitude and relative distribution of the components in the energy balance and other energy flows as operating conditions vary is discussed in the following pages.

7.2 Indicated thermal efficiencies

As expected, the detailed study into the effect of operating and design variables on rates of heat release anticipates the effect of such variables on the engine indicated thermal efficiency, accordingly, only general observations are appropriate in this section. Efficiency data are presented in Tables 7.1 - 7.3 and graphical output in Figures II.2 - II.19 (Appendix II).

When compared with the original TaskII arrangement, the Hrcc was found effective in increasing the thermal efficiency by 3 percentage points at stoichiometric conditions at all speeds, around 6 percentage points at the mixture strength for maximum efficiency and was able to maintain higher efficiency levels with extended lean mixture operation: at the mid-range speed the thermal efficiency increased to 25% at stoichiometric operation, to 29.5% at the optimum mixture strength (excess air ratio of 1.15) and to 24% at the lean mixture limit (excess air ratio of 1.61). At stoichiometric conditions and at the lean mixture limit, irrespective of speed or compression ratio, the performance of the 3-2 chamber was in general lower than that of the Hrcc arrangement but exceeded that of the TaskII configuration. At stoichiometric air-to-fuel ratios, slightly improved thermal efficiencies of around 1 percentage point were evident for all chambers with increasing speed, whilst at the lean mixture limit a more positive

effect was apparent: the performance of the 3-2 chamber at equal air-to-fuel ratio improving by 3.5 percentage points. Adverse changes in geometry are thought to account for the poor performance of the 3-2 chamber at higher compression ratios. This was discussed in detail in Section 5.7.2.

The effects of parametric changes on engine performance and emission levels were investigated in a preliminary study on a similar engine, (1.30), in which the efficiency of the 3-2 arrangement was found comparable with that established for the Hrcc and the engine used in this study. Although the causes for these discrepancies have not been positively identified, it is probable that the high levels of blowby and frictional losses measured on the engine used in this study are at least partly responsible (see Sections 7.5 and 7.10). Whilst discouraging in that the development process has realised only relative (although significant) improvements in efficiency, the objectives of the study have not been compromised and furthermore, the performance of the current engine in its original configuration is illustrative as it is representative of the performance of, and problems associated with, similar off-the-shelf units.

Considering the relative performance of the 3-2 and Hrcc arrangements discussed above and the potential for reductions in frictional and blowby losses, the observed improvement in efficiency is encouraging.

7.3 Engine heat transfer

Introduction

A simplified analysis of the correlation for the instantaneous, spatially-averaged heat transfer coefficient based on the Nusselt, Prandtl and Reynolds number relationship for turbulent flow in pipes or over flat plates (see Section 4.3.5) shows gas temperature, pressure and velocity substantially controlling the engine heat transfer coefficient, (4.37):

$$h = 3.26 B^{-0.2} P^{0.8} T^{-0.55} w^{0.8}$$

where:

B -	cylinder bore	(m)
h -	heat transfer coefficient	($W/m^2.K$)
P -	gas pressure	(kPa)
T -	gas temperature	(K)
w -	gas velocity	(m/s)

It is to be expected therefore that changes in operating or design variables such as chamber arrangement, engine speed, excess air ratio, compression ratio and ignition timing will affect the engine heat transfer through changes in the gas velocities or properties together with any changes in wall temperature or geometry.

Discussion of the experimental results

The calorimetry on which the graphs in this and the following section dealing with exhaust heat transfer are derived is presented in a more extensive and detailed format in Appendix II. With respect to the data in Appendix II the following observations are pertinent at the outset; although linear relationships between engine and exhaust heat transfer and the exhaust temperatures with respect to the excess air ratio are suggested, and furthermore, the substantial data accrued to support such relationships are characterised by remarkably low scatter, it has been reported, (1.29, 4.18, 7.3, 7.4), that non-linear relationships are to be expected, particularly around the stoichiometric air-to-fuel ratio. Such inconsistency is not necessarily a cause for concern, primarily since the bulk of measurements were obtained at weak conditions, but also in light of the small variation in the magnitude of the quantities measured with changing mixture strength.

Engine heat transfer data (including piston friction) under all conditions investigated are shown as a proportion of incoming fuel energy against the excess air ratio in Figure 7.1. It is evident that the effect of all operating variables, with the exception of the excess air ratio, is small. Although not indicative of a functional relationship, the data are noted to deviate by around +/- 2 percentage points from a line of best fit. The coolant load is typically 32% of

fuel energy at the stoichiometric mixture strength, reducing to around 25% at the lean mixture limit.

Also included in Figure 7.1 are the predicted engine heat transfers at the operating points where pressure-crankangle data were obtained. These data are remarkably consistent with the measured values, showing a similar deviation from a line of best fit and a relative magnitude of around half the corresponding experimental values, consistent with the findings of other workers (2.9). Piston friction (see Section 7.10) accounts for some 2 to 3% of the fuel energy, depending on the operating condition, hence the engine heat transfer to the coolant is approximately equally distributed between the working and exhaust/blowdown portions of the cycle. A comparison of the experimental and theoretical heat transfers at each operating point is included in the figures of Appendix I.

The influences of ignition timing, compression ratio, engine speed and chamber arrangement are presented against a base of excess air ratio in Figures 7.2 - 7.7. These figures show that the chamber arrangement is the most significant variable influencing the heat transfer together with the excess air ratio identified earlier. Noting the weak influences of compression ratio, engine speed and ignition timing, it is illustrative to consider the performance of each configuration under all operating conditions with changes in mixture strength. The data are well correlated according to a line of best fit. The results of this analysis are compared with the corresponding theoretical values in Figure 7.8 and again a good measure of agreement is noted.

Over the range of mixture strength, Figure 7.8 indicates that a consistently higher proportion of the fuel energy (1 - 2%) appears in the engine coolant when the performance of the Hrcc is compared with the 3-2 arrangement. With the TaskII chamber, at the stoichiometric condition, heat transfer as a proportion of fuel energy exceeds that of the other configurations by around 3 percentage points falling rapidly with weakening mixtures to a level comparable with the 3-2 chamber. Whilst recognising the limitations of the experimental evidence it is possible to propose a number of important chamber-specific variables thought likely to influence the relative performance of the

configurations. It was established in Section 5.7.5 that the TaskII chamber is relatively intolerant of weakening mixtures and although combustion rates in this configuration in general exceed those in the 3-2 chamber at stoichiometric conditions, the slowest rates are apparent at leaner mixtures. It was also noted that the Hrcc promotes the fastest rates of heat release. The predicted peak gas temperatures (see Figure 7.9) are consistent with the combustion rates; higher temperatures corresponding to faster rates of heat release. At stoichiometric conditions this suggests that it is the surface area of the TaskII chamber (around twice that of the other arrangements) that is the significant factor in heat transfer, whereas at weaker conditions the gas temperature appears to predominate. Rapid rates of heat release, centred closely around tdc, suggest that it is the gas temperature which is the significant variable influencing the heat transfer in the Hrcc when compared with the 3-2 chamber where surface areas are similar.

Whilst the effect of compression ratio on engine heat transfer is small, at around +/- 1% of fuel energy over the range of excess air (see Figure 7.3), the significance of the influence of adverse geometrical effects referred to in Section 5.7.2 is unclear.

The closed cycle predictions (see Figure 7.10) indicate a strong dependence on ignition timing, whilst the measured quantities, with the exception of the TaskII configuration, show only a moderate dependence (see Figure 7.2). This suggests, as expected, that the lower gas temperatures at exhaust valve opening which are associated with advancing ignition result in a proportionally smaller contribution from the blowdown/exhaust portion of the cycle. The stronger dependence on spark timing evident for the slower burning TaskII configuration is to be anticipated because initiating combustion later in the stroke has a greater volume effect with longer burn duration than with shorter (assuming that burn duration remains unchanged with spark timing) since the rate of volume change is small around tdc.

No clear effect can be attributed to variations in engine speed (see Figure 7.4). The TaskII configuration shows the greatest dependency consistent with the strong influence of engine speed on combustion

rates noted in Section 5.7.4. Similar indeterminacy is apparent from the cycle simulation (see Figure 7.11).

Conclusions

It may be concluded that the engine heat transfer from a unit of this type running within the likely range of operating and design variables will not vary by more than +/- 2% of fuel energy at a given excess air ratio, falling from around 32% of fuel energy at stoichiometric conditions to around 25% at the lean mixture limit.

A thermally efficient configuration may reject a greater proportion of fuel energy to the engine coolant than a less efficient arrangement. Although the least efficient TaskII configuration rejects the greatest proportion of fuel energy to the coolant, the most efficient Hrcc does not reject the least. (In the next section the most efficient chamber is shown to reject the least proportion of fuel energy to the exhaust.)

The effects of the ignition timing, excess air ratio and engine speed are most pronounced for the slower burning TaskII configuration.

7.4 Exhaust heat transfer

Introduction

Reducing a time-and spatially-averaged Nusselt, Prandtl and Reynolds number relationship found appropriate to convective heat transfer in straight sections of exhaust pipe (Malchow et al., cited in 2.8, 2.9) with the gas conductivity- and viscosity-to-temperature relationships developed by Woschni, (4.37), the heat transfer coefficient is seen to be strongly dependent on pipe diameter, gas temperature and velocity, since pressure changes are small. Hence the influence of design and operating variables on the exhaust heat transfer will arise mostly through changes promoted in the gas temperature and velocity, since geometry and wall temperature are sensibly constant for all operating conditions.

Discussion of the experimental results

Figures II.2 - II.19 (Appendix II) show that for all speeds around the stoichiometric air-to-fuel ratio the Hrcc configuration exhibits the lowest exhaust temperatures whilst the 3-2 (nominal configuration) chamber has the highest. As the mixture weakens, the highest temperatures are in general evident for the TaskII configuration and the lowest for the Hrcc. Increasing engine speed effects around a 75 K rise in temperature for all chambers at the stoichiometric air-to-fuel ratio with a lesser influence as the mixture weakens. Temperatures reduce with excess air: the TaskII configuration least and the 3-2 chamber most; the latter around 100 K for the nominal arrangement at average speed over the range of excess air. Temperatures decrease markedly with advancing ignition timing: typically 100 K for 15 degrees advance (excluding the Hrcc where a reduced dependence is evident, producing only half the fall in temperature). Slight reductions in temperature are noted with increasing compression ratio at constant speed over the range of excess air.

Predicted temperatures at exhaust valve opening are illustrated in Figures 7.12 - 7.14 for all operating conditions at the three speeds. These data are noted to be consistent trend-wise with the measured mean exhaust temperatures. Around the stoichiometric air-to-fuel ratio at all speeds, the Hrcc configuration exhibits the lowest temperatures whilst the 3-2 (nominal configuration) chamber has the highest. As the mixture weakens, the highest temperatures are evident for the TaskII configuration and the lowest for the Hrcc. The ignition timing and excess air ratio have a marked effect on the gas temperature, for example, in the case of the 3-2 chamber at the mid-range speed a 15 degree advance produces a 200 K decrease in temperature and a reduction of around 300 K is apparent over the range of excess air. Only slight variations in temperature are evident between speeds at constant air-to-fuel ratio for a given chamber, or for changes in the compression ratio for the 3-2 chamber. These are small enough to be indistinguishable from any inconsistency following from the range in optimum ignition timing setting.

The effects of ignition timing, compression ratio, engine speed and chamber arrangement on exhaust heat transfer, expressed as a percentage of fuel energy, are presented against a base of excess air in Figures 7.2 - 7.7. Broadly, the heat transfer under all operating conditions varies at a given excess air ratio by +/- 4% of fuel energy, rising from 27% of fuel energy at the stoichiometric mixture strength to 30% at the lean mixture limit.

Heat transfer to the exhaust is noted to increase with speed by around 3% of fuel energy, irrespective of mixture strength or chamber arrangement (see Figure 7.4). The observed influence of engine speed on exhaust temperatures anticipates this effect on heat transfer.

Heat transfer to the exhaust is least for the Hrcc configuration, most for the 3-2 chamber at the stoichiometric condition, but most for the TaskII chamber at weaker mixtures over the range of speed considered (see Figures 7.5 - 7.7). These observations are consistent with the measured mean exhaust temperatures and the predicted temperatures at exhaust valve opening. All other factors being equal (such as blowby and unburned hydrocarbons) the Hrcc characteristics are implied by the highest thermal efficiencies and, with respect to the 3-2 chamber, the moderately higher engine heat transfer identified earlier. When compared with the 3-2 chamber (nominal configuration) at stoichiometric mixture strengths, the TaskII configuration features lower thermal efficiency and higher engine heat transfer. The sum of these two terms exceeds that in the 3-2 arrangement and hence the lower exhaust heat transfer is to be expected. As the excess air ratio increases, engine heat transfer and thermal efficiencies reduce significantly in the TaskII chamber with poor tolerance to weakening mixtures and markedly higher exhaust heat transfer results.

Increases in exhaust heat transfer of around 2 to 4% of fuel energy are noted as the ignition timing retards by about 15 degrees. This is consistent with the observed changes in mean exhaust gas temperature and the predicted gas temperature at exhaust valve opening. It is evident that reducing engine heat transfer is broadly reflected in increasing exhaust heat transfer with due consideration to the thermal efficiency and unburned fuel (see Figure 7.2).

To interpret the observed influence of compression ratio on exhaust heat transfer, it is illustrative, initially, to consider this influence in general on engine performance. It is widely recognised that improved efficiency, slightly reduced engine heat transfer and diminished exhaust heat transfer result from increasing compression ratio; the latter from lower burned gas temperatures late in the expansion stroke. Such beneficial effects persist until the compression ratio for maximum efficiency is reached. This restriction on the compression ratio is thought to be influenced primarily by the changing combustion chamber geometry adversely affecting burn rates as quenching becomes more significant and the flame shape increasingly deviates from the spherical form. Heat transfer rises slightly with unfavourable changes in the surface area-to-volume ratio. The increasing importance of crevice volumes and frictional losses and/or detonation limiting the optimum spark timing are additional factors.

Although Figure 7.3 shows that the measured exhaust heat transfer reduces steadily with increasing compression ratio, consistent trend-wise with the observed reduction in mean exhaust gas temperatures noted earlier, higher engine efficiency together with reduced engine and exhaust heat transfer are evident at stoichiometric conditions only as the compression ratio is increased from 9 to 10:1, any further increases resulting in lower engine efficiency and in general increased engine heat transfer. Thermal efficiencies are detailed in Table 7.3. It is most probable that the observed trend of exhaust heat transfer is reflecting deteriorating combustion quality rather than the expected beneficial effects of higher compression ratio setting. The combustion characteristics of this particular chamber with increasing compression ratio were discussed in detail in Section 5.7.2, and in Chapter 8 increasing hydrocarbon levels with higher compression ratios are also discussed.

Conclusions

The influence of design and operating variables on exhaust heat transfer is more pronounced than the influence on engine heat transfer. The exhaust heat transfer under all operating conditions investigated varies by +/- 4% of fuel energy at a given excess air ratio, rising

from around 27% of fuel energy at the stoichiometric mixture strength to around 30% at the lean mixture limit.

The predicted gas temperatures at exhaust valve opening and the measured mean exhaust gas temperatures are consistent trend-wise.

The reclaimed heat over all operating conditions represents only one third to one half of the total exhaust heat transfer, since a measurable loss was present at the exhaust manifold, exhaust gas was removed for emissions sampling and combustion products left the heat exchanger without condensing. There is potential for further improvement in this area; with suitable modifications to the heat exchanger including a water-cooled manifold and a condensing stage (possibly located in the proximity of the evaporator in the heat pump package) it should be possible to reclaim almost all of the exhaust heat loss.

The total heat transfer for the three chambers over virtually all operating conditions investigated accounts for 58% of fuel energy +/- 2% of fuel energy at the stoichiometric air-to-fuel ratio and 56% of fuel energy +/- 3% of fuel energy at the lean mixture limit (see Figures 7.15 - 7.16). Excluding the setting of 9:1, where the total heat transfer exceeds the spread noted for the influence of the other variables, the effect of compression ratio on total heat transfer is negligible at less than +/- 1% of fuel energy over the range of excess air.

7.5 Crankcase blowby

Introduction

Crankcase blowby can be responsible for significant energy losses. It also influences exhaust hydrocarbon emission levels through in-cylinder flow dynamics. Increased levels of blowby have been found to reduce exhaust hydrocarbons (7.5). Gases collecting in the crankcase are usually (although currently not a feature of the Task engine) recycled through the inlet manifold to reduce atmospheric pollutant levels and maintain efficiency. This study was conducted to establish the

proportion the blowby represented in an overall energy balance, to evaluate the mechanical design and to provide a simplified correlation for the engine model for validation and prototype development.

Experimental methodology

Motoring tests were used to investigate crankcase blowby. Firing conditions were simulated using a high compression ratio cylinder head together with a heated lubrication and coolant facility. This procedure was preferred to measurements made on the firing engine because the composition of the blowby gas was unknown, although a previous study has assumed the composition to be air, (7.7).

Air mass flow rates were determined at the inlet manifold and the crankcase exit to atmosphere using volume flow, pressure and temperature measurements. The effects of pulsating flow were minimised at inlet by use of a laminar air flow meter and at crankcase exit the flow was directed through a plenum. In-cylinder pressure was displayed continually on an oscilloscope.

The crankcase and rocker box were sealed prior to testing and the condition of the valves and valve seats were checked. Engine speed was varied from 15 to 35 rev/sec and the compression ratio from 14 to 21:1, producing peak cylinder pressures of around 30 and 45 bar respectively.

Discussion of results and comparison with published data

The measured blowby expressed as a percentage of incoming charge is presented in Figure 7.17 and shows a strong pressure and time dependence. The blowby flow rates were observed to increase from around 2.5 to about 4.5 litres/min as the compression ratio increased from 14 to 21:1. That the data obtained under motoring conditions at the higher compression ratio simulated typical firing conditions was corroborated by a simplified analysis of measurements made with the engine firing at the lower compression ratio. In comparison with previous work, (7.5, 7.6, 7.8), blowby flow rates were found comparable with those of firing engines but excessively high when referenced to the mass of incoming charge where a value of around 1 to 2.5% is usual, (2.8, 2.9, 7.7).

Energy loss to blowby

The mass loss to blowby during the experimental programme was estimated at each operating point based on a simple speed correlation determined from the blowby measurements at the higher compression ratio according to:

$$m_l = -0.3N + 14.26$$

where m_l is the mass loss to blowby (percentage of incoming charge) and N the engine speed in rev/sec.

In the absence of experimental data, the proportion of reactants to products within the blowby was set to a nominal value of 0.6, consistent with published work, (2.9). The energy loss then comprised an enthalpy term referred to standard conditions together with the energy of the unburned fuel. The magnitude of this loss was estimated at around 4.5, 3.5 and 2.5% of the incoming fuel energy at speeds of 25, 30 and 35 rev/sec respectively.

A blowby allowance was incorporated into the closed cycle engine simulation based on the known mass at inlet valve closure and the above speed correlation; the method is detailed further in Section 4.3.8.

Conclusions

Energy loss to blowby is significant, particularly at low speed, accounting for some 4.5% of fuel energy.

Blowby flow rates are comparable with those reported from previous studies of engines with larger capacity although excessive when referred to the incoming charge. The possibility of mechanical defect or a scaling effect should be addressed.

A mechanical configuration incorporating features to minimise blowby implies more, rather than less, piston rings with gas tight joints. A piston ring of low width to minimise flutter and running in a smooth cylindrical bore is also desirable. Such features often have a detrimental effect on production complexity, friction and mechanical

strength or are influenced by operational factors such as wear. In the shorter term the AEconoseal piston ring assembly described in Reference 7.6 appears to offer a compromise between these conflicting requirements.

The ring gap area was measured at the middle of the range applicable to production engines, a reduction in area would be desirable.

7.6 Ambient loss

Introduction

The ambient loss is usually assigned the value of the outstanding quantity in the energy balance, although a detailed energy audit reported in Reference 7.3 refers to direct measurement techniques. Direct measurement is attractive because it precludes cumulative measurement errors. Agreement of results obtained by both methods is a further confirmation of the reliability of the data.

An enclosure comprising an aluminium skin lined with medium density Rockwool glass fibres was manufactured to surround the engine in order that noise and heat transfer to the atmosphere were kept to a minimum (see Plate 2.1). Providing the heat transfer characteristics of the enclosure are known, the ambient loss can be obtained from the atmospheric and cabinet temperatures recorded during the test. Since only a small range in coolant and ambient temperatures was noted during the experimental programme it is to be expected that the ambient loss should remain reasonably constant.

Experimental methodology

A 1 kW heating element was installed within the cabinet coupled to a variac and watt meter. With the temperature of the engine increased to operating levels using the oil and coolant heating facilities, the energy input was then controlled by the heating element alone and conditions allowed to stabilise. Measurements of cabinet and ambient air temperatures were recorded periodically over several hours. The procedure was repeated at various levels of energy input and the

relationship between energy input and the cabinet-to-ambient temperature difference determined. The air temperature within the enclosure was also measured throughout the test programme over a wide range of operating and test conditions.

Discussion of the experimental results

Using the above relationship and the temperature difference between the enclosure and atmosphere together with the test data, the ambient loss was calculated for each test condition and was found to represent from 7 to 14% of the fuel input. The ambient loss determined by difference in the energy balance was found to represent from 10 to 20% of the fuel input, comparing favourably with a previous study of a single-cylinder engine, (7.4). The ambient losses determined by this latter method are included in the figures of Appendix II.

The difference between the ambient loss calculated from the energy balance and the loss calculated by the enclosure method, expressed as a proportion of incoming fuel energy, is illustrated in Figure 7.18 for the 3-2 and Hrcc arrangements; it is less than 6% for 75% of all readings and represents the outstanding energy term. Ambient losses assigned the value of the outstanding term in the energy balances accounted for around 700 +/- 300 W over the range of operating conditions whereas those estimated from the enclosure tests accounted for around 550 +/- 220 W. Considering the number of experimental measurements and calculations involved in the energy balance term and that the enclosure tests would underestimate heat transfer because air movement both within the enclosure arising from engine ancillaries and outside from the dynamometer fan were not simulated, there is remarkably good agreement.

Conclusions

The ambient loss represents a significant proportion of the fuel energy that remains unclaimed. A reduction is desirable through effective lagging or enclosure.

Recognising that the engine of the current integrated engine/compressor configuration has the surface area of a four-cylinder arrangement, the measured engine ambient loss is higher than that which could be achieved utilising an independent unit. Single-cylinder units are however, disadvantaged in comparison with multi-cylinder engines because the external surface area does not diminish in proportion to the number of cylinders. The relative merits therefore of either independent or integrated engine/compressor units in a heat pump require further study.

7.7 Unburned hydrocarbons

The effect of operating and design variables on this term follows from the discussion of such effects on emission levels described later in Chapter 8; more general statements concerning the magnitude and the most significant variables influencing this loss are described in this section. The data referred to are presented in Figures II.2 - II.19 (Appendix II).

Minimum losses of around 2 to 3% of incoming fuel energy are noted to occur over a range of excess air ratios from about 1.1 to 1.3. The losses increase when mixture strengths are enriched or weakened outside this range, rising typically to 3 or 4% at the stoichiometric air-to-fuel ratio and the lean mixture limit. All tests conducted with the 3-2 configuration at compression ratios greater than 12:1 and the Hrcc show significantly higher losses at the lean mixture limit at around 5 to 7%.

7.8 Losses at the gas analyser

The analyser loss was determined from measurements of the flow rate through the positive displacement analyser sample pump, together with the thermodynamic properties of exhaust gas. The latter were calculated using the method detailed in Section 2.5 and the loss was referred to standard conditions. The magnitude of this term varied from around 0.7 to 1.2% of fuel energy, depending on operating conditions.

7.9 Oil heat transfer

The oil heat transfer was determined from measurements of the flow rate through the remote, gear-type oil pump together with the measured oil temperatures at engine inlet and outlet and appropriate thermodynamic properties. Inspection of the early test data showed that this quantity was small at typically 35 W, and no significant difference was noted as operating conditions were varied. Accordingly, subsequent heat transfers were based on representative values from the earlier work and varied from about 0.6 to 1.3% of fuel energy depending on operating conditions. The oil temperatures were, however, continuously monitored.

7.10 Frictional losses

7.10.1 Introduction

Quantifying engine friction and component contributions in the form of generalised correlations or sub-models in an engine model is of interest from the aspect of prototype development since the effect of parametric changes can be readily investigated without recourse to experimental method; also the dominant parameters are identified. Generalised correlations are also of value as a diagnostic tool in the evaluation of the mechanical design, providing a datum against which the experimental data can be compared. The objective is to further understanding of the mechanisms involved and to apply this to component design in order that improved efficiency can be achieved through reduction in frictional loss. Engine friction also has some bearing on the sizing of coolant systems. Piston friction particularly has been found to account for a significant proportion of heat transfer to the cooling jacket, (7.3, 7.9); at high engine speeds up to 60%, (7.3). Since frictional losses remain sensibly constant at a given speed they become substantially more significant as the output is reduced through either quality or quantity governing. (Reducing the output by quality governing is the favoured approach in this work because pumping losses are smaller.) The importance of frictional loss in the Task engine with reducing output is illustrated in Figure 7.19 over a typical range in operating conditions. The frictional loss rises from around 20 to around 30% of the indicated power over the range in output considered.

Friction data are extremely limited and no evidence of such data relating to engines of a similar size to the Task unit has been noted in the literature.

Types of lubrication

The various regimes of lubrication are conveniently represented on a Stribeck diagram where the coefficient of friction is plotted against a dimensionless duty parameter - defined as the product of the lubricant's dynamic viscosity and the sliding speed between surfaces divided by the loading force per unit area. Since the various engine components are subjected to large variations in loading and speed the coefficient of friction can vary from around 0.2 to 0.001 under normal operating conditions, with boundary, mixed and hydrodynamic regimes in evidence, (7.10). Typical operating modes for the major engine components are documented in References 2.4 and 7.10 - 7.12, these are illustrated in the Stribeck diagram of Figure 7.20.

Component friction

Piston assembly friction arises from a radially-directed static ring tension augmented by gas pressure together with inertial forces. It is dominated by the ring friction, which is typically responsible for around 80% of the piston assembly frictional loss, (7.11). Other contributions arise from the skirt, gudgeon pin and big end. The piston assembly usually accounts for around 50 to 75% of the engine friction, (4.44, 7.13, 7.14).

During normal running, piston rings can operate under both boundary and hydrodynamic conditions, the former regime promoted at top and bottom dead centres as reducing oil film thickness ensues due to abrupt changes in temperature, speed and load , (7.10, 7.11, 7.14). Higher sliding velocities, reduced loads and temperatures at other piston positions promote the hydrodynamic mode. The oil film thickness between the top ring and cylinder liner has been observed to change markedly throughout the engine cycle, with a minimum thickness of around 0.5 μm at top dead centre during combustion, rising to around 8 μm at other piston positions, (7.15). It has been reported that a film thickness of

around 1 μm is required to prevent asperity contact, (2.9, 7.10), although this is dependent on the surface finish of components. Other piston assembly components; skirt, gudgeon pin and big end operate under the hydrodynamic condition during normal running.

Crankshaft journal bearings are subjected to loads of varying magnitude and direction since these arise from gas pressure and accelerations of the piston connecting rod mechanism. Providing an adequate hydrodynamic film is maintained, which is the usual condition under normal running, the viscous regime predominates and high loads are supported with low frictional losses. Crankshaft journal bearings are usually responsible for around 10 - 15% of the engine friction, (4.44, 7.14).

Valve trains carry high loads throughout the speed range. The spring force is predominant at low speeds whilst inertial forces are most significant at high speeds, (7.10). The rocker arm fulcrum and the cam follower/camshaft interface are the major sources of frictional loss, with the latter thought to contribute the most, (7.10, 7.16). High loads and low sliding velocities promote a predominantly boundary-to-mixed regime, (7.10, 7.16), although Dyson, (7.17), cites evidence to suggest that the hydrodynamic mode is of significance at the cam follower/camshaft interface. Other interfaces, the camshaft chain/tensioner and valve stem/rockers operate in the boundary mode, (2.9).

7.10.2 Experimental methodology

The contribution of individual components to the total frictional loss was investigated by motoring the engine in various stages of disassembly. A high compression ratio cylinder head together with heated lubrication and coolant systems were used to simulate, as far as was possible, the actual conditions in the firing engine. At each stage of disassembly, the motoring speed was varied from 15 to 35 rev/sec. A 15W/40 multigrade oil was used throughout the test programme at a pressure of 30 psi. Oil viscosity was evaluated at the sump temperature at 36 +/- 7 centistokes over the range of observation. Pressure-crankangle data were obtained where appropriate and the indicated and pumping powers calculated by integrating the pressure-volume diagram.

Prior to testing, the coolant and lubricating oil were allowed to warm up for several hours while circulating around the engine. The load cell was calibrated over the expected range of observation. Valve timing and clearances, ignition timing and compression ratio were set where appropriate. During the tests, the temperatures around the oil and coolant circuits were allowed to stabilise following any change in operating conditions. To minimise the effect of hysteresis, average values of friction load were obtained from measurements made with the speed both increasing and decreasing. Load cell calibration was repeated after each test.

Calibration procedures for temperature, static and in-cylinder pressure measurements are detailed in Appendix IV. Running clearances were also measured and compared with recommended specifications (see Table 7.4).

Stages of disassembly

Motoring tests were conducted with the engine in the following stages of disassembly:

Stage I comprised the fully assembled engine with a modified high compression ratio combustion chamber. This arrangement produced peak cylinder pressures between 45 and 50 bar depending on the engine speed.

Stage II comprised the fully assembled engine at a compression ratio of 13:1, producing peak pressures around 30 bar.

Stage III comprised the full engine with the sparking plug removed.

Stage IV comprised the full engine with the cylinder head and valve train mechanism removed. Coolant flow was maintained by directing the usual water flow from the block to the cylinder head back into the cooling system. Oil flow to the rocker assembly was restricted.

Stage V comprised the crankshaft and compressor rear bearing.

Stage VI comprised the crankshaft only - driven directly from the dynamometer using a purpose made dummy shaft.

Stage VII considered the dynamometer only.

Contributions from ancillaries such as the camshaft-driven oil pump and the crankshaft encoder assembly were also investigated.

The contribution from the camshaft journal bearings was investigated independently by rotating the camshaft in the mechanism illustrated in Figure 7.21 and measuring the resistive torque. This provided additional information on the distribution of the losses associated with the valve train.

7.10.3 Experimental results

Component contributions and engine friction at various compression ratios are illustrated in Figure 7.22. All components illustrate, to a greater or lesser degree, hydrodynamic and boundary friction; the former condition linearly dependent and the latter independent of speed. In addition, the dynamometer shows a dependence on the square of the engine speed indicating turbulent dissipation at the fan. The data are well correlated by the following relationships:

Crankshaft:

$$fmep = 1602N + 13135$$

Piston and connecting rod assembly:

$$fmep = 388N + 46210$$

Valve train:

$$fmep = 7140$$

Camshaft bearings:

$$fmep = 233N + 100$$

Compressor rear bearing:

$$fmep = 181N + 8428$$

Dynamometer:

$$fmep = 10.1N^2 + 209N + 177$$

Engine friction without load: $fmep = 2104N + 64109$

Engine friction with load (compression ratio settings of 13 and 21:1):

$$fmep = 1155N + 104769$$

Motoring tests, with the engine fully assembled, were also conducted throughout the experimental programme at each change in engine configuration. These tests were undertaken as part of the calibration procedure used to verify the accuracy of the pressure-crankangle measuring system. This procedure is detailed in Reference 2.3. The pumping mep from all such data was found to be well correlated by:

$$fmep = 170N^{1.42}$$

The pumping mep from all firing data was found to vary as:

$$fmep = 7.26N^2$$

where:

$fmep$ - friction mean effective pressure (N/m^2)
N - engine speed (rev/sec)

No measurable contribution from the encoder mechanism was evident. Investigations were also undertaken to evaluate the contribution from the original camshaft-operated oil pump, which was replaced in the early stages of the work by a remote lubrication system. These tests were inconclusive because the engine sump did not include a heating facility, precluding satisfactory temperature control and allowing significant changes in oil viscosity.

7.10.4 Discussion of the results and comparison with previous work

Only limited information can be obtained from the direct comparison of frictional data since these are influenced by such factors as engine geometry, oil viscosity, loading and mechanical design. The correlations of Bishop, (2.4), account for many such variations but do exclude the influence of oil viscosity; a value of 15.5 centistokes being used throughout his work. (These correlations are detailed in

Section 4.3.7.) Both firing and motoring tests consistent with the range of experimental observation have shown however, that piston friction is only weakly dependent on oil viscosity, (4.43, 7.1, 7.11); the dependency increasing slightly with simulated combustion pressures, (4.43, 7.1). It has been suggested that measured piston friction conforms to the theoretical relationship for sliding bearings in which the coefficient of friction varies as the square root of the oil viscosity - at higher viscosities a lesser dependence is therefore to be expected, (7.1, 7.11). On the other hand, journal bearing friction is directly proportional to oil viscosity and hence this influence is of greater significance when comparing friction data.

The correlations of Bishop, together with appropriate engine-specific data presented by other workers, have been used in this work for comparative purposes, with the objectives of identifying areas where further reductions in frictional loss can be achieved and to assess the mechanical design and the suitability of generalised correlations for an overall engine model.

Figures 7.22 and 7.23 present the correlations of Bishop together with the experimental data.

Piston assembly friction

The hydrodynamic and boundary regimes are respectively represented by a quantity varying linearly with speed superimposed on a speed independent term. The boundary term of around 45 kPa reduces from 85 to 75% of the piston friction load as the speed increases from 15 to 35 rev/sec. Total piston assembly friction reduces from 57 to 43% of the total frictional loss at no load conditions as the speed increases.

Previous workers, (2.4, 7.14) and Leary, (cited in 7.1), have identified significantly smaller boundary friction contributions at around 20, 30 and 35 kPa respectively, the latter obtained under firing conditions and including an extra ring. Neglecting the influence of gas pressure in Leary's result and noting that as a first approximation ring friction is taken as 7 kPa per ring, (2.4, 4.44, 7.14), the measured boundary term is around twice that reported by these workers.

It is improbable that compression ring tension is a major contributor, since the measured blowby was high (see Section 7.5) although increased blowby has been found to result from pressure reversals between the lower rings initiating 'ring flutter', (7.10), a problem that did occur in the early development stages of the engine, (1.28). The piston skirt is also unlikely to be a significant factor since the running clearance was within the recommended limits (see Table 7.4) and no evidence of undue wear was noted.

Running clearance has a marked effect on bearing friction power and minimum film thickness (see Figure 7.24). Typically, as radial clearances exceed 0.02 mm, the minimum film thickness approaches that usually required to promote complete hydrodynamic lubrication (around 1.0 to 2.0 μm) and mixed lubrication ensues with increased frictional loss and bearing wear, (7.10). Table 7.4 shows that the big end radial clearance is around three times the recommended value and that the side clearance is also excessive. It is possible therefore that the big end operated in the mixed regime, the excessive side clearance exacerbating oil leakage, further impairing the formation of the film.

It is also likely that oil metering to the piston may have been insufficient to promote full hydrodynamic lubrication, particularly when it is noted that the experimental programme was conducted with a dry sump lubrication system and that the piston/small end design called for a splash oil feed from a drilling in the connecting rod - a feature omitted in the Task engine. To some extent this deficiency would be offset by the big end side and running clearances.

In light of the crankshaft/connecting rod assembly modifications undertaken at an earlier stage (see Section 3.1), a further inspection was conducted which revealed witness marks on both the crankshaft and connecting rod thrust surfaces, indicating a possible misalignment.

Crankshaft

Compared with previous studies, (4.44, 7.14), a disproportionate contribution from the crankshaft is evident in both the hydrodynamic and boundary regimes. The latter term, at around 20 kPa, reduces from

about 50 to about 30% of the crankshaft friction as the speed increases from 15 to 35 rev/sec. Crankshaft friction increases from 40 to 50% of the total frictional loss under no load conditions as the speed increases over the range. Some speed independent term is to be expected due to constant spring loading at the oil seals and could conceivably arise at thrust surfaces. Typically, front and rear seals have been found to represent about 25% of the crankshaft contribution at 25 rev/sec, (7.14). However, the Task configuration included only a single rear oil seal. While running clearances were within tolerances (see Table 7.4), oil supply to the main bearings is intimately related to leakage at the big end, excessive clearance, as noted earlier, impairing the supply. It is probable that this, together with the other mechanical defects referred to above, were responsible for promoting the boundary regime.

The strong dependence on engine speed in the hydrodynamic condition can in part be attributed to over-sized main bearings. The geometrical parameter K (see Section 4.3.7) evaluated for this engine at 2.52 is around three times as large as that usually found in spark-ignition engines. Compared with Bishop's correlation, the stronger dependence on engine speed is consistent with a higher oil viscosity.

Valve train mechanism

The valve train mechanism shows no measurable dependence on engine speed, suggesting the dominance of the boundary mode arising at the interfaces. This source reduces from around 7.5 to 5% of the total frictional loss at no load conditions as the speed increases from 15 to 35 rev/sec. The hydrodynamic contribution at the camshaft bearings was established using the mechanism illustrated in Figure 7.21 and was found to be small, rising from 6 to 12% of the valve train friction as the speed increased from 15 to 35 rev/sec. Over a similar range of observation, comparative testing of four common valve train mechanisms has also shown a weak dependence on speed for the push rod-operated over-head valve arrangement utilised on the Task engine (7.12).

Both the valve train mechanism and camshaft journal contributions were found to show close agreement with the correlations of Bishop.

The effect of gas pressure

The initial increment in gas loading to a compression ratio of 13:1 is seen to increase the engine friction by around 9 to 25% depending on the speed (see Figure 7.22), further increases producing no measurable effect. In marked contrast to the above data and a further study by Roensch, (cited in 7.1), is Bishop's correlation (see Figure 7.23) which indicates a far stronger dependence on compression ratio increase during motoring. Constant gas pressure applied to the space above the piston during motoring, (4.43), also appears to have a similar influence on the engine friction as the experimental measurements when cycle-averaged pressures are taken to represent the constant gas load.

Additionally, other workers have considered this influence directly by varying the load on the firing engine, (7.13, 7.15, 7.18). It is evident from these studies that there is a lack of consensus with respect to the influence of gas pressure on engine friction. It has been reported to increase the piston friction, possibly through greater radial tension of the rings, (2.4, 2.9, 4.43) and to a lesser extent increase the bearing friction, (2.9). Other workers however, (7.3, 7.13), suggest that engine mechanical friction, piston friction and bearing friction are largely insensitive to changes in load. Furuhama, (7.15), considers that it is the increasing temperature associated with increasing load that is responsible for greater ring friction; higher temperatures lowering the viscosity of the oil and thereby reducing the oil film thickness.

Pumping

The correlations of Section 7.10.3 confirm low pumping losses for the quality governed engine running at slow speed; rising from around 10 to 60 W as the speed increases from 15 to 35 rev/sec under motoring conditions. The modest proportion of these losses with respect to engine output suggests only a small advantage is to be gained by developing an open loop sub-model, with the pumping losses adequately represented by the correlations developed. The functional form of both motoring and firing correlations corresponds to those presented by other workers for wot operation (see References 2.4 and 4.44

respectively). Engine specific characteristics evidently influence the speed dependency in these relationships, the experimental motoring data are, however, well represented by Bishop's generalised correlation, viz.:

$$fmep = 304\, N^{1.7} \Big/ \left(\frac{CGH^2}{V_S}\right)^{1.28}$$

Smaller pumping losses were measured for the firing engine. Inspection of the pressure-volume diagram suggests that a dynamic effect is present after blowdown during firing operation so that mean exhaust system pressure is not achieved until later in the stroke. The firing data agree most closely with the firing data of Millington, (4.44), viz.:

$$fmep = 400\bar{S}_p^2$$

where:

C	- number of cylinders	
$fmep$	- friction mean effective pressure	(N/m^2)
G	- number of intake valves per cylinder	
H	- intake valve head diameter	(mm)
N	- engine speed	(rev/sec)
$\bar{S}_p$	- mean piston speed	(m/s)
Vs	- swept volume	(cm^3)

Heat and mass transfer

Heat and mass transfer are noted to relate inversely to engine speed since they are both time dependent; a strong pressure dependence is also indicated (see Figure 7.22). Both results are consistent trend-wise with Bishop but show a stronger dependence on speed together with a significantly greater contribution. The rate at which heat and mass transfer losses diminish with increasing speed is evidently sufficient to maintain an almost constant total motoring loss. Usual motoring losses increase with speed (see for example Reference 4.44) which suggests the influence of the high levels of crankcase blowby noted in Section 7.5.

Total frictional loss

Correlations for total motoring frictional losses including the effects of heat and mass loss, accessories and pumping work are typically of the form:

$$fmep = A + BN + CN^2$$

where the terms mainly represent boundary, hydrodynamic and turbulent dissipation effects. Pressure and geometric dependency or mechanical configuration are reflected in the values of the constants, A, B and C. The total motoring frictional loss for the Ricardo E6 engine at a compression ratio of 8:1 was found to correlate to such a function, with the constants set to values applicable to small, swirl-chamber IDI compression-ignition engines, (4.44). SAE standard J816b, (2.5), suggests a correlation of similar functional form for firing frictional and pumping losses, together with a pressure dependency correction determined from brake power measurements.

Fujii et al., (7.19), present a correlation which may be written in the form:

$$fmep = A + BN^2$$

where the values of A and B are constant for a given engine but are functions of geometry. Whilst the relationship does benefit from geometric generality it was not found representative of the experimental data.

Recognising the conflicting evidence surrounding the influence of gas loading on engine friction (discussed earlier under 'The effect of gas pressure') and that information obtained from motoring tests is of limited value when applied to the firing engine (partly because the pressure-crankangle phasing is altered, although other factors are discussed in Section 7.10.5), there is evidence to suggest an approximate relationship between the influence on engine friction of a constant gas load under motoring conditions and the influence arising from firing pressures, (7.1). Using this result, together with the correlations of Bishop and Millington, a relationship with the advantages of geometrical generality and pressure dependence and which

closely represents the experimental data is proposed to describe engine mechanical friction, the influence of gas pressure and pumping losses viz.:

$$fmep = 370.10^3 \frac{S}{B^2} n + 756.10^3 \frac{M}{BS} \bar{S}_p + 2083 imep + 414 \frac{B}{S} NK$$

$$+393.10^3 [30 - 0.24N] \frac{GH^{1.75}}{B^2 S} + 600 \bar{S}_p^2$$

The terms describe piston ring wall tension, viscous piston friction, a gas pressure term, journal bearing friction, valve train friction and pumping losses respectively. (Heat/mass loss or ancillaries are neglected.) The nomenclature and units were defined in Section 4.3.7. This correlation was included in the engine model as a generalised tool for prototype development.

7.10.5 The utility of progressive disassembly

Whilst the utility of progressive disassembly is recognised as a reliable indication of the proportion of frictional loss associated with each component, these losses are influenced to some extent by the temperatures and pressures in the firing engine. Higher piston and cylinder wall temperatures reduce the viscosity of the oil in the bore and hence reduce piston viscous friction. On the other hand, combustion temperatures tend to reduce mechanical clearances and the thickness of the hydrodynamic film at the top of the bore, promoting boundary lubrication. Combustion pressure may also increase ring tension and bearing loads, (7.18). Engine friction data derived from the firing pressure-crankangle data and brake power measurements do indicate some reduction compared with the motoring engine, although scatter in the data precludes quantifying any difference. Under firing conditions, reductions in engine friction of around 10% have been reported when compared with measurements made under motoring conditions, (7.13).

7.10.6 Conclusions

In light of the preliminary stage of the engine development and the scope for further improvement of the mechanical design, it is probable that the correlations of Bishop accurately represent the motoring

frictional losses of the main components of the Task engine in the production stage of development.

Further work is required to improve the mechanical design, particularly with reference to the crankshaft and piston assembly where excessive boundary friction was noted. A reduction in the bearing surface area, consistent with the demands for durability and the likely range in speed and mean effective pressure, is desirable.

Recent developments in piston design discussed in References 7.6 and 7.11, including reduction in the number, area and tension of piston rings and the area of piston skirt, would be beneficial in reducing the engine friction. The AEconoguide piston discussed in Reference 7.6 and referred to in Section 7.5 incorporates many such features, suggesting a possible alternative for future work.

Correlations, supported by comparative data, have assisted the analysis of engine friction data in the form of a diagnostic tool. Engine-specific correlations obtained from the experimental data, together with a more generalised relationship describing mechanical and pumping losses have been incorporated into an engine model for validation purposes, energy flow analysis and for use as a tool in prototype development.

7.11 Miscellaneous observations

Ignition timing

The ignition timing was set to the minimum advance for best efficiency, excluding those tests where the effects of ignition timing were investigated. If the ignition timing is retarded from a very advanced setting, negative compression work diminishes; with very retarded ignition positive expansion work also reduces. The optimum setting achieves the most favourable balance between these two trends and hence maximises the net work for the working loop; as a rough empirical guide, corresponding peak pressures occur between 5 and 20 degrees atdc, (2.9, 7.20). The optimum setting depends on the design and operating conditions which influence the rate of combustion and is

therefore implied by the detailed discussion in Chapter 5. The purpose of this section is to outline the most significant variables influencing the optimum spark timing and typical settings. The data referred to are presented in graphical form in Appendix II.

Around stoichiometric air-to-fuel ratios, an optimum ignition advance of 25 to 30 degrees was typical for all operating conditions; the 3-2 configuration at compression ratios exceeding 12:1 and the Hrcc were notable exceptions with 20 and 15 degrees advance respectively. At the lean mixture limit, the optimum ignition setting advanced to around 35 to 45 degrees for most configurations depending on the speed; the 3-2 arrangement at compression ratios exceeding 12:1 and the Hrcc again characterised by lesser advance at 30 to 35 and 25 degrees respectively.

Noise levels

Noise levels, at 1 metre from the enclosure, were obtained at 3 speeds for a typical operating condition. These were recorded at 61, 65 and 71 dBA at 20, 25 and 35 rev/sec respectively, compared with the levels recorded by previous workers (discussed in Section 1.5) of 50 to 65 dBA between 30 and 35 rev/sec for complete heat pump units, (1.22, 1.23, 1.27). The measurements from the Task engine did, however, include an unknown contribution from the dynamometer fan.

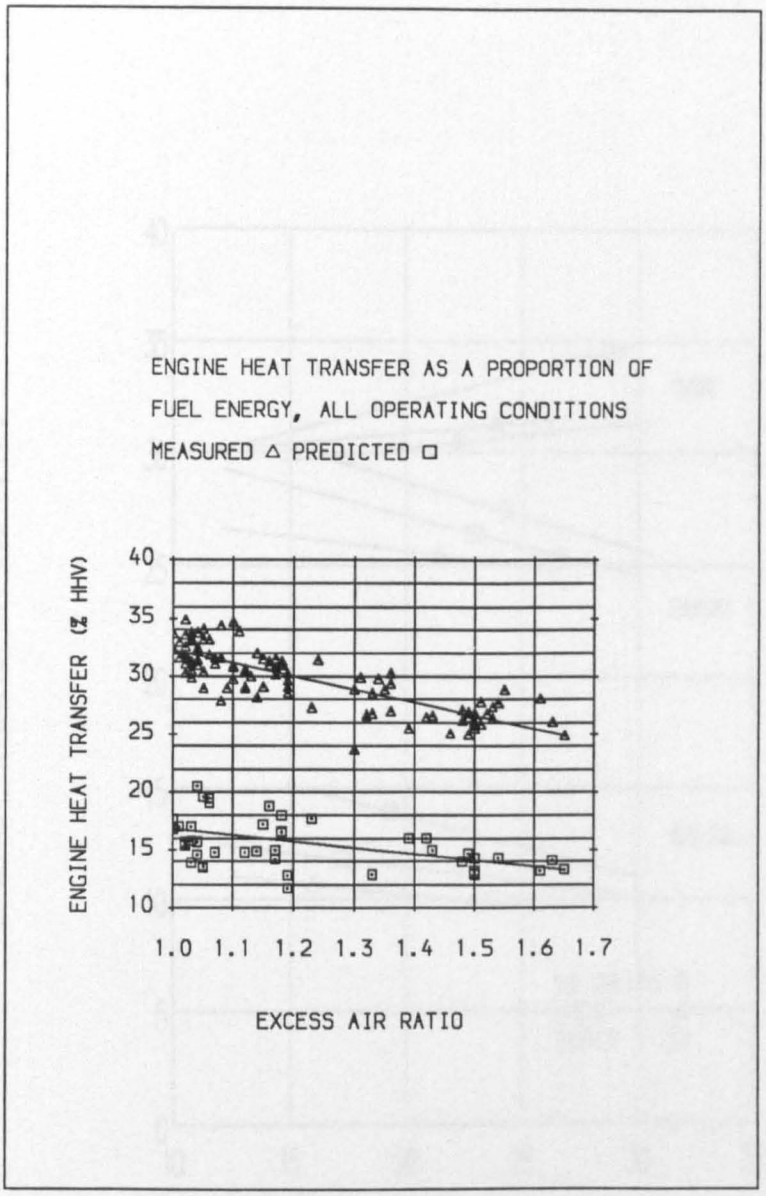

Figure 7.1 Measured and predicted engine heat transfer for all operating conditions.

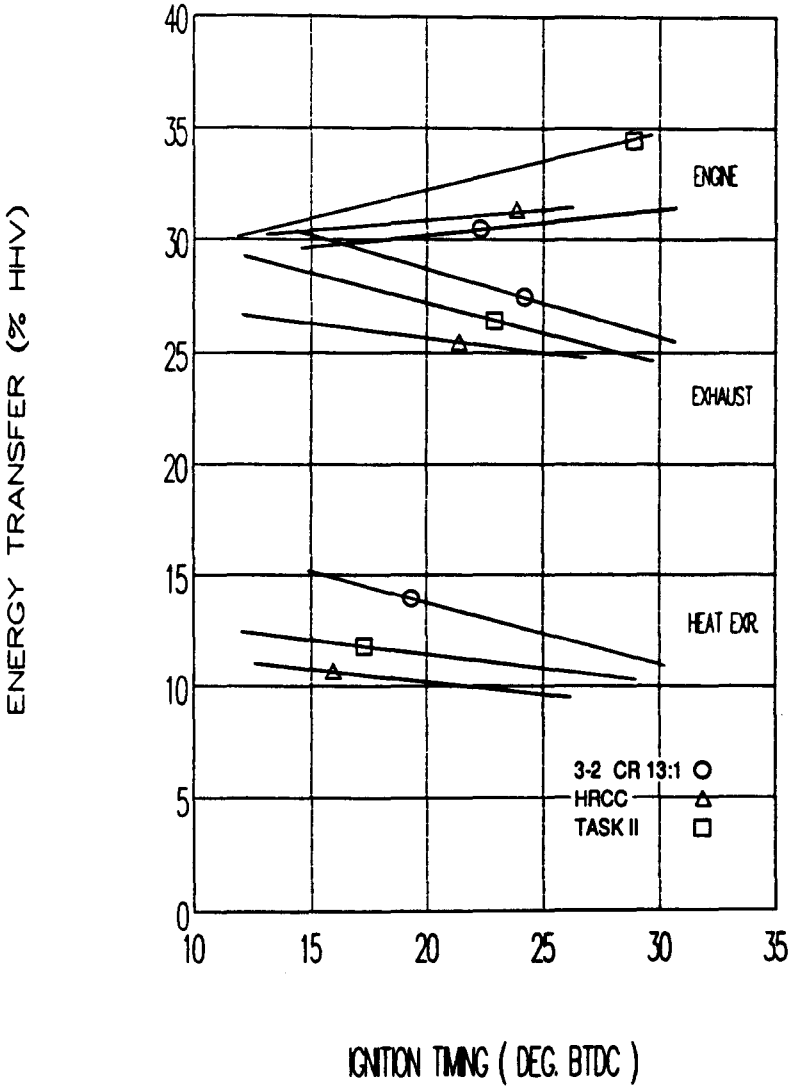

Figure 7.2 Effect of ignition timing on engine and total exhaust heat transfer. Excess air 1.2, 1800 rpm.

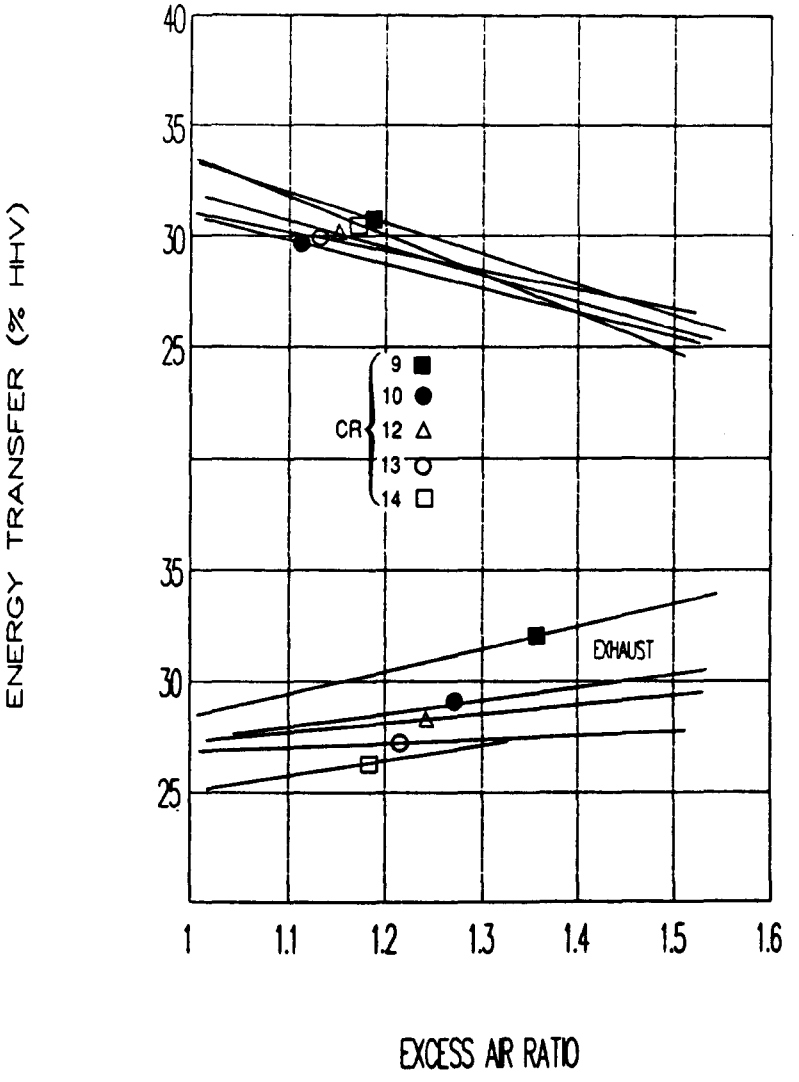

Figure 7.3 Effect of compression ratio on engine and total exhaust heat transfer. Chamber 3-2, 1800 rpm.

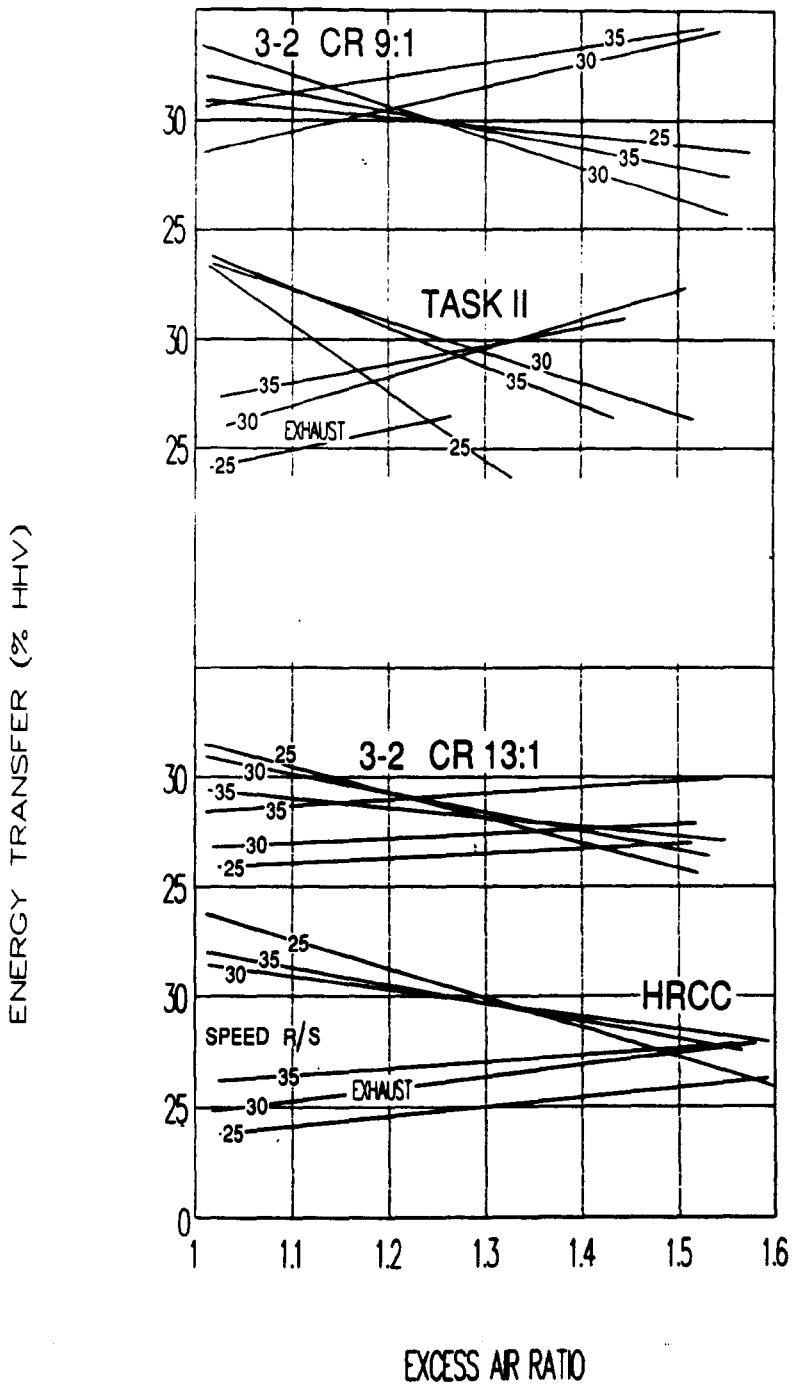

Figure 7.4 Effect of engine speed on engine and total exhaust heat transfer.

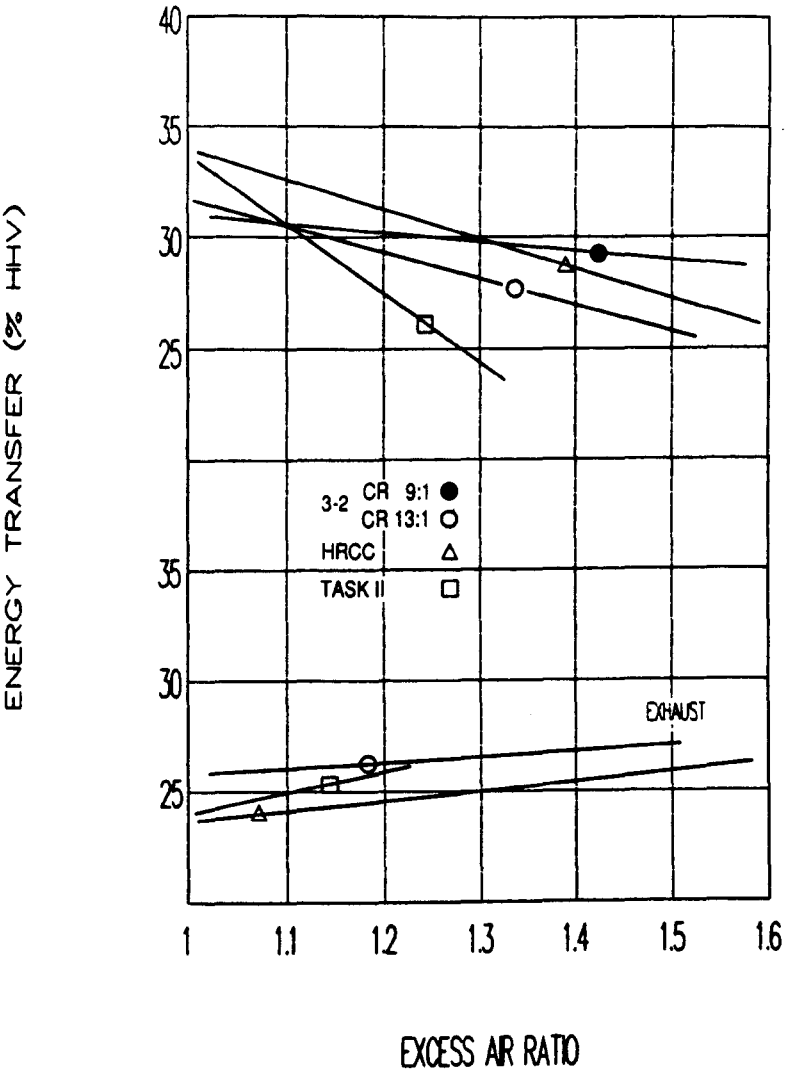

Figure 7.5 Effect of chamber on engine and total exhaust heat transfer at 25 r/s.

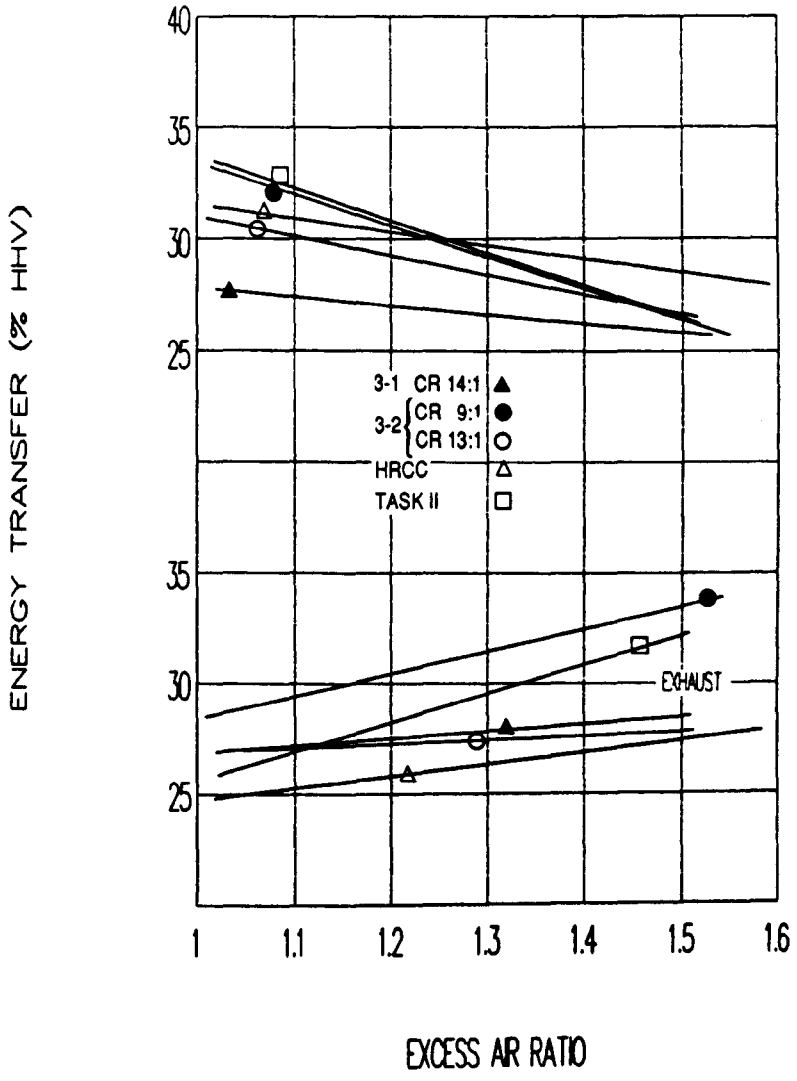

Figure 7.6 Effect of chamber on engine and total exhaust heat transfer at 30 r/s. (3-1: engine only unit, results from preliminary study, reference 1.30).

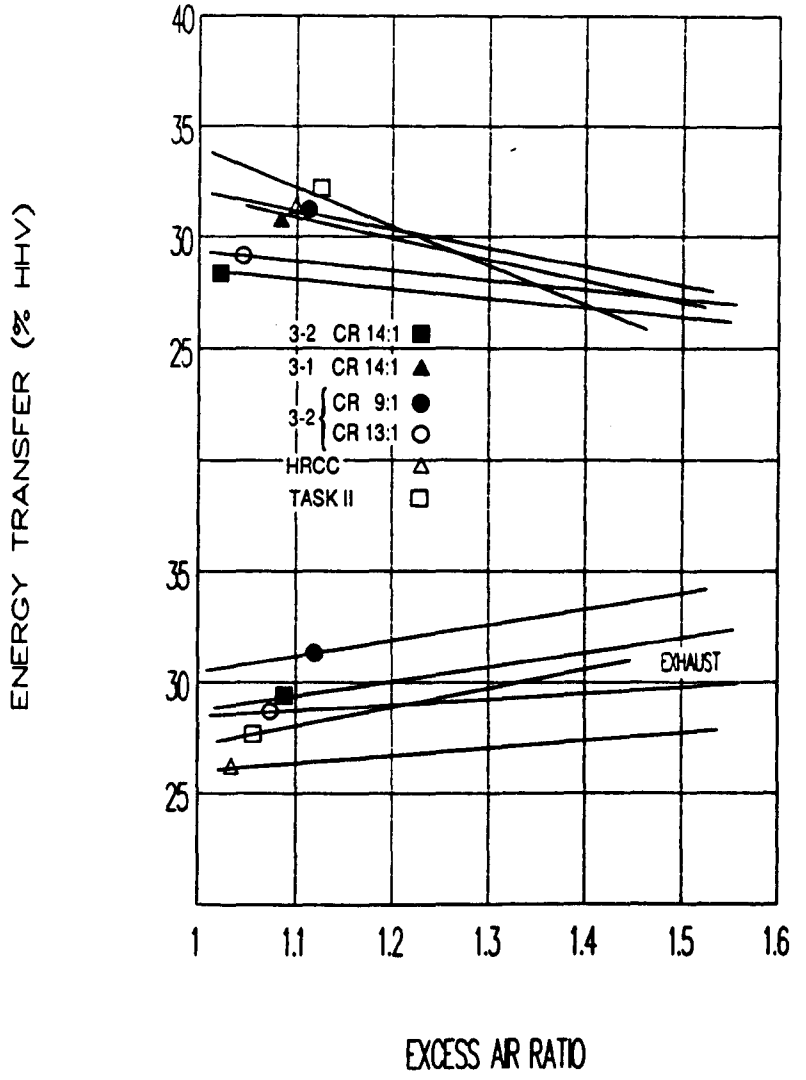

Figure 7.7 Effect of chamber on engine and total exhaust heat transfer at 35 r/s. (3-1: engine only unit, results from preliminary study, reference 1.30).

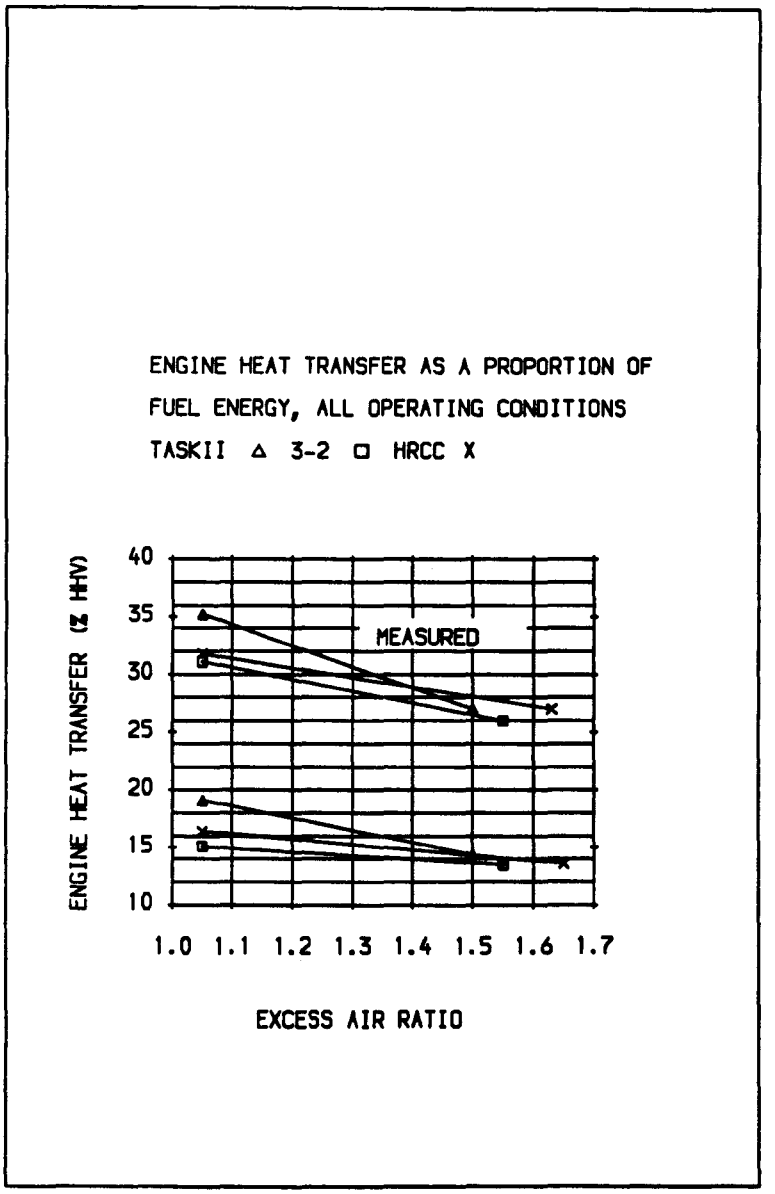

Figure 7.8 Measured and predicted engine heat transfer for three chambers.

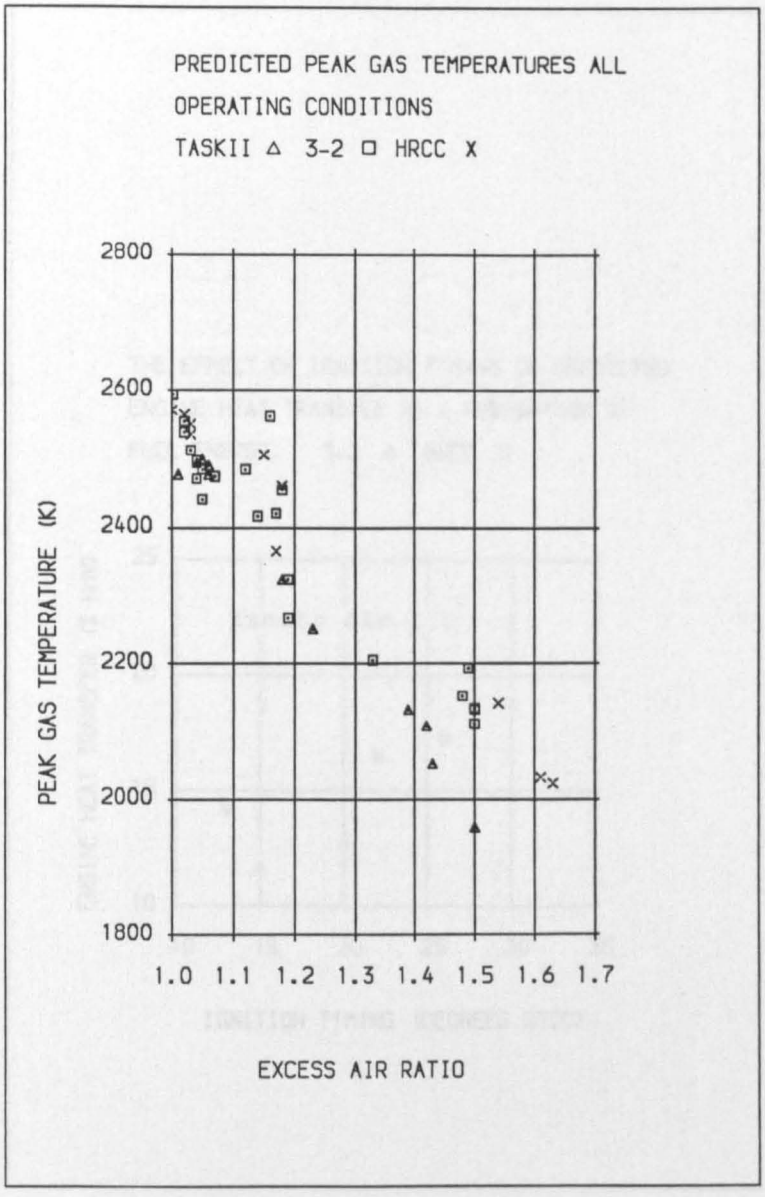

Figure 7.9 Predicted peak gas temperatures all operating conditions.

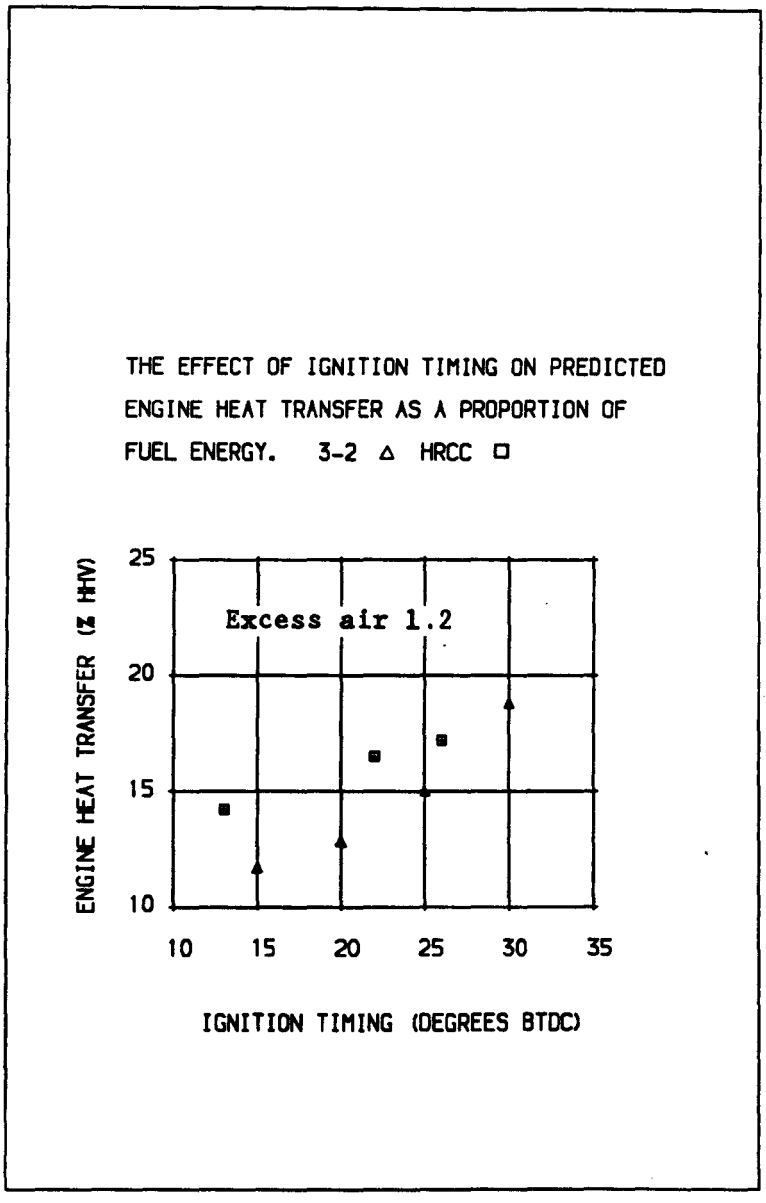

Figure 7.10 Influence of ignition timing on the predicted engine heat transfer.

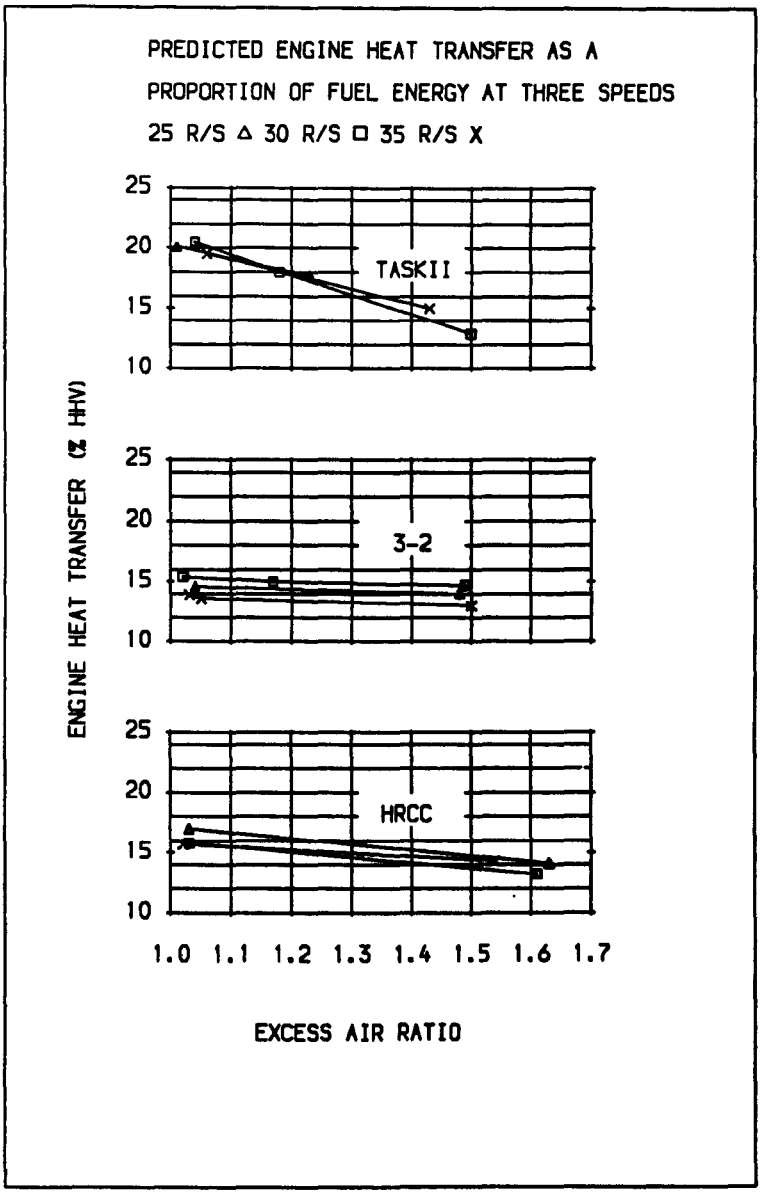

Figure 7.11 Influence of engine speed on predicted engine heat transfer for three chambers.

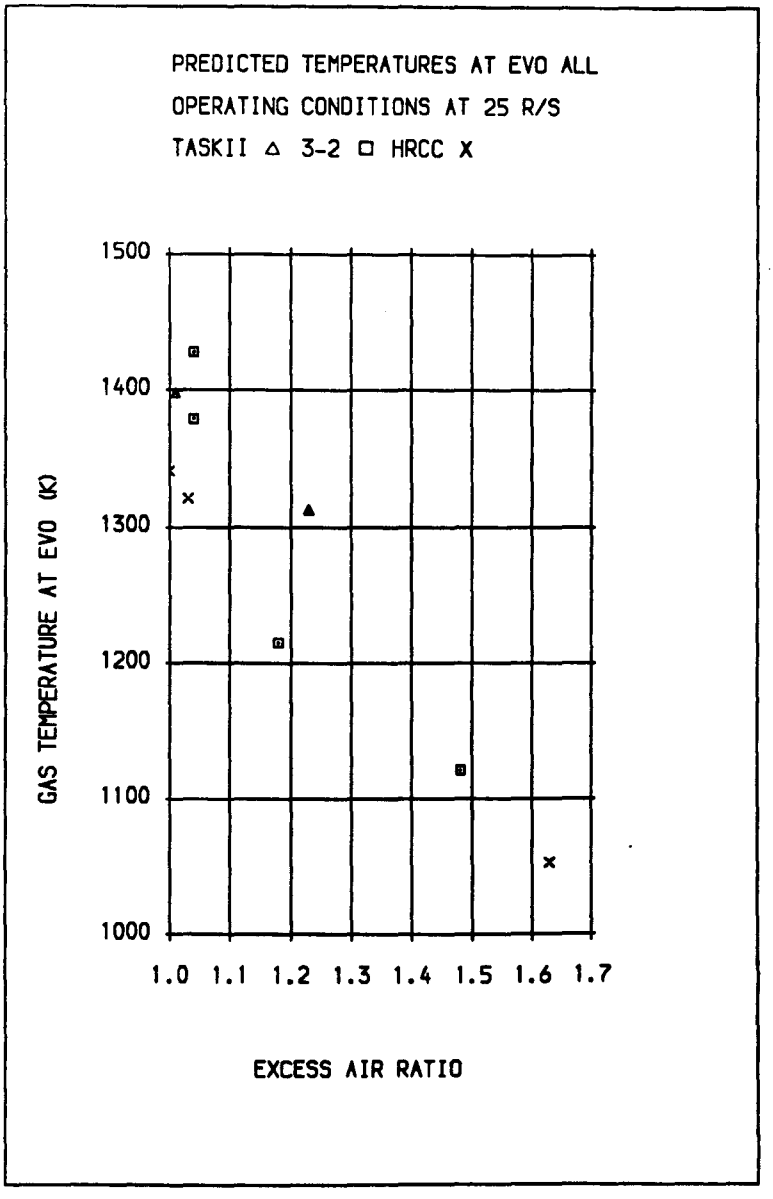

Figure 7.12 Predicted temperatures at exhaust valve opening at 25 r/s.

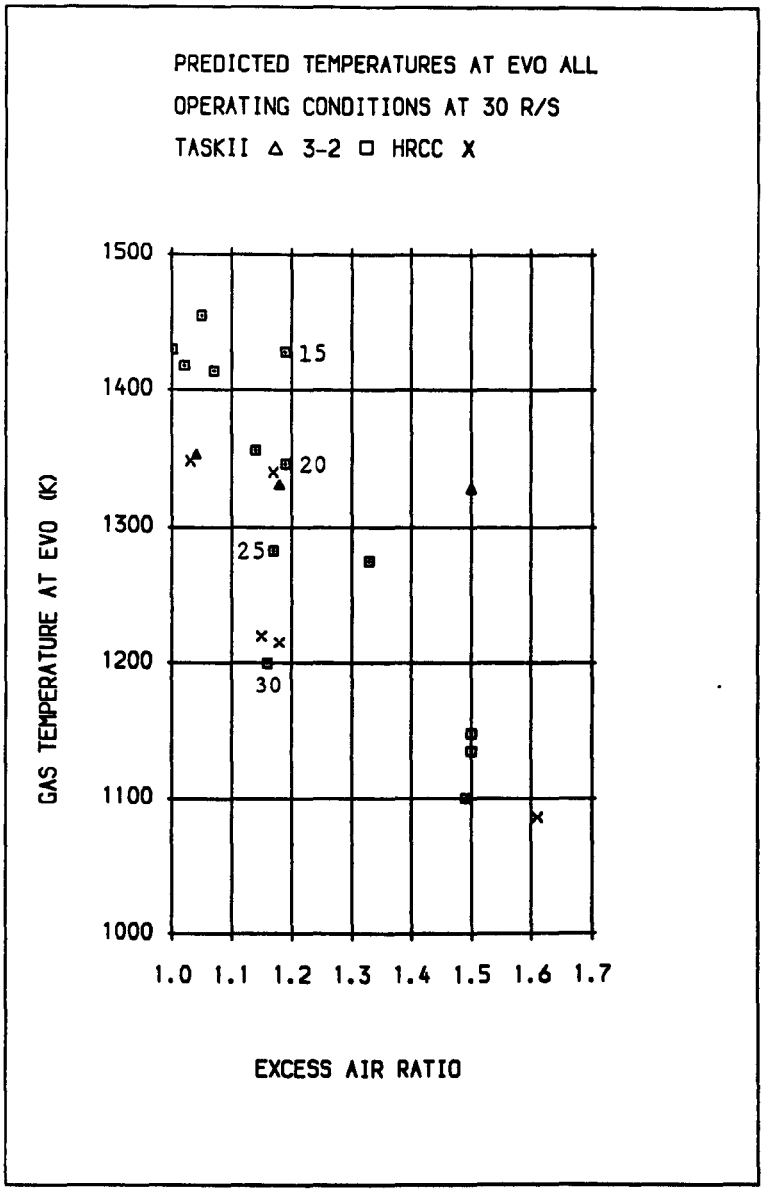

Figure 7.13 Predicted temperatures at exhaust valve opening at 30 r/s. Numbers adjacent to markers refer to ignition timing, (degrees btdc).

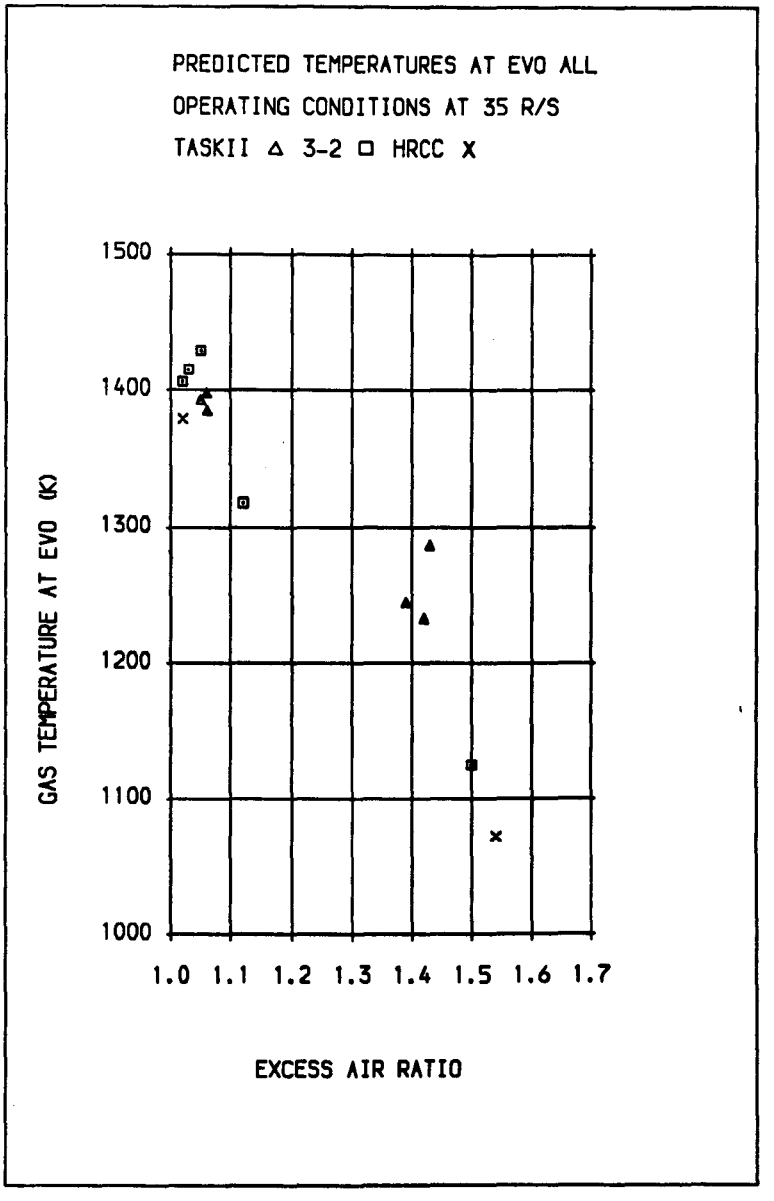

Figure 7.14 Predicted temperatures at exhaust valve opening at 35 r/s.

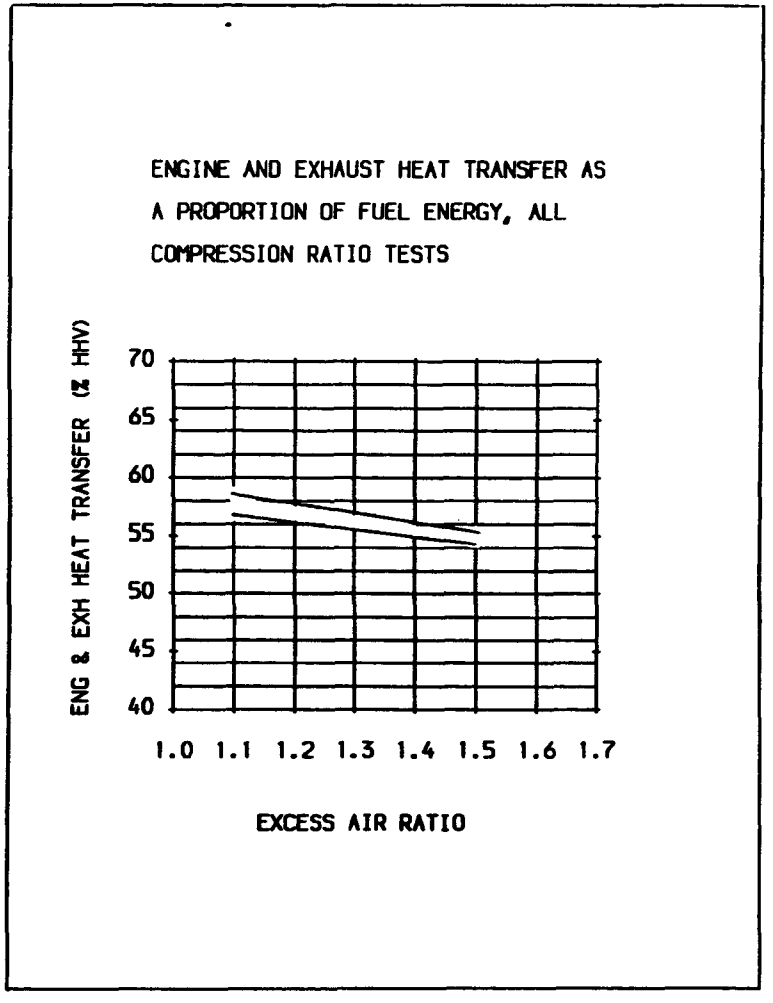

Figure 7.16 Range in the total heat transfer to engine and exhaust.

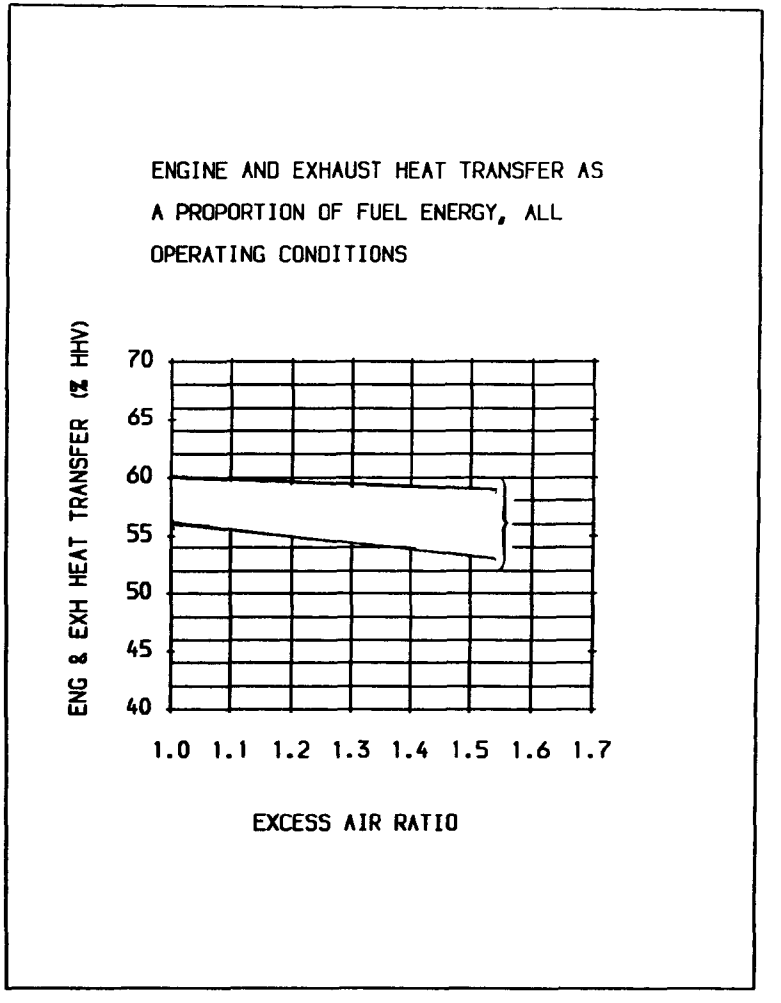

Figure 7.15 Range in the total heat transfer to engine and exhaust.

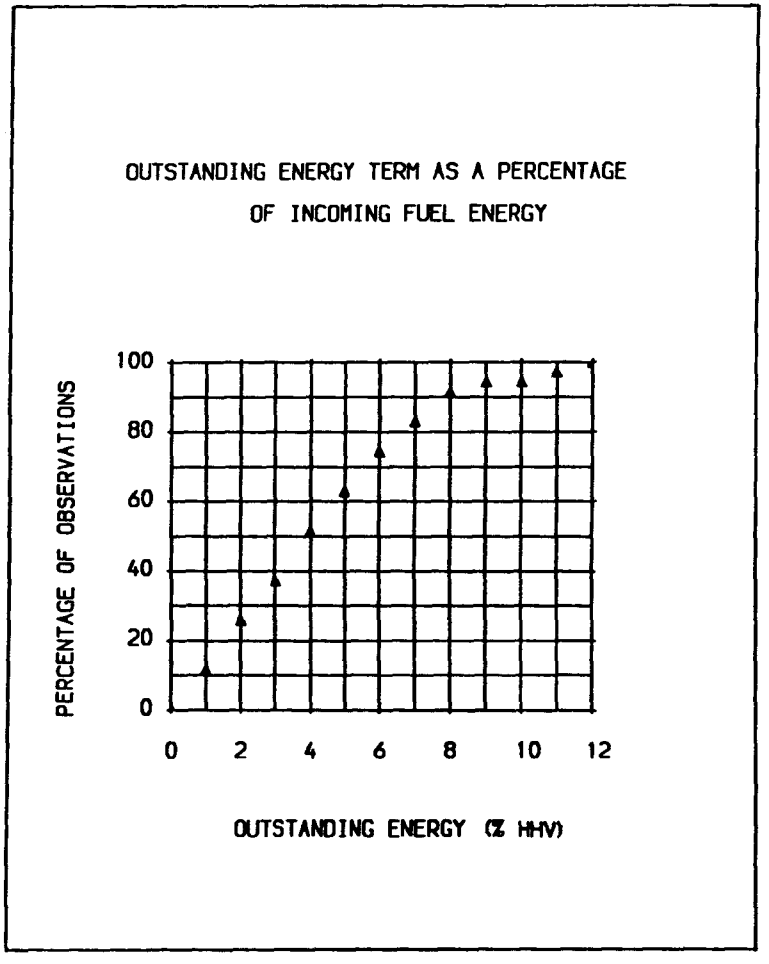

Figure 7.18 The outstanding energy term with the ambient loss assigned the value of the enclosure loss.

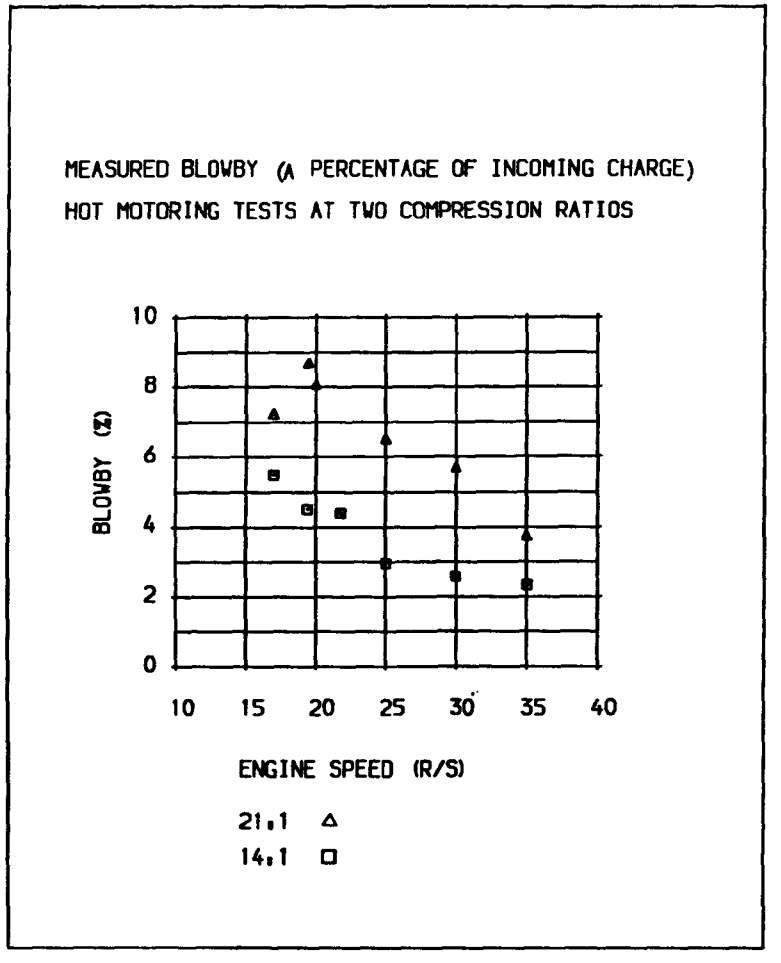

Figure 7.17 The effect of speed and compression ratio on blowby under simulated firing conditions.

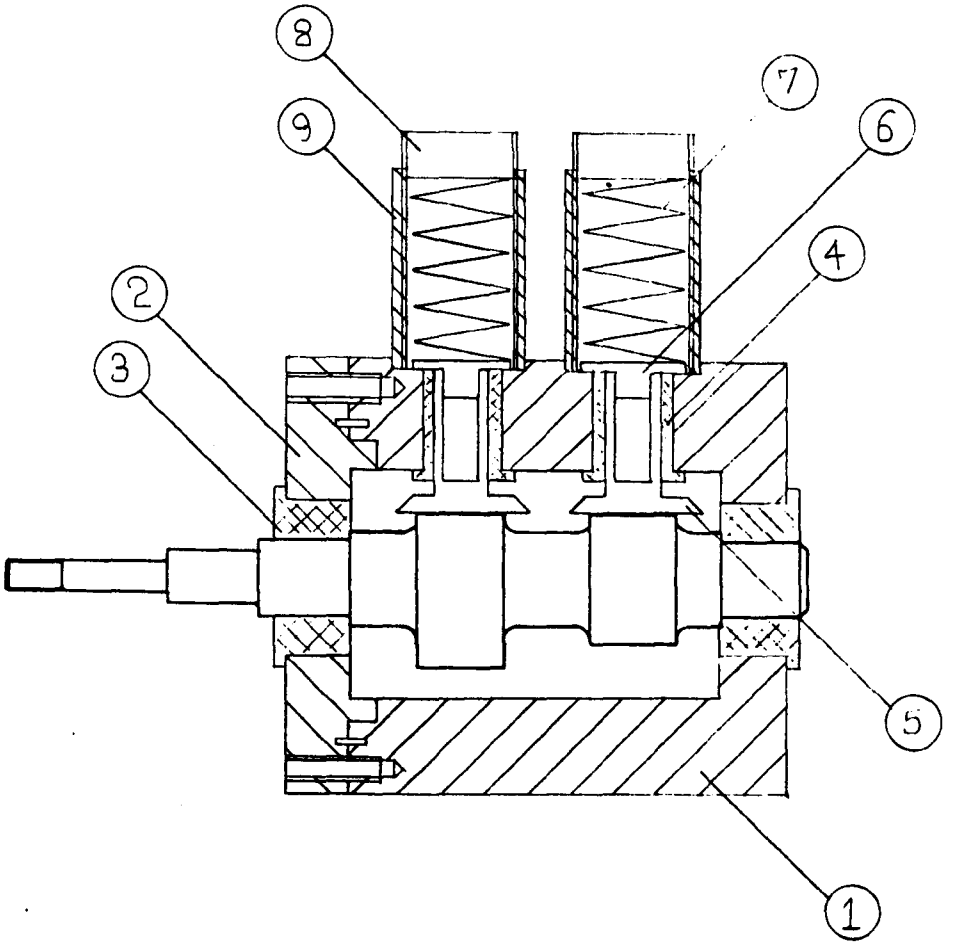

Nº	DESCRIPTION/MATERIAL	Nº OFF
1	MAINBODY PART 1 : ALUMININUM	1
2	MAINBODY PART 2 : ALUMINIUM	1
3	INSERT : CAST IRON	2
4	INSERT : CAST IRON	2
5	CAM FOLLOWER	2
6	CAP	2
7	SPRING	2
8	SCRW	2
9	CYLINDER : ALUMINIUM	2

Figure 7.21 Mechanism for measuring the camshaft friction.

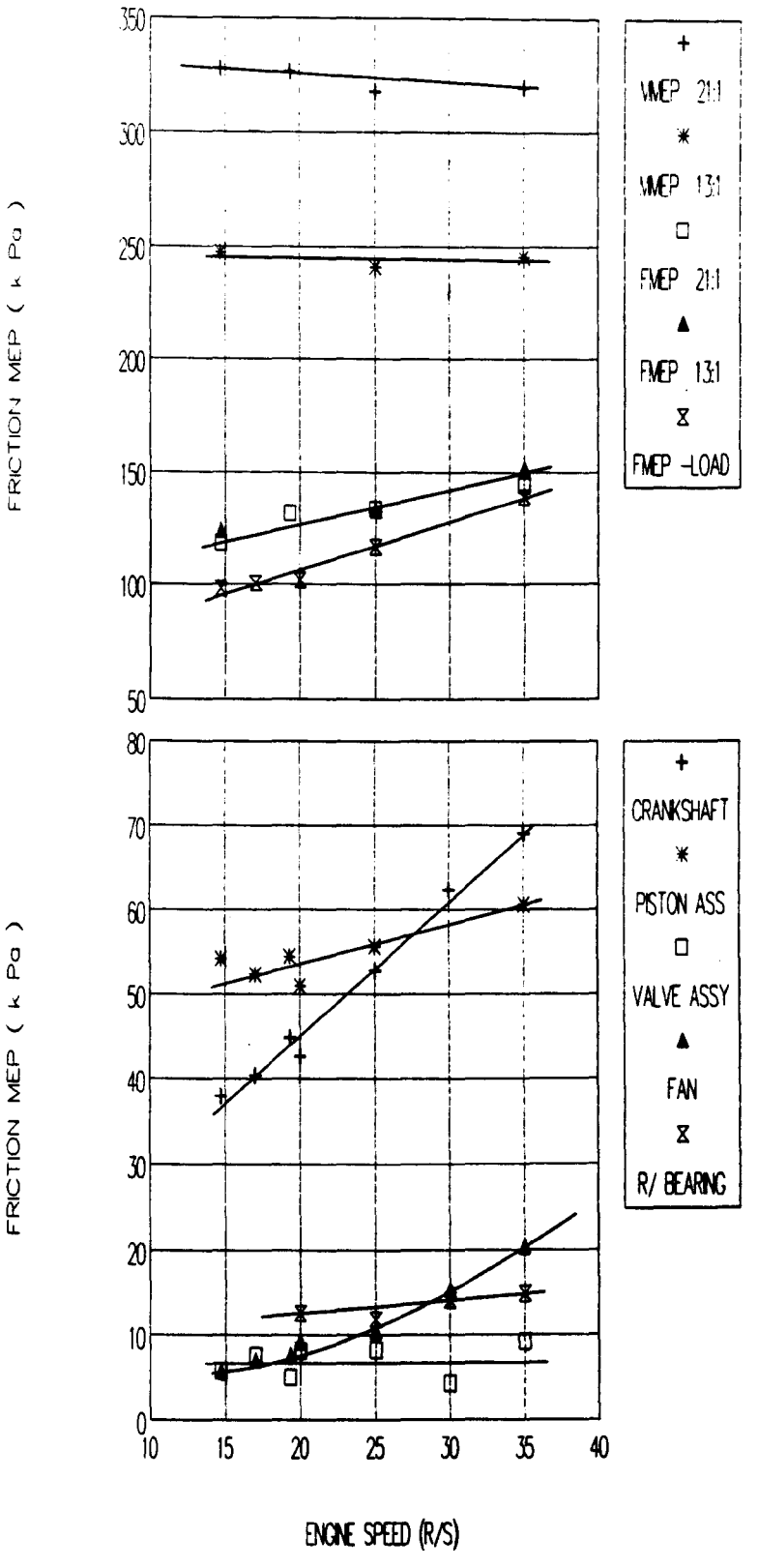

Figure 7.22 Engine component friction and engine friction at various compression ratios and under simulated firing conditions.

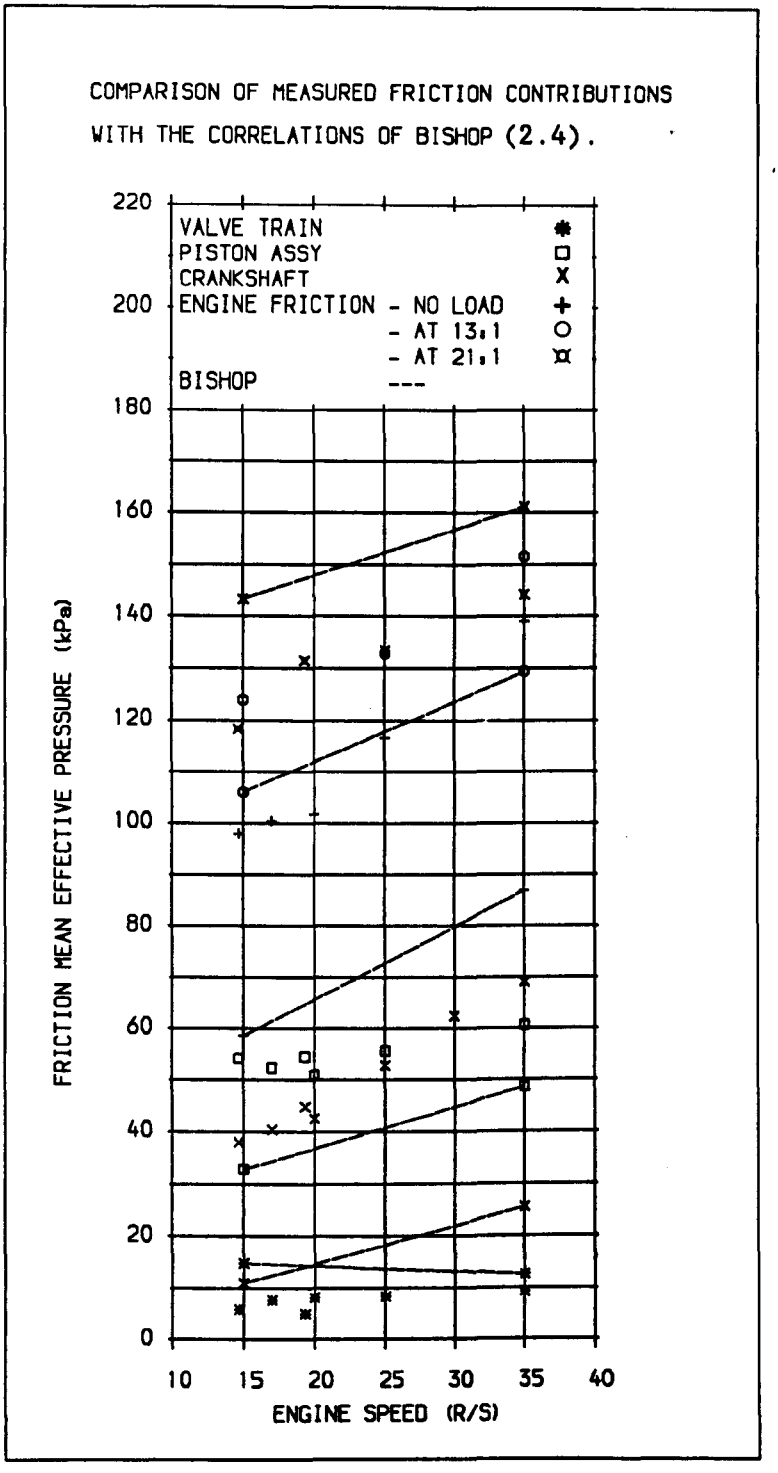

Figure 7.23 Comparison of the measured friction contributions with the correlations of Bishop, (2.4).

Table 7.1 Indicated thermal efficiencies.

Chamber: TaskII

Speed (rev/ sec)	Excess air	Thermal effy
	1.01	22.1
25	1.23	23.5
	1.04	22.0
30	1.18	23.6
	1.50	21.8
	1.06	22.9
35	1.42	24.5

Table 7.2 Indicated thermal efficiencies.

Chamber: Hrcc

Speed (rev/ sec)	Excess air	Thermal effy
	1.00	24.9
25	1.63	21.5
	1.03	24.9
30	1.15	29.4
	1.61	23.9
	1.02	25.7
35	1.54	28.3

Table 7.3 Indicated thermal efficiencies.

Chamber: 3-2 at 9:1

Speed (rev/ sec)	Excess air	Thermal effy
	1.00	22.3
30	1.50	24.8

Chamber: 3-2 at 10:1

Speed (rev/ sec)	Excess air	Thermal effy
	1.07	25.6
30	1.14	25.9
	1.33	25.5

Chamber: 3-2 at 12:1

Speed (rev/ sec)	Excess air	Thermal effy
25	1.04	24.4
	1.05	23.9
30	1.50	26.5
35	1.02	25.0

Chamber: 3-2 at 13:1

Speed (rev/ sec)	Excess air	Thermal effy
	1.04	23.0
25	1.18	22.8
	1.48	22.0
	1.02	23.9
30	1.17	23.3
	1.49	23.1
	1.03	23.3
35	1.12	23.7
	1.50	25.5

Table 7.4 Running clearances based on diameter (cold).

	measured	recommended
Piston skirt	: 0.05 mm	0.015 to 0.055 mm (Honda)
Ring gap		
Top compression	: 0.5 mm	0.5 mm (Honda)
Second compression	: 0.85 mm	0.5 mm (Honda)
Big end	: 0.26 mm	0.059 to 0.089 mm (Glacier)
Side clearance	: 0.88 mm	
Main bearings		
Front	: 0.05 mm	-0.068 to 0.108 mm (Glacier)
Rear	: mm	
Side clearance	:	0.102 to 0.152 mm (Bell)
Gudgeon pin offset	: 1.1 mm	

References

7.1 Taylor, C.F.
The internal combustion engine in theory and practice, Vol. 1.
M.I.T. Press, Massachusetts, 1985.

7.2 Paul, G.R., Billinton, M.A.
Tests on very small four-stroke spark ignition engines.
Instn. Mech. Engrs. International Conference on the Small Spark Ignition Engine, paper C372/017, London, 1989.

7.3 Alkidas, A.C., Cole, R.M.
Heat losses from a divided-chamber diesel engine.
Proc. Instn. Mech. Engrs., Vol. 197C, pp. 151-158, 1983.

7.4 Alkidas, A.C., Cole, R.M.
The distribution of heat rejection from a single-cylinder divided-chamber diesel engine.
SAE paper 810959, 1981.

7.5 Wentworth, J.T.
Piston and ring variables affect exhaust hydrocarbon emissions.
SAE paper 680109, 1968.

7.6 Parker, D.A.
The tribology of automotive components: development of verified predictive design techniques.
Proc. Instn. Mech. Engrs., Vol. 204, pp. 1-19, 1990.

7.7 Daniel, W.A.
Why engine variables affect exhaust hydrocarbon emissions.
SAE paper 700108, 1970.

7.8 Bull, B., Voisey, M.A.
An investigation of the sources of blowby in single-cylinder supercharged diesel engines.
Proc. Instn. Mech. Engrs., Vol. 192, pp. 39-48, 1978.

7.9 Woschni, G.
Prediction of thermal loading of supercharged diesel engines.
SAE paper 790821, 1979.

7.10 Rosenberg, R.C.
General friction considerations for engine design.
SAE paper 821576, 1982.

7.11 Furuhama, S., Takiguchi, M., Tomizawa, K.
Effect of piston and piston ring designs on the piston friction forces in diesel engines.
SAE paper 810977, 1981.

7.12 Armstrong, W.B., Buuck, B.A.
Valve gear energy consumption: effect of design and operating parameters.
SAE paper 810787, 1981.

7.13 Brown, W.L.
The caterpillar imep meter and engine friction.
SAE paper 730150, 1973.

7.14 Kovach, J.T., Tsakiris, E.A., Wong, L.T.
Engine friction reduction for improved fuel economy.
SAE paper 820085, 1982.

7.15 Furuhama, S., Asahi, C., Hiruma, M.
Measurements of piston ring oil film thickness in an operating engine.
ASLE preprint 82-LC-6C-1, 1982.

7.16 Staron, J.T., Willermet, P.A.
An analysis of valve train friction in terms of lubrication principles.
SAE paper 830165, 1983.

7.17 Dyson, A.
Kinematics and wear patterns of cam and finger follower automotive valve gear.
Tribology International, pp. 121-132, June 1980.

7.18 Gish, R.E., McCullough, J.D., Retzloff, J.B., Mueller, H.T.
Determination of true engine friction.
SAE Trans., Vol. 66, pp. 649-667, 1958.

7.19 Fujii, I., Yagi, S., Sono, H., Kamiya, H.
Total engine friction in four stroke S.I. motorcycle engine.
SAE paper 880268, 1988.

7.20 Benson, R.S, Whitehouse, N.D.
Internal combustion engines, Vol. I.
Pergamon Press, Oxford, 1979.

CHAPTER 8 - EMISSIONS

Summary

The influence of operating and design variables on exhaust emission levels is discussed in the context of simple established models describing the main mechanisms of pollutant formation, with the objectives of understanding the experimental data and subsequently evaluating a lean burn strategy.

8.1 Formation of pollutants

The mechanisms governing the formation of atmospheric pollutants are several and complex, measured exhaust concentrations often differing substantially from the concentrations calculated from assumptions of chemical equilibria. The purpose of this section is to detail briefly, simple established models describing the main mechanisms of pollutant formation and observations from previous experimental studies of relevance to this work.

Oxides of nitrogen

Both nitric oxide and nitrogen dioxide are formed within the engine cylinder; exhaust levels of the former around 100 times greater than those of the latter, (8.1). Based on extensive measurement, Lavoie et al., (8.2), concluded that whilst nitric oxide forms within the reaction zone, the levels are negligible in the lean regime and post-flame production predominates. It was also concluded that the formation and decomposition of nitric oxide in the post-flame gases are rate limited, and due to the temperature gradient within the engine cylinder a nitric oxide concentration gradient is also present. Additionally, it was shown that the nitric oxide concentration freezes early in the expansion stroke at values above equilibrium levels and before the other constituents of the combustion products depart appreciably from equilibrium levels. References 1.55 and 8.3, for example, suggest that freezing occurs at temperatures around 2000 K.

The extended Zeldovich mechanism is generally held to describe the significant reactions governing the oxidation of atmospheric nitrogen within the engine cylinder:

$$O + N_2 = NO + N$$

$$N + O_2 = NO + O$$

$$N + OH = NO + H$$

The rate of formation of NO according to the above mechanism follows:

$$\frac{d[NO]}{dt} = k_1^+[O][N_2] + k_2^+[N][O_2] + k_3^+[N][OH] - k_1^-[NO][N] - k_2^-[NO][O] - k_3^-[NO][H] \quad (\text{mol/cm}^3\text{s})$$

where the forward (k_i^+) and reverse (k_i^-) rate constants ($\text{cm}^3/\text{mol.s}$) have been established experimentally. A similar treatment obtains a relationship for the rate of formation of monatomic nitrogen:

$$\frac{d[N]}{dt} = k_1^+[O][N_2] - k_2^+[N][O_2] - k_3^+[N][OH] - k_1^-[NO][N] + k_2^-[NO][O] + k_3^-[NO][H] \quad (\text{mol/cm}^3\text{s})$$

With the assumption that the concentrations of O, O_2, OH, H and N_2 follow chemical equilibria and the concentration of monatomic nitrogen remains essentially unchanged ($\frac{d[N]}{dt} \simeq 0$), the rate of formation of NO can be rearranged:

$$\frac{d[NO]}{dt} = \frac{2R_1\{1 - ([NO]/[NO]_e)^2\}}{1 + ([NO]/[NO]_e)R_1/(R_2 + R_3)}$$

where:

$$R_1 = k_1^+[\text{O}]_e[\text{N}_2]_e = k_1^-[\text{NO}]_e[\text{N}]_e \quad (\text{mol/cm}^3\text{s})$$

$$R_2 = k_2^+[\text{N}]_e[\text{O}_2]_e = k_2^-[\text{NO}]_e[\text{O}]_e \quad (\text{mol/cm}^3\text{s})$$

$$R_3 = k_3^+[N]_e[OH]_e = k_3^-[NO]_e[H]_e \quad (mol/cm^3.s)$$

$[\ ]_e$ denotes the equilibrium concentration.

A further simplification from Reference 2.9 illustrates the dependency of the rate of NO formation. At the initial condition the above relationship reduces to:

$$\frac{d[NO]}{dt} = 2R_1 = 2k_1^+[O]_e[N_2]_e$$

$$[NO]/[NO]_e << 1$$

Using the relationship for the equilibrium monatomic oxygen concentration and substituting for the forward rate constant, k_1^+:

$$\frac{d[NO]}{dt} = \frac{6 \times 10^{16}}{T^{1/2}} \exp\left(\frac{-69,090}{T}\right)[O_2]_e^{1/2}[N_2]_e \quad (mol/cm^3.s)$$

Hence high temperatures and oxygen concentrations favour high rates of NO formation.

Due to compression, early burning elements in the burned gas attain higher temperatures than late burning elements and consequently are richer in NO. Charge inhomogeneity may also ameliorate or enhance the concentration of NO in burned gas elements depending on the local oxygen concentration, (5.15).

Unburned hydrocarbons

Quenching of the flame at the cool cylinder walls or at the entrance to small crevice volumes, absorption and desorption of fuel by deposits or oil layers on the chamber walls and bulk gas quenching in slow burning cycles are the mechanisms thought to influence hydrocarbon emission levels. Since natural gas is inherently a clean-burning fuel and comparative studies with propane-fuelled engines, (8.4), have suggested that the oil layer mechanism is strongly dependent on the solubility of the fuel in the oil, only the quenching mechanisms are considered of significance in this investigation.

The Peclet number, p_e, is useful in understanding the quenching processes at the cylinder walls or at entrances to crevices within the combustion space. It is defined as the ratio of the heat release within the flame to the heat loss to the walls when quenching just occurs.

Reference 2.9 details the following formulation for a pair of parallel plates:

$$p_e = \frac{\rho_u S_l c_{p,f} d_{q2}}{k_f}$$

where d_{q2} is the two-plate quench distance.

For a flame front propagating normally to and parallel with a confining wall:

$$p_e = \frac{\rho_u S_l c_{p,u} d_{q1}}{k_u} \approx 8$$

where d_{q1} is the one-plate quench distance. In spark-ignition engines, typical two-plate quench distances are of the order of 0.2 to 1 mm and one-plate quench distances 0.04 to 0.2 mm.

Exhaust hydrocarbon levels from the piston top-land crevice volume have been found to conform closely with the above mechanism; equal levels measured at zero and 0.2 mm clearance (d_{q2}) with higher levels measured at intermediary values, (8.5).

Bulk gas quenching is promoted by retarded or extended heat-release timing because the cylinder pressure and temperature are lower later in the expansion stroke. These influence the burn rate through the laminar flame speed dependency and can cause the flame to be extinguished. Weak mixture strengths, retarded ignition timing, high levels of residual fraction and exhaust gas recirculation are the conditions where bulk gas quenching is most likely to occur. The condition may vary in severity from partial burning cycles to complete misfire for a few or more slower burning cycles.

It has been established with rapid gas sampling techniques, (4.48) and concluded from theoretical studies, (7.7), that post-combustion

hydrocarbon levels in the engine cylinder preceding blowdown are up to twice the average exhaust concentrations, suggesting the importance of in-cylinder oxidation mechanisms. Sampling of the quench layer has shown that hydrocarbons from this source diffuse into the bulk gas and rapidly oxidise implying an insignificant contribution to the level of unburned hydrocarbons in the exhaust, (4.47). Such conclusions are supported by experiments in high-pressure bombs where unburned hydrocarbons were found to be formed predominantly through the crevice mechanism, (8.6). Substantial oxidation has also been observed in the exhaust system with strong dependency on residence time, oxygen concentration and temperature, (7.7, 8.7).

Based on such observations it may be concluded that post-combustion oxidation is significant and that the crevice and bulk gas quenching mechanisms are probably the dominant sources of exhaust hydrocarbons in this application under normal conditions. Both the oxidation and bulk gas quenching mechanisms are likely to be promoted at the weaker mixture strengths associated with reduced burn rates and excess oxygen, although the oxidation process in these conditions is likely to be inhibited by lower temperatures. It is also to be expected that increased levels of turbulence will both promote oxidation and enhance combustion quality with a positive influence on exhaust levels of unburned hydrocarbons. The oxidation mechanism is attractive from the perspective of emission control.

8.2 Discussion of experimental results

The figures referred to in the following section have been collated from the substantial and detailed experimental data presented in graphical form in Appendix II.

8.2.1 Oxides of carbon

Exhaust gas concentrations of oxygen, carbon monoxide and carbon dioxide are presented in Figures 8.1 - 8.3 against a base of excess air ratio for all the operating conditions investigated. It is evident that the excess air ratio is the predominant variable controlling the level of these exhaust gases. The concentration of carbon monoxide reduces

rapidly from stoichiometric levels to around 0.05 to 0.1% at excess air ratios of 1.1, remaining unchanged to the lean mixture limit. Carbon dioxide reduces from around 9.5% at the stoichiometric air-to-fuel ratio to around 7% at the lean mixture limit. In comparison with petrol fuels of lower hydrogen-to-carbon atomic ratios, where stoichiometric concentrations of exhaust products are of the order of 14%, carbon dioxide emission levels from natural gas-fuelled engines are favourable. Conversely, carbon monoxide levels have been found to be independent of fuel type, (1.5). The presence of carbon monoxide and oxygen at the stoichiometric mixture strength is a consequence of incomplete combustion.

8.2.2 Oxides of nitrogen

Ignition timing

All chambers show a marked dependence on the timing of the spark; around 150 ppm/degree advance for the 3-2 and Hrcc configurations with 75 ppm/degree advance for the TaskII arrangement (see Figure 8.4). In the case of the 3-2 chamber this represents a reduction of 2500 ppm from the most advanced to the most retarded condition. Advanced combustion phasing promotes markedly increased pressures and temperatures as main stage combustion closes progressively to tdc where the volume is smaller; higher NO_x concentration follows from the strong temperature dependency. (The combustion characteristics and predicted burned gas temperatures at these operating conditions were discussed in Section 5.7.3.) Of interest is the relative tolerance to spark advance evident in the TaskII chamber. Although in this case the data are unsupported by pressure analysis, this arrangement operates at a lower compression ratio of 9:1. An equal increment in spark advance has, therefore, a lesser influence on the total volume in the combustion space and hence a lesser effect on burned gas temperatures would be expected.

Compression ratio

Figure 8.5 illustrates the effect of compression ratio at optimum timing on the levels of NO_x in the exhaust. It is evident that the

effect of compression ratio cannot be described simply, contradictory trends are evident at stoichiometric and lean mixture strengths, and phasing with respect to the mixture strength also appears to be a factor. It is probable that the influence of compression ratio setting is augmented by changes in chamber geometry, as discussed in Section 5.7.2, and a strong dependence on the spark timing. In the range of mixture strength of interest in a lean burn strategy (excess air ratios greater than 1.2) NO_x levels in general reduce with reducing compression ratio. The range in NO_x levels with changing compression ratio varies from around 300 to 800 ppm depending on the mixture strength. Whilst this represents a significant proportional increase, particularly at weak mixture strengths where the baseline level is low, the effect of compression ratio is small in light of the effects of ignition timing described above. Understanding of the influence of this design variable would be enhanced with a rate-controlled NO_x formation model and precise measurements of the residual fraction, which is known to reduce with increasing compression ratio and affect NO_x levels in the exhaust through dilution of the charge, (1.57). Despite higher burned gas temperatures which would be expected to follow increases in compression ratio, previous studies, (1.20, 1.21, 1.57), have reported that NO_x levels are only weakly dependent on compression ratio. The latter reference considered the effect of changing geometry to be a contributory factor as the compression ratio changed.

Engine speed

The effect of engine speed on exhaust NO_x levels for various configurations is detailed in Figure 8.6. The speed dependency is evidently complicated by the influence of mixture strength and chamber geometry. Only for excess air ratios greater than around 1.25 is a clear reducing trend with reducing speed apparent for all chambers. The range in NO_x concentration with changes in speed at such mixture strengths is modest, not exceeding 400 ppm and approaching equality at the lean mixture limit. This does however represent a significant proportional change since baseline levels are low. The range in peak NO_x levels is greater but not exceeding around 650 ppm for all the arrangements investigated; the proportional change this represents is diminished with respect to weaker mixture strengths.

Inspection of the peak pressure measurements at operating points where pressure analysis was conducted, does suggest some qualitative correlation with the observed levels of NO_x in the exhaust; this follows since the pressures are indicative of in-cylinder temperatures. Although limited in detail and resolution, comparison is possible over a wide range of operating conditions. Table 8.1 ranks the measurements.

In light of previous studies it is not surprising that the speed dependency cannot be stated simply. Over a similar range of increasing engine speed, NO_x emissions have been found to increase modestly by around 300 ppm at slightly weak mixture strengths and optimum ignition timing, (8.8) and decrease at weak mixture strengths at constant spark timing, (1.56). A contrary trend with rich mixtures was also reported by the latter study.

Furthermore, because the observed speed dependency is small in relation to that of the spark timing, it is difficult to establish the effect of speed alone, particularly when it is noted that a tolerance of about +/-2 degrees is usual for the minimum advance for maximum efficiency. (Over this range engine output remains substantially unchanged.) Such considerations are of most concern around peak NO_x levels where the effect of ignition timing is pronounced in relation to weaker mixtures where little effect, if any, is apparent (refer to Figure II.10 in Appendix II which compares the performance of the 3-2 chamber at the lean mixture limit with significant change in ignition timing or see References 1.52 and 2.2).

Chamber configuration

The effect of chamber arrangement on the levels of NO_x in the exhaust at three speeds is detailed in Figures 8.7 - 8.9. Following slower rates of heat release, markedly lower cylinder pressures and burned gas temperatures, the TaskII arrangement is characterised by significantly lower NO_x emissions. Peak levels are some 700 to 1200 ppm lower when compared with the highest peak level at any speed and reduced levels persist to the lean mixture limit. The relationship between the remaining chambers and NO_x emissions is less clearly defined but does correlate qualitatively with peak cylinder pressures (indicative of

burned gas temperatures) at operating points where pressure analysis was undertaken. Table 8.2 details the comparison.

Excess air ratio

The effect of excess air ratio on the level of NO_x in the exhaust is evidently pronounced and common to all the operating and design conditions investigated. NO_x concentrations rise steeply from stoichiometric mixture strengths to reach a maximum value between excess air ratios of 1.05 to 1.15 and then fall less steeply towards the lean mixture limit. Competition between the temperature and oxygen dependency set the mixture strength for maximum NO_x production. As the preceding discussion suggests, other operating and design variables interact with the excess air dependency, influencing the rate of increase or decrease of NO_x levels with changes in mixture strength and the peak values.

8.2.3 Unburned hydrocarbons

Ignition timing

It is unlikely that the influence of the crevice quench mechanism on unburned hydrocarbon levels in the exhaust will vary significantly with changes in the ignition timing, since the geometry remains unchanged, although the two-plate quench distance is a function of the gas properties and the laminar flame speed. A previous study, (7.7), concluded that the increase in gas density arising from higher pressures at advanced settings promoted only a slight increase in the significance of the crevice mechanism.

A range of burn rates exist on a cycle-to-cycle basis at a given operating point due to mixture inhomogeneity and flow field variations. The optimum spark timing caters for the average cycle; it is retarded in the case of slow burning cycles and advanced with respect to the faster burning cycles. It was established in Section 5.7.3 that retarded ignition timing effects extended burn duration for the mean cycle. In comparison to the advanced condition, later and longer burn durations are most likely to promote bulk gas quenching and increase

hydrocarbon levels. On the other hand, the significance of post-combustion oxidation, although unknown, is likely to be most marked at retarded spark timing where the in-cylinder temperatures late in the expansion stroke are the highest.

Since the residual fraction has been found insensitive to changes in spark timing, (1.57), the significance of bulk gas quenching is unlikely to be influenced by this mechanism as the timing of the spark advances.

Figure 8.4 shows the effect of ignition timing on the three chambers investigated; optimum timing is at 25 degrees advance for the TaskII and 3-2 chambers and 22 degrees advance for the Hrcc arrangement. Both the TaskII and Hrcc configurations are characterised by an upturn in exhaust hydrocarbon emission levels at the retarded and advanced conditions, suggesting an interplay between the bulk gas quenching and post-combustion oxidation mechanisms. It is probable, at the retarded settings, that enhanced post-combustion oxidation is unable to maintain equilibrium with increasing hydrocarbons from quenching, whereas at advanced spark timings where quenching is less likely, the influence of oxidation also diminishes.

A contrary trend is noted for the 3-2 chamber where unburned hydrocarbon levels diminish with retarded ignition. Inspection of the pressure analysis data (see Tables 5.5 - 5.6) shows that although the burn duration reduces with advancing ignition in keeping with the Hrcc, in contrast, the duration of the latter stage of combustion (50 to 90% mass consumed) increases, and the crankangle at which this portion of heat release commences closes to tdc where the chamber depth is of the order of 5 to 6 mm (see Figure 5.27). This suggests that excessive wall quenching and hence high hydrocarbon levels are promoted at advanced ignition settings with this chamber. Thus it would appear that chamber geometry, bulk gas quenching and post-combustion oxidation are influencing the levels of exhaust hydrocarbons in the 3-2 chamber. Further discussion of such geometrical effects is included in Sections 5.7.2 and 5.7.3.

Compression ratio

Unburned hydrocarbon levels in the exhaust increase steadily with increasing compression ratio while the significance of compression ratio setting increases as the mixture weakens (see Figure 8.5). At near stoichiometric air-to-fuel ratios the spread in hydrocarbon levels is around 550 ppm over the range of compression ratio settings and at the lean mixture limit the spread has increased to around 1200 ppm. Since crevice volumes account for a greater proportion of the chamber volume as the compression ratio increases and the surface area-to-volume ratio is greater, it might be expected that levels of unburned hydrocarbons in the exhaust increase with increasing compression ratio, all other factors being equal. It was evident from the pressure analysis (see Section 5.7.2 and Tables 5.3 - 5.4) that retarded combustion-crankangle phasing together with reduced rates of heat release ensued through compression ratio increase. It is also probable therefore, that the bulk gas quenching mechanism increases in significance with increasing compression ratio and contributes to the level of hydrocarbon emissions, since this mechanism is promoted by lower cylinder pressures and temperatures occurring later in the expansion stroke. The extent of in-cylinder and exhaust hydrocarbon oxidation as an ameliorating factor in the above mechanisms is however unknown as the compression ratio increases. Similarly, a lesser, but unknown, influence from the residual fraction on the bulk gas quenching mechanism would be anticipated with increases in the compression ratio setting.

Engine speed

In general, for all the configurations investigated, the levels of exhaust hydrocarbons diminish from 25 to 30 rev/sec and then increase from 30 to 35 revs/sec (see Figure 8.10). The speed effect is evidently further complicated by the influence of the excess air ratio; at near stoichiometric mixture strengths and the lean mixture limit the speed dependency is noted to change for all chambers.

These data are puzzling in light of previous investigations (see for example References 7.5, 7.7 and 8.8) where modest reductions in exhaust

hydrocarbon levels over a similar range of increasing speed have been reported. In these studies, the influence of speed on hydrocarbon levels has been attributed largely to a reduced contribution from the crevice mechanism, (7.7 and 8.5). The latter study suggests that this arises from a reduction in the piston top-land crevice volume under the influence of higher in-cylinder temperatures. Furthermore, as the speed increases, enhanced turbulence, lower levels of residuals and higher in-cylinder temperatures during combustion would be expected to reduce the influence of bulk gas quenching. It is also to be expected that enhanced turbulence and greater temperatures will promote oxidation, although the residence time is shorter.

Noting the contrast between the observed performance with increasing speed and the expected positive influence on exhaust unburned hydrocarbon levels of all these factors (excluding the residence time) it is possible that the effect of crankcase blowby is an additional contributory factor. This is suggested by the strong speed dependency noted for this engine in Section 7.5, the influence of this variable on unburned hydrocarbon levels reported in Reference 7.5 and the fact that the observed performance is common to all chambers.

Chamber configuration

The effect of chamber arrangement on the levels of unburned hydrocarbons in the exhaust is detailed in Figures 8.7 - 8.9. At all speeds the TaskII configuration benefits from the lowest levels, although a rapid upturn is noted at the lean mixture limit at the lower speed through rapidly deteriorating combustion quality (see Table 5.10). Recognising the influence of compression ratio on hydrocarbon emissions (referred to in the earlier section) and the similarity of the performance of the TaskII chamber with the 3-2 configuration at an equal setting of 9:1, suggests that the lower emission levels arise from a compression ratio effect.

Despite the significantly faster rates of heat release and enhanced combustion stability promoted by the Hrcc arrangement (see for example Tables 5.13 - 5.15 comparing rates of combustion at stoichiometric conditions between chambers), the difference in levels of hydrocarbon

emissions is slight when compared with the 3-2 chamber (excluding weaker mixture strengths at the lower speed where the former configuration is effective in reducing levels by around 500 ppm). Such results are difficult to interpret in light of the available data, since the conditions least favourable to bulk gas quenching occur with rapid, stable and advanced heat release where temperatures are high late in the combustion process. On the other hand, extended and retarded heat release promotes bulk gas quenching, but also higher temperatures late in the expansion and early in the exhaust stroke make oxidation more likely. From a geometric viewpoint it is unlikely that the crevice mechanism predominates with either configuration, although changes in the gas properties and laminar flame speed may influence the two-plate quench distance and mass of charge entering the crevices. It is also unlikely that there are significant differences between the residual fraction when comparing these chambers, by noting the similarity of the relevant operating and design variables known to influence this quantity. These include changes in manifold and exhaust pressures, air-to-fuel ratio, speed, valve timing, compression ratio and volumetric efficiency, (1.57). In the case of the Hrcc arrangement, predicted temperatures at exhaust valve opening are lower (see Figures 7.12 - 7.14) and the measured time-averaged exhaust temperatures are markedly lower (see Figures II.2 - II.19 in Appendix II) suggesting the tentative conclusion that the observed levels of exhaust hydrocarbons result through competition in each chamber between the bulk gas quenching and oxidation mechanisms.

Excess air ratio

For all the conditions investigated, unburned hydrocarbons rise steeply from minima at excess air ratios between 1.1 to 1.25 as the mixture strength is enriched or weakened. This is thought to arise primarily through competition between the influences of temperature and oxygen concentration on the bulk gas quenching and oxidation mechanisms, (2.9). Reference 7.7 also emphasises the importance of the crevice mechanism with weakening mixture strengths since it was concluded that around 25 - 50% of the exhaust hydrocarbons arise from this source and the fuel density within the crevices diminishes as the excess air ratio increases. As discussed in previous sections, other operating and

design variables interact with the excess air dependency, which can strongly influence hydrocarbon levels as the mixture strength is varied.

8.3 Conclusions

Carbon monoxide can be maintained below 0.1% over a wide range of operating conditions provided the excess air ratio is greater than 1.1. A useful reduction in CO_2 levels can be achieved with weak mixture operation. Stoichiometric CO_2 emissions in natural gas-fuelled engines are around two thirds those of petrol-fuelled engines.

Effect of ignition timing

Peak NO_x levels are strongly dependent on spark timing, the dependency is most notable with the rapid burning chambers at around 150 ppm/degree advance. There is considerable scope for emission control with retarded ignition setting.

In the absence of unfavourable geometric effects, exhaust hydrocarbon levels are lowest at optimum spark timings, although several degrees of spark retard can be tolerated without undue effect on hydrocarbon emission levels; in the case of the Hrcc, around + 50 ppm/degree retard. Noting the dependence of NO_x on spark timing (- 150 ppm/degree retard) a larger reduction in this pollutant can be achieved through retarded timing than the corresponding increase in unburned hydrocarbons.

Effect of compression ratio

The effect of compression ratio setting on the levels of NO_x is small in light of the influence of spark timing; it is most marked at weak mixture strengths where relatively small absolute increases are significant because the baseline level is low. A clear relationship between NO_x levels and compression ratio setting is not in evidence. This is thought to be a result of changing combustion chamber geometry and the strong influence of spark timing; further understanding would benefit from a more rigorous theoretical base. A careful choice of

compression ratio setting is implied from the perspective of a lean burn strategy since NO_x levels, in general, diminish with reducing compression ratio in the weak regime.

A lower compression ratio is effective in reducing unburned hydrocarbon emissions and is of increasing influence as the mixture weakens. A lean burn strategy therefore favours a low compression ratio.

Effect of engine speed

The effect of speed on NO_x production is complicated by the influence of mixture strength and chamber geometry. Over the range of excess air most attractive to a lean burn strategy, the levels of NO_x in the exhaust diminish with reducing speed for all the chambers investigated; a slow running engine is implied. From the stoichiometric mixture strength to an excess air ratio of around 1.25, the geometry of the combustion chamber and the air-to-fuel ratio influence the level of NO_x and no clear speed dependency is evident. The magnitude of the speed effect is small in relation to that of the spark timing. Further understanding of the processes involved would be enhanced by a rate-controlled NO_x model with positive effect on the design process and predictive capability.

Given the complexity of the processes involved and the interaction between them, it is doubtful, even with additional and substantial experimental data, that a complete understanding of the influence of speed on unburned hydrocarbon levels could be achieved and consequently more general conclusions are appropriate. Over the range of likely operating conditions between the upturn in emission levels at the stoichiometric mixture strength and the lean mixture limit and in the absence of excessive crankcase blowby, exhaust hydrocarbons reduce with increasing speed. A higher speed is implied for a lean burn strategy.

The effect of chamber geometry

Solely on the basis of reducing the levels of exhaust NO_x, a slow burning chamber is most effective. Under such conditions however, a thermally efficient engine is unlikely. In comparison with the 3-2

arrangement, the Hrcc configuration offers a compromise between high thermal efficiency - implied by rapid combustion - and lower levels of NO_x in the envelope of conditions encompassing weaker mixture strengths and slow speed.

When compared with the 3-2 chamber, the faster burning and most stable Hrcc configuration is effective in reducing unburned hydrocarbon emissions at low speed but has negligible effect at the higher speeds.

The effect of mixture strength

There is considerable scope for reducing NO_x emissions through weakening mixture strength. Enhanced rates of combustion and extended stable lean mixture operation suggest the Hrcc is most suited to this type of emission control.

Minimal unburned hydrocarbon emissions occur at excess air ratios of around 1.1 to 1.25, increasing as the mixture is enriched or weakened. From the perspective of a lean burn strategy a compromise between NO_x and unburned hydrocarbon levels is indicated since minimum unburned hydrocarbons occur around the mixture strength for maximum NO_x production and the latter reduces as the former increases with weakening mixtures.

In light of the evidence for substantial post-combustion oxidation cited in this chapter, after-burning may have potential for further reductions in unburned hydrocarbons, particularly at weak mixture strengths where free oxygen is available. Low exhaust temperatures suggest some form of additional heat input which does have the disadvantage of extra complexity in usual engine applications; however, with reclaimed heat a primary concern, some modification to an existing exhaust heat exchanger may be possible. It may prove attractive, in circumstances where the heating load is low or where heat only is required from CHP units, to incorporate such a function.

Also, the evidence cited (References 4.48 and 7.7) for the predominance of crevice unburned hydrocarbons in the exhaust, suggests the importance of detailed attention to mechanical tolerances and possibly

revisions to the design of the piston around the top-land and areas surrounding other crevices such as the spark plug threads, head gasket etc.

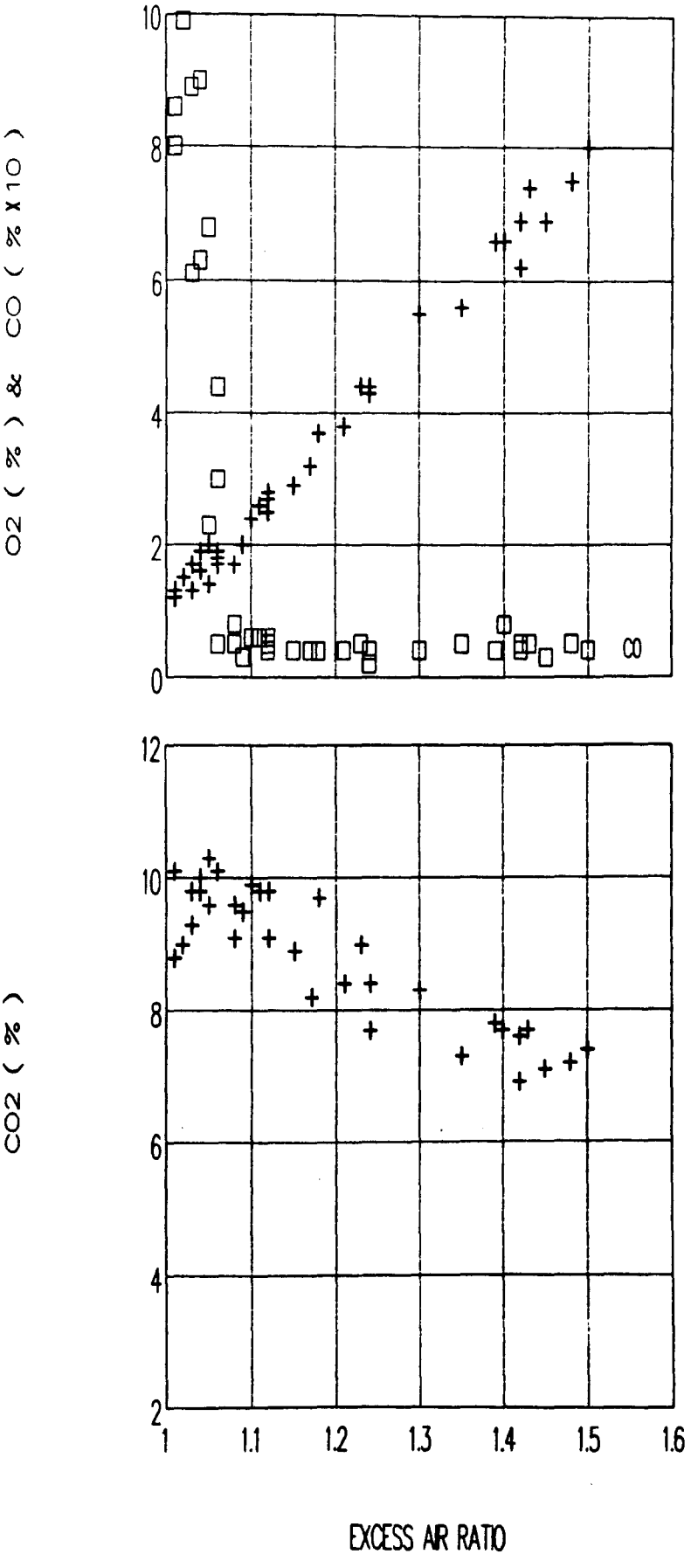

Figure 8.1 Exhaust concentration of oxides of carbon and oxygen for the TaskII chamber under all operating conditions.

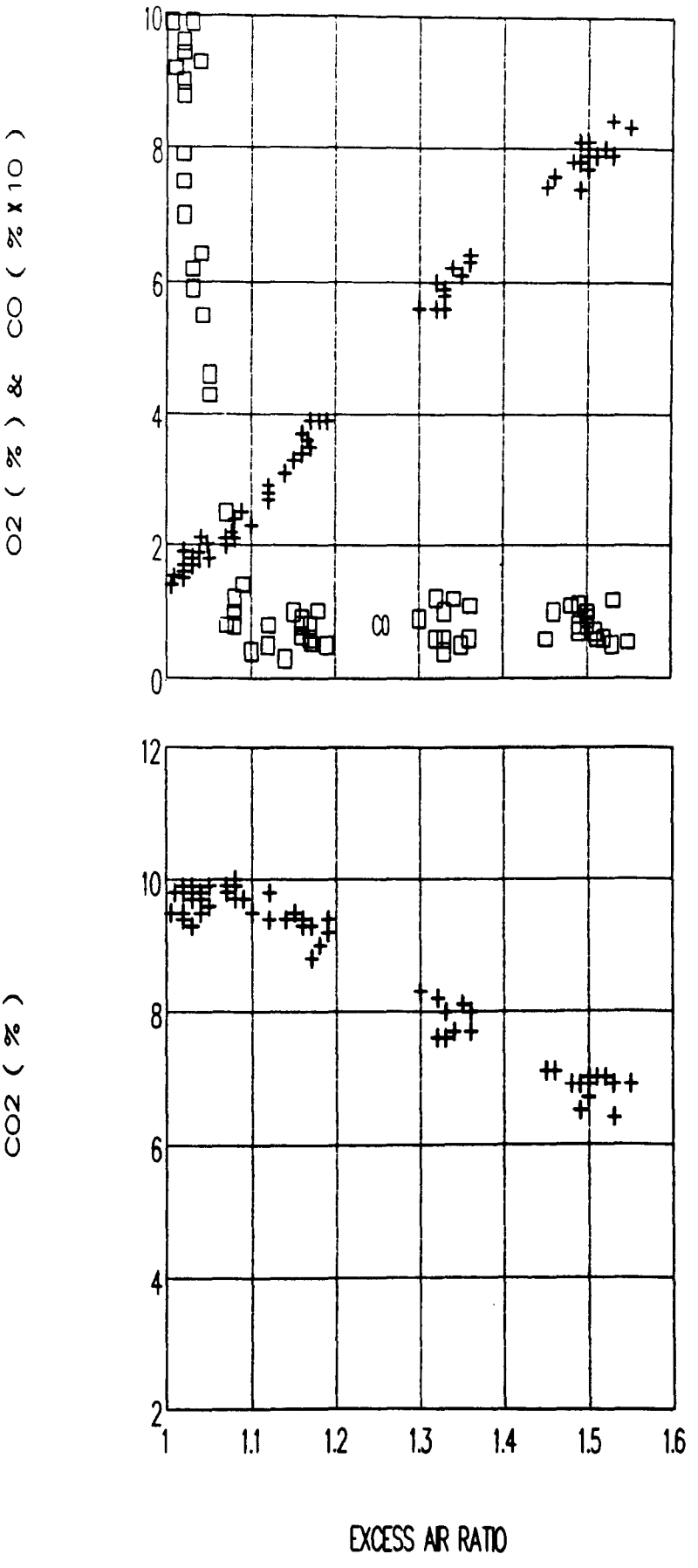

Figure 8.2 Exhaust concentration of oxides of carbon and oxygen for the 3-2 chamber under all operating conditions.

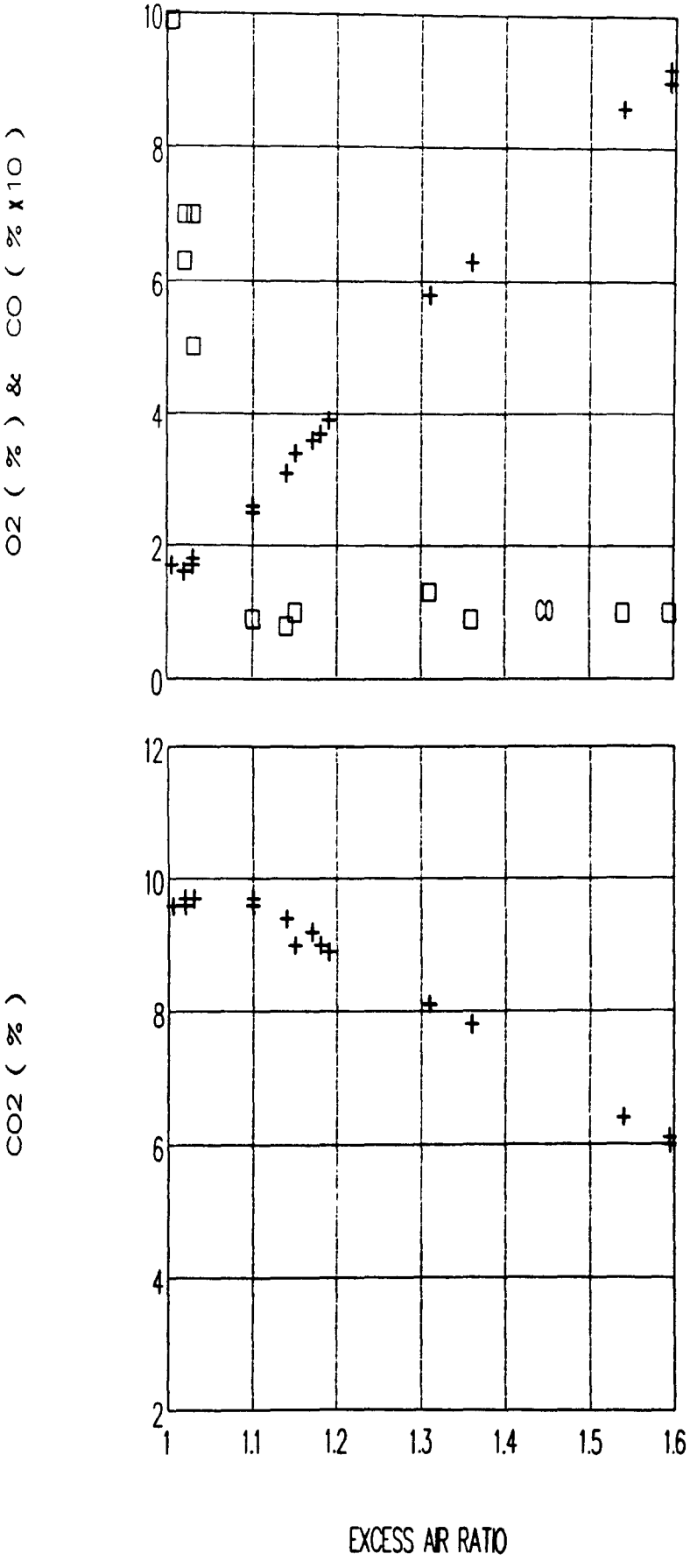

Figure 8.3 Exhaust concentration of oxides of carbon and oxygen for the Hrcc under all operating conditions.

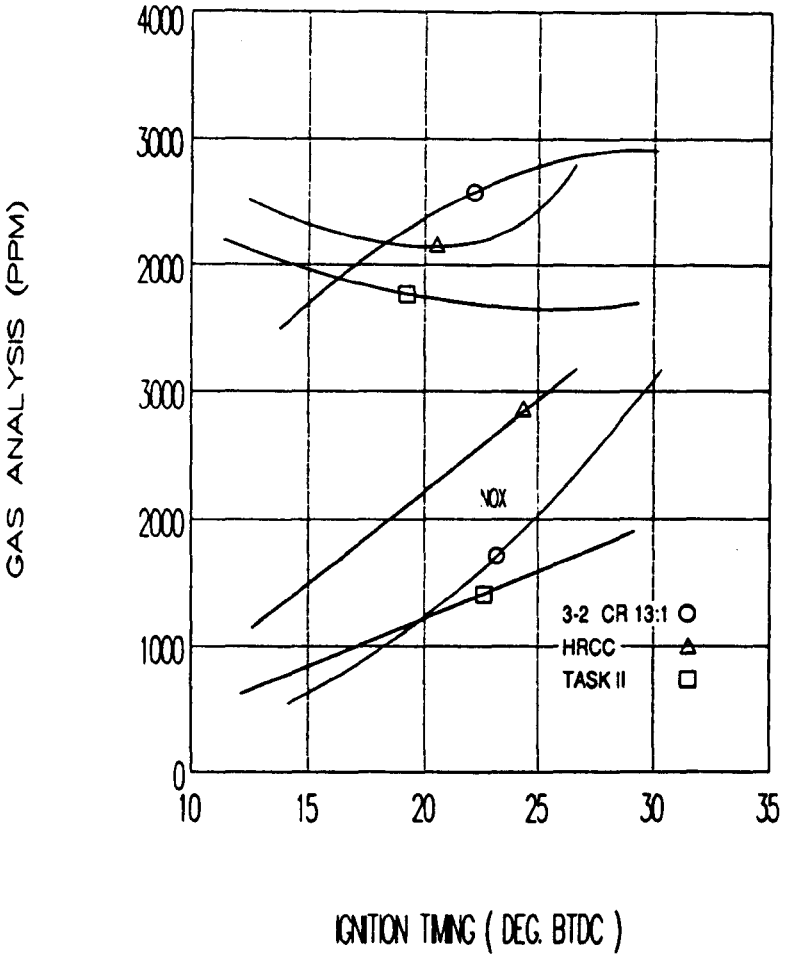

Figure 8.4 The influence of ignition timing on the exhaust concentration of oxides of nitrogen and unburned hydrocarbons for three chambers. Excess air at 1.2, 1800 rpm.

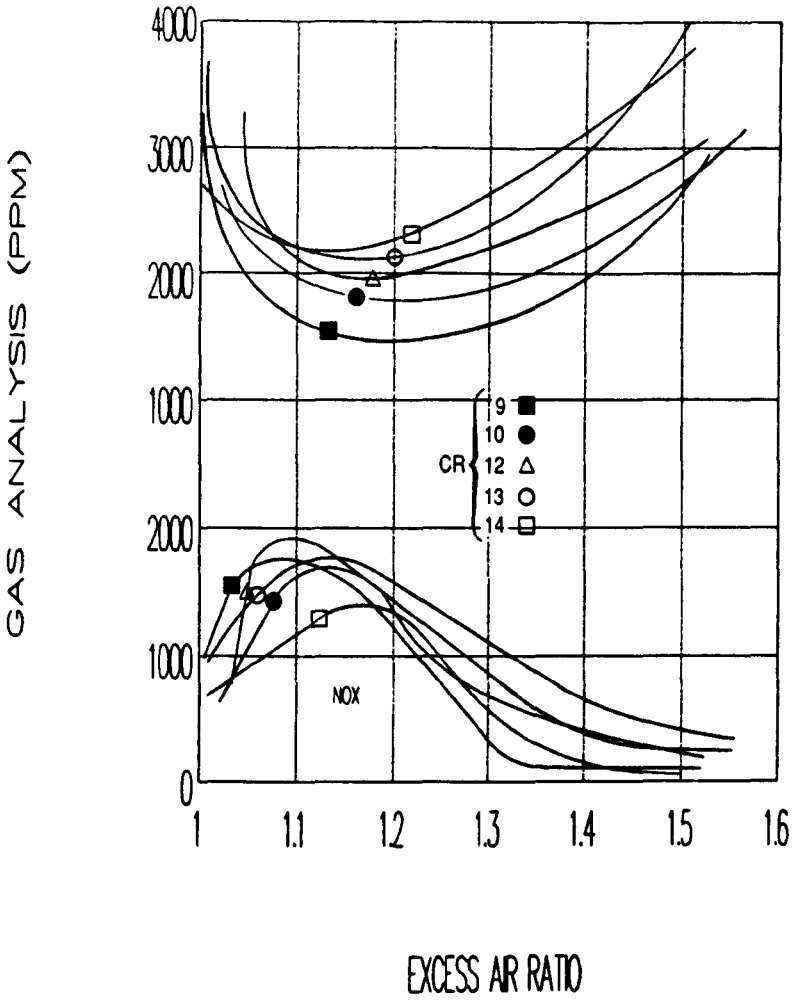

Figure 8.5 The influence of compression ratio on the exhaust concentration of oxides of nitrogen and unburned hydrocarbons for the 3-2 chamber, 1800 rpm.

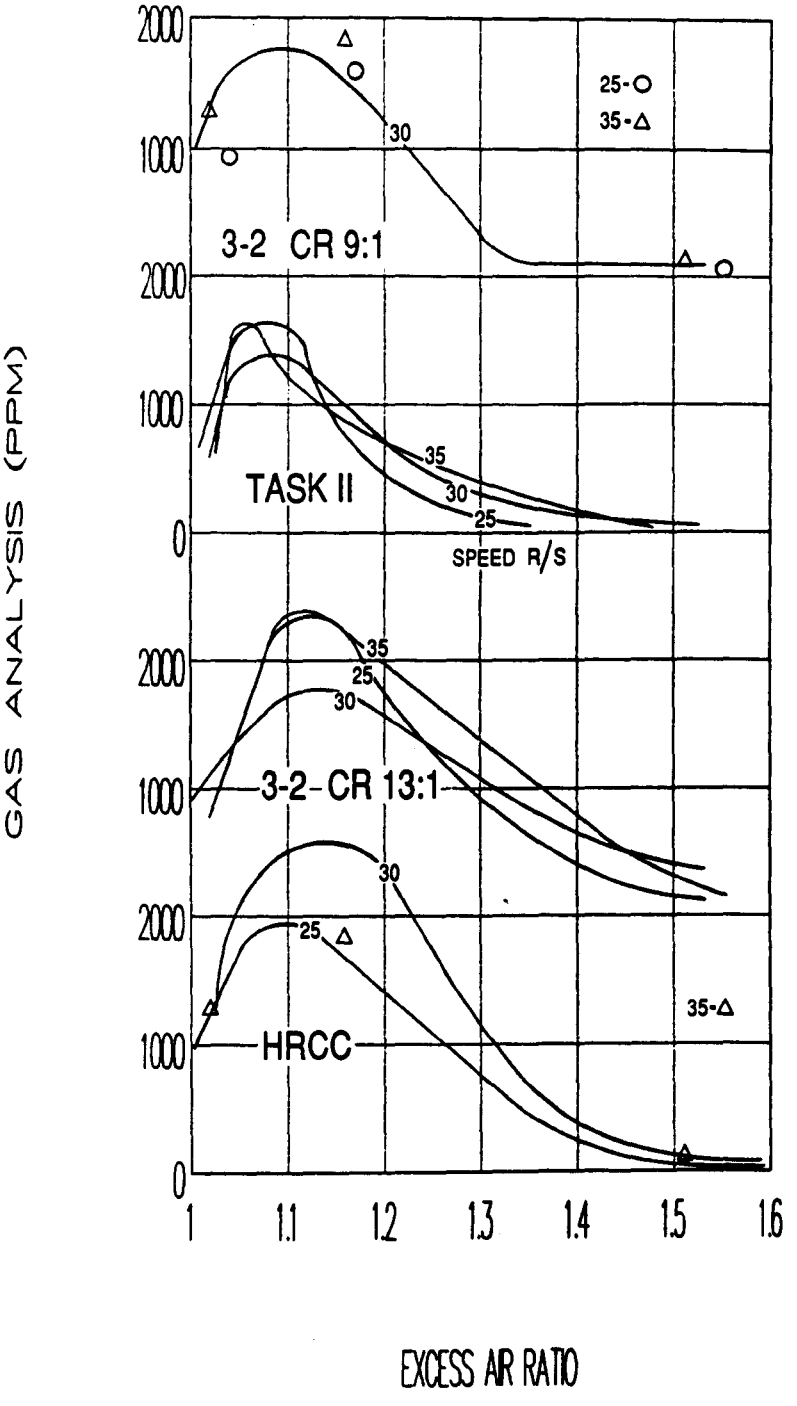

Figure 8.6 The influence of engine speed on the exhaust concentration of oxides of nitrogen for various chambers.

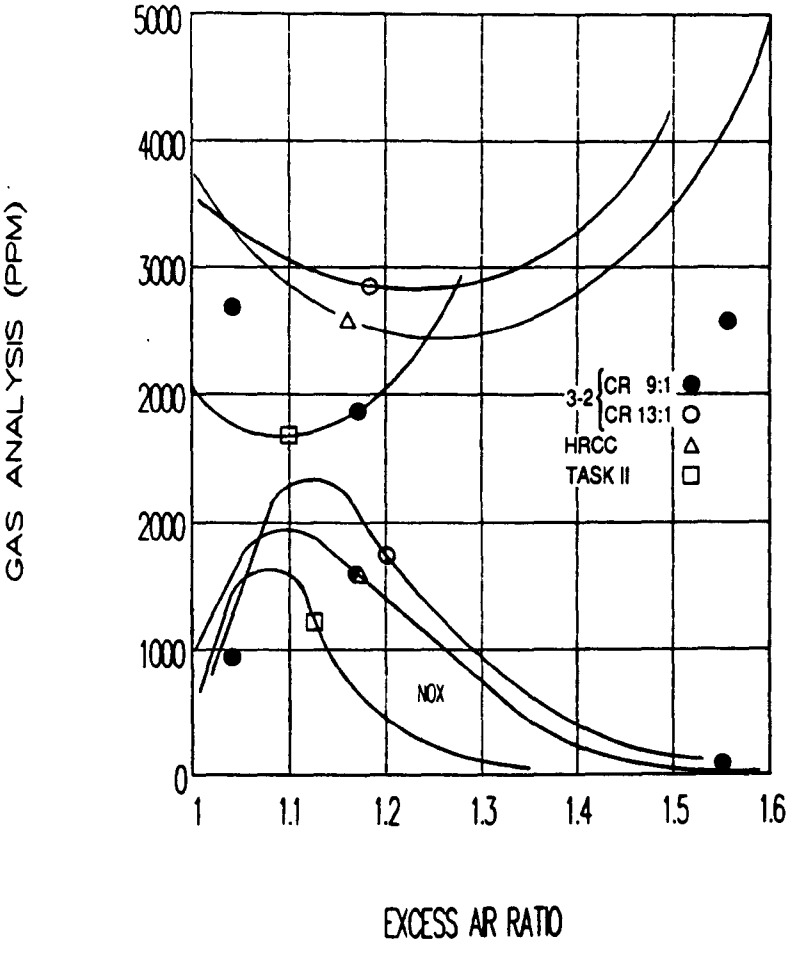

Figure 8.7 The influence of chamber arrangement on the exhaust concentration of oxides of nitrogen and unburned hydrocarbons at 25 r/s. (Points only- 3-2 at 9:1)

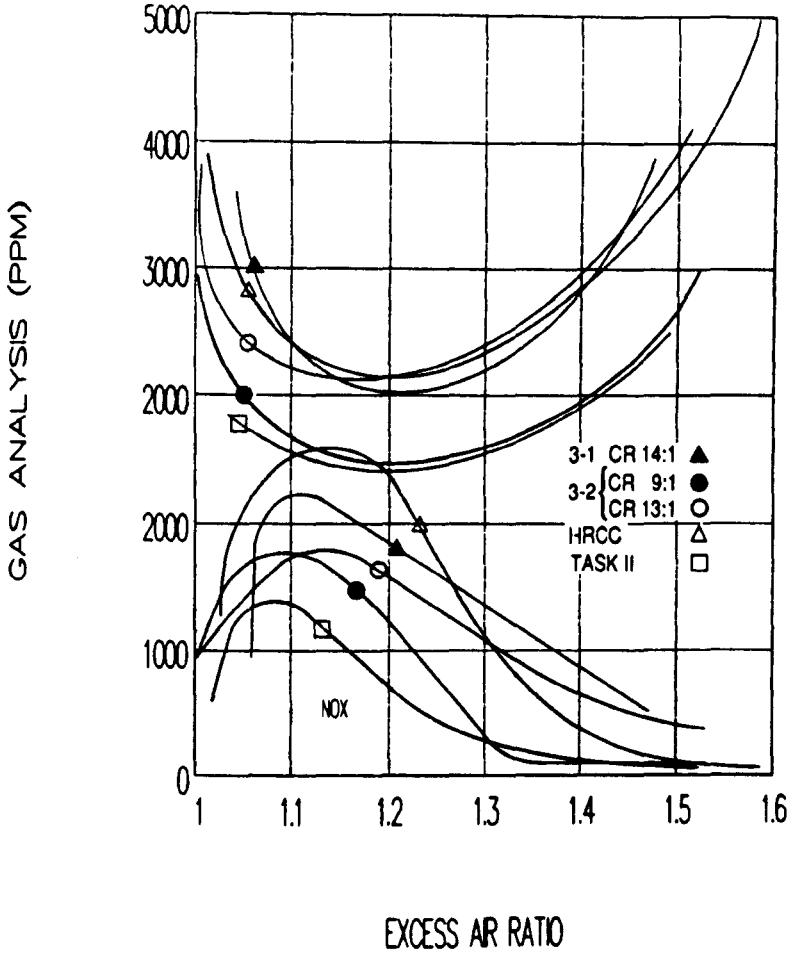

Figure 8.8 The influence of chamber arrangement on the exhaust concentration of oxides of nitrogen and unburned hydrocarbons at 30 r/s. (3-1: engine only unit, results from preliminary study, reference 1.30).

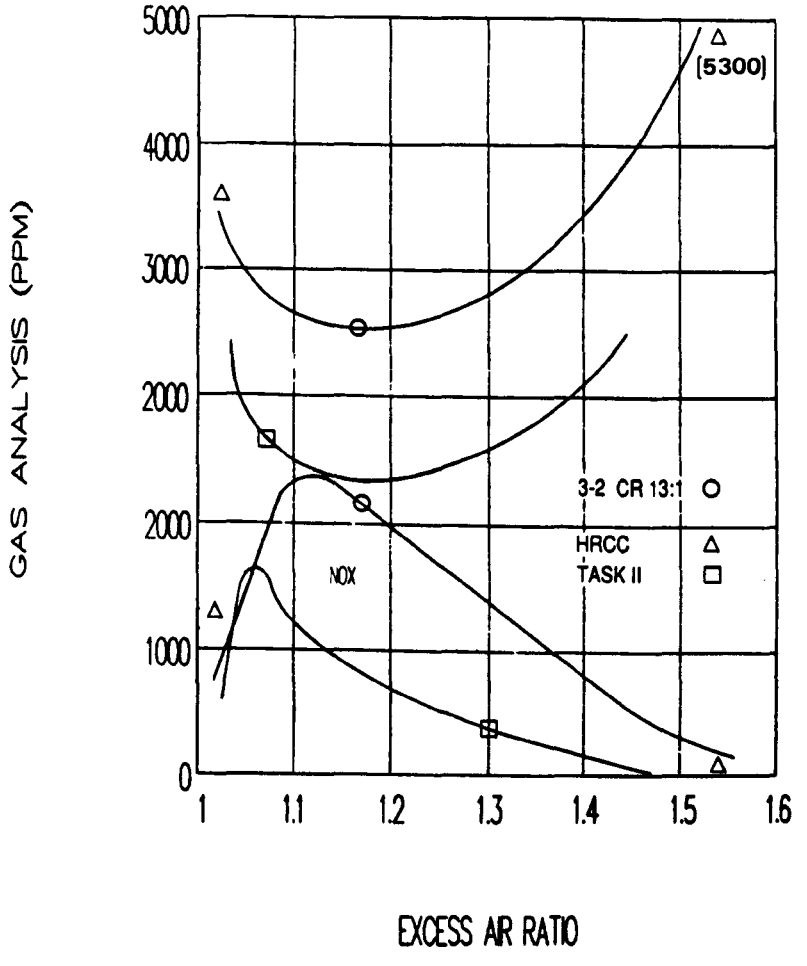

Figure 8.9 The influence of chamber arrangement on the exhaust concentration of oxides of nitrogen and unburned hydrocarbons at 35 r/s.

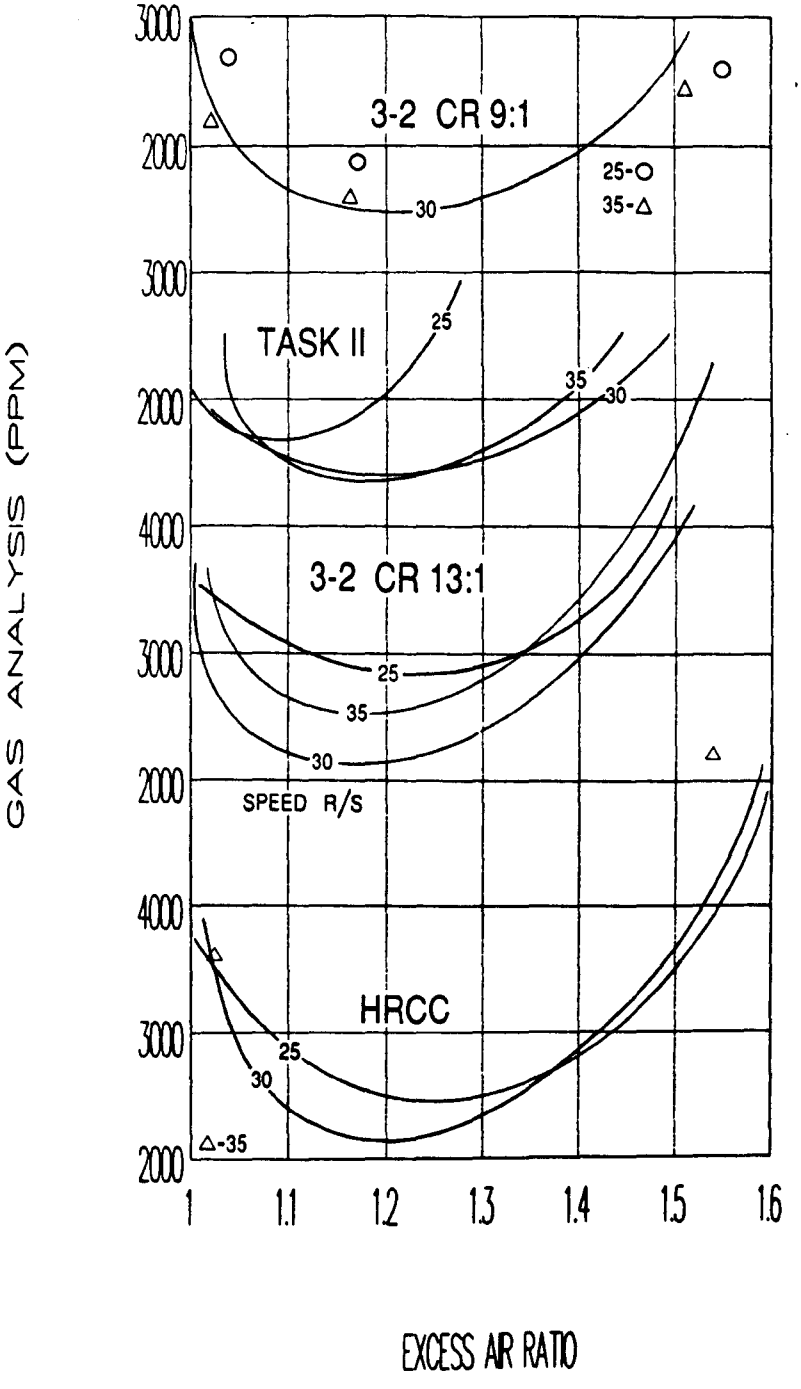

Figure 8.10 The influence of engine speed on the exhaust concentration of unburned hydrocarbons for various chambers.

Table 8.1 Qualitative comparison of exhaust NOx and peak cylinder pressures, the effect of engine speed. Variables are ranked in descending order, 1 to 3.

Chamber: 3-2 Cr: 13:1 Excess air: 1.17

Fil	Speed (rev/sec)	NOx	Pmax
46	25	2	2
41	30	3	3
49	35	1	1

Chamber: 3-2 Cr: 13:1 Excess air: 1.50

Fil	Speed (rev/sec)	NOx	Pmax
47	25	3	3
40	30	1	1
1	35	2	2

Chamber: Hrcc Cr: 13:1 Excess air: 1.03

Fil	Speed (rev/sec)	NOx	Pmax
11	25	2	2
9	30	1	1

Chamber: Hrcc Cr: 13:1 Excess air: 1.62

Fil	Speed (rev/sec)	NOx	Pmax
14	25	2	2
10	30	1	1

Table 8.2 Qualitative comparison of exhaust NOx and peak cylinder pressures, the effect of chamber. Variables are ranked in descending order, 1 to 3.

Speed: 25 rev/sec Cr: 13:1 Excess air: 1.04

Fil	Chamber	NOx	Pmax
45	3-2	2	2
11	Hrcc	1	1

Speed: 30 rev/sec Cr: 13:1 Excess air: 1.03

Fil	Chamber	NOx	Pmax
39	3-2	1	1
9	Hrcc	1	1

Speed: 30 rev/sec Cr: 13:1 Excess air: 1.17

Fil	Chamber	NOx	Pmax
41	3-2	2	2
15	Hrcc	1	1

References

8.1 Hilliard, J.C., Wheeler, R.W.
Nitrogen dioxide in engine exhaust.
SAE paper 790691, 1979.

8.2 Lavoie, G.A., Heywood, J.B., Keck, J.C.
Experimental and theoretical study of nitric oxide formation in internal combustion engines.
Combust. Sci. Technol., Vol. 1, pp. 313-326, 1970.

8.3 Annand, W.J.D.
Calculation of nitric oxide and carbon monoxide concentrations in spark-ignition engines.
Proc. Instn. Mech. Engrs., Vol. 188 41/74, pp. 431-436, 1974.

8.4 Kaiser, E.W., LoRusso, J.A., Lavoie, G.A., Adamczyk, A.A.
The effect of oil layers on the hydrocarbon emissions from spark-ignited engines.
Combust. Sci. Technol., Vol. 28, pp. 69-73, 1982.

8.5 Haskell, W.W., Legate, C.E.
Exhaust hydrocarbon emissions from gasoline engines - surface phenomena.
SAE paper 720255, 1972.

8.6 Adamczyk, A.A., Kaiser, E.W., Cavolowsky, J.A., Lavoie, G.A.
An experimental study of hydrocarbon emissions from closed vessel explosions.
Proceedings of Eighteenth International Symposium on Combustion, The Combustion Institute, pp. 1695-1702, 1981.

8.7 Nakagawa, Y., Etoh, Y., Maruyama, R.
A fundamental analysis of HC and CO oxidation reaction in the exhaust system.
JSAE Rev., No. 1, pp. 98-106, 1978.

8.8 Lavoie, G.A., Blumberg, P.N.
A fundamental model for predicting fuel consumption, NOx and HC emissions of the conventional spark-ignited engine.
Combust. Sci. Technol., Vol. 21, pp. 225-258, 1980.

CHAPTER 9 - FLOW

Summary

The utility of valve discharge and swirl data is outlined briefly, together with the limitations of steady state flow analysis. The objectives of the study and the experimental facility are described. The performance of the three chambers is discussed with reference to previous studies and the implications for volumetric efficiency are considered with reference to the measured values.

Introduction

Steady state flow apparatus is extensively used in the design process for the measurement of valve discharge and swirl coefficients due to simplicity in comparison with direct measurements from an engine. Such data have been used to evaluate and optimise induction systems following the comparative testing of various configurations or as input to flow or closed cycle thermodynamic models.

An immediate objection to this method of investigation is that flow dynamic and pressure characteristics or the swirl profile are not represented; swirl is also modified during the compression process (this latter point was referred to in Sections 1.8 and 4.2.1). Since only comparative testing was undertaken, these issues are beyond the scope of this work. It is of interest to note that numerous studies discussed in Uzkan et al., (9.1), have concluded that steady state flow discharge coefficients are able to predict dynamic performance over the normal engine speed range with reasonable accuracy.

Objectives

The scope of this work extended only to comparative measurements of swirl and valve discharge coefficients for the three configurations at a baseline condition, with the objectives of evaluating the design and eliminating the effects of these variables from the initial stages of the experimental programme. It was envisaged, particularly in view of the lean burn strategy, that the study should eventually include some

investigation into the swirl since this has been found effective in promoting burn rates (see Section 1.8). Accordingly, some features were incorporated in the Hrcc design and a number of perspex prototypes produced so the effect of this parameter could be investigated independently. However, as the programme proceeded it became clear that there was insufficient time available to conduct this work.

Experimental facility

Following Partington, (9.2) and Uzkan et al., (9.1), a steady state flow rig was produced (see Figure 9.1) which consists of a perspex tube with the bore diameter equal to that of the cylinder on the Task engine. At one end of the tube a plate is incorporated which allows the mounting of a port/combustion chamber configuration in a position corresponding to its actual position on the engine. At a distance of approximately 1.5 times the bore diameter downstream from the cylinder head face, the tube widens to contain an aluminium honeycomb with small cells of large aspect ratio, capable of straightening the flow completely. The other end of the tube supports a longitudinal shaft running in low friction bearings on which the honeycomb is mounted. The widening of the bore has been found necessary in order to reduce blowby.

Compressed air is supplied to the port through a diaphragm type pressure regulator and pressure box which provides a constant, but adjustable, pressure differential between the inlet port and cylinder. The angular momentum of the flow produced by the port exerts a torque on the honeycomb which is restrained by a cantilevered beam and link arrangement attached to the longitudinal shaft. Valve lift is varied by a threaded adjuster on the end of the valve stem. The flow straightener and tube are easily replaced for measurements of the valve flow coefficients.

Experimental methodology

A pressure differential of 2.5 kPa was maintained between the port inlet and cylinder. For valve discharge measurements, the valve lift was increased incrementally from the minimum to the maximum value and

measurements of pressure, temperature and volume flow rate obtained at the collector together with the upstream stagnation and static pressures at the valve. The procedure was repeated for each configuration and for the measurement of swirl, where additionally, the load at the torque arm was noted. Software was developed to process the results and produce graphical and tabulated output. Calibration procedures are detailed in Appendix IV.

Flow area and swirl coefficient definition

Three distinct stages of minimum flow area development have been noted with increasing valve lift, (9.3). The flow coefficient is defined in terms of, and is inseparable from, an arbitrary reference area which may be the minimum flow area or some other characteristic area such as that of the valve curtain (valve circumference times valve lift), valve head, or valve port.

The swirl-generating capabilities of the port/valve arrangements are measured by a dimensionless parameter, the swirl coefficient. The several definitions which are used for impulse-type meters have been reviewed and related through a series of expressions developed by Uzkan et al., (9.1). In order that the experimental data were readily comparable with published work, the flow area and swirl coefficient definitions were consistent with those of Reference 9.1. The flow area was based on the geometrical minimum area of flow corresponding to small values of L/d ratios (typically less than 0.125) according to:

$$A_f = \pi d_v L(1 + L/d_v \sin\phi\cos\phi)\cos\phi$$

The swirl coefficient was defined according to:

$$C_s = T_q/(\dot{m} v_{is} B/2)$$

Discussion of experimental results

The flow and swirl coefficients for the configurations investigated are illustrated in Figure 9.2. Low swirl is evident for all configurations, with slight increases noted at higher lifts for the 3-2 and Hrcc arrangements, consistent with the tangential orientation of the inlet

tract in these designs. Typical high swirl ports produce swirl numbers considerably in excess of these values at around 0.25 for L/d ratios of 0.25, (9.1, 9.2). No significant variation between geometries is evident for the valve flow coefficients, the small reduction for the Hrcc at higher lifts in keeping with the slight increase in swirl observed. The peak value of around unity at L/d ratios of about 0.04 is consistent with other observations, (9.1).

Volumetric efficiency

The measured volumetric efficiencies (see Appendix II) reflect the implications of the flow coefficients, with similar values noted for all chambers. At stoichiometric mixture strengths, a small range from 86 to 90% is evident for all operating and design variables with a slight but consistent increase of around 5 percentage points noted as the excess air ratio increases towards the lean mixture limit. Such a dependency with weakening mixtures is reported in Reference 7.1 for gas-fuelled engines and probably reflects lower in-cylinder and residual gas temperatures at leaner air-to-fuel ratios.

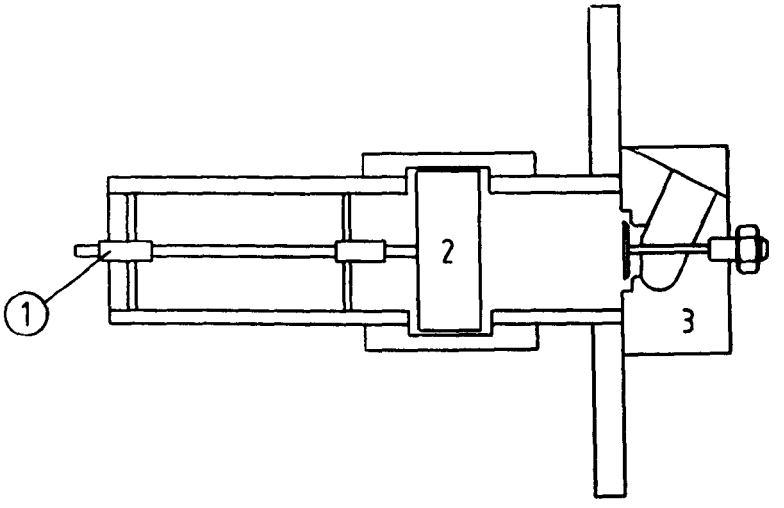

1. Low friction bearings
2. Aluminium honeycomb
3. Inlet port/combustion chamber configuration

Figure 9.1 Steady state flow rig.

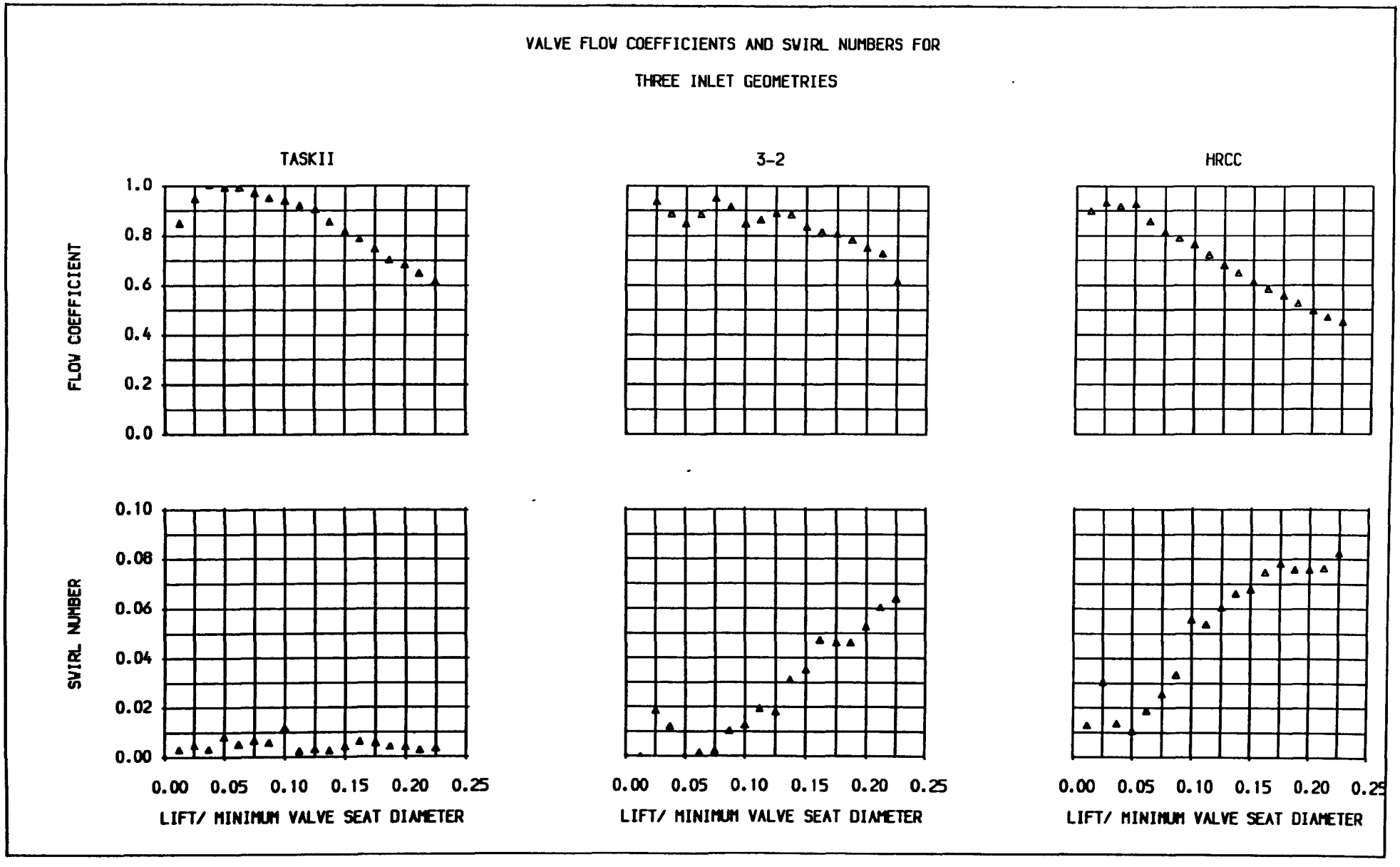

Figure 9.2 Valve flow coefficients and swirl numbers for three inlet geometries.

References

9.1 Uzkan, T., Borgnakke, C., Morel, T.
Characterisation of flow produced by a high swirl inlet port.
SAE paper 830266, 1983.

9.2 Partington, G.D.
Development and application of a fully machined helical inlet port for high speed DI engines.
Instn. Mech. Engrs., paper C121/82, 1982.

9.3 Kastner, L.J., Williams, T.J., White, J.B.
Poppet inlet valve characteristics and their influence on the induction process.
Proc. Instn. Mech. Engrs., Vol. 178, Pt. 1, No. 36, pp. 955-975, 1963-64.

CHAPTER 10 - CONCLUSIONS

The following chapter outlines the main conclusions drawn. Further detail is presented at the closure to preceding chapters and in the summaries of Chapter 5.

10.1 Parametric tests

A parametric investigation of the performance of the engine over a wide range of operating and design variables, consistent with an envelope of conditions appropriate to a lean burn strategy, has produced a wealth of original benchmark data with respect to rates of heat release, energy flows and emission levels.

Diminishing rates of heat release arising through weakening mixture strengths are appreciably ameliorated using higher compression ratios, with a positive influence on thermal efficiency and combustion stability, but the choice of compression ratio is intimately related to the geometry of the chamber.

Geometric or spatial arrangement of the combustion chamber may unfavourably influence the early stages of flame growth with retarded heat-release timing.

Although rates of heat release are influenced positively by increasing engine speed, the effect on combustion stability and the limit of stable lean mixture operation is less clearly defined.

The fastest rates of heat release, enhanced combustion stability and a lesser dependency on changes in ignition timing, excess air ratio and engine speed are promoted by the Hrcc together with extended lean mixture operation which is particularly pronounced at slow speed.

Significantly improved thermal efficiencies are realised with the Hrcc: a 6 percentage point increase when compared with the original configuration at the optimum mixture strength.

The influence of operating and design variables on the total heat transfer to the engine coolant and exhaust is small, falling from around 58% of fuel energy +/- 2% of fuel energy at the stoichiometric air-to-fuel ratio to 56 +/- 3% at the lean mixture limit. A stronger dependency on excess air ratio is evident, however, for the engine heat transfer; falling from 32 to 25% of fuel energy with weakening mixtures but similarly insensitive to other design and operating conditions. The exhaust heat transfer increases from 27% of fuel energy +/- 4% of fuel energy to 30 +/- 4% over the range in mixture strength.

The energy loss to blowby is notable, particularly at slow speed, accounting for some 4.5% of fuel energy.

The ambient loss, at 10 to 20% of fuel energy, represents a significant proportion of fuel energy that remains unclaimed.

Minimum losses from unburned fuel occur at excess air ratios between 1.1 and 1.3 and account for 2 to 3% of fuel energy but these may increase significantly at the lean mixture limit to around 7%.

The motored mechanical loss varies from 4 to 7% of fuel energy over the range of speed and mixture strength. The contributions of the piston assembly, crankshaft and the valve train vary from 57 to 43%, 40 to 50% and 8 to 5% respectively of the total mechanical loss over the range of increasing speed.

Carbon monoxide can be maintained below 0.1% over a wide range of operating conditions provided the excess air ratio is greater than 1.1. Stoichiometric CO_2 emission levels in natural gas-fuelled engines are around two thirds those of petrol-fuelled units and these levels reduce by around 25% as the lean mixture limit is approached.

In general and in keeping with previous studies - although differing in the range of experimental observation - exhaust concentrations of NO_x reduce significantly with slower rates of combustion, retarded ignition timing and weakening mixtures and show a small and less clearly defined dependence on compression ratio and engine speed. However, at excess air ratios greater than about 1.25, the influence of compression ratio

is considerably more marked and NO_x levels in general diminish with reduced settings. In this regime NO_x also diminishes with reducing engine speed. In very lean conditions NO_x levels are only weakly dependent on ignition timing.

In the regime where NO_x levels diminish with reducing compression ratio, this ameliorating influence on hydrocarbon levels is also most pronounced. In contrast however, increased engine speed and advanced timing have a positive effect on unburned hydrocarbon levels whilst the excess air ratio for maximum NO_x levels is around that for minimum levels of unburned hydrocarbons.

10.2 Engine modelling

Modelling techniques have been developed and used as diagnostic tools in conjunction with the experimental data to investigate the influence of operating and design variables on rates of heat release and energy flows. The models have been validated using the experimental data over a wide range of operating conditions and incorporated into a thermodynamic engine model for use as a sub-model in an overall heat pump model.

The turbulent entrainment model for flame development has good predictive capability when applied to lean combustion of natural gas at high compression ratio. The capability is limited with very lengthy flame development periods.

The utility of the Weibe function in combustion modelling is significantly enhanced with rapid burning chambers where rates of heat release are least dependent on operating variables. A single function can, therefore, be used over a wide range of operating conditions; this also considerably reduces experimental work.

The trend-wise dependence of the output from the closed cycle heat transfer model conforms closely with the measured dependence as operating conditions change. The proportion of closed cycle heat transfer is approximately half that of the measured and in the absence of experimental data this distribution is in keeping with previous

work. Predicted temperatures at exhaust valve opening and measured mean exhaust temperatures are also consistent trend-wise.

In light of the preliminary stage of the engine development and the scope for further improvement of the mechanical design, it is probable that established correlations accurately represent the motoring frictional losses of the main components of the Task engine in the production stage of development. Subject to such considerations, the friction sub-model, incorporating geometric generality for the main engine components, together with generalised pressure dependency and pumping terms representative of firing engines, has good predictive capability when compared with the experimental data.

10.3 Lean burn strategy

Considerable progress has been achieved in the development of a conceptual design for heat pump and CHP applications, based on a lean, fast-burning combustion process in a low speed engine together with close control of other operating variables. A compact, high compression ratio combustion chamber has promoted extended lean mixture operation at higher thermal efficiencies and at low speed without attendant penalty in emission levels. In light of work conducted in a preliminary study on a similar engine, further increases in performance are expected solely through attention to the mechanical tolerancing of engine components. Although higher engine efficiencies and lower emission levels are still necessary to meet heat pump performance targets, it is thought that the lean burn approach for this application is likely to become increasingly attractive with further development as a method of producing heat or heat and power with relatively low environmental penalty. Some areas for improvement in the shorter term are outlined in the following chapter.

CHAPTER 11 - FUTURE WORK

The possibilities for future work are seemingly limitless, as a cursory inspection of the literature dealing with petrol-fuelled engines will confirm. However, in the shorter term and arising specifically from the conclusions reached and the problems encountered during this work, the following areas are thought to be worthy of further attention.

11.1 Engine design

A number of modifications to the engine design are desirable both from the perspective of the lean burn strategy and general mechanical reliability.

Further study of the chamber arrangement is thought to be advantageous since this was found to be a significant factor in influencing rates of heat release. A restriction on the aspect ratio may be implied from this work. As a first step, the influence of this variable together with, and inseparable from, that of the compression ratio setting may form the basis of a future study, possibly coupled with a swirl investigation.

The blowby and friction measurements emphasise the importance of attention to mechanical tolerancing. The former is of particular concern at the slow speeds envisaged for the operating strategy and suggests the additional measure of manifold recycling. A reduction in frictional loss is attractive since this reflects directly in shaft power. Attention to tolerancing and detail design is also implied by the evidence cited in Chapter 8 for the predominance of crevice unburned hydrocarbons in the exhaust.

Modifications are required to the crankshaft and piston assembly where excessive boundary friction was noted, probably resulting from misalignment and/or excessive clearances.

Recent developments in piston design outlined in Section 7.10.6, including reduction in the number, area and tension of rings and the area of piston skirt would be beneficial in reducing the engine

friction. The AEconoguide piston referred to in Sections 7.5 and 7.10.6 incorporates many such features, evidently without detrimental effect on piston ring blowby, and appears worthy of further investigation.

Reduction in bearing surface area, consistent with the demands for durability and the likely range in engine speed and mean effective pressure is desirable.

A more robust shaft coupling would be preferable, possibly incorporating a conventional splined fitting.

Since only one third to one half of the exhaust heat transfer was reclaimed, due mainly to a condensing loss, a secondary condensing heat exchanger (possibly located in the proximity of the evaporator in the heat pump package) could be installed at minimal cost for this low temperature application. Additionally, the smaller, but useful, loss at the exhaust port exit could be reclaimed utilising a water-cooled manifold.

Further work is required to improve the method of enclosure, to reduce both the ambient heat loss and the noise levels.

Improvement in volumetric efficiency may be possible by cooling the charge utilising the low temperature at the evaporator.

11.2 Operating strategy

Considerable further work is required in the area of engine management with respect to the operating strategy.

In the regime most attractive for the lean burn strategy, and with the exception of compression ratio, the variables that influence hydrocarbon emissions positively have an adverse effect on NO_x levels. However, it may be possible to control for minimum NO_x levels in light of the evidence for substantial post-combustion oxidation cited in Section 8.1. After-burning may have the potential for reductions in the unburned hydrocarbons, particularly at these weak mixture strengths where free oxygen is available. Low exhaust temperatures suggest some

form of additional heat input which does have the disadvantage of extra complexity in usual engine applications, however, with reclaimed heat a primary concern some modification to an existing exhaust heat exchanger should be possible. Such a heat only function may prove attractive in circumstances where the heating load is low or where heat only is required from CHP units.

11.3 Engine model

The utility of the Weibe function has been demonstrated for specific and rapid burning chambers. Coupled with the flame development model this should allow flexibility in specifying heat-release schedules, from which considerable information can be produced from the engine model in its present form without recourse to an extensive experimental programme. The output could take the form of extended engine maps or nomograms providing the basis of input to an overall heat pump model as a first step in future development. The engine model is limited however in predictive capability with respect to unburned hydrocarbons and NO_x emission levels and further work in this area is desirable, possibly incorporating a rate-controlled model for NO_x.

The several areas of contention noted throughout this work emphasise the extreme complexity of the processes involved. Although applicable to other processes such as friction and emission levels, the interaction of compression ratio, ignition timing and combustion chamber configuration on rates of heat release illustrates the point. This does suggest the utility of placing the engine model on a more fundamental basis to further understanding and enhance the predictive capability.

APPENDIX I - COMBUSTION ANALYSIS AND ENGINE MODEL OUTPUT

Introduction

Figures I.2 - I.57 compare the experimental pressure data analysis and engine performance with the engine model output for all the operating conditions investigated. Each figure corresponds to a single operating point. Selected data from this appendix form the basis of the tabulated and graphical figures included in Chapters 5, 6 and 7. The last characters in the test reference label identify the chamber arrangement (TaskII, 3-2, Hrcc and Ricardo E6 engine).

Contents

	page/figure no
TaskII chamber	I.2
Bathtub (3-2 chamber)	I.13
Hrcc arrangement	I.37
Ricardo E6 (disc chamber)	I.49
Influence of a 7% increase in the inducted mass	
nominal	I.13
+ 7%	I.14
Effect of a 2^0 error in the pressure-crankangle phasing	
nominal	I.35
+ 2 degrees	I.36
Effect of the range in the Weibe parameters: Hrcc	
nominal	I.40
parameters selected to promote the fastest burn	I.41
parameters selected to promote the slowest burn	I.42

TEST DATE	13/03/89
TEST REFERENCE	T38M2B04TII
COMPRESSION RATIO	9.00
SPEED (RPM)	1515.00
IGNITION (DEG BTDC)	21
EXCESS AIR RATIO	1.01
CHAMBER AREA (CM**2)	67.51
ATMOSPHERIC PRESS (BAR)	1.00730
PRESS TDC EXHAUST (BAR)	0.90730
PRESSURE IVC (BAR)	1.16593
RESIDUAL FRACTION (%)	7.00
BLOWBY COEFFICIENT	1.99
BLOWBY % OF CHARGE	6.8

DERIVED MASS BURNED CRITERIA

SRT OF HT RLS DABDC		350.0	
0 - 1%	DEG.	14	mS 1.5
0 - 10%	DEG.	23	mS 2.5
0 - 50%	DEG.	40	mS 4.4
0 - 90%	DEG.	55	mS 6.1
0 - 100%	DEG.	65	mS 7.2
1 - 90%	DEG.	41	mS 4.5
dP/dθ MAX (BARS/DEG)		0.52	
	AT	359.0	DEG
MAX PRESSURE (BARS)		27.87	
AT		381.0	DEG

WEIBE MASS BURNED CRITERIA

SRT OF HT RLS DABDC		350.0	
0 - 1%	DEG.	16	mS 1.8
0 - 10%	DEG.	23	mS 2.5
0 - 50%	DEG.	39	mS 4.3
0 - 90%	DEG.	59	mS 6.5
0 - 100%	DEG.	65	mS 7.2
1 - 90%	DEG.	43	mS 4.7
dP/dθ MAX (BARS/DEG)		0.68	
	AT	364.0	DEG
MAX PRESSURE (BARS)		30.27	
AT		379.0	DEG

HEAT TRANSFER

ENGINE MEASURED (kW)	1.551
ENGINE PREDICTED (kW)	0.944
PREDICTED/MEASURED (%)	60.9
MAX BURNED GAS TEMP (K)	2478.4
AT	372.0 DEG
BURNED GAS TEMP EVO (K)	1398.2
GAS TEMP AT IVC (K)	382.0
WALL TEMPERATURE (K)	400.0

STATISTICAL DATA

	MEAN	SD	% DIS
WORK (J)	82.16	0.890	1.1
POWER (kW)	1.037	0.011	1.1
PMAX (BAR)	28.31	2.800	9.9
AT DEG	21.1	3.700	17.5

GAS ANALYSIS

	MODEL	MEASURED
CO2 (%)	9.6	10.1
CO (PPM)	0.0	8000.0
O2 (%)	0.2	1.2
NOx (PPM)	3299.1	805.0
UHC (PPM)		1776.0

FUEL GROSS CV (kJ/kG) 53408.4
STOICH A/F RATIO 16.58

	MODEL	MEASD
POWER (kW)	1.176	1.035
FRICTN PWR (kW)	0.187	
PUMPNG PWR (kW)		0.002
INDICATD MEP (BAR)	7.37	6.49
INDICATED EFFICNCY	0.250	0.220
BRAKE POWER (kW)	0.991	0.830
BRAKE TH EFFICNCY	0.211	0.177

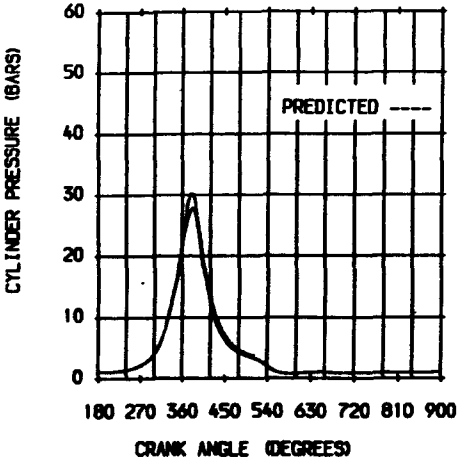

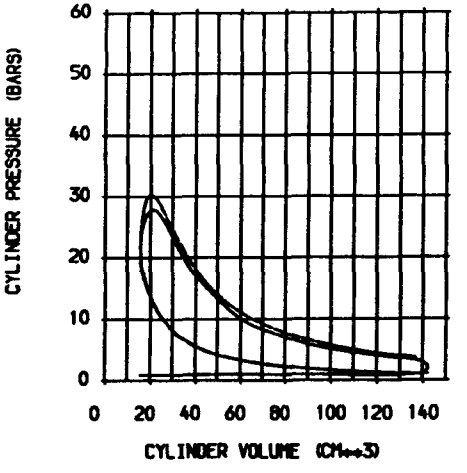

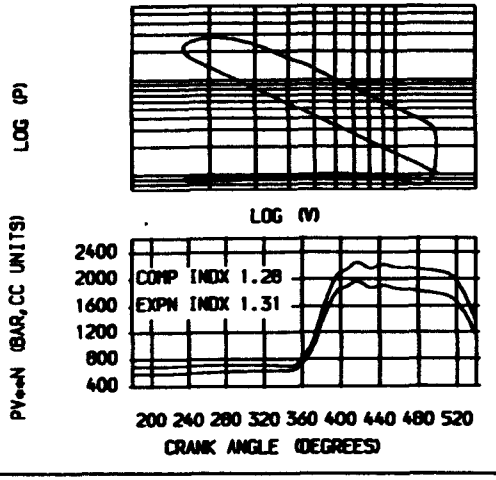

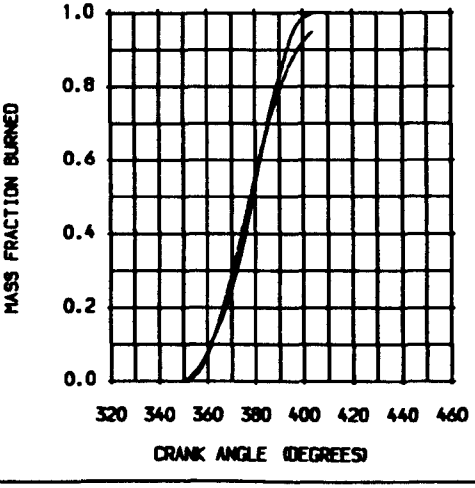

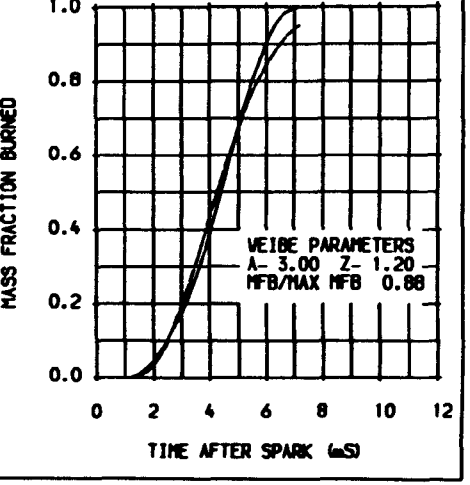

TEST DATE	13/03/89
TEST REFERENCE	T38M2905TII
COMPRESSION RATIO	9.00
SPEED (RPM)	1513.00
IGNITION (DEG BTDC)	33
EXCESS AIR RATIO	1.23
CHAMBER AREA (CM**2)	67.51
ATMOSPHERIC PRESS (BAR)	1.00730
PRESS TOC EXHAUST (BAR)	0.90730
PRESSURE IVC (BAR)	1.16093
RESIDUAL FRACTION (%)	7.00
BLOWBY COEFFICIENT	1.99
BLOWBY % OF CHARGE	6.8

DERIVED MASS BURNED CRITERIA

SRT OF HT RLS DABDC		348.0	
0 - 1%	DEG.	25	2.8
0 - 10%	DEG.	36	4.0
0 - 50%	DEG.	57	6.3
0 - 90%	DEG.	82	9.0
0 - 100%	DEG.	93	10.2
1 - 90%	DEG.	57	6.3
dP/dθ MAX (BARS/DEG)		0.47	
	AT	355.0	DEG
MAX PRESSURE (BARS)		25.06	
	AT	378.0	DEG

VEIBE MASS BURNED CRITERIA

SRT OF HT RLS DABDC		348.0	
0 - 1%	DEG.	26	2.9
0 - 10%	DEG.	36	4.0
0 - 50%	DEG.	57	6.3
0 - 90%	DEG.	85	9.4
0 - 100%	DEG.	93	10.2
1 - 90%	DEG.	59	6.5
dP/dθ MAX (BARS/DEG)		0.43	
	AT	359.0	DEG
MAX PRESSURE (BARS)		24.95	
	AT	376.0	DEG

HEAT TRANSFER

ENGINE MEASURED (kW)	1.082
ENGINE PREDICTED (kW)	0.701
PREDICTED/MEASURED (%)	64.8
MAX BURNED GAS TEMP (K)	2251.3
AT	369.0 DEG
BURNED GAS TEMP EVO (K)	1313.3
GAS TEMP AT IVC (K)	376.5
WALL TEMPERATURE (K)	400.0

STATISTICAL DATA

	MEAN	SD	% DIS
WORK (J)	73.99	2.110	2.9
POWER (kW)	0.933	0.027	2.9
PMAX (BAR)	25.71	3.300	12.8
AT DEG	16.9	6.700	39.7

GAS ANALYSIS

	MODEL	MEASURED
CO2 (%)	8.0	9.0
CO (PPM)	0.0	500.0
O2 (%)	3.6	4.4
NOx (PPM)	5694.7	511.0
UHC (PPM)		1084.0

FUEL GROSS CV (kJ/kG) 53408.4
STOICH A/F RATIO 16.58

	MODEL	MEASD
POWER (kW)	0.967	0.935
FRICTN PWR (kW)	0.187	
PUMPNG PWR (kW)		-0.002
INDICATD MEP (BAR)	6.07	5.87
INDICATED EFFICNCY	0.245	0.236
BRAKE POWER (kW)	0.778	0.711
BRAKE TH EFFICNCY	0.196	0.179

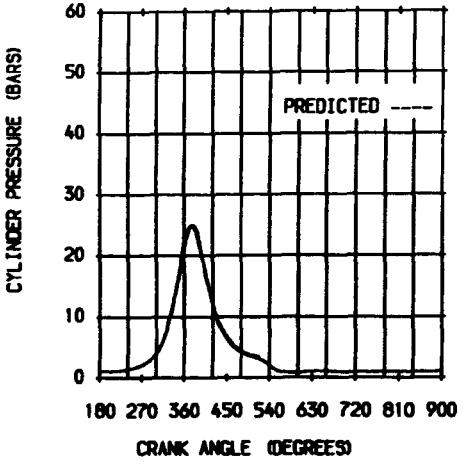

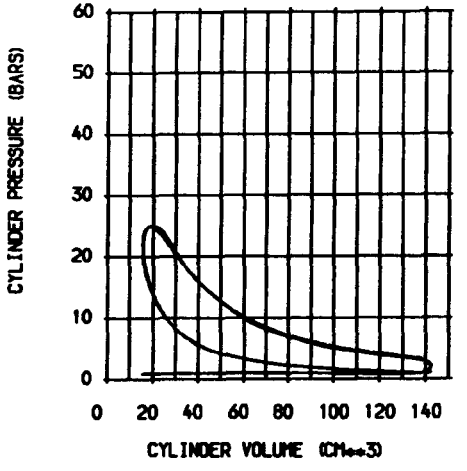

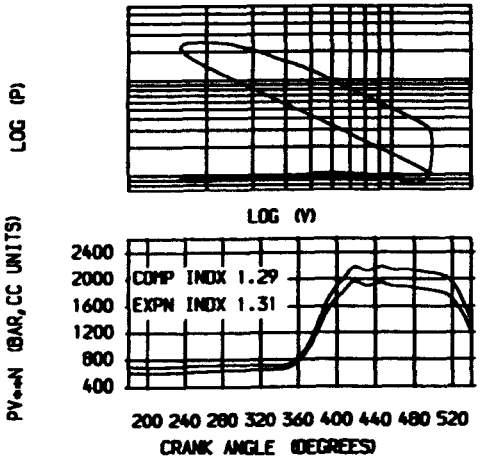

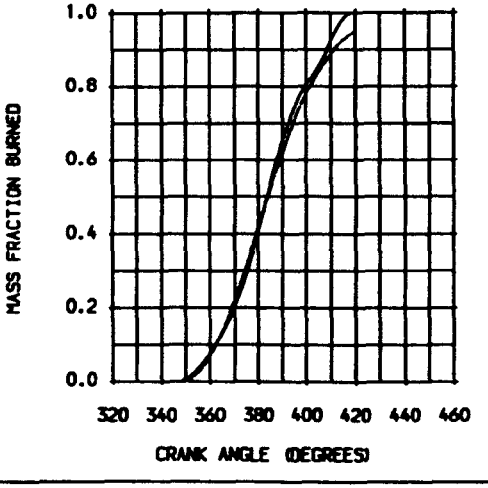

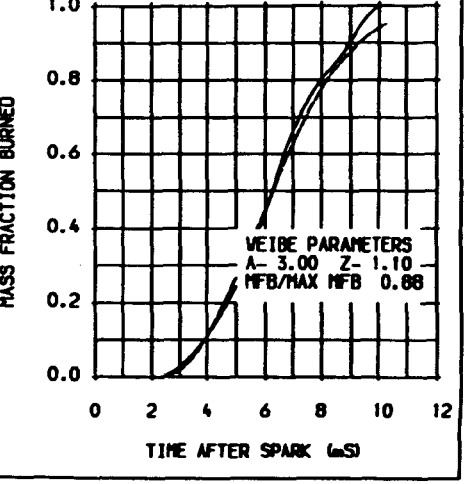

TEST DATE	13/03/89
TEST REFERENCE	T38M25DITII
COMPRESSION RATIO	9.00
SPEED (RPM)	1814.00
IGNITION (DEG BTDC)	26
EXCESS AIR RATIO	1.04
CHAMBER AREA (CM**2)	67.51
ATMOSPHERIC PRESS (BAR)	1.00730
PRESS TDC EXHAUST (BAR)	0.90730
PRESSURE IVC (BAR)	1.21044
RESIDUAL FRACTION (%)	7.00
BLOWBY COEFFICIENT	1.84
BLOWBY % OF CHARGE	5.3

DERIVED MASS BURNED CRITERIA

SRT OF HT RLS DABDC	344.0		
0 - 1%	DEG.	13	mS 1.2
0 - 10%	DEG.	22	mS 2.0
0 - 50%	DEG.	37	mS 3.4
0 - 90%	DEG.	55	mS 5.1
0 - 100%	DEG.	68	mS 6.2
1 - 90%	DEG.	42	mS 3.9
dP/dθ MAX (BARS/DEG)		0.80	
	AT	364.0	DEG
MAX PRESSURE (BARS)		34.07	
	AT	375.0	DEG

WEIBE MASS BURNED CRITERIA

SRT OF HT RLS DABDC	344.0		
0 - 1%	DEG.	14	mS 1.3
0 - 10%	DEG.	21	mS 1.9
0 - 50%	DEG.	37	mS 3.4
0 - 90%	DEG.	59	mS 5.4
0 - 100%	DEG.	68	mS 6.2
1 - 90%	DEG.	45	mS 4.1
dP/dθ MAX (BARS/DEG)		1.06	
	AT	358.0	DEG
MAX PRESSURE (BARS)		37.15	
	AT	374.0	DEG

HEAT TRANSFER

ENGINE MEASURED (kW)	1.939
ENGINE PREDICTED (kW)	1.161
PREDICTED/MEASURED (%)	59.9
MAX BURNED GAS TEMP (K)	2502.8
AT	366.0 DEG
BURNED GAS TEMP EVO (K)	1353.7
GAS TEMP AT IVC (K)	378.5
WALL TEMPERATURE (K)	400.0

STATISTICAL DATA

	MEAN	SD	% DIS
WORK (J)	83.59	1.190	1.4
POWER (kW)	1.264	0.018	1.4
PMAX (BAR)	34.47	2.700	7.9
AT DEG	15.1	1.800	12.3

GAS ANALYSIS

	MODEL	MEASURED
CO2 (%)	9.3	9.8
CO (PPM)	0.0	9000.0
O2 (%)	0.7	1.9
NOx (PPM)	4546.0	929.0
UHC (PPM)		1812.0

FUEL GROSS CV (kJ/kG) 53408.4
STOICH A/F RATIO 16.58

	MODEL	MEASD
POWER (kW)	1.505	1.261
FRICTN PWR (kW)	0.244	
PUMPNG PWR (kW)		0.003
INDICATD MEP (BAR)	7.88	6.60
INDICATED EFFICNCY	0.262	0.220
BRAKE POWER (kW)	1.264	1.078
BRAKE TH EFFICNCY	0.220	0.188

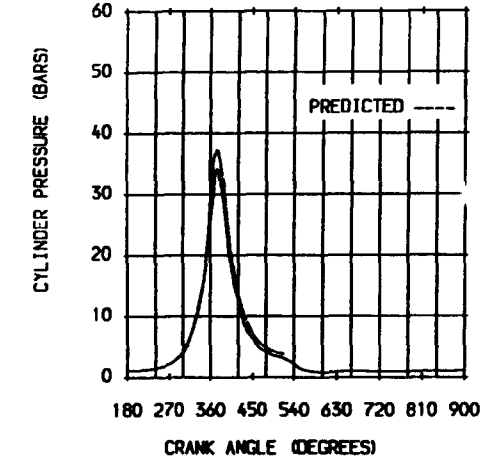

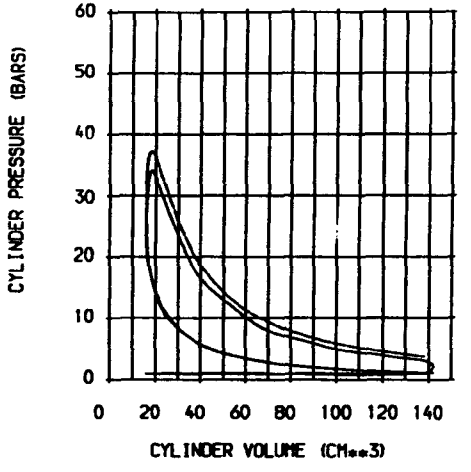

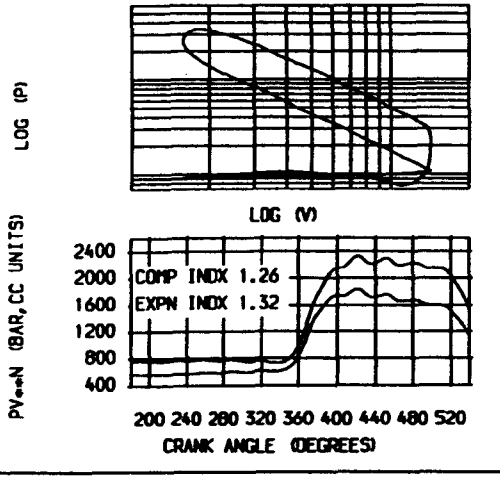

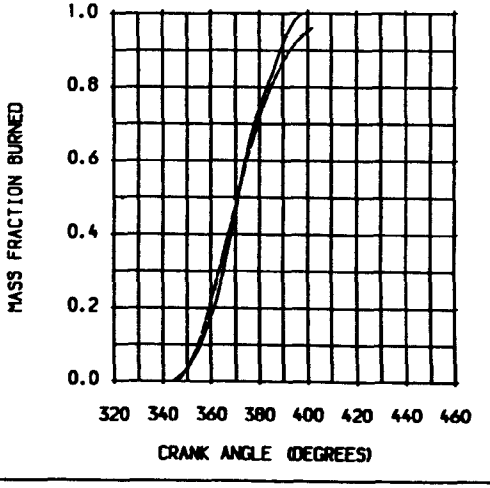

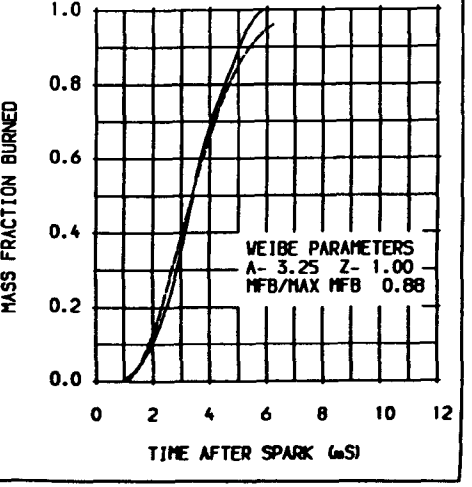

TEST DATE	13/03/89
TEST REFERENCE	T38M2602TII
COMPRESSION RATIO	9.00
SPEED (RPM)	1807.00
IGNITION (DEG BTDC)	25
EXCESS AIR RATIO	1.18
CHAMBER AREA (CM**2)	67.51
ATMOSPHERIC PRESS (BAR)	1.00730
PRESS TDC EXHAUST (BAR)	0.90730
PRESSURE IVC (BAR)	1.18424
RESIDUAL FRACTION (%)	7.00
BLOWBY COEFFICIENT	1.85
BLOWBY % OF CHARGE	5.3

DERIVED MASS BURNED CRITERIA

SRT OF HT RLS DABDC		348.0		
0 - 1%	DEG.	17	BS	1.6
0 - 10%	DEG.	27	BS	2.5
0 - 50%	DEG.	44	BS	4.1
0 - 90%	DEG.	71	BS	6.5
0 - 100%	DEG.	89	BS	8.2
1 - 90%	DEG.	54	BS	5.0
dP/dθ MAX (BARS/DEG)		0.59		
	AT	361.0	DEG	
MAX PRESSURE (BARS)		28.73		
AT		379.0	DEG	

WEIBE MASS BURNED CRITERIA

SRT OF HT RLS DABDC		348.0		
0 - 1%	DEG.	18	BS	1.7
0 - 10%	DEG.	26	BS	2.4
0 - 50%	DEG.	45	BS	4.2
0 - 90%	DEG.	69	BS	6.4
0 - 100%	DEG.	89	BS	8.2
1 - 90%	DEG.	51	BS	4.7
dP/dθ MAX (BARS/DEG)		0.60		
	AT	361.0	DEG	
MAX PRESSURE (BARS)		29.19		
AT		377.0	DEG	

HEAT TRANSFER

ENGINE MEASURED (kW)	1.581
ENGINE PREDICTED (kW)	0.914
PREDICTED/MEASURED (%)	57.8
MAX BURNED GAS TEMP (K)	2324.3
AT	370.0 DEG
BURNED GAS TEMP EVO (K)	1330.9
GAS TEMP AT IVC (K)	372.0
WALL TEMPERATURE (K)	400.0

STATISTICAL DATA

	MEAN	SD	% DIS
WORK (J)	79.74	1.100	1.4
POWER (kW)	1.201	0.017	1.4
PMAX (BAR)	29.27	2.900	9.9
AT DEG	18.9	3.000	15.7

GAS ANALYSIS

	MODEL	MEASURED
CO2 (%)	8.3	9.7
CO (PPM)	0.0	400.0
O2 (%)	2.9	3.7
NOx (PPM)	5914.4	836.0
UHC (PPM)		1138.0

FUEL GROSS CV (kJ/kG) 53408.4
STOICH A/F RATIO 16.58

	MODEL	MEASD
POWER (kW)	1.328	1.204
FRICTN PWR (kW)	0.243	
PUMPNG PWR (kW)		-0.003
INDICATD MEP (BAR)	6.98	6.33
INDICATED EFFICNCY	0.262	0.237
BRAKE POWER (kW)	1.082	1.001
BRAKE TH EFFICNCY	0.213	0.197

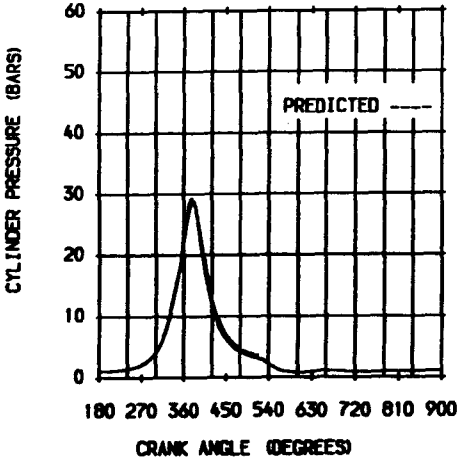

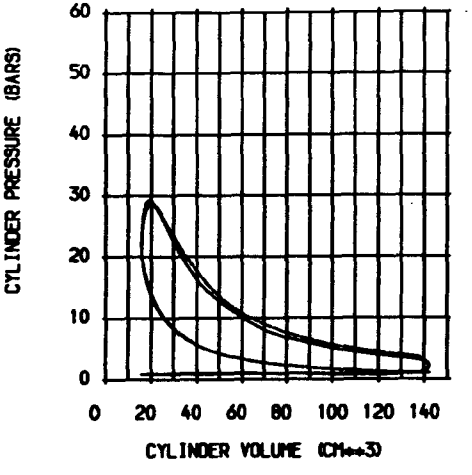

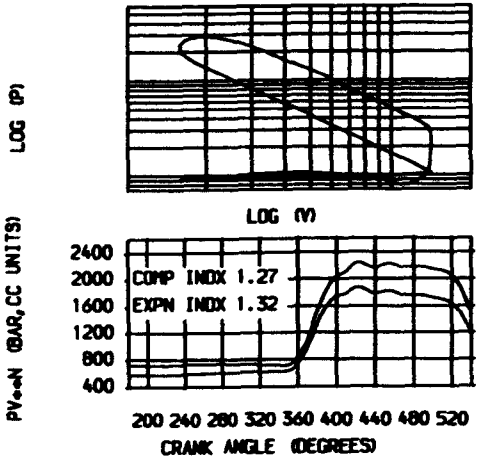

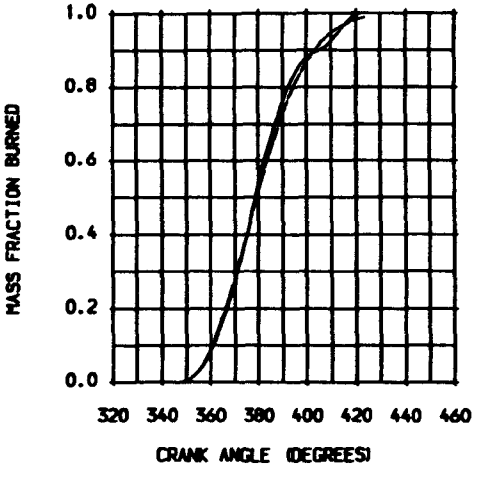

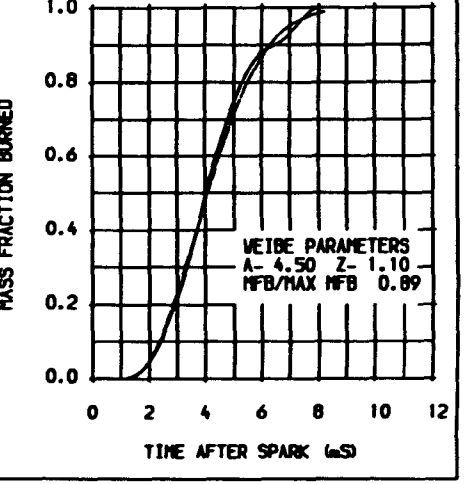

TEST DATE	13/03/89
TEST REFERENCE	T38M2602TII
COMPRESSION RATIO	9.00
SPEED (RPM)	1807.00
IGNITION (DEG BTDC)	25
EXCESS AIR RATIO	1.18
CHAMBER AREA (CM**2)	67.51
ATMOSPHERIC PRESS (BAR)	1.00730
PRESS TDC EXHAUST (BAR)	0.90730
PRESSURE IVC (BAR)	1.18424
RESIDUAL FRACTION (%)	7.00
BLOWBY COEFFICIENT	1.85
BLOWBY % OF CHARGE	5.3

DERIVED MASS BURNED CRITERIA

SRT OF HT RLS DABDC		348.0		
0 - 1%	DEG.	17	mS	1.6
0 - 10%	DEG.	27	mS	2.5
0 - 50%	DEG.	44	mS	4.1
0 - 90%	DEG.	71	mS	6.5
0 - 100%	DEG.	89	mS	8.2
1 - 90%	DEG.	54	mS	5.0
dP/dθ MAX (BARS/DEG)		0.59		
	AT	361.0	DEG	
MAX PRESSURE (BARS)		28.73		
AT		379.0	DEG	

VEIBE MASS BURNED CRITERIA

SRT OF HT RLS DABDC		348.0		
0 - 1%	DEG.	18	mS	1.7
0 - 10%	DEG.	26	mS	2.4
0 - 50%	DEG.	45	mS	4.2
0 - 90%	DEG.	69	mS	6.4
0 - 100%	DEG.	89	mS	8.2
1 - 90%	DEG.	51	mS	4.7
dP/dθ MAX (BARS/DEG)		0.60		
	AT	361.0	DEG	
MAX PRESSURE (BARS)		29.19		
AT		377.0	DEG	

HEAT TRANSFER

ENGINE MEASURED (kW)	1.581
ENGINE PREDICTED (kW)	0.914
PREDICTED/MEASURED (%)	57.8
MAX BURNED GAS TEMP (K)	2324.3
AT	370.0 DEG
BURNED GAS TEMP EVO (K)	1330.9
GAS TEMP AT IVC (K)	372.0
WALL TEMPERATURE (K)	400.0

STATISTICAL DATA

	MEAN	SD	% DIS
WORK (J)	79.74	1.100	1.4
POWER (kW)	1.201	0.017	1.4
PMAX (BAR)	29.27	2.900	9.9
AT DEG	18.9	3.000	15.7

GAS ANALYSIS

	MODEL	MEASURED
CO2 (%)	8.3	9.7
CO (PPM)	0.0	400.0
O2 (%)	2.9	3.7
NOx (PPM)	5914.4	836.0
UHC (PPM)		1138.0

FUEL GROSS CV (kJ/kG) 53408.4
STOICH A/F RATIO 16.58

	MODEL	MEASD
POWER (kW)	1.328	1.204
FRICTN PWR (kW)	0.243	
PUMPNG PWR (kW)		-0.003
INDICATD MEP (BAR)	6.98	6.33
INDICATED EFFICNCY	0.262	0.237
BRAKE POWER (kW)	1.082	1.001
BRAKE TH EFFICNCY	0.213	0.197

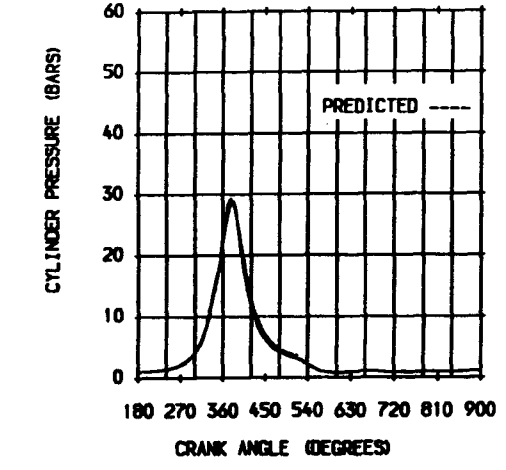

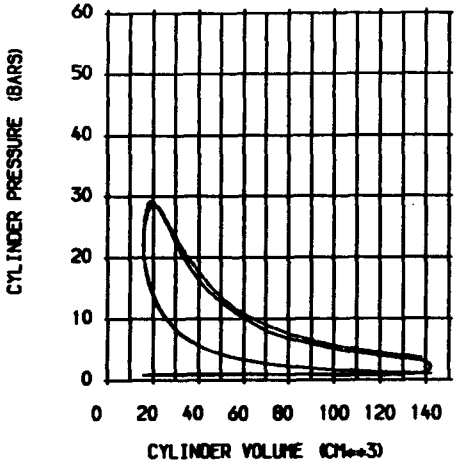

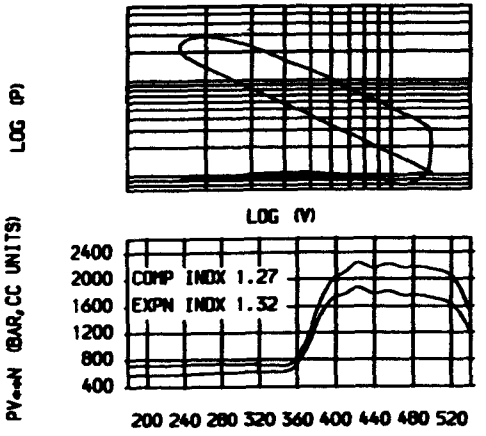

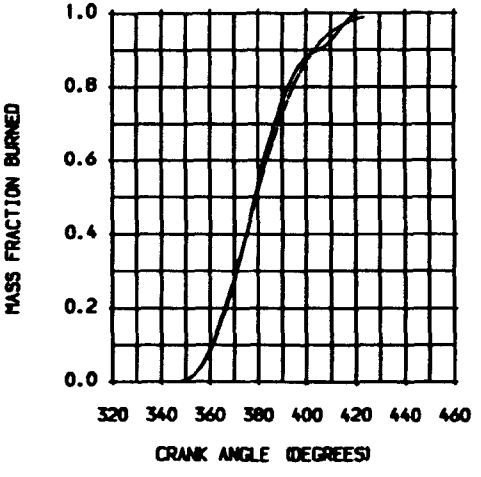

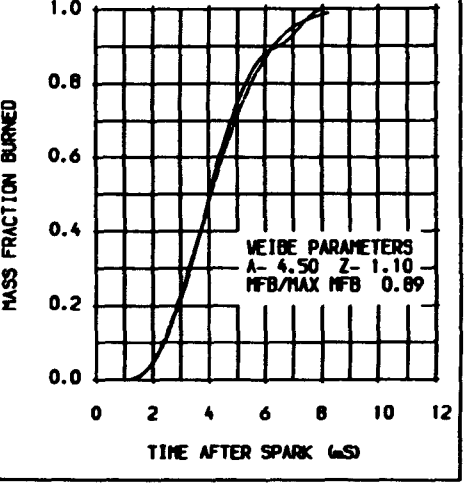

TEST DATE	13/03/89
TEST REFERENCE	T38M27D3TII
COMPRESSION RATIO	9.00
SPEED (RPM)	1806.00
IGNITION (DEG BTDC)	33
EXCESS AIR RATIO	1.50
CHAMBER AREA (CM**2)	67.51
ATMOSPHERIC PRESS (BAR)	1.00730
PRESS TDC EXHAUST (BAR)	0.90730
PRESSURE IVC (BAR)	1.11986
RESIDUAL FRACTION (%)	7.00
BLOWBY COEFFICIENT	1.85
BLOWBY % OF CHARGE	5.3

DERIVED MASS BURNED CRITERIA

SRT OF HT RLS DABDC		354.0		
0 - 1%	DEG.	31	mS	2.9
0 - 10%	DEG.	47	mS	4.3
0 - 50%	DEG.	76	mS	7.0
0 - 90%	DEG.	111	mS	10.2
0 - 100%	DEG.	131	mS	12.1
1 - 90%	DEG.	80	mS	7.4
dP/dθ MAX (BARS/DEG)		0.28		
	AT	355.0	DEG	
MAX PRESSURE (BARS)		20.64		
	AT	366.0	DEG	

WEIBE MASS BURNED CRITERIA

SRT OF HT RLS DABDC		354.0		
0 - 1%	DEG.	33	mS	3.0
0 - 10%	DEG.	46	mS	4.2
0 - 50%	DEG.	77	mS	7.1
0 - 90%	DEG.	121	mS	11.2
0 - 100%	DEG.	131	mS	12.1
1 - 90%	DEG.	88	mS	8.1
dP/dθ MAX (BARS/DEG)		0.18		
	AT	355.0	DEG	
MAX PRESSURE (BARS)		19.19		
	AT	366.0	DEG	

HEAT TRANSFER

ENGINE MEASURED (kW)	1.082
ENGINE PREDICTED (kW)	0.533
PREDICTED/MEASURED (%)	49.2
MAX BURNED GAS TEMP (K)	1957.8
AT	361.0 DEG
BURNED GAS TEMP EVO (K)	1328.3
GAS TEMP AT IVC (K)	343.5
WALL TEMPERATURE (K)	400.0

STATISTICAL DATA

	MEAN	SD	% DIS
WORK (J)	60.01	5.640	9.5
POWER (kW)	0.903	0.085	9.5
PMAX (BAR)	20.89	1.400	6.7
AT DEG	6.1	3.500	57.4

GAS ANALYSIS

	MODEL	MEASURED
CO2 (%)	6.6	7.4
CO (PPM)	0.0	400.0
O2 (%)	6.5	8.0
NOx (PPM)	3841.9	0.0
UHC (PPM)		1836.0

FUEL GROSS CV (kJ/kG) 53408.4
STOICH A/F RATIO 16.58

	MODEL	MEASD
POWER (kW)	0.843	0.915
FRICTN PWR (kW)	0.242	
PUMPNG PWR (kW)		-0.012
INDICATD MEP (BAR)	4.43	4.81
INDICATED EFFICNCY	0.203	0.221
BRAKE POWER (kW)	0.589	0.672
BRAKE TH EFFICNCY	0.142	0.162

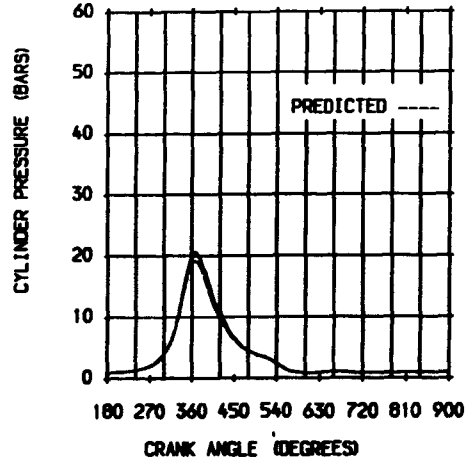

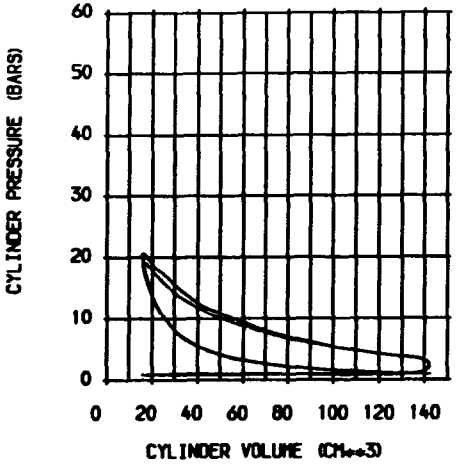

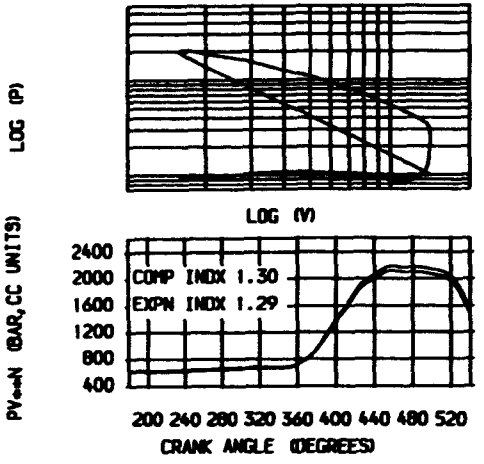

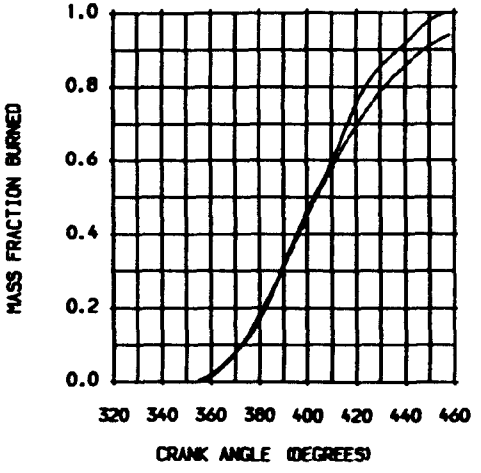

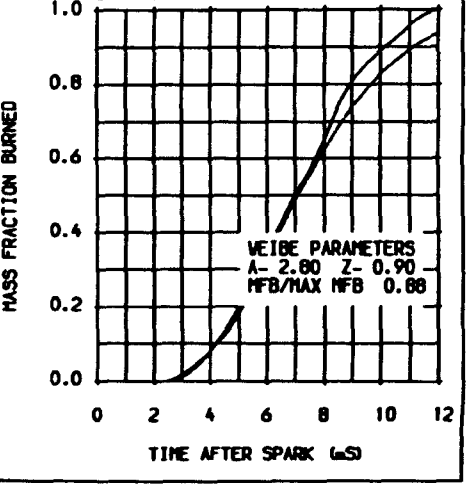

TEST DATE	29/03/89
TEST REFERENCE	T39M3403TII
COMPRESSION RATIO	8.95
SPEED (RPM)	2105.00
IGNITION (DEG BTDC)	28
EXCESS AIR RATIO	1.05
CHAMBER AREA (CM**2)	67.51
ATMOSPHERIC PRESS (BAR)	1.01320
PRESS TDC EXHAUST (BAR)	0.91320
PRESSURE IVC (BAR)	1.24565
RESIDUAL FRACTION (%)	7.00
BLOWBY COEFFICIENT	1.54
BLOWBY % OF CHARGE	3.8

DERIVED MASS BURNED CRITERIA

SRT OF HT RLS DABDC		344.0	
0 - 1%	DEG.	15	DS 1.2
0 - 10%	DEG.	23	DS 1.8
0 - 50%	DEG.	40	DS 3.2
0 - 90%	DEG.	59	DS 4.7
0 - 100%	DEG.	76	DS 6.0
1 - 90%	DEG.	44	DS 3.5
dP/dθ MAX	(BARS/DEG)	0.85	
	AT	355.0	DEG
MAX PRESSURE	(BARS)	33.33	
	AT	376.0	DEG

VEIBE MASS BURNED CRITERIA

SRT OF HT RLS DABDC		344.0	
0 - 1%	DEG.	16	DS 1.3
0 - 10%	DEG.	24	DS 1.9
0 - 50%	DEG.	41	DS 3.2
0 - 90%	DEG.	64	DS 5.1
0 - 100%	DEG.	76	DS 6.0
1 - 90%	DEG.	48	DS 3.8
dP/dθ MAX	(BARS/DEG)	0.95	
	AT	358.0	DEG
MAX PRESSURE	(BARS)	35.61	
	AT	374.0	DEG

HEAT TRANSFER

ENGINE MEASURED (kW)		2.221
ENGINE PREDICTED (kW)		1.276
PREDICTED/MEASURED (%)		57.4
MAX BURNED GAS TEMP (K)		2500.4
	AT	367.0 DEG
BURNED GAS TEMP EVO (K)		1392.5
GAS TEMP AT IVC (K)		396.0
WALL TEMPERATURE (K)		400.0

STATISTICAL DATA

	MEAN	SD	% DIS
WORK (J)	81.24	1.290	1.6
POWER (kW)	1.425	0.023	1.6
PMAX (BAR)	33.71	2.600	7.6
AT DEG	15.9	2.100	13.2

GAS ANALYSIS

	MODEL	MEASURED
CO2 (%)	9.2	9.6
CO (PPM)	0.0	6800.0
O2 (%)	0.9	2.0
NOx (PPM)	4865.5	1073.0
UHC (PPM)		2627.0
FUEL GROSS CV (kJ/kG)		53319.0
STOICH A/F RATIO		16.61

	MODEL	MEASD
POWER (kW)	1.716	1.430
FRICTN PWR (kW)	0.306	
PUMPNG PWR (kW)		-0.005
INDICATD MEP (BAR)	7.74	6.45
INDICATED EFFICNCY	0.265	0.219
BRAKE POWER (kW)	1.405	1.155
BRAKE TH EFFICNCY	0.215	0.177

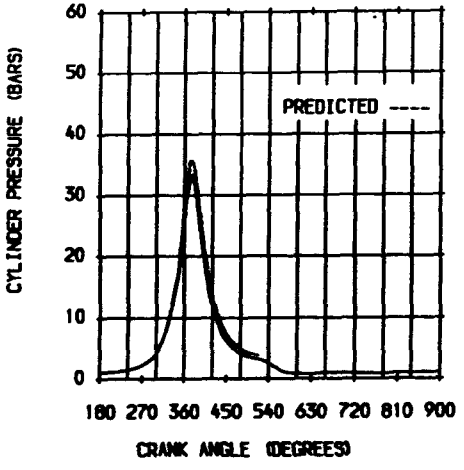

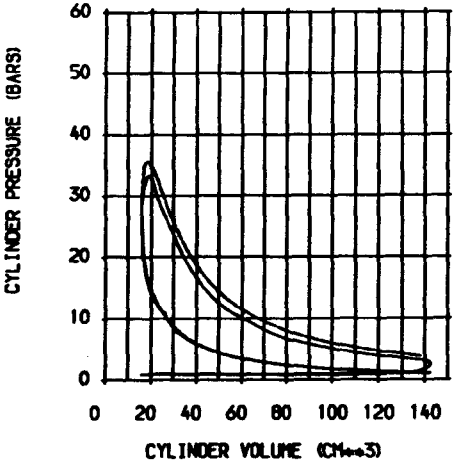

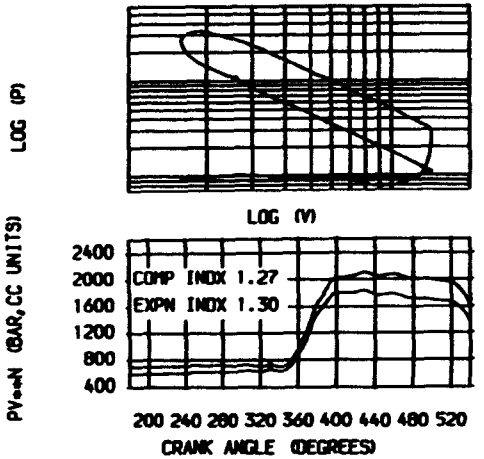

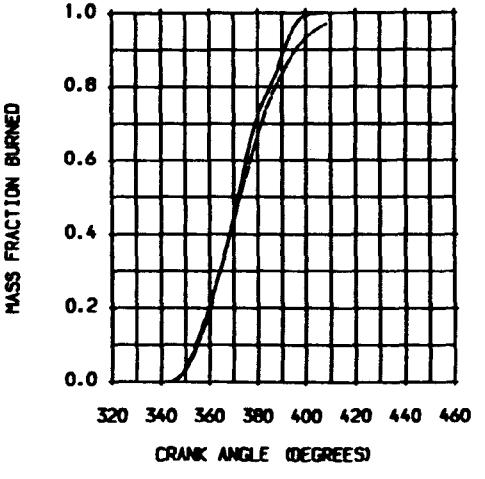

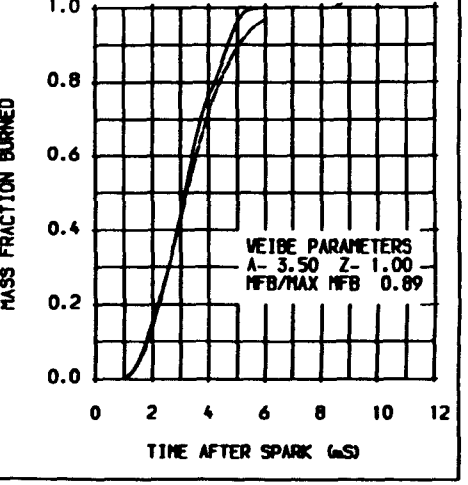

TEST DATE	29/03/89
TEST REFERENCE	T59M3201TII
COMPRESSION RATIO	8.95
SPEED (RPM)	2117.00
IGNITION (DEG BTDC)	28
EXCESS AIR RATIO	1.06
CHAMBER AREA (CM**2)	67.51
ATMOSPHERIC PRESS (BAR)	1.01320
PRESS TDC EXHAUST (BAR)	0.91321
PRESSURE IVC (BAR)	1.22253
RESIDUAL FRACTION (%)	7.00
BLOWBY COEFFICIENT	1.52
BLOWBY % OF CHARGE	3.8

DERIVED MASS BURNED CRITERIA

SRT OF HT RLS DABDC		346.0	
0 - 1%	DEG.	16	mS 1.3
0 - 10%	DEG.	24	mS 1.9
0 - 50%	DEG.	41	mS 3.2
0 - 90%	DEG.	60	mS 4.7
0 - 100%	DEG.	70	mS 5.5
1 - 90%	DEG.	44	mS 3.5
dP/dθ MAX (BARS/DEG)		0.96	
	AT	363.0	DEG
MAX PRESSURE (BARS)		33.79	
	AT	376.0	DEG

WEIBE MASS BURNED CRITERIA

SRT OF HT RLS DABDC		346.0	
0 - 1%	DEG.	17	mS 1.3
0 - 10%	DEG.	24	mS 1.9
0 - 50%	DEG.	41	mS 3.2
0 - 90%	DEG.	65	mS 5.1
0 - 100%	DEG.	70	mS 5.5
1 - 90%	DEG.	48	mS 3.8
dP/dθ MAX (BARS/DEG)		0.94	
	AT	358.0	DEG
MAX PRESSURE (BARS)		34.69	
	AT	375.0	DEG

HEAT TRANSFER

ENGINE MEASURED (kW)	2.037
ENGINE PREDICTED (kW)	1.220
PREDICTED/MEASURED (%)	59.9
MAX BURNED GAS TEMP (K)	2490.9
AT	367.0 DEG
BURNED GAS TEMP EVO (K)	1385.1
GAS TEMP AT IVC (K)	395.0
WALL TEMPERATURE (K)	400.0

STATISTICAL DATA

	MEAN	SD	% DIS
WORK (J)	82.87	0.460	0.6
POWER (kW)	1.462	0.008	0.6
PMAX (BAR)	34.04	2.100	6.8
AT DEG	16.0	1.600	11.2

GAS ANALYSIS

	MODEL	MEASURED
CO2 (%)	9.1	9.8
CO (PPM)	0.0	4400.0
O2 (%)	1.1	2.0
NOx (PPM)	5090.4	1132.0
UHC (PPM)		2469.0
FUEL GROSS CV (kJ/kG)		53319.0
STOICH A/F RATIO	16.61	

	MODEL	MEASD
POWER (kW)	1.685	1.469
FRICTN PWR (kW)	0.308	
PUMPNG PWR (kW)		-0.007
INDICATD MEP (BAR)	7.56	6.59
INDICATED EFFICNCY	0.265	0.230
BRAKE POWER (kW)	1.370	1.190
BRAKE TH EFFICNCY	0.214	0.186

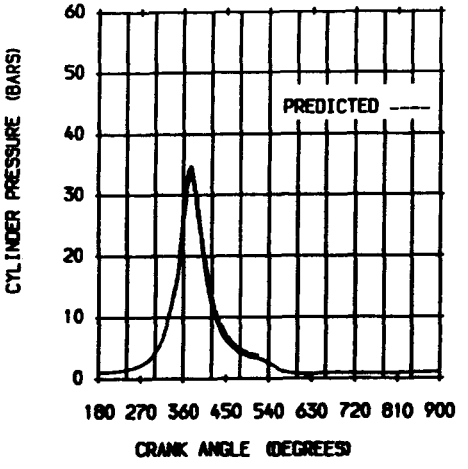

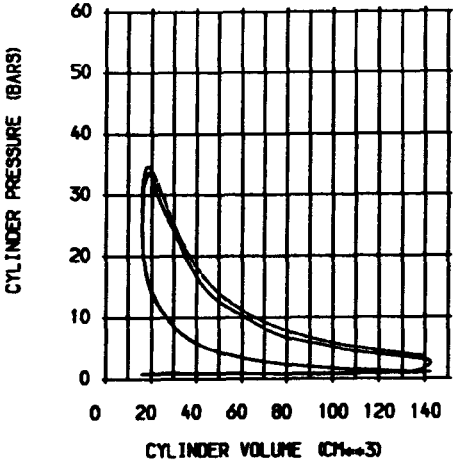

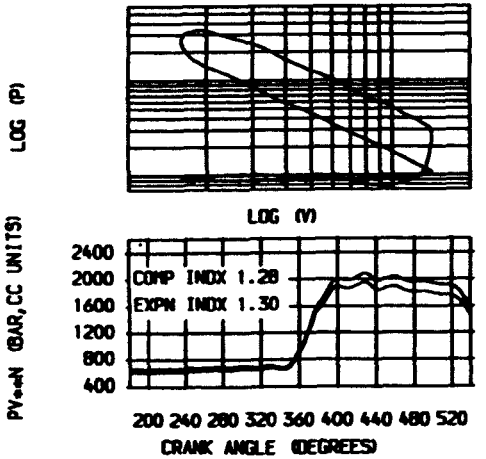

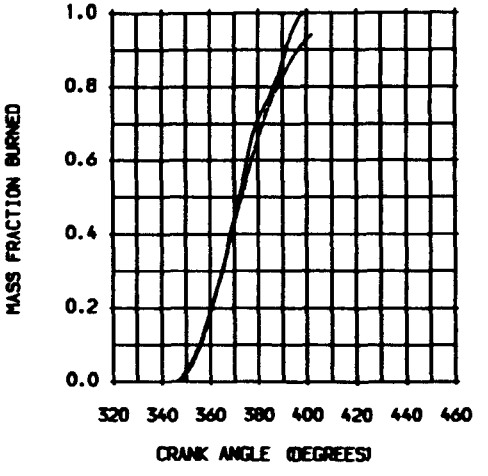

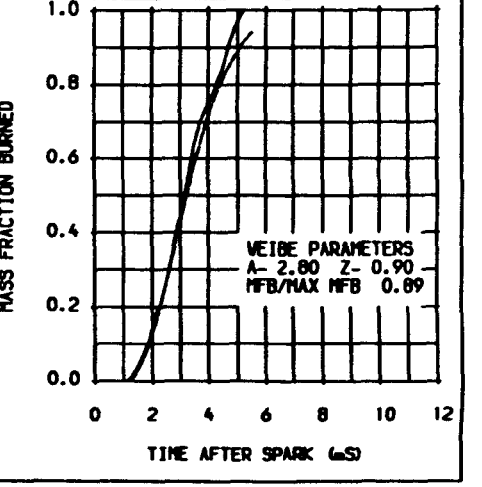

TEST DATE	13/03/89
TEST REFERENCE	T38M3006TII
COMPRESSION RATIO	9.00
SPEED (RPM)	2105.00
IGNITION (DEG BTDC)	28
EXCESS AIR RATIO	1.06
CHAMBER AREA (CM**2)	67.51
ATMOSPHERIC PRESS (BAR)	1.00730
PRESS TDC EXHAUST (BAR)	0.90730
PRESSURE IVC (BAR)	1.21698
RESIDUAL FRACTION (%)	7.00
BLOWBY COEFFICIENT	1.54
BLOWBY % OF CHARGE	3.8

DERIVED MASS BURNED CRITERIA

SRT OF HT RLS DABDC	342.0	
0 - 1%	DEG. 14	DEG 1.1
0 - 10%	DEG. 25	DEG 2.0
0 - 50%	DEG. 44	DEG 3.5
0 - 90%	DEG. 62	DEG 4.9
0 - 100%	DEG. 74	DEG 5.9
1 - 90%	DEG. 48	DEG 3.8
dP/dθ MAX (BARS/DEG)	0.62	
	AT	357.0 DEG
MAX PRESSURE (BARS)	30.96	
	AT	378.0 DEG

WEIBE MASS BURNED CRITERIA

SRT OF HT RLS DABDC	342.0	
0 - 1%	DEG. 16	DEG 1.3
0 - 10%	DEG. 25	DEG 2.0
0 - 50%	DEG. 43	DEG 3.4
0 - 90%	DEG. 66	DEG 5.2
0 - 100%	DEG. 74	DEG 5.9
1 - 90%	DEG. 50	DEG 4.0
dP/dθ MAX (BARS/DEG)	0.77	
	AT	358.0 DEG
MAX PRESSURE (BARS)	32.92	
	AT	376.0 DEG

HEAT TRANSFER

ENGINE MEASURED (kW)	2.062
ENGINE PREDICTED (kW)	1.210
PREDICTED/MEASURED (%)	58.7
MAX BURNED GAS TEMP (K)	2478.3
AT	368.0 DEG
BURNED GAS TEMP EVO (K)	1397.8
GAS TEMP AT IVC (K)	399.5
WALL TEMPERATURE (K)	400.0

STATISTICAL DATA

	MEAN	SD	% DIS
WORK (J)	82.35	1.340	1.6
POWER (kW)	1.445	0.023	1.6
PMAX (BAR)	31.51	3.100	9.7
AT DEG	17.8	3.300	18.4

GAS ANALYSIS

	MODEL	MEASURED
CO2 (%)	9.1	10.4
CO (PPM)	0.0	500.0
O2 (%)	1.1	1.7
NOx (PPM)	4970.9	2020.0
UHC (PPM)		1683.0
FUEL GROSS CV (kJ/kG)		53408.4
STOICH A/F RATIO		16.58

	MODEL	MEASD
POWER (kW)	1.649	1.449
FRICTN PWR (kW)	0.306	
PUMPNG PWR (kW)		-0.004
INDICATD MEP (BAR)	7.44	6.54
INDICATED EFFICNCY	0.265	0.234
BRAKE POWER (kW)	1.340	1.210
BRAKE TH EFFICNCY	0.216	0.195

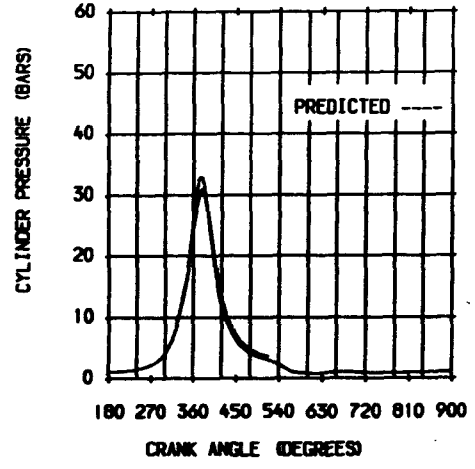

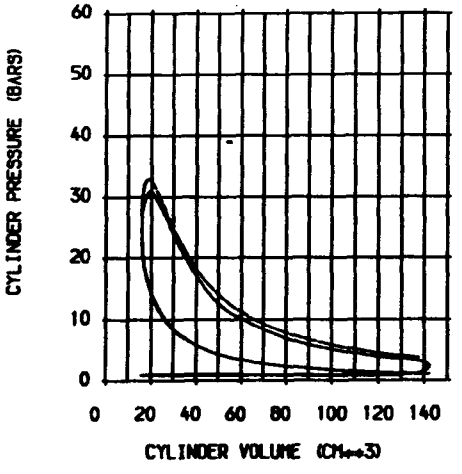

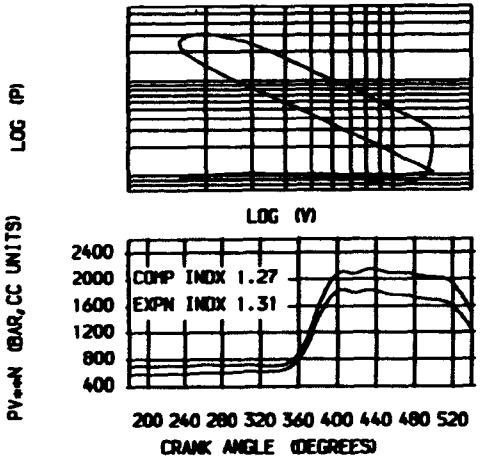

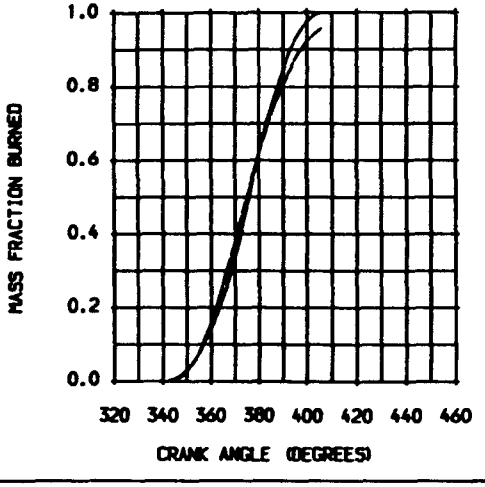

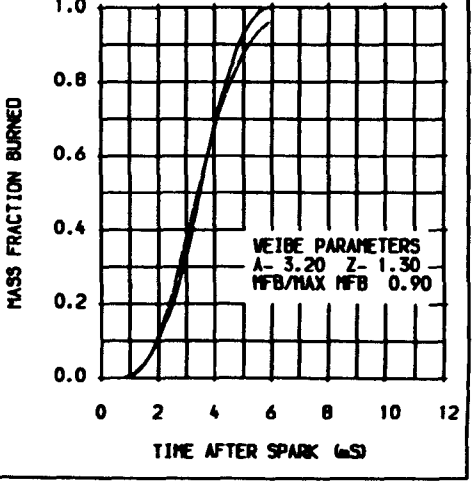

TEST DATE	13/03/89
TEST REFERENCE	T38M3107TII
COMPRESSION RATIO	9.00
SPEED (RPM)	2105.00
IGNITION (DEG BTDC)	40
EXCESS AIR RATIO	1.43
CHAMBER AREA (CM**2)	67.51
ATMOSPHERIC PRESS (BAR)	1.00730
PRESS TDC EXHAUST (BAR)	0.90730
PRESSURE IVC (BAR)	1.09711
RESIDUAL FRACTION (%)	7.00
BLOWBY COEFFICIENT	1.54
BLOWBY % OF CHARGE	3.8

DERIVED MASS BURNED CRITERIA

SRT OF HT RLS DABDC		337.0	
0 - 1%	DEG. 25	MS	2.0
0 - 10%	DEG. 42	MS	3.3
0 - 50%	DEG. 69	MS	5.5
0 - 90%	DEG. 98	MS	7.8
0 - 100%	DEG. 132	MS	10.5
1 - 90%	DEG. 73	MS	5.8
dP/dθ MAX (BARS/DEG)		0.43	
	AT	352.0	DEG
MAX PRESSURE (BARS)		23.10	
	AT	373.0	DEG

WEIBE MASS BURNED CRITERIA

SRT OF HT RLS DABDC		337.0	
0 - 1%	DEG. 27	MS	2.1
0 - 10%	DEG. 43	MS	3.4
0 - 50%	DEG. 71	MS	5.6
0 - 90%	DEG. 104	MS	8.2
0 - 100%	DEG. 132	MS	10.5
1 - 90%	DEG. 77	MS	6.1
dP/dθ MAX (BARS/DEG)		0.42	
	AT	348.0	DEG
MAX PRESSURE (BARS)		22.30	
	AT	370.0	DEG

HEAT TRANSFER

ENGINE MEASURED (kW)	1.281
ENGINE PREDICTED (kW)	0.723
PREDICTED/MEASURED (%)	56.4
MAX BURNED GAS TEMP (K)	2052.9
AT	363.0 DEG
BURNED GAS TEMP EVO (K)	1287.2
GAS TEMP AT IVC (K)	354.5
WALL TEMPERATURE (K)	400.0

STATISTICAL DATA

	MEAN	SD	% DIS
WORK (J)	75.01	5.660	7.6
POWER (kW)	1.316	0.099	7.6
PMAX (BAR)	23.56	2.200	9.4
AT DEG	13.0	5.000	38.6

GAS ANALYSIS

	MODEL	MEASURED
CO2 (%)	6.9	7.8
CO (PPM)	0.0	500.0
O2 (%)	5.9	7.4
NOx (PPM)	4677.0	0.0
UHC (PPM)		2574.0

FUEL GROSS CV (kJ/kG) 53408.4
STOICH A/F RATIO 16.58

	MODEL	MEASD
POWER (kW)	1.167	1.333
FRICTN PWR (kW)	0.306	
PUMPNG PWR (kW)		-0.018
INDICATD MEP (BAR)	5.27	6.01
INDICATED EFFICNCY	0.243	0.277
BRAKE POWER (kW)	0.843	0.852
BRAKE TH EFFICNCY	0.175	0.177

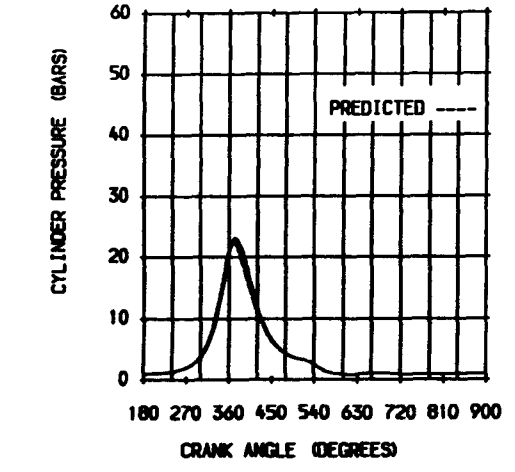

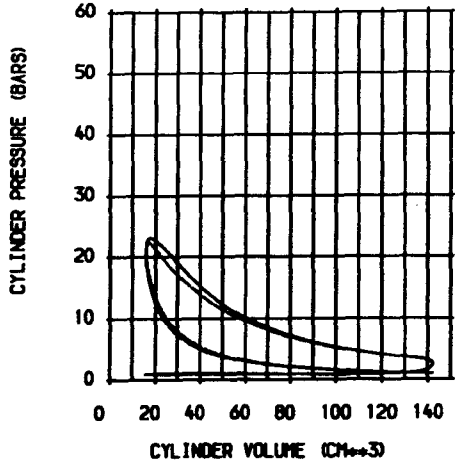

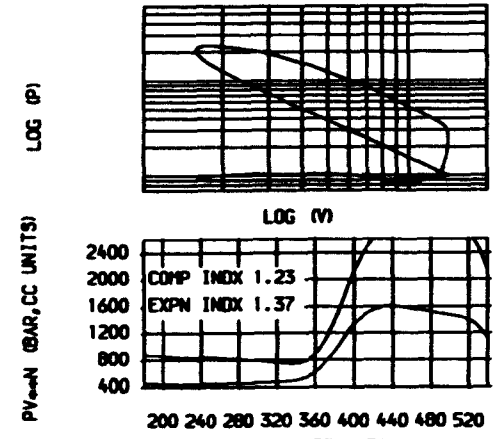

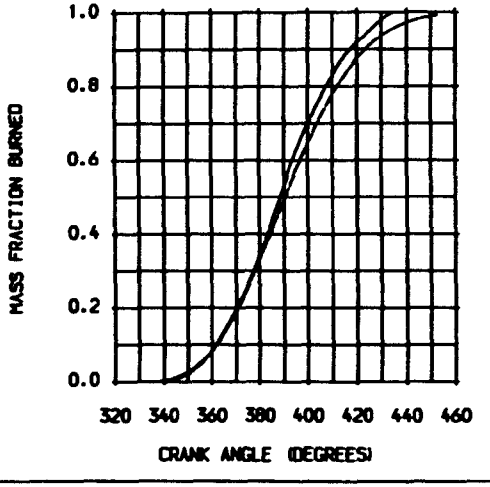

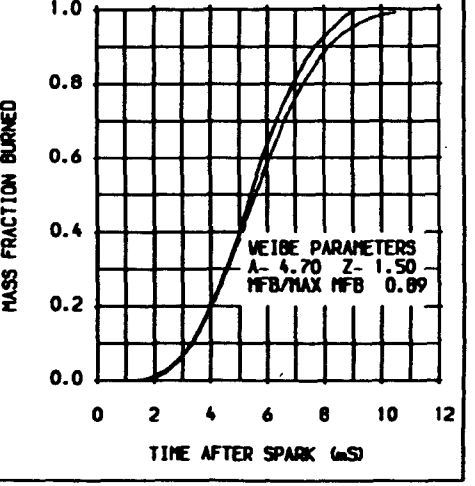

TEST DATE	29/03/89
TEST REFERENCE	139M3302TII
COMPRESSION RATIO	8.95
SPEED (RPM)	2116.00
IGNITION (DEG BTDC)	38
EXCESS AIR RATIO	1.42
CHAMBER AREA (CM**2)	67.51
ATMOSPHERIC PRESS (BAR)	1.01320
PRESS TDC EXHAUST (BAR)	0.91321
PRESSURE IVC (BAR)	1.15043
RESIDUAL FRACTION (%)	7.00
BLOWBY COEFFICIENT	1.52
BLOWBY % OF CHARGE	3.8

DERIVED MASS BURNED CRITERIA

SRT OF HT RLS DABDC		344.0	
0 - 1%	DEG. 26	DEG	2.0
0 - 10%	DEG. 36	DEG	2.8
0 - 50%	DEG. 61	DEG	4.8
0 - 90%	DEG. 92	DEG	7.2
0 - 100%	DEG. 110	DEG	8.7
1 - 90%	DEG. 66	DEG	5.2
dP/dθ MAX (BARS/DEG)		0.68	
	AT	353.0	DEG
MAX PRESSURE (BARS)		27.13	
	AT	374.0	DEG

WEIBE MASS BURNED CRITERIA

SRT OF HT RLS DABDC		344.0	
0 - 1%	DEG. 27	DEG	2.1
0 - 10%	DEG. 36	DEG	2.8
0 - 50%	DEG. 60	DEG	4.7
0 - 90%	DEG. 93	DEG	7.3
0 - 100%	DEG. 110	DEG	8.7
1 - 90%	DEG. 66	DEG	5.2
dP/dθ MAX (BARS/DEG)		0.57	
	AT	355.0	DEG
MAX PRESSURE (BARS)		26.80	
	AT	372.0	DEG

HEAT TRANSFER

ENGINE MEASURED (kW)	1.331
ENGINE PREDICTED (kW)	0.804
PREDICTED/MEASURED (%)	60.4
MAX BURNED GAS TEMP (K)	2107.5
AT	365.0 DEG
BURNED GAS TEMP EVO (K)	1232.6
GAS TEMP AT IVC (K)	358.0
WALL TEMPERATURE (K)	400.0

STATISTICAL DATA

	MEAN	SD	% DIS
WORK (J)	69.80	1.420	2.2
POWER (kW)	1.231	0.025	2.2
PMAX (BAR)	27.48	3.400	13.3
AT DEG	12.6	4.500	38.7

GAS ANALYSIS

	MODEL	MEASURED
CO2 (%)	7.0	7.6
CO (PPM)	0.0	400.0
O2 (%)	5.8	6.9
NOx (PPM)	5298.4	69.0
UHC (PPM)		1966.0
FUEL GROSS CV (kJ/kG)		53319.0
STOICH A/F RATIO		16.61

	MODEL	MEASD
POWER (kW)	1.308	1.248
FRICTN PWR (kW)	0.308	
PUMPNG PWR (kW)		-0.017
INDICATD MEP (BAR)	5.87	5.60
INDICATED EFFICNCY	0.260	0.248
BRAKE POWER (kW)	0.982	0.912
BRAKE TH EFFICNCY	0.195	0.181

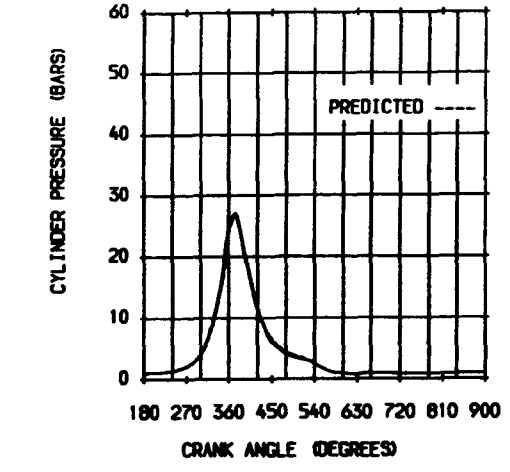

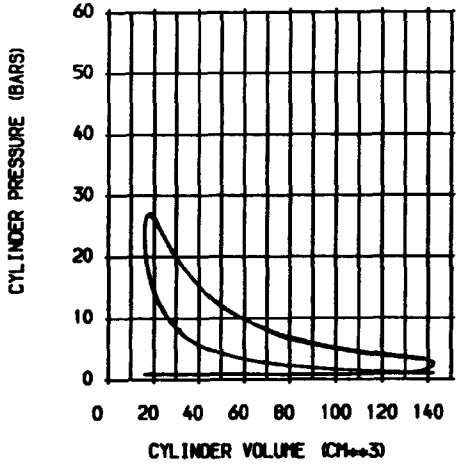

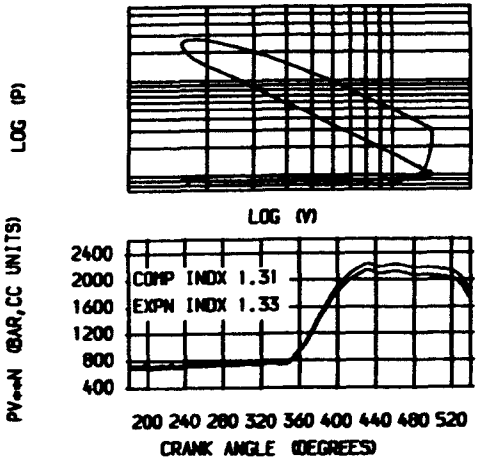

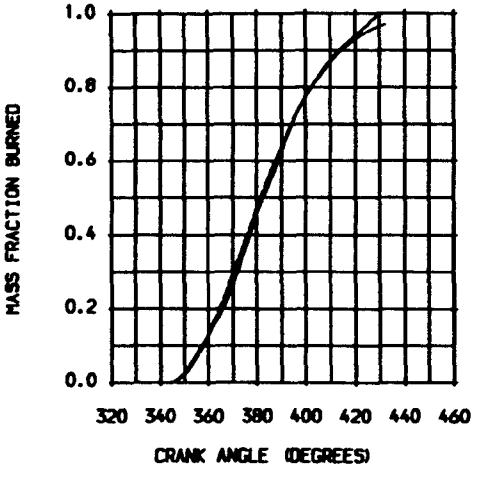

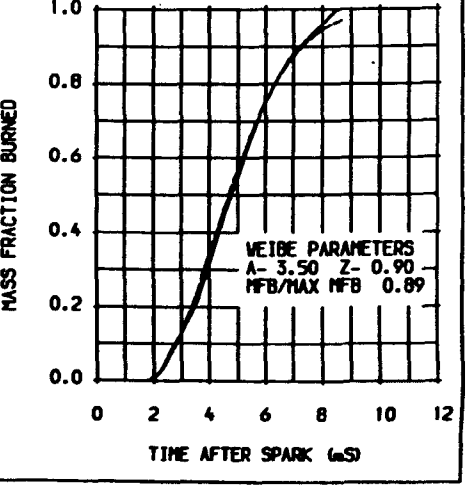

TEST DATE	29/03/89
TEST REFERENCE	T39M3504TII
COMPRESSION RATIO	8.95
SPEED (RPM)	2111.00
IGNITION (DEG BTDC)	38
EXCESS AIR RATIO	1.39
CHAMBER AREA (CM**2)	67.51
ATMOSPHERIC PRESS (BAR)	1.01320
PRESS TDC EXHAUST (BAR)	0.91320
PRESSURE IVC (BAR)	1.15851
RESIDUAL FRACTION (%)	7.00
BLOWBY COEFFICIENT	1.53
BLOWBY % OF CHARGE	3.8

DERIVED MASS BURNED CRITERIA

SRT OF HT RLS DABDC		344.0		
0 - 1%	DEG.	26	mS	2.1
0 - 10%	DEG.	36	mS	2.8
0 - 50%	DEG.	58	mS	4.6
0 - 90%	DEG.	90	mS	7.1
0 - 100%	DEG.	109	mS	8.6
1 - 90%	DEG.	64	mS	5.1
dP/dθ MAX (BARS/DEG)		0.66		
	AT	355.0	DEG	
MAX PRESSURE (BARS)		28.44		
	AT	375.0	DEG	

VEIBE MASS BURNED CRITERIA

SRT OF HT RLS DABDC		344.0		
0 - 1%	DEG.	26	mS	2.1
0 - 10%	DEG.	36	mS	2.8
0 - 50%	DEG.	60	mS	4.7
0 - 90%	DEG.	92	mS	7.3
0 - 100%	DEG.	109	mS	8.6
1 - 90%	DEG.	66	mS	5.2
dP/dθ MAX (BARS/DEG)		0.59		
	AT	355.0	DEG	
MAX PRESSURE (BARS)		27.36		
	AT	373.0	DEG	

HEAT TRANSFER

ENGINE MEASURED (kW)	1.317	
ENGINE PREDICTED (kW)	0.827	
PREDICTED/MEASURED (%)	62.8	
MAX BURNED GAS TEMP (K)	2131.8	
AT	365.0	DEG
BURNED GAS TEMP EVO (K)	1245.0	
GAS TEMP AT IVC (K)	357.5	
WALL TEMPERATURE (K)	400.0	

STATISTICAL DATA

	MEAN	SD	% DIS
WORK (J)	71.65	1.890	2.6
POWER (kW)	1.260	0.033	2.6
PMAX (BAR)	28.81	3.400	11.9
AT DEG	13.9	3.800	27.2

GAS ANALYSIS

	MODEL	MEASURED
CO2 (%)	7.1	7.8
CO (PPM)	0.0	400.0
O2 (%)	5.5	6.6
NOx (PPM)	5452.5	170.0
UHC (PPM)		2088.0

FUEL GROSS CV (kJ/kG) 53319.0
STOICH A/F RATIO 16.61

	MODEL	MEASD
POWER (kW)	1.343	1.275
FRICTN PWR (kW)	0.307	
PUMPNG PWR (kW)		-0.017
INDICATD MEP (BAR)	6.04	5.74
INDICATED EFFICNCY	0.260	0.247
BRAKE POWER (kW)	1.019	0.965
BRAKE TH EFFICNCY	0.197	0.187

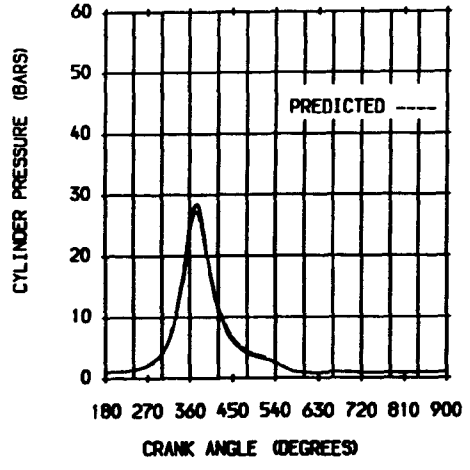

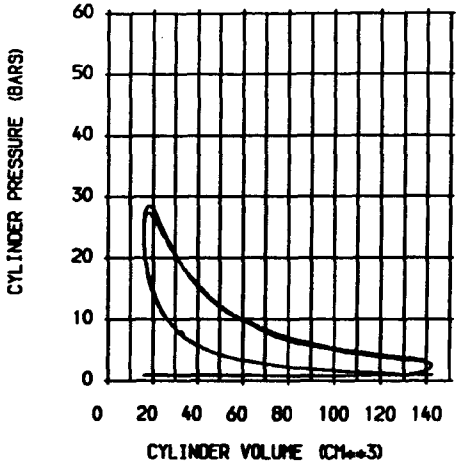

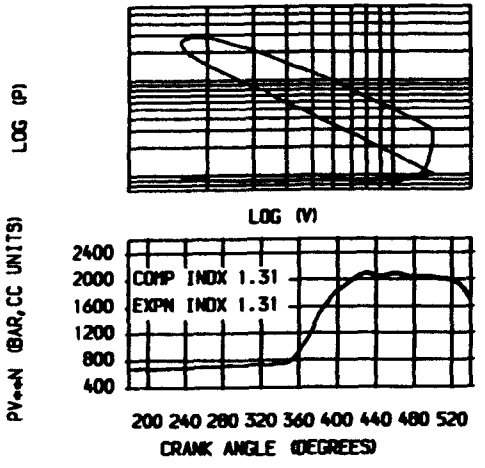

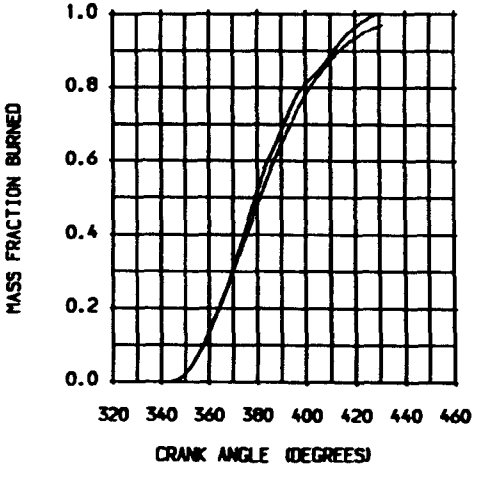

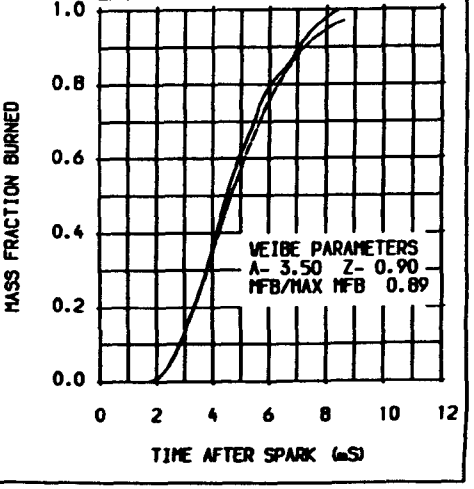

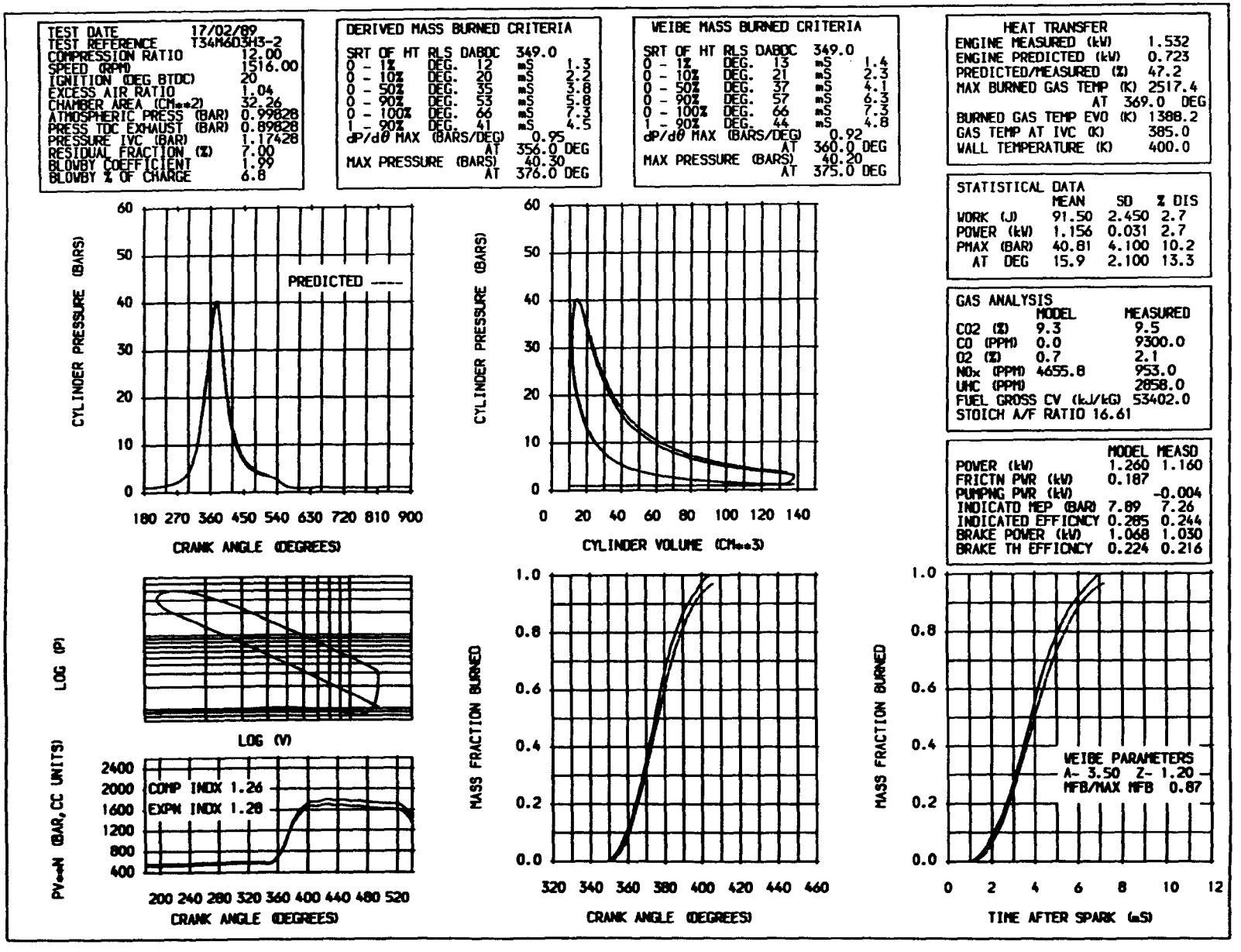
TEST DATE 17/02/89
TEST REFERENCE T34M6D3H3-2
COMPRESSION RATIO 12.00
SPEED (RPM) 1516.00
IGNITION (DEG BTDC) 20
EXCESS AIR RATIO 1.04
CHAMBER AREA (CM**2) 32.26
ATMOSPHERIC PRESS (BAR) 0.99828
PRESS TDC EXHAUST (BAR) 0.89828
PRESSURE IVC (BAR) 1.17428
RESIDUAL FRACTION (%) 7.00
BLOWBY COEFFICIENT 1.99
BLOWBY % OF CHARGE 6.8
DERIVED MASS BURNED CRITERIA
SRT OF HT RLS DABDC 349.0
0 - 1% DEG. 12 mS 1.3
0 - 10% DEG. 20 mS 2.2
0 - 50% DEG. 35 mS 3.8
0 - 90% DEG. 53 mS 5.8
0 - 100% DEG. 66 mS 7.3
1 - 90% DEG. 41 mS 4.5
dP/dθ MAX (BARS/DEG) 0.95
AT 356.0 DEG
MAX PRESSURE (BARS) 40.30
AT 376.0 DEG
WEIBE MASS BURNED CRITERIA
SRT OF HT RLS DABDC 349.0
0 - 1% DEG. 13 mS 1.4
0 - 10% DEG. 21 mS 2.3
0 - 50% DEG. 37 mS 4.1
0 - 90% DEG. 57 mS 6.3
0 - 100% DEG. 66 mS 7.3
1 - 90% DEG. 44 mS 4.8
dP/dθ MAX (BARS/DEG) 0.92
AT 360.0 DEG
MAX PRESSURE (BARS) 40.20
AT 375.0 DEG
HEAT TRANSFER
ENGINE MEASURED (kW) 1.532
ENGINE PREDICTED (kW) 0.723
PREDICTED/MEASURED (%) 47.2
MAX BURNED GAS TEMP (K) 2517.4
AT 369.0 DEG
BURNED GAS TEMP EVO (K) 1388.2
GAS TEMP AT IVC (K) 385.0
WALL TEMPERATURE (K) 400.0
STATISTICAL DATA
MEAN SD % DIS
WORK (J) 91.50 2.450 2.7
POWER (kW) 1.156 0.031 2.7
PMAX (BAR) 40.81 4.100 10.2
AT DEG 15.9 2.100 13.3
GAS ANALYSIS
MODEL MEASURED
CO2 (%) 9.3 9.5
CO (PPM) 0.0 9300.0
O2 (%) 0.7 2.1
NOx (PPM) 4655.8 953.0
UHC (PPM) 2858.0
FUEL GROSS CV (kJ/kG) 53402.0
STOICH A/F RATIO 16.61
MODEL MEASD
POWER (kW) 1.260 1.160
FRICTN PWR (kW) 0.187
PUMPNG PWR (kW) -0.004
INDICATD MEP (BAR) 7.89 7.26
INDICATED EFFICNCY 0.285 0.244
BRAKE POWER (kW) 1.068 1.030
BRAKE TH EFFICNCY 0.224 0.216
CYLINDER PRESSURE (BARS)
PREDICTED
CRANK ANGLE (DEGREES)
CYLINDER PRESSURE (BARS)
CYLINDER VOLUME (CM**3)
LOG (P)
LOG (V)
PV**N (BAR,CC UNITS)
COMP INDX 1.26
EXPN INDX 1.28
CRANK ANGLE (DEGREES)
MASS FRACTION BURNED
CRANK ANGLE (DEGREES)
MASS FRACTION BURNED
WEIBE PARAMETERS
A- 3.50 Z- 1.20
MFB/MAX MFB 0.87
TIME AFTER SPARK (mS)

TEST DATE	17/02/89
TEST REFERENCE	T34M60JH3-2
COMPRESSION RATIO	12.00
SPEED (RPM)	1516.00
IGNITION (DEG BTDC)	20
EXCESS AIR RATIO	1.04
CHAMBER AREA (CM**2)	32.26
ATMOSPHERIC PRESS (BAR)	0.99828
PRESS TDC EXHAUST (BAR)	0.89828
PRESSURE IVC (BAR)	1.17428
RESIDUAL FRACTION (%)	7.00
BLOWBY COEFFICIENT	1.99
BLOWBY % OF CHARGE	6.8

DERIVED MASS BURNED CRITERIA

SRT OF HT RLS DABOC		349.0	
0 - 1%	DEG. 12	DEG	1.3
0 - 10%	DEG. 20	DEG	2.2
0 - 50%	DEG. 35	DEG	3.8
0 - 90%	DEG. 53	DEG	5.8
0 - 100%	DEG. 66	DEG	7.3
1 - 90%	DEG. 41	DEG	4.5
dP/dθ MAX (BARS/DEG)		0.95	
	AT	356.0	DEG
MAX PRESSURE (BARS)		40.30	
	AT	376.0	DEG

WEIBE MASS BURNED CRITERIA

SRT OF HT RLS DABOC		349.0	
0 - 1%	DEG. 13	DEG	1.4
0 - 10%	DEG. 21	DEG	2.3
0 - 50%	DEG. 37	DEG	4.1
0 - 90%	DEG. 57	DEG	6.3
0 - 100%	DEG. 66	DEG	7.3
1 - 90%	DEG. 44	DEG	4.8
dP/dθ MAX (BARS/DEG)		1.01	
	AT	361.0	DEG
MAX PRESSURE (BARS)		42.42	
	AT	375.0	DEG

HEAT TRANSFER

ENGINE MEASURED (kW)	1.532
ENGINE PREDICTED (kW)	0.745
PREDICTED/MEASURED (%)	48.6
MAX BURNED GAS TEMP (K)	2498.2
AT	369.0 DEG
BURNED GAS TEMP EVO (K)	1378.7
GAS TEMP AT IVC (K)	357.5
WALL TEMPERATURE (K)	400.0

STATISTICAL DATA

	MEAN	SD	% DIS
WORK (J)	91.50	2.450	2.7
POWER (kW)	1.156	0.031	2.7
PMAX (BAR)	40.81	4.100	10.2
AT DEG	15.9	2.100	13.3

GAS ANALYSIS

	MODEL	MEASURED
CO2 (%)	9.3	9.5
CO (PPM)	0.0	9300.0
O2 (%)	0.7	2.1
NOx (PPM)	4443.1	953.0
UHC (PPM)		2858.0
FUEL GROSS CV (kJ/kG)		53402.0
STOICH A/F RATIO	16.61	

	MODEL	MEASD
POWER (kW)	1.376	1.160
FRICTN PWR (kW)	0.187	
PUMPNG PWR (kW)		-0.004
INDICATD MEP (BAR)	8.62	7.26
INDICATED EFFICNCY	0.290	0.244
BRAKE POWER (kW)	1.185	1.030
BRAKE TH EFFICNCY	0.249	0.216

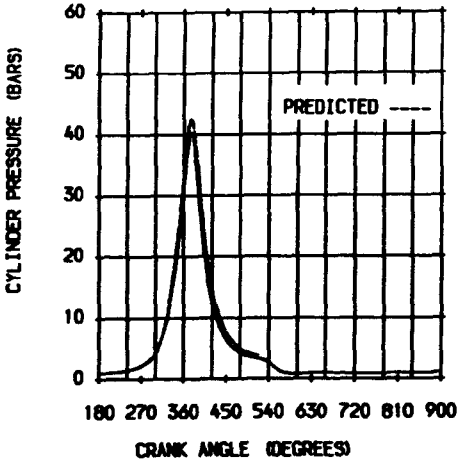

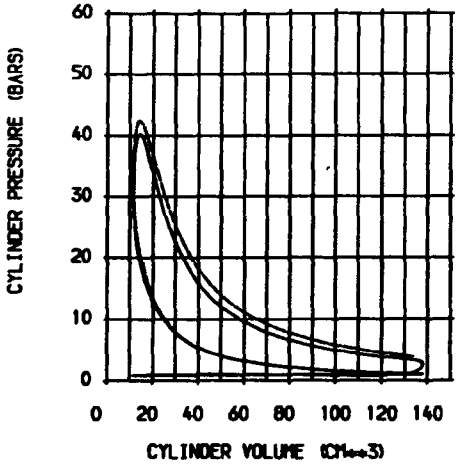

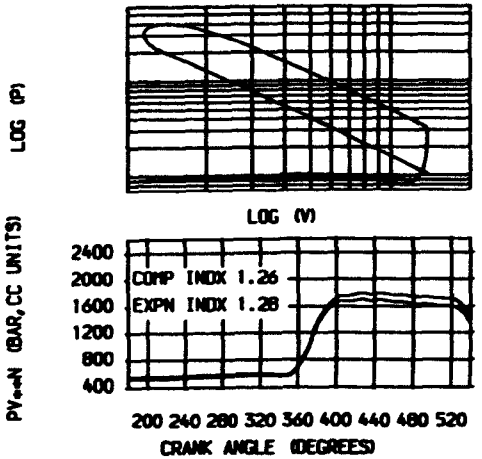

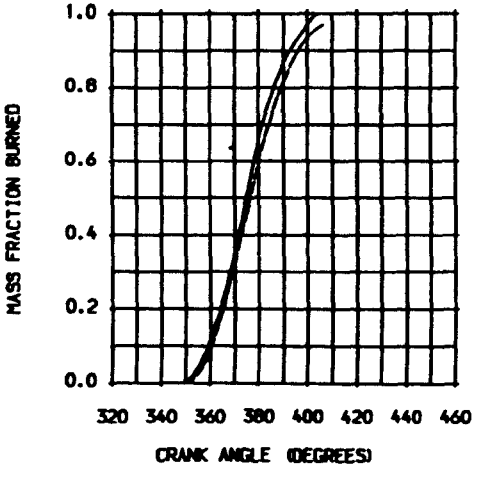

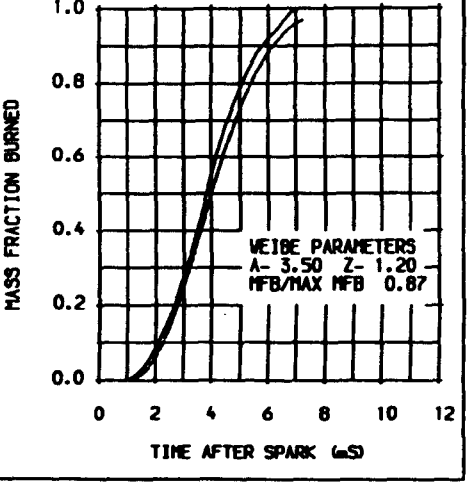

TEST DATE	01/02/89
TEST REFERENCE	T32M4501H3-2
COMPRESSION RATIO	13.00
SPEED (RPM)	1525.00
IGNITION (DEG BTDC)	16
EXCESS AIR RATIO	1.04
CHAMBER AREA (CM**2)	31.65
ATMOSPHERIC PRESS (BAR)	1.02597
PRESS TDC EXHAUST (BAR)	0.92596
PRESSURE IVC (BAR)	1.21512
RESIDUAL FRACTION (%)	7.00
BLOWBY COEFFICIENT	1.99
BLOWBY % OF CHARGE	6.7

DERIVED MASS BURNED CRITERIA

SRT OF HT RLS DABDC		351.0	
0 - 1%	DEG. 10	mS	1.1
0 - 10%	DEG. 20	mS	2.2
0 - 50%	DEG. 38	mS	4.2
0 - 90%	DEG. 60	mS	6.6
0 - 100%	DEG. 72	mS	7.9
1 - 90%	DEG. 50	mS	5.5
dP/dθ MAX (BARS/DEG)		0.82	
	AT	356.0	DEG
MAX PRESSURE (BARS)		38.27	
	AT	371.0	DEG

WEIBE MASS BURNED CRITERIA

SRT OF HT RLS DABDC		351.0	
0 - 1%	DEG. 12	mS	1.3
0 - 10%	DEG. 21	mS	2.3
0 - 50%	DEG. 39	mS	4.3
0 - 90%	DEG. 61	mS	6.7
0 - 100%	DEG. 72	mS	7.9
1 - 90%	DEG. 49	mS	5.4
dP/dθ MAX (BARS/DEG)		0.68	
	AT	358.0	DEG
MAX PRESSURE (BARS)		39.74	
	AT	374.0	DEG

HEAT TRANSFER

ENGINE MEASURED (kW)	1.519
ENGINE PREDICTED (kW)	0.715
PREDICTED/MEASURED (%)	47.0
MAX BURNED GAS TEMP (K)	2471.8
AT	368.0 DEG
BURNED GAS TEMP EVO (K)	1428.2
GAS TEMP AT IVC (K)	361.5
WALL TEMPERATURE (K)	400.0

STATISTICAL DATA

	MEAN	SD	% DIS
WORK (J)	88.71	1.180	1.3
POWER (kW)	1.127	0.015	1.3
PMAX (BAR)	38.65	2.900	7.6
AT DEG	10.9	3.000	27.9

GAS ANALYSIS

	MODEL	MEASURED
CO2 (%)	9.3	9.7
CO (PPM)	0.0	5500.0
O2 (%)	0.7	1.9
NOx (PPM)	4199.1	969.0
UHC (PPM)		3379.9

FUEL GROSS CV (kJ/kG) 53989.5
STOICH A/F RATIO 16.72

	MODEL	MEASD
POWER (kW)	1.348	1.133
FRICTN PWR (kW)	0.189	
PUMPNG PWR (kW)		-0.006
INDICATD MEP (BAR)	8.39	7.06
INDICATED EFFICNCY	0.276	0.231
BRAKE POWER (kW)	1.153	0.927
BRAKE TH EFFICNCY	0.236	0.189

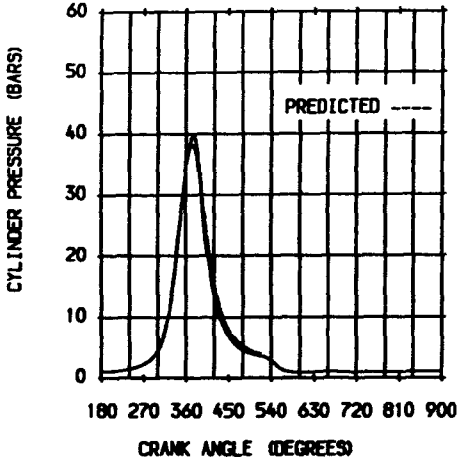

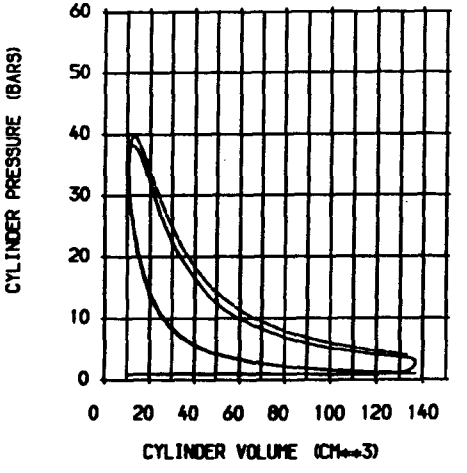

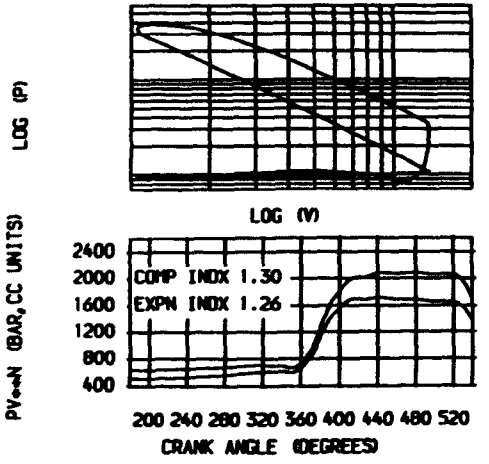

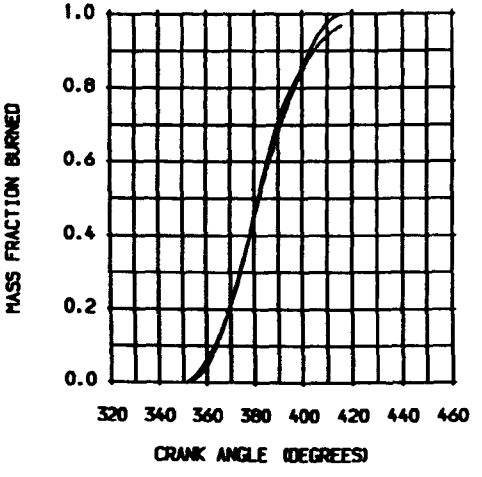

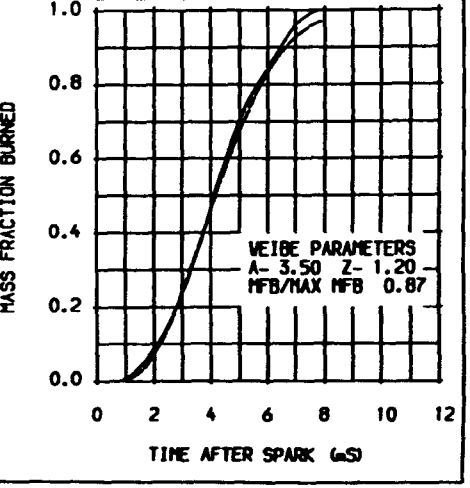

TEST DATE	01/02/89
TEST REFERENCE	T32M4603H3-2
COMPRESSION RATIO	13.00
SPEED (RPM)	1515.00
IGNITION (DEG BTDC)	22
EXCESS AIR RATIO	1.18
CHAMBER AREA (CM**2)	31.65
ATMOSPHERIC PRESS (BAR)	1.02597
PRESS TDC EXHAUST (BAR)	0.92596
PRESSURE IVC (BAR)	1.25008
RESIDUAL FRACTION (%)	7.00
BLOWBY COEFFICIENT	1.99
BLOWBY % OF CHARGE	6.8

DERIVED MASS BURNED CRITERIA

SRT OF HT	RLS	DABDC	346.0	
0 - 1%	DEG.	10	AS	1.1
0 - 10%	DEG.	17	AS	1.9
0 - 50%	DEG.	30	AS	3.3
0 - 90%	DEG.	45	AS	5.0
0 - 100%	DEG.	53	AS	5.8
1 - 90%	DEG.	35	AS	3.9
dP/dθ MAX	(BARS/DEG)		1.27	
		AT	354.0	DEG
MAX PRESSURE	(BARS)		48.23	
		AT	370.0	DEG

WEIBE MASS BURNED CRITERIA

SRT OF HT	RLS	DABDC	346.0	
0 - 1%	DEG.	12	AS	1.3
0 - 10%	DEG.	19	AS	2.1
0 - 50%	DEG.	32	AS	3.5
0 - 90%	DEG.	47	AS	5.2
0 - 100%	DEG.	53	AS	5.8
1 - 90%	DEG.	35	AS	3.9
dP/dθ MAX	(BARS/DEG)		1.68	
		AT	359.0	DEG
MAX PRESSURE	(BARS)		55.48	
		AT	372.0	DEG

HEAT TRANSFER

ENGINE MEASURED (kW)	1.346
ENGINE PREDICTED (kW)	0.711
PREDICTED/MEASURED (%)	52.8
MAX BURNED GAS TEMP (K)	2454.5
AT	367.0 DEG
BURNED GAS TEMP EVO (K)	1215.2
GAS TEMP AT IVC (K)	376.5
WALL TEMPERATURE (K)	400.0

STATISTICAL DATA

	MEAN	SD	% DIS
WORK (J)	77.59	3.320	4.3
POWER (kW)	0.980	0.042	4.3
PMAX (BAR)	49.08	5.100	10.4
AT DEG	10.1	2.000	19.7

GAS ANALYSIS

	MODEL	MEASURED
CO2 (%)	8.3	9.0
CO (PPM)	0.0	1000.0
O2 (%)	2.9	3.9
NOx (PPM)	7487.3	1985.0
UHC (PPM)		3129.0

FUEL GROSS CV (kJ/kG) 53989.5
STOICH A/F RATIO 16.72

	MODEL	MEASD
POWER (kW)	1.341	0.982
FRICTN PWR (kW)	0.187	
PUMPNG PWR (kW)		-0.003
INDICATD MEP (BAR)	8.41	6.16
INDICATED EFFICNCY	0.315	0.229
BRAKE POWER (kW)	1.151	0.910
BRAKE TH EFFICNCY	0.268	0.212

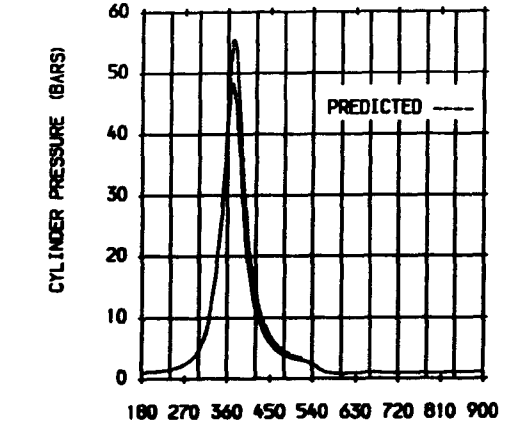

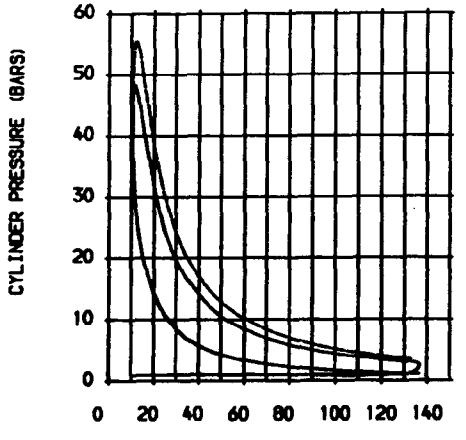

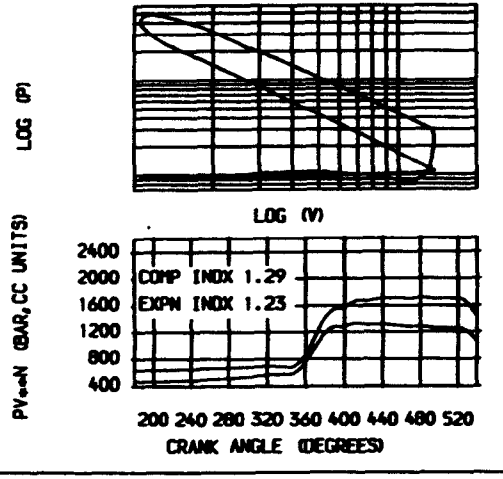

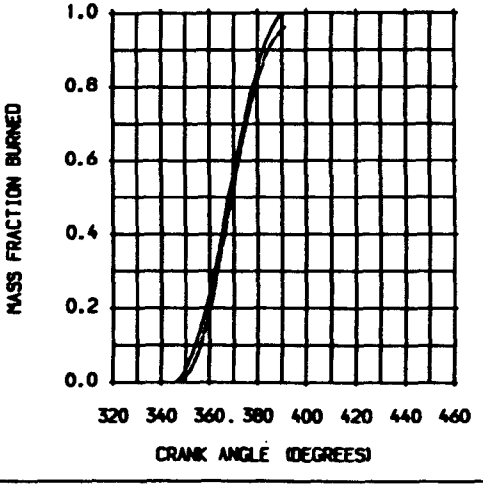

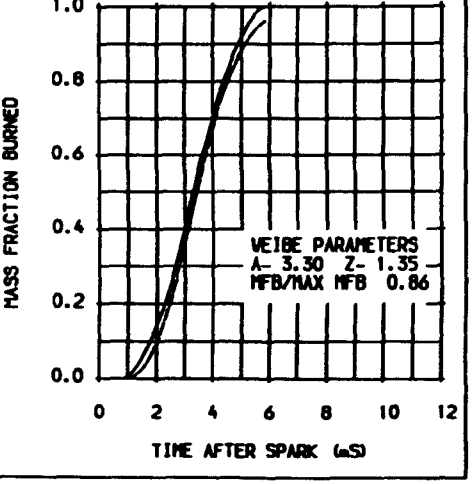

TEST DATE	01/02/89
TEST REFERENCE	T32M470SH3-2
COMPRESSION RATIO	13.00
SPEED (RPM)	1500.00
IGNITION (DEG BTDC)	29
EXCESS AIR RATIO	1.48
CHAMBER AREA (CM**2)	31.65
ATMOSPHERIC PRESS (BAR)	1.02597
PRESS TDC EXHAUST (BAR)	0.92596
PRESSURE IVC (BAR)	1.20679
RESIDUAL FRACTION (%)	7.00
BLOWBY COEFFICIENT	1.99
BLOWBY % OF CHARGE	6.8

DERIVED MASS BURNED CRITERIA

SRT OF HT RLS DABDC		344.0	
0 - 1%	DEG. 16	MS	1.8
0 - 10%	DEG. 24	MS	2.7
0 - 50%	DEG. 44	MS	4.9
0 - 90%	DEG. 72	MS	8.0
0 - 100%	DEG. 83	MS	9.2
1 - 90%	DEG. 56	MS	6.2
dP/dθ MAX (BARS/DEG)		1.14	
	AT	352.0	DEG
MAX PRESSURE (BARS)		42.74	
	AT	366.0	DEG

WEIBE MASS BURNED CRITERIA

SRT OF HT RLS DABDC		344.0	
0 - 1%	DEG. 17	MS	1.9
0 - 10%	DEG. 26	MS	2.9
0 - 50%	DEG. 46	MS	5.1
0 - 90%	DEG. 74	MS	8.2
0 - 100%	DEG. 83	MS	9.2
1 - 90%	DEG. 57	MS	6.3
dP/dθ MAX (BARS/DEG)		1.17	
	AT	353.0	DEG
MAX PRESSURE (BARS)		43.65	
	AT	368.0	DEG

HEAT TRANSFER

ENGINE MEASURED (kW)	0.919
ENGINE PREDICTED (kW)	0.490
PREDICTED/MEASURED (%)	53.3
MAX BURNED GAS TEMP (K)	2151.5
AT	363.0 DEG
BURNED GAS TEMP EVO (K)	1121.2
GAS TEMP AT IVC (K)	357.5
WALL TEMPERATURE (K)	400.0

STATISTICAL DATA

	MEAN	SD	% DIS
WORK (J)	61.75	1.590	2.6
POWER (kW)	0.772	0.020	2.6
PMAX (BAR)	42.97	3.700	8.8
AT DEG	6.2	1.500	25.1

GAS ANALYSIS

	MODEL	MEASURED
CO2 (%)	6.7	6.9
CO (PPM)	0.0	1100.0
O2 (%)	6.4	7.8
NOx (PPM)	6172.3	348.0
UHC (PPM)		4139.0
FUEL GROSS CV (kJ/kG)	53989.5	
STOICH A/F RATIO	16.72	

	MODEL	MEASD
POWER (kW)	0.995	0.780
FRICTN PWR (kW)	0.184	
PUMPNG PWR (kW)		-0.008
INDICATD MEP (BAR)	6.30	4.94
INDICATED EFFICNCY	0.286	0.222
BRAKE POWER (kW)	0.803	0.694
BRAKE TH EFFICNCY	0.229	0.198

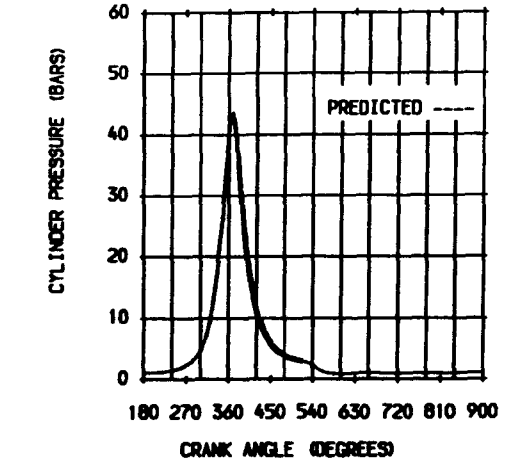

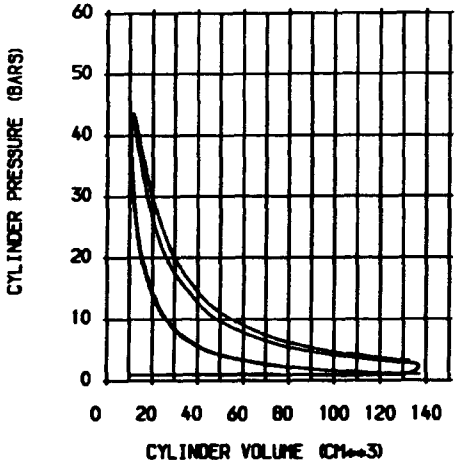

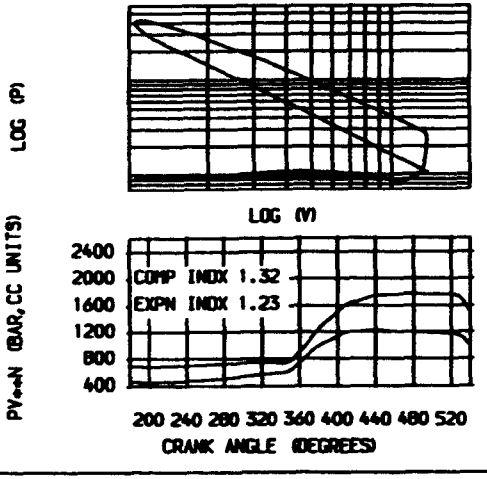

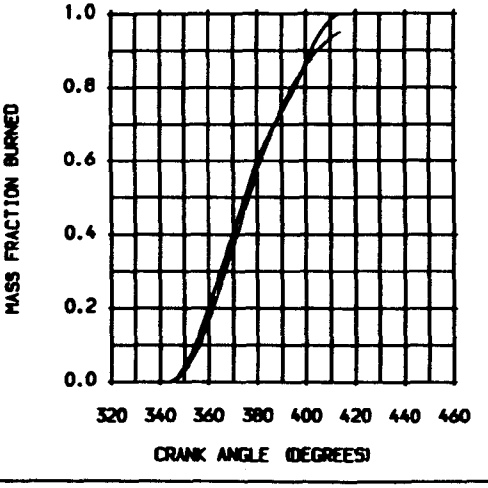

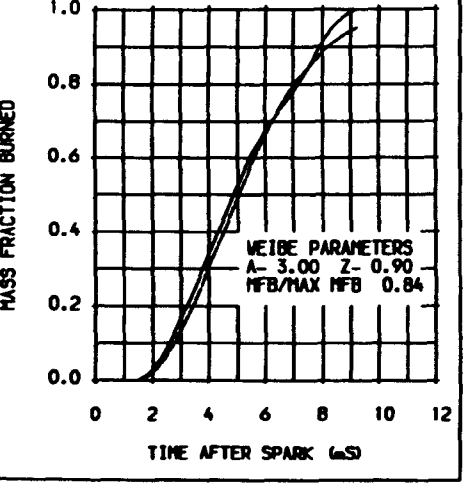

TEST DATE	08/03/89
TEST REFERENCE	T37M2301H3-2
COMPRESSION RATIO	9.00
SPEED (RPM)	1814.00
IGNITION (DEG BTDC)	30
EXCESS AIR RATIO	1.00
CHAMBER AREA (CM**2)	35.56
ATMOSPHERIC PRESS (BAR)	1.01056
PRESS TDC EXHAUST (BAR)	0.91056
PRESSURE IVC (BAR)	1.19472
RESIDUAL FRACTION (%)	7.00
BLOWBY COEFFICIENT	1.84
BLOWBY % OF CHARGE	5.3

DERIVED MASS BURNED CRITERIA

SRT OF HT RLS DABDC	339.0	
0 - 1%	DEG. 13	mS 1.2
0 - 10%	DEG. 20	mS 1.8
0 - 50%	DEG. 34	mS 3.1
0 - 90%	DEG. 51	mS 4.7
0 - 100%	DEG. 60	mS 5.5
1 - 90%	DEG. 38	mS 3.5
dP/dθ MAX (BARS/DEG)	1.26	
	AT	360.0 DEG
MAX PRESSURE (BARS)	40.35	
	AT	372.0 DEG

VEIBE MASS BURNED CRITERIA

SRT OF HT RLS DABDC	339.0	
0 - 1%	DEG. 14	mS 1.3
0 - 10%	DEG. 21	mS 1.9
0 - 50%	DEG. 35	mS 3.2
0 - 90%	DEG. 52	mS 4.8
0 - 100%	DEG. 60	mS 5.5
1 - 90%	DEG. 38	mS 3.5
dP/dθ MAX (BARS/DEG)	1.40	
	AT	357.0 DEG
MAX PRESSURE (BARS)	43.71	
	AT	372.0 DEG

HEAT TRANSFER

ENGINE MEASURED (kW)	1.958
ENGINE PREDICTED (kW)	1.029
PREDICTED/MEASURED (%)	52.5
MAX BURNED GAS TEMP (K)	2594.1
AT	366.0 DEG
BURNED GAS TEMP EVO (K)	1429.8
GAS TEMP AT IVC (K)	382.0
WALL TEMPERATURE (K)	400.0

STATISTICAL DATA

	MEAN	SD	% DIS
WORK (J)	85.72	1.820	2.1
POWER (kW)	1.296	0.027	2.1
PMAX (BAR)	41.19	3.300	7.9
AT DEG	11.5	2.400	20.6

GAS ANALYSIS

	MODEL	MEASURED
CO2 (%)	9.6	9.5
CO (PPM)	0.0	10000.0
O2 (%)	0.0	1.4
NOx (PPM)	4028.6	1037.0
UHC (PPM)		3190.0
FUEL GROSS CV (kJ/kG)		53506.6
STOICH A/F RATIO	16.64	

	MODEL	MEASD
POWER (kW)	1.646	1.303
FRICTN PWR (kW)	0.244	
PUMPNG PWR (kW)		-0.007
INDICATD MEP (BAR)	8.62	6.82
INDICATED EFFICNCY	0.284	0.224
BRAKE POWER (kW)	1.395	1.149
BRAKE TH EFFICNCY	0.240	0.198

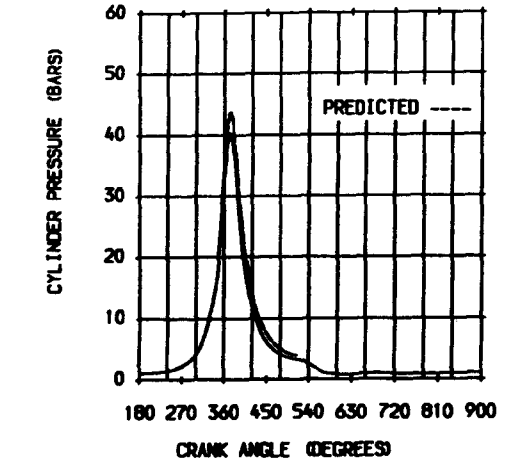

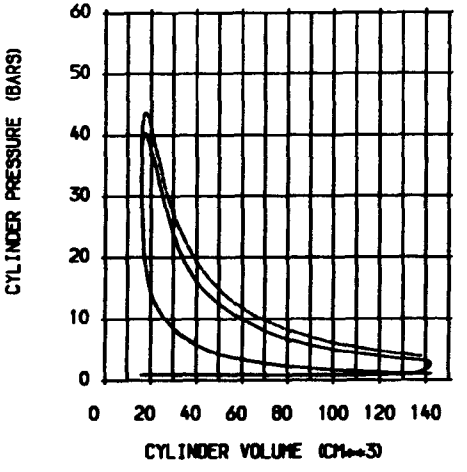

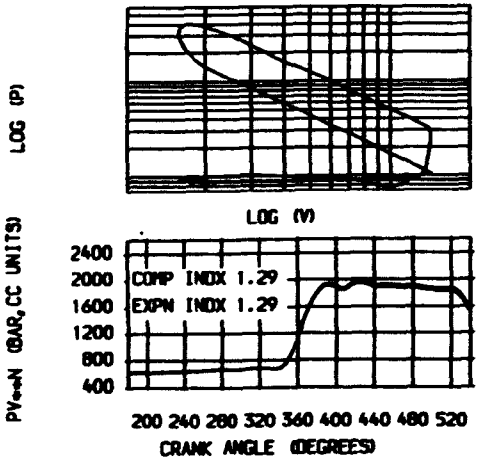

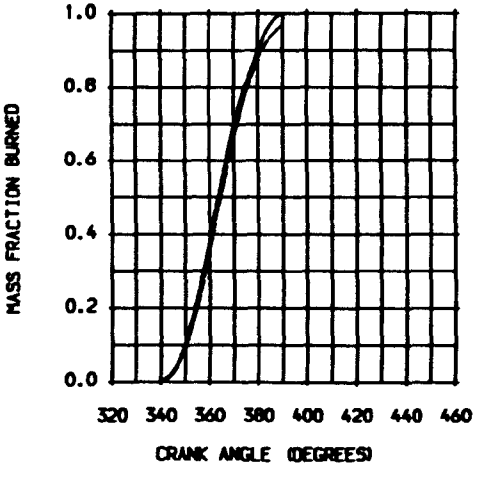

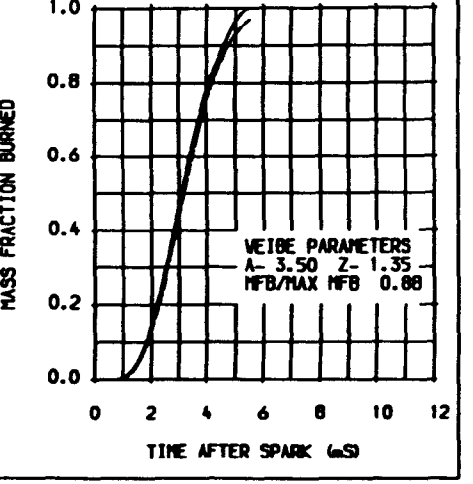

TEST DATE	08/03/89
TEST REFERENCE	T37M2402H3-2
COMPRESSION RATIO	9.00
SPEED (RPM)	1805.00
IGNITION (DEG BTDC)	43
EXCESS AIR RATIO	1.50
CHAMBER AREA (CM**2)	35.56
ATMOSPHERIC PRESS (BAR)	1.01056
PRESS TDC EXHAUST (BAR)	0.91056
PRESSURE IVC (BAR)	1.14466
RESIDUAL FRACTION (%)	7.00
BLOWBY COEFFICIENT	1.85
BLOWBY % OF CHARGE	5.3

DERIVED MASS BURNED CRITERIA

SRT OF HT RLS DABOC		336.0	
0 - 1%	DEG. 23	mS	2.1
0 - 10%	DEG. 33	mS	3.0
0 - 50%	DEG. 51	mS	4.7
0 - 90%	DEG. 71	mS	6.6
0 - 100%	DEG. 82	mS	7.6
1 - 90%	DEG. 48	mS	4.4
dP/dθ MAX (BARS/DEG)		0.79	
	AT	354.0	DEG
MAX PRESSURE (BARS)		31.34	
	AT	370.0	DEG

WEIBE MASS BURNED CRITERIA

SRT OF HT RLS DABOC		336.0	
0 - 1%	DEG. 24	mS	2.2
0 - 10%	DEG. 33	mS	3.0
0 - 50%	DEG. 52	mS	4.8
0 - 90%	DEG. 75	mS	6.9
0 - 100%	DEG. 82	mS	7.6
1 - 90%	DEG. 51	mS	4.7
dP/dθ MAX (BARS/DEG)		0.89	
	AT	354.0	DEG
MAX PRESSURE (BARS)		33.82	
	AT	371.0	DEG

HEAT TRANSFER

ENGINE MEASURED (kW)	1.060
ENGINE PREDICTED (kW)	0.586
PREDICTED/MEASURED (%)	55.2
MAX BURNED GAS TEMP (K)	2133.6
AT	365.0 DEG
BURNED GAS TEMP EVO (K)	1148.2
GAS TEMP AT IVC (K)	353.5
WALL TEMPERATURE (K)	400.0

STATISTICAL DATA

	MEAN	SD	% DIS
WORK (J)	67.67	1.820	2.7
POWER (kW)	1.018	0.027	2.7
PMAX (BAR)	31.54	3.800	12.2
AT DEG	9.8	1.900	19.4

GAS ANALYSIS

	MODEL	MEASURED
CO2 (%)	6.6	6.9
CO (PPM)	0.0	800.0
O2 (%)	6.5	7.9
NOx (PPM)	6011.5	139.0
UHC (PPM)		3453.0

FUEL GROSS CV (kJ/kG) 53506.6
STOICH A/F RATIO 16.64

	MODEL	MEASD
POWER (kW)	1.192	1.036
FRICTN PWR (kW)	0.242	
PUMPNG PWR (kW)		-0.019
INDICATD MEP (BAR)	6.27	5.45
INDICATED EFFICNCY	0.290	0.252
BRAKE POWER (kW)	0.931	0.859
BRAKE TH EFFICNCY	0.227	0.209

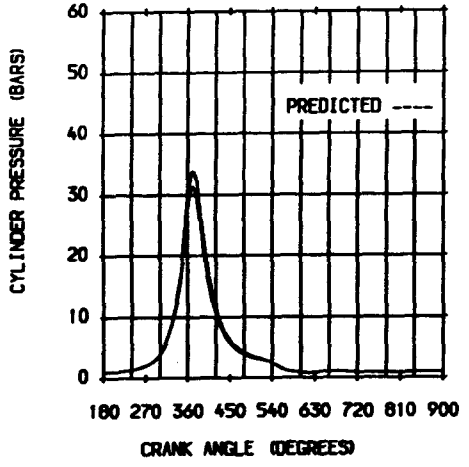

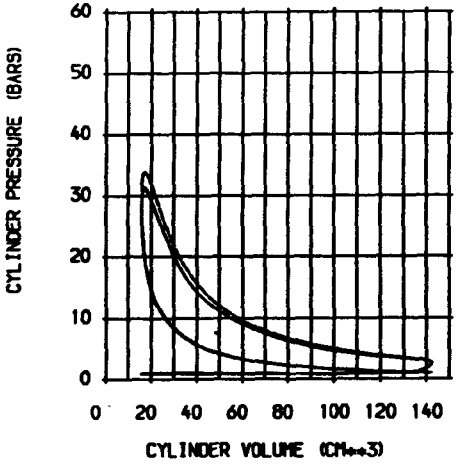

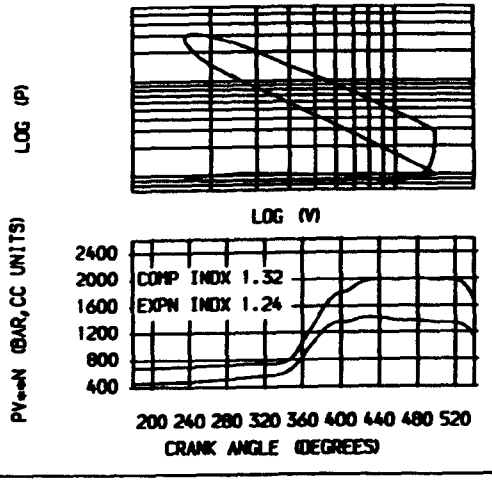

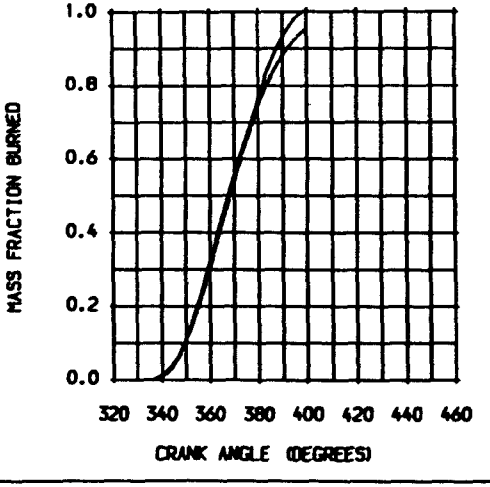

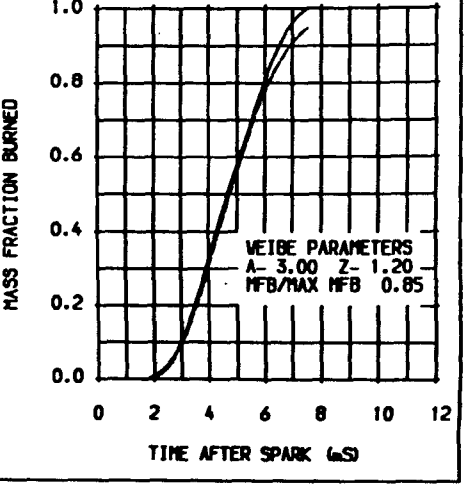

TEST DATE	02/05/89
TEST REFERENCE	T40M3602H3-2
COMPRESSION RATIO	10.00
SPEED (RPM)	1829.00
IGNITION (DEG BTDC)	24
EXCESS AIR RATIO	1.07
CHAMBER AREA (CM**2)	34.26
ATMOSPHERIC PRESS (BAR)	1.01623
PRESS TDC EXHAUST (BAR)	0.91622
PRESSURE IVC (BAR)	1.17652
RESIDUAL FRACTION (%)	7.00
BLOWBY COEFFICIENT	1.83
BLOWBY % OF CHARGE	5.2

DERIVED MASS BURNED CRITERIA

SRT OF HT RLS DABDC		346.0	
0 - 1%	DEG. 13	mS	1.2
0 - 10%	DEG. 21	mS	1.9
0 - 50%	DEG. 40	mS	3.6
0 - 90%	DEG. 56	mS	5.1
0 - 100%	DEG. 67	mS	6.1
1 - 90%	DEG. 43	mS	3.9
dP/dθ MAX (BARS/DEG)		0.85	
	AT	352.0	DEG
MAX PRESSURE (BARS)		35.38	
	AT	376.0	DEG

WEIBE MASS BURNED CRITERIA

SRT OF HT RLS DABDC		346.0	
0 - 1%	DEG. 15	mS	1.4
0 - 10%	DEG. 23	mS	2.1
0 - 50%	DEG. 40	mS	3.6
0 - 90%	DEG. 60	mS	5.5
0 - 100%	DEG. 67	mS	6.1
1 - 90%	DEG. 45	mS	4.1
dP/dθ MAX (BARS/DEG)		0.91	
	AT	360.0	DEG
MAX PRESSURE (BARS)		37.47	
	AT	376.0	DEG

HEAT TRANSFER

ENGINE MEASURED (kW)	1.763	
ENGINE PREDICTED (kW)	0.840	
PREDICTED/MEASURED (%)	47.6	
MAX BURNED GAS TEMP (K)	2474.6	
AT	370.0	DEG
BURNED GAS TEMP EVO (K)	1413.6	
GAS TEMP AT IVC (K)	360.5	
WALL TEMPERATURE (K)	400.0	

STATISTICAL DATA

	MEAN	SD	% DIS
WORK (J)	95.14	2.150	2.3
POWER (kW)	1.450	0.033	2.3
PMAX (BAR)	35.91	3.800	10.6
AT DEG	16.3	2.200	13.5

GAS ANALYSIS

	MODEL	MEASURED
CO2 (%)	9.1	9.8
CO (PPM)	0.0	2500.0
O2 (%)	1.3	2.0
NOx (PPM)	5201.2	1329.0
UHC (PPM)		2124.0
FUEL GROSS CV (kJ/kG)		53611.5
STOICH A/F RATIO		16.67

	MODEL	MEASD
POWER (kW)	1.627	1.462
FRICTN PWR (kW)	0.247	
PUMPNG PWR (kW)		-0.013
INDICATD MEP (BAR)	8.45	7.59
INDICATED EFFICNCY	0.287	0.258
BRAKE POWER (kW)	1.367	1.255
BRAKE TH EFFICNCY	0.241	0.221

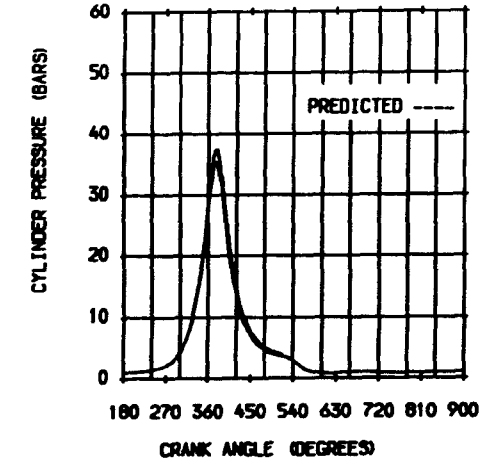

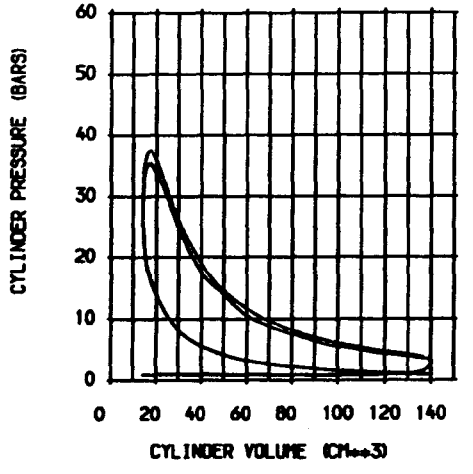

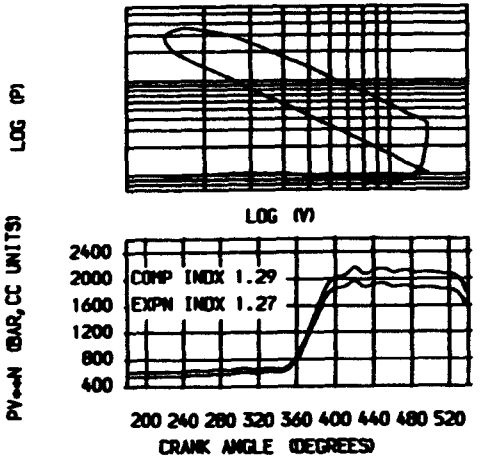

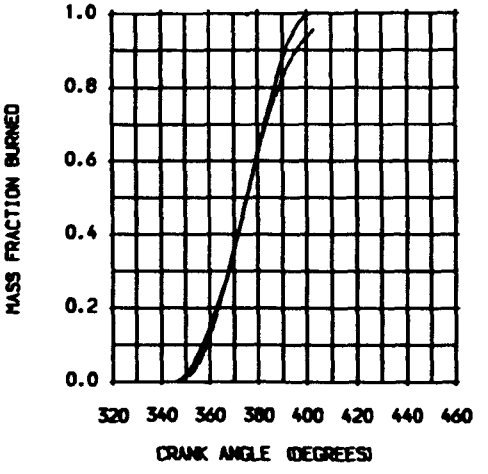

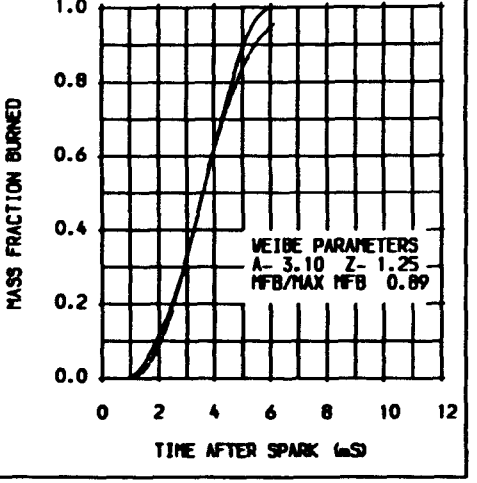

TEST DATE	02/05/89
TEST REFERENCE	T40M3703H3-2
COMPRESSION RATIO	10.00
SPEED (RPM)	1837.00
IGNITION (DEG BTDC)	26
EXCESS AIR RATIO	1.14
CHAMBER AREA (CM**2)	34.26
ATMOSPHERIC PRESS (BAR)	1.01623
PRESS TDC EXHAUST (BAR)	0.91622
PRESSURE IVC (BAR)	1.16708
RESIDUAL FRACTION (%)	7.00
BLOWBY COEFFICIENT	1.83
BLOWBY % OF CHARGE	5.2

DERIVED MASS BURNED CRITERIA

SRT OF HT RLS DABDC		346.0	
0 - 1%	DEG.	15	1.4
0 - 10%	DEG.	23	2.1
0 - 50%	DEG.	40	5.6
0 - 90%	DEG.	57	5.2
0 - 100%	DEG.	76	6.9
1 - 90%	DEG.	42	3.8
dP/dθ MAX (BARS/DEG)		0.88	
	AT	357.0	DEG
MAX PRESSURE (BARS)		36.43	
	AT	375.0	DEG

WEIBE MASS BURNED CRITERIA

SRT OF HT RLS DABDC		346.0	
0 - 1%	DEG.	17	1.5
0 - 10%	DEG.	25	2.3
0 - 50%	DEG.	41	5.7
0 - 90%	DEG.	60	5.4
0 - 100%	DEG.	76	6.9
1 - 90%	DEG.	43	3.9
dP/dθ MAX (BARS/DEG)		0.95	
	AT	360.0	DEG
MAX PRESSURE (BARS)		37.86	
	AT	376.0	DEG

HEAT TRANSFER

ENGINE MEASURED (kW)	1.513
ENGINE PREDICTED (kW)	0.799
PREDICTED/MEASURED (%)	52.8
MAX BURNED GAS TEMP (K)	2417.2
AT	370.0 DEG
BURNED GAS TEMP EVO (K)	1356.3
GAS TEMP AT IVC (K)	358.0
WALL TEMPERATURE (K)	400.0

STATISTICAL DATA

	MEAN	SD	% DIS
WORK (J)	90.73	2.340	2.6
POWER (kW)	1.389	0.036	2.6
PMAX (BAR)	36.89	3.500	9.4
AT DEG	14.7	2.400	16.4

GAS ANALYSIS

	MODEL	MEASURED
CO2 (%)	8.5	9.4
CO (PPM)	0.0	300.0
O2 (%)	2.4	3.1
NOx (PPM)	6283.3	1718.0
UHC (PPM)		1690.0
FUEL GROSS CV (kJ/kG)		53611.5
STOICH A/F RATIO	16.67	

	MODEL	MEASD
POWER (kW)	1.582	1.402
FRICTN PWR (kW)	0.249	
PUMPNG PWR (kW)		-0.013
INDICATD MEP (BAR)	8.18	7.25
INDICATED EFFICNCY	0.295	0.261
BRAKE POWER (kW)	1.320	1.259
BRAKE TH EFFICNCY	0.246	0.235

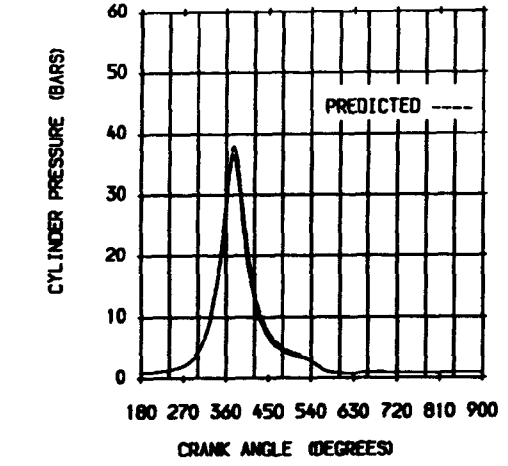

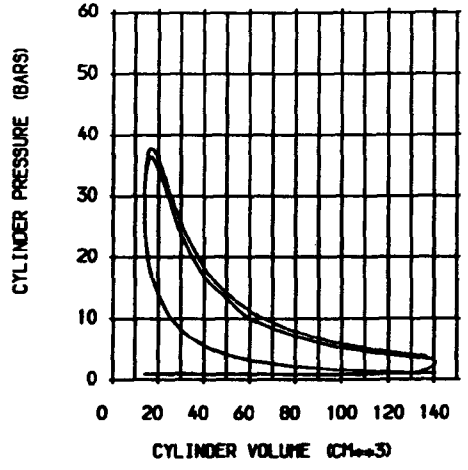

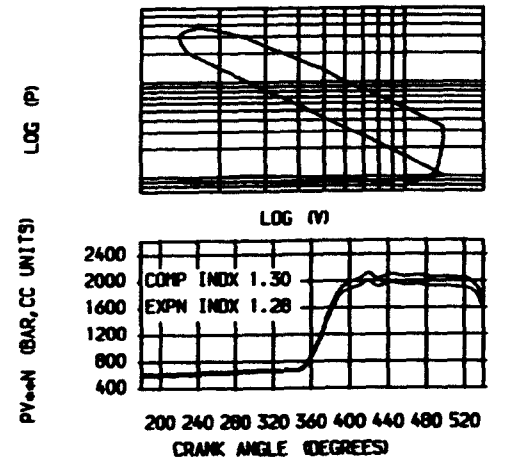

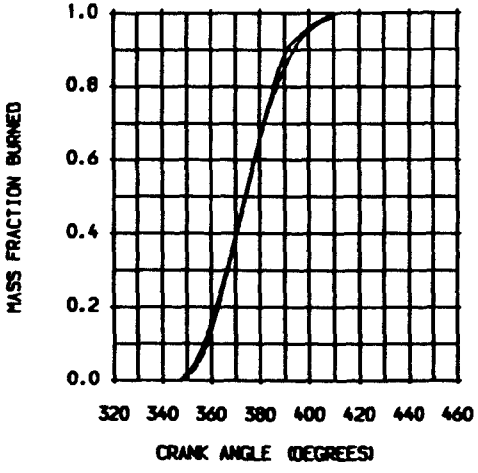

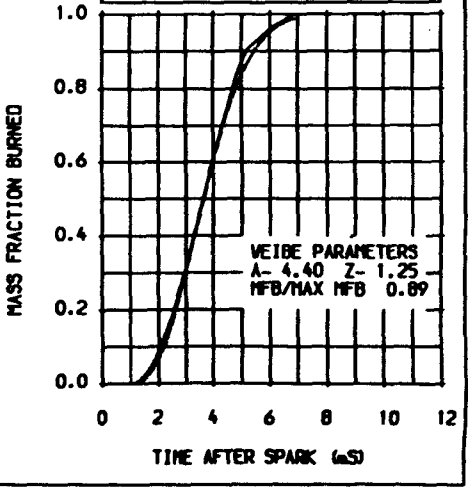

TEST DATE	02/05/89
TEST REFERENCE	T40M38D4H3-2
COMPRESSION RATIO	10.00
SPEED (RPM)	1835.00
IGNITION (DEG BTDC)	32
EXCESS AIR RATIO	1.33
CHAMBER AREA (CM**2)	34.26
ATMOSPHERIC PRESS (BAR)	1.01623
PRESS TOC EXHAUST (BAR)	0.91622
PRESSURE IVC (BAR)	1.12268
RESIDUAL FRACTION (%)	7.00
BLOWBY COEFFICIENT	1.83
BLOWBY % OF CHARGE	5.2

DERIVED MASS BURNED CRITERIA

SRT OF HT RLS DABOC		340.0		
0 - 1%	DEG.	18	mS	1.6
0 - 10%	DEG.	28	mS	2.5
0 - 50%	DEG.	51	mS	4.6
0 - 90%	DEG.	85	mS	7.7
0 - 100%	DEG.	95	mS	8.6
1 - 90%	DEG.	67	mS	6.1
dP/dθ MAX (BARS/DEG)		0.80		
	AT	352.0	DEG	
MAX PRESSURE (BARS)		33.13		
	AT	373.0	DEG	

WEIBE MASS BURNED CRITERIA

SRT OF HT RLS DABOC		340.0		
0 - 1%	DEG.	18	mS	1.6
0 - 10%	DEG.	29	mS	2.6
0 - 50%	DEG.	52	mS	4.7
0 - 90%	DEG.	81	mS	7.4
0 - 100%	DEG.	95	mS	8.6
1 - 90%	DEG.	63	mS	5.7
dP/dθ MAX (BARS/DEG)		0.75		
	AT	354.0	DEG	
MAX PRESSURE (BARS)		32.13		
	AT	372.0	DEG	

HEAT TRANSFER

ENGINE MEASURED (kW)		1.271
ENGINE PREDICTED (kW)		0.614
PREDICTED/MEASURED (%)		48.3
MAX BURNED GAS TEMP (K)		2204.8
	AT	365.0 DEG
BURNED GAS TEMP EVO (K)		1275.3
GAS TEMP AT IVC (K)		338.5
WALL TEMPERATURE (K)		400.0

STATISTICAL DATA

	MEAN	SD	% DIS
WORK (J)	79.26	1.820	2.3
POWER (kW)	1.212	0.028	2.3
PMAX (BAR)	33.42	3.500	10.7
AT DEG	12.1	2.000	16.2

GAS ANALYSIS

	MODEL	MEASURED
CO2 (%)	7.4	8.0
CO (PPM)	0.0	400.0
O2 (%)	4.8	5.8
NOx (PPM)	6007.5	770.0
UHC (PPM)		1950.0

FUEL GROSS CV (kJ/kG) 53611.5
STOICH A/F RATIO 16.67

	MODEL	MEASD
POWER (kW)	1.316	1.230
FRICTN PWR (kW)	0.248	
PUMPNG PWR (kW)		-0.018
INDICATD MEP (BAR)	6.81	6.36
INDICATED EFFICNCY	0.279	0.259
BRAKE POWER (kW)	1.050	1.105
BRAKE TH EFFICNCY	0.221	0.233

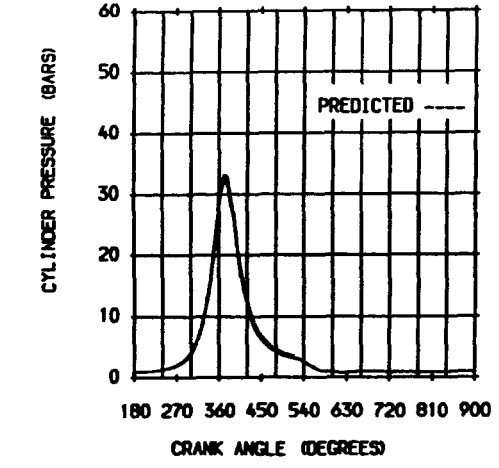

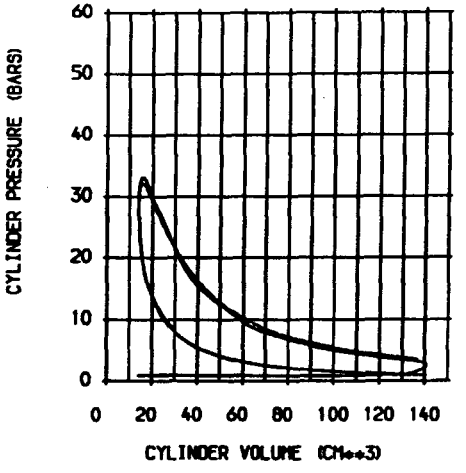

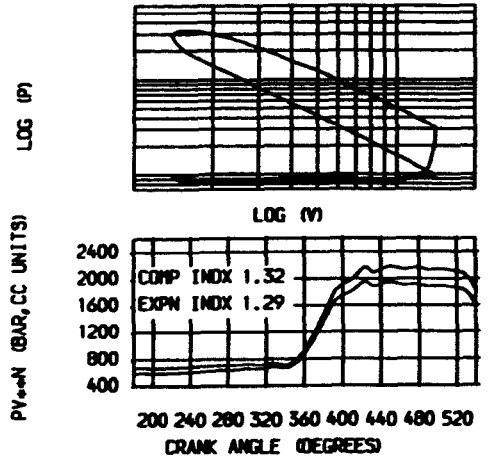

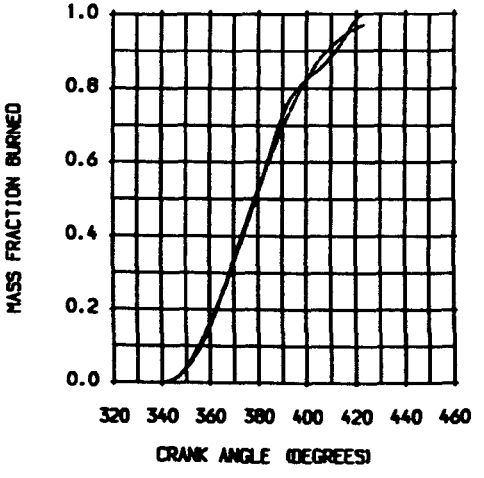

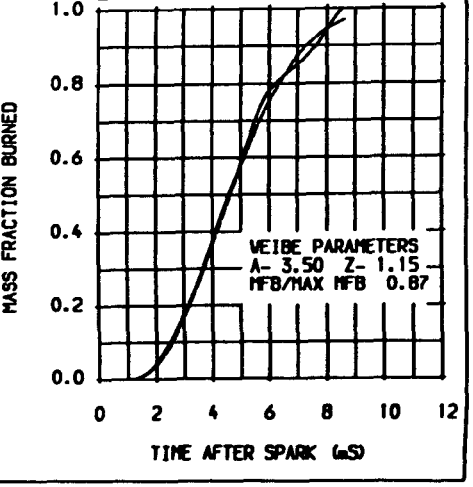

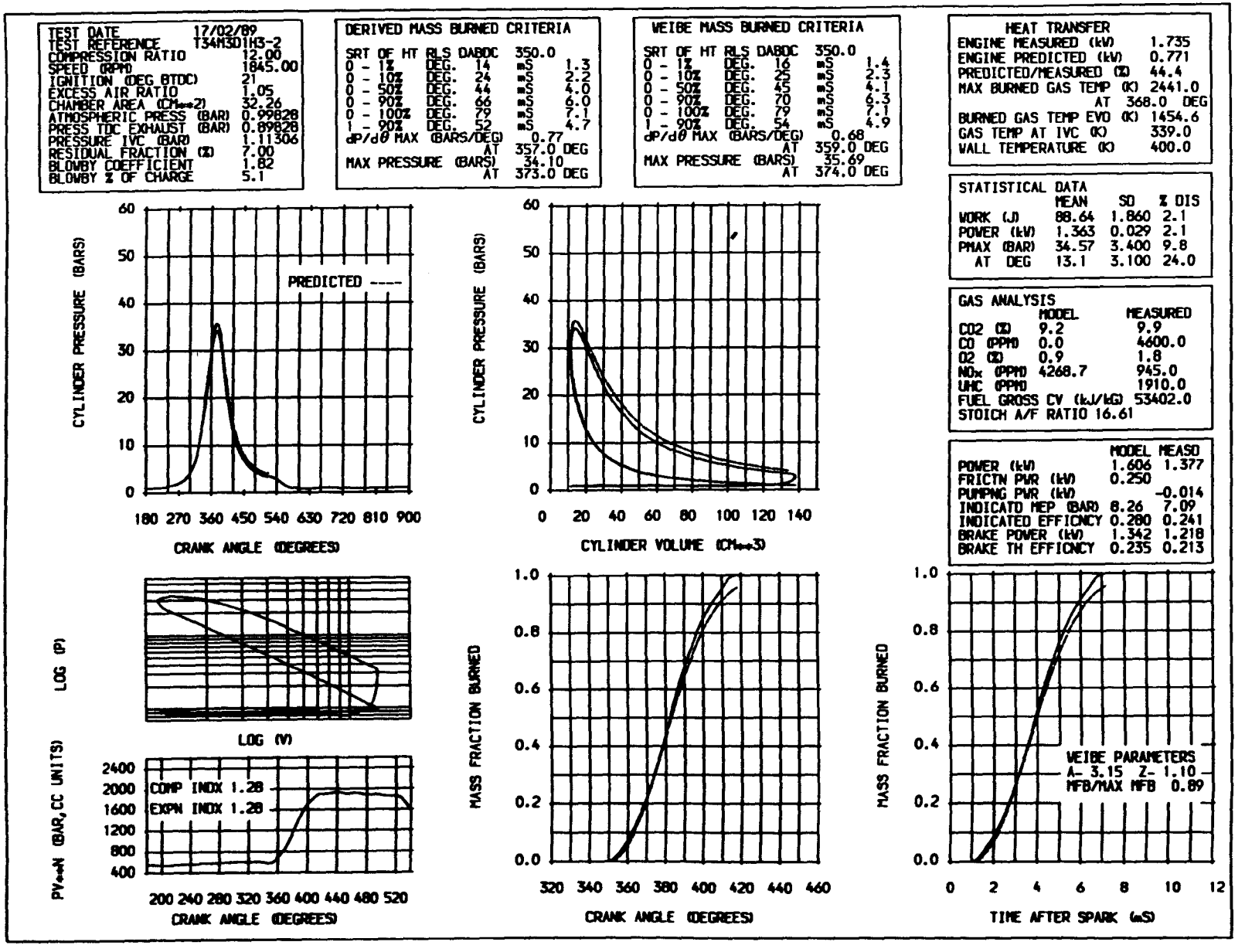
TEST DATE 17/02/89
TEST REFERENCE T34M3D1H3-2
COMPRESSION RATIO 12.00
SPEED (RPM) 1845.00
IGNITION (DEG BTDC) 21
EXCESS AIR RATIO 1.05
CHAMBER AREA (CM**2) 32.26
ATMOSPHERIC PRESS (BAR) 0.99828
PRESS TDC EXHAUST (BAR) 0.89828
PRESSURE IVC (BAR) 1.11306
RESIDUAL FRACTION (%) 7.00
BLOWBY COEFFICIENT 1.82
BLOWBY % OF CHARGE 5.1
DERIVED MASS BURNED CRITERIA
SRT OF HT RLS DABDC 350.0
0 - 1% DEG. 14 MS 1.3
0 - 10% DEG. 24 MS 2.2
0 - 50% DEG. 44 MS 4.0
0 - 90% DEG. 66 MS 6.0
0 - 100% DEG. 79 MS 7.1
1 - 90% DEG. 52 MS 4.7
dP/dθ MAX (BARS/DEG) 0.77
AT 357.0 DEG
MAX PRESSURE (BARS) 34.10
AT 373.0 DEG
WEIBE MASS BURNED CRITERIA
SRT OF HT RLS DABDC 350.0
0 - 1% DEG. 16 MS 1.4
0 - 10% DEG. 25 MS 2.3
0 - 50% DEG. 45 MS 4.1
0 - 90% DEG. 70 MS 6.3
0 - 100% DEG. 79 MS 7.1
1 - 90% DEG. 54 MS 4.9
dP/dθ MAX (BARS/DEG) 0.68
AT 359.0 DEG
MAX PRESSURE (BARS) 35.69
AT 374.0 DEG
HEAT TRANSFER
ENGINE MEASURED (kW) 1.735
ENGINE PREDICTED (kW) 0.771
PREDICTED/MEASURED (%) 44.4
MAX BURNED GAS TEMP (K) 2441.0
AT 368.0 DEG
BURNED GAS TEMP EVO (K) 1454.6
GAS TEMP AT IVC (K) 339.0
WALL TEMPERATURE (K) 400.0
STATISTICAL DATA
MEAN SD % DIS
WORK (J) 88.64 1.860 2.1
POWER (kW) 1.363 0.029 2.1
PMAX (BAR) 34.57 3.400 9.8
AT DEG 13.1 3.100 24.0
GAS ANALYSIS
MODEL MEASURED
CO2 (%) 9.2 9.9
CO (PPM) 0.0 4600.0
O2 (%) 0.9 1.8
NOx (PPM) 4268.7 945.0
UHC (PPM) 1910.0
FUEL GROSS CV (kJ/kG) 53402.0
STOICH A/F RATIO 16.61
MODEL MEASD
POWER (kW) 1.606 1.377
FRICTN PWR (kW) 0.250
PUMPNG PWR (kW) -0.014
INDICATD MEP (BAR) 8.26 7.09
INDICATED EFFICNCY 0.280 0.241
BRAKE POWER (kW) 1.342 1.218
BRAKE TH EFFICNCY 0.235 0.213
CYLINDER PRESSURE (BARS)
PREDICTED ----
CRANK ANGLE (DEGREES)
CYLINDER VOLUME (CM**3)
LOG (P)
LOG (V)
PV**N (BAR,CC UNITS)
COMP INDX 1.28
EXPN INDX 1.28
MASS FRACTION BURNED
WEIBE PARAMETERS
A- 3.15 Z- 1.10
MFB/MAX MFB 0.89
TIME AFTER SPARK (mS)

TEST DATE	17/02/89
TEST REFERENCE	T34M7D4H3-2
COMPRESSION RATIO	12.00
SPEED (RPM)	1808.00
IGNITION (DEG BTDC)	37
EXCESS AIR RATIO	1.50
CHAMBER AREA (CM**2)	32.26
ATMOSPHERIC PRESS (BAR)	0.99828
PRESS TDC EXHAUST (BAR)	0.89828
PRESSURE IVC (BAR)	1.12416
RESIDUAL FRACTION (%)	7.00
BLOWBY COEFFICIENT	1.85
BLOWBY % OF CHARGE	5.3

DERIVED MASS BURNED CRITERIA

SRT OF HT RLS DABDC		344.0	
0 - 1%	DEG.	23	2.1 mS
0 - 10%	DEG.	31	2.9 mS
0 - 50%	DEG.	54	5.0 mS
0 - 90%	DEG.	84	7.7 mS
0 - 100%	DEG.	95	8.8 mS
1 - 90%	DEG.	61	5.6 mS
dP/dθ MAX (BARS/DEG)		1.05	
	AT	351.0	DEG
MAX PRESSURE (BARS)		38.26	
	AT	369.0	DEG

WEIBE MASS BURNED CRITERIA

SRT OF HT RLS DABDC		344.0	
0 - 1%	DEG.	25	2.3 mS
0 - 10%	DEG.	33	3.0 mS
0 - 50%	DEG.	54	5.0 mS
0 - 90%	DEG.	85	7.8 mS
0 - 100%	DEG.	95	8.8 mS
1 - 90%	DEG.	60	5.5 mS
dP/dθ MAX (BARS/DEG)		1.06	
	AT	354.0	DEG
MAX PRESSURE (BARS)		39.28	
	AT	369.0	DEG

HEAT TRANSFER

ENGINE MEASURED (kW)	1.060
ENGINE PREDICTED (kW)	0.539
PREDICTED/MEASURED (%)	50.9
MAX BURNED GAS TEMP (K)	2111.4
AT	363.0 DEG
BURNED GAS TEMP EVO (K)	1135.1
GAS TEMP AT IVC (K)	338.5
WALL TEMPERATURE (K)	400.0

STATISTICAL DATA

	MEAN	SD	% DIS
WORK (J)	72.03	2.400	3.3
POWER (kW)	1.085	0.036	3.3
PMAX (BAR)	38.50	4.300	11.3
AT DEG	7.9	1.900	24.1

GAS ANALYSIS

	MODEL	MEASURED
CO2 (%)	6.6	6.9
CO (PPM)	0.0	900.0
O2 (%)	6.5	7.7
NOx (PPM)	5707.0	304.0
UHC (PPM)		2389.0

FUEL GROSS CV (kJ/kG) 53402.0
STOICH A/F RATIO 16.61

	MODEL	MEASD
POWER (kW)	1.206	1.101
FRICTN PWR (kW)	0.243	
PUMPNG PWR (kW)		-0.016
INDICATD MEP (BAR)	6.33	5.78
INDICATED EFFICNCY	0.295	0.269
BRAKE POWER (kW)	0.947	0.956
BRAKE TH EFFICNCY	0.231	0.233

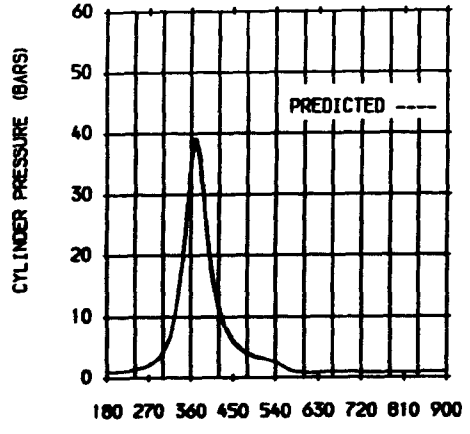

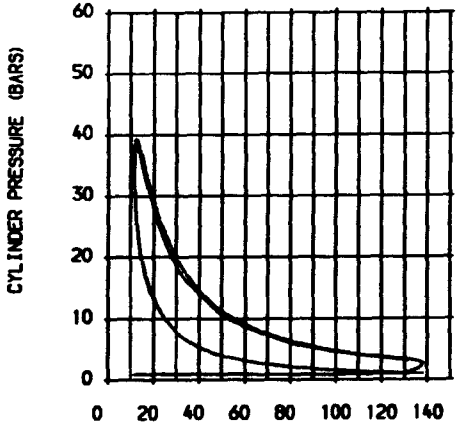

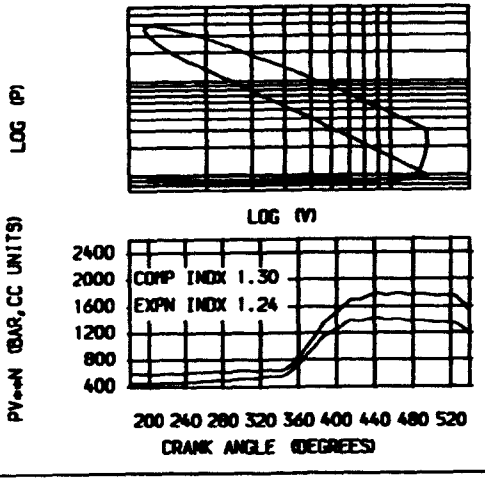

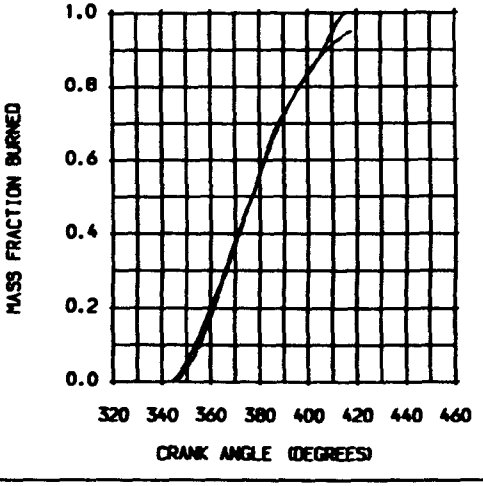

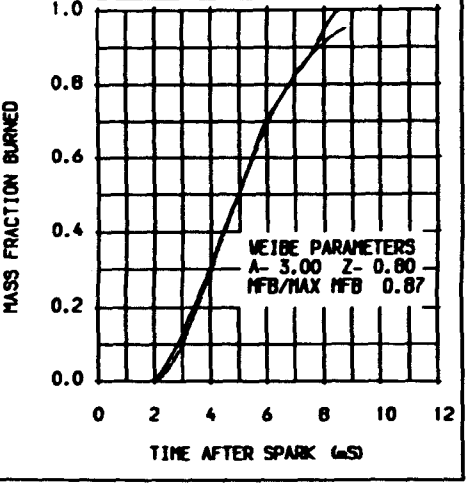

TEST DATE	10/01/89
TEST REFERENCE	T31M3901H3-2
COMPRESSION RATIO	13.00
SPEED (RPM)	1825.00
IGNITION (DEG BTDC)	22
EXCESS AIR RATIO	1.02
CHAMBER AREA (CM**2)	31.65
ATMOSPHERIC PRESS (BAR)	1.02890
PRESS TDC EXHAUST (BAR)	0.92889
PRESSURE IVC (BAR)	1.21693
RESIDUAL FRACTION (%)	7.00
BLOWBY COEFFICIENT	1.84
BLOWBY % OF CHARGE	5.2

DERIVED MASS BURNED CRITERIA

SRT OF HT RLS DABDC		346.0	
0 - 1%	DEG. 11	mS	1.0
0 - 10%	DEG. 20	mS	1.8
0 - 50%	DEG. 38	mS	3.5
0 - 90%	DEG. 62	mS	5.7
0 - 100%	DEG. 81	mS	7.4
1 - 90%	DEG. 51	mS	4.7
dP/dθ MAX (BARS/DEG)		1.20	
	AT	354.0	DEG
MAX PRESSURE (BARS)		46.61	
	AT	372.0	DEG

WEIBE MASS BURNED CRITERIA

SRT OF HT RLS DABDC		346.0	
0 - 1%	DEG. 13	mS	1.2
0 - 10%	DEG. 21	mS	1.9
0 - 50%	DEG. 39	mS	3.6
0 - 90%	DEG. 62	mS	5.7
0 - 100%	DEG. 81	mS	7.4
1 - 90%	DEG. 49	mS	4.5
dP/dθ MAX (BARS/DEG)		1.21	
	AT	357.0	DEG
MAX PRESSURE (BARS)		46.89	
	AT	372.0	DEG

HEAT TRANSFER

ENGINE MEASURED (kW)	1.739
ENGINE PREDICTED (kW)	0.888
PREDICTED/MEASURED (%)	51.1
MAX BURNED GAS TEMP (K)	2539.3
AT	366.0 DEG
BURNED GAS TEMP EVO (K)	1417.7
GAS TEMP AT IVC (K)	373.5
WALL TEMPERATURE (K)	400.0

STATISTICAL DATA

	MEAN	SD	% DIS
WORK (J)	90.02	2.770	3.1
POWER (kW)	1.369	0.042	3.1
PMAX (BAR)	47.39	4.400	9.3
AT DEG	11.3	2.600	22.9

GAS ANALYSIS

	MODEL	MEASURED
CO2 (%)	9.5	9.8
CO (PPM)	0.0	9000.0
O2 (%)	0.4	1.9
NOx (PPM)	4089.9	1234.0
UHC (PPM)		3624.0

FUEL GROSS CV (kJ/kG) 53647.1
STOICH A/F RATIO 16.69

	MODEL	MEASD
POWER (kW)	1.658	1.380
FRICTN PWR (kW)	0.246	
PUMPNG PWR (kW)		-0.012
INDICATD MEP (BAR)	8.63	7.18
INDICATED EFFICNCY	0.289	0.240
BRAKE POWER (kW)	1.400	1.288
BRAKE TH EFFICNCY	0.244	0.224

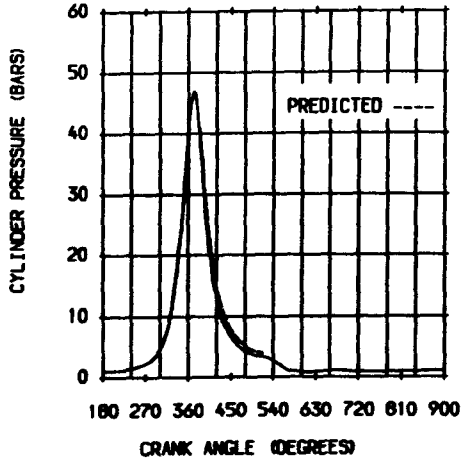

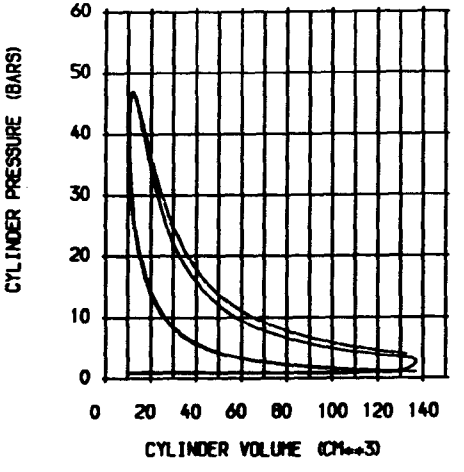

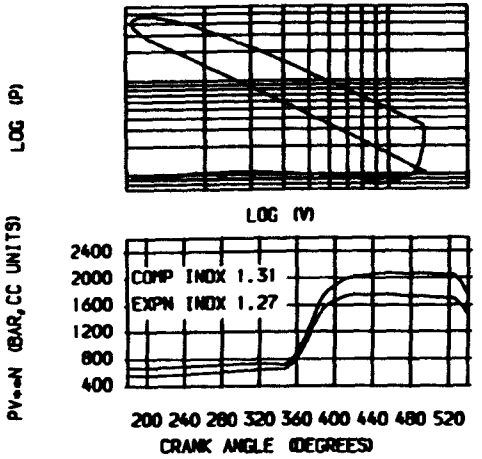

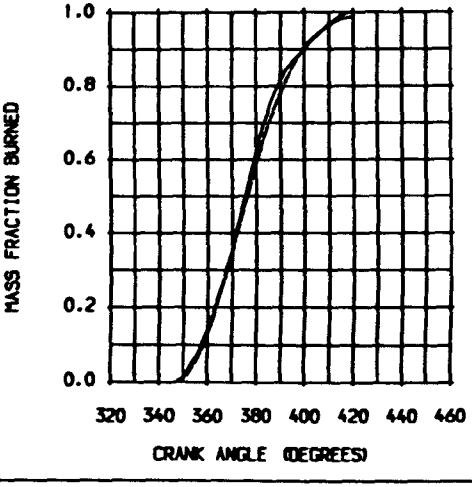

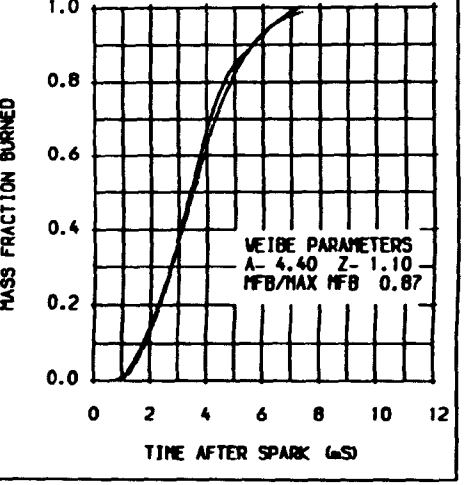

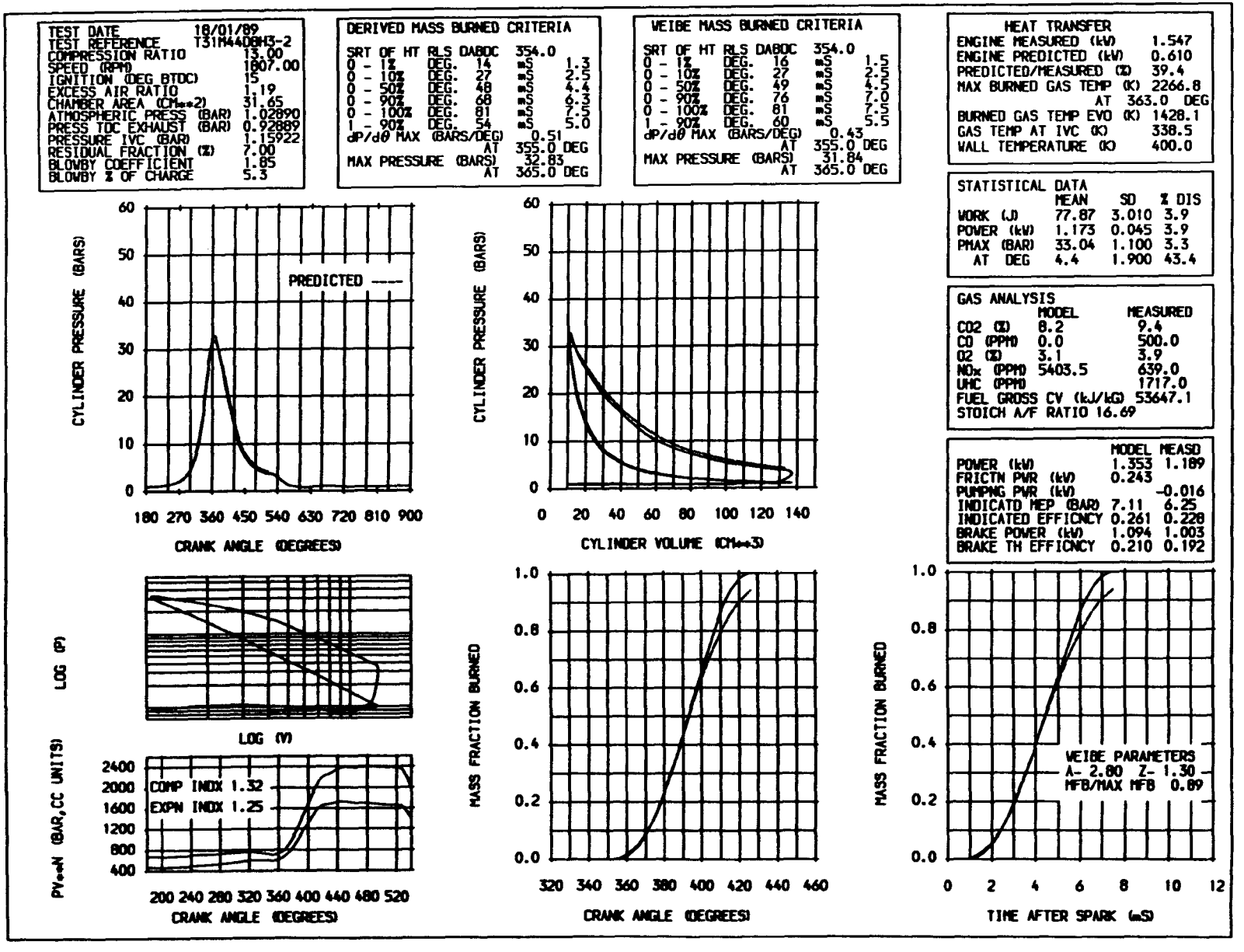
TEST DATE 18/01/89
TEST REFERENCE T31M4408H3-2
COMPRESSION RATIO 13.00
SPEED (RPM) 1807.00
IGNITION (DEG BTDC) 15
EXCESS AIR RATIO 1.19
CHAMBER AREA (CM**2) 31.65
ATMOSPHERIC PRESS (BAR) 1.02890
PRESS TDC EXHAUST (BAR) 0.92889
PRESSURE IVC (BAR) 1.15922
RESIDUAL FRACTION (%) 7.00
BLOWBY COEFFICIENT 1.85
BLOWBY % OF CHARGE 5.3
DERIVED MASS BURNED CRITERIA
SRT OF HT RLS DABDC 354.0
0 - 1% DEG. 14 mS 1.3
0 - 10% DEG. 27 mS 2.5
0 - 50% DEG. 48 mS 4.4
0 - 90% DEG. 68 mS 6.3
0 - 100% DEG. 81 mS 7.5
1 - 90% DEG. 54 mS 5.0
dP/dθ MAX (BARS/DEG) 0.51
AT 355.0 DEG
MAX PRESSURE (BARS) 32.83
AT 365.0 DEG
WEIBE MASS BURNED CRITERIA
SRT OF HT RLS DABDC 354.0
0 - 1% DEG. 16 mS 1.5
0 - 10% DEG. 27 mS 2.5
0 - 50% DEG. 49 mS 4.5
0 - 90% DEG. 76 mS 7.0
0 - 100% DEG. 81 mS 7.5
1 - 90% DEG. 60 mS 5.5
dP/dθ MAX (BARS/DEG) 0.43
AT 355.0 DEG
MAX PRESSURE (BARS) 31.84
AT 365.0 DEG
HEAT TRANSFER
ENGINE MEASURED (kW) 1.547
ENGINE PREDICTED (kW) 0.610
PREDICTED/MEASURED (%) 39.4
MAX BURNED GAS TEMP (K) 2266.8
AT 363.0 DEG
BURNED GAS TEMP EVO (K) 1428.1
GAS TEMP AT IVC (K) 338.5
WALL TEMPERATURE (K) 400.0
STATISTICAL DATA
MEAN SD % DIS
WORK (J) 77.87 3.010 3.9
POWER (kW) 1.173 0.045 3.9
PMAX (BAR) 33.04 1.100 3.3
AT DEG 4.4 1.900 43.4
GAS ANALYSIS
MODEL MEASURED
CO2 (%) 8.2 9.4
CO (PPM) 0.0 500.0
O2 (%) 3.1 3.9
NOx (PPM) 5403.5 639.0
UHC (PPM) 1717.0
FUEL GROSS CV (kJ/kG) 53647.1
STOICH A/F RATIO 16.69
MODEL MEASD
POWER (kW) 1.353 1.189
FRICTN PWR (kW) 0.243
PUMPNG PWR (kW) -0.016
INDICATD MEP (BAR) 7.11 6.25
INDICATED EFFICNCY 0.261 0.228
BRAKE POWER (kW) 1.094 1.003
BRAKE TH EFFICNCY 0.210 0.192
CYLINDER PRESSURE (BARS)
PREDICTED
CRANK ANGLE (DEGREES)
CYLINDER VOLUME (CM**3)
LOG (P)
LOG (V)
PV**N (BAR,CC UNITS)
COMP INDX 1.32
EXPN INDX 1.25
MASS FRACTION BURNED
WEIBE PARAMETERS
A- 2.80 Z- 1.30
MFB/MAX MFB 0.89
TIME AFTER SPARK (mS)

TEST DATE	18/01/89
TEST REFERENCE	T31M4307M3-2
COMPRESSION RATIO	13.00
SPEED (RPM)	1807.00
IGNITION (DEG BTDC)	20
EXCESS AIR RATIO	1.19
CHAMBER AREA (CM**2)	31.65
ATMOSPHERIC PRESS (BAR)	1.02890
PRESS TDC EXHAUST (BAR)	0.92889
PRESSURE IVC (BAR)	1.17031
RESIDUAL FRACTION (%)	7.00
BLOWBY COEFFICIENT	1.85
BLOWBY % OF CHARGE	5.3

DERIVED MASS BURNED CRITERIA

SRT OF HT RLS DABDC	348.0	
0 - 1%	DEG. 12	MS 1.1
0 - 10%	DEG. 24	MS 2.2
0 - 50%	DEG. 45	MS 4.2
0 - 90%	DEG. 67	MS 6.2
0 - 100%	DEG. 80	MS 7.4
1 - 90%	DEG. 55	MS 5.1
dP/dθ MAX (BARS/DEG)	0.85	
	AT 353.0	DEG
MAX PRESSURE (BARS)	38.09	
	AT 368.0	DEG

WEIBE MASS BURNED CRITERIA

SRT OF HT RLS DABDC	348.0	
0 - 1%	DEG. 13	MS 1.2
0 - 10%	DEG. 23	MS 2.1
0 - 50%	DEG. 44	MS 4.1
0 - 90%	DEG. 72	MS 6.6
0 - 100%	DEG. 80	MS 7.4
1 - 90%	DEG. 59	MS 5.4
dP/dθ MAX (BARS/DEG)	0.82	
	AT 355.0	DEG
MAX PRESSURE (BARS)	39.17	
	AT 370.0	DEG

HEAT TRANSFER

ENGINE MEASURED (kW)	1.485
ENGINE PREDICTED (kW)	0.665
PREDICTED/MEASURED (%)	44.8
MAX BURNED GAS TEMP (K)	2323.7
AT	365.0 DEG
BURNED GAS TEMP EVO (K)	1345.9
GAS TEMP AT IVC (K)	342.0
WALL TEMPERATURE (K)	400.0

STATISTICAL DATA

	MEAN	SD	% DIS
WORK (J)	82.04	1.850	2.3
POWER (kW)	1.235	0.028	2.3
PMAX (BAR)	38.38	3.000	7.9
AT DEG	7.4	2.400	32.1

GAS ANALYSIS

	MODEL	MEASURED
CO2 (%)	8.2	9.2
CO (PPM)	0.0	600.0
O2 (%)	3.1	4.1
NOx (PPM)	6045.5	1227.0
UHC (PPM)		2401.0

FUEL GROSS CV (kJ/kG) 53647.1
STOICH A/F RATIO 16.69

	MODEL	MEASD
POWER (kW)	1.467	1.251
FRICTN PWR (kW)	0.243	
PUMPNG PWR (kW)		-0.016
INDICATD MEP (BAR)	7.71	6.57
INDICATED EFFICNCY	0.284	0.241
BRAKE POWER (kW)	1.208	1.097
BRAKE TH EFFICNCY	0.233	0.211

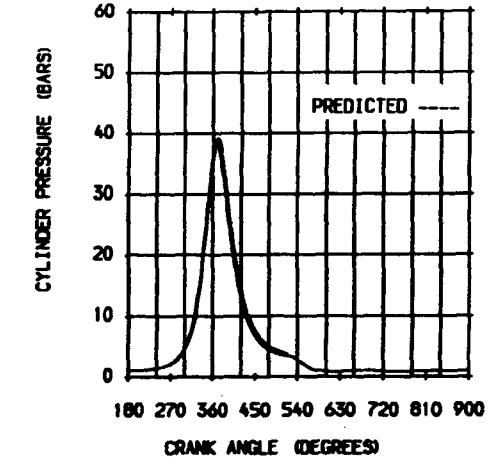

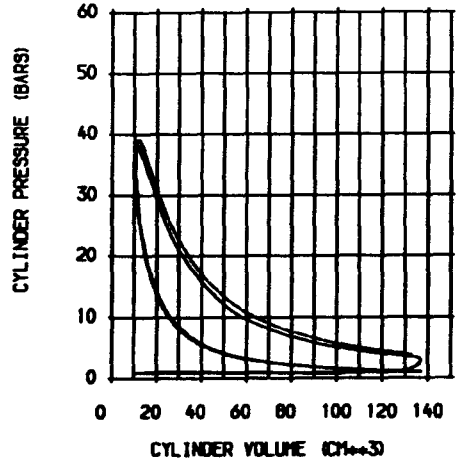

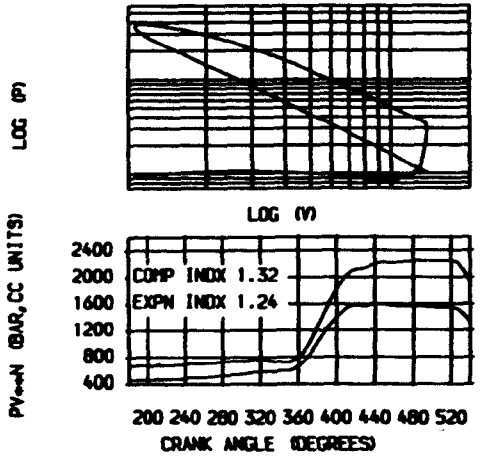

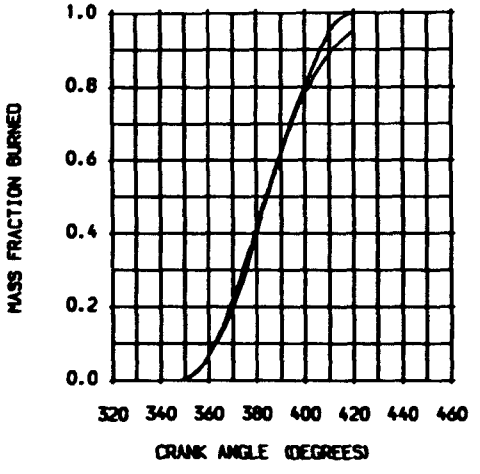

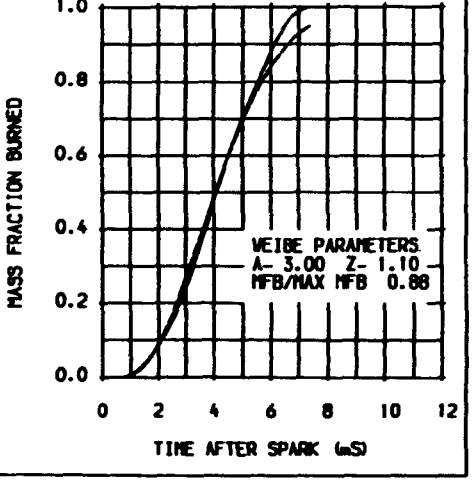

TEST DATE	18/01/89
TEST REFERENCE	T31M41D5H3-2
COMPRESSION RATIO	13.00
SPEED (RPM)	1806.00
IGNITION (DEG BTDC)	25
EXCESS AIR RATIO	1.17
CHAMBER AREA (CM**2)	31.65
ATMOSPHERIC PRESS (BAR)	1.02890
PRESS TDC EXHAUST (BAR)	0.92889
PRESSURE IVC (BAR)	1.20195
RESIDUAL FRACTION (%)	7.00
BLOWBY COEFFICIENT	1.85
BLOWBY % OF CHARGE	5.3

DERIVED MASS BURNED CRITERIA

SRT OF HT RLS DABDC		344.0	
0 - 1%	DEG.	12	1.1
0 - 10%	DEG.	20	1.8
0 - 50%	DEG.	39	3.6
0 - 90%	DEG.	63	5.8
0 - 100%	DEG.	79	7.3
1 - 90%	DEG.	51	4.7
dP/dθ MAX (BARS/DEG)		1.23	
	AT	352.0	DEG
MAX PRESSURE (BARS)		46.31	
	AT	370.0	DEG

VEIBE MASS BURNED CRITERIA

SRT OF HT RLS DABDC		344.0	
0 - 1%	DEG.	13	1.2
0 - 10%	DEG.	22	2.0
0 - 50%	DEG.	39	3.6
0 - 90%	DEG.	62	5.7
0 - 100%	DEG.	79	7.3
1 - 90%	DEG.	49	4.5
dP/dθ MAX (BARS/DEG)		1.38	
	AT	356.0	DEG
MAX PRESSURE (BARS)		49.28	
	AT	371.0	DEG

HEAT TRANSFER

ENGINE MEASURED (kW)	1.578
ENGINE PREDICTED (kW)	0.770
PREDICTED/MEASURED (%)	48.8
MAX BURNED GAS TEMP (K)	2420.5
AT	365.0 DEG
BURNED GAS TEMP EVO (K)	1282.5
GAS TEMP AT IVC (K)	359.0
WALL TEMPERATURE (K)	400.0

STATISTICAL DATA

	MEAN	SD	% DIS
WORK (J)	79.24	2.590	3.3
POWER (kW)	1.193	0.039	3.3
PMAX (BAR)	46.82	4.100	8.9
AT DEG	9.5	1.900	20.3

GAS ANALYSIS

	MODEL	MEASURED
CO2 (%)	8.4	9.3
CO (PPM)	0.0	800.0
O2 (%)	2.8	3.9
NOx (PPM)	6880.6	2096.0
UHC (PPM)		2770.0

FUEL GROSS CV (kJ/kG) 53647.1
STOICH A/F RATIO 16.69

	MODEL	MEASD
POWER (kW)	1.569	1.206
FRICTN PWR (kW)	0.242	
PUMPNG PWR (kW)		-0.013
INDICATD MEP (BAR)	8.25	6.34
INDICATED EFFICNCY	0.305	0.235
BRAKE POWER (kW)	1.314	1.096
BRAKE TH EFFICNCY	0.256	0.214

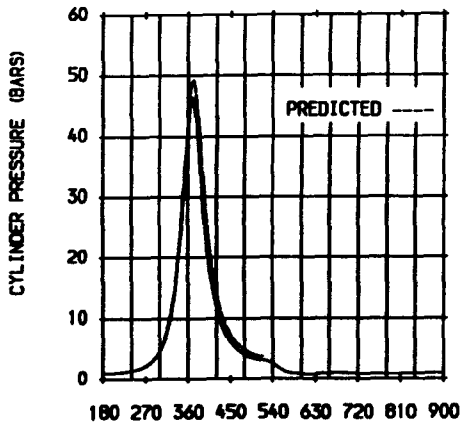

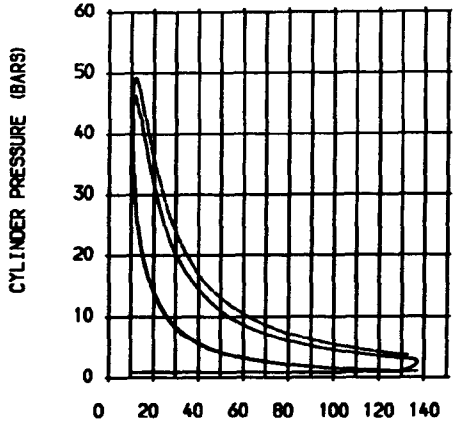

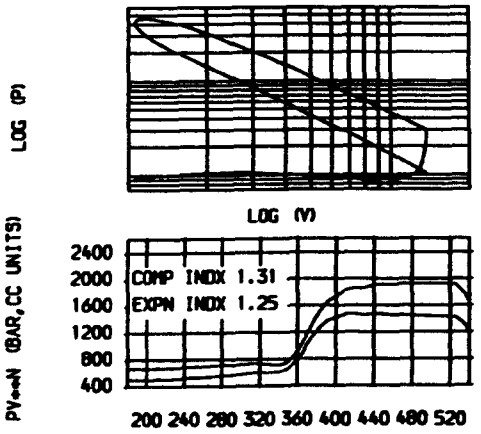

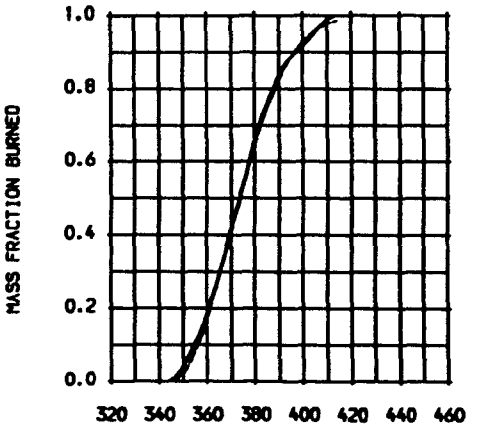

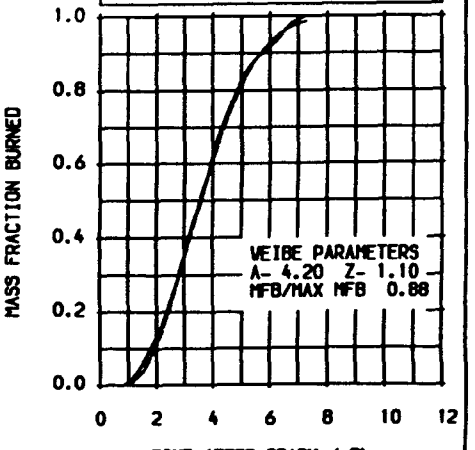

TEST DATE	18/01/89
TEST REFERENCE	T31M42D6H3-2
COMPRESSION RATIO	13.00
SPEED (RPM)	1806.00
IGNITION (DEG BTDC)	30
EXCESS AIR RATIO	1.16
CHAMBER AREA (CM**2)	31.65
ATMOSPHERIC PRESS (BAR)	1.02890
PRESS TDC EXHAUST (BAR)	0.92889
PRESSURE IVC (BAR)	1.27806
RESIDUAL FRACTION (%)	7.00
BLOWBY COEFFICIENT	1.85
BLOWBY % OF CHARGE	5.3

DERIVED MASS BURNED CRITERIA

SRT OF HT RLS DABDC		337.0		
0 - 1%	DEG.	10	MS	0.9
0 - 10%	DEG.	17	MS	1.6
0 - 50%	DEG.	29	MS	2.7
0 - 90%	DEG.	44	MS	4.1
0 - 100%	DEG.	55	MS	5.1
1 - 90%	DEG.	34	MS	3.1
dP/dθ MAX (BARS/DEG)		2.05		
	AT	358.0	DEG	
MAX PRESSURE (BARS)		58.89		
	AT	366.0	DEG	

WEIBE MASS BURNED CRITERIA

SRT OF HT RLS DABDC		337.0		
0 - 1%	DEG.	11	MS	1.0
0 - 10%	DEG.	17	MS	1.6
0 - 50%	DEG.	30	MS	2.8
0 - 90%	DEG.	45	MS	4.2
0 - 100%	DEG.	55	MS	5.1
1 - 90%	DEG.	34	MS	3.1
dP/dθ MAX (BARS/DEG)		2.69		
	AT	354.0	DEG	
MAX PRESSURE (BARS)		71.20		
	AT	367.0	DEG	

HEAT TRANSFER

ENGINE MEASURED (kW)		1.612
ENGINE PREDICTED (kW)		0.968
PREDICTED/MEASURED (%)		60.0
MAX BURNED GAS TEMP (K)		2561.6
	AT	362.0 DEG
BURNED GAS TEMP EVO (K)		1199.5
GAS TEMP AT IVC (K)		384.5
WALL TEMPERATURE (K)		400.0

STATISTICAL DATA

	MEAN	SD	% DIS
WORK (J)	73.85	3.870	5.3
POWER (kW)	1.111	0.058	5.3
PMAX (BAR)	61.85	6.400	10.4
AT DEG	5.9	3.100	52.7

GAS ANALYSIS

	MODEL	MEASURED
CO2 (%)	8.4	9.4
CO (PPM)	0.0	900.0
O2 (%)	2.7	3.7
NOx (PPM)	8489.3	3109.0
UHC (PPM)		2910.0
FUEL GROSS CV (kJ/kG)		53647.1
STOICH A/F RATIO	16.69	

	MODEL	MEASD
POWER (kW)	1.648	1.115
FRICTN PWR (kW)	0.242	
PUMPNG PWR (kW)		-0.003
INDICATD MEP (BAR)	8.67	5.86
INDICATED EFFICNCY	0.321	0.217
BRAKE POWER (kW)	1.403	1.049
BRAKE TH EFFICNCY	0.273	0.204

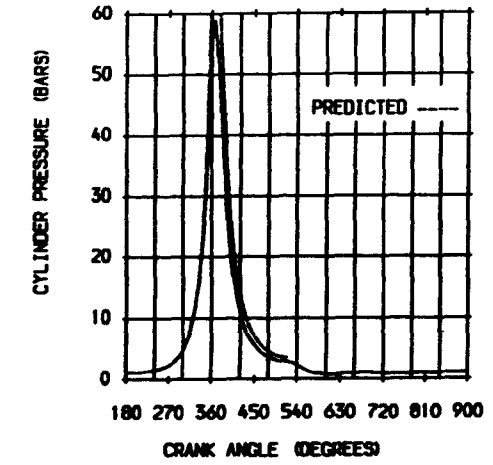

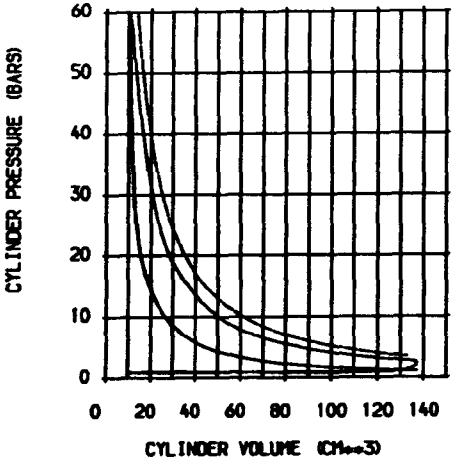

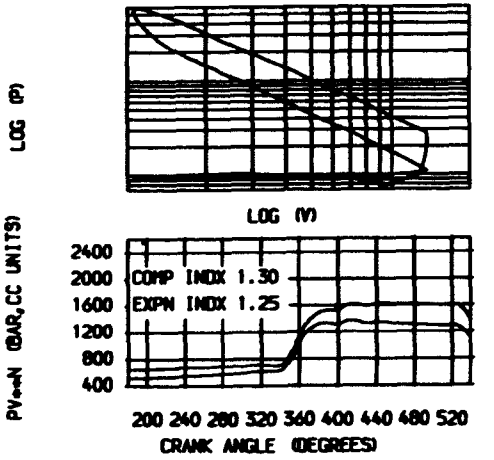

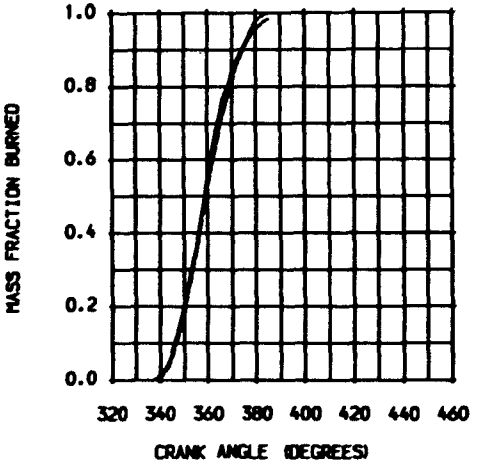

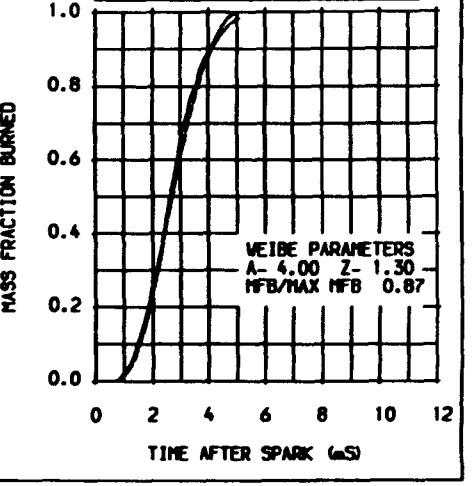

TEST DATE	10/01/89
TEST REFERENCE	T31M40D4H3-2
COMPRESSION RATIO	13.00
SPEED (RPM)	1807.00
IGNITION (DEG BTDC)	37
EXCESS AIR RATIO	1.49
CHAMBER AREA (CM**2)	31.65
ATMOSPHERIC PRESS (BAR)	1.02890
PRESS TOC EXHAUST (BAR)	0.92889
PRESSURE IVC (BAR)	1.19273
RESIDUAL FRACTION (%)	7.00
BLOWBY COEFFICIENT	1.85
BLOWBY % OF CHARGE	5.5

DERIVED MASS BURNED CRITERIA

SRT OF HT RLS DABOC	334.0	
0 - 1%	DEG. 15	mS 1.4
0 - 10%	DEG. 24	mS 2.2
0 - 50%	DEG. 46	mS 4.2
0 - 90%	DEG. 81	mS 7.5
0 - 100%	DEG. 95	mS 8.8
1 - 90%	DEG. 66	mS 6.1
dP/dθ MAX (BARS/DEG)		1.51
	AT	349.0 DEG
MAX PRESSURE (BARS)		49.37
	AT	366.0 DEG

WEIBE MASS BURNED CRITERIA

SRT OF HT RLS DABOC	334.0	
0 - 1%	DEG. 16	mS 1.5
0 - 10%	DEG. 26	mS 2.4
0 - 50%	DEG. 48	mS 4.4
0 - 90%	DEG. 77	mS 7.1
0 - 100%	DEG. 95	mS 8.8
1 - 90%	DEG. 61	mS 5.6
dP/dθ MAX (BARS/DEG)		1.53
	AT	351.0 DEG
MAX PRESSURE (BARS)		50.39
	AT	366.0 DEG

HEAT TRANSFER

ENGINE MEASURED (kW)	1.125
ENGINE PREDICTED (kW)	0.615
PREDICTED/MEASURED (%)	54.7
MAX BURNED GAS TEMP (K)	2192.5
AT	361.0 DEG
BURNED GAS TEMP EVO (K)	1100.1
GAS TEMP AT IVC (K)	350.5
WALL TEMPERATURE (K)	400.0

STATISTICAL DATA

	MEAN	SD	% DIS
WORK (J)	64.29	2.210	3.5
POWER (kW)	0.968	0.033	3.5
PMAX (BAR)	49.59	4.800	9.8
AT DEG	5.5	1.200	22.8

GAS ANALYSIS

	MODEL	MEASURED
CO2 (%)	6.7	6.9
CO (PPM)	0.0	1100.0
O2 (%)	6.4	8.1
NOx (PPM)	6814.6	523.0
UHC (PPM)		4119.0

FUEL GROSS CV (kJ/kG) 53647.1
STOICH A/F RATIO 16.69

	MODEL	MEASD
POWER (kW)	1.247	0.981
FRICTN PWR (kW)	0.243	
PUMPNG PWR (kW)		-0.013
INDICATD MEP (BAR)	6.55	5.15
INDICATED EFFICNCY	0.299	0.234
BRAKE POWER (kW)	0.992	0.861
BRAKE TH EFFICNCY	0.237	0.205

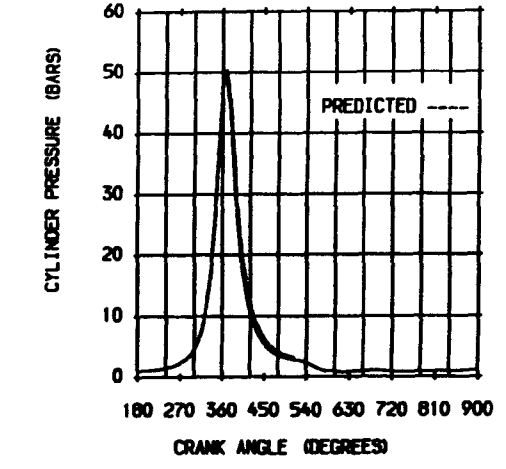

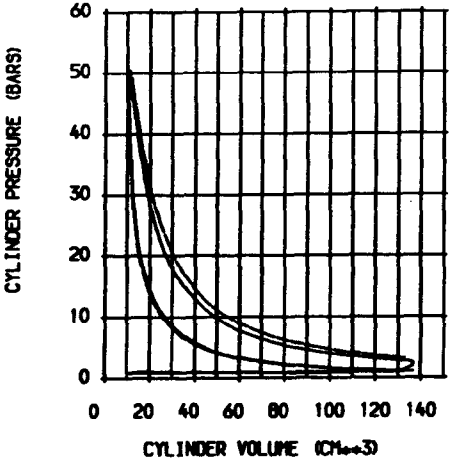

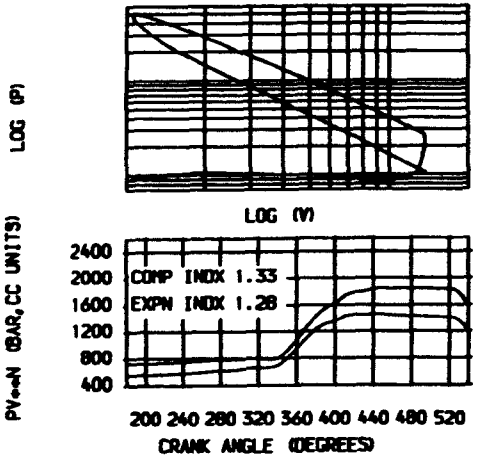

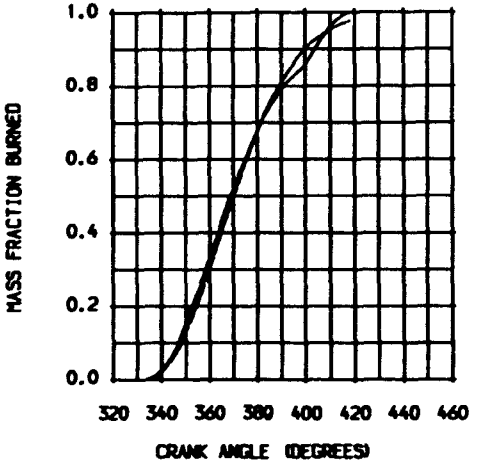

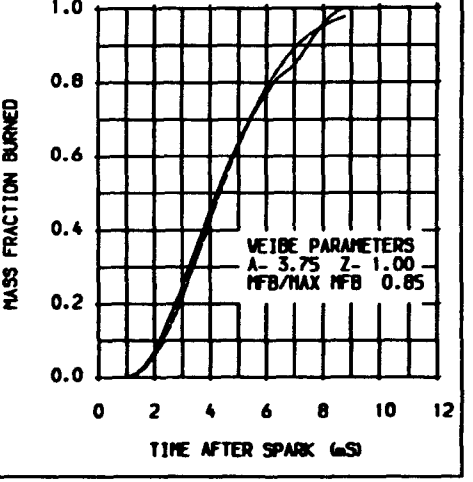

TEST DATE	17/02/89
TEST REFERENCE	T34M8DSH3-2
COMPRESSION RATIO	12.00
SPEED (RPM)	2105.00
IGNITION (DEG BTDC)	24
EXCESS AIR RATIO	1.02
CHAMBER AREA (CM**2)	32.26
ATMOSPHERIC PRESS (BAR)	0.99828
PRESS TDC EXHAUST (BAR)	0.89828
PRESSURE IVC (BAR)	1.19853
RESIDUAL FRACTION (%)	7.00
BLOWBY COEFFICIENT	1.54
BLOWBY % OF CHARGE	3.8

DERIVED MASS BURNED CRITERIA

SRT OF HT RLS DABDC		344.0	
0 - 1%	DEG. 12	MS	1.0
0 - 10%	DEG. 20	MS	1.6
0 - 50%	DEG. 36	MS	2.9
0 - 90%	DEG. 53	MS	4.2
0 - 100%	DEG. 64	MS	5.1
1 - 90%	DEG. 41	MS	3.2
dP/dθ MAX (BARS/DEG)		1.09	
	AT	358.0	DEG
MAX PRESSURE (BARS)		44.27	
	AT	372.0	DEG

WEIBE MASS BURNED CRITERIA

SRT OF HT RLS DABDC		344.0	
0 - 1%	DEG. 13	MS	1.0
0 - 10%	DEG. 22	MS	1.7
0 - 50%	DEG. 37	MS	2.9
0 - 90%	DEG. 56	MS	4.4
0 - 100%	DEG. 64	MS	5.1
1 - 90%	DEG. 43	MS	3.4
dP/dθ MAX (BARS/DEG)		1.31	
	AT	359.0	DEG
MAX PRESSURE (BARS)		48.35	
	AT	374.0	DEG

HEAT TRANSFER

ENGINE MEASURED (kW)	2.122	
ENGINE PREDICTED (kW)	1.032	
PREDICTED/MEASURED (%)	48.6	
MAX BURNED GAS TEMP (K)	2555.4	
AT	368.0	DEG
BURNED GAS TEMP EVO (K)	1405.7	
GAS TEMP AT IVC (K)	370.5	
WALL TEMPERATURE (K)	400.0	

STATISTICAL DATA

	MEAN	SD	% DIS
WORK (J)	94.90	2.250	2.4
POWER (kW)	1.665	0.039	2.4
PMAX (BAR)	45.57	4.900	10.7
AT DEG	12.4	2.900	23.8

GAS ANALYSIS

	MODEL	MEASURED
CO2 (%)	9.5	9.5
CO (PPM)	0.0	9400.0
O2 (%)	0.4	1.6
NOx (PPM)	4251.4	1172.0
UHC (PPM)		2642.0
FUEL GROSS CV (kJ/kG)		53402.0
STOICH A/F RATIO	16.61	

	MODEL	MEASD
POWER (kW)	2.038	1.684
FRICTN PWR (kW)	0.306	
PUMPNG PWR (kW)		-0.019
INDICATD MEP (BAR)	9.19	7.59
INDICATED EFFICNCY	0.308	0.253
BRAKE POWER (kW)	1.713	1.513
BRAKE TH EFFICNCY	0.257	0.227

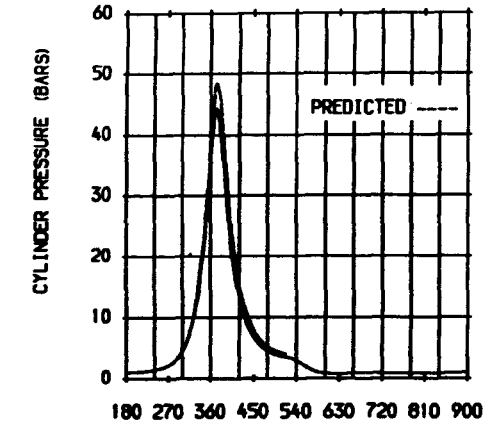

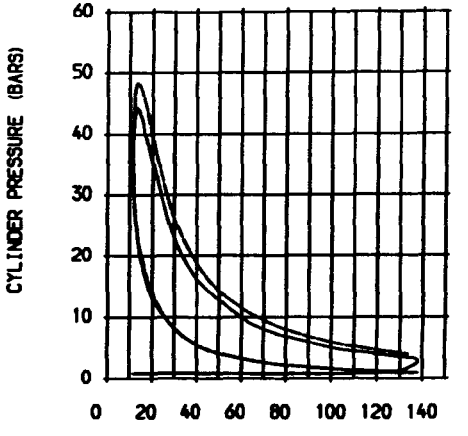

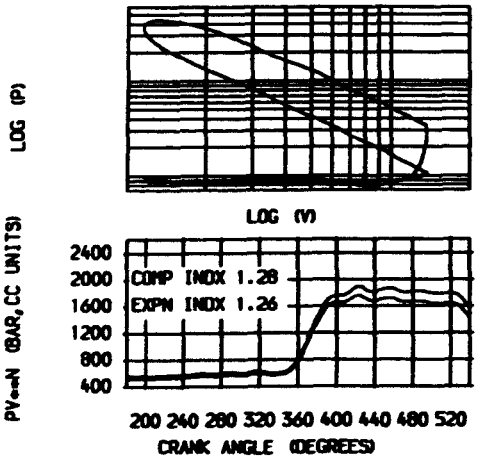

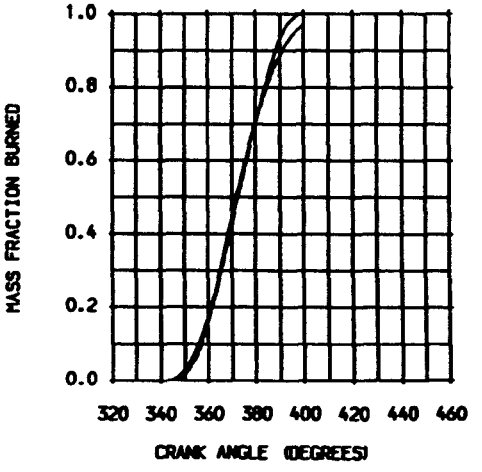

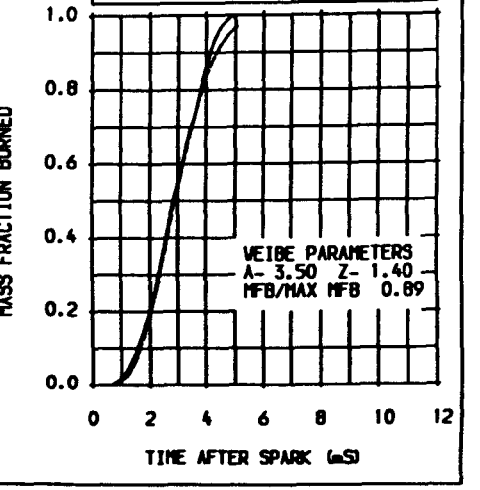

TEST DATE	01/02/89
TEST REFERENCE	T32M48D6H5-2
COMPRESSION RATIO	13.00
SPEED (RPM)	2105.00
IGNITION (DEG BTDC)	19
EXCESS AIR RATIO	1.03
CHAMBER AREA (CM**2)	31.65
ATMOSPHERIC PRESS (BAR)	1.02597
PRESS TDC EXHAUST (BAR)	0.92596
PRESSURE IVC (BAR)	1.19735
RESIDUAL FRACTION (%)	7.00
BLOWBY COEFFICIENT	1.54
BLOWBY % OF CHARGE	3.8

DERIVED MASS BURNED CRITERIA

SRT OF HT RLS DABDC		349.0	
0 - 1%	DEG. 10	mS	0.8
0 - 10%	DEG. 18	mS	1.4
0 - 50%	DEG. 35	mS	2.8
0 - 90%	DEG. 51	mS	4.0
0 - 100%	DEG. 61	mS	4.8
1 - 90%	DEG. 41	mS	3.2
dP/dθ MAX (BARS/DEG)		1.13	
	AT	354.0	DEG
MAX PRESSURE (BARS)		44.77	
	AT	371.0	DEG

WEIBE MASS BURNED CRITERIA

SRT OF HT RLS DABDC		349.0	
0 - 1%	DEG. 12	mS	1.0
0 - 10%	DEG. 20	mS	1.6
0 - 50%	DEG. 37	mS	2.9
0 - 90%	DEG. 58	mS	4.6
0 - 100%	DEG. 61	mS	4.8
1 - 90%	DEG. 46	mS	3.6
dP/dθ MAX (BARS/DEG)		1.11	
	AT	359.0	DEG
MAX PRESSURE (BARS)		46.82	
	AT	374.0	DEG

HEAT TRANSFER

ENGINE MEASURED (kW)	2.050
ENGINE PREDICTED (kW)	0.951
PREDICTED/MEASURED (%)	46.4
MAX BURNED GAS TEMP (K)	2512.9
AT	368.0 DEG
BURNED GAS TEMP EVO (K)	1414.6
GAS TEMP AT IVC (K)	353.5
WALL TEMPERATURE (K)	400.0

STATISTICAL DATA

	MEAN	SD	% DIS
WORK (J)	91.16	1.960	2.2
POWER (kW)	1.599	0.034	2.2
PMAX (BAR)	45.35	4.600	10.2
AT DEG	11.2	2.500	22.7

GAS ANALYSIS

	MODEL	MEASURED
CO2 (%)	9.4	9.7
CO (PPM)	0.0	6200.0
O2 (%)	0.6	1.7
NOx (PPM)	4194.7	1135.0
UHC (PPM)		3260.0
FUEL GROSS CV (kJ/kG)		53989.5
STOICH A/F RATIO		16.72

	MODEL	MEASD
POWER (kW)	2.064	1.625
FRICTN PWR (kW)	0.306	
PUMPNG PWR (kW)		-0.026
INDICATD MEP (BAR)	9.31	7.33
INDICATED EFFICNCY	0.302	0.237
BRAKE POWER (kW)	1.732	1.417
BRAKE TH EFFICNCY	0.253	0.207

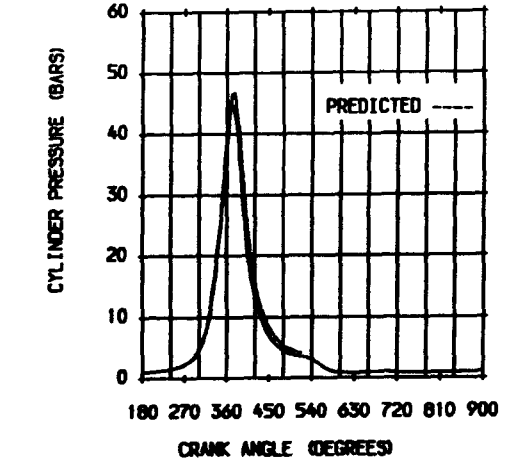

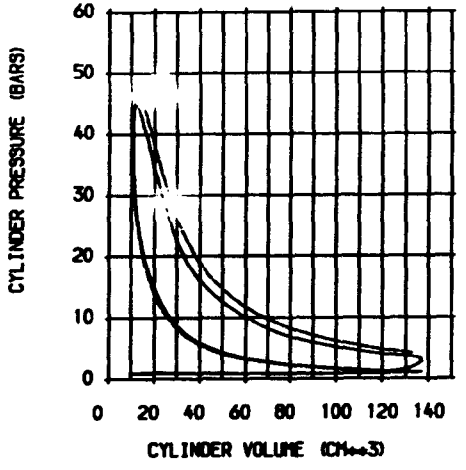

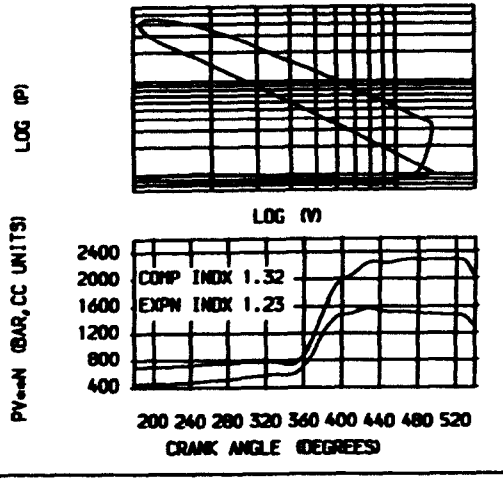

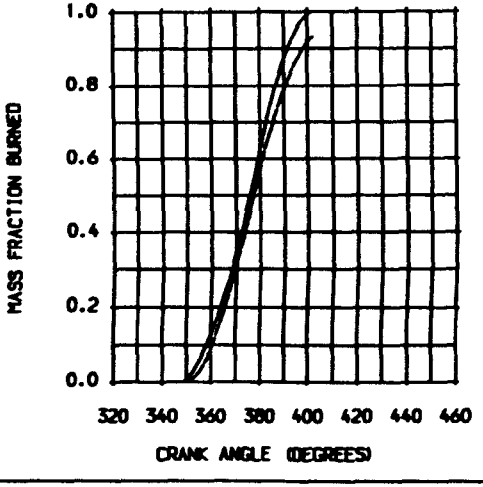

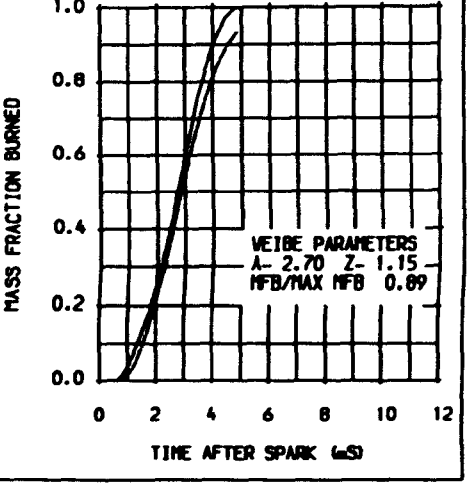

TEST DATE	11/02/89
TEST REFERENCE	T33M202H3-2
COMPRESSION RATIO	13.00
SPEED (RPM)	2107.00
IGNITION (DEG BTDC)	19
EXCESS AIR RATIO	1.05
CHAMBER AREA (CM**2)	31.65
ATMOSPHERIC PRESS (BAR)	1.02397
PRESS TDC EXHAUST (BAR)	0.92396
PRESSURE IVC (BAR)	1.17883
RESIDUAL FRACTION (%)	7.00
BLOWBY COEFFICIENT	1.54
BLOWBY % OF CHARGE	3.8

DERIVED MASS BURNED CRITERIA

SRT OF HT RLS DABOC	349.0	
0 - 1%	DEG. 11	mS 0.9
0 - 10%	DEG. 19	mS 1.5
0 - 50%	DEG. 39	mS 3.1
0 - 90%	DEG. 63	mS 5.0
0 - 100%	DEG. 78	mS 6.2
1 - 90%	DEG. 52	mS 4.1
dP/dθ MAX (BARS/DEG)	1.13	
	AT	357.0 DEG
MAX PRESSURE (BARS)	43.57	
	AT	372.0 DEG

VEIBE MASS BURNED CRITERIA

SRT OF HT RLS DABOC	349.0	
0 - 1%	DEG. 12	mS 0.9
0 - 10%	DEG. 20	mS 1.6
0 - 50%	DEG. 39	mS 3.1
0 - 90%	DEG. 63	mS 5.0
0 - 100%	DEG. 78	mS 6.2
1 - 90%	DEG. 51	mS 4.0
dP/dθ MAX (BARS/DEG)	1.06	
	AT	358.0 DEG
MAX PRESSURE (BARS)	44.47	
	AT	372.0 DEG

HEAT TRANSFER

ENGINE MEASURED (kW)	1.954
ENGINE PREDICTED (kW)	0.914
PREDICTED/MEASURED (%)	46.8
MAX BURNED GAS TEMP (K)	2485.4
AT	367.0 DEG
BURNED GAS TEMP EVO (K)	1428.6
GAS TEMP AT IVC (K)	348.5
WALL TEMPERATURE (K)	400.0

STATISTICAL DATA

	MEAN	SD	% DIS
WORK (J)	95.38	2.030	2.1
POWER (kW)	1.675	0.036	2.1
PMAX (BAR)	44.12	4.000	9.0
AT DEG	11.1	2.400	21.4

GAS ANALYSIS

	MODEL	MEASURED
CO2 (%)	9.2	9.6
CO (PPM)	0.0	4300.0
O2 (%)	0.9	2.0
NOx (PPM)	4643.2	1181.0
UHC (PPM)		3745.0

FUEL GROSS CV (kJ/kG) 53989.5
STOICH A/F RATIO 16.72

	MODEL	MEASD
POWER (kW)	1.972	1.689
FRICTN PWR (kW)	0.306	
PUMPNG PWR (kW)		-0.026
INDICATD MEP (BAR)	8.89	7.61
INDICATED EFFICNCY	0.293	0.251
BRAKE POWER (kW)	1.640	1.405
BRAKE TH EFFICNCY	0.244	0.209

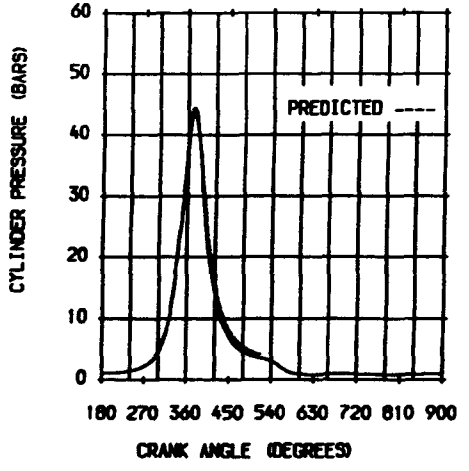

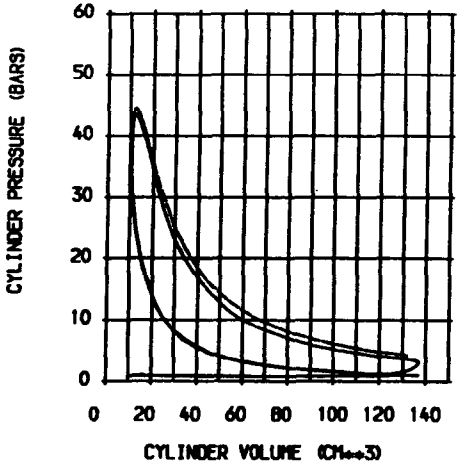

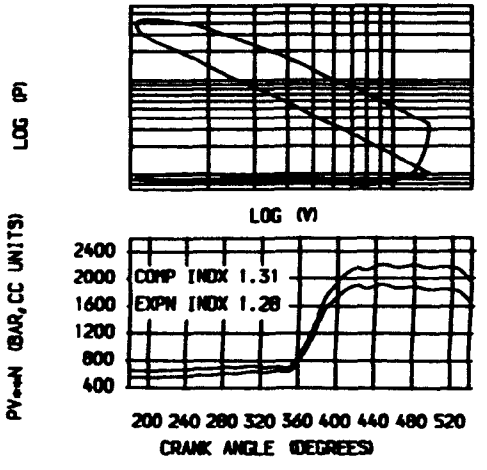

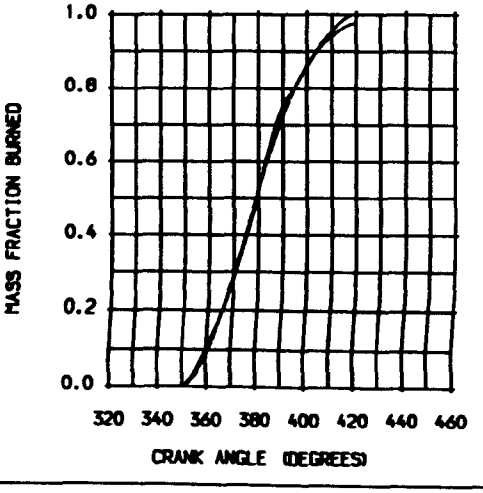

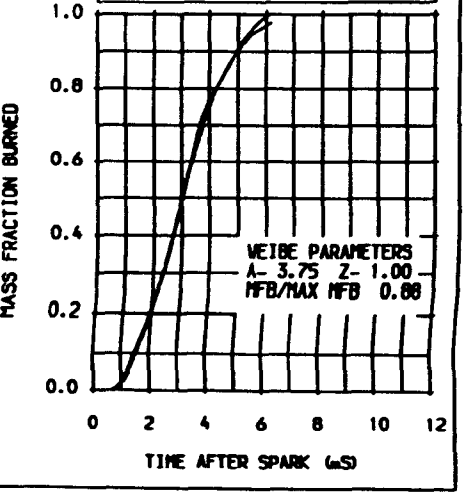

TEST DATE	01/02/89
TEST REFERENCE	T32M490BH3-2
COMPRESSION RATIO	13.00
SPEED (RPM)	2106.00
IGNITION (DEG BTDC)	23
EXCESS AIR RATIO	1.12
CHAMBER AREA (CM**2)	31.65
ATMOSPHERIC PRESS (BAR)	1.02597
PRESS TDC EXHAUST (BAR)	0.92596
PRESSURE IVC (BAR)	1.24175
RESIDUAL FRACTION (%)	7.00
BLOWBY COEFFICIENT	1.54
BLOWBY % OF CHARGE	3.8

DERIVED MASS BURNED CRITERIA

SRT OF HT RLS DABDC		346.0	
0 - 1%	DEG. 11	MS	0.9
0 - 10%	DEG. 18	MS	1.4
0 - 50%	DEG. 33	MS	2.6
0 - 90%	DEG. 52	MS	4.1
0 - 100%	DEG. 63	MS	5.0
1 - 90%	DEG. 41	MS	3.2
dP/dθ MAX (BARS/DEG)			1.38
		AT	356.0 DEG
MAX PRESSURE (BARS)			51.15
		AT	370.0 DEG

VEIBE MASS BURNED CRITERIA

SRT OF HT RLS DABDC		346.0	
0 - 1%	DEG. 13	MS	1.0
0 - 10%	DEG. 21	MS	1.7
0 - 50%	DEG. 36	MS	2.8
0 - 90%	DEG. 56	MS	4.4
0 - 100%	DEG. 63	MS	5.0
1 - 90%	DEG. 43	MS	3.4
dP/dθ MAX (BARS/DEG)			1.49
		AT	358.0 DEG
MAX PRESSURE (BARS)			52.86
		AT	372.0 DEG

HEAT TRANSFER

ENGINE MEASURED (kW)	1.841
ENGINE PREDICTED (kW)	0.937
PREDICTED/MEASURED (%)	50.9
MAX BURNED GAS TEMP (K)	2484.8
AT	367.0 DEG
BURNED GAS TEMP EVO (K)	1317.6
GAS TEMP AT IVC (K)	367.5
WALL TEMPERATURE (K)	400.0

STATISTICAL DATA

	MEAN	SD	% DIS
WORK (J)	85.45	3.300	3.9
POWER (kW)	1.500	0.058	3.9
PMAX (BAR)	52.30	5.100	9.8
AT DEG	9.8	2.100	21.8

GAS ANALYSIS

	MODEL	MEASURED
CO2 (%)	8.7	9.4
CO (PPM)	0.0	800.0
O2 (%)	2.1	2.9
NOx (PPM)	6598.5	2372.0
UHC (PPM)		2568.0
FUEL GROSS CV (kJ/kG)		53989.5
STOICH A/F RATIO		16.72

	MODEL	MEASD
POWER (kW)	2.005	1.523
FRICTN PWR (kW)	0.306	
PUMPNG PWR (kW)		-0.023
INDICATD MEP (BAR)	9.04	6.86
INDICATED EFFICNCY	0.317	0.241
BRAKE POWER (kW)	1.676	1.349
BRAKE TH EFFICNCY	0.265	0.213

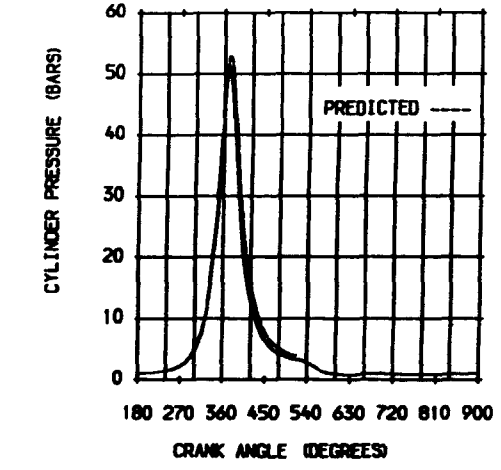

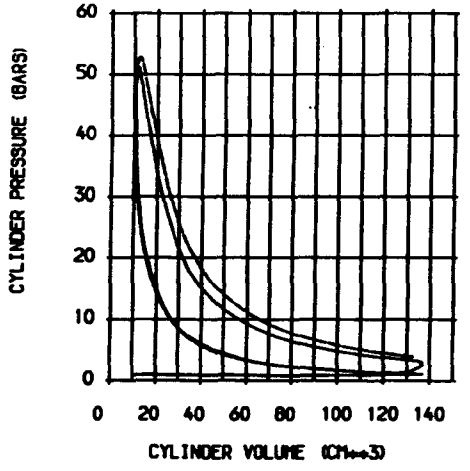

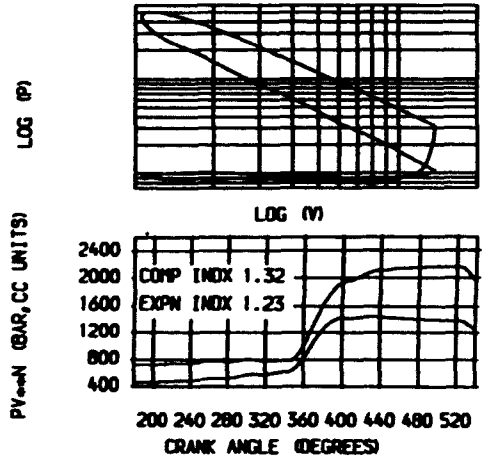

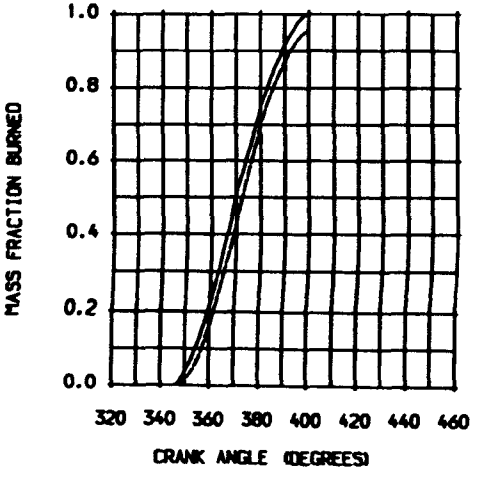

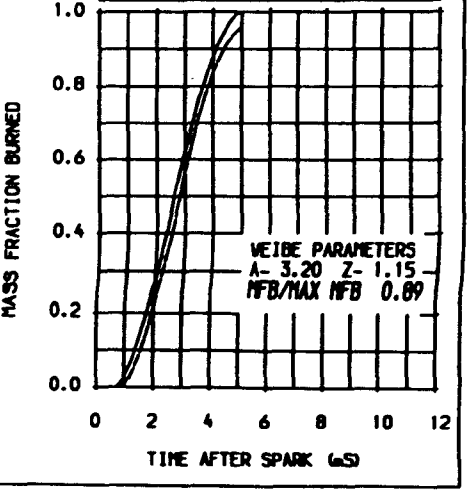

TEST DATE	11/02/89
TEST REFERENCE	T33M1D1H3-2
COMPRESSION RATIO	13.00
SPEED (RPM)	2105.00
IGNITION (DEG BTDC)	33
EXCESS AIR RATIO	1.50
CHAMBER AREA (CM**2)	31.65
ATMOSPHERIC PRESS (BAR)	1.02397
PRESS IDC EXHAUST (BAR)	0.92396
PRESSURE IVC (BAR)	1.14929
RESIDUAL FRACTION (%)	7.00
BLOWBY COEFFICIENT	1.54
BLOWBY % OF CHARGE	3.8

DERIVED MASS BURNED CRITERIA

SRT OF HT RLS DABDC		342.0		
0 - 1%	DEG.	18	mS	1.4
0 - 10%	DEG.	26	mS	2.1
0 - 50%	DEG.	50	mS	4.0
0 - 90%	DEG.	84	mS	6.7
0 - 100%	DEG.	95	mS	7.5
1 - 90%	DEG.	66	mS	5.2
dP/dθ MAX (BARS/DEG)		1.37		
	AT	351.0	DEG	
MAX PRESSURE (BARS)		46.31		
	AT	367.0	DEG	

WEIBE MASS BURNED CRITERIA

SRT OF HT RLS DABDC		342.0		
0 - 1%	DEG.	19	mS	1.5
0 - 10%	DEG.	28	mS	2.2
0 - 50%	DEG.	48	mS	3.8
0 - 90%	DEG.	77	mS	6.1
0 - 100%	DEG.	95	mS	7.5
1 - 90%	DEG.	58	mS	4.6
dP/dθ MAX (BARS/DEG)		1.30		
	AT	353.0	DEG	
MAX PRESSURE (BARS)		45.53		
	AT	368.0	DEG	

HEAT TRANSFER

ENGINE MEASURED (kW)	1.301
ENGINE PREDICTED (kW)	0.632
PREDICTED/MEASURED (%)	48.6
MAX BURNED GAS TEMP (K)	2132.0
AT	363.0 DEG
BURNED GAS TEMP EVO (K)	1125.0
GAS TEMP AT IVC (K)	335.5
WALL TEMPERATURE (K)	400.0

STATISTICAL DATA

	MEAN	SD	% DIS
WORK (J)	70.70	2.020	2.9
POWER (kW)	1.240	0.036	2.9
PMAX (BAR)	46.59	4.500	9.8
AT DEG	6.6	1.500	22.7

GAS ANALYSIS

	MODEL	MEASURED
CO2 (%)	6.6	6.7
CO (PPM)	0.0	1000.0
O2 (%)	6.5	8.1
NOx (PPM)	5990.5	159.0
UHC (PPM)		4069.0
FUEL GROSS CV (kJ/kG)	53989.5	
STOICH A/F RATIO	16.72	

	MODEL	MEASD
POWER (kW)	1.489	1.268
FRICTN PWR (kW)	0.306	
PUMPNG PWR (kW)		-0.028
INDICATD MEP (BAR)	6.72	5.72
INDICATED EFFICNCY	0.305	0.261
BRAKE POWER (kW)	1.155	0.907
BRAKE TH EFFICNCY	0.238	0.187

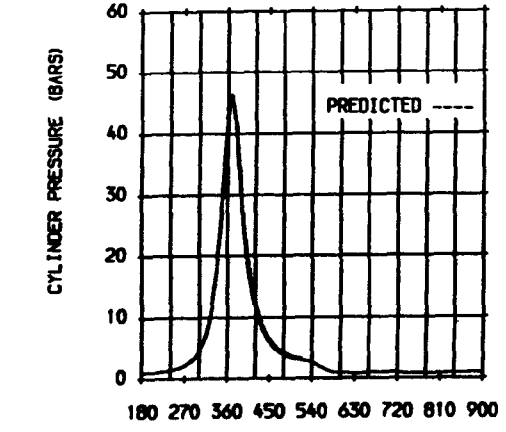

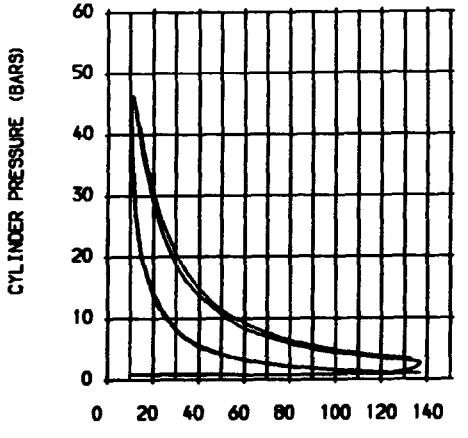

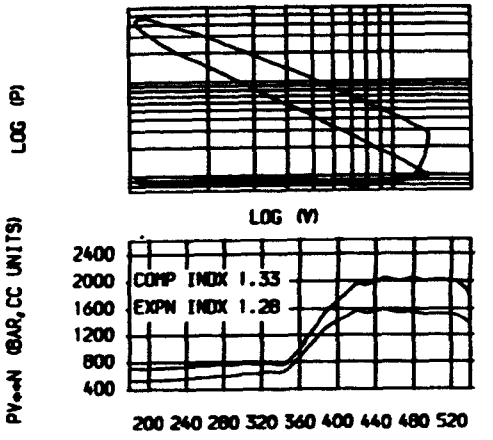

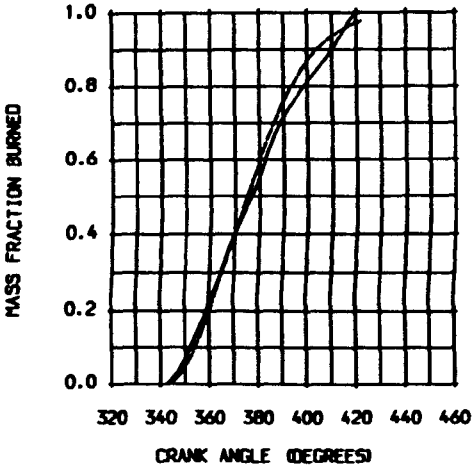

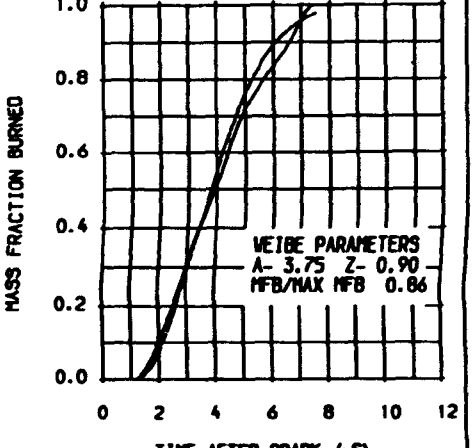

TEST DATE	11/02/89
TEST REFERENCE	T33M1D1H3-2
COMPRESSION RATIO	13.00
SPEED (RPM)	2105.00
IGNITION (DEG BTDC)	33
EXCESS AIR RATIO	1.50
CHAMBER AREA (CM**2)	31.65
ATMOSPHERIC PRESS (BAR)	1.02397
PRESS TDC EXHAUST (BAR)	0.94172
PRESSURE IVC (BAR)	1.14596
RESIDUAL FRACTION (%)	7.00
BLOWBY COEFFICIENT	1.54
BLOWBY % OF CHARGE	3.8

DERIVED MASS BURNED CRITERIA

SRT OF HT RLS DABDC		344.0	
0 - 1%	DEG. 20	mS	1.6
0 - 10%	DEG. 28	mS	2.2
0 - 50%	DEG. 49	mS	3.9
0 - 90%	DEG. 83	mS	6.6
0 - 100%	DEG. 97	mS	7.7
1 - 90%	DEG. 63	mS	5.0
dP/dθ MAX (BARS/DEG)		1.37	
	AT	353.0	DEG
MAX PRESSURE (BARS)		46.31	
	AT	369.0	DEG

WEIBE MASS BURNED CRITERIA

SRT OF HT RLS DABDC		344.0	
0 - 1%	DEG. 21	mS	1.7
0 - 10%	DEG. 29	mS	2.3
0 - 50%	DEG. 49	mS	3.9
0 - 90%	DEG. 79	mS	6.3
0 - 100%	DEG. 97	mS	7.7
1 - 90%	DEG. 58	mS	4.6
dP/dθ MAX (BARS/DEG)		1.25	
	AT	354.0	DEG
MAX PRESSURE (BARS)		44.67	
	AT	368.0	DEG

HEAT TRANSFER

ENGINE MEASURED (kW)	1.301
ENGINE PREDICTED (kW)	0.622
PREDICTED/MEASURED (%)	47.8
MAX BURNED GAS TEMP (K)	2124.5
AT	363.0 DEG
BURNED GAS TEMP EVO (K)	1130.3
GAS TEMP AT IVC (K)	334.5
WALL TEMPERATURE (K)	400.0

STATISTICAL DATA

	MEAN	SD	% DIS
WORK (J)	70.70	2.020	2.9
POWER (kW)	1.240	0.036	2.9
PMAX (BAR)	46.59	4.500	9.8
AT DEG	6.6	1.500	22.7

GAS ANALYSIS

	MODEL	MEASURED
CO2 (%)	6.6	6.7
CO (PPM)	0.0	1000.0
O2 (%)	6.5	8.1
NOx (PPM)	5887.0	159.0
UHC (PPM)		4069.0
FUEL GROSS CV (kJ/kG)		53989.5
STOICH A/F RATIO		16.72

	MODEL	MEASD
POWER (kW)	1.481	1.445
FRICTN PWR (kW)	0.306	
PUMPNG PWR (kW)		-0.030
INDICATD MEP (BAR)	6.68	6.52
INDICATED EFFICNCY	0.303	0.297
BRAKE POWER (kW)	1.145	0.907
BRAKE TH EFFICNCY	0.236	0.187

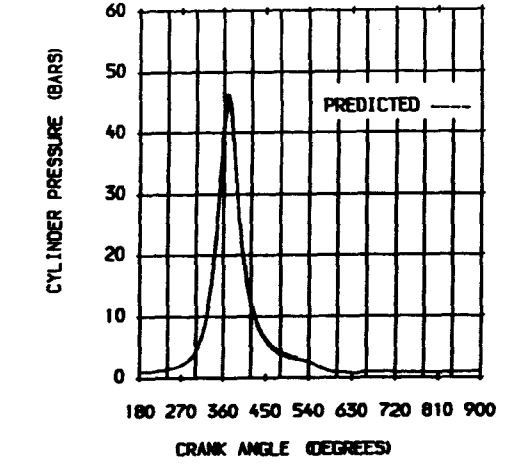

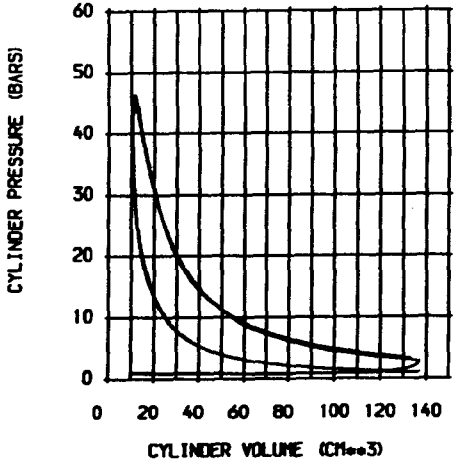

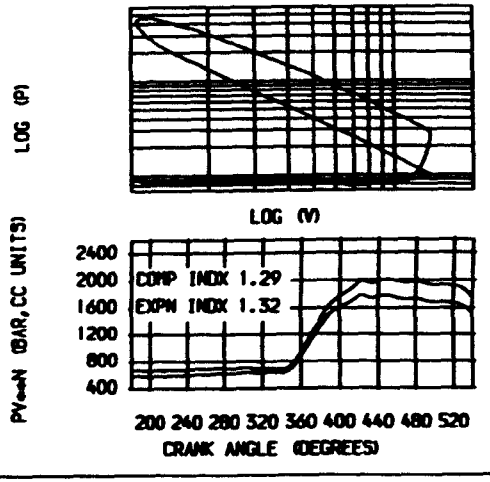

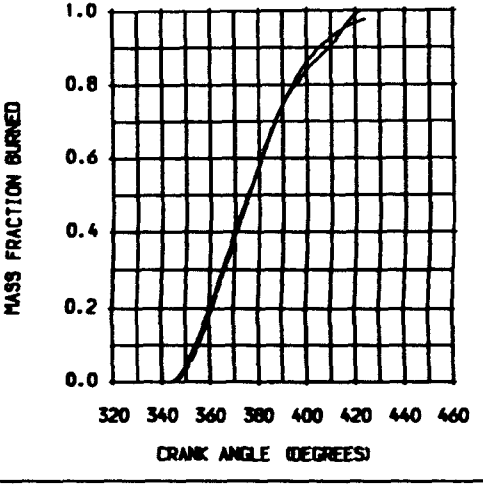

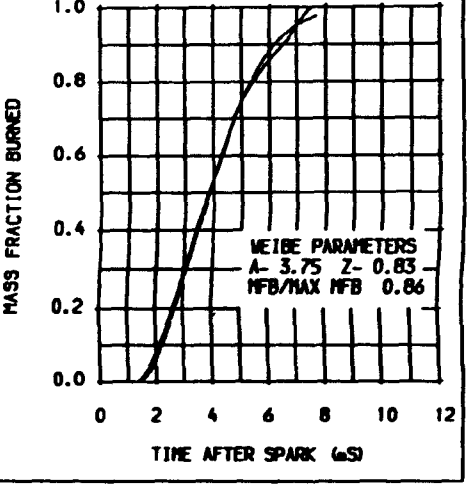

TEST DATE	01/03/89
TEST REFERENCE	T35M22012HRCC
COMPRESSION RATIO	13.00
SPEED (RPM)	1518.00
IGNITION (DEG BTDC)	14
EXCESS AIR RATIO	1.01
CHAMBER AREA (CM**2)	34.00
ATMOSPHERIC PRESS (BAR)	0.98194
PRESS TDC EXHAUST (BAR)	0.88194
PRESSURE IVC (BAR)	1.16277
RESIDUAL FRACTION (%)	7.00
BLOWBY COEFFICIENT	1.99
BLOWBY % OF CHARGE	6.8

DERIVED MASS BURNED CRITERIA

SRT OF HT RLS DABDC		354.0	
0 - 1%	DEG. 10	%S	1.1
0 - 10%	DEG. 15	%S	1.6
0 - 50%	DEG. 26	%S	2.9
0 - 90%	DEG. 39	%S	4.3
0 - 100%	DEG. 48	%S	5.3
1 - 90%	DEG. 29	%S	3.2
dP/dθ MAX (BARS/DEG)		1.40	
	AT	363.0	DEG
MAX PRESSURE (BARS)		46.49	
	AT	374.0	DEG

WEIBE MASS BURNED CRITERIA

SRT OF HT RLS DABDC		354.0	
0 - 1%	DEG. 11	%S	1.2
0 - 10%	DEG. 15	%S	1.6
0 - 50%	DEG. 27	%S	3.0
0 - 90%	DEG. 42	%S	4.6
0 - 100%	DEG. 48	%S	5.3
1 - 90%	DEG. 31	%S	3.4
dP/dθ MAX (BARS/DEG)		1.54	
	AT	363.0	DEG
MAX PRESSURE (BARS)		49.01	
	AT	374.0	DEG

HEAT TRANSFER

ENGINE MEASURED (kW)	1.492	
ENGINE PREDICTED (kW)	0.782	
PREDICTED/MEASURED (%)	52.4	
MAX BURNED GAS TEMP (K)	2571.3	
AT	370.0	DEG
BURNED GAS TEMP EVO (K)	1341.4	
GAS TEMP AT IVC (K)	381.0	
WALL TEMPERATURE (K)	400.0	

STATISTICAL DATA

	MEAN	SD	% DIS
WORK (J)	90.61	0.510	0.5
POWER (kW)	1.146	0.007	0.5
PMAX (BAR)	47.13	2.600	5.6
AT DEG	14.1	1.400	9.9

GAS ANALYSIS

	MODEL	MEASURED
CO2 (%)	9.5	9.6
CO (PPM)	0.0	10000.0
O2 (%)	0.2	1.7
NOx (PPM)	4027.0	1145.0
UHC (PPM)		4826.0

FUEL GROSS CV (kJ/kG) 53395.7
STOICH A/F RATIO 16.47

	MODEL	MEASD
POWER (kW)	1.346	1.154
FRICTN PWR (kW)	0.188	
PUMPNG PWR (kW)		-0.008
INDICATD MEP (BAR)	8.42	7.22
INDICATED EFFICNCY	0.296	0.251
BRAKE POWER (kW)	1.150	1.011
BRAKE TH EFFICNCY	0.250	0.220

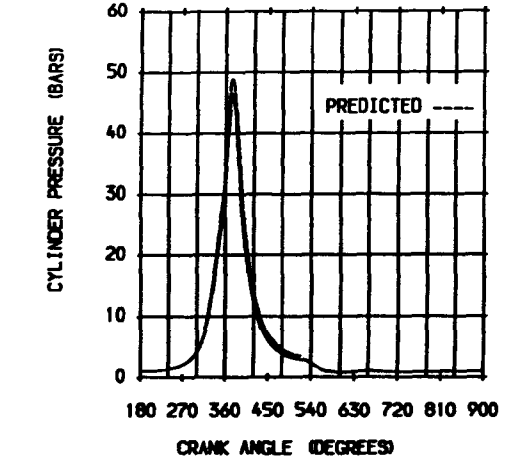

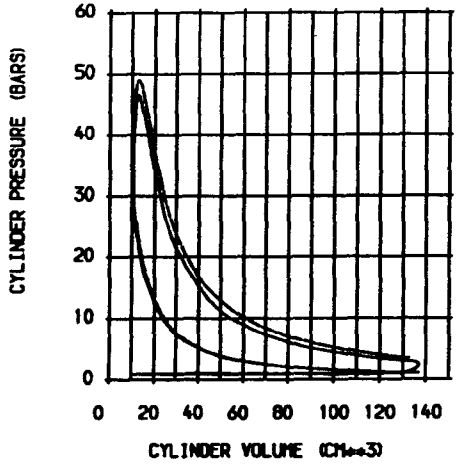

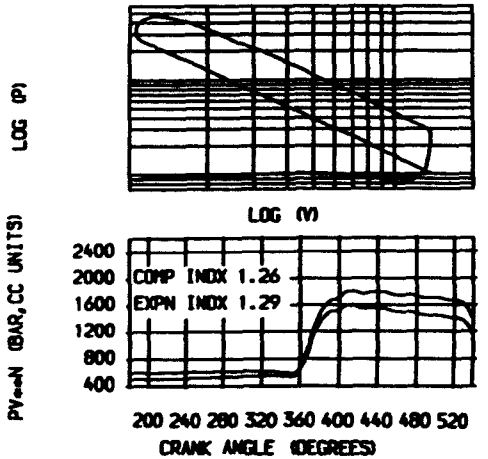

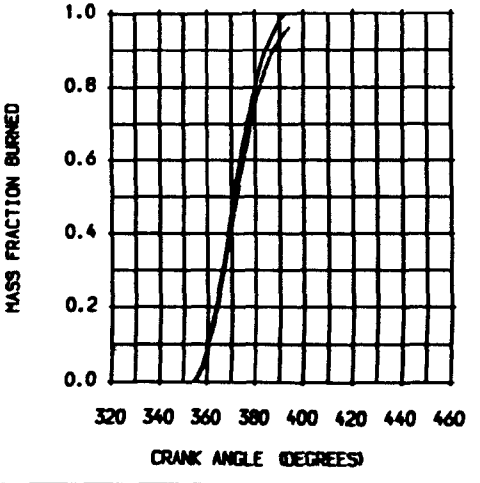

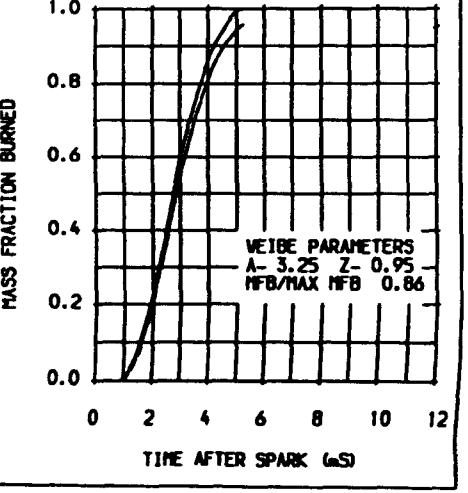

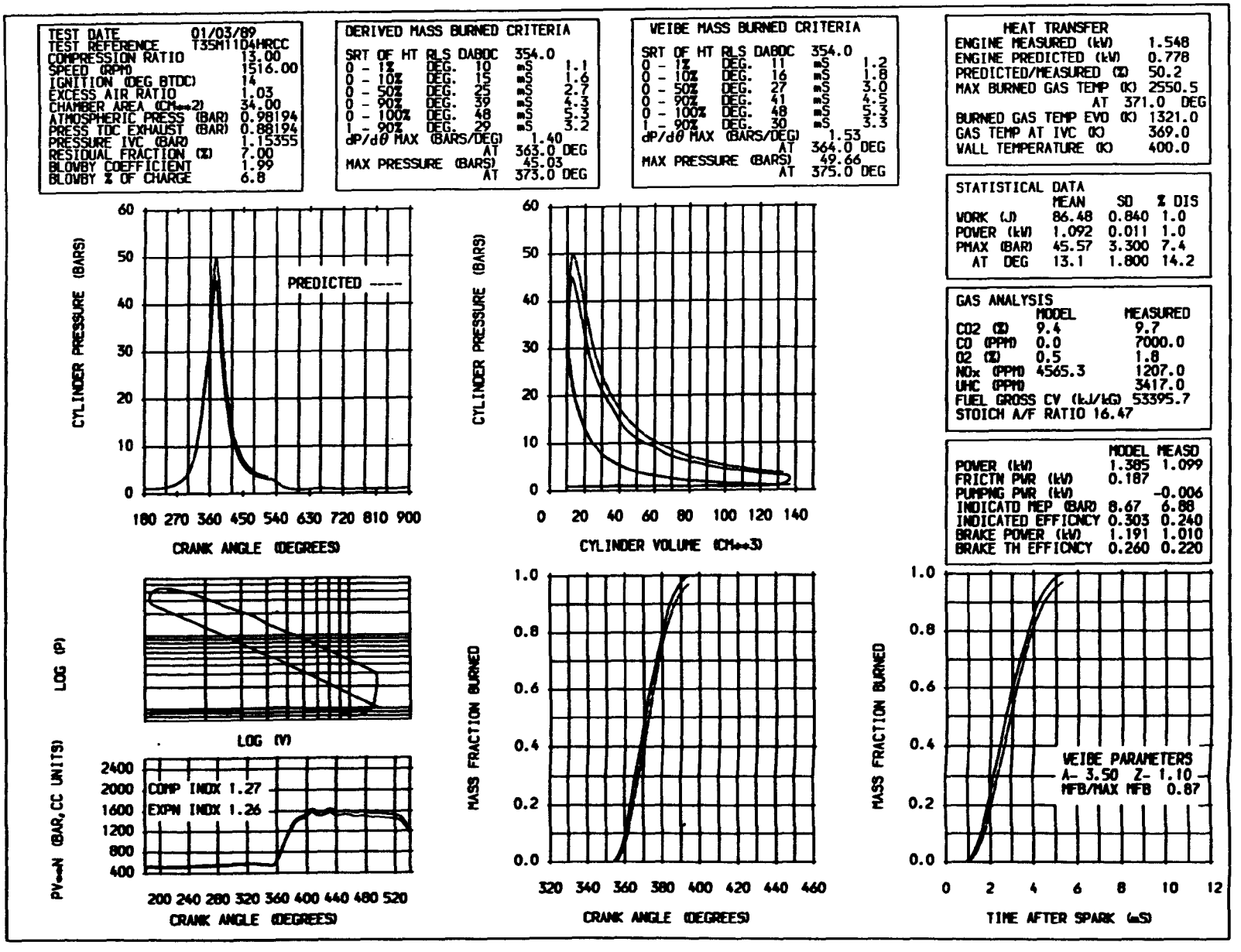
TEST DATE 01/03/89
TEST REFERENCE T35M11D4HRCC
COMPRESSION RATIO 13.00
SPEED (RPM) 1516.00
IGNITION (DEG BTDC) 14
EXCESS AIR RATIO 1.03
CHAMBER AREA (CM**2) 34.00
ATMOSPHERIC PRESS (BAR) 0.98194
PRESS TDC EXHAUST (BAR) 0.88194
PRESSURE IVC (BAR) 1.15355
RESIDUAL FRACTION (%) 7.00
BLOWBY COEFFICIENT 1.99
BLOWBY % OF CHARGE 6.8
DERIVED MASS BURNED CRITERIA
SRT OF HT RLS DABDC 354.0
0 - 1% DEG. 10 DEG 1.1
0 - 10% DEG. 15 DEG 1.6
0 - 50% DEG. 25 DEG 2.7
0 - 90% DEG. 39 DEG 4.3
0 - 100% DEG. 48 DEG 5.3
1 - 90% DEG. 29 DEG 3.2
dP/dθ MAX (BARS/DEG) 1.40
AT 363.0 DEG
MAX PRESSURE (BARS) 45.03
AT 373.0 DEG
VEIBE MASS BURNED CRITERIA
SRT OF HT RLS DABDC 354.0
0 - 1% DEG. 11 DEG 1.2
0 - 10% DEG. 16 DEG 1.8
0 - 50% DEG. 27 DEG 3.0
0 - 90% DEG. 41 DEG 4.5
0 - 100% DEG. 48 DEG 5.4
1 - 90% DEG. 30 DEG 3.3
dP/dθ MAX (BARS/DEG) 1.53
AT 364.0 DEG
MAX PRESSURE (BARS) 49.66
AT 375.0 DEG
HEAT TRANSFER
ENGINE MEASURED (kW) 1.548
ENGINE PREDICTED (kW) 0.778
PREDICTED/MEASURED (%) 50.2
MAX BURNED GAS TEMP (K) 2550.5
AT 371.0 DEG
BURNED GAS TEMP EVO (K) 1321.0
GAS TEMP AT IVC (K) 369.0
WALL TEMPERATURE (K) 400.0
STATISTICAL DATA
MEAN SD % DIS
WORK (J) 86.48 0.840 1.0
POWER (kW) 1.092 0.011 1.0
PMAX (BAR) 45.57 3.300 7.4
AT DEG 13.1 1.800 14.2
GAS ANALYSIS
MODEL MEASURED
CO2 (%) 9.4 9.7
CO (PPM) 0.0 7000.0
O2 (%) 0.5 1.8
NOx (PPM) 4565.3 1207.0
UHC (PPM) 3417.0
FUEL GROSS CV (kJ/kG) 53395.7
STOICH A/F RATIO 16.47
MODEL MEASD
POWER (kW) 1.385 1.099
FRICTN PWR (kW) 0.187
PUMPNG PWR (kW) -0.006
INDICATD MEP (BAR) 8.67 6.88
INDICATED EFFICNCY 0.303 0.240
BRAKE POWER (kW) 1.191 1.010
BRAKE TH EFFICNCY 0.260 0.220
CYLINDER PRESSURE (BARS)
PREDICTED -----
CRANK ANGLE (DEGREES)
CYLINDER VOLUME (CM**3)
LOG (P)
LOG (V)
PV**N (BAR,CC UNITS)
COMP INDX 1.27
EXPN INDX 1.26
MASS FRACTION BURNED
VEIBE PARAMETERS
A- 3.50 Z- 1.10
MFB/MAX MFB 0.87
TIME AFTER SPARK (mS)

TEST DATE	01/03/89
TEST REFERENCE	T35M140SHRCC
COMPRESSION RATIO	13.00
SPEED (RPM)	1512.00
IGNITION (DEG BTDC)	24
EXCESS AIR RATIO	1.63
CHAMBER AREA (CM**2)	34.00
ATMOSPHERIC PRESS (BAR)	0.98194
PRESS TDC EXHAUST (BAR)	0.88194
PRESSURE IVC (BAR)	1.15361
RESIDUAL FRACTION (%)	7.00
BLOWBY COEFFICIENT	1.99
BLOWBY % OF CHARGE	6.8

DERIVED MASS BURNED CRITERIA

SRT OF HT RLS DABDC		352.0	
0 - 1%	DEG. 19	mS	2.1
0 - 10%	DEG. 25	mS	2.8
0 - 50%	DEG. 40	mS	4.4
0 - 90%	DEG. 83	mS	9.1
0 - 100%	DEG. 96	mS	10.6
1 - 90%	DEG. 64	mS	7.1
dP/dθ MAX (BARS/DEG)		0.82	
	AT	361.0	DEG
MAX PRESSURE (BARS)		37.84	
	AT	370.0	DEG

WEIBE MASS BURNED CRITERIA

SRT OF HT RLS DABDC		352.0	
0 - 1%	DEG. 20	mS	2.2
0 - 10%	DEG. 26	mS	2.9
0 - 50%	DEG. 42	mS	4.6
0 - 90%	DEG. 62	mS	6.8
0 - 100%	DEG. 96	mS	10.6
1 - 90%	DEG. 42	mS	4.6
dP/dθ MAX (BARS/DEG)		0.71	
	AT	359.0	DEG
MAX PRESSURE (BARS)		37.80	
	AT	371.0	DEG

HEAT TRANSFER

ENGINE MEASURED (kW)	0.804
ENGINE PREDICTED (kW)	0.433
PREDICTED/MEASURED (%)	53.9
MAX BURNED GAS TEMP (K)	2023.3
AT	367.0 DEG
BURNED GAS TEMP EVO (K)	1052.6
GAS TEMP AT IVC (K)	356.0
WALL TEMPERATURE (K)	400.0

STATISTICAL DATA

	MEAN	SD	% DIS
WORK (J)	56.49	2.560	4.7
POWER (kW)	0.712	0.032	4.7
PMAX (BAR)	38.15	3.400	9.2
AT DEG	9.4	1.700	18.9

GAS ANALYSIS

	MODEL	MEASURED
CO2 (%)	6.1	6.0
CO (PPM)	0.0	1000.0
O2 (%)	7.6	9.2
NOx (PPM)	4969.1	0.0
UHC (PPM)		4888.0

FUEL GROSS CV (kJ/kG) 53395.7
STOICH A/F RATIO 16.47

	MODEL	MEASD
POWER (kW)	0.888	0.722
FRICTN PWR (kW)	0.187	
PUMPNG PWR (kW)		-0.010
INDICATD MEP (BAR)	5.57	4.53
INDICATED EFFICNCY	0.288	0.234
BRAKE POWER (kW)	0.691	0.631
BRAKE TH EFFICNCY	0.224	0.205

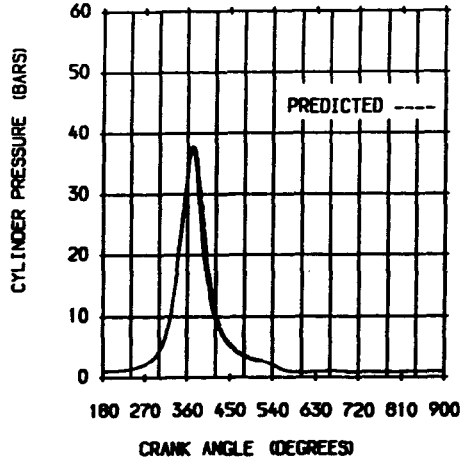

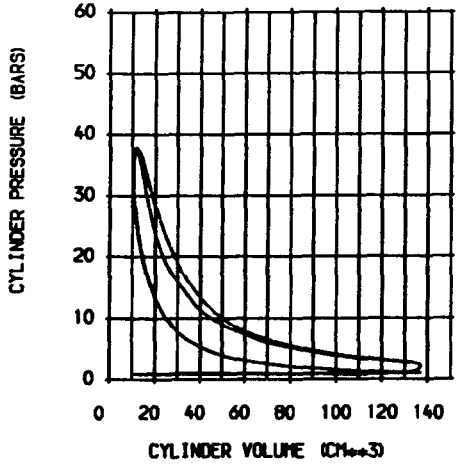

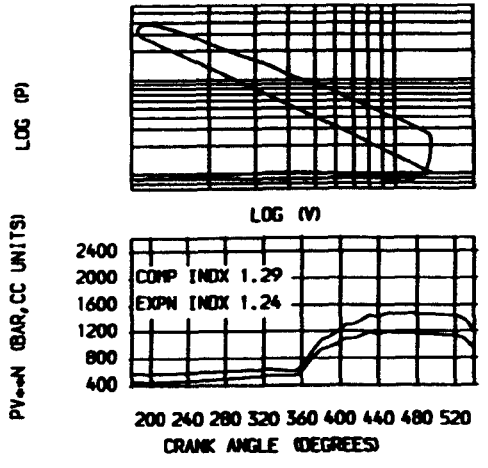

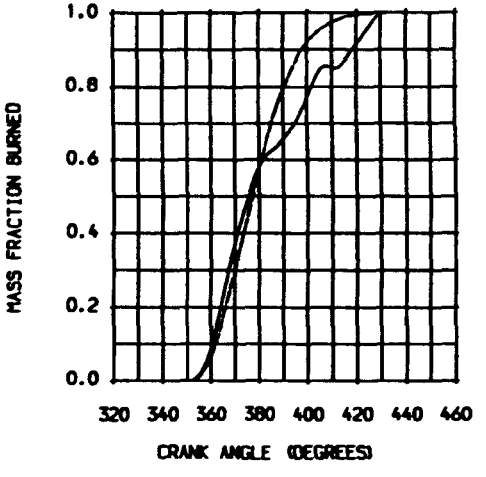

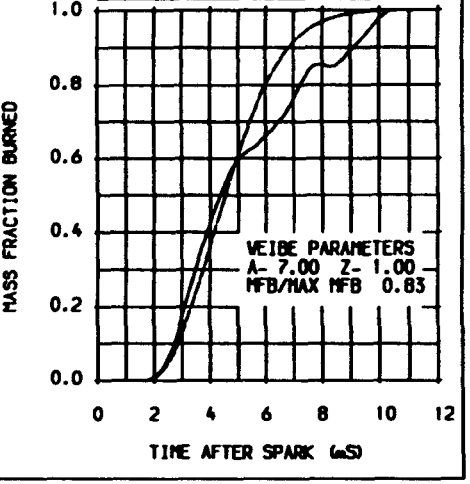

TEST DATE	01/03/89
TEST REFERENCE	T35M902HRCC
COMPRESSION RATIO	13.00
SPEED (RPM)	1815.00
IGNITION (DEG BTDC)	16
EXCESS AIR RATIO	1.03
CHAMBER AREA (CM**2)	34.00
ATMOSPHERIC PRESS (BAR)	0.98194
PRESS IDC EXHAUST (BAR)	0.83194
PRESSURE IVC (BAR)	1.09444
RESIDUAL FRACTION (%)	7.00
BLOWBY COEFFICIENT	1.84
BLOWBY % OF CHARGE	5.3

DERIVED MASS BURNED CRITERIA

SRT OF HT RLS DABDC		353.0	
0 - 1%	DEG. 11	mS	1.0
0 - 10%	DEG. 16	mS	1.5
0 - 50%	DEG. 28	mS	2.6
0 - 90%	DEG. 44	mS	4.0
0 - 100%	DEG. 56	mS	5.1
1 - 90%	DEG. 33	mS	3.0
dP/dθ MAX (BARS/DEG)		1.47	
	AT	362.0	DEG
MAX PRESSURE (BARS)		45.95	
	AT	372.0	DEG

WEIBE MASS BURNED CRITERIA

SRT OF HT RLS DABDC		353.0	
0 - 1%	DEG. 12	mS	1.1
0 - 10%	DEG. 17	mS	1.6
0 - 50%	DEG. 30	mS	2.8
0 - 90%	DEG. 47	mS	4.3
0 - 100%	DEG. 56	mS	5.1
1 - 90%	DEG. 35	mS	3.2
dP/dθ MAX (BARS/DEG)		1.44	
	AT	362.0	DEG
MAX PRESSURE (BARS)		47.44	
	AT	374.0	DEG

HEAT TRANSFER

ENGINE MEASURED (kW)	1.686
ENGINE PREDICTED (kW)	0.853
PREDICTED/MEASURED (%)	50.6
MAX BURNED GAS TEMP (K)	2535.9
AT	369.0 DEG
BURNED GAS TEMP EVO (K)	1348.3
GAS TEMP AT IVC (K)	355.5
WALL TEMPERATURE (K)	400.0

STATISTICAL DATA

	MEAN	SD	% DIS
WORK (J)	89.02	0.390	0.4
POWER (kW)	1.346	0.006	0.4
PMAX (BAR)	46.31	2.900	6.4
AT DEG	12.1	1.400	11.5

GAS ANALYSIS

	MODEL	MEASURED
CO2 (%)	9.4	9.7
CO (PPM)	0.0	5000.0
O2 (%)	0.5	1.7
NOx (PPM)	4429.6	1394.0
UHC (PPM)		3660.0

FUEL GROSS CV (kJ/kG) 53395.7
STOICH A/F RATIO 16.47

	MODEL	MEASD
POWER (kW)	1.641	1.359
FRICTN PWR (kW)	0.244	
PUMPNG PWR (kW)		-0.013
INDICATD MEP (BAR)	8.58	7.11
INDICATED EFFICNCY	0.305	0.251
BRAKE POWER (kW)	1.383	1.292
BRAKE TH EFFICNCY	0.256	0.239

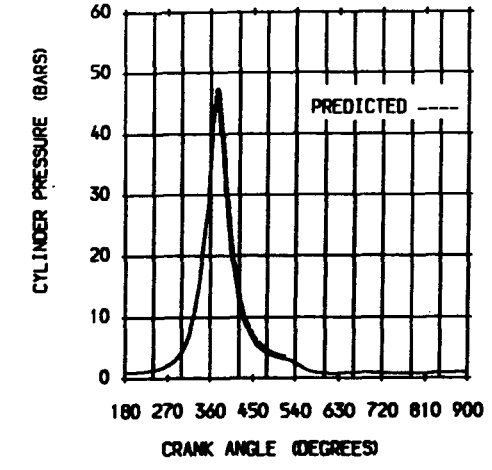

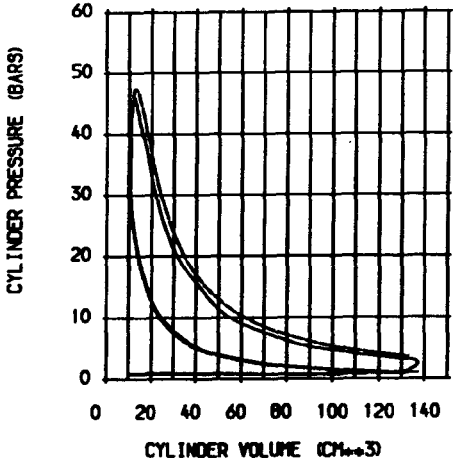

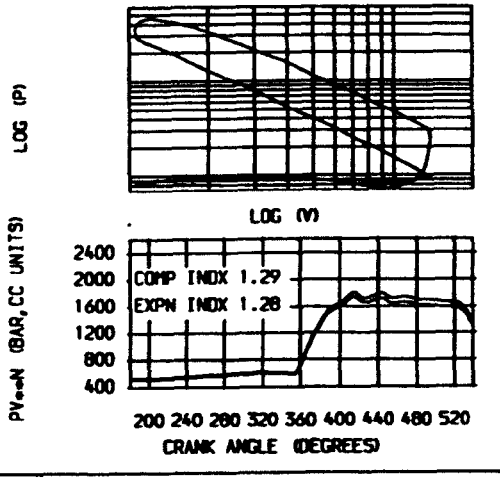

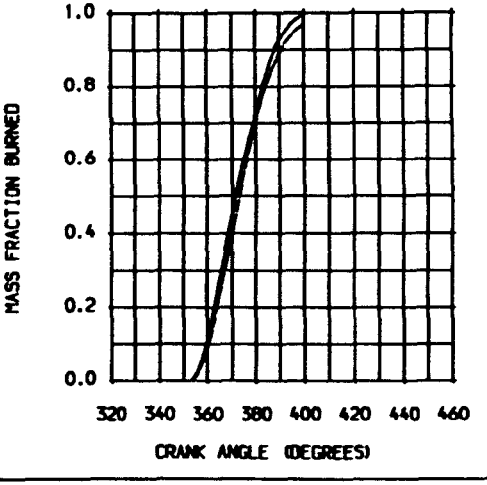

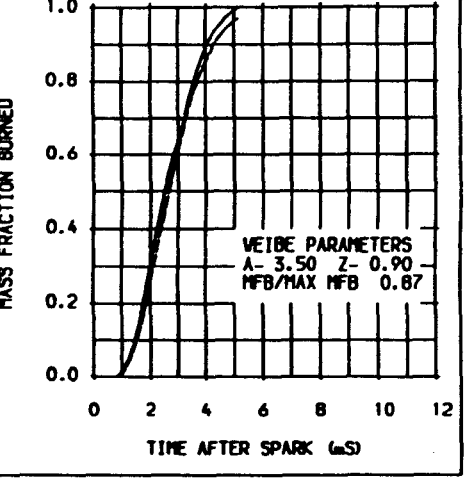

TEST DATE	01/03/89
TEST REFERENCE	T35M902HRCC
COMPRESSION RATIO	13.00
SPEED (RPM)	1815.00
IGNITION (DEG BTDC)	16
EXCESS AIR RATIO	1.03
CHAMBER AREA (CM**2)	34.00
ATMOSPHERIC PRESS (BAR)	0.98194
PRESS TDC EXHAUST (BAR)	0.83194
PRESSURE IVC (BAR)	1.09444
RESIDUAL FRACTION (%)	7.00
BLOWBY COEFFICIENT	1.84
BLOWBY % OF CHARGE	5.3

DERIVED MASS BURNED CRITERIA

SRT OF HT RLS DABOC		353.0	
0 - 1%	DEG. 11	mS	1.0
0 - 10%	DEG. 16	mS	1.5
0 - 50%	DEG. 28	mS	2.6
0 - 90%	DEG. 44	mS	4.0
0 - 100%	DEG. 56	mS	5.1
1 - 90%	DEG. 33	mS	3.0
dP/dθ MAX (BARS/DEG)		1.47	
	AT	362.0	DEG
MAX PRESSURE (BARS)		45.95	
	AT	372.0	DEG

WEIBE MASS BURNED CRITERIA

SRT OF HT RLS DABOC		353.0	
0 - 1%	DEG. 11	mS	1.0
0 - 10%	DEG. 16	mS	1.5
0 - 50%	DEG. 28	mS	2.6
0 - 90%	DEG. 45	mS	4.1
0 - 100%	DEG. 56	mS	5.1
1 - 90%	DEG. 34	mS	3.1
dP/dθ MAX (BARS/DEG)		1.69	
	AT	361.0	DEG
MAX PRESSURE (BARS)		49.90	
	AT	373.0	DEG

HEAT TRANSFER

ENGINE MEASURED (kW)	1.686
ENGINE PREDICTED (kW)	0.873
PREDICTED/MEASURED (%)	51.8
MAX BURNED GAS TEMP (K)	2549.3
AT	369.0 DEG
BURNED GAS TEMP EVO (K)	1334.1
GAS TEMP AT IVC (K)	355.5
WALL TEMPERATURE (K)	400.0

STATISTICAL DATA

	MEAN	SD	% DIS
WORK (J)	89.02	0.390	0.4
POWER (kW)	1.346	0.006	0.4
PMAX (BAR)	46.31	2.900	6.4
AT DEG	12.1	1.400	11.5

GAS ANALYSIS

	MODEL	MEASURED
CO2 (%)	9.4	9.7
CO (PPM)	0.0	5000.0
O2 (%)	0.5	1.7
NOx (PPM)	4554.3	1394.0
UHC (PPM)		3660.0
FUEL GROSS CV (kJ/kG)		53395.7
STOICH A/F RATIO		16.47

	MODEL	MEASD
POWER (kW)	1.653	1.359
FRICTN PWR (kW)	0.244	
PUMPNG PWR (kW)		-0.013
INDICATD MEP (BAR)	8.65	7.11
INDICATED EFFICNCY	0.307	0.251
BRAKE POWER (kW)	1.396	1.292
BRAKE TH EFFICNCY	0.258	0.239

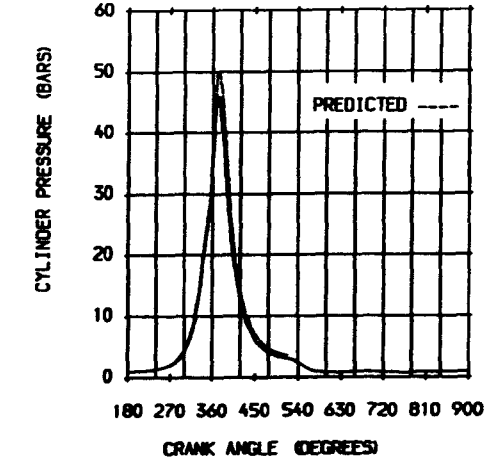

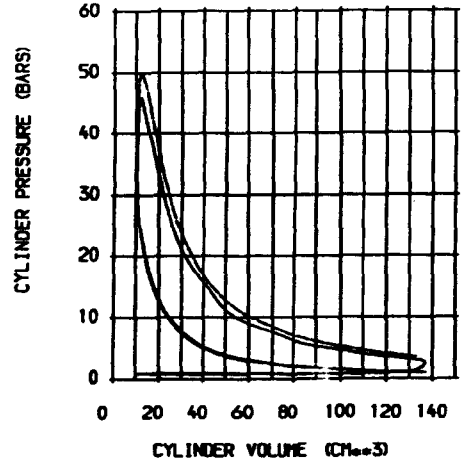

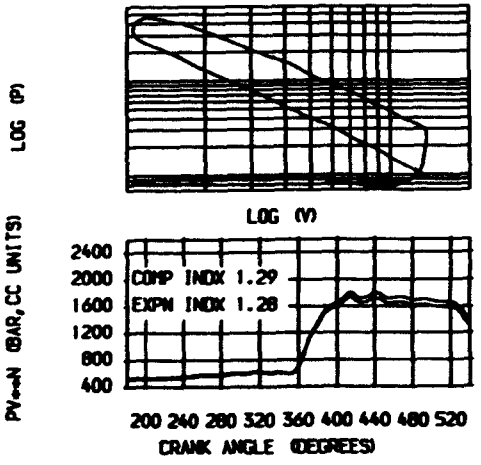

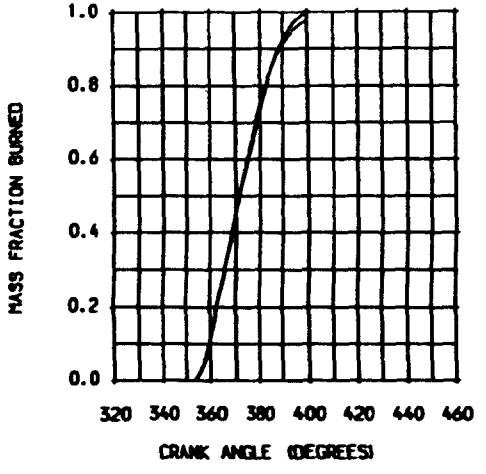

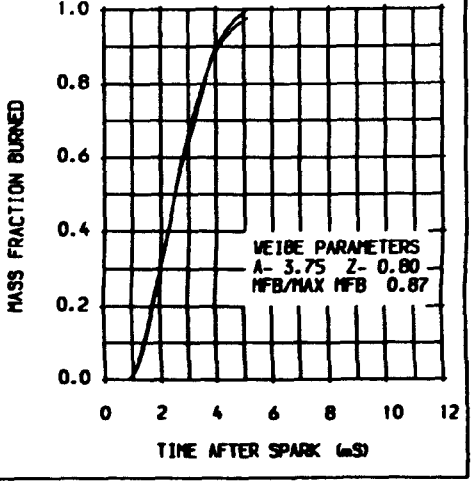

TEST DATE	01/03/89
TEST REFERENCE	T35M902HRCC
COMPRESSION RATIO	13.00
SPEED (RPM)	1815.00
IGNITION (DEG BTDC)	16
EXCESS AIR RATIO	1.03
CHAMBER AREA (CM**2)	34.00
ATMOSPHERIC PRESS (BAR)	0.98194
PRESS TDC EXHAUST (BAR)	0.83194
PRESSURE IVC (BAR)	1.09444
RESIDUAL FRACTION (%)	7.00
BLOWBY COEFFICIENT	1.84
BLOWBY % OF CHARGE	5.3

DERIVED MASS BURNED CRITERIA

SRT OF HT RLS DABOC		353.0	
0 - 1%	DEG. 11	mS	1.0
0 - 10%	DEG. 16	mS	1.5
0 - 50%	DEG. 28	mS	2.6
0 - 90%	DEG. 44	mS	4.0
0 - 100%	DEG. 56	mS	5.1
1 - 90%	DEG. 33	mS	3.0
dP/dθ MAX (BARS/DEG)		1.47	
	AT	362.0	DEG
MAX PRESSURE (BARS)		45.95	
	AT	372.0	DEG

WEIBE MASS BURNED CRITERIA

SRT OF HT RLS DABOC		353.0	
0 - 1%	DEG. 12	mS	1.1
0 - 10%	DEG. 19	mS	1.7
0 - 50%	DEG. 32	mS	2.9
0 - 90%	DEG. 49	mS	4.5
0 - 100%	DEG. 56	mS	5.1
1 - 90%	DEG. 37	mS	3.4
dP/dθ MAX (BARS/DEG)		1.10	
	AT	363.0	DEG
MAX PRESSURE (BARS)		43.90	
	AT	376.0	DEG

HEAT TRANSFER

ENGINE MEASURED (kW)	1.686
ENGINE PREDICTED (kW)	0.827
PREDICTED/MEASURED (%)	49.1
MAX BURNED GAS TEMP (K)	2515.5
AT	371.0 DEG
BURNED GAS TEMP EVO (K)	1369.3
GAS TEMP AT IVC (K)	355.5
WALL TEMPERATURE (K)	400.0

STATISTICAL DATA

	MEAN	SD	% DIS
WORK (J)	89.02	0.390	0.4
POWER (kW)	1.346	0.006	0.4
PMAX (BAR)	46.31	2.900	6.4
AT DEG	12.1	1.400	11.5

GAS ANALYSIS

	MODEL	MEASURED
CO2 (%)	9.4	9.7
CO (PPM)	0.0	5000.0
O2 (%)	0.5	1.7
NOx (PPM)	4243.2	1394.0
UHC (PPM)		3660.0
FUEL GROSS CV (kJ/kG)		53395.7
STOICH A/F RATIO		16.47

	MODEL	MEASD
POWER (kW)	1.622	1.359
FRICTN PWR (kW)	0.244	
PUMPNG PWR (kW)		-0.013
INDICATD MEP (BAR)	8.48	7.11
INDICATED EFFICNCY	0.301	0.251
BRAKE POWER (kW)	1.365	1.292
BRAKE TH EFFICNCY	0.253	0.239

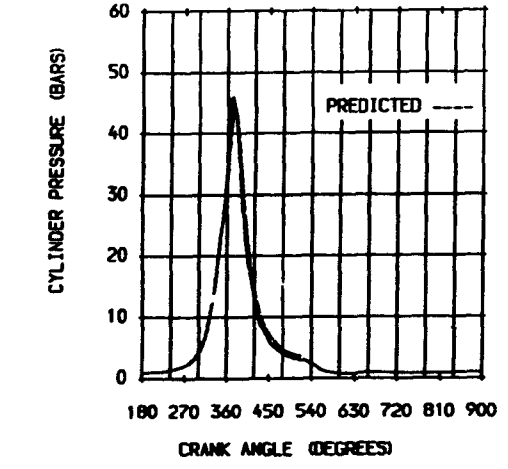

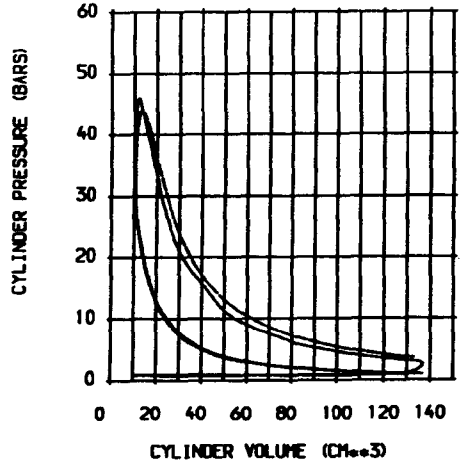

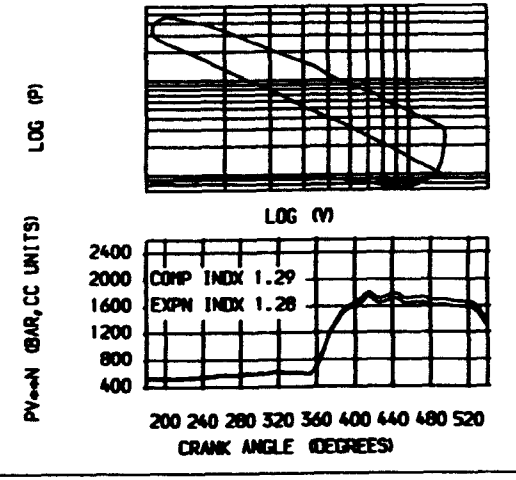

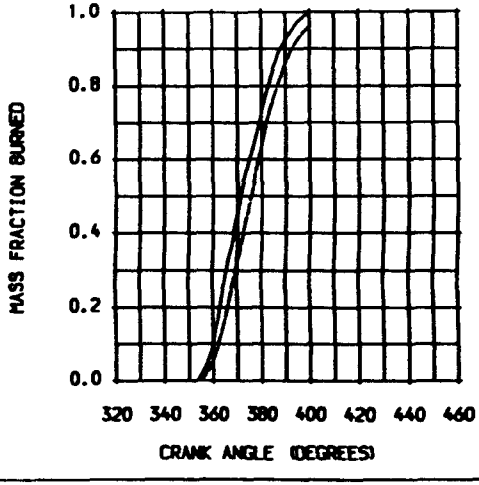

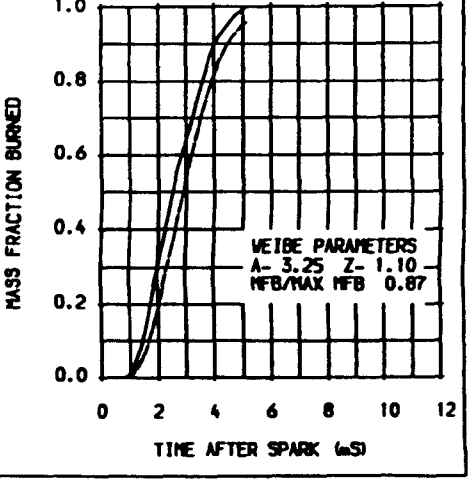

TEST DATE	01/03/89
TEST REFERENCE	T35M1608HRCC
COMPRESSION RATIO	13.00
SPEED (RPM)	1813.00
IGNITION (DEG BTDC)	13
EXCESS AIR RATIO	1.17
CHAMBER AREA (CM**2)	34.00
ATMOSPHERIC PRESS (BAR)	0.98194
PRESS TDC EXHAUST (BAR)	0.88194
PRESSURE IVC (BAR)	1.13576
RESIDUAL FRACTION (%)	7.00
BLOWBY COEFFICIENT	1.84
BLOWBY % OF CHARGE	5.3

DERIVED MASS BURNED CRITERIA

SRT OF HT RLS DABDC		357.0		
0 - 1%	DEG.	12	mS	1.1
0 - 10%	DEG.	19	mS	1.7
0 - 50%	DEG.	34	mS	3.1
0 - 90%	DEG.	59	mS	5.4
0 - 100%	DEG.	69	mS	6.3
1 - 90%	DEG.	47	mS	4.3
dP/dθ MAX (BARS/DEG)		0.67		
	AT	366.0	DEG	
MAX PRESSURE (BARS)		36.74		
	AT	374.0	DEG	

WEIBE MASS BURNED CRITERIA

SRT OF HT RLS DABDC		357.0		
0 - 1%	DEG.	13	mS	1.2
0 - 10%	DEG.	20	mS	1.8
0 - 50%	DEG.	35	mS	3.2
0 - 90%	DEG.	56	mS	5.1
0 - 100%	DEG.	69	mS	6.3
1 - 90%	DEG.	43	mS	4.0
dP/dθ MAX (BARS/DEG)		0.56		
	AT	365.0	DEG	
MAX PRESSURE (BARS)		36.33		
	AT	376.0	DEG	

HEAT TRANSFER

ENGINE MEASURED (kW)	1.514
ENGINE PREDICTED (kW)	0.683
PREDICTED/MEASURED (%)	45.1
MAX BURNED GAS TEMP (K)	2365.8
AT	371.0 DEG
BURNED GAS TEMP EVO (K)	1339.5
GAS TEMP AT IVC (K)	367.5
WALL TEMPERATURE (K)	400.0

STATISTICAL DATA

	MEAN	SD	% DIS
WORK (J)	79.54	1.320	1.7
POWER (kW)	1.202	0.020	1.7
PMAX (BAR)	37.00	2.600	7.3
AT DEG	14.2	3.000	21.4

GAS ANALYSIS

	MODEL	MEASURED
CO2 (%)	8.4	9.2
CO (PPM)	0.0	0.0
O2 (%)	2.8	3.6
NOx (PPM)	6233.4	1328.0
UHC (PPM)		2421.0

FUEL GROSS CV (kJ/kG) 53395.7
STOICH A/F RATIO 16.47

	MODEL	MEASD
POWER (kW)	1.396	1.224
FRICTN PWR (kW)	0.244	
PUMPNG PWR (kW)		-0.017
INDICATD MEP (BAR)	7.31	6.41
INDICATED EFFICNCY	0.291	0.255
BRAKE POWER (kW)	1.136	1.149
BRAKE TH EFFICNCY	0.236	0.239

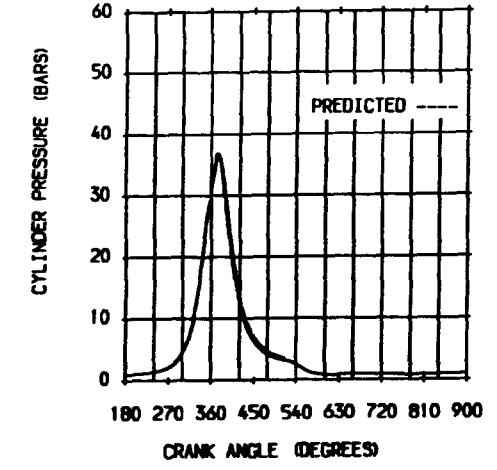

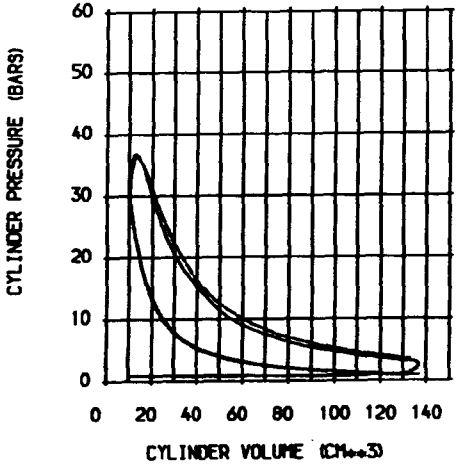

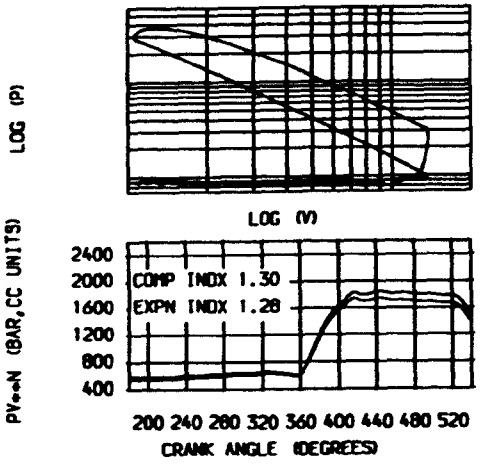

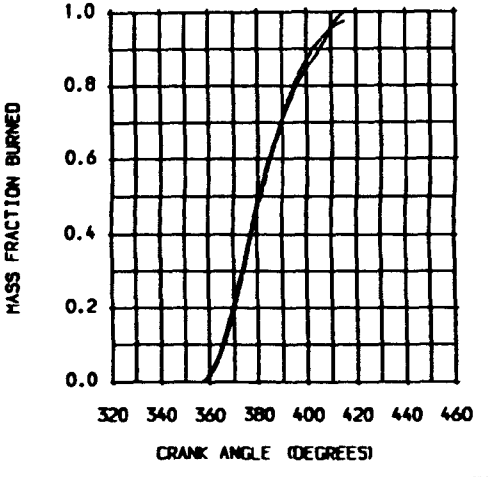

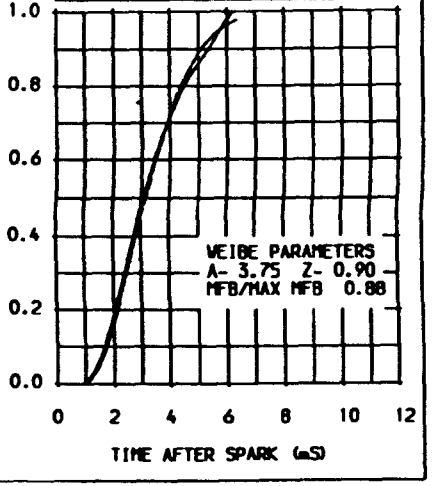

TEST DATE	01/03/89
TEST REFERENCE	T35M15D6HRCC
COMPRESSION RATIO	13.00
SPEED (RPM)	1813.00
IGNITION (DEG BTDC)	22
EXCESS AIR RATIO	1.18
CHAMBER AREA (CM**2)	34.00
ATMOSPHERIC PRESS (BAR)	0.98194
PRESS TDC EXHAUST (BAR)	0.88194
PRESSURE IVC (BAR)	1.14723
RESIDUAL FRACTION (%)	7.00
BLOWBY COEFFICIENT	1.84
BLOWBY % OF CHARGE	5.3

DERIVED MASS BURNED CRITERIA

SRT OF HT RLS DABOC 348.0

0 - 1%	DEG. 12	mS	1.1
0 - 10%	DEG. 17	mS	1.6
0 - 50%	DEG. 27	mS	2.5
0 - 90%	DEG. 46	mS	4.2
0 - 100%	DEG. 54	mS	5.0
1 - 90%	DEG. 34	mS	3.1

dP/dθ MAX (BARS/DEG) 1.89 AT 359.0 DEG

MAX PRESSURE (BARS) 51.54 AT 368.0 DEG

WEIBE MASS BURNED CRITERIA

SRT OF HT RLS DABOC 348.0

0 - 1%	DEG. 13	mS	1.2
0 - 10%	DEG. 18	mS	1.7
0 - 50%	DEG. 30	mS	2.8
0 - 90%	DEG. 47	mS	4.3
0 - 100%	DEG. 54	mS	5.0
1 - 90%	DEG. 34	mS	3.1

dP/dθ MAX (BARS/DEG) 1.84 AT 358.0 DEG

MAX PRESSURE (BARS) 53.78 AT 371.0 DEG

HEAT TRANSFER

ENGINE MEASURED (kW)	1.489
ENGINE PREDICTED (kW)	0.793
PREDICTED/MEASURED (%)	53.3
MAX BURNED GAS TEMP (K)	2461.4 AT 366.0 DEG
BURNED GAS TEMP EVO (K)	1215.1
GAS TEMP AT IVC (K)	371.5
WALL TEMPERATURE (K)	400.0

STATISTICAL DATA

	MEAN	SD	% DIS
WORK (J)	80.15	0.730	0.9
POWER (kW)	1.211	0.011	0.9
PMAX (BAR)	51.92	2.700	5.2
AT DEG	7.9	1.400	17.7

GAS ANALYSIS

	MODEL	MEASURED
CO2 (%)	8.3	9.0
CO (PPM)	0.0	0.0
O2 (%)	2.9	3.7
NOx (PPM)	7578.2	2511.0
UHC (PPM)		2168.0

FUEL GROSS CV (kJ/kG) 53395.7

STOICH A/F RATIO 16.47

	MODEL	MEASD
POWER (kW)	1.526	1.224
FRICTN PWR (kW)	0.244	
PUMPNG PWR (kW)		-0.013
INDICATD MEP (BAR)	7.99	6.41
INDICATED EFFICNCY	0.321	0.255
BRAKE POWER (kW)	1.269	1.149
BRAKE TH EFFICNCY	0.264	0.239

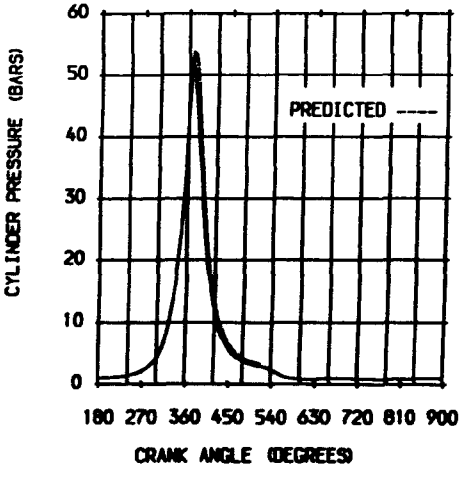

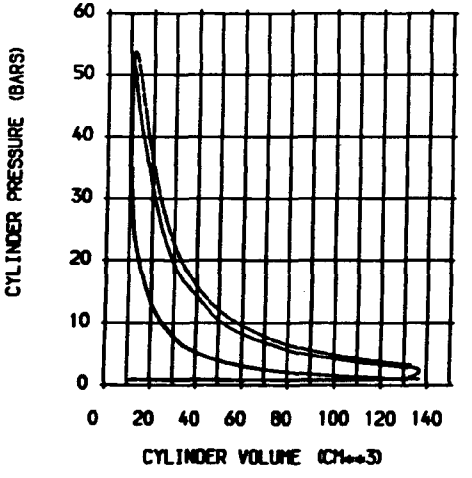

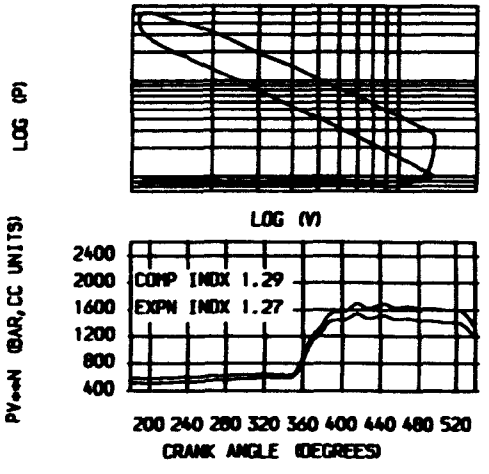

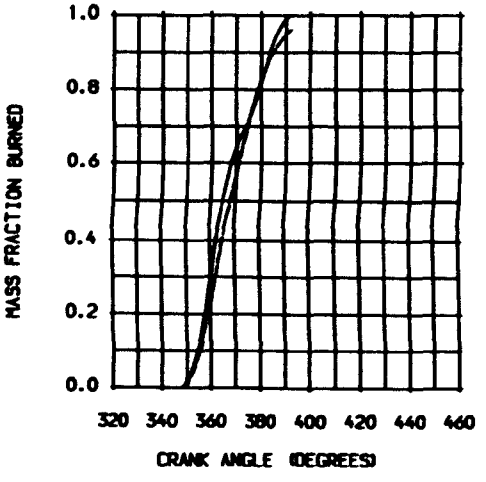

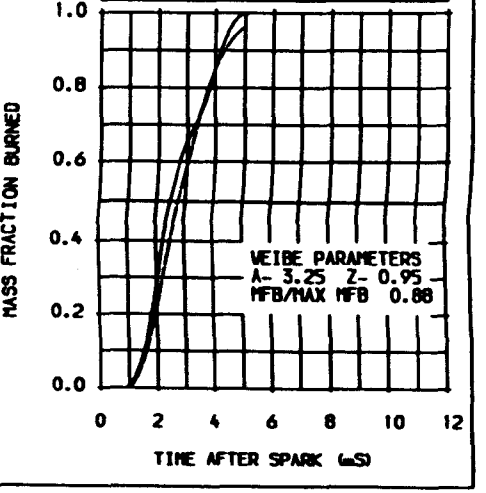

TEST DATE	01/03/89
TEST REFERENCE	T35M1809HRCC
COMPRESSION RATIO	13.00
SPEED (RPM)	1815.00
IGNITION (DEG BTDC)	26
EXCESS AIR RATIO	1.15
CHAMBER AREA (CM**2)	34.00
ATMOSPHERIC PRESS (BAR)	0.98194
PRESS TDC EXHAUST (BAR)	0.88194
PRESSURE IVC (BAR)	1.12090
RESIDUAL FRACTION (%)	7.00
BLOWBY COEFFICIENT	1.84
BLOWBY % OF CHARGE	5.3

DERIVED MASS BURNED CRITERIA

SRT OF HT RLS DABDC		346.0	
0 - 1%	DEG.	14	1.3
0 - 10%	DEG.	20	1.8
0 - 50%	DEG.	30	2.8
0 - 90%	DEG.	50	4.6
0 - 100%	DEG.	58	5.3
1 - 90%	DEG.	36	3.3
dP/dθ MAX (BARS/DEG)		2.44	
	AT	359.0	DEG
MAX PRESSURE (BARS)		56.61	
	AT	368.0	DEG

WEIBE MASS BURNED CRITERIA

SRT OF HT RLS DABDC		346.0	
0 - 1%	DEG.	14	1.3
0 - 10%	DEG.	19	1.7
0 - 50%	DEG.	32	2.9
0 - 90%	DEG.	50	4.6
0 - 100%	DEG.	58	5.3
1 - 90%	DEG.	36	3.3
dP/dθ MAX (BARS/DEG)		2.06	
	AT	356.0	DEG
MAX PRESSURE (BARS)		55.69	
	AT	369.0	DEG

HEAT TRANSFER

ENGINE MEASURED (kW)		1.508
ENGINE PREDICTED (kW)		0.825
PREDICTED/MEASURED (%)		54.7
MAX BURNED GAS TEMP (K)		2506.2
	AT	364.0 DEG
BURNED GAS TEMP EVO (K)		1220.0
GAS TEMP AT IVC (K)		372.0
WALL TEMPERATURE (K)		400.0

STATISTICAL DATA

	MEAN	SD	% DIS
WORK (J)	94.22	8.020	8.6
POWER (kW)	1.425	0.121	8.6
PMAX (BAR)	57.38	2.800	4.9
AT DEG	7.5	2.100	28.2

GAS ANALYSIS

	MODEL	MEASURED
CO2 (%)	8.5	9.0
CO (PPM)	0.0	1000.0
O2 (%)	2.5	3.4
NOx (PPM)	7548.4	3068.0
UHC (PPM)		2657.0
FUEL GROSS CV (kJ/kG)		53395.7
STOICH A/F RATIO		16.47

	MODEL	MEASD
POWER (kW)	1.505	1.440
FRICTN PWR (kW)	0.244	
PUMPNG PWR (kW)		-0.015
INDICATD MEP (BAR)	7.87	7.53
INDICATED EFFICNCY	0.316	0.301
BRAKE POWER (kW)	1.246	1.102
BRAKE TH EFFICNCY	0.260	0.230

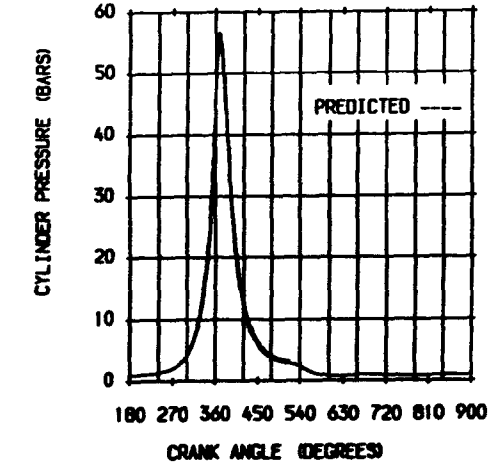

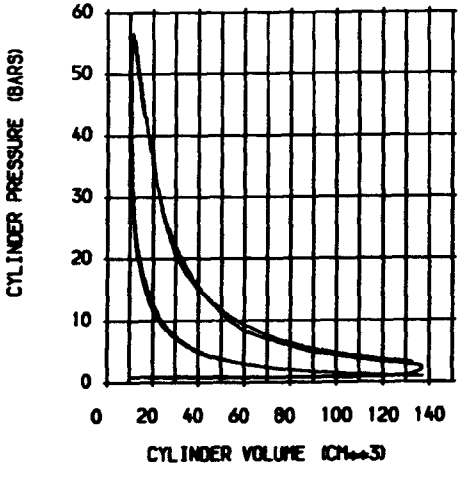

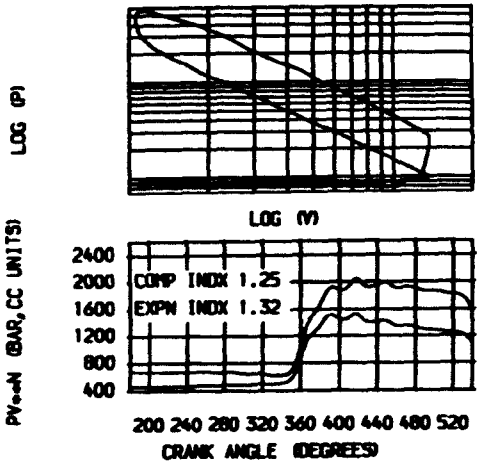

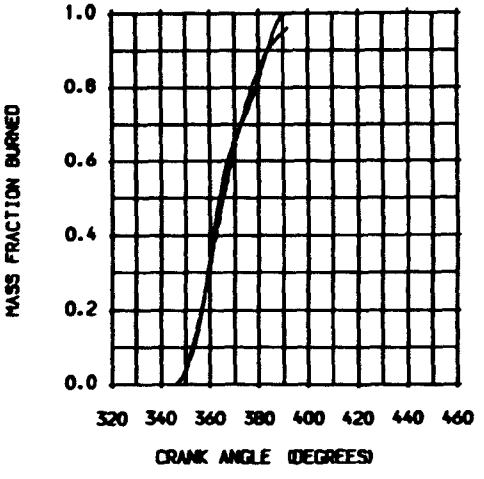

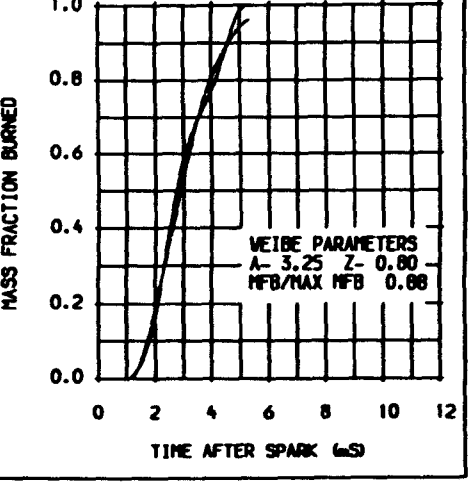

TEST DATE	01/03/89
TEST REFERENCE	T35M1003HRCC
COMPRESSION RATIO	13.00
SPEED (RPM)	1810.00
IGNITION (DEG BTDC)	25
EXCESS AIR RATIO	1.61
CHAMBER AREA (CM**2)	34.00
ATMOSPHERIC PRESS (BAR)	0.98194
PRESS TDC EXHAUST (BAR)	0.88194
PRESSURE IVC (BAR)	1.13613
RESIDUAL FRACTION (%)	7.00
BLOWBY COEFFICIENT	1.85
BLOWBY % OF CHARGE	5.3

DERIVED MASS BURNED CRITERIA

SRT OF HT RLS DABDC		352.0	
0 - 1%	DEG.	20	1.8
0 - 10%	DEG.	27	2.5
0 - 50%	DEG.	46	4.2
0 - 90%	DEG.	92	8.5
0 - 100%	DEG.	107	9.9
1 - 90%	DEG.	72	6.6
dP/dθ MAX (BARS/DEG)		0.81	
	AT	361.0	DEG
MAX PRESSURE (BARS)		38.90	
	AT	369.0	DEG

WEIBE MASS BURNED CRITERIA

SRT OF HT RLS DABDC		352.0	
0 - 1%	DEG.	20	1.8
0 - 10%	DEG.	27	2.5
0 - 50%	DEG.	44	4.1
0 - 90%	DEG.	68	6.3
0 - 100%	DEG.	107	9.9
1 - 90%	DEG.	48	4.4
dP/dθ MAX (BARS/DEG)		0.71	
	AT	358.0	DEG
MAX PRESSURE (BARS)		37.18	
	AT	370.0	DEG

HEAT TRANSFER

ENGINE MEASURED (kW)	1.043	
ENGINE PREDICTED (kW)	0.492	
PREDICTED/MEASURED (%)	47.2	
MAX BURNED GAS TEMP (K)	2031.9	
AT	366.0	DEG
BURNED GAS TEMP EVO (K)	1085.6	
GAS TEMP AT IVC (K)	353.5	
WALL TEMPERATURE (K)	400.0	

STATISTICAL DATA

	MEAN	SD	% DIS
WORK (J)	59.01	2.920	5.0
POWER (kW)	0.890	0.044	5.0
PMAX (BAR)	39.10	2.800	7.2
AT DEG	8.8	1.200	14.0

GAS ANALYSIS

	MODEL	MEASURED
CO2 (%)	6.2	6.1
CO (PPM)	0.0	1000.0
O2 (%)	7.5	9.0
NOx (PPM)	5026.2	0.0
UHC (PPM)		4681.0

FUEL GROSS CV (kJ/kG) 53395.7
STOICH A/F RATIO 16.47

	MODEL	MEASD
POWER (kW)	1.070	0.906
FRICTN PWR (kW)	0.243	
PUMPNG PWR (kW)		-0.018
INDICATD MEP (BAR)	5.61	4.75
INDICATED EFFICNCY	0.289	0.244
BRAKE POWER (kW)	0.808	0.862
BRAKE TH EFFICNCY	0.217	0.232

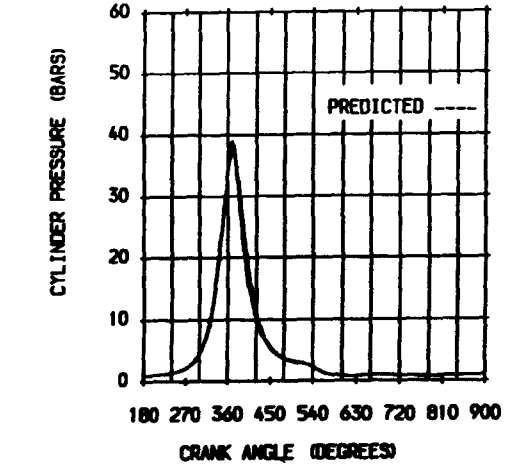

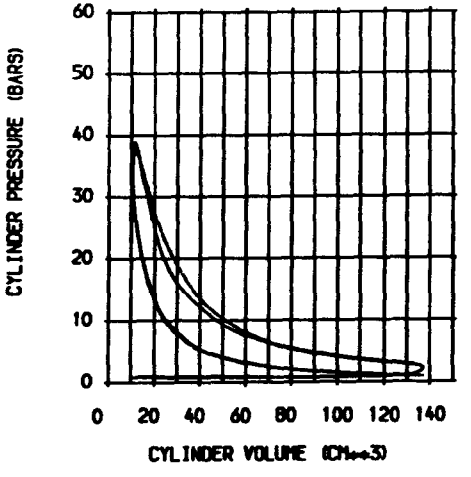

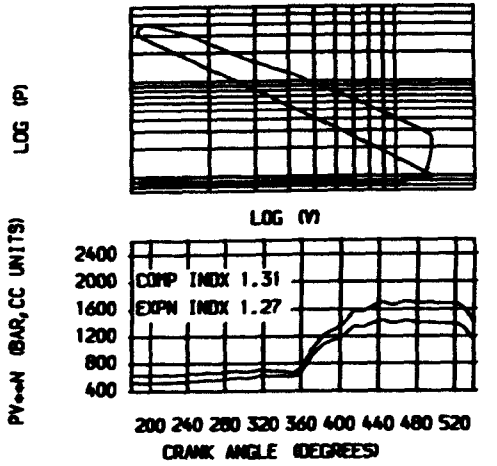

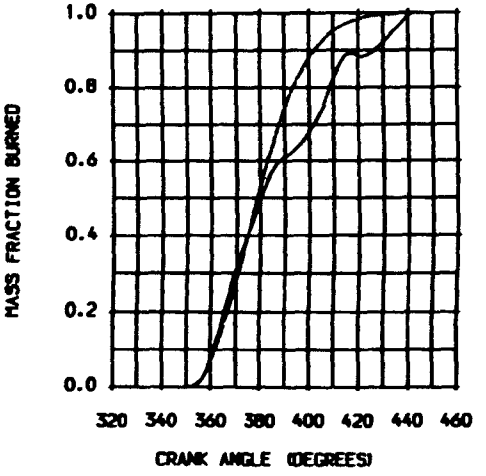

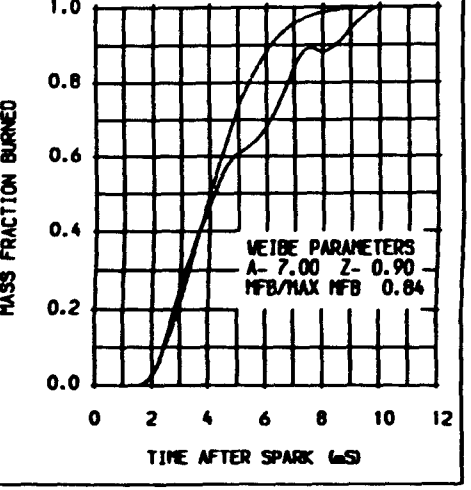

TEST DATE	01/03/89
TEST REFERENCE	T3SM2001OHRCC
COMPRESSION RATIO	13.00
SPEED (RPM)	2116.00
IGNITION (DEG BTDC)	15
EXCESS AIR RATIO	1.02
CHAMBER AREA (CM**2)	34.00
ATMOSPHERIC PRESS (BAR)	0.98194
PRESS TDC EXHAUST (BAR)	0.88194
PRESSURE IVC (BAR)	1.16499
RESIDUAL FRACTION (%)	7.00
BLOWBY COEFFICIENT	1.52
BLOWBY % OF CHARGE	3.8

DERIVED MASS BURNED CRITERIA

SRT OF HT RLS DABDC		353.0	
0 - 1%	DEG.	10	0.8
0 - 10%	DEG.	16	1.3
0 - 50%	DEG.	27	2.1
0 - 90%	DEG.	44	3.5
0 - 100%	DEG.	53	4.2
1 - 90%	DEG.	34	2.7
dP/dθ MAX (BARS/DEG)		1.42	
	AT	363.0	DEG
MAX PRESSURE (BARS)		47.79	
	AT	372.0	DEG

WEIBE MASS BURNED CRITERIA

SRT OF HT RLS DABDC		353.0	
0 - 1%	DEG.	11	0.9
0 - 10%	DEG.	16	1.3
0 - 50%	DEG.	28	2.2
0 - 90%	DEG.	45	3.5
0 - 100%	DEG.	53	4.2
1 - 90%	DEG.	34	2.7
dP/dθ MAX (BARS/DEG)		1.56	
	AT	362.0	DEG
MAX PRESSURE (BARS)		50.44	
	AT	374.0	DEG

HEAT TRANSFER

ENGINE MEASURED (kW)	2.063	
ENGINE PREDICTED (kW)	1.012	
PREDICTED/MEASURED (%)	49.0	
MAX BURNED GAS TEMP (K)	2565.1	
AT	369.0	DEG
BURNED GAS TEMP EVO (K)	1378.5	
GAS TEMP AT IVC (K)	372.5	
WALL TEMPERATURE (K)	400.0	

STATISTICAL DATA

	MEAN	SD	% DIS
WORK (J)	93.96	0.480	0.5
POWER (kW)	1.657	0.009	0.5
PMAX (BAR)	48.18	3.200	6.8
AT DEG	12.6	1.500	12.1

GAS ANALYSIS

	MODEL	MEASURED
CO2 (%)	9.5	9.6
CO (PPM)	0.0	7000.0
O2 (%)	0.4	1.6
NOx (PPM)	4334.7	1286.0
UHC (PPM)		3593.0

FUEL GROSS CV (kJ/kG) 53395.7
STOICH A/F RATIO 16.47

	MODEL	MEASD
POWER (kW)	2.001	1.687
FRICTN PWR (kW)	0.308	
PUMPING PWR (kW)		-0.030
INDICATD MEP (BAR)	8.98	7.57
INDICATED EFFICNCY	0.311	0.261
BRAKE POWER (kW)	1.663	1.439
BRAKE TH EFFICNCY	0.257	0.223

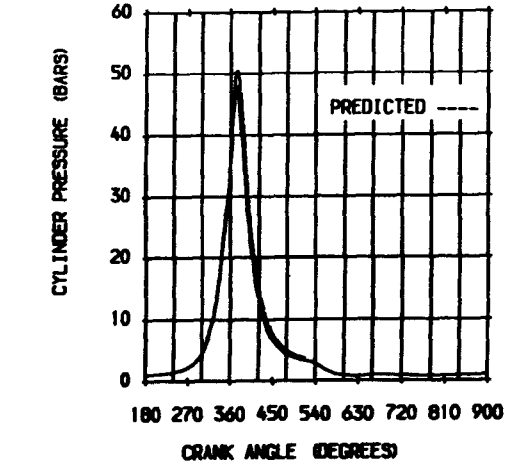

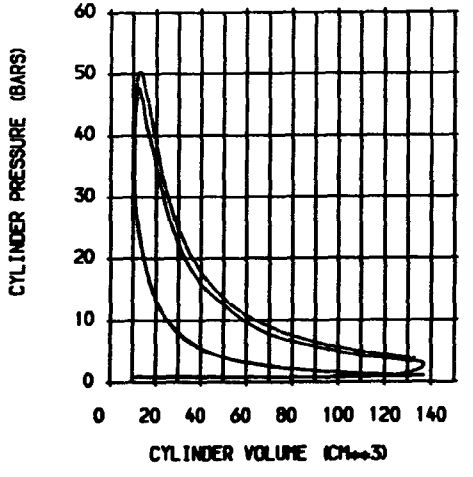

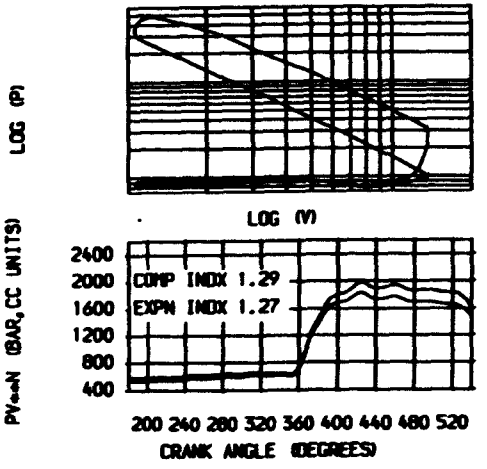

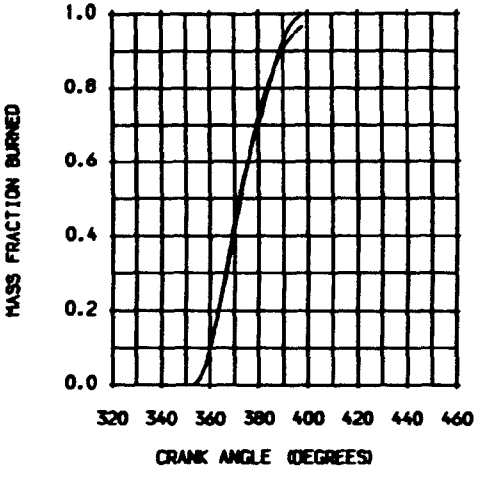

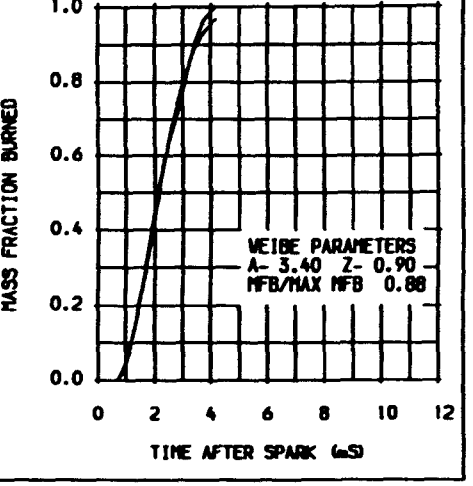

TEST DATE	01/03/89
TEST REFERENCE	T35M21D11HRCC
COMPRESSION RATIO	13.00
SPEED (RPM)	2100.00
IGNITION (DEG BTDC)	26
EXCESS AIR RATIO	1.54
CHAMBER AREA (CM**2)	34.00
ATMOSPHERIC PRESS (BAR)	0.98194
PRESS TDC EXHAUST (BAR)	0.88194
PRESSURE IVC (BAR)	1.13977
RESIDUAL FRACTION (%)	7.00
BLOWBY COEFFICIENT	1.55
BLOWBY % OF CHARGE	3.9

DERIVED MASS BURNED CRITERIA

SRT OF HT RLS DABDC		346.0	
0 - 1%	DEG. 15	mS	1.2
0 - 10%	DEG. 22	mS	1.7
0 - 50%	DEG. 39	mS	3.1
0 - 90%	DEG. 79	mS	6.3
0 - 100%	DEG. 94	mS	7.5
1 - 90%	DEG. 64	mS	5.1
dP/dθ MAX (BARS/DEG)		1.37	
	AT	359.0	DEG
MAX PRESSURE (BARS)		47.23	
	AT	369.0	DEG

WEIBE MASS BURNED CRITERIA

SRT OF HT RLS DABDC		346.0	
0 - 1%	DEG. 15	mS	1.2
0 - 10%	DEG. 22	mS	1.7
0 - 50%	DEG. 37	mS	2.9
0 - 90%	DEG. 58	mS	4.6
0 - 100%	DEG. 94	mS	7.5
1 - 90%	DEG. 43	mS	3.4
dP/dθ MAX (BARS/DEG)		1.35	
	AT	356.0	DEG
MAX PRESSURE (BARS)		46.27	
	AT	369.0	DEG

HEAT TRANSFER

ENGINE MEASURED (kW)	1.231
ENGINE PREDICTED (kW)	0.634
PREDICTED/MEASURED (%)	51.5
MAX BURNED GAS TEMP (K)	2140.5
AT	365.0 DEG
BURNED GAS TEMP EVO (K)	1072.1
GAS TEMP AT IVC (K)	357.0
WALL TEMPERATURE (K)	400.0

STATISTICAL DATA

	MEAN	SD	% DIS
WORK (J)	71.77	3.120	4.4
POWER (kW)	1.256	0.055	4.4
PMAX (BAR)	47.62	3.400	7.2
AT DEG	8.8	1.500	17.5

GAS ANALYSIS

	MODEL	MEASURED
CO2 (%)	6.5	6.4
CO (PPM)	0.0	1000.0
O2 (%)	6.9	8.6
NOx (PPM)	6280.6	91.0
UHC (PPM)		5224.0

FUEL GROSS CV (kJ/kG) 53395.7
STOICH A/F RATIO 16.47

	MODEL	MEASD
POWER (kW)	1.369	1.285
FRICTN PWR (kW)	0.305	
PUMPNG PWR (kW)		-0.036
INDICATD MEP (BAR)	6.19	5.81
INDICATED EFFICNCY	0.308	0.289
BRAKE POWER (kW)	1.029	1.015
BRAKE TH EFFICNCY	0.232	0.229

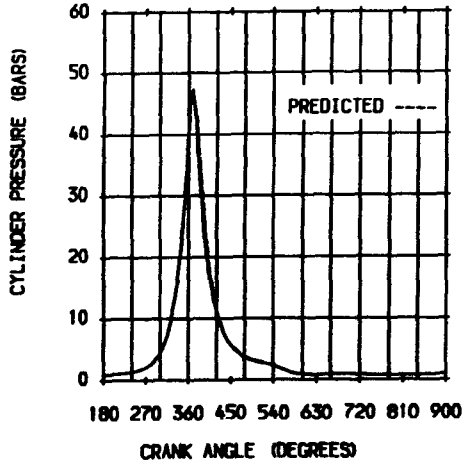

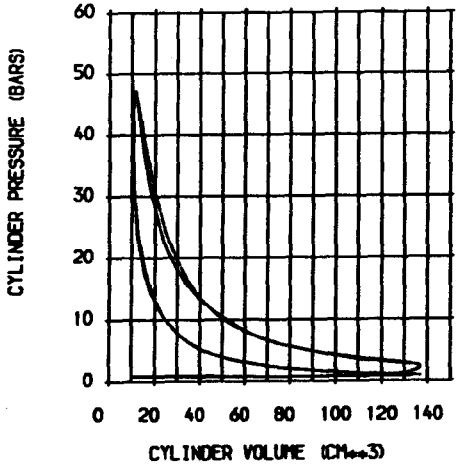

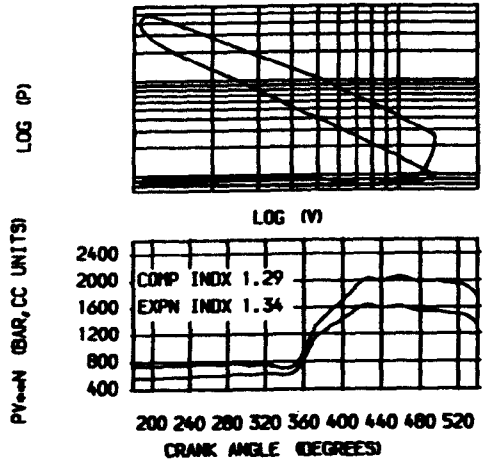

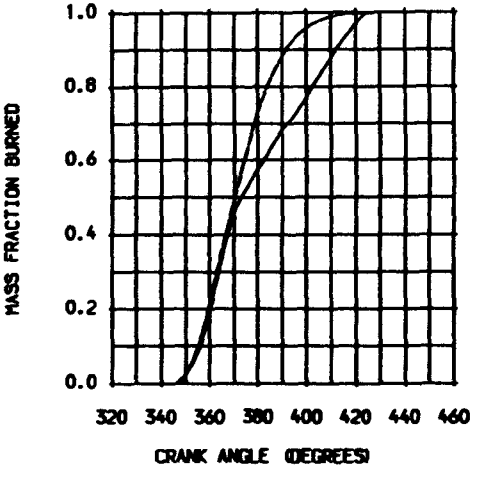

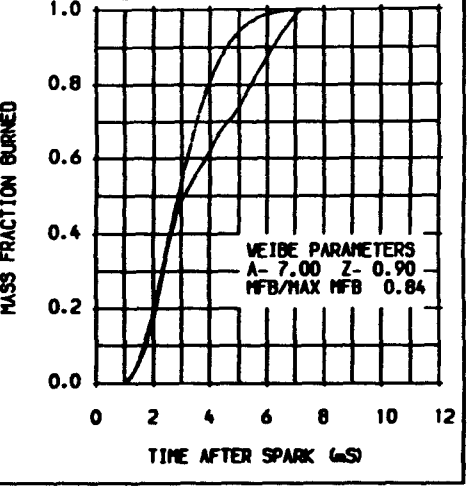

TEST DATE	30/08/89
TEST REFERENCE	T46M5601RIC
COMPRESSION RATIO	8.00
SPEED (RPM)	1800.00
IGNITION (DEG BTDC)	30
EXCESS AIR RATIO	1.00
CHAMBER AREA (CM**2)	118.00
ATMOSPHERIC PRESS (BAR)	1.00430
PRESS TDC EXHAUST (BAR)	1.00429
PRESSURE IVC (BAR)	1.06256
RESIDUAL FRACTION (%)	7.00
BLOWBY COEFFICIENT	1.00
BLOWBY % OF CHARGE	2.8

DERIVED MASS BURNED CRITERIA

SRT OF HT RLS DABDC		341.0	
0 - 1%	DEG. 18	mS	1.7
0 - 10%	DEG. 29	mS	2.7
0 - 50%	DEG. 42	mS	3.9
0 - 90%	DEG. 55	mS	5.1
0 - 100%	DEG. 70	mS	6.5
1 - 90%	DEG. 37	mS	3.4
dP/dθ MAX (BARS/DEG)		1.24	
	AT	368.0	DEG
MAX PRESSURE (BARS)		39.04	
	AT	378.0	DEG

WEIBE MASS BURNED CRITERIA

SRT OF HT RLS DABDC		341.0	
0 - 1%	DEG. 19	mS	1.8
0 - 10%	DEG. 28	mS	2.6
0 - 50%	DEG. 42	mS	3.9
0 - 90%	DEG. 57	mS	5.3
0 - 100%	DEG. 70	mS	6.5
1 - 90%	DEG. 38	mS	3.5
dP/dθ MAX (BARS/DEG)		1.00	
	AT	364.0	DEG
MAX PRESSURE (BARS)		35.24	
	AT	379.0	DEG

HEAT TRANSFER

ENGINE MEASURED (kW)	0.000
ENGINE PREDICTED (kW)	3.776
PREDICTED/MEASURED (%)	0.0
MAX BURNED GAS TEMP (K)	2542.9
AT	373.0 DEG
BURNED GAS TEMP EVO (K)	1538.4
GAS TEMP AT IVC (K)	359.0
WALL TEMPERATURE (K)	400.0

STATISTICAL DATA

	MEAN	SD	% DIS
WORK (J)	452.57	5.290	1.2
POWER (kW)	6.789	0.080	1.2
PMAX (BAR)	39.64	3.600	9.1
AT DEG	18.8	3.000	16.0

GAS ANALYSIS

	MODEL	MEASURED
CO2 (%)	9.6	0.0
CO (PPM)	0.0	0.0
O2 (%)	0.0	0.0
NOx (PPM)	3560.0	0.0
UHC (PPM)		0.0
FUEL GROSS CV (kJ/kG)		53402.0
STOICH A/F RATIO		16.61

	MODEL	MEASD
POWER (kW)	6.358	6.535
FRICTN PWR (kW)	1.723	
PUMPNG PWR (kW)		-0.106
INDICATD MEP (BAR)	8.45	8.70
INDICATED EFFICNCY	0.287	0.278
BRAKE POWER (kW)	4.635	5.580
BRAKE TH EFFICNCY	0.197	0.237

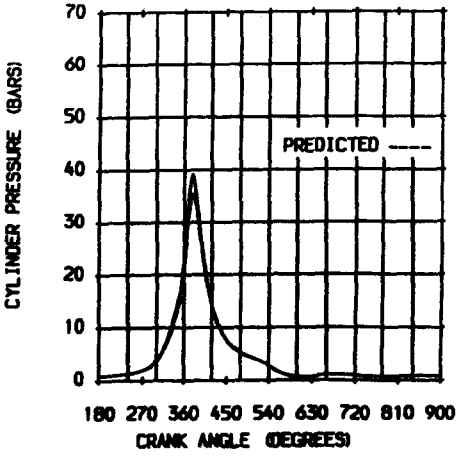

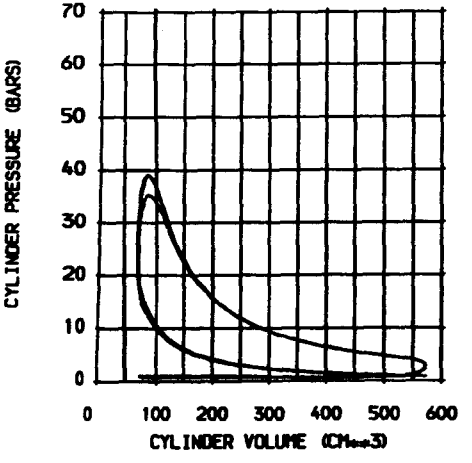

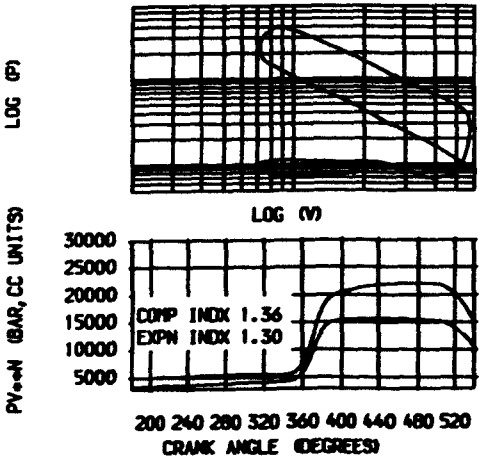

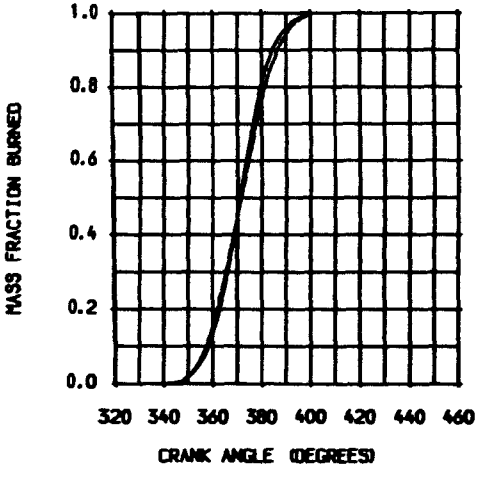

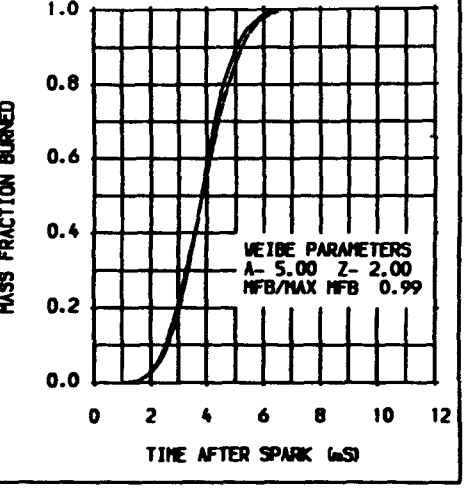

TEST DATE	30/08/89
TEST REFERENCE	T46MS702RIC
COMPRESSION RATIO	9.00
SPEED (RPM)	1800.00
IGNITION (DEG BTDC)	28
EXCESS AIR RATIO	1.00
CHAMBER AREA (CM**2)	108.90
ATMOSPHERIC PRESS (BAR)	1.00430
PRESS TDC EXHAUST (BAR)	1.00429
PRESSURE IVC (BAR)	1.03815
RESIDUAL FRACTION (%)	7.00
BLOWBY COEFFICIENT	1.00
BLOWBY % OF CHARGE	2.8

DERIVED MASS BURNED CRITERIA

SRT OF HT RLS DABDC		342.0	
0 - 1%	DEG.	17	MS 1.6
0 - 10%	DEG.	27	MS 2.5
0 - 50%	DEG.	40	MS 3.7
0 - 90%	DEG.	53	MS 4.9
0 - 100%	DEG.	68	MS 6.3
1 - 90%	DEG.	36	MS 3.3
dP/dθ MAX (BARS/DEG)		1.33	
	AT	367.0	DEG
MAX PRESSURE (BARS)		43.03	
	AT	378.0	DEG

WEIBE MASS BURNED CRITERIA

SRT OF HT RLS DABDC		342.0	
0 - 1%	DEG.	18	MS 1.7
0 - 10%	DEG.	26	MS 2.4
0 - 50%	DEG.	40	MS 3.7
0 - 90%	DEG.	54	MS 5.0
0 - 100%	DEG.	68	MS 6.3
1 - 90%	DEG.	36	MS 3.3
dP/dθ MAX (BARS/DEG)		1.24	
	AT	364.0	DEG
MAX PRESSURE (BARS)		40.66	
	AT	378.0	DEG

HEAT TRANSFER

ENGINE MEASURED (kW)	0.000	
ENGINE PREDICTED (kW)	3.720	
PREDICTED/MEASURED (%)	0.0	
MAX BURNED GAS TEMP (K)	2537.5	
AT	373.0	DEG
BURNED GAS TEMP EVO (K)	1488.3	
GAS TEMP AT IVC (K)	326.0	
WALL TEMPERATURE (K)	400.0	

STATISTICAL DATA

	MEAN	SD	% DIS
WORK (J)	463.53	6.010	1.3
POWER (kW)	6.953	0.090	1.3
PMAX (BAR)	43.72	4.700	10.9
AT DEG	18.0	3.000	16.9

GAS ANALYSIS

	MODEL	MEASURED
CO2 (%)	9.6	0.0
CO (PPM)	0.0	0.0
O2 (%)	0.0	0.0
NOx (PPM)	3418.9	0.0
UHC (PPM)		0.0

FUEL GROSS CV (kJ/kG) 53402.0
STOICH A/F RATIO 16.61

	MODEL	MEASD
POWER (kW)	6.923	6.692
FRICTN PWR (kW)	1.715	
PUMPNG PWR (kW)		-0.098
INDICATD MEP (BAR)	9.20	8.91
INDICATED EFFICNCY	0.307	0.296
BRAKE POWER (kW)	5.208	5.882
BRAKE TH EFFICNCY	0.230	0.260

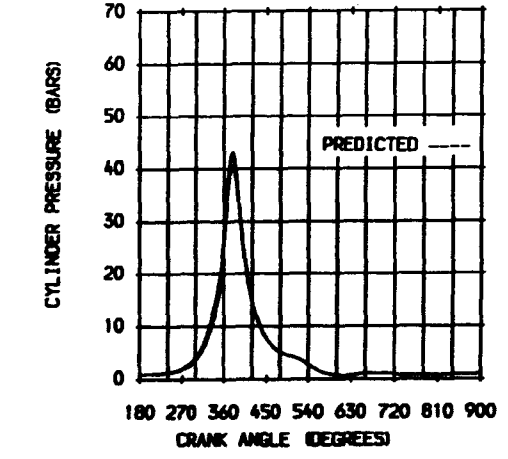

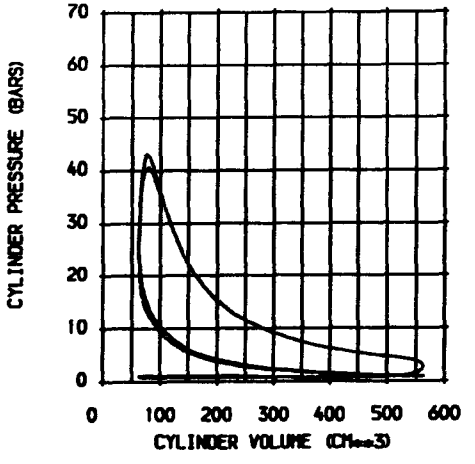

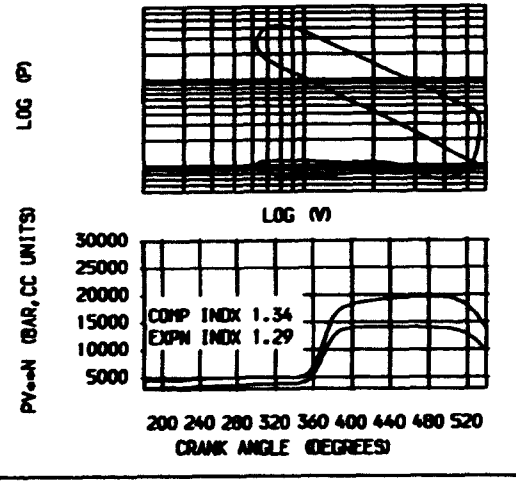

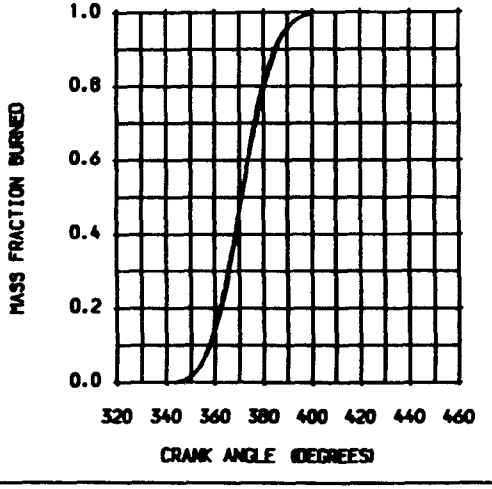

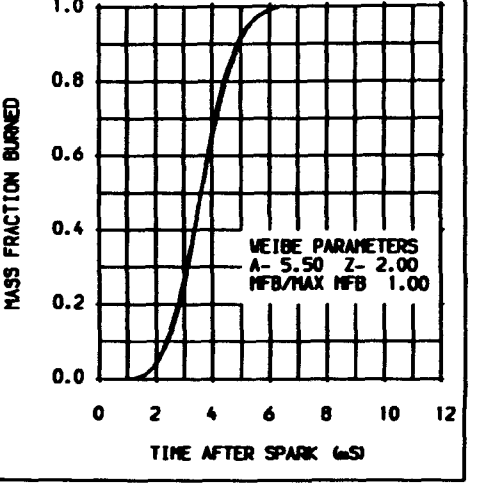

TEST DATE	30/08/89
TEST REFERENCE	T46M5803RIC
COMPRESSION RATIO	10.00
SPEED (RPM)	1800.00
IGNITION (DEG BTDC)	28
EXCESS AIR RATIO	1.02
CHAMBER AREA (CM**2)	101.90
ATMOSPHERIC PRESS (BAR)	1.00430
PRESS TDC EXHAUST (BAR)	1.00429
PRESSURE IVC (BAR)	1.06145
RESIDUAL FRACTION (%)	7.00
BLOWBY COEFFICIENT	1.30
BLOWBY % OF CHARGE	2.8

DERIVED MASS BURNED CRITERIA

SRT OF HT RLS DABDC		343.0		
0 - 1%	DEG.	17	mS	1.6
0 - 10%	DEG.	26	mS	2.4
0 - 50%	DEG.	39	mS	3.6
0 - 90%	DEG.	54	mS	5.0
0 - 100%	DEG.	68	mS	6.3
1 - 90%	DEG.	37	mS	3.4
dP/dθ MAX (BARS/DEG)		1.45		
	AT	365.0	DEG	
MAX PRESSURE (BARS)		47.45		
	AT	376.0	DEG	

WEIBE MASS BURNED CRITERIA

SRT OF HT RLS DABDC		343.0		
0 - 1%	DEG.	18	mS	1.7
0 - 10%	DEG.	27	mS	2.5
0 - 50%	DEG.	40	mS	3.7
0 - 90%	DEG.	54	mS	5.0
0 - 100%	DEG.	68	mS	6.3
1 - 90%	DEG.	36	mS	3.3
dP/dθ MAX (BARS/DEG)		1.33		
	AT	364.0	DEG	
MAX PRESSURE (BARS)		44.09		
	AT	378.0	DEG	

HEAT TRANSFER

ENGINE MEASURED (kW)	0.000
ENGINE PREDICTED (kW)	3.604
PREDICTED/MEASURED (%)	0.0
MAX BURNED GAS TEMP (K)	2536.6
AT	372.0 DEG
BURNED GAS TEMP EVO (K)	1452.3
GAS TEMP AT IVC (K)	328.5
WALL TEMPERATURE (K)	400.0

STATISTICAL DATA

	MEAN	SD	% DIS
WORK (J)	472.61	7.720	1.6
POWER (kW)	7.089	0.116	1.6
PMAX (BAR)	48.18	6.100	12.7
AT DEG	16.7	3.200	19.0

GAS ANALYSIS

	MODEL	MEASURED
CO2 (%)	9.5	0.0
CO (PPM)	0.0	0.0
O2 (%)	0.3	0.0
NOx (PPM)	3903.1	0.0
UHC (PPM)		0.0

FUEL GROSS CV (kJ/kG) 53402.0
STOICH A/F RATIO 16.61

	MODEL	MEASD
POWER (kW)	7.045	6.825
FRICTN PWR (kW)	1.707	
PUMPNG PWR (kW)		-0.090
INDICATD MEP (BAR)	9.36	9.08
INDICATED EFFICNCY	0.317	0.308
BRAKE POWER (kW)	5.338	5.969
BRAKE TH EFFICNCY	0.241	0.269

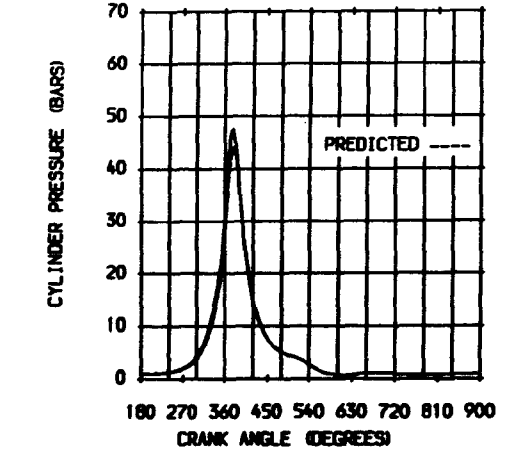

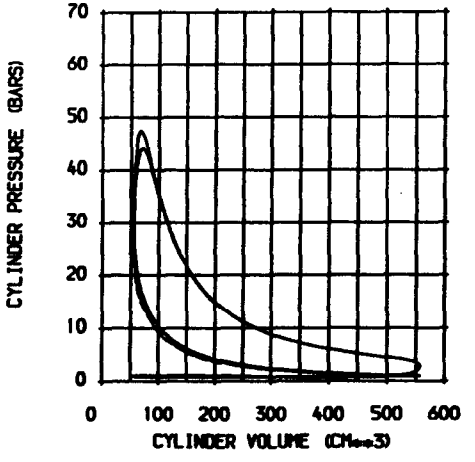

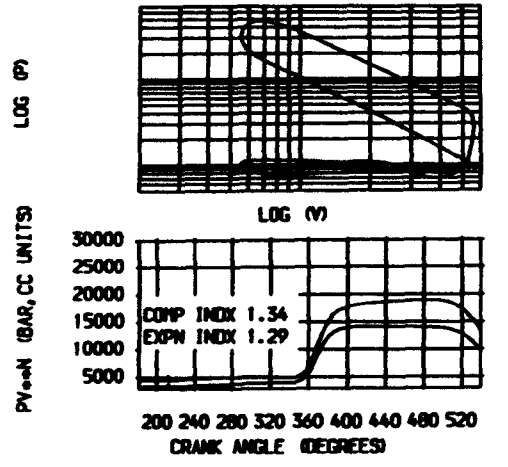

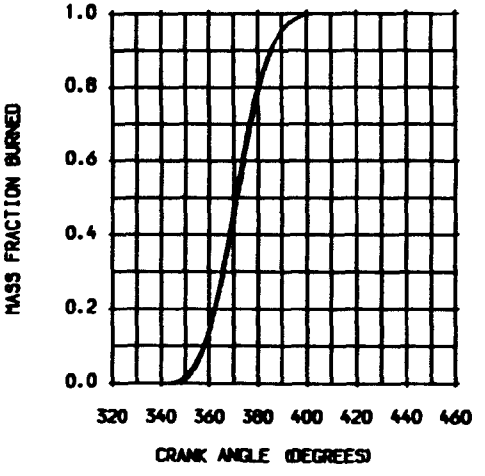

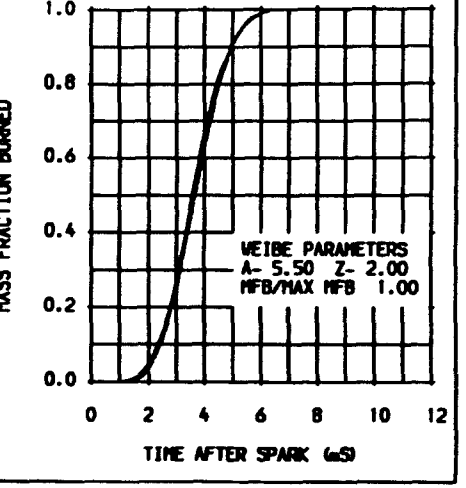

TEST DATE	30/08/89
TEST REFERENCE	T46M5904RIC
COMPRESSION RATIO	11.00
SPEED (RPM)	1800.00
IGNITION (DEG BTDC)	27
EXCESS AIR RATIO	1.20
CHAMBER AREA (CM**2)	96.30
ATMOSPHERIC PRESS (BAR)	1.00430
PRESS TDC EXHAUST (BAR)	1.00429
PRESSURE IVC (BAR)	1.08199
RESIDUAL FRACTION (%)	7.00
BLOWBY COEFFICIENT	1.00
BLOWBY % OF CHARGE	2.8

DERIVED MASS BURNED CRITERIA

SRT OF HT RLS DABDC		342.0		
0 - 1%	DEG.	15	mS	1.4
0 - 10%	DEG.	24	mS	2.2
0 - 50%	DEG.	37	mS	3.4
0 - 90%	DEG.	52	mS	4.8
0 - 100%	DEG.	67	mS	6.2
1 - 90%	DEG.	37	mS	3.4
dP/dθ MAX (BARS/DEG)		1.67		
	AT	365.0	DEG	
MAX PRESSURE (BARS)		52.96		
	AT	375.0	DEG	

WEIBE MASS BURNED CRITERIA

SRT OF HT RLS DABDC		342.0		
0 - 1%	DEG.	15	mS	1.4
0 - 10%	DEG.	23	mS	2.1
0 - 50%	DEG.	36	mS	3.3
0 - 90%	DEG.	51	mS	4.7
0 - 100%	DEG.	67	mS	6.2
1 - 90%	DEG.	36	mS	3.3
dP/dθ MAX (BARS/DEG)		1.54		
	AT	360.0	DEG	
MAX PRESSURE (BARS)		49.13		
	AT	374.0	DEG	

HEAT TRANSFER

ENGINE MEASURED (kW)	0.000
ENGINE PREDICTED (kW)	3.072
PREDICTED/MEASURED (%)	0.0
MAX BURNED GAS TEMP (K)	2417.5
AT	369.0 DEG
BURNED GAS TEMP EVO (K)	1290.6
GAS TEMP AT IVC (K)	347.5
WALL TEMPERATURE (K)	400.0

STATISTICAL DATA

	MEAN	SD	% DIS
WORK (J)	484.33	6.120	1.3
POWER (kW)	7.265	0.092	1.3
PMAX (BAR)	53.54	6.000	11.2
AT DEG	15.3	2.400	15.8

GAS ANALYSIS

	MODEL	MEASURED
CO2 (%)	8.1	0.0
CO (PPM)	0.0	0.0
O2 (%)	3.3	0.0
NOx (PPM)	7401.9	0.0
UHC (PPM)		0.0
FUEL GROSS CV (kJ/kG)		53402.0
STOICH A/F RATIO		16.61

	MODEL	MEASD
POWER (kW)	6.402	7.002
FRICTN PWR (kW)	1.700	
PUMPNG PWR (kW)		-0.088
INDICATD MEP (BAR)	8.51	9.32
INDICATED EFFICNCY	0.338	0.370
BRAKE POWER (kW)	4.702	6.227
BRAKE TH EFFICNCY	0.249	0.329

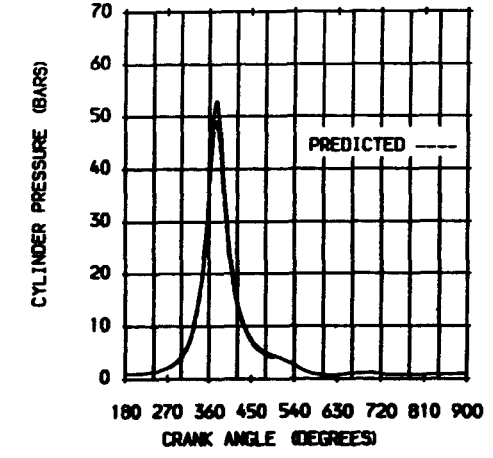

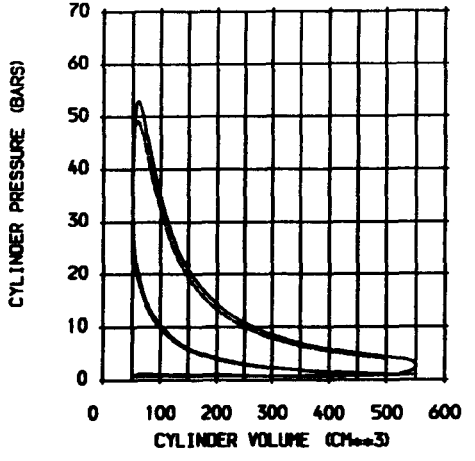

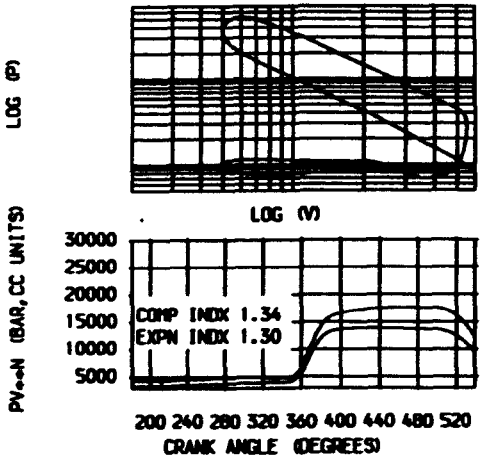

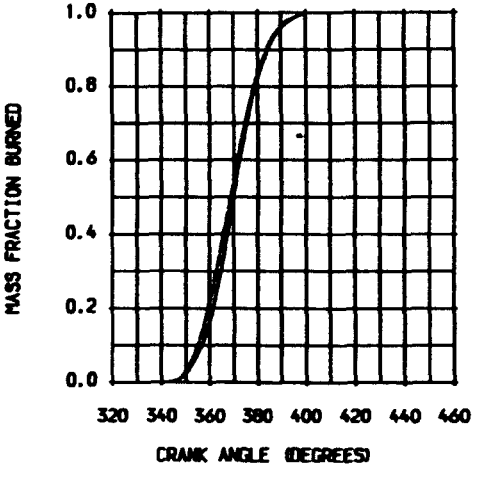

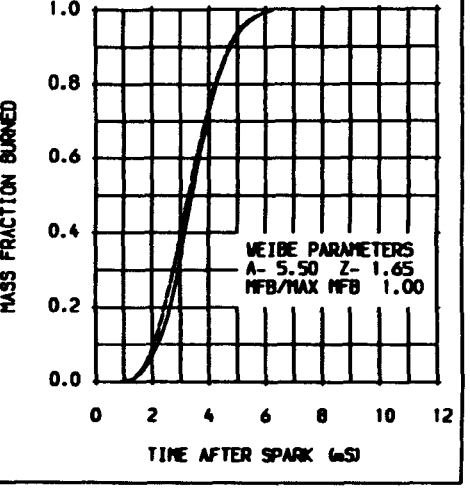

TEST DATE	30/08/89
TEST REFERENCE	T46M60DSRIC
COMPRESSION RATIO	12.00
SPEED (RPM)	1800.00
IGNITION (DEG BTDC)	27
EXCESS AIR RATIO	1.03
CHAMBER AREA (CM**2)	91.70
ATMOSPHERIC PRESS (BAR)	1.00430
PRESS TDC EXHAUST (BAR)	1.00429
PRESSURE IVC (BAR)	1.17801
RESIDUAL FRACTION (%)	7.00
BLOWBY COEFFICIENT	1.00
BLOWBY % OF CHARGE	2.8

DERIVED MASS BURNED CRITERIA

SRT OF HT RLS DABDC		343.0		
0 - 1%	DEG.	14	mS	1.3
0 - 10%	DEG.	23	mS	2.1
0 - 50%	DEG.	36	mS	3.3
0 - 90%	DEG.	51	mS	4.7
0 - 100%	DEG.	69	mS	6.4
1 - 90%	DEG.	37	mS	3.4
dP/dθ MAX (BARS/DEG)				1.85
		AT		364.0 DEG
MAX PRESSURE (BARS)				56.53
		AT		373.0 DEG

WEIBE MASS BURNED CRITERIA

SRT OF HT RLS DABDC		343.0		
0 - 1%	DEG.	15	mS	1.4
0 - 10%	DEG.	23	mS	2.1
0 - 50%	DEG.	36	mS	3.3
0 - 90%	DEG.	52	mS	4.8
0 - 100%	DEG.	69	mS	6.4
1 - 90%	DEG.	37	mS	3.4
dP/dθ MAX (BARS/DEG)				1.88
		AT		360.0 DEG
MAX PRESSURE (BARS)				57.32
		AT		373.0 DEG

HEAT TRANSFER

ENGINE MEASURED (kW)	0.000
ENGINE PREDICTED (kW)	3.794
PREDICTED/MEASURED (%)	0.0
MAX BURNED GAS TEMP (K)	2575.9
AT	368.0 DEG
BURNED GAS TEMP EVO (K)	1394.8
GAS TEMP AT IVC (K)	346.5
WALL TEMPERATURE (K)	400.0

STATISTICAL DATA

	MEAN	SD	% DIS
WORK (J)	489.07	6.460	1.3
POWER (kW)	7.336	0.097	1.3
PMAX (BAR)	59.15	7.400	12.7
AT DEG	14.0	2.500	18.0

GAS ANALYSIS

	MODEL	MEASURED
CO2 (%)	9.4	0.0
CO (PPM)	0.0	0.0
O2 (%)	0.5	0.0
NOx (PPM)	4751.3	0.0
UHC (PPM)		0.0

FUEL GROSS CV (kJ/kG) 53402.0
STOICH A/F RATIO 16.61

	MODEL	MEASD
POWER (kW)	7.484	7.069
FRICTN PWR (kW)	1.693	
PUMPNG PWR (kW)		-0.080
INDICATD MEP (BAR)	9.95	9.41
INDICATED EFFICNCY	0.334	0.316
BRAKE POWER (kW)	5.791	6.313
BRAKE TH EFFICNCY	0.259	0.282

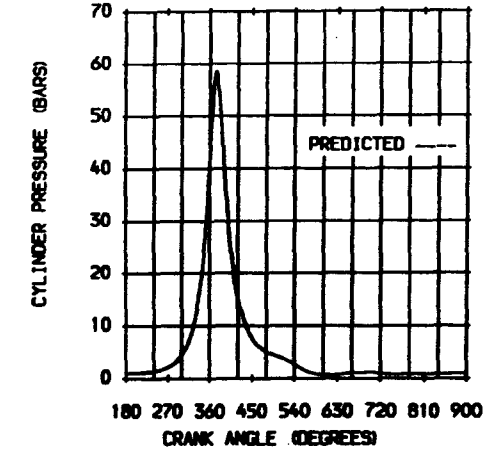

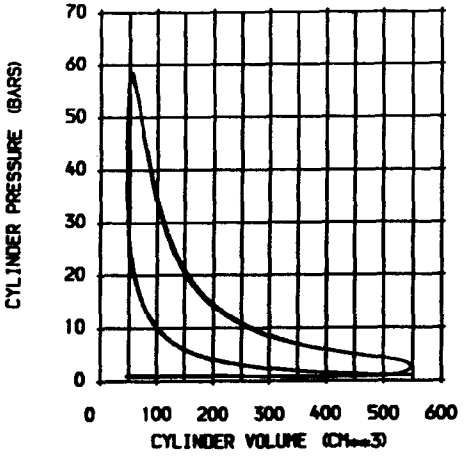

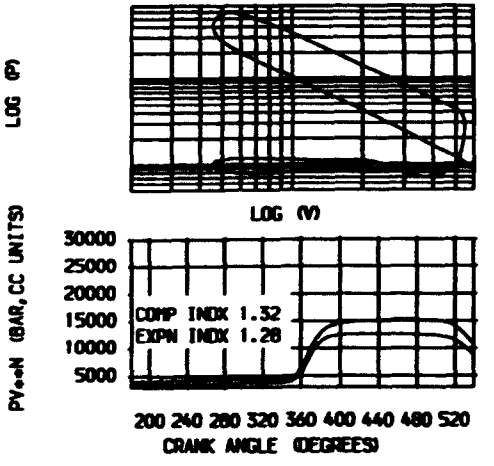

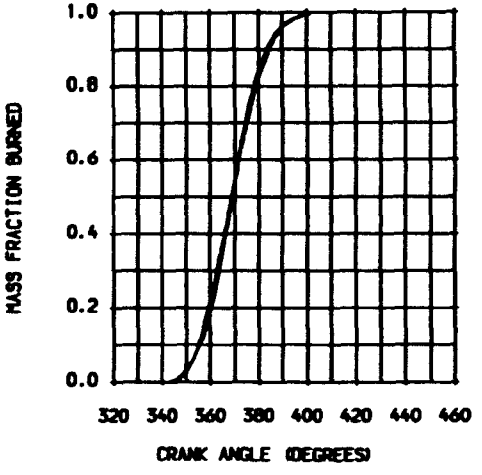

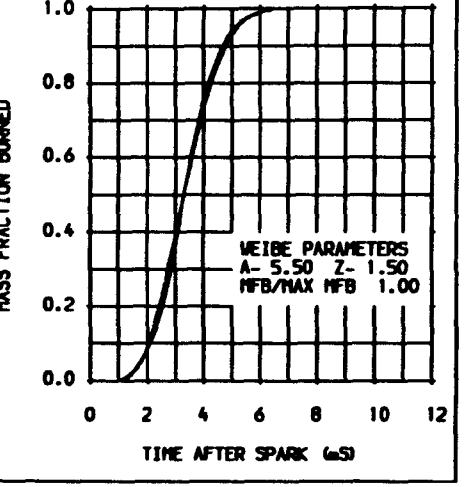

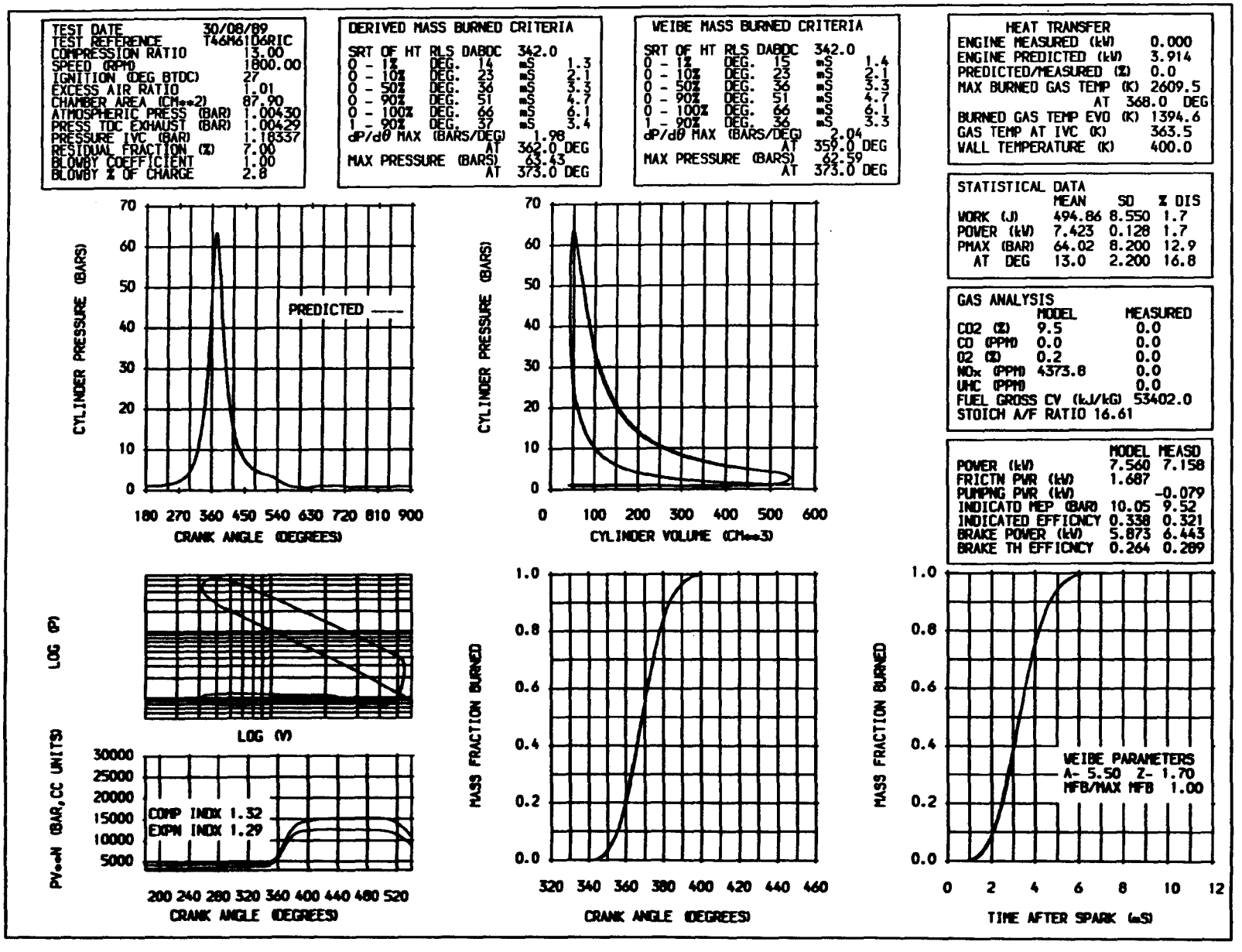
TEST DATE 30/08/89
TEST REFERENCE T46M6106RIC
COMPRESSION RATIO 13.00
SPEED (RPM) 1800.00
IGNITION (DEG BTDC) 27
EXCESS AIR RATIO 1.01
CHAMBER AREA (CM**2) 87.90
ATMOSPHERIC PRESS (BAR) 1.00430
PRESS TDC EXHAUST (BAR) 1.00429
PRESSURE IVC (BAR) 1.18337
RESIDUAL FRACTION (%) 7.00
BLOWBY COEFFICIENT 1.00
BLOWBY % OF CHARGE 2.8
DERIVED MASS BURNED CRITERIA
SRT OF HT RLS DABDC 342.0
0 - 1% DEG. 14 1.3
0 - 10% DEG. 23 2.1
0 - 50% DEG. 36 3.3
0 - 90% DEG. 51 4.7
0 - 100% DEG. 66 6.1
1 - 90% DEG. 37 3.4
dP/dθ MAX (BARS/DEG) 1.98
AT 362.0 DEG
MAX PRESSURE (BARS) 63.43
AT 373.0 DEG
WEIBE MASS BURNED CRITERIA
SRT OF HT RLS DABDC 342.0
0 - 1% DEG. 15 1.4
0 - 10% DEG. 23 2.1
0 - 50% DEG. 36 3.3
0 - 90% DEG. 51 4.7
0 - 100% DEG. 66 6.1
1 - 90% DEG. 36 3.3
dP/dθ MAX (BARS/DEG) 2.04
AT 359.0 DEG
MAX PRESSURE (BARS) 62.59
AT 373.0 DEG
HEAT TRANSFER
ENGINE MEASURED (kW) 0.000
ENGINE PREDICTED (kW) 3.914
PREDICTED/MEASURED (%) 0.0
MAX BURNED GAS TEMP (K) 2609.5
AT 368.0 DEG
BURNED GAS TEMP EVO (K) 1394.6
GAS TEMP AT IVC (K) 363.5
WALL TEMPERATURE (K) 400.0
STATISTICAL DATA
MEAN SD % DIS
WORK (J) 494.86 8.550 1.7
POWER (kW) 7.423 0.128 1.7
PMAX (BAR) 64.02 8.200 12.9
AT DEG 13.0 2.200 16.8
GAS ANALYSIS
MODEL MEASURED
CO2 (%) 9.5 0.0
CO (PPM) 0.0 0.0
O2 (%) 0.2 0.0
NOx (PPM) 4373.8 0.0
UHC (PPM) 0.0
FUEL GROSS CV (kJ/kG) 53402.0
STOICH A/F RATIO 16.61
MODEL MEASD
POWER (kW) 7.560 7.158
FRICTN PWR (kW) 1.687
PUMPNG PWR (kW) -0.079
INDICATD MEP (BAR) 10.05 9.52
INDICATED EFFICNCY 0.338 0.321
BRAKE POWER (kW) 5.873 6.443
BRAKE TH EFFICNCY 0.264 0.289
CYLINDER PRESSURE (BARS)
PREDICTED
CRANK ANGLE (DEGREES)
CYLINDER VOLUME (CM**3)
LOG (P)
LOG (V)
PV**N (BAR,CC UNITS)
COMP INDX 1.32
EXPN INDX 1.29
MASS FRACTION BURNED
WEIBE PARAMETERS
A- 5.50 Z- 1.70
MFB/MAX MFB 1.00
TIME AFTER SPARK (mS)

TEST DATE	30/08/89
TEST REFERENCE	T46M6207RIC
COMPRESSION RATIO	14.00
SPEED (RPM)	1800.00
IGNITION (DEG BTDC)	27
EXCESS AIR RATIO	1.00
CHAMBER AREA (CM**2)	84.60
ATMOSPHERIC PRESS (BAR)	1.00430
PRESS TDC EXHAUST (BAR)	1.00429
PRESSURE IVC (BAR)	1.19743
RESIDUAL FRACTION (%)	7.00
BLOWBY COEFFICIENT	1.00
BLOWBY % OF CHARGE	2.8

DERIVED MASS BURNED CRITERIA

SRT OF HT RLS DABDC		342.0	
0 - 1%	DEG.	13	mS 1.2
0 - 10%	DEG.	23	mS 2.1
0 - 50%	DEG.	37	mS 3.4
0 - 90%	DEG.	51	mS 4.7
0 - 100%	DEG.	67	mS 6.2
1 - 90%	DEG.	38	mS 3.5
dP/dθ MAX (BARS/DEG)		2.04	
	AT	363.0	DEG
MAX PRESSURE (BARS)		67.72	
	AT	372.0	DEG

WEIBE MASS BURNED CRITERIA

SRT OF HT RLS DABDC		342.0	
0 - 1%	DEG.	14	mS 1.3
0 - 10%	DEG.	22	mS 2.0
0 - 50%	DEG.	36	mS 3.3
0 - 90%	DEG.	52	mS 4.8
0 - 100%	DEG.	67	mS 6.2
1 - 90%	DEG.	38	mS 3.5
dP/dθ MAX (BARS/DEG)		2.26	
	AT	358.0	DEG
MAX PRESSURE (BARS)		67.05	
	AT	371.0	DEG

HEAT TRANSFER

ENGINE MEASURED (kW)	0.000
ENGINE PREDICTED (kW)	3.937
PREDICTED/MEASURED (%)	0.0
MAX BURNED GAS TEMP (K)	2618.5
AT	366.0 DEG
BURNED GAS TEMP EVO (K)	1387.1
GAS TEMP AT IVC (K)	357.5
WALL TEMPERATURE (K)	400.0

STATISTICAL DATA

	MEAN	SD	% DIS
WORK (J)	503.17	6.520	1.3
POWER (kW)	7.548	0.098	1.3
PMAX (BAR)	68.19	7.900	11.7
AT DEG	12.6	2.000	15.7

GAS ANALYSIS

	MODEL	MEASURED
CO2 (%)	9.6	0.0
CO (PPM)	0.0	0.0
O2 (%)	0.0	0.0
NOx (PPM)	4025.4	0.0
UHC (PPM)		0.0
FUEL GROSS CV (kJ/kG)		53402.0
STOICH A/F RATIO		16.61

	MODEL	MEASD
POWER (kW)	7.729	7.281
FRICTN PWR (kW)	1.681	
PUMPNG PWR (kW)		-0.073
INDICATD MEP (BAR)	10.27	9.69
INDICATED EFFICNCY	0.342	0.312
BRAKE POWER (kW)	6.048	6.529
BRAKE TH EFFICNCY	0.259	0.280

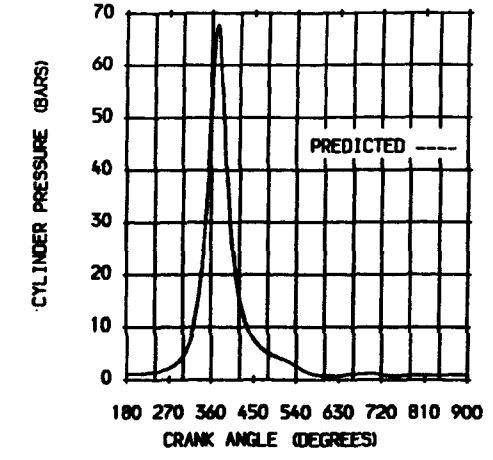

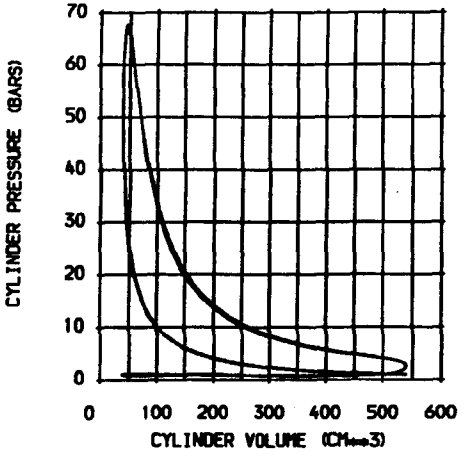

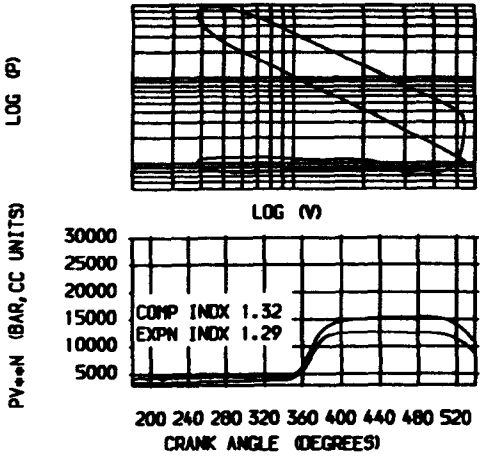

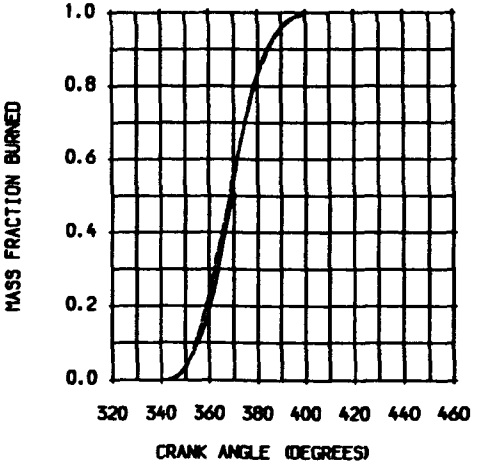

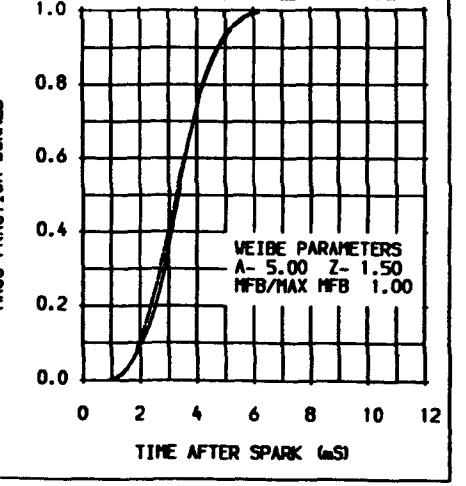

TEST DATE	30/08/89
TEST REFERENCE	T46M6308RIC
COMPRESSION RATIO	15.00
SPEED (RPM)	1800.00
IGNITION (DEG BTDC)	22
EXCESS AIR RATIO	1.01
CHAMBER AREA (CM**2)	81.81
ATMOSPHERIC PRESS (BAR)	1.00430
PRESS TDC EXHAUST (BAR)	1.00429
PRESSURE IVC (BAR)	1.21360
RESIDUAL FRACTION (%)	7.00
BLOWBY COEFFICIENT	1.00
BLOWBY % OF CHARGE	2.8

DERIVED MASS BURNED CRITERIA

SRT OF HT RLS DABDC				347.0
0 - 1%	DEG.	13	mS	1.2
0 - 10%	DEG.	24	mS	2.2
0 - 50%	DEG.	39	mS	5.6
0 - 90%	DEG.	57	mS	5.3
0 - 100%	DEG.	76	mS	7.0
1 - 90%	DEG.	44	mS	4.1
dP/dθ MAX (BARS/DEG)				1.57
		AT		354.0 DEG
MAX PRESSURE (BARS)				58.02
		AT		375.0 DEG

WEIBE MASS BURNED CRITERIA

SRT OF HT RLS DABDC				347.0
0 - 1%	DEG.	15	mS	1.4
0 - 10%	DEG.	23	mS	2.1
0 - 50%	DEG.	39	mS	5.6
0 - 90%	DEG.	58	mS	5.4
0 - 100%	DEG.	76	mS	7.0
1 - 90%	DEG.	43	mS	4.0
dP/dθ MAX (BARS/DEG)				1.45
		AT		359.0 DEG
MAX PRESSURE (BARS)				56.63
		AT		373.0 DEG

HEAT TRANSFER

ENGINE MEASURED (kW)	0.000
ENGINE PREDICTED (kW)	3.479
PREDICTED/MEASURED (%)	0.0
MAX BURNED GAS TEMP (K)	2534.4
AT	368.0 DEG
BURNED GAS TEMP EVO (K)	1434.1
GAS TEMP AT IVC (K)	334.0
WALL TEMPERATURE (K)	400.0

STATISTICAL DATA

	MEAN	SD	% DIS
WORK (J)	499.00	10.500	2.3
POWER (kW)	7.485	0.158	2.3
PMAX (BAR)	58.26	7.700	14.2
AT DEG	15.3	1.600	11.1

GAS ANALYSIS

	MODEL	MEASURED
CO2 (%)	9.5	0.0
CO (PPM)	0.0	0.0
O2 (%)	0.2	0.0
NOx (PPM)	3674.7	0.0
UHC (PPM)		0.0
FUEL GROSS CV (kJ/kG)		53402.0
STOICH A/F RATIO		16.61

	MODEL	MEASD
POWER (kW)	7.822	7.217
FRICTN PWR (kW)	1.676	
PUMPNG PWR (kW)		-0.086
INDICATD MEP (BAR)	10.40	9.60
INDICATED EFFICNCY	0.336	0.311
BRAKE POWER (kW)	6.146	6.529
BRAKE TH EFFICNCY	0.265	0.282

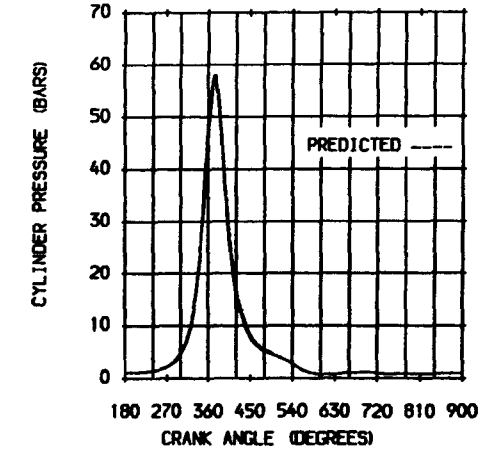

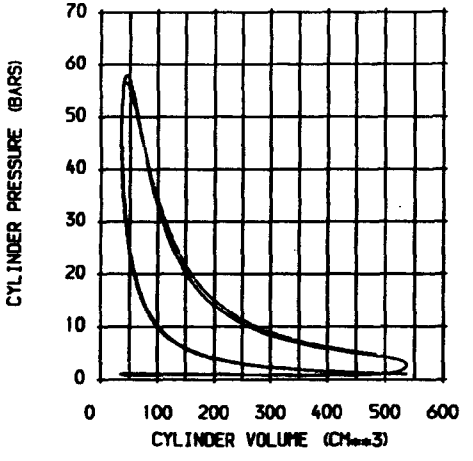

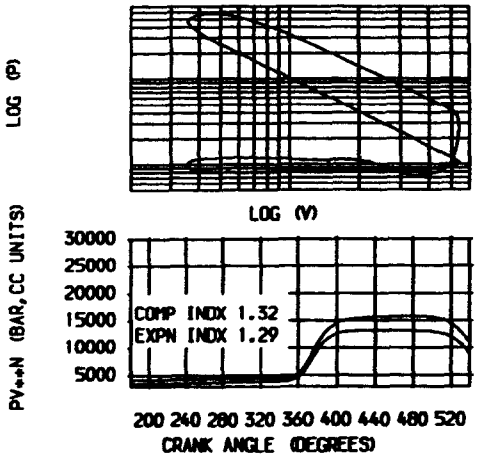

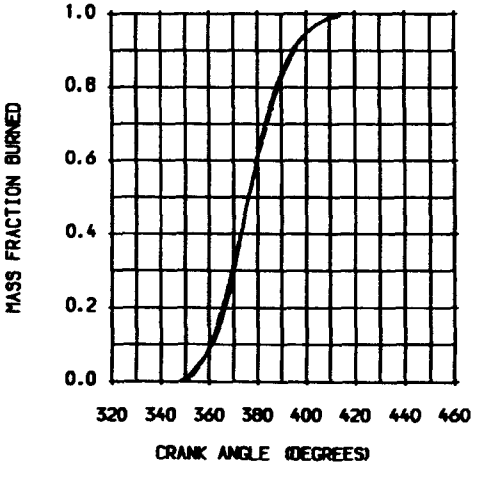

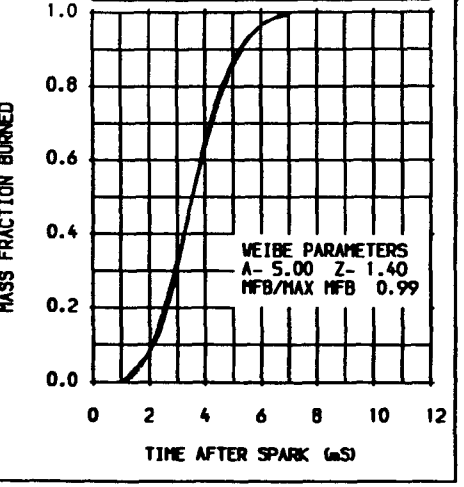

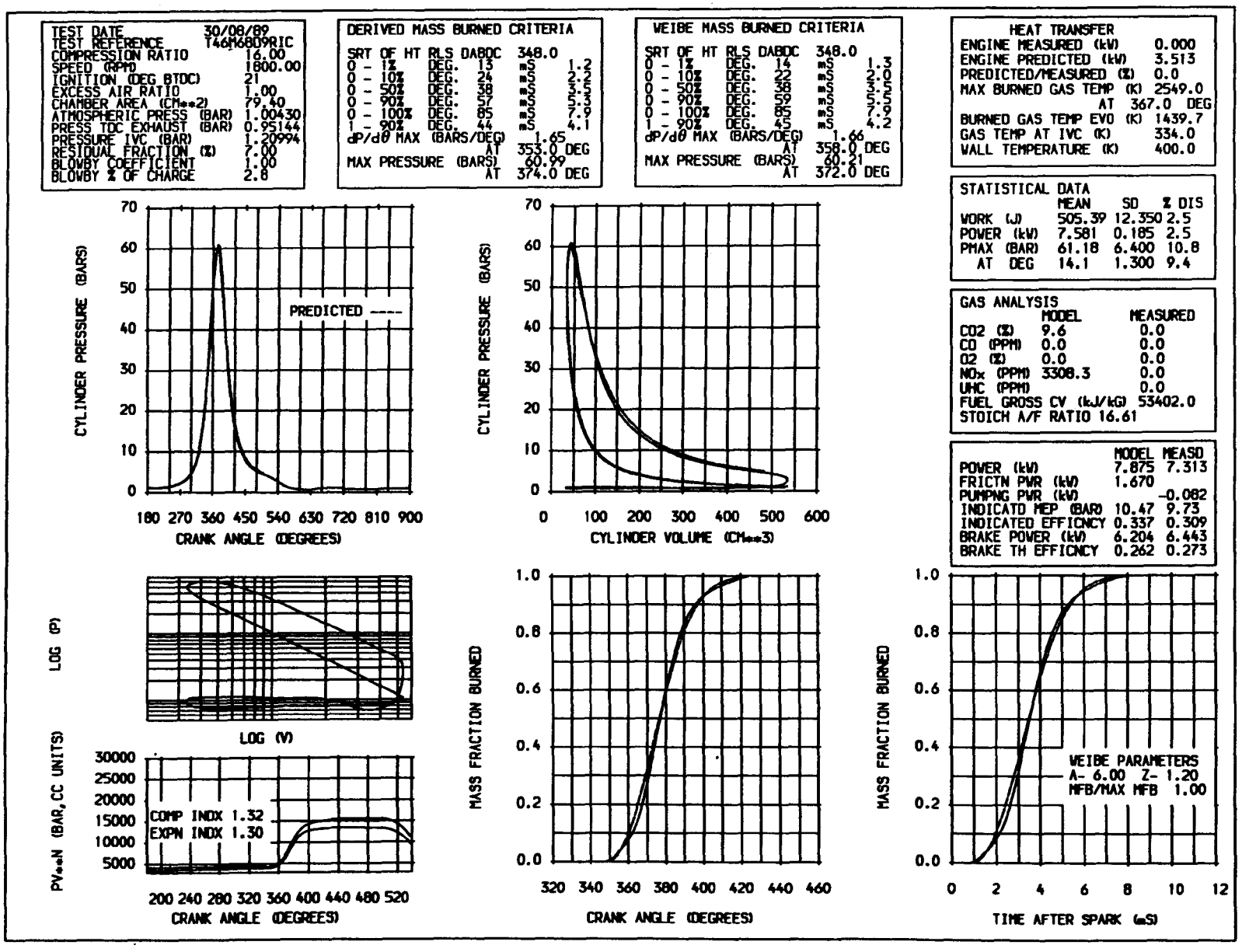
TEST DATE 30/08/89
TEST REFERENCE T46M6809RIC
COMPRESSION RATIO 16.00
SPEED (RPM) 1800.00
IGNITION (DEG BTDC) 21
EXCESS AIR RATIO 1.00
CHAMBER AREA (CM**2) 79.40
ATMOSPHERIC PRESS (BAR) 1.00430
PRESS TDC EXHAUST (BAR) 0.95144
PRESSURE IVC (BAR) 1.20994
RESIDUAL FRACTION (%) 7.00
BLOWBY COEFFICIENT 1.00
BLOWBY % OF CHARGE 2.8
DERIVED MASS BURNED CRITERIA
SRT OF HT RLS DABDC 348.0
0 - 1% DEG. 13 mS 1.2
0 - 10% DEG. 24 mS 2.2
0 - 50% DEG. 38 mS 3.5
0 - 90% DEG. 57 mS 5.3
0 - 100% DEG. 85 mS 7.9
1 - 90% DEG. 44 mS 4.1
dP/dθ MAX (BARS/DEG) 1.65
AT 353.0 DEG
MAX PRESSURE (BARS) 60.99
AT 374.0 DEG
WEIBE MASS BURNED CRITERIA
SRT OF HT RLS DABDC 348.0
0 - 1% DEG. 14 mS 1.3
0 - 10% DEG. 22 mS 2.0
0 - 50% DEG. 38 mS 3.5
0 - 90% DEG. 59 mS 5.5
0 - 100% DEG. 85 mS 7.9
1 - 90% DEG. 45 mS 4.2
dP/dθ MAX (BARS/DEG) 1.66
AT 358.0 DEG
MAX PRESSURE (BARS) 60.21
AT 372.0 DEG
HEAT TRANSFER
ENGINE MEASURED (kW) 0.000
ENGINE PREDICTED (kW) 3.513
PREDICTED/MEASURED (%) 0.0
MAX BURNED GAS TEMP (K) 2549.0
AT 367.0 DEG
BURNED GAS TEMP EVO (K) 1439.7
GAS TEMP AT IVC (K) 334.0
WALL TEMPERATURE (K) 400.0
STATISTICAL DATA
MEAN SD % DIS
WORK (J) 505.39 12.350 2.5
POWER (kW) 7.581 0.185 2.5
PMAX (BAR) 61.18 6.400 10.8
AT DEG 14.1 1.300 9.4
GAS ANALYSIS
MODEL MEASURED
CO2 (%) 9.6 0.0
CO (PPM) 0.0 0.0
O2 (%) 0.0 0.0
NOx (PPM) 3308.3 0.0
UHC (PPM) 0.0
FUEL GROSS CV (kJ/kG) 53402.0
STOICH A/F RATIO 16.61
MODEL MEASD
POWER (kW) 7.875 7.313
FRICTN PWR (kW) 1.670
PUMPNG PWR (kW) -0.082
INDICATD MEP (BAR) 10.47 9.73
INDICATED EFFICNCY 0.337 0.309
BRAKE POWER (kW) 6.204 6.443
BRAKE TH EFFICNCY 0.262 0.273
CYLINDER PRESSURE (BARS)
PREDICTED
CRANK ANGLE (DEGREES)
CYLINDER VOLUME (CM**3)
LOG (P)
LOG (V)
PV**N (BAR,CC UNITS)
COMP INDX 1.32
EXPN INDX 1.30
MASS FRACTION BURNED
WEIBE PARAMETERS
A- 6.00 Z- 1.20
MFB/MAX MFB 1.00
TIME AFTER SPARK (mS)

APPENDIX II - PERFORMANCE DATA AND ENERGY TRANSFERS

Introduction

Figures II.2 - II.19 comprise the experimental engine performance and energy transfer data for all the operating conditions investigated. Selected data from this appendix form the basis of the graphical figures included in Chapters 7 and 8.

TASKII, REF. T182138TII

SPEED: 25 R/S, CR: 9:1

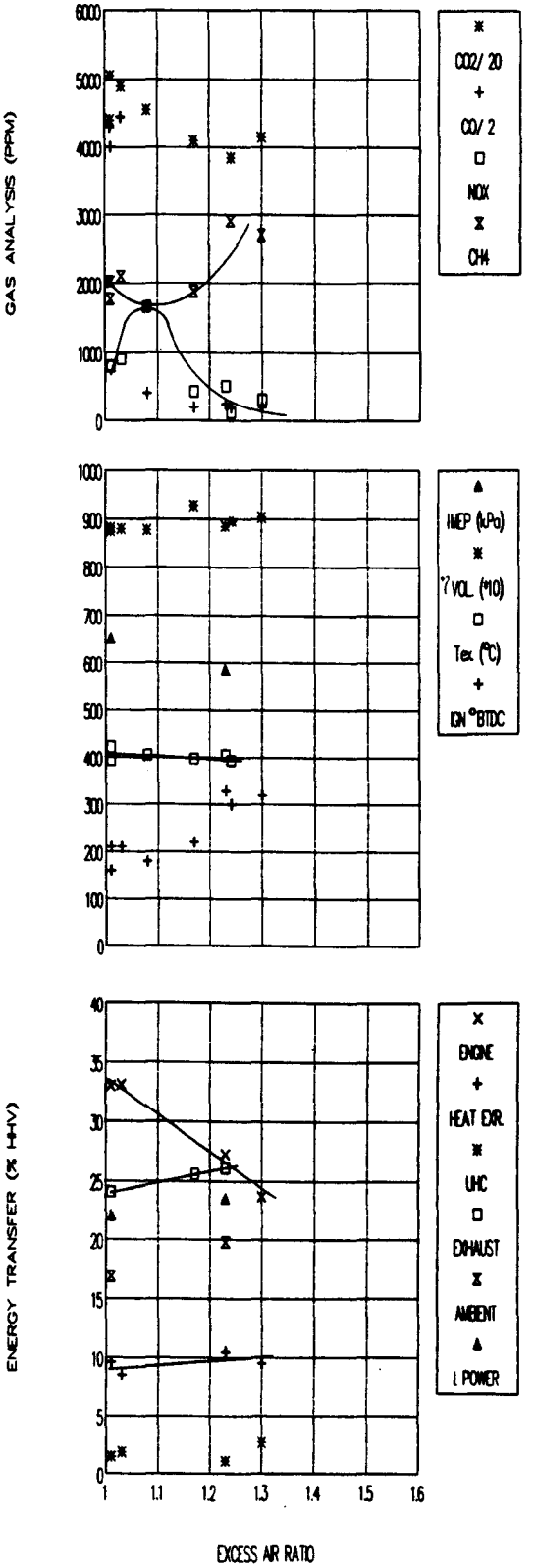

TASKII, REF. T192138TII

SPEED: 30 R/S, CR: 9:1

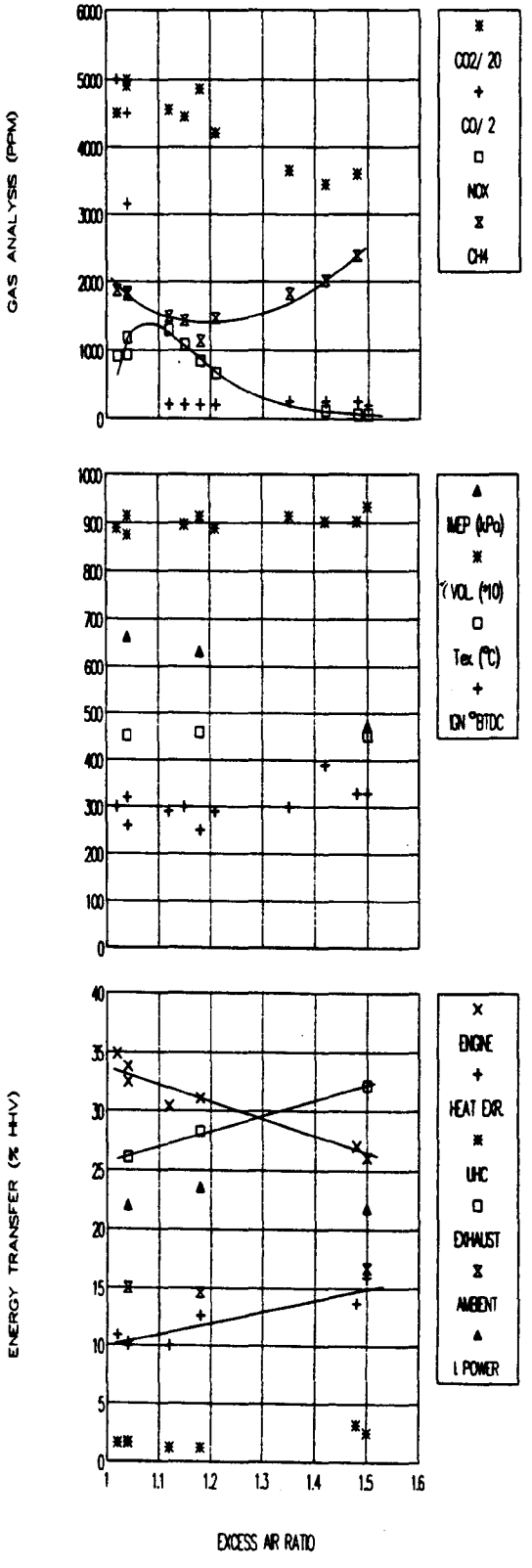

EFFECT OF IGNITION TIMING ON TASKII

SPEED: 30 R/S, XAIR: 1.11, CR: 9: 1

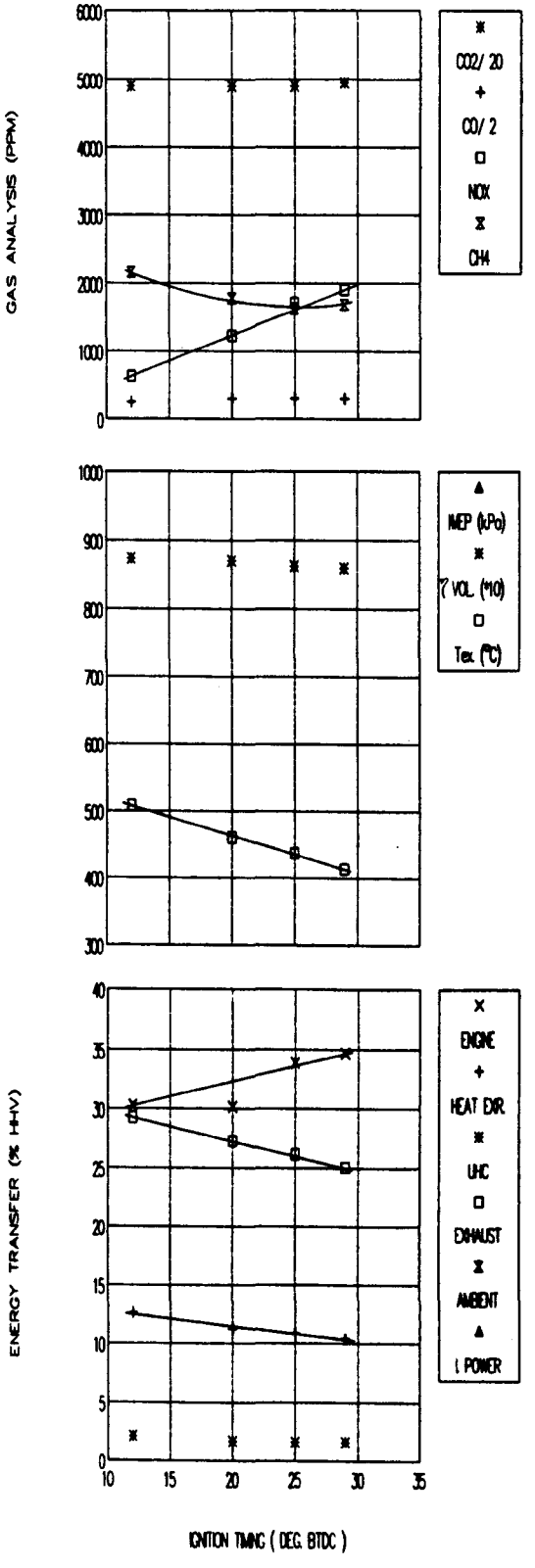

TASK II, REF. T2021223839TII

SPEED: 35 R/S, CR: 9:1

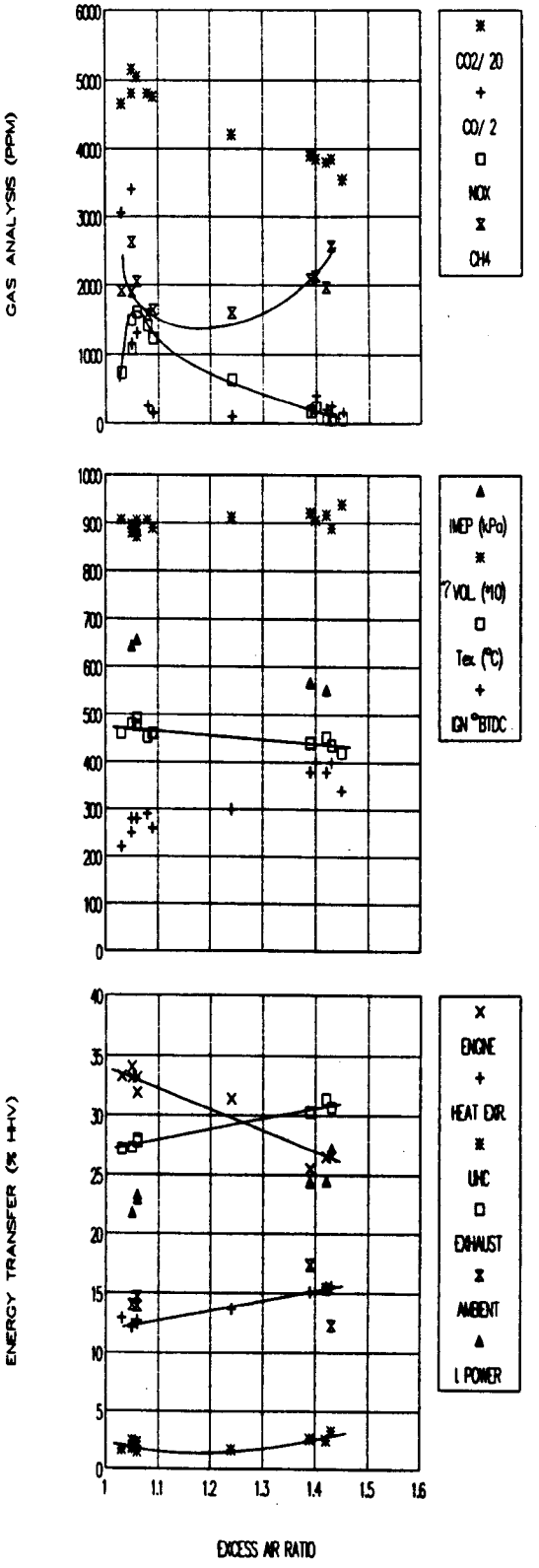

HEAD 3-2, REF. T24H3CH2

SPEED: 25 R/S, CR: 9:1

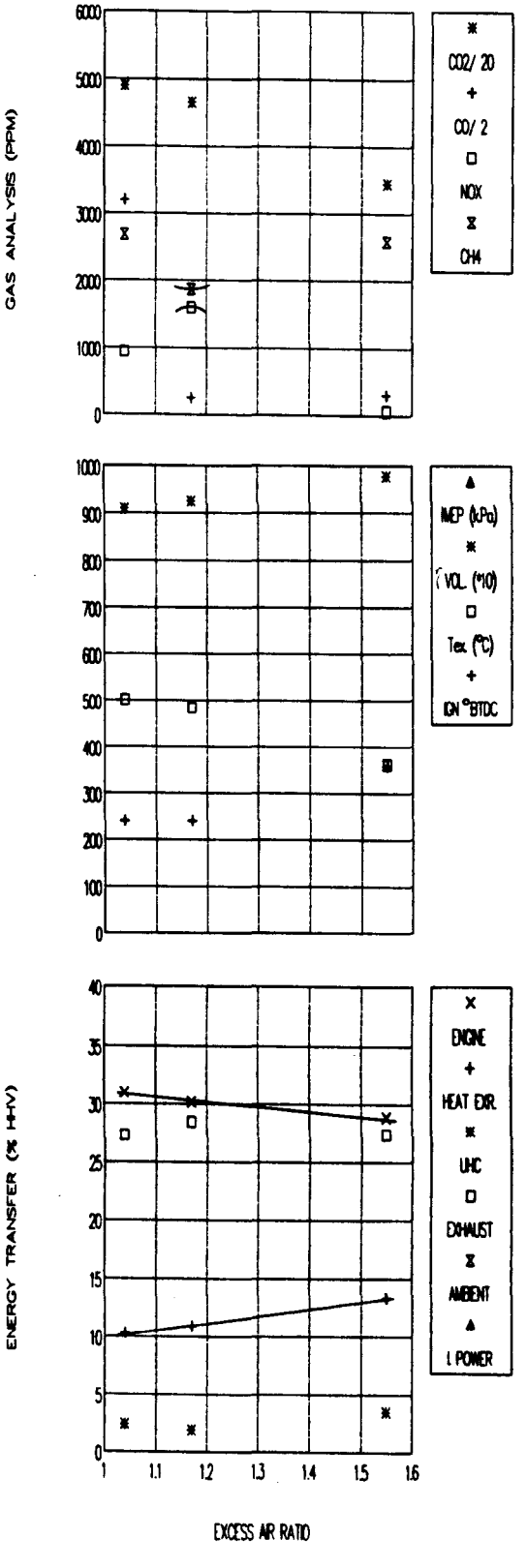

HEAD 3-2, REF. T2437H3CH2

SPEED: 30 R/S, CR: 9:1

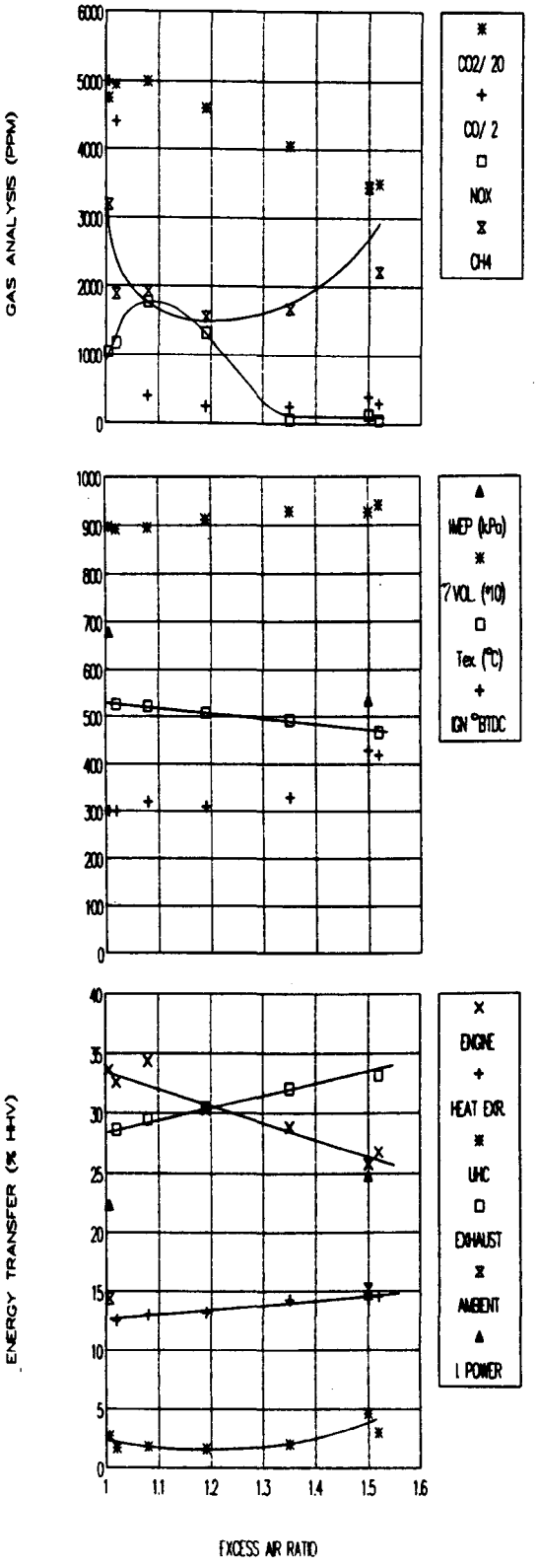

HEAD 3-2, REF. T24H3CH2

SPEED: 35 R/S, CR: 9:1

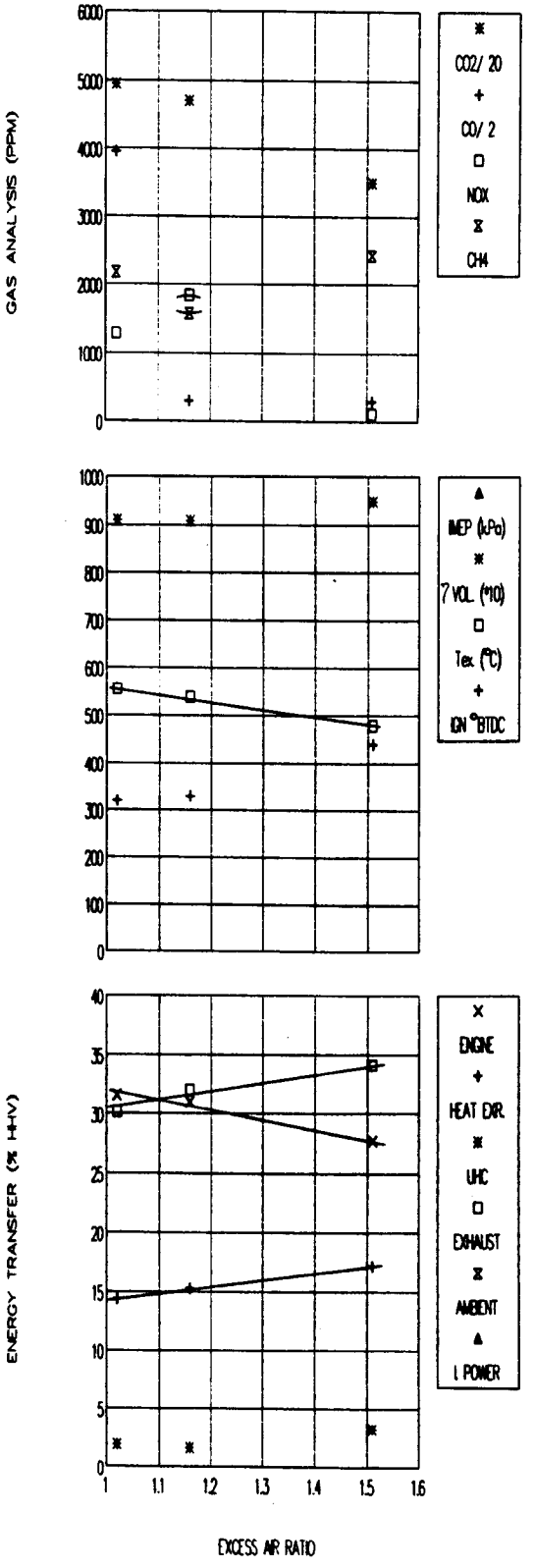

HEAD 3-2, REF. T2540H3CH2

SPEED: 30 R/S, CR: 10:1

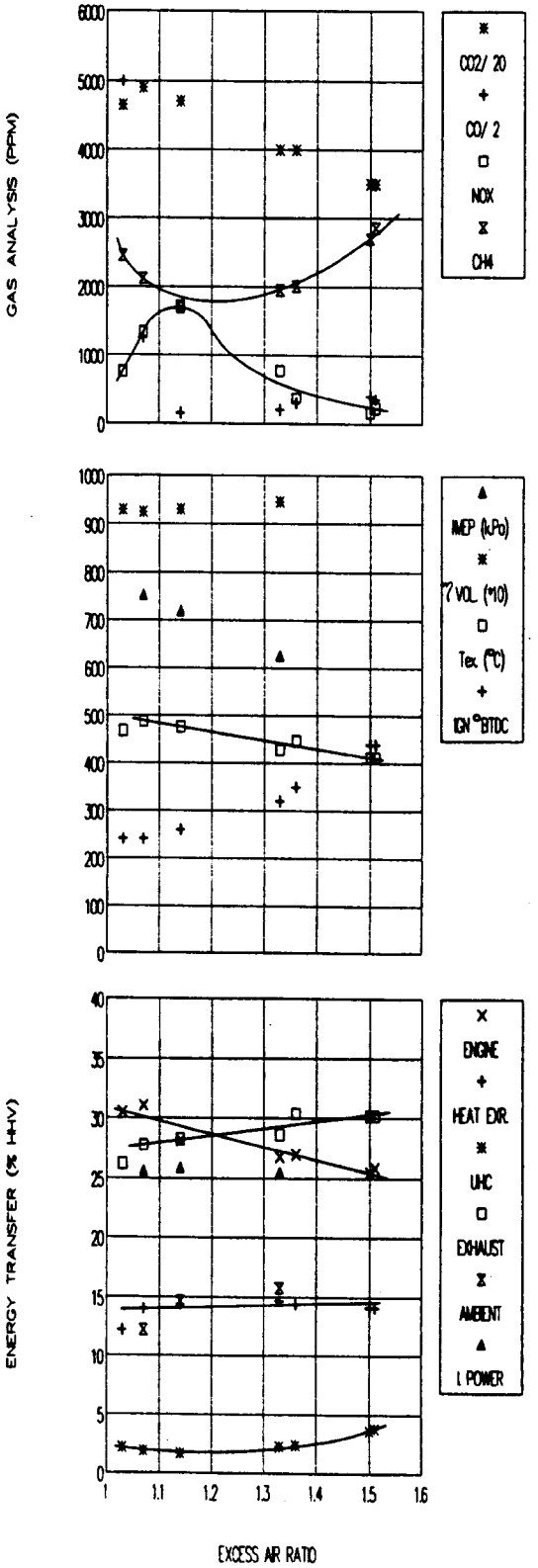

HEAD 3-2, REF. T2634H3CH2

SPEED: 30 R/S, CR: 12:1

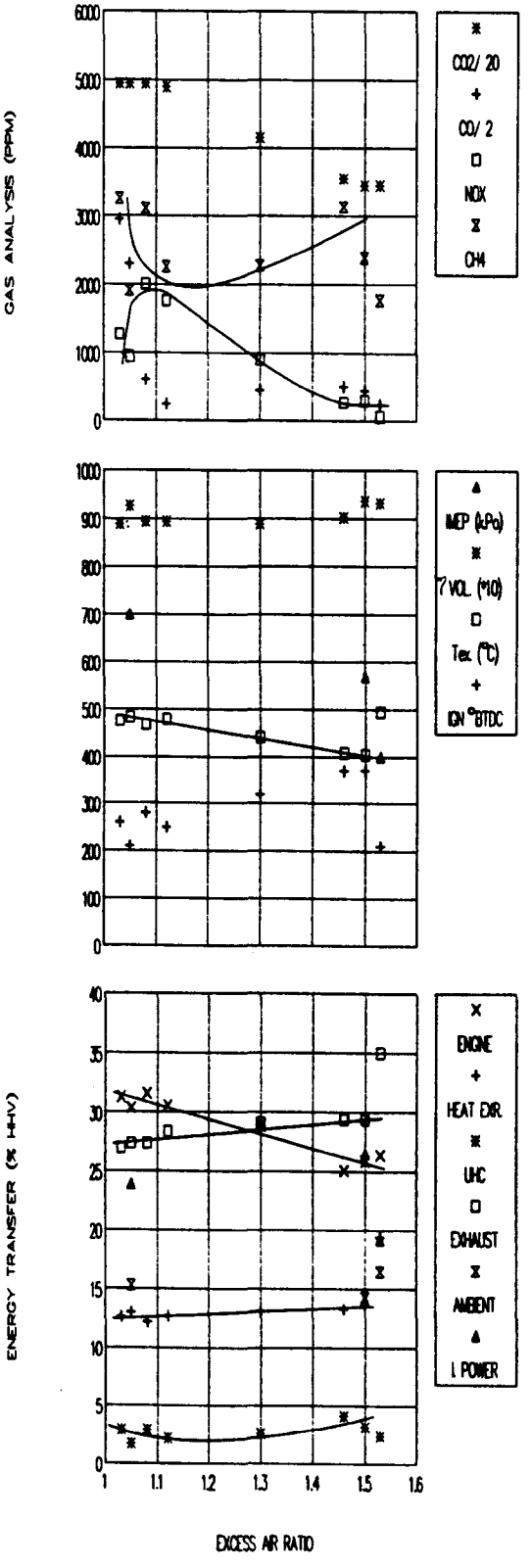

HEAD 3-2, REF. T2932H3CH2

SPEED: 25 R/S, CR: 13:1

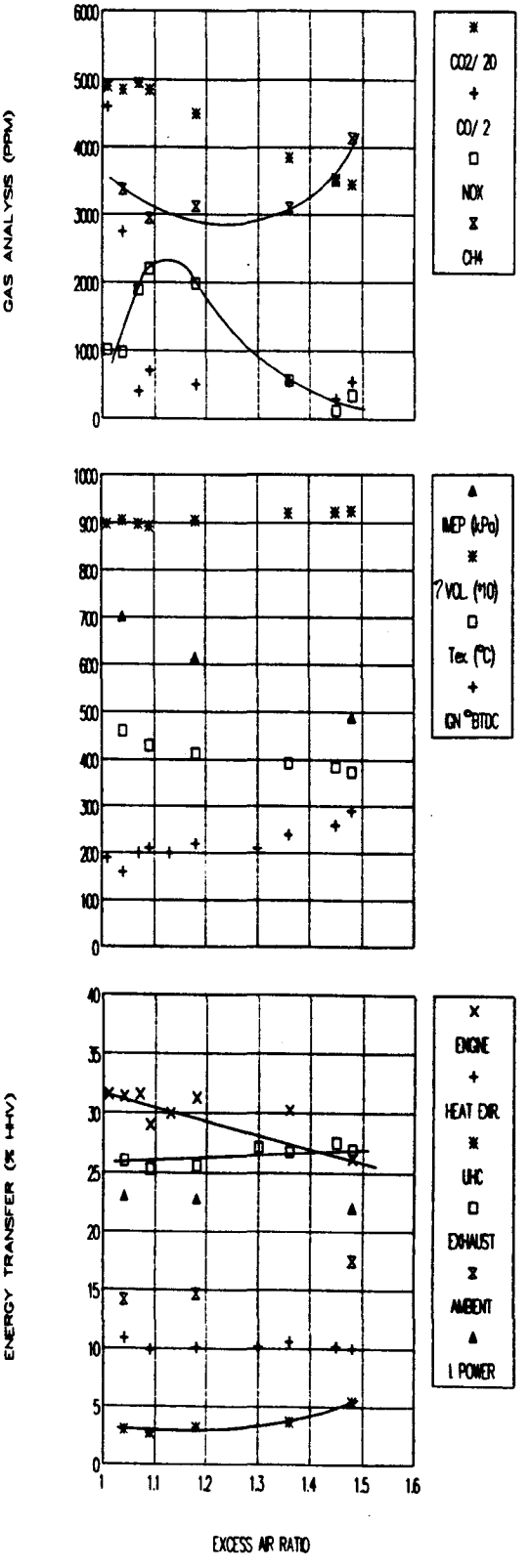

HEAD 3-2, REF. T3031H3CH2

SPEED: 30 R/S, CR: 13:1

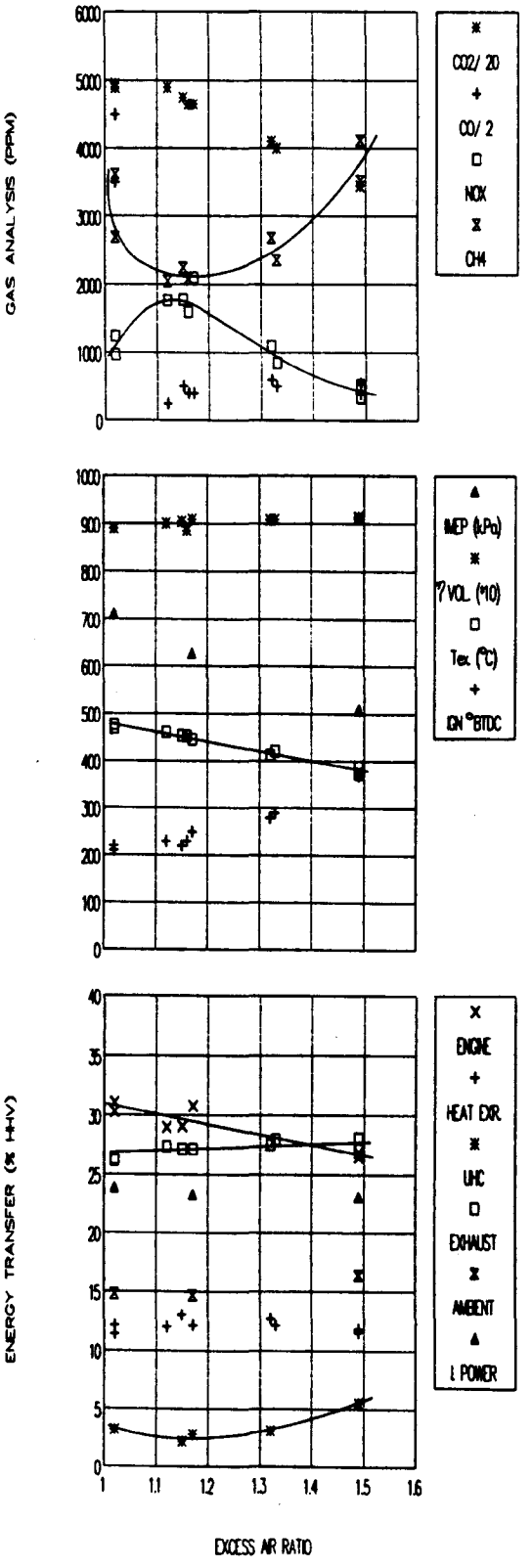

EFFECT OF IGNITION TIMING, HEAD 3-2

SPEED: 30 R/S, XAIR: 1.17, CR: 13: 1

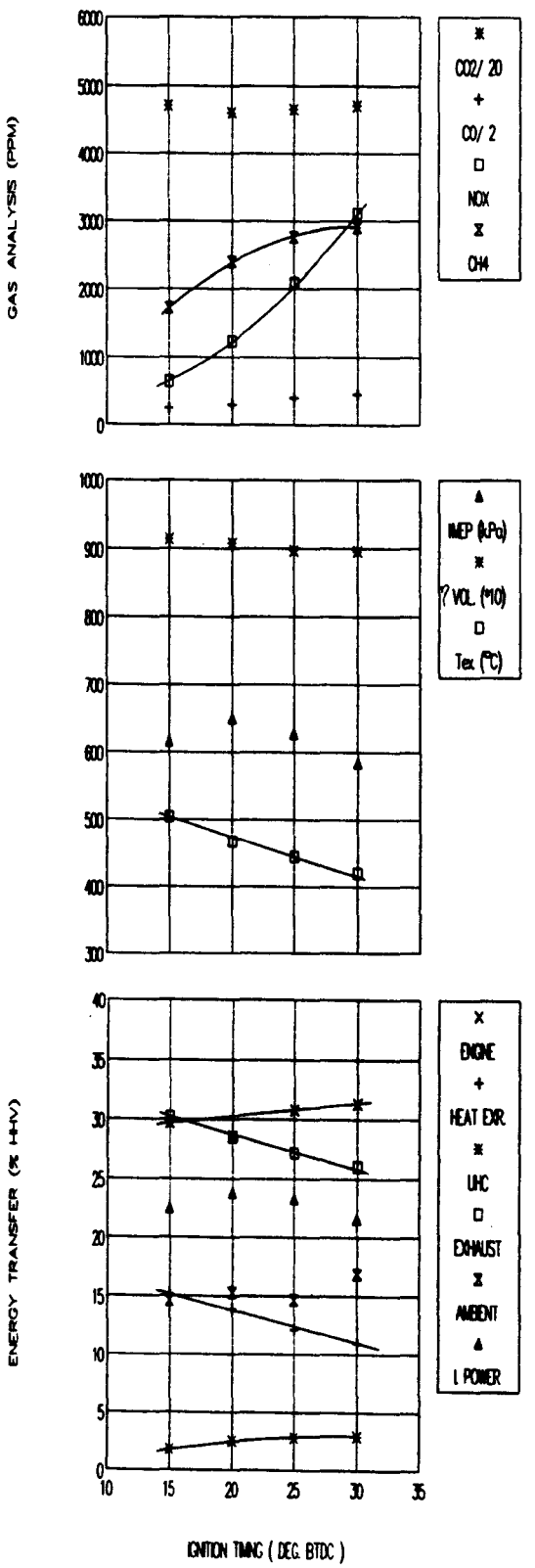

HEAD 3-2, REF. T273233H3CH2

SPEED: 35 R/S, CR: 13:1

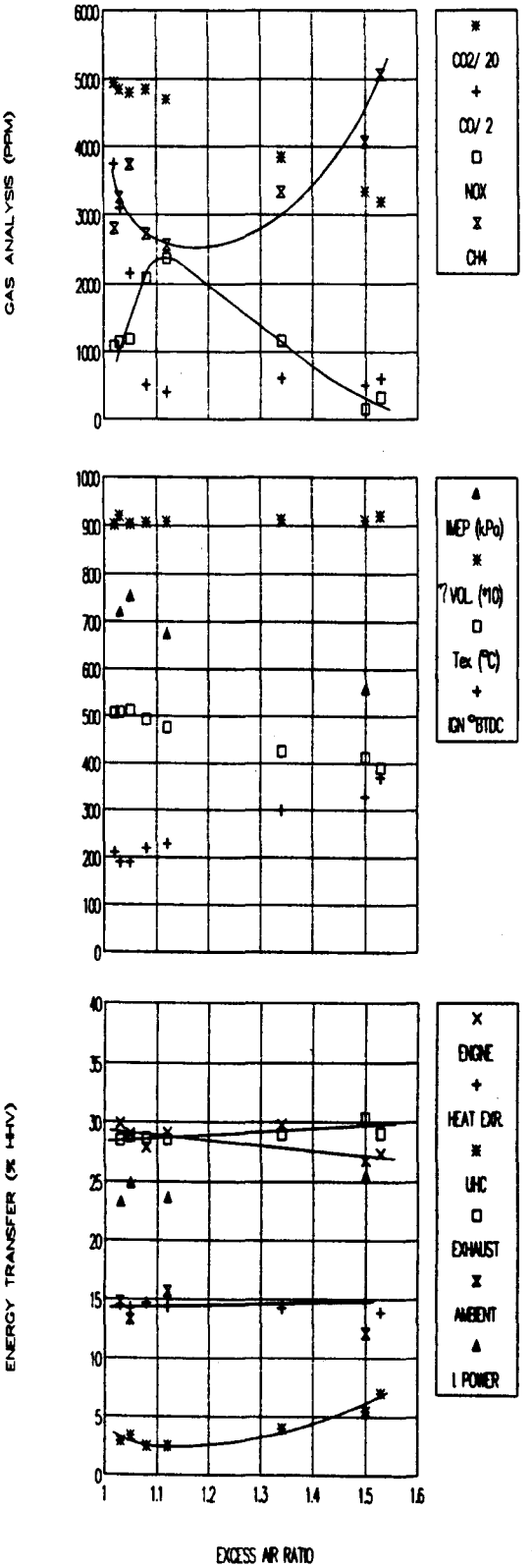

HEAD 3-2, REF. T43H3CH2

SPEED: 30 R/S, CR: 14:1

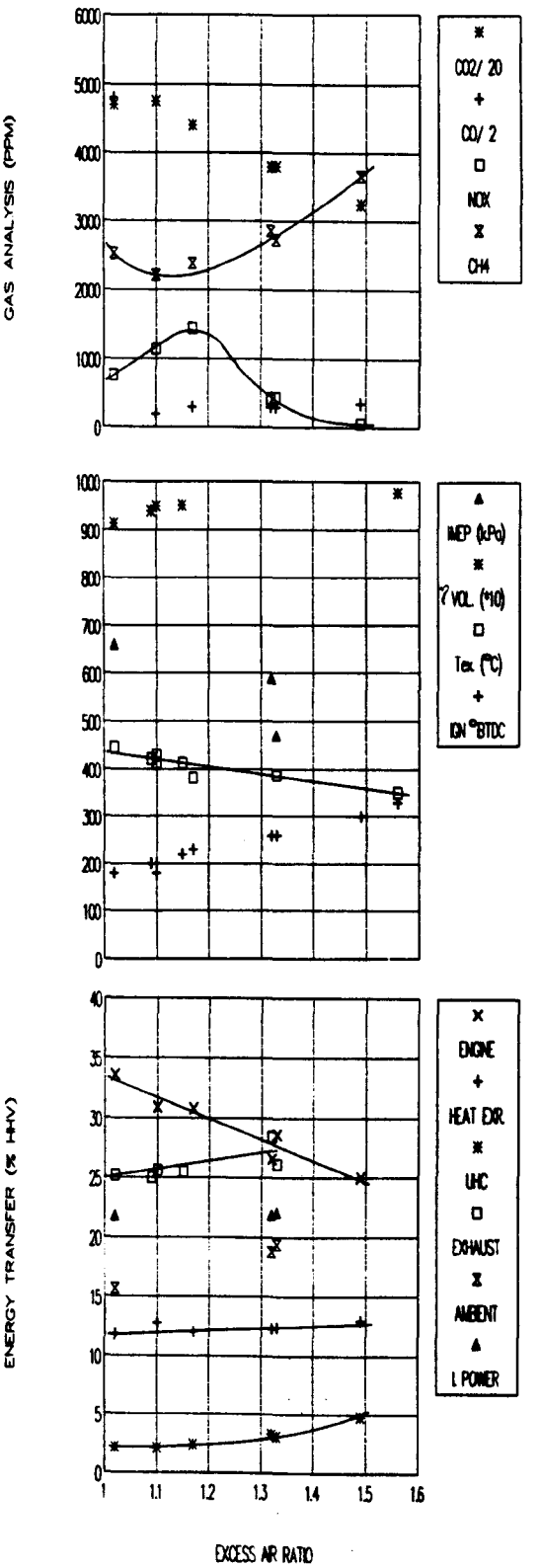

HRCC, REF. T3536HRCC

SPEED: 25 R/S, CR: 13:1

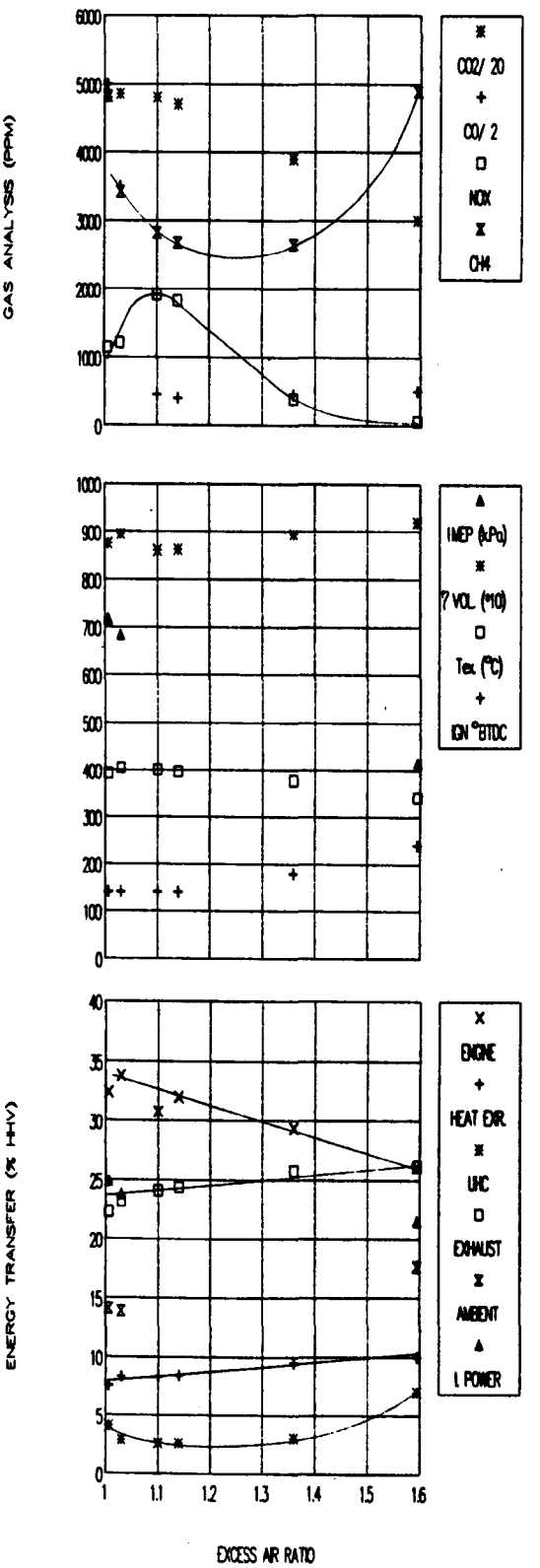

HRCC, REF. T3536HRCC

SPEED: 30 R/S, CR: 13:1

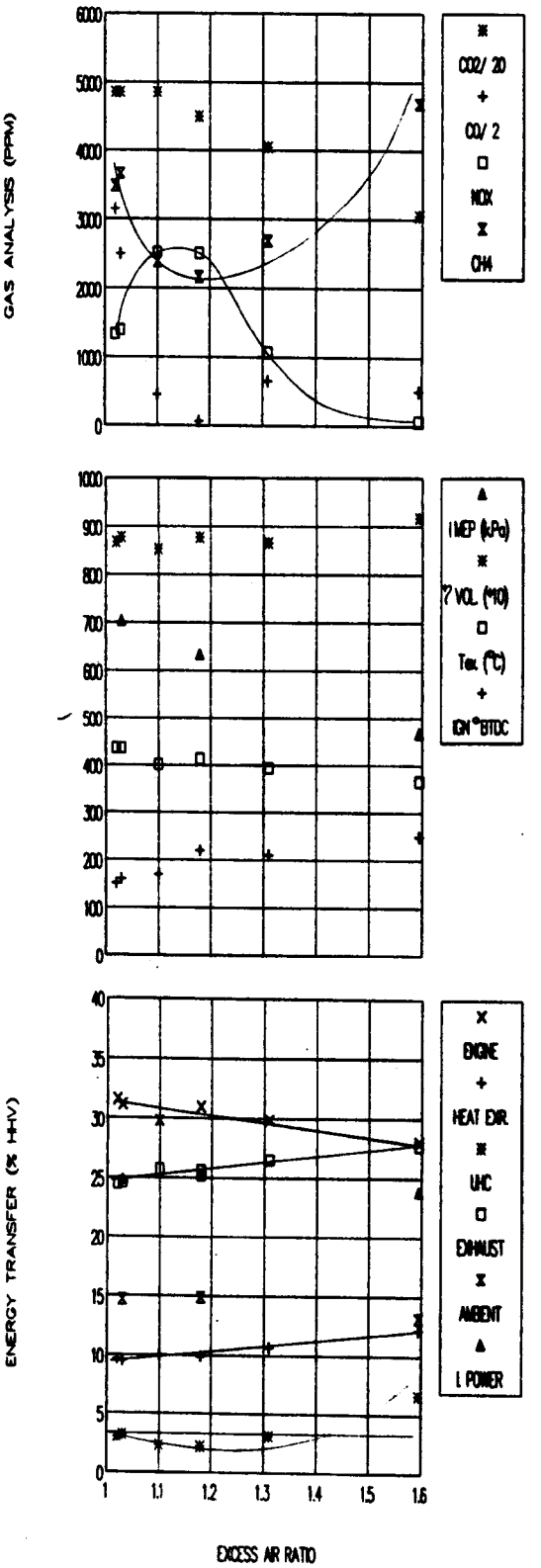

EFFECT OF IGNITION TIMING ON HRCC

SPEED: 30 R/S, XAIR: 1.16, CR: 13: 1

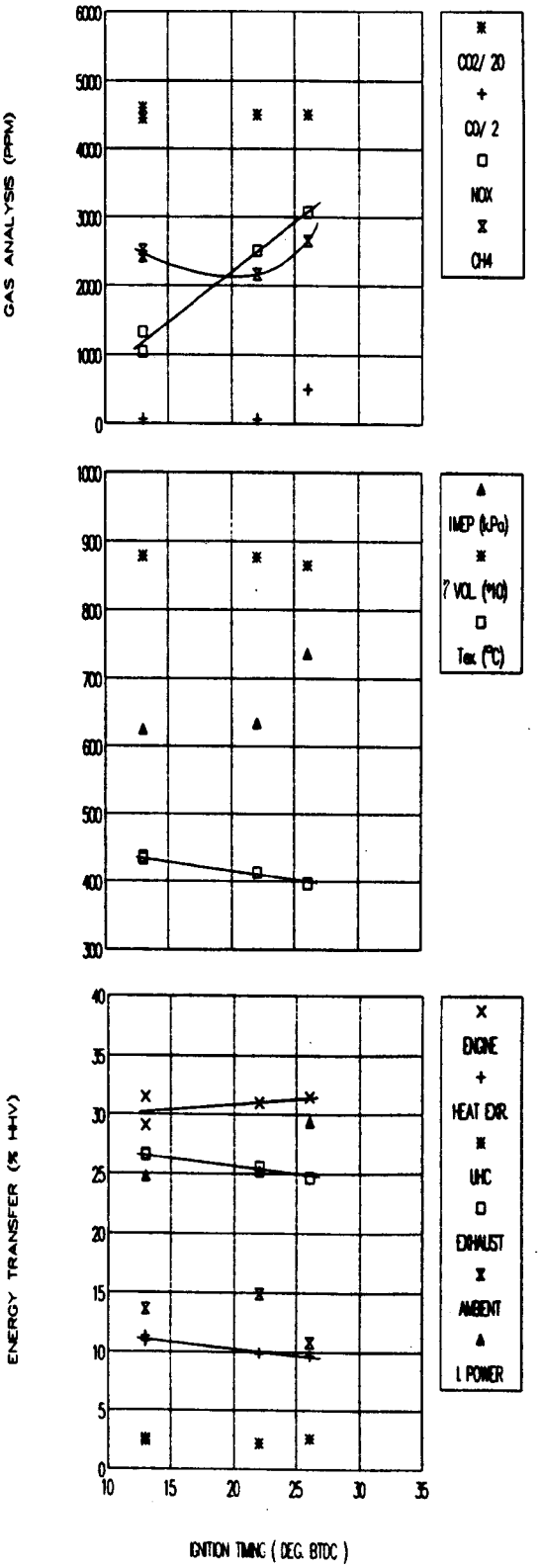

HRCC, REF. T35HRCC

SPEED: 35 R/S, CR: 13:1

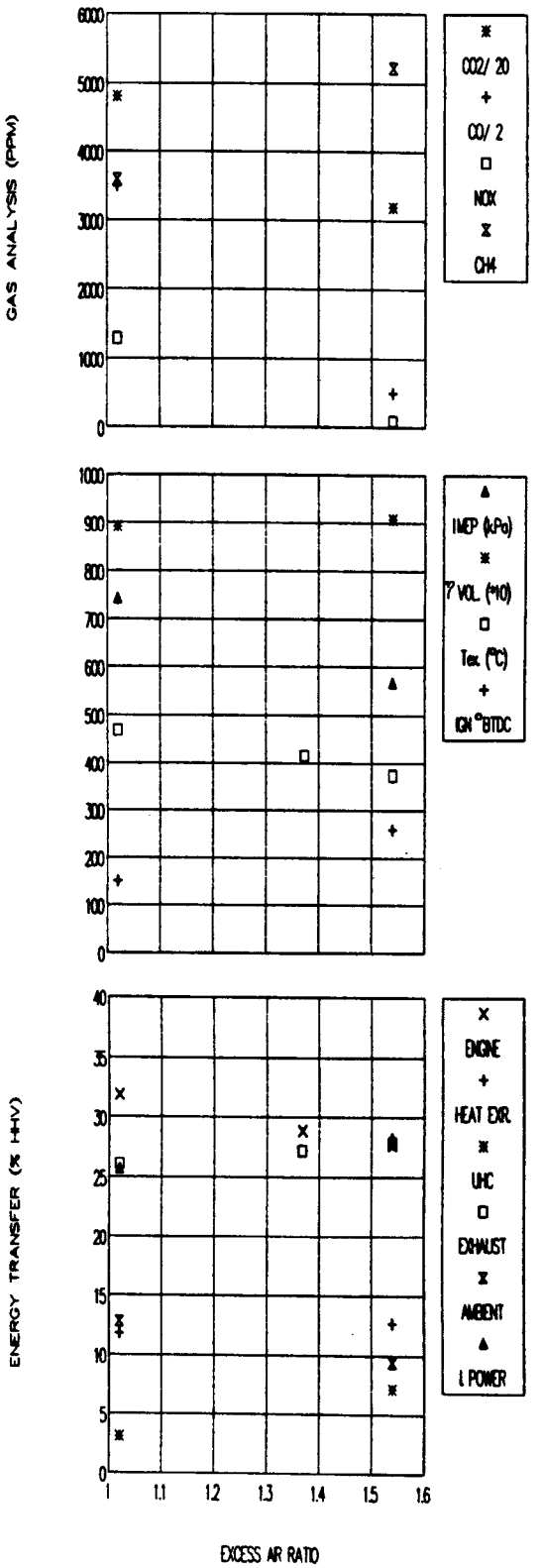

APPENDIX III - COMPUTER PROGRAMMES

Introduction

The following pages include the listings of the performance analysis programme and the thermodynamic engine model. Representative output from the extensive software developed for the single cycle analysis of pressure-crankangle data is also presented. Output from the mean cycle analysis is illustrated in the various figures in Appendix I.

```
C  ********************************************************
C  *     PROGRAMME TO EVALUATE TEST RESULTS                *
C  ********************************************************
C
C
C
C      INPUT DATA REQUIRED
C      *******************
C      *******************
C
C
C      NTEST     -- TEST NUMBER
C      NDAT      -- NUMBER OF DATA POINTS
C      W         -- BRAKE LOAD (N)
C      RH        -- RELATIVE HUMIDITY
C      TIGN      -- IGNITION TIMING (DEG BTDC)
C*     GP        -- GAS POWER (KW)
C      GCV       -- GROSS CALORIFIC VALUE (MJ/M3) BASED ON GAS QUALITY
C      DATA
C      NCV       -- NET CALORIFIC VALUE (MJ/M3) BASED ON BG ANALYSIS
C*     SPEED     -- ENGINE SPEED (REV/S)
C**    ML        -- MOTORING LOAD (N)
C      BORE      -- BORE DIA. (MM)
C      STR       -- STROKE (MM)
C      CR        -- COMPRESSION RATIO
C      IHEAD     -- HEAD TYPE (1-TASK ENGINE ONLY,2-TASK ENGINE AND
C                   COMPRESSOR,3-BATHTUB,4-HRCC)
C      ICAM      -- CAMSHAFT TYPE(1-TASK A,2-TASK B,3-TASK C,4-OXPOLY D)
C      IVO       -- INLET VALVE OPENING (DEG.BTDC)
C      IVC       -- INLET VALVE CLOSING (DEG.ABDC)
C      EVO       -- EXHAUST VALVE OPENING (DEG.BBDC)
C      EVC       -- EXHAUST VALVE CLOSING (DEG.ATDC)
C      IVL       -- INLET VALVE LIFT (MM)
C      EVL       -- EXHAUST VALVE LIFT (MM)
C      IVD       -- INLET VALVE DIA. (MM)
C      EVD       -- EXHAUST VALVE DIA. (MM)
C
C      TEMPERATURE MEASUREMENTS (DEG C)
C      ********************************
C      T1        -- EXHAUST GAS IN TO HEAT EXCHANGER
C      T2        -- EXHAUST GAS OUT OF HEAT EXCHANGER
C**    T3        -- COOLANT IN TO BLOCK
C**    T4        -- COOLANT OUT OF HEAD
C**    T5        -- COOLANT IN TO EXHAUST HEAT EXCHANGER
C**    T6        -- COOLANT OUT OF EXHAUST HEAT EXCHANGER
C      T7        -- W/W HEAT EXCHANGER COLD IN
C      T8        -- W/W HEAT EXCHANGER COLD OUT
C**    T9        -- W/W HEAT EXCHANGER HOT IN
C**    T10       -- W/W HEAT EXCHANGER HOT OUT
C      T11       -- OIL IN TO BLOCK
C*     T12       -- AIR TEMPERATURE AT MIXER
C*     T13       -- GAS TEMPERATURE AT MIXER
C*     TMAN      -- MANIFOLD TEMPERATURE BASED ON ADIABATIC MIXING OF
C                   GAS AND AIR STREAMS
```

```
C*    T14       -- EXHAUST GAS OUT OF CYLINDER HEAD
C**   T15       -- GAS SAMPLE TEMPERATURE
C     TATM      -- ATMOSPHERIC TEMPERATURE
C     TGAS      -- TEMPERATURE OF GAS AT SATURATOR
C
C     GAS ANALYSIS (PPM & %)
C     **********************
C**   G1        -- CO2
C**   G2        -- CO
C** * G3        -- O2
C**   G4        -- NOX
C**   G5        -- CH4
C
C     FLOW MEASUREMENT
C     ****************
C*    WFH       -- HOT WATER FLOW RATE (L/MIN)
C     WFC       -- COLD WATER FLOW RATE (CC/S)
C     GF        -- GAS FLOW (DM**3/HR)
C     AFW       -- AIR FLOW (MM H2O)
C
C     PRESSURE MEASUREMENT
C     ********************
C     PATM      -- ATMOSPHERIC PRESSURE(MBAR)
C     PGAS      -- GAS PRESSURE (MM H2O)
C*    PIN       -- MANIFOLD PRESSURE (MM H2O)
C     PG1       -- PARTIAL PRESSURE OF WATER VAPOUR IN GAS WITH
C                  GAS SATURATED AT SAME TEMPERATURE (MBAR)
C     PG2       -- PARTIAL PRESSURE OF WATER VAPOUR IN AIR WITH
C                  AIR SATURATED AT SAME TEMPERATURE (MBAR)
C     POIL      -- ENGINE OIL PRESSURE (PSI)
C
C
C     GAS QUALITY DATA ON TEST DATE
C     *****************
C     CO2       -- CARBON DIOXIDE IN FUEL (%)
C     CH4       -- METHANE IN FUEL (%)
C     C2H6      -- ETHANE IN FUEL (%)
C     C3H8      -- PROPANE IN FUEL (%)
C     C4H10     -- ISOBUTANE IN FUEL (%)
C     N2        -- NITROGEN IN FUEL (%)
C     SG        -- RELATIVE DENSITY OF FUEL
C     STV       -- STOICHIOMETRIC AIR TO FUEL RATIO BY VOLUME
C
C     INDICATED POWER
C     ***************
C     PTHETA    -- INTEGRATED PRESSURE VOLUME (W)
C
C
C     FORMAT FOR INPUT DATA
C     *********************
C     *********************
C
C
C     BORE,STR,CR,IHEAD,ICAM,IVO,IVC,EVO,EVC,IVL,EVL,IVD,EVD
```

```
C     NDATE
C     NTEST,NDAT
C     SG,STV
C     CO2,CH4,N2,C2H6,C3H8,C4H10 (GAS QUALITY ON THE TEST DATE)
C     PATM,TATM,RH,PG1,PG2,GCV,NCV,POIL,TGAS
C     PTHETA(1) TO PTHETA(NDAT)
C     W,SPEED,GF,GP,WFH,WFC,TIGN
C     PGAS,PIN,AFW
C     T1
C
C     T14
C     G1
C
C     G5
C     ML
C
C
C
C     ENGINE PERFORMANCE DATA CALCULATED
C     **********************************
C     **********************************
C
C
C*    MP      -- MOTORING POWER (KW)
C*    MMEP    -- MOTORING M.E.P. (BAR)
C*    FRSAE   -- FRICTION POWER ACCORDING TO SAE J816B (KW)
C*    EFR     -- ENGINE FRICTION 20.75:1 (W)
C*    EFR2    -- ENGINE FRICTION NO LOAD (W)
C*    PISFR   -- PISTON FRICTION (W)
C*    CRKFR   -- CRANKSHAFT FRICTION (W)
C*    VTFR    -- VALVE TRAIN FRICTION (W)
C*    MFRB    -- MOTORING FRICTION, BISHOP, (W)
C*    PISFRB -- PISTON FRICTION, BISHOP, (W)
C*    JBFRB   -- JOURNAL BEARING FRICTION, BISHOP, (W)
C*    VTFRB   -- VALVE TRAIN FRICTION, BISHOP, (W)
C*    VPFRB   -- VALVE PUMPING FRICTION, BISHOP (W)
C*    BBFRB   -- HEAT AND MASS LOSS, BISHOP (W)
C*    PUFRB   -- PUMPS FRICTION, BISHOP, (W)
C*    ENFRB   -- JBFRB+PISFRB+VTFRB: ENGINE FRICTION, BISHOP (W)
C                (PISTON FRICTION EVALUATED AT CR OF TEST)
C*    BLWBY   -- ENERGY LOSS TO BLOWBY, FUEL AND HEAT (W)
C     PTHETA -- INTEGRATED INDICATED POWER (W)
C*    IP      -- INDICATED POWER - BRAKE POWER+ENGINE FRICTION (KW)
C*    IPC     -- CORRECTED INDICATED POWER TO SAE J1349 (KW)
C*    IMEP    -- INDICATED M.E.P. BASED ON BRAKE POWER AND
C                ENGINE FRICTION (BAR)
C*    PIMEP   -- INDICATED M.E.P. BASED ON INTEGRATED P/VOL (BAR)
C*    ITEFF   -- INDICATED THERMAL EFFICIENCY (%)
C*    FC      -- FAN AND REAR BEARING LOAD (N)
C*    FAP     -- FAN AND REAR BEARING POWER (W)
C*    TQ      -- TORQUE (NM)
C*    BP      -- BRAKE POWER (KW)
C*    BPC     -- CORRECTED BRAKE POWER TO SAE J1349 (KW)
C*    TEFF    -- BRAKE THERMAL EFFICIENCY
```

```
C     TEFFI  -- 1/BRAKE THERMAL EFFICIENCY
C*    E      -- VOLUME RATIO OF UNBURNT METHANE IN EXHAUST TO
C               VOLUME INDUCTED
C*    CH4LS  -- FUEL LOSS TO ATMOSPHERE (W)
C*    BMEP   -- BRAKE MEAN EFFECTIVE PRESSURE (BAR)
C*    PHI    -- FUEL / AIR EQUIVALENCE
C***  ALPHA  -- NUMBER OF CARBON ATOMS PER MOL OF FUEL
C***  BETA   -- NUMBER OF HYDROGEN ATOMS PER MOL OF FUEL
C***  DELTA  -- NUMBER OF OXYGEN ATOMS PER MOL OF FUEL
C***  GAMMA  -- NUMBER OF NITROGEN ATOMS PER MOL OF FUEL
C***  STM    -- STOICHIOMETRIC AIR TO FUEL RATIO BY MASS
C***  RMM    -- RELATIVE MOLECULAR MASS OF FUEL
C     PS1    -- PARTIAL PRESSURE OF WATER VAPOUR IN GAS (MBAR)
C*    PS2    -- PARTIAL PRESSURE OF WATER VAPOUR IN AIR (MBAR)
C     PS1STP -- PARTIAL PRESSURE OF WATER VAPOUR IN GAS AT STP (MBAR)
C*    PMAN     -- ATMOSPHERIC + MANIFOLD + VAPOUR PRESSURE (N/M**2)
C*    MDOTG  -- MEASURED DRY GAS MASS FLOW RATE (KG/S)
C*    AFRC   -- AIR/FUEL RATIO BY MASS
C*    AFRM   -- AIR/FUEL RATIO BY MASS BASED ON AIR FLOW
C*    EXAIR  -- EXCESS AIR RATIO
C*    EXAIRM -- EXCESS AIR RATIO BASED ON AIR FLOW
C*    MDOTA  -- CALCULATED DRY AIR MASS FLOW RATE (KG/S)
C*    MDOTAM -- WET AIR MASS FLOW RATE BASED ON AIR FLOW (KG/S)
C*    VDOTA  -- CALCULATED DRY AIR VOLUME FLOW RATE (M**3/S)
C*    VDOTAM -- WET AIR VOLUME FLOW RATE BASED ON AIR FLOW (KG/S)
C     VDOTG  -- MEASURED DRY GAS VOLUME FLOW RATE (L/HR)
C     VDOTO  -- OIL VOLUME FLOW RATE (M**3/S)
C     AVDOT  -- VOLUME FLOW RATE OF EXHAUST
C               TO GAS ANALYSER (M**3/S)
C*    Z      -- MASS RATIO OF BLOWBY TO INCOMING CHARGE
C*    MS2    -- WATER VAPOUR WITH AIR MASS FLOW RATE (KG/S)
C     MS2M   -- WATER VAPOUR WITH AIR MASS FLOW RATE BASED ON AIR FLOW
C               (KG/S)
C*    MS1    -- WATER VAPOUR WITH GAS MASS FLOW RATE (KG/S)
C*    MDOTS  -- MASS FLOW RATE OF WATER VAPOUR IN TO ENGINE (KG/S)
C     MDOTSM -- MASS FLOW RATE OF WATER VAPOUR IN TO ENGINE BASED
C               ON MEASURED AIR FLOW (KG/S)
C*    AMDOT  -- MASS FLOW RATE OF EXHAUST GAS TO
C               GAS ANALYSER (KG/S)
C     ROEA   -- DENSITY OF AIR AT MANIFOLD (KG/M**3)
C*    ROEI   -- DENSITY OF AIR AND GAS AT INLET MANIFOLD (KG/M**3)
C     VEDIC  -- VOLUMETRIC EFFICIENCY BASED ON DRY AIR AT THE INLET
C               MANIFOLD CONDITIONS AND THE CALCULATED AIR FLOW RATE
C     VEDIM  -- VOLUMETRIC EFFICIENCY BASED ON DRY AIR AT THE INLET
C               MANIFOLD CONDITIONS AND THE MEASURED AIR FLOW RATE
C     VEWAC  -- VOLUMETRIC EFFICIENCY BASED ON WET AIR IN THE
C               ATMOSPHERE AND THE CALCULATED AIR FLOW RATE
C     VEWAM  -- VOLUMETRIC EFFICIENCY BASED ON WET AIR IN THE
C               ATMOSPHERE AND THE MEASURED AIR FLOW RATE
C     VEDAC  -- VOLUMETRIC EFFICIENCY AIR ONLY BASED ON DRY AIR IN
C               THE ATMOSPHERE AND THE CALCULATED AIR FLOW RATE
C     VEDAM  -- VOLUMETRIC EFFICIENCY AIR ONLY BASED ON DRY AIR IN
C               THE ATMOSPHERE AND THE MEASURED AIR FLOW RATE
C*    VE     -- VOLUMETRIC EFFICIENCY AIR AND GAS BASED ON INLET
```

```
C                MANIFOLD CONDITIONS
C      QTOTH  -- TOTAL HEAT TRANSFER TO COOLANT BASED ON HOT SIDE (W)
C      QTOTC  -- TOTAL HEAT TRANSFER TO COOLANT BASED ON COLD SIDE (W)
C*     QEN    -- HEAT TRANSFER TO COOLANT FROM ENGINE (W)
C*     QEXH   -- HEAT TRANSFER TO COOLANT FROM EXHAUST BASED ON
C                HOT SIDE (W)
C*     QEXC   -- HEAT TRANSFER TO COOLANT FROM EXHAUST BASED ON
C                COLD SIDE (W)
C*     QEXL   -- HEAT LOSS FROM EXHAUST MANIFOLD (W)
C*     QLEX   -- ENERGY LOSS FROM EXHAUST TO ATMOSPHERE (W)
C*     QAN    -- ENERGY LOSS TO GAS ANALYSERS (W)
C      QENC   -- ENERGY LOSS TO ENGINE ENCLOSURE (W)
C*     QENEX  -- HEAT TRANSFER TO ENGINE + EXHAUST HEAT EXCHANGER
C                HOT SIDE (W)
C*     QOIL   -- HEAT TRANSFER TO OIL (W)
C*     AMB    -- HEAT LOSS TO AMBIENT (W)
C*     BLBY   -- ENERGY LOSS TO BLOWBY (W)
C      BTOTH  -- ENERGY BALANCE:TOTAL HEAT TRANSFER TO COOLANT
C                BASED ON HOT SIDE (%)
C      BTOTC  -- ENERGY BALANCE:TOTAL HEAT TRANSFER TO COOLANT
C                BASED ON COLD SIDE (%)
C*     BEN    -- ENERGY BALANCE:HEAT TRANSFER TO COOLANT FROM
C                ENGINE(%)
C*     BEXH   -- ENERGY BALANCE:HEAT TRANSFER TO COOLANT FROM
C                EXHAUST BASED ON HOT SIDE (%)
C      BEXC   -- ENERGY BALANCE:HEAT TRANSFER TO COOLANT FROM
C                EXHAUST BASED ON COLD SIDE (%)
C*     BENEX  -- ENERGY BALANCE:HEAT TRANSFER TO COOLANT +
C                EXHAUST HEAT EXCHANGER HOT SIDE (%)
C*     BLEX   -- ENERGY BALANCE:ENERGY LOSS FROM EXHAUST TO ATMOSPHERE
C                (%)
C*     BEXL   -- ENERGY BALANCE:ENERGY LOSS FROM MANIFOLD (%)
C*     BIP    -- ENERGY BALANCE:SHAFT POWER + ENGINE FRICTION (%)
C*     BPTHA  -- ENERGY BALANCE:INTEGRATED INDICATED POWER (%)
C*     BCH4LS -- ENERGY BALANCE:UNBURNT FUEL (%)
C*     BBLBY  -- ENERGY BALANCE:BLOWBY (%)
C*     BAN    -- ENERGY BALANCE: ENERGY TO GAS ANALYSER (%)
C*     BOIL   -- ENERGY BALANCE: ENERGY TO OIL (W)
C      BENG   -- ENERGY BALANCE:ENERGY TO ENGINE
C                ENCLOSURE (%)
C*     BPISFR -- ENERGY BALANCE:PISTON FRICTON (%)
C      BEFR   -- ENERGY BALANCE:MEASURED ENGINE FRICTION
C                AT 20.75:1 (%)
C*     BBP    -- ENERGY BALANCE:ENERGY TO SHAFT (%)
C      BMP    -- ENERGY BALANCE:ENERGY TO MOTOR THE ENGINE (%)
C*     SUM    -- ENERGY BALANCE: ALL MEASURED ENERGY TRANSFERS (%)
C**** COBP   -- CARBON MONOXIDE IN EXHAUST BRAKE POWER BASIS (G/kWHR)
C**** CO2BP  -- CARBON DIOXIDE IN EXHAUST BRAKE POWER BASIS (G/kWHR)
C**** O2BP   -- OXYGEN IN EXHAUST BRAKE POWER BASIS (G/kWHR)
C**** CH4BP  -- METHANE IN EXHAUST BRAKE POWER BASIS (G/kWHR)
C**** NOXBP  -- OXIDES OF NITROGEN IN EXHAUST BRAKE POWER BASIS
C                (G/kWHR)
C**** COCP,COHP ETC REFER TO CHP AND HEAT PUMP MODE RESPECTIVELY
C
```

```
C
C
      REAL MDOTG,MDOTA,MDOTS,MS1,MS2,MDOTAM,IVO,IVC,ILIFT,IVD
     X,ML,MP,MMEP,MS1M,MS2M,MDOTSM,ITEFF,IP,IMEP,MW,N2,N,NCV,IPC
     X,MMEPB,MFRB,JBMEPB,JBFRB,NOXM,MASSF,NOXM1,MWEX,K1,K2,K3
     X,IPSAE,MESAE,MASCY,NOXBP,NOXCP,NOXHP
C
      COMMON ALPHA,BETA,GAMMA,DELTA
C
      DIMENSION W(50),SPEED(50),T(15,50),GF(50),GP(50),G(5,50),
     XWFH(50),WFC(50),TIGN(50),BP(50),TEFF(50),BMEP(50),PHI(50)
     X,VEDIC(50),VEDAC(50),VE(50),QTOTH(50),QEN(50),PGAS(50),PIN(50),
     XAFW(50),FC(50),AFRC(50),G2PLT(50),G4PLT(50),TEFFI(50),EXAIRM(50)
     X,EXAIR(50),FAP(50),QTOTC(50),QEXH(50),QEXC(50),QLEX(50),BLBY(50)
     X,BTOTH(50),BTOTC(50),BEN(50),BEXH(50),BEXC(50),BBP(50),BMP(50)
     X,BLEX(50),AFRM(50),ML(50),MMEP(50),MP(50),TEFG(50),G5PLT(50)
     X,VEDIM(50),VEWAM(50),VEWAC(50),VEDAM(50),TQ(50),ITEFF(50),IP(50)
     X,IMEP(50),MW(10),QEXL(50),BEXL(50),CH4LS(50),BCH4LS(50)
     X,BBLBY(50),Z(50),PISFR(50),BPISFR(50),EFR(50),BIP(50),IPC(50)
     X,BPC(50),PUFRB(50),VTFRB(50),JBFRB(50),PISFRB(50),MFRB(50)
     X,CRKFR(50),VTFR(50),FRSAE(50),TMAN(50),GW(5,50),GW1(5,50)
     X,COM(50),CO2M(50),CH4M(50),NOXM(50),O2M(50),COM1(50),CO2M1(50)
     X,O2M1(50),CH4M1(50),NOXM1(50),QAN(50),VPFRB(50),BBFRB(50)
     X,EFRB(50),BAN(50),BOIL(50),EFR2(50),BEFR(50),BENC(50),SUM(50)
     X,BENEX(50),QENEX(50),AMB(50),PTHETA(50),BPTHA(50),PIMEP(50)
     X,MASCY(50),COBP(50),CO2BP(50),O2BP(50),CH4BP(50),NOXBP(50)
     X,COCP(50),CO2CP(50),O2CP(50),CH4CP(50),NOXCP(50),COHP(50),
     XCO2HP(50),O2HP(50),CH4HP(50),NOXHP(50)
C
C
C     SET MOLECULAR WEIGHTS (H,C,N,O,CO2,CH4,N2,C2H6,C3H8,C4H10)
C     ***************************************************
C
      DATA MW/1.00797,12.011,14.008,15.994,44.01,16.043,28.013,
     X30.07,44.097,58.124/
C
C
C
C     OPEN DATA FILE AND READ IN EXPERIMENTAL DATA
C     ********************************************
C
      OPEN(UNIT=5,FILE='TEST.DAT')
      READ(5,*)BORE,STR,CR,IHEAD,ICAM,IVO,IVC,EVO,EVC,
     XILIFT,ELIFT,IVD,EVD
      READ(5,*)NDATE
      READ(5,*)NTEST,NDAT
      READ(5,*)SG,STV
      READ(5,*)CO2,CH4,N2,C2H6,C3H8,C4H10
      READ(5,*)PATM,TATM,RH,PG1,PG2,GCV,NCV,POIL,TGAS
      DO 10 I=1,NDAT
      READ(5,*)W(I),SPEED(I),GF(I),GP(I),WFH(I),WFC(I),TIGN(I)
     X,PTHETA(I)
C
```

```
C     CALIBRATE SPEED (300 < N < 1200 RPM)
C
      IF(SPEED(I).LT.5.0.OR.SPEED(I).GT.40.0)
     XPRINT*,'SPEED CORRELATIONS INNAPROPRIATE'
      IF(SPEED(I).LT.20.0)SPEED(I)=SPEED(I)*0.473+12.288
C
C     CALIBRATE GAS FLOW RATE
C
      GP(I)=GP(I)*GCV/38.6
C
      READ(5,*)PGAS(I),PIN(I),AFW(I)
C
C     CALIBRATE COOLANT FLOW RATE
C
      IF(NTEST.LE.3)WFH(I)=WFH(I)*0.9275+0.1095
      IF(NTEST.GT.3.AND.NTEST.LE.6)WFH(I)=WFH(I)*0.938+0.023
      IF(NTEST.GT.6.AND.NTEST.LE.19)WFH(I)=WFH(I)*1.027-0.06
      IF(NTEST.GT.19)WFH(I)=WFH(I)*1.03-0.077
C
C     CALIBRATE MANIFOLD PRESSURE
C
      IF(PIN(I).GE.14.)PIN(I)=PIN(I)*1.163-1.698
C
      DO 15 J=1,15
      READ(5,*)T(J,I)
   15 CONTINUE
C
C     CALIBRATE GAS AND AIR INLET TEMPERATURES AND THE EXHAUST
C     TEMPERATURE (GAS AND AIR TO MIG EXHAUST TO T1 AND MIG)
C
      T(12,I)=T(12,I)*1.08+0.696
      IF(NTEST.GT.34)T(13,I)=T(13,I)*1.139-1.2
      T(14,I)=T(14,I)*0.7876+27.188
C
C     CORRECT THERMOCOUPLES FOR RADIATIVE HEAT TRANSFER
C
C     READ IN GAS ANALYSIS AND CORRECT OXYGEN CONCENTRATION
C
      DO 20 K=1,5
      READ(5,*)G(K,I)
      IF(K.EQ.3)G(K,I)=G(K,I)-1.0
   20 CONTINUE
      READ(5,*)ML(I)
   10 CONTINUE
C     PRINT*,'ENTER THE HEAT TRANSFER TO THE ENGINE ENCLOSURE (W)'
C     READ(1,*)QENC
      CLOSE (UNIT=5)
C     PRINT*,T(3,1),T(4,1),T(5,1),T(6,1),WFH(1)
C
C
```

```
C      CALCULATE RESULTS
C      *****************
C
C      OIL PROPRTIES BASED ON SAE 15W/40. VISCOSITY AT 65 DEG.C,
C      DENSITY SEE SHELL DATA. SPECIFIC HEAT AT 60 DEG. C
C
       ROOIL=885.0
       VISCK=43.0/1E6
       CPOIL=2047.0
       VDOTO=15.47/1E6
C
       TCV=15.0
       TCK=65.0
       HFG=2258.0
       PI=3.1416
       VS=0.12638
C
C      UNBURNT MIXTURE/TOTAL MASS WITHIN RING CREVICE
C
       UNM=0.6
C
C      CP VALUES FOR AIR AND METHANE AT CRANKCASE TEMPERATURE OF 338K
C      SEE ROGERS AND MAYHEW STEAM TABLES.
C
       CPAIR=1007.2
       CPG=2328.0
C
       PBAR=PATM/1000.0
       PS1STP=17.04
       ROASTP=1.224799
C
C      CALCULATE COMPOSITION OF GAS, STOICHIOMETRIC A/F RATIO BY MASS
C      AND CALORIFIC VALUE ON MASS BASIS
C
       C=MW(2)/100.0*(CH4+CO2+2*C2H6+3*C3H8+4*C4H10)
       HY=MW(1)/100.0*(4*CH4+6*C2H6+8*C3H8+10*C4H10)
       O=MW(4)/100.0*CO2*2.0
       N=MW(3)/100.0*N2*2.0
       RMM=C+HY+O+N
       ALPHA=C/MW(2)
       BETA=HY/MW(1)
       GAMMA=O/MW(4)
       DELTA=N/MW(3)
       STM=STV/SG
       GCVM=GCV/ROASTP/SG
C      PRINT*,RMM
C
       DO 25 I=1,NDAT
C
       Q2=VS/1E3*SPEED(I)/2.0
C
C      CALCULATE ENGINE FRICTION AT 20.75:1 AND NO LOAD
C
       ENMEP=1155.0*SPEED(I)+104769
```

```
      EFR(I)=ENMEP*Q2
      ENMEP2=2104*SPEED(I)+64109
      EFR2(I)=ENMEP2*Q2
C
C     CALCULATE PISTON FRICTION
C
      PSMEP=388.0*SPEED(I)+46210
      PISFR(I)=PSMEP*Q2
C
C     CALCULATE THE CRANKSHAFT FRICTION
C
      CKMEP=1602.0*SPEED(I)+13135
      CRKFR(I)=CKMEP*Q2
C
C     CALCULATE VALVE TRAIN FRICTION
C
      VTMEP=156.0*SPEED(I)+3957
      VTFR(I)=VTMEP*Q2
C
C     CALCULATE POWER REQUIRED TO DRIVE DYNAMOMETER AND
C     THE ENGINE REAR BEARING
C
      RBMEP=478.2*SPEED(I)-456.0
      FANMEP=10.1*SPEED(I)**2.0+209.0*SPEED(I)+177.0
C     PRINT*,RBMEP,FANMEP
      FBMEP=RBMEP+FANMEP
      FC(I)=FBMEP*VS/1E3/PI
      FAP(I)=FBMEP*Q2
C
C     CALCULATE MOTORING POWER
C
      MP(I)=(ML(I)-FC(I))*2.0*PI*SPEED(I)*0.25/1000.0
C
C     CALCULATE FRICTION COMPONENTS ACCORDING TO BISHOP
C
      UP=2*STR*SPEED(I)/1000.0
      RE=UP*BORE/VISCK/1000.0
      EM=37.265/2.0
      K1=1.8
      K2=0.666
      K3=0.053
C
C     MOTORING POWER
C
      MMEPB=5089.0*SPEED(I)+5385.0*CR+80671.5
      MFRB(I)=MMEPB*Q2
C
C     PISTON FRICTION
C
C     wall tension of rings
C
      PFWT=369.97*1E3*STR*3.0/(BORE**2.0)
C
```

```
C     gas pressure on rings
C
      PFGP=411.08*1E3*STR/(BORE**2.0)*
     X(0.088*CR+0.182*(CR**(1.33-0.024*UP)))
C
C     piston and rings viscous friction
C
      PFVISC=756.04*1E3*EM*UP/BORE/STR
C
      PSMEPB=PFWT+PFGP+PFVISC
      PISFRB(I)=PSMEPB*Q2
C
C     JOURNAL BEARING FRICTION
C
C     crankshaft
C
      CKFR=413.7*BORE/STR*SPEED(I)*K1
C
C     con rod
C
      CRDFR=413.7*BORE/STR*SPEED(I)*K2
C
C     camshaft
C
      CMFR=413.7*BORE/STR*SPEED(I)*K3
C
      JBMEPB=CKFR+CRDFR+CMFR
      JBFRB(I)=JBMEPB*Q2
C
C     VALVE TRAIN FRICTION
C
      VTMEPB=393166.4*(30.0-0.24*SPEED(I))*IVD**1.75
     X/BORE**2.0/STR
CB    VTMEPG=VTMEPB+CMFR
C
C     Piston friction no load
C
CB    PSMEPG=PSMEPB+CRDFR-PFGP
C
C    Piston friction with load (includes gas pressure on rings)
C
CB    PSMEPG=PSMEPB+CRDFR
      VTFRB(I)=VTMEPB*Q2
C
C     VALVE PUMPING
C
      EF=IVD**2.0/VS/1000.0
      VPMEPB=304.18*SPEED(I)**1.7/EF**1.28
      VPFRB(I)=Q2*VPMEPB
C
C     PUMPS FRICTION
C
      PUMEPB=39.52*SPEED(I)**1.5
      PUFRB(I)=PUMEPB*Q2
```

```
C
C     HEAT AND MASS LOSS
C
      BBMEPB=6.895*1E3*(1.72*CR**0.4-(0.49+0.015*CR)
     X*((0.06*SPEED(I))**1.185))
      BBFRB(I)=BBMEPB*Q2
C
C     ENGINE FRICTION AT TEST COMPRESSION RATIO
C
      ENMEPB=PSMEPB+JBMEPB+VTMEPB
      EFRB(I)=ENMEPB*Q2
CB    ENMEPG=PSMEPG+CKFR+VTMEPG
CB    PRINT*,VTMEPG,CKFR,PSMEPG,ENMEPG
C
C     CALCULATE MASS RATIO OF BLOWBY/INCOMING CHARGE
C
      Z(I)=(-0.3*SPEED(I)+14.26)/100
C
C     CALCULATE POWER AND THERMAL EFFICIENCY
C
      TQ(I)= (W(I)+FC(I))*0.25
      BP(I)=TQ(I)*2*PI*SPEED(I)/1000
      TEFF(I)=BP(I)/GP(I)*100.0
      TEFFI(I)=1.0/TEFF(I)
      IP(I)=EFR(I)/1000.0+BP(I)
      ITEFF(I)=IP(I)/GP(I)*100.0
C     PRINT*,TEFF(I),ITEFF(I)
C
C     CORRECT BRAKE POWER ACCORDING TO SAE J1349
C
      PS2=PG2*RH
      PA=PATM-PS2
      PMAN=PA*100.0-PIN(I)*9.81
      IPC(I)=IP(I)*(99000/PMAN)*((T(12,I)+273.0)/298.0)**0.5
      BPC(I)=IPC(I)-EFR(I)/1000.0
C     PRINT*,IPC(I),BPC(I)
C
C
C     CALCULATE MEAN EFFECTIVE PRESSURES
C
      BMEP(I)=20*BP(I)/VS/SPEED(I)
      MMEP(I)=20*MP(I)/VS/SPEED(I)
      IMEP(I)=IP(I)/SPEED(I)/VS*20.0
      PIMEP(I)=0.02*PTHETA(I)/VS/SPEED(I)
C
C     CALCULATE FRICTION POWER ACCORDING TO SAE J816B
C
      Z10=16.3761+2.28629*(SPEED(I)*0.06)+0.297053
     X*(SPEED(I)*0.06)**2.0
      Z20=0.01*(5.44659-0.02495*(SPEED(I)*0.06)
     X-0.174376*(SPEED(I)*0.06)**2.0)
      MESAE=1.0/(1.0+(6.89*Z10-BMEP(I)*Z20*100.0)
     X/(BMEP(I)*100.0))
      IPSAE=BP(I)/MESAE
```

```
      FRSAE(I)=(IPSAE-BP(I))*1000.0
C
C     CALCULATE EXCESS AIR RATIO BASED ON EXHAUST GAS ANALYSIS
C
      Y2=BETA/ALPHA/2.0*(G(1,I)/100+G(2,I)/100)/
     X(1+G(2,I)/100/3.5/G(1,I)*100)
      PHI(I)=2*(1+0.25*BETA/ALPHA-0.5*GAMMA/ALPHA)*
     X(G(1,I)/100+G(2,I)/100+G(5,I)*1E-6)/(2*G(1,I)/100
     X+Y2+2*G(3,I)/100+G(2,I)/100)
      EXAIR(I)=1.0/PHI(I)
      AFRC(I)=STM/PHI(I)
C
C     CALCULATE WET SPECIES CONCENTRATION ACCORDING TO SPINDT
C
      Y2W=Y2/(Y2+1)
      GW(1,I)=G(1,I)/100.0*(1-Y2W)
      GW(2,I)=G(2,I)/100.0*(1-Y2W)
      GW(3,I)=G(3,I)/100.0*(1-Y2W)
      GW(4,I)=G(4,I)/1E6
      GW(5,I)=G(5,I)/1E6*(1-Y2W)
C
C     CALCULATE WET SPECIES CONCENTRATION ACCORDING TO SAE J1088
C
      CORR=1.0-(1.21/AFRC(I)+0.0407)
      GW1(1,I)=G(1,I)*CORR/100.0
      GW1(2,I)=G(2,I)*CORR/100.0
      GW1(3,I)=G(3,I)*CORR/100.0
      GW1(4,I)=G(4,I)/1E6
      GW1(5,I)=G(5,I)*CORR/1E6
C
C     CALCULATE EXHAUST ON MASS BASIS ACCORDING TO SAE J1088
C
      VDOTG=GF(I)
      MDOTG=VDOTG*1E-3*ROASTP*SG/3600
      MDOTA=MDOTG*AFRC(I)
      MASSF=(MDOTA+MDOTG)*1000.0*3600.0
      MASCY(I)=(MDOTA+MDOTG)*1000.0*2.0/SPEED(I)
C     PRINT*,MASCY,PTHETA(I)
C     PRINT*,MDOTG,MDOTA
      COM1(I)=GW1(2,I)*MASSF*(MW(2)+MW(4))/29.0
      CO2M1(I)=GW1(1,I)*MASSF*(MW(2)+2*MW(4))/29.0
      O2M1(I)=GW1(3,I)*MASSF*2.0*MW(4)/29.0
      CH4M1(I)=GW1(5,I)*MASSF*(MW(2)+4*MW(1))/29.0
      NOXM1(I)=GW1(4,I)*MASSF*(MW(3)+2*MW(4))/29.0
C
C     CALCULATE EXHAUST ON MASS BASIS ACCORDING TO SPINDT
C
      CALL GASPR(PBAR,PHI(I),TCV,H,CP,MWEX,VM)
      COM(I)=GW(2,I)*MASSF*(MW(2)+MW(4))/MWEX
      CO2M(I)=GW(1,I)*MASSF*(MW(2)+2*MW(4))/MWEX
      O2M(I)=GW(3,I)*MASSF*2.0*MW(4)/MWEX
      CH4M(I)=GW(5,I)*MASSF*(MW(2)+4*MW(1))/MWEX
      NOXM(I)=GW(4,I)*MASSF*(MW(3)+2*MW(4))/MWEX
C     PRINT*,COM1(1),CO2M1(1),O2M1(1),CH4M1(1),NOXM1(1)
```

```
C     PRINT*,COM(1),CO2M(1),O2M(1),CH4M(1),NOXM(1)
C
C     CALCULATE EXCESS AIR RATIO BASED ON GAS AND AIR FLOWS
C
      TA=TATM+273.15
      VDOTAM=0.4622/3600*AFW(I)
C
C     CALCULATE AIR AND GAS VOLUME FLOW IN L/MIN FOR BLOWBY COMPARISON
C
      AIR=462.2/60.*AFW(I)
      GAS=GF(I)/60.
      AGMESD=GAS+AIR
C     PRINT*,AGMESD
      MDOTAM=VDOTAM*PATM*100/287/TA
      DIFAIR=(MDOTA-MDOTAM)/MDOTA
C     PRINT*,DIFAIR
      AFRM(I)=MDOTAM/MDOTG
      EXAIRM(I)= AFRM(I)/STM
C
C     CALCULATE MASS FLOW RATE OF VAPOUR WITH GAS AND AIR
C
      PS1=PG1
      PG=PATM+PGAS(I)*0.0981-PS1
      VDOTA=MDOTA*287*TA/PA/100
      MS2=PS2*100.0*VDOTA/8314.0*18.0/TA
      MS2M= PS2*100.0*VDOTAM/8314.0*18.0/TA
      MS1=101325.0/(PG*100)/288.15*VDOTG*1E-3/3600*PS1*100*18/8314
      MDOTS=MS1+MS2
      PRINT*, VDOTA,VDOTG
C
C     CALCULATE MANIFOLD TEMPERATURE OF MIXTURE BASED ON ADIABATIC
C     MIXING OF GAS AND AIR STREAMS ( CPG1- LINEAR INTERPOLATION FOR
C     METHANE 2-52 DEG. C, CPAIR1- AIR AT 26.85 DEG. C )
C
      CPG1=2.68/1E3*T(13,I)+2.154
      CPAIR1=1.0049
      TMAN(I)=(MDOTG*CPG1*(T(13,I)+273.15)+MDOTA*CPAIR1*
     X(T(12,I)+273.15))/(MDOTG*CPG1+MDOTA*CPAIR1)
C     PRINT*,TMAN(I)
C
C     CALCULATE VOLUMETRIC EFFICIENCIES BASED ON:
C
      F=1/(1+1/AFRC(I)*29/RMM+MDOTS/MDOTA*29/18)
      F2=1/(1+MDOTG/MDOTAM*29/RMM+MDOTS/MDOTAM*29/18)
      ROEA=29.0/8314.0*(PATM*100.0-PIN(I)*9.81)/(T(12,I)+273.15)*F
      ROEA2=29.0/8314.0*(PATM*100.0-PIN(I)*9.81)/(T(12,I)+273.15)*F2
C
C     DRY AIR AT INLET MANIFOLD AND CALCULATED AIR FLOW
C
      VEDIC(I)=2*MDOTA/SPEED(I)/126.0/1E-6/ROEA*100
C
C     DRY AIR AT INLET MANIFOLD AND MEASURED AIR FLOW
C
      VEDIM(I)=2*MDOTAM/SPEED(I)/126.0/1E-6/ROEA2*100
```

```
C
C     WET AIR IN THE ATMOSPHERE AND MEASURED AIR FLOW
C
      VEWAM(I)=2*MDOTAM/SPEED(I)/126.0/1E-6/(PATM*100)*287*TA
C
C     WET AIR IN THE ATMOSPHERE AND THE CALCULATED AIR FLOW
C
      VEWAC(I)=2*MDOTA/SPEED(I)/126.0/1E-6/(PATM*100)*287*TA*100.0
C
C     DRY AIR IN THE ATMOSPHERE AND THE CALCULATED AIR FLOW
C
      VEDAC(I)=2*MDOTA/SPEED(I)/126/1E-6/PA/100*287*TA*100
C
C     DRY AIR IN THE ATMOSPHERE AND THE MEASURED AIR FLOW
C
      VEDAM(I)=2*MDOTAM/SPEED(I)/126/1E-6/PA/100*287*TA*100
C
C     AIR AND GAS AT THE MANIFOLD AND THE CALCULATED FLOWS
C
      RI=8314*(MDOTG/RMM+MDOTA/29+MDOTS/18)/(MDOTA+MDOTG+MDOTS)
      ROEI=(PATM*100.0-PIN(I)*9.81)/RI/TMAN(I)
      VE(I)=2*(MDOTA+MDOTG)/ROEI/126/1E-8/SPEED(I)
C
C     CALCULATE ENERGY TRANSFERS
C
      CALL GASPR(PBAR,PHI(I),T(14,I),H,CP,MWEX,VM)
      HX1=H
      CALL GASPR(PBAR,PHI(I),T(1,I),H,CP,MWEX,VM)
      HX2=H
      VM2=VM
      CALL GASPR(PBAR,PHI(I),T(2,I),H,CP,MWEX,VM)
      HX3=H
      CALL GASPR(PBAR,PHI(I),TCV,H,CP,MWEX,VM)
      HX4=H
      CALL GASPR(PBAR,PHI(I),TCK,H,CP,MWEX,VM)
      HX5=H
C     PRINT*,HX1,HX2,HX3,HX4,HX5
C
C     CALCULATE VOLUME OF UNBURNT METHANE PER VOLUME
C     PARTICIPATING IN COMBUSTION
C
      X=AFRC(I)*SG/4.76
      Y=1-G(1,I)/100-G(2,I)/100-G(3,I)/100-G(5,I)/1E6
      E=G(5,I)/1E6*X*3.76/Y
C
C     CALCULATE HEAT AND CHEMICAL ENERGY LOSS TO BLOWBY
C
C     ASSUME PROPORTIONS OF UNBURNED AND BURNED FUEL WITHIN RING
C     CAVITY OF 60 AND 40% RESPECTIVELY,
C     CRANKCASE TEMPERATURE OF 338K, ATMOSPHERIC PRESSURE
C
      Z1=Z(I)*(MDOTA+MDOTG)
      Z2=Z(I)*(MDOTA+MDOTG)*UNM
      Z3=Z(I)*(MDOTA+MDOTG)*(1-UNM)
```

```
C
      FLOSS =Z2/(AFRC(I)+1)/SG/ROASTP*GCV*1E6
      HLOSS1=Z2*(1/(AFRC(I)+1))*CPG*(TCK-TCV)
      HLOSS2=Z2*(AFRC(I)/(AFRC(I)+1))*CPAIR*(TCK-TCV)
      HLOSS3=Z3*(HX5-HX4)*1000.0
      HLOSS4=Z3/(AFRC(I)+1)/SG/ROASTP*(1-E)*(GCV-NCV)*1E6
      BLBY(I)=FLOSS+HLOSS1+HLOSS2+HLOSS3+HLOSS4
C     PRINT*,FLOSS,HLOSS1,HLOSS2,HLOSS3,HLOSS4,BLBY(I)
C
C     CALCULATE ENERGY OF THE UNBURNT FUEL IN THE EXHAUST PIPE
C
C     non reactive volume flow of methane to blowby
C
      X1=Z2/(AFRC(I)+1)/SG/ROASTP
C
      CH4LS(I)=E*(VDOTG/3600.0/1000.0-X1)*GCV*1E6
C
C     CALCULATE ENERGY LOSS TO GAS ANALYSERS
C
      AVDOT=7.5*1E-3/60.0
      AMDOT=AVDOT/VM2
      HLOSSA=AMDOT*(HX2-HX4)*1000.0
      HLOSSB=AMDOT/(AFRC(I)+1)/SG/
     XROASTP*(1-E)*(GCV-NCV)*1E6
      QAN(I)=HLOSSA+HLOSSB
C     PRINT*,QAN(I),HLOSSA,HLOSSB,AMDOT,VM2
C
C     CALCULATE HEAT TRANSFER TO OIL BASED ON MEASURED OIL FLOW,
C     DENSITY OF OIL AT 65 DEG. C, MEAN TEMPERATURE DIFFERENCE
C     OF 1.4 DEG. C, SPECIFIC HEAT CAPACITY AT 60 DEG. C
C
      QOIL=VDOTO*ROOIL*CPOIL*1.4
C
      HOIL=VDOTO*ROOIL*CPOIL*(T(11,I)-61.0)
C
      QTOTH(I)=WFH(I)/60.0*4.18*(T(9,I)-T(10,I))*1000.0
C     PRINT*,QTOTH(I)
      IF(NTEST.EQ.35)QTOTH(I)=QTOTH(I)-HOIL
      QTOTC(I)=WFC(I)/1000.0*4.18*(T(8,I)-T(7,I))*1000.0
      QEN(I)=WFH(I)/60.0*4.18*(T(4,I)-T(3,I))*1000.0
      IF(NTEST.EQ.35)QEN(I)=QEN(I)-HOIL
      QEXL(I)=(MDOTG+MDOTA-Z1)*(HX1-HX2)*1000.0
      QEXH(I)=(MDOTA+MDOTG-Z1-AMDOT)*(HX2-HX3)*1000.0
      QEXC(I)=WFH(I)/60.0*4.18*(T(6,I)-T(5,I))*1000.0
      QENEX(I)=QEN(I)+QEXH(I)
      HLOSI=(MDOTG+MDOTA-Z1-AMDOT)*(HX3-HX4)*1000.0
      HLOSII=(1-E)*(VDOTG*1E-3/3600.0-X1)*(GCV-NCV)*1E6
      QLEX(I)=(HLOSI+HLOSII-HLOSS4-HLOSSB)
C     PRINT*,QEXH(I),QEXL(I),HLOSI,QLEX(I),QOIL
C
C     CALCULATE ENERGY BALANCES
C
      BPISFR(I)=PISFR(I)/GP(I)/10.0
      BEFR(I)=EFR(I)/GP(I)/10.0
```

```
      BTOTH(I)=QTOTH(I)/GP(I)/10.0
      BTOTC(I)=QTOTC(I)/GP(I)/10.0
      BEN(I)=QEN(I)/GP(I)/10.0
      BEXH(I)=QEXH(I)/GP(I)/10.0
      BENEX(I)=BEXH(I)+BEN(I)
      BEXL(I)=QEXL(I)/GP(I)/10.0
      BLEX(I)=QLEX(I)/GP(I)/10.0
      BEXC(I)=QEXC(I)/GP(I)/10.0
      BBP(I)=BP(I)/GP(I)*100.0
      BIP(I)=IP(I)/GP(I)*100.0
      BPTHA(I)=PTHETA(I)/GP(I)/10.0
      BMP(I)=MP(I)/GP(I)*100.0
      BCH4LS(I)=CH4LS(I)/1000.0/GP(I)*100.0
      BBLBY(I)=BLBY(I)/1000.0/GP(I)*100.0
      BAN(I)=QAN(I)/1000.0/GP(I)*100.0
      BOIL(I)=QOIL/GP(I)/10.0
C     BENC(I)=QENC/GP(I)/10.0
      SUM(I)=BENEX(I)+BEXL(I)+BLEX(I)+BCH4LS(I)+BPTHA(I)
     X+BBLBY(I)+BAN(I)-BPISFR(I)
      AMB(I)=(100-SUM(I))*GP(I)*10.0
C
C     CALCULATE EXHAUST ON MASS TO BRAKE POWER BASIS ACCORDING
C     TO SPINDT
C
      COBP(I)=COM(I)/BP(I)
      CO2BP(I)=CO2M(I)/BP(I)
      O2BP(I)=O2M(I)/BP(I)
      CH4BP(I)=CH4M(I)/BP(I)
      NOXBP(I)=NOXM(I)/BP(I)
C
C     CALCULATE EXHAUST ON MASS TO BRAKE POWER AND HEAT RECLAIMED
C     BASIS ACCORDING TO SPINDT
C
      COCP(I)=COM(I)/(BP(I)+QENEX(I)/1000.)
      CO2CP(I)=CO2M(I)/(BP(I)+QENEX(I)/1000.)
      O2CP(I)=O2M(I)/(BP(I)+QENEX(I)/1000.)
      CH4CP(I)=CH4M(I)/(BP(I)+QENEX(I)/1000.)
      NOXCP(I)=NOXM(I)/(BP(I)+QENEX(I)/1000.)
C
C     CALCULATE EXHAUST ON MASS TO HEAT PUMP OUTPUT BASIS ACCORDING
C     TO SPINDT. COP AT 3
C
      COP=3.
      COHP(I)=COM(I)/(BP(I)*COP+QENEX(I)/1000.)
      CO2HP(I)=CO2M(I)/(BP(I)*COP+QENEX(I)/1000.)
      O2HP(I)=O2M(I)/(BP(I)*COP+QENEX(I)/1000.)
      CH4HP(I)=CH4M(I)/(BP(I)*COP+QENEX(I)/1000.)
      NOXHP(I)=NOXM(I)/(BP(I)*COP+QENEX(I)/1000.)
C
      G5PLT(I)=G(5,I)
      G4PLT(I)=G(4,I)
      G2PLT(I)=G(2,I)
   25 CONTINUE
C     PRINT*,COBP(1),CO2BP(1),O2BP(1),CH4BP(1),NOXBP(1)
```

```
C     PRINT*,COCP(1),CO2CP(1),O2CP(1),CH4CP(1),NOXCP(1)
C     PRINT*,COHP(1),CO2HP(1),O2HP(1),CH4HP(1),NOXHP(1)
C
C
C
C     WRITE OUT ENGINE CONFIGURATION
C     ******************************
C
      OPEN(UNIT=6,FILE='OUT')
      WRITE(6,31)
   31 FORMAT(1H1,/,/,/,56X,'********************',/,56X,
     X'ENGINE CONFIGURATION',/,56X,'********************')
      WRITE(6,32)BORE,STR,CR,IHEAD,ICAM,IVO,IVC
     X,EVO,EVC,ILIFT,ELIFT,IVD,EVD
   32 FORMAT(/,/,1X,'BORE (MM)',50X,F4.1,/,1X,'STROKE (MM)',48X
     X,F4.1,/
     X,1X,'COMPRESSION RATIO',42X,F4.1,/,1X,'HEAD TYPE',51X,
     XI1,/,1X,'CAMSHAFT TYPE',47X,I1,
     X/,1X,'INLET VALVE OPENS DEG. BTDC',32X,F4.1,/,1X,
     X'INLET VALVE CLOSES DEG. ABDC',31X,F4.1,/,1X,
     X'EXHAUST VALVE OPENS DEG. BBDC',30X,F4.1,/,1X
     X,'EXHAUST VALVE CLOSES DEG. ATDC',29X,F4.1,/,1X,
     X'INLET VALVE LIFT (MM)',39X,F3.1,/,1X,'EXHAUST VALVE LIFT (MM)
     X',33X,F3.1,/,1X,'INLET VALVE DIA. (MM)',38X,F4.1,/
     X,1X,'EXHAUST VALVE DIA. (MM)',36X,F4.1)


C     WRITE OUT ENGINE TEST CONDITIONS
C     ********************************
C
      WRITE(6,34)
   34 FORMAT(/,/,/,/,58X,'****************',/,58X,'TEST CONDITIONS'
     X,/,58X,'****************')
      WRITE(6,35)NTEST,NDATE,NDAT,PATM,TATM,RH,PG1,PG2,GCV,POIL,TGAS
   35 FORMAT(/,/,1X,'TEST NUMBER',51X,I3,/,1X,'DATE',54X,I7,
     X/,1X,'NUMBER OF DATA SETS',43X,I3,/,1X,'ATMOSPHERIC
     XPRESSURE(MBAR)
     X',35X,F7.2,/,1X,'ATMOSPHERIC TEMPERATURE(DEG.C)',33X,
     XF5.2,/,1X,'RELATIVE HUMIDITY',47X,F4.2,/
     X,1X,'PARTIAL PRESSURE OF WATER VAPOUR IN GAS(MBAR)'
     X,16X,F7.2,/,1X,'PARTIAL PRESSURE OF WATER VAPOUR IN AIR(MBAR)
     X',11X,F7.2,/ ,1X,'GAS CALORIFIC VALUE(MJ/M**3)'
     X,33X,F7.2,/,1X,'OIL PRESSURE(PSI)',44X,F7.2,
     X/,1X,'TEMPERATURE OF GAS AT SATURATOR(DEG.C)',23X,F7.2)
C
C
C     WRITE OUT RESULTS OF CALCULATIONS
C     *********************************
C
C
      WRITE(6,39)
   39 FORMAT(1H1,/,/,54X,'******************',/,54X,'ENGINE
     XPERFORMANCE',/,54X,'******************')
      WRITE(6,40)
```

```
   40 FORMAT(/,/,'TORQ',' BMEP ','IMEP ','MMEP ','PIMEP'
     X,' VDIC',' VDIM',' VWAC',' VDAC',' VDAM',' VG&A'
     X,' PHI ',' XARC',' XARM ',' AFM  ','AFC ')
      DO 30 I=1,NDAT
      WRITE(6,45)TQ(I),BMEP(I),IMEP(I),MMEP(I),PIMEP(I),VEDIC(I),
     XVEDIM(I),VEWAC(I),VEDAC(I),VEDAM(I),VE(I),PHI(I),EXAIR(I)
     X,EXAIRM(I),AFRM(I),AFRC(I)
   45 FORMAT(5(F4.2,1X),1X,6(F4.1,1X),3(F4.2,1X),F4.1,1X,F4.1)
   30 CONTINUE
C
C
C     WRITE OUT THE EXPERIMENTAL DATA
C     ********************************
C
      WRITE(6,49)
   49 FORMAT(1H1,/,/,/,60X,'*********',/,60X,'TEST DATA',/,60X
     X,'*********')
      WRITE(6,50)
   50 FORMAT(/,/,'LOAD',' SPEED ','GASFLOW',' GPWR',' WFH ','WFC',
     X' TIGN ','PGAS ','PMAN ','AFW ','CO2 ',' CO ',' O2 ',' NOX ',
     X'HC  ','ML')
      DO 55 I=1,NDAT

      WRITE(6,60)W(I),SPEED(I),GF(I),GP(I),WFH(I),WFC(I),
      XTIGN(I),PGAS(I),PIN(I),AFW(I),G(1,I),G(2,I),
      XG(3,I),G(4,I),G(5,I),ML(I)
   60 FORMAT(F4.1,1X,F5.2,1X,F7.3,1X,F5.3,F4.1,F4.1,F5.1,
     X1X,F5.1,1X,F4.1,F4.1,F4.1,1X,F4.2,F4.1,1X,F5.0,F5.0,F4.1)
   55 CONTINUE
      WRITE(6,95)
   95 FORMAT(/,/,/,1X,' T1  ',' T2  ','T3  ','T4  ','T5  ','T6
     X','T7  ','T8  ','T9  ','T10 ','T11 ','T12 ','T13 ','  T14
     X',' T15 ')
      DO 90 I=1,NDAT
      WRITE(6,85)T(1,I),T(2,I),T(3,I),T(4,I),T(5,I),T(6,I),T(7,I),
     XT(8,I),T(9,I),T(10,I),T(11,I),T(12,I),T(13,I),T(14,I),T(15,I)
   85 FORMAT(1X,F5.1,1X,12(F4.1,1X),1X,2(F5.1,1X))
   90 CONTINUE
      CLOSE(UNIT=5)
C
C
C
C     OPEN DATA FILES AND WRITE OUT DATA FOR POLYGRAPH
C     ************************************************
C
C     OPEN(UNIT=6,FILE='BMEPA')
C     CALL PDATA(EXAIR,BMEP,NDAT)
C     CLOSE (UNIT=6)
C     OPEN(UNIT=6,FILE='COA')
C     CALL PDATA(EXAIR,G2PLT,NDAT)
C     CLOSE(UNIT=6)
C     OPEN(UNIT=6,FILE='EFFA')
C     CALL PDATA(EXAIR,TEFF,NDAT)
C     CLOSE(UNIT=6)
```

```
C     OPEN(UNIT=6,FILE='EFFBMEP')
C     CALL PDATA(BMEP,TEFF,NDAT)
C     CLOSE(UNIT=6)
C     OPEN(UNIT=6,FILE='NOA')
C     CALL PDATA(EXAIR,G4PLT,NDAT)
C     CLOSE(UNIT=6)
C     OPEN(UNIT=6,FILE='CH4A')
C     CALL PDATA(EXAIR,G5PLT,NDAT)
C     CLOSE(UNIT=6)
C
C     WRITE OUT ENERGY BALANCES TO FILE
C
      OPEN(UNIT=6,FILE='EGYBAL')
C
      WRITE(6,68)
   68 FORMAT(' QENEX',' QEN ','QEXH ','QEXC ','CH4L ',
     X'QEXL ','QANR ','QLEX ','BLBY ','PTHET',' BP  ','AMBT ',
     X'SPEED',' XAIR',' TIGN')
      DO 76 I=1,NDAT
      BP(I)=BP(I)*1000.0
      WRITE(6,81)QENEX(I),QEN(I),QEXH(I),QEXC(I),CH4LS(I),
     XQEXL(I),QAN(I),QLEX(I),BLBY(I),PTHETA(I),BP(I),AMB(I)
     X,SPEED(I),EXAIR(I),TIGN(I)
   81 FORMAT(1X,13(F5.0),1X,F4.2,1X,F4.1)
   76 CONTINUE
C
      WRITE(6,71)
   71 FORMAT(/,/,'QENEX',' ENG ',' EXH ',' OIL ',' UHC ',' EXM
     X','GASAN',' EXA ',' BLBY',' BIP ',' BP  ','PISFR',' SUM ','BPTH
     X',' GSPR')
      DO 61 I=1,NDAT
      WRITE(6,62)BENEX(I),BEN(I),BEXH(I),BOIL(I),BCH4LS(I),BEXL(I)
     X,BAN(I),BLEX(I),BBLBY(I),BIP(I),BBP(I),BPISFR(I)
     X,SUM(I),BPTHA(I),GP(I)
   62 FORMAT(14(F4.1,1X),1X,F5.3)
   61 CONTINUE
      CLOSE (UNIT=6)
C
C     WRITE FRICTION LOSSES TO DATA FILE
C
      OPEN(UNIT=6,FILE='FRLSS')
      WRITE(6,72)
   72 FORMAT('ENFR  ','PISFR ','JBRFR ','VTRFR ','MGPWR ','ENFRLD',
     X' ENFR ','PISFR ','CRKFR ','VTRFR ',' FBFR ','MGPWR ','FRSAE ')
      DO 74 I=1,NDAT
      WRITE(6,73)EFRB(I),PISFRB(I),JBFRB(I),VTFRB(I),MFRB(I),EFR(I)
     X,EFR2(I),PISFR(I),CRKFR(I),VTFR(I),FAP(I),MP(I)*1000.0,FRSAE(I)
   73 FORMAT(13(F5.1,1X))
   74 CONTINUE
      CLOSE(UNIT=6)
C
C     WRITE DATA FOR MODEL AND PLOTTING PROGRAMME
C
      OPEN(UNIT=6,FILE='EM.DTA')
```

```
      PCAL=0.1
      T1=400.0
      TWALL=400.0
      CEE=3.0
      EF=0.07
      FS=1./STM
      DO 999 I=1,NDAT
      IF(PTHETA(I).GT.0.0)THEN
      WRITE(6,989)I,PTHETA(I)/1000.
      WRITE(6,988)TIGN(I)
      WRITE(6,987)EXAIR(I)
      WRITE(6,986)PATM/1000.,PCAL
      CORR1=1.0-BBLBY(I)/100.-BCH4LS(I)/100.-0.06
      WRITE(6,985)T1,TWALL,CEE,EF,CORR1,MASCY(I),QEN(I)/1000.
      WRITE(6,984)G(1,I),G(2,I)*1E4,G(3,I),G(4,I),G(5,I)
      WRITE(6,983)BP(I)/1000.,GP(I)
      WRITE(6,982)GCVM*1000.,FS
      WRITE(6,981)ALPHA,BETA,DELTA,GAMMA
      ENDIF
999   CONTINUE
989   FORMAT(I4,2X,F5.3)
988   FORMAT(F4.1)
987   FORMAT(F4.2)
986   FORMAT(F7.5,2X,F4.2)
985   FORMAT(7F9.3)
984   FORMAT(5F9.2)
983   FORMAT(F5.3,2X,F5.3)
982   FORMAT(F7.1,2X,F6.4)
981   FORMAT(4F7.3)
      CLOSE (UNIT=6)
      STOP
      END

C
C
C
C
C
C
C
C
C
C
      SUBROUTINE PDATA(X,Y,N)
      DIMENSION X(30),Y(30)
      DO 65 I=1,N
      WRITE(6,60)X(I),Y(I)
   60 FORMAT(F7.2,8X,F7.2)
   65 CONTINUE
      RETURN
      END
C
C
C
C
```

```
      PCAL=0.1
      T1=400.0
      TWALL=400.0
      CEE=3.0
      EF=0.07
      FS=1./STM
      DO 999 I=1,NDAT
      IF(PTHETA(I).GT.0.0)THEN
      WRITE(6,989)I,PTHETA(I)/1000.
      WRITE(6,988)TIGN(I)
      WRITE(6,987)EXAIR(I)
      WRITE(6,986)PATM/1000.,PCAL
      CORR1=1.0-BBLBY(I)/100.-BCH4LS(I)/100.-0.06
      WRITE(6,985)T1,TWALL,CEE,EF,CORR1,MASCY(I),QEN(I)/1000.
      WRITE(6,984)G(1,I),G(2,I)*1E4,G(3,I),G(4,I),G(5,I)
      WRITE(6,983)BP(I)/1000.,GP(I)
      WRITE(6,982)GCVM*1000.,FS
      WRITE(6,981)ALPHA,BETA,DELTA,GAMMA
      ENDIF
999   CONTINUE
989   FORMAT(I4,2X,F5.3)
988   FORMAT(F4.1)
987   FORMAT(F4.2)
986   FORMAT(F7.5,2X,F4.2)
985   FORMAT(7F9.3)
984   FORMAT(5F9.2)
983   FORMAT(F5.3,2X,F5.3)
982   FORMAT(F7.1,2X,F6.4)
981   FORMAT(4F7.3)
      CLOSE (UNIT=6)
      STOP
      END

C
C
C
C
C
C
C
C
C
      SUBROUTINE PDATA(X,Y,N)
      DIMENSION X(30),Y(30)
      DO 65 I=1,N
      WRITE(6,60)X(I),Y(I)
   60 FORMAT(F7.2,8X,F7.2)
   65 CONTINUE
      RETURN
      END
C
C
C
C
```

```
C
C
      SUBROUTINE GASPR(P,PHI,T,H,CP,MWEX,VM)
      COMMON ALPHA,BETA,GAMMA,DELTA
      REAL M,MW,NU,MWEX
      DIMENSION A(7,6),TABLE(6),M(6),NU(6),Y(6),CPO(6),HO(6),SO(6)
C
C
C
C     SET CONSTANTS FOR SPECIFIC HEAT,ENTHALPY AND ENTROPY
C     ****************************************************
C     POLYNOMIALS AS FUNCTIONS OF TEMPERATURE
C     ***************************************
      DATA A/
     1.24007797E1,.87350957E-2,-.6607878E-5,.20021861E-8,
     1.63274039E-15,-.48377527E5,.96951457E1,
     2.40701275E1,-.11084499E-2,.41521180E-5,-.29637404E-8,
     2.80702103E-12,-.30279722E5,-.32270046E0,
     3.36748261E1,-.12081500E-2,.23240102E-5,-.63217559E-9,
     3-.22577253E-12,-.10611588E4,.23580424E1,
     4.36255985E1,-.18782184E-2,.70554544E-5,-.67635137E-8,
     4.21555993E-11,-.10475226E4,.43052778E1,
     5.37100928E1,-.16190964E-2,.36923594E-5,-.20319674E-8,
     5.23953344E-12,-.14356310E5,.2955535E1,
     6.30574451E1,.26765200E-2,-.58099162E-5,.55210391E-8,
     6-.18122739E-11,-.98890474E3,-.22997056E1/
C
C
C
C     SET MOLECULAR WEIGHTS (CO2,H2O,N2,O2,CO,H2)
C     *******************************************
C
      DATA M/44.01,18.02,28.008,32.000,28.01,2.018/
C
C
C     SET GAS CONSTANT AND TABLE
C     **************************
C
      DATA RO/8.315/, TABLE/-1.0,1.0,0.0,0.0,1.0,-1.0/
C
      T=T+273.15
      EPS=0.21/(ALPHA+0.25*BETA-0.5*GAMMA)
      NU(1)=ALPHA*PHI*EPS
      NU(2)=BETA*PHI*EPS/2.0
      NU(3)=0.79+DELTA*PHI*EPS/2.0
      NU(4)=0.21*(1.0-PHI)
      NU(5)=0.0
      NU(6)=0.0
C
C     COMPUTE MOLE FRACTIONS
C
      TMOLES=0.0
      DO 30 I=1,6
      TMOLES=TMOLES+NU(I)
```

```
   30 CONTINUE
      DO 40 I=1,6
      Y(I)=NU(I)/TMOLES
   40 CONTINUE
C
C
C     COMPUTE COMPONENT PROPERTIES
C
      DO 60 I=1,6
      CP0(I)=A(1,I)+A(2,I)*T+A(3,I)*T**2+A(4,I)*T**3+
     &A(5,I)*T**4
      H0(I)=A(1,I)+A(2,I)/2.0*T+A(3,I)/3.0*T**2+A(4,I)/4.0*T**3
     &+A(5,I)/5.0*T**4+A(6,I)/T
C     S0(I)=A(1,I)*ALOG(T)+A(2,I)*T+A(3,I)/2.0*T**2+
C    &A(4,I)/3.0*T**3+A(5,I)/4.0*T**4+A(7,I)
   60 CONTINUE
C
C
C     COMPUTE PROPERTIES OF MIXTURE
C
      H=0.0
      S=0.0
      CP=0.0
      MW=0.0
      DO 70 I=1,6
      H=H+H0(I)*Y(I)
C     S=S+Y(I)*(S0(I)-ALOG(Y(I)))
     .CP=CP+CP0(I)*Y(I)+H0(I)*T*TABLE(I)
      MW=MW+Y(I)*M(I)
   70 CONTINUE
      R=R0/MW
      H=R*T*H
      U=H-R*T
      VM=R*T/P*1E-2
C     S=R*(-ALOG(0.9869*P)+S)
      CP=R*CP
C
      MWEX=MW
      T=T-273.15
      RETURN
      END
C
C
C
C
```

```
C
C          XXXXXXX   XX    XX   XXXXXXX   XXXXXXX
C          XX        XXX  XXX   XX   XX    XX   XX
C          XXXXX     XX XX XX   XX   XX    XX   XX
C          XX        XX    XX   XX   XX    XX   XX
C          XXXXXXX   XX    XX   XXXXXXX   XXXXXXXX
C
C
C     Thermodynamic rate model of a fuel inducted spark ignition
C     engine with arbitrary heat release.
C
C
C
C
C                              VARIABLES
C                              ---------
C
C     B - Engine bore (m)
C     S - Engine stroke (m)
C     RPM - Engine speed (rev/min)
C     OMEGA - Engine speed (rad/s)
C     L - Con rod length (m)
C     T - Temperature (K)
C     P - Pressure (K)
C     TW - Wall temperature (K)
C     TU - Unburned gas temperature (K)
C     TB - Burned gas temperature (K)
C     V - Cylinder volume (m**3)
C     THETAS - Start of heat release (deg)
C     THETAB - Burn duration (deg)
C     FRAC - Residual fraction
C     H - Heat transfer coefficient (W/m**2 K)
C     C - Blowby coefficient (1/s)
C     AFR - Air fuel ratio
C     THETA - Crank angle (deg)
C
C
C     Y1 - Six dimensional composition vector - mole fractions
C     Y1(1) - CO2,  Y1(2) - H2O,  Y1(3) - N2,  Y1(4) - O2,  Y1(5) -
C     CO,  Y1(6) - H2
C     Y2 - Ten dimensional composition vector - mole fractions
C     Y2(1) - CO2,  Y2(2) - H2O,  Y2(3) - N2,  Y2(4) - O2,  Y2(5) -
C     CO,  Y2(6) - H2,  Y2(7) - H,  Y2(8) - O,  Y2(9) - OH,
C     Y2(10) - NO
C
C     CR - Compression ratio
C     VC - Clearance volume
C     IMEP - Indicated mean effective pressure
C
C     AFMS - Stoichiometric A/F ratio by mass
C     CV - Calorific value of the fuel kJ/kg
C     EM - Blowby multiplier
C
C     ALPHA,BETA,GAMA,DELTA - See AFRES
```

```
C
C
C                              DIMENSION ARRAYS
C                              ----------------
C
C
      IMPLICIT REAL*8(A-H,O-Z)
      EXTERNAL RATES
      REAL*8  IMEP,MNOT,M,MG,MEND
      REAL*8 INDEX1,INDEX2,INDEXE,INDXCM,INDXEM
      REAL*4 PMEAN,TMEAN
      CHARACTER*13 REFN
      CHARACTER*12 FUELN
      CHARACTER*8 DATE
      CHARACTER*1 IHEAD
      CHARACTER ANS
      COMMON/ENGINE/R,B,S,EPS,RPM,C,THETAB,THETAS,PHI,F,
     /P1,T1,TW,MNOT,OMEGA,UNOT,UFINAL,ACOMB,THEVO,THIVC
      COMMON/FUEL/AO,FS
      COMMON/FUEN/FUELN
      COMMON/RESULT/THETAG(361),YG(6,361),VOLG(361),XG(361),MG(361)
     &,CO2G,H2OG,GN2,O2G,COG,H2G,HG,OG,OHG,GNO,Y2MAXG
     &,QEN,PMAXE,TPMAXE,PMAXT,TPMAXT,PMAX1,TPMAX1,PMAX,TPMAX
     &,TBMAX,TTBMAX,TEVO
      COMMON/WEIBE/CORR,WA,WZ
      COMMON/ABDG/ALPHA,BETA,DELTA,GAMA
C
      DIMENSION Y1(6),Y(6),W(6,7),Y2(10),PCHEK(360),PMEAN(361),
     &TMEAN(361)
C
      DATA Y/1.,0.,350.,3*0.0/,
     /THIVC/-140./,THEVO/157./,TOL/1D-6/,
     /PI/3.141593/,Y2/10*.0/
C
      THETA=THIVC
      THETAE=THIVC+1.
C
C     DETERMINE CHAMBER TYPE
C
      PRINT*, 'Give chamber type: 1 for TaskII,  2 for 3-2,  3 for
     &Hrcc'
      READ(1,9)IHEAD
  9   FORMAT(A1)
C     READ IN THE EXPERIMENTAL PRESSURE THETA DATA AND DATA
C
      TEVO=0.0
      PMAX=0.0
      PMAXE=0.0
      TPMAXE=0.0
      TPMAX=0.0
      Y2MAX=0.0
      PMAXT=0.0
      TPMAXT=0.0
      PMAX1=0.0
```

```
      TPMAX1=0.0
      TBMAX=0.0
      TTBMAX=0.0
      OPEN(5,FILE='MEAN')
      READ(5,21)REFN
      READ(5,21)DATE
21    FORMAT(A13)
      READ(5,*)IGN
      READ(5,*)EXAIR
      READ(5,*)R,VS,EPS
      READ(5,*)SPEED
      READ(5,*)INDEX1,INDEX2,INDEXE
      READ(5,*)PATM,PCAL
      READ(5,*)ENDC,STC,INDXCM,INDXEM
      READ(5,*)WA,WZ,ACOMB,T1,TW,C,F,CORR
     &,EMASS,QEN
      READ(5,*)CO2,CO,O2,ENOX,UHC
      READ(5,*)WM,WSD,WDISP,PRM,PRSD,PRDISP,PSM,PSSD,PSDISP
     &,TIM,TISD,TIDISP
      READ(5,*)BPWRE,GP
      READ(5,*)GCV,FS
      READ(5,*)ALPHA,BETA,DELTA,GAMA
C
      PHI=1.0/EXAIR
      RPM=SPEED
      OMEGA = RPM*PI/30.
      THETAS=STC-360.0
      THETAB=ENDC-STC
      AO=GCV
C
      DO 24 I=1,360
      READ(5,*)PMEAN(I),TMEAN(I)
      TMEAN(I)=TMEAN(I)-360
      PMEAN(I)=PMEAN(I)-PCAL
C
C     CALCULATE THE MAXIMUM RATE OF PRESSURE RISE AND PEAK PRESSURE
C
      IF(TMEAN(I).GT.THETAS.AND.TMEAN(I).LT.THETAS+THETAB)THEN
      PRISE=PMEAN(I)-PMEAN(I-1)
      IF(PRISE.GT.PMAXE)THEN
      PMAXE=PRISE
      TPMAXE=TMEAN(I)
      ENDIF
      IF(PMEAN(I).GT.PMAX)THEN
      PMAX=PMEAN(I)
      TPMAX=TMEAN(I)
      ENDIF
      ENDIF
24    CONTINUE
      CLOSE(UNIT=5)
C
```

```
C     CALCULATE EXPERIMENTAL MASS INDUCTED CONSIDERING RESIDUALS
C
      RM=F*EMASS/(1-F)
      EMASST=EMASS+RM
C
C     SET BLOWBY COEFFICIENT TO ALLOW MEASURED BLOWBY
C
      RADEVO=THEVO*PI/180.
      RADIVC=(ABS(THIVC)-180.)*PI/180.
      BLBYE=-0.3*RPM/60.+14.26
444   EMEND=DEXP(-C*(RADEVO+RADIVC+PI)/OMEGA)
      MEND=EMEND*EMASST
      BLBYT=(EMASST-MEND)/EMASS*100.
      IF(BLBYT-BLBYE.GT.0.1)THEN
      C=C-0.01
      GO TO 444
      ENDIF
      IF(BLBYE-BLBYT.GT.0.1)THEN
      C=C+0.01
      GO TO 444
      ENDIF
      PRINT*,C
C     DETERMINE PRESSURE AT IVC
C
      KTHIVC=ABS(THIVC)
      P1=PMEAN(181-KTHIVC)
C
11    Y(1)=P1
      PCHEK(1)=P1
      Y(3)=T1
      CALL AUXLRY(THETA, V, X, EM,EMEOC)
      CALL AFRES(Y(1), Y(3), PHI, F, HU, U, VU, SU, Y1, CP,
     &     DLVLT, DLVLP)
      MNOT = V/VU
      IF(ABS(MNOT-EMASST).GT.0.001)THEN
      IF(MNOT-EMASST.GT.0.001)T1=T1+0.5
      IF(EMASST-MNOT.GT.0.001)T1=T1-0.5
      GO TO 11
      ENDIF
      M=EM*MNOT
      UNOT = MNOT*U
      PRINT 10
10    FORMAT(5X,'THETA', 4X,'VOLUME', 3X,'BURN FRAC', 2X,'PRESSURE'
     &,3X,  'BURN TEMP' ,2X, 'T UNBURN' ,3X, 'WORK' ,3X, 'HEAT LOSS'
     &,5X,        'MASS',3X, 'H-LEAK')
      PRINT 15
15    FORMAT(4X,'DEG ATDC' ,2X, 'CM**3' ,6X, '--' ,8X, 'BARS' ,7X,
     &'KELVIN',5X, 'KELVIN' ,3X, 'JOULES' ,4X, 'JOULES' ,6X, 'GRAMES'
     &,2X,        'JOULES')
      PRINT 20,THETA,V,X,(Y(J),J=1,5),M,Y(6),MNOT,Y(6)
20    FORMAT(4X,F5.0,6X,F5.0,4X,F5.3,6X,F5.2,7X,F5.0,5X,F5.0,
     &       5X,F5.0,3X,F5.0,7X,F5.3,3X,F5.2)
      THETAG(1)=THETA
      VOLG(1)=V
```

```
      XG(1)=X
      DO 5 J=1,6
5     YG(J,1)=Y(J)
      MG(1)=M
C
C     INTEGRATE THE RATE EQUATIONS 4.80 - 4.85 AND PRINT ANSWERS
C     EVERY 1 DEGREE
C
      CHEK2=0.
C
      DO 30 I = 1,THEVO-THIVC
C
C     Call subroutine to solve differential equation
C
      IFAIL=0
      CALL D02BAF(THETA,THETAE,6,Y,TOL,RATES,W,IFAIL)
      IF(TOL.LT.0)THEN
C     PRINT*,'** WARNING ** TOL less than zero'
C     PRINT*,'Resetting TOL to 0.000001'
      TOL=1D-2
      ENDIF
C
C     CALCULATE PEAK NOx VALUE
C
      IF(THETA.GT.THETAS.AND.THETA.LT.THETAS+THETAB)THEN
      CALL EQUIL(Y(1), Y(2), PHI, HH, UU, VV, SS, Y2, CC, VLT, VLP,
     &          IER,THETA)
      IF(Y2(10).GT.Y2MAX)Y2MAX=Y2(10)
      ENDIF
C
C     CALCULATE EMISSIONS AT EVO LESS 2 DEGREES
C
      DIF=THEVO-THETA
      IF(DIF.LT.3..AND.DIF.GT.1.9)THEN
      CALL EQUIL(Y(1), Y(2), PHI, HH, UU, VV, SS, Y2, CC, VLT, VLP,
     &          IER,THETA)
      Y2MAXG=Y2MAX*1E6
      CO2G=Y2(1)*100.
      H2OG=Y2(2)*100.
      GN2=Y2(3)*100.
      O2G=Y2(4)*100.
      COG=Y2(5)*1E6
      H2G=Y2(6)*1E6
      HG=Y2(7)*1E6
      OG=Y2(8)*1E6
      OHG=Y2(9)*1E6
      GNO=Y2(10)*1E6
      ENDIF
C
C     EXIT PROGRAMME AND SELECT NEW VALUE OF CORR IF THE % AGE
C     ERROR BETWEEN EXPERIMENTAL AND PREDICTED PEAK PRESSURES
C     IS GREATER THAN X %
C
C     PCHEK(I+1)=Y(1)
```

```
C      IF(PCHEK(I+1).LT.PCHEK(I).AND.(PCHEK(I)-PMAX)/PMAX.GT.0.05)
C     &GO TO 999
C
       CALL AUXLRY(THETAE, V, X, EM,EMEOC)
       M = EM*MNOT
       THETA=THETAE
       THETAE=THETA+1
       IF(THETAS .GE. THETA .AND. THETAS .LT. THETAE)
      &CALL TINITL(Y(1), Y(3), PHI, F, Y(2))
       IF(THETA .GT. THETAS + THETAB) Y(3) = 0.
       PRINT 20, THETA, V, X, (Y(J),J=1,5), M, Y(6)
       THETAG(I+1)=THETA
       VOLG(I+1)=V
       XG(I+1)=X
       DO 6 J=1,6
6      YG(J,I+1)=Y(J)
       MG(I+1)=M
C
C      CALCULATE THE MAXIMUM RATE OF PRESSURE RISE AND PEAK PRESSURE
C
       IF(THETA.GT.THETAS.AND.THETA.LT.THETAS+THETAB)THEN
       PRIST=YG(1,I+1)-YG(1,I)
       IF(PRIST.GT.PMAXT)THEN
       PMAXT=PRIST
       TPMAXT=THETAG(I+1)
       ENDIF
       IF(YG(1,I+1).GT.PMAX1)THEN
       PMAX1=YG(1,I+1)
       TPMAX1=THETAG(I+1)
       ENDIF
       ENDIF
C
C      CALCULATE MAXIMUM BURNT GAS TEMPERATURE
C
       IF(THETA.GT.THETAS.AND.THETA.LT.THETAS+THETAB)THEN
       IF(Y(2).GT.TBMAX)THEN
       TBMAX=Y(2)
       TTBMAX=THETAG(I+1)
       ENDIF
       ENDIF
C
C      CALCULATE LAMINAR FLAME SPEED ACCORDING TO KUEHL AT X=0.00001
C
C
       IF(X.GT.0.00001.AND.CHEK2.LT.1.)THEN
C
C      CALCULATE LAMINAR FLAME SPEED FOR PROPANE BASED ON METGHALCHI
C
C
       COEFH=0.364
       BEM=34.2
       BPHI=-138.7
       PHIM=1.08
       TNOWT=298.
```

```
      ALFA=2.18-0.8*(1./EXAIR-1.)
      BEETA=-0.16+0.22*(1./EXAIR-1.)
      SLO=BEM+BPHI*(1./EXAIR-PHIM)**2
      ULAMH=SLO/100.*(Y(3)/TNOWT)**ALFA*(Y(1)/1.01325)**BEETA
C
C     CALCULATE LAMINAR FLAME SPEED FOR METHANE BASED ON BABKIN AND
C     KOSACHENKO SEE BAILEY P 63
C
      COEFBK=0.31
      U1BK=(1E4/Y(2)+900./Y(3))**2.64
      UUBK=0.00055*Y(3)-0.662
      U2BK=(Y(1)/1.01325)**UUBK
      ULAMBK=1E2/U1BK*U2BK
C
C     CALCULATE LAMINAR FLAME SPEED FOR PROPANE BASED ON KUEHL
C
      COEFF=0.483
      U1=(1E4/Y(2)+900./Y(3))**4.938
      UU=-0.09676
      U2=(Y(1)/13.6/9.81*100.*39.3701)**UU
      ULAM=1.087E4/U1*U2
C
C     REPLACE S IN AFRES BELOW WITH DUMMY VARIABLE S IS STROKE
C
      CALL AFRES(Y(1), Y(3), PHI, F, HL, U, VU, SS, Y1, CP, DLVLT,
     &           DLVLP)
      CALL TRANSP(Y(3),Y1,CP,MU,LAMBDA)
      VCL=VS/(R-1.)
      CALL AUXLRY(THETA, V, X, EM,EMEOC)
C
C     WORK OUT GASKET THICKNESS AND CHAMBER DEPTH FOR A CHAMBER
C
      DEPTH=0.00425
      GASTH=(126.38/(R-1)-8.3)*0.000437
      IF(IHEAD.EQ.'1')THEN
      DEPTH=0.0075
      GASTH=0.00039
      ENDIF
      IF(IHEAD.EQ.'3')THEN
      DEPTH=0.0034
      GASTH=0.001369
      ENDIF
      HTIGN=(V-VCL)*4./PI/B**2.*1E-2 + DEPTH + GASTH
      SPBAR=SPEED/60.*2.*S*1E-2
      THDLAY=COEFF*(SPBAR*MU*VU*1E-4)**(1./3.)*(HTIGN/ULAM)**(2./3.)
      THDLBK=COEFBK*(SPBAR*MU*VU*1E-4)**(1./3.)*(HTIGN/ULAMBK)
     X**(2./3.)
      THDLH=COEFH*(SPBAR*MU*VU*IE-4)**(1./3.)*(HTIGN/ULAMH)**(2./3.)
      PRINT*,ULAM,ULAMBK,ULAMH
      PRINT*, THDLAY,THDLBK,THDLH
      PRINT*,THDLBK,HTIGN,ULAMBK
      CHEK2=CHEK2+1.
      ENDIF
30    CONTINUE
```

```
C
C     COLLECT BURNT GAS TEMPERATURE AT EVO
C
      TEVO=Y(2)
C
C     COMPUTE AND WRITE THE ETA, IMEP AND ERRORS
C
      CALL EQUIL(Y(1), Y(2), PHI, HB, U, VB, SB, Y2, CP, DLVLT, DLVLP,
     &          IER,THETA)
      UFINAL = U*M
      ERROR1 = 1.0 - VB*M/V
      ERROR2 = 1.0 + Y(4)/(UFINAL - UNOT + Y(5) + Y(6))
      ETA = Y(4)/MNOT*(1. + PHI*FS*(1. - F))/PHI/FS/(1. -F)/AO
      IMEP = Y(4)/(PI/4.*B**2*S)*10.
      PRINT 40, ETA, IMEP, ERROR1, ERROR2
40    FORMAT('ETA = ',1PE11.4,' IMEP = ',1PE11.4,' ERROR1 =',1PE11.4,
     &       ' ERROR = ',1PE11.4)
      PRINT*,'Graphics ?'
      READ(1,1)ANS
1     FORMAT(A1)
      IF(ANS.EQ.'Y')CALL PICTUR(PMEAN,TMEAN)
      CALL WRIT1
      CALL WRIT2(BLBYT)
      PRINT 555
555   FORMAT('Spool EMODR.LIST for complete set of results')
999   STOP
      END
C
C
C************************  Subroutine RATES  ***************************
C
C
      SUBROUTINE RATES(THETA, Y, YPRIME)
      IMPLICIT REAL*8(A-H,O-Z)
      REAL*8 M,MNOT,MU,LAMBDA
      DIMENSION Y1(6),Y2(10),YT(10)
      DIMENSION Y(6),YPRIME(6)
      COMMON /ENGINE/ R, BORE, STROKE, EPS, RPM, CEE, THETAB,
     &                THETAS, PHI, F, P1, T1, TW, MNOT, OMEGA, UNOT,
     &                UFINAL,ACOMB,THEVO,THIVC
      COMMON/WEIBE/CORR,WA,WZ
      DATA PI/3.141593/, Y2/10*0.0/
      CALL AUXLRY(THETA, V, X, EM,EMEOC)
      M = EM*MNOT
      RAD = THETA*PI/180.
      DUMB = DSQRT(1. - (EPS*DSIN(RAD))**2)
      DV = PI/8.*BORE**2*STROKE*DSIN(RAD)*(1. + EPS*DCOS(RAD)/DUMB)
      A = (DV + V*CEE/OMEGA)/M
      C11 = (PI*BORE**2/4. +ACOMB+ 4. *V/BORE)/OMEGA/M/10000.
      CO = DSQRT(X)
C
```

```
C     THREE DIFFERENT COMPUTATIONS ARE REQUIRED DEPENDING
C     UPON THE SIZE OF THE MASS FRACTION BURNED
C
      XEOC=1.0-DEXP(-WA*((THETAB)/(THETAB))
     X**(WZ+1))
      XEOC=XEOC*CORR/EMEOC/(1+(F/(1-F)))
      IF(XEOC-X.LE.0.001)GO TO 20
      IF( X .GT. .00001 ) GO TO 10
C
C     COMPRESSION
C
      CALL AFRES(Y(1), Y(3), PHI, F, HL, U, VU, S, Y1, CP, DLVLT,
     &          DLVLP)
C
C     Determine heat transfer coefficient
C
      DO 888 I=1,6
      YT(I)=Y1(I)
888   CONTINUE
      DO 889 I=7,10
889   YT(I)=0.0
      CALL TRANSP(Y(3),Y1,CP,MU,LAMBDA)
      CALL WOCHNI(V,Y(1),VU,MU,LAMBDA,HEATU,THETA)
CE    CALL EICH(Y(1),Y(3),HEATU)
      C1U=HEATU*C11
      B = C1U*VU/CP*DLVLT*(1.0 - TW/Y(3))
      C = 0
      D = 0
      E = VU**2/CP/Y(3)*DLVLT**2 + 10.*VU/Y(1)*DLVLP
      YPRIME(1) = (A + B + C)/(D + E)*10.
      YPRIME(2) = 0.
      YPRIME(3) = -C1U/CP*(Y(3) - TW) + VU/CP*DLVLT*YPRIME(1)/10.
      GO TO 30
C
C     COMBUSTION
C
10    CONTINUE
      CALL AFRES(Y(1), Y(3), PHI, F, HU, U, VU, S, Y1, CPU, DLVLTU,
     &          DLVLPU)
      CALL EQUIL(Y(1), Y(2), PHI, HB, U, VB, S, Y2, CPB, DLVLTB,
     &DLVLPB, IER,THETA)
C
C     Determine heat transfer coefficients for burned and
C     unburned gas.
C
      DO 890 I=1,6
890   YT(I)=Y1(I)
      DO 891 I=7,10
891   YT(I)=0.0
      CALL TRANSP(Y(3),Y1,CPU,MU,LAMBDA)
      CALL WOCHNI(V,Y(1),VU,MU,LAMBDA,HEATU,THETA)
CE    CALL EICH(Y(1),Y(3),HEATU)
      CALL TRANSP(Y(2),Y2,CPB,MU,LAMBDA)
      CALL WOCHNI(V,Y(1),VB,MU,LAMBDA,HEATB,THETA)
```

```
CE     CALL EICH(Y(1),Y(2),HEATB)
       C1U=HEATU*C11
       C1B=HEATB*C11
       B = C1B*VB/CPB*DLVLTB*CO*(1. - TW/Y(2)) + VU/CPU*DLVLTU*
      &    (1. - CO)*(1. - TW/Y(3))*C1U
C      DX = 0.5*SIN(PI*(THETA - THETAS)/THETAB)*180./THETAB
       DX=CORR/EM/(1+(F/(1-F)))*DEXP(-WA*((THETA-THETAS)/(THETAB))**
      &(0.8+1))*(WA/THETAB/PI*180.0*(0.8+1)*((THETA-THETAS)/THETAB)
      &**0.8)
       C = -(VB - VU)*DX - VB/Y(2)*DLVLTB*(HU - HB)/CPB*(DX - (X -
      &    X**2)*CEE/OMEGA)
       D = X*(VB**2/CPB/Y(2)*DLVLTB**2 + 10.*VB/Y(1)*DLVLPB)
       E = (1. - X)*(VU**2/CPU/Y(3)*DLVLTU**2 + 10.*VU/Y(1)*DLVLPU)
       HL = (1.0 - X**2)*HU + X**2*HB
       YPRIME(1) = (A + B+ C)/(D + E)*10.
       YPRIME(2) = -C1B/CPB/CO*(Y(2) - TW) + VB/CPB*DLVLTB*
      &             YPRIME(1)/10. + (HU - HB)/CPB*(DX/X - (1. - X)*
      &             CEE/OMEGA)
       YPRIME(3) = -C1U/CPU/(1. + CO)*(Y(3) - TW) + VU/CPU*DLVLTU*
      &            YPRIME(1)/10.
       GO TO 30
C
C      EXPANSION
C
20     CALL EQUIL(Y(1), Y(2), PHI, HL, U, VB, S, Y2,CP, DLVLT, DLVLP,
      &         IER,THETA)
C
C      Determine heat transfer coefficient for products
C
       CALL TRANSP(Y(2),Y2,CPB,MU,LAMBDA)
       CALL WOCHNI(V,Y(1),VB,MU,LAMBDA,HEATB,THETA)
CE     CALL EICH(Y(1),Y(2),HEATB)
       C1B=HEATB*C11
       C1U=0.0
C
C      *******
C
       B = C1B*VB/CP*DLVLT*(1. - TW/Y(2))
       C = 0.
       D = VB**2/CP/Y(2)*DLVLT**2 + 10.*VB/Y(1)*DLVLP
       E = 0.
       YPRIME(1) = (A + B + C)/(D + E)*10.
       YPRIME(2) = -C1B/CP*(Y(2) - TW) + VB/CP*DLVLT*YPRIME(1)/10.
       YPRIME(3) = 0.
C
C      ALL CASES
C
30     YPRIME(4) = Y(1)*DV/10.
       YPRIME(5) = M*(CO*(Y(2) - TW)*C1B + (1. - CO)*C1U*(Y(3) - TW))
       YPRIME(6) = CEE*M/OMEGA*HL
       DO 40 I = 1,6
40     YPRIME(I) = YPRIME(I)*PI/180.
       RETURN
       END
```

```
C
C
      SUBROUTINE AUXLRY(THETA, V, X, EM,EMEOC)
      IMPLICIT REAL*8(A-H,O-Z)
      COMMON/ENGINE/ R, B, S, EPS, RPM, C, THETAB, THETAS,
     &               PHI, F, P1, T1, TW, EMNOT, OMEGA, UNOT, UFINAL
     &,ACOMB,THEVO,THIVC
      COMMON/WEIBE/CORR,WA,WZ
      DATA PI/3.141593/
      RAD = THETA*PI/180.
      RADEOC=(THETAS+THETAB)*PI/180.
      RADIVC=(ABS(THIVC)-180.)*PI/180.0
      VTDC = PI/4.*B**2*S/(R - 1.)
      V = VTDC*(1. + (R - 1.)/2.*(1. - DCOS(RAD) + 1./EPS*(1. -
     &    DSQRT(1. - (EPS*DSIN(RAD))**2))))
      EM = DEXP(-C*(RAD+RADIVC + PI)/OMEGA)
      EMEOC=DEXP(-C*(RADEOC+RADIVC+PI)/OMEGA)
      X=1.0-DEXP(-WA*((THETAB)/(THETAB))
     X**(WZ+1))
      X=X*CORR/EMEOC/(1+(F/(1-F)))
      IF(THETA.LE.THETAS)X=0.0
      IF(THETA.GT.THETAS.AND.THETA.LT.THETAS+THETAB)THEN
C     X = 0.5*(1. - DCOS(PI*(THETA - THETAS)/THETAB))
      X=1.0-DEXP(-WA*((THETA-THETAS)/(THETAB))
     X**(WZ+1))
      X=X*CORR/EM/(1+(F/(1-F)))
      ENDIF
      RETURN
      END
C
C
      BLOCK DATA
      IMPLICIT REAL*8(A-H,O-Z)
      CHARACTER*12 FUELN
      COMMON/ENGINE/ R, B, S, EPS, RPM, C, THETAB, THETAS,
     &               PHI, F, P1, T1, TW, EMNOT, OMEGA, UNOT, UFINAL
     &,ACOMB,THEVO,THIVC
      COMMON/FUEL/AO,FS
      COMMON/FUEN/FUELN
      COMMON/ABDG/ALPHA,BETA,DELTA,GAMA
      DATA  B/5.405/, S/5.508/, THEVO/157./, THIVC/-140./
      DATA FUELN/'Methane'/
      END
C
C
      SUBROUTINE TINITL(P, TU, PHI, F, TB)
      IMPLICIT REAL*8(A-H,O-Z)
      DIMENSION Y1(6), Y2(10)
      DATA MAXITS/50/, TOL/.001/, Y2/10*0.0/
      TB = 3000.
      CALL AFRES(P, TU, PHI, F, HU, U, V, S, Y1, CP, DLVLT, DLVLP)
      DO 10 I = 1,MAXITS
      CALL EQUIL(P, TB, PHI, HB, U, V, S, Y2, CP,DLVLT, DLVLP, IER,
     &THETA)
```

```
      DELT = (HU - HB)/CP
      TB = TB + DELT
      IF(DABS(DELT/TB) .LT. TOL) RETURN
10    CONTINUE
      WRITE(1,20)
20    FORMAT('CONVERGENCE FAILURE IN TINITL')
      RETURN
      END
C
C
C
C**********************   AFRES   **********************
C
C
C
C
      SUBROUTINE AFRES(P,T,PHI,F,H,U,V,S,Y,CP,DLVLT,DLVLP)
C
C
C     Subroutine to determine the properties of a mixture of fuel,
C     air and residual exhaust gas.
C
C     Given:
C     Pressure  P   (bar)
C     Temperature  T  (K)
C     Air - fuel ratio by mass  AFR
C     Exhaust gas residual mass fraction  FRAC
C
C     Returns:
C     Specific enthalpy of mixxture  (H)  (kJ/kg)
C     Specific internal energy of mixture  (U)  (kJ/kg)
C     Specific volume of mixture  V  (m**3/kg)
C     Specific entropy of mixture  S  (kJ/kg K)
C     A six dimensional composition vector of mole fractions
C     showing composition of exhaust gas (cold) - Y(I) where
C     1.  CO2,  2.  H2O,  3.  N2,  4.  O2,  5.  CO,  6.  H2
C     Specific heat at constant pressure of mixture  CP  (kJ/kg K)
C     LDVDTP derivative of log vol with respect to log temp at const T
C     LDVDPT derivative of log vol with respect to log pres at const P
C
C     Requires fuel data in COMMON/FUEL/
C     ALPHA - number of C atoms in molecule
C     BETA - number of H atoms in molecule
C     GAMA - number of O atoms in molecule
C     DELTA - number of N atoms in molecule
C     Constants AO, BO, CO, DO, EO for ideal gas properties of fuel
C     CP/R=AO+BO*T+CO*T*T
C
C     Also requires ideal gas data for exhaust gases in
C     COMMON/GASES/  -  A(I,J)
C
C
      IMPLICIT REAL*8 (A-H,O-Z)
      REAL*8 M, MW,MRES,MFA,MFUEL,K,NU,N2
```

```
      LOGICAL RICH,LEAN
      DIMENSION A(7,6),TABLE(6),M(6)
      DIMENSION NU(6),Y(6),CPO(6),HO(6),SO(6)
C
      COMMON/ABDG/ALPHA,BETA,DELTA,GAMA
      DATA AO/1.971324/,BO/7.871586E-03/,CO/-1.048592E-06/,DO/
     /-9.930422E+03/,EO/8.873728/
      DATA A/
     1.24007797D+01,.87350957D-02,-.6607878D-05,.20021861D-08,
     1.63274039D-15,-.48377527D+05,.96951457D+01,
     2.40701275D+01,-.11084499D-02,.41521180D-05,-.29637404D-08,
     2.80702103D-12,-.30279722D+05,-.32270046D+00,
     3.36748261D+01,-.12081500D-02,.23240102D-05,-.63217559D-09,
     3-.22577253D-12,-.10611588D+04,.23580424D+01,
     4.36255985D+01,-.18782184D-02,.70554544D-05,-.67635137D-08,
     4.21555993D-11,-.10475226D+04,.43052778D+01,
     5.37100928D+01,-.16190964D-02,.36923594D-05,-.20319674D-08,
     5.23953344D-12,-.14356310D+05,.2955535D+01,
     6.30574451D+01,.26765200D-02,-.58099162D-05,.5521039D-08,
     6-.18122739D-11,-.98890474D+03,-.22997056D+01/
C
      DATA RO/8.314/,TABLE/-1.,1.,0.,0.,1.,-1./,M/44.01,18.02,
     1       28.008,32.,28.01,2.018/
C     Determine stoichiometric A/F ratio by mass AFMS
C
C
      EPS= 0.21/(ALPHA+0.25*BETA-0.5*GAMA)
C
C     Stoichiometric A/F ratio by volume AFVS
C
C
C     Fuel air equivalence
C
C
C     Rich or lean?
C
      RICH=PHI.GT.1.0
      LEAN=.NOT.RICH
      DLVLT=1.0
      DLVLP=-1.0
      IF(LEAN)THEN
      NU(1)=ALPHA*PHI*EPS
      NU(2)=BETA*PHI*EPS/2
      NU(3)=0.79+DELTA*PHI*EPS/2
      NU(4)=0.21*(1.0-PHI)
      NU(5)=0.0
      NU(6)=0.0
      DCDT=0
      ELSE
      Z=1000/T
      K=EXP(2.743+Z*(-1.761+Z*(-1.611+Z*.2803)))
      DKDT=-K*(-1.761+Z*(-3.222+Z*.8409))/1000
      A1=1.0-K
      B=.42-PHI*EPS*(2*ALPHA-GAMA)+K*(.42*(PHI-1)+ALPHA*PHI*
```

```
     /EPS)
      C=-0.42*ALPHA*PHI*EPS*(PHI-1)*K
      NU(5)=(-B+DSQRT(B*B-4*A1*C))/2/A1
      DCDT=DKDT*(NU(5)**2-NU(5)*(.42*(PHI-1)+ALPHA*PHI*EPS
     /)+.42*ALPHA*PHI*EPS*(PHI-1))/(2*NU(5)*A1+B)
      NU(1)=ALPHA*PHI*EPS-NU(5)
      NU(2)=.42-PHI*EPS*(2*ALPHA-GAMA)+NU(5)
      NU(3)=0.79+DELTA*PHI*EPS/2
      NU(4)=0.0
      NU(6)=0.42*(PHI-1)-NU(5)
      ENDIF
C
C     Compute mole fractions and molecular weight of residuals
C
      TMOLES=0
      DO 30 I=1,6
30    TMOLES=TMOLES+NU(I)
      MRES=0
      DO 40 I=1,6
      Y(I)=NU(I)/TMOLES
40    MRES=MRES+Y(I)*M(I)
C
C     Compute mole fractions and molecular weight of fuel air
C
      FUEL=EPS*PHI/(1+EPS*PHI)
      O2=0.21/(1+EPS*PHI)
      N2=0.79/(1+EPS*PHI)
      MFA=FUEL*(12.01*ALPHA+1.008*BETA+16*GAMA+14.01*DELTA
     /)+32*O2+28.02*N2
C
C     Compute mole fractions of fuel air residual gas
C
      YRES=F/(F+MRES/MFA*(1-F))
      DO 50 I=1,6
50    Y(I)=Y(I)*YRES
      YFUEL=FUEL*(1-YRES)
      Y(3)=Y(3)+N2*(1-YRES)
      Y(4)=Y(4)+O2*(1-YRES)
C
C     Compute component properties
C
      DO 60 I=1,6
      CPO(I)=A(1,I)+A(2,I)*T+A(3,I)*T**2+A(4,I)*T**3+A(5,I)*T**4
      HO(I)=A(1,I)+A(2,I)/2*T+A(3,I)/3*T**2+A(4,I)/4*T**3
     /+A(5,I)/5*T**4+A(6,I)/T
60    SO(I)=A(1,I)*DLOG(T)+A(2,I)*T+A(3,I)/2*T**2
     /+A(4,I)/3*T**3+A(5,I)/4*T**4+A(7,I)
C
      MFUEL=12.01*ALPHA+1.008*BETA+16.0*GAMA+14.01*DELTA
      CPFUEL=AO+BO*T+CO*T**2
      HFUEL=AO+BO/2.*T+CO/3*T**2+DO/T
      SOFUEL=AO*DLOG(T)+BO*T+CO/2.*T**2+EO
C
```

```
C     Compute properties of mixture
C
      H=HFUEL*YFUEL
      IF(YFUEL.GT.0.0)THEN
      S=(SOFUEL-DLOG(YFUEL))*YFUEL
      ELSE
      S=0.0
      ENDIF
      CP=CPFUEL*YFUEL
      MW=MFUEL*YFUEL
      DO 70 I=1,6
      H=H+HO(I)*Y(I)
      IF(Y(I).GT.0.0)THEN
      S=S+Y(I)*(SO(I)-DLOG(Y(I)))
      ELSE
      S=S
      ENDIF
      CP=CP+CPO(I)*Y(I)+HO(I)*T*TABLE(I)*DCDT*YRES/TMOLES
70    MW=MW+Y(I)*M(I)
      R=RO/MW
      H=R*T*H
      U=H-R*T
      V=10*R*T/P
      S=R*(-DLOG(.9869*P)+S)
      CP=R*CP
C
C
      RETURN
      END
C
C
C
C*********************  Subroutine EQUIL  **********************
C
C
C     This subroutine computes the composition and properties of
C     equilibrium combustion products.
C
C
C
      SUBROUTINE EQUIL(P,T,PHI,H,U,V,S,Y,CP,DLVLT,DLVLP,IER,THETA)
      IMPLICIT REAL*8 (A-H,O-Z)
      REAL*8 M, MW, K, KP, MT, MP
      LOGICAL CHECK
      DIMENSION M(10), K(6), C(6), Y(10), D(3), B(4), A(4,4), YO(6),
     &          KP(5,6), DFDT(4), DCDT(6), DKDT(6), DCDP(6),
     &          DYDT(10), DYDP(10), AO(7,0), DFDP(4), CPO(10), HO(10),
     &          SO(10),  BS(4), WK1(4), WK2(4)
      DIMENSION AA(4,4)
      COMMON/ABDG/ALPHA,BETA,DELTA,GAMMA
C
C
C
```

```
C     SPECIFIC HEAT DATA FROM GORDON AND MCBRIDE (1971)
C
      DATA AO/
     1  .44608041D+01, .30981719D-02, -.12392571D-05, .22741325D-09,
     1 -.15525954D-13,-.48961442D+05, -.98635982D+00,
     2  .27167633D+01, .29451374D-02, -.80224374D-06, .10226682D-09,
     2 -.48472145D-14,-.29905826D+05,  .66305671D+01,
     3  .28963194D+01, .15154866D-02, -.57235277D-06, .99807393D-10,
     3 -.65223555D-14,-.90586184D+03,  .61615148D+01,
     4  .36219535D+01, .73618264D-03, -.19652228D-06, .36201558D-10,
     4 -.28945627D-14,-.12019825D+04,  .36150960D+01,
     5  .29840696D+01, .14891390D-02, -.57899684D-06, .10364577D-09,
     5 -.69353550D-14,-.14245228D+05,  .63479156D+01,
     6  .31001901D+01, .51119464D-03,  .52644210D-07,-.34909973D-10,
     6  .36945345D-14,-.87738042D+03, -.19629421D+01,
     7  .25000000D+01,0., 0., 0., 0.,  .25471627D05, -.46011763D+00,
     8  .55420596D+01,-.27550619D-04, -.31028033D-08, .45510674D-11,
     8 -.43680515D-15, .29230803D+05,  .49203080D+01,
     9  .29106427D+01, .95931650D-03, -.19441702D-06, .13756646D-10,
     9  .14224542D-15, .39353815D+04,  .54423445D+01,
     £  .31890000D+01, .13382281D-02, -.52899318D-06, .95919332D-10,
     £ -.64847932D-14, .98283290D+04,  .67458126D+01/
C
C     EQUILIBRIUM CONSTANT DATA FROM OLIKARA AND BORMAN (1975)
C
      DATA KP/
     1  .432168D+00, -.112464D+05,  .267269D+01, -.745744D-04,
     1  .242484D-08,
     2  .310805D+00, -.129540D+05,  .321779D+01, -.738336D-04,
     2  .344645D-08,
     3 -.141784D+00, -.213308D+04,  .853461D+00,  .355015D-04,
     3 -.310227D-08,
     4  .150789D-01, -.470959D+04,  .646096D+00,  .272805D-05,
     4 -.154444D-08,
     5 -.752364D+00,  .124210D+05, -.260286D+01,  .259556D-03,
     5 -.162687D-07,
     6 -.415302D-02,  .148627D+05, -.475746D+01,  .124699D-03,
     6 -.900227D-08/
C
C     MOLECULAR WEIGHTS
C
       DATA   M/44.01, 18.02, 28.008, 32., 28.01, 2.018, 1.009, 16.,
     &        17.009, 30.004/
C
C     OTHER DATA
C
      DATA MAXITS/100/, TOL/3.0E-05/, RO/8.31434/
C
C     MAKE SURE SOLID CARBON WILL NOT FORM
C
      IER = 2
      EPS = .210/(ALPHA + 0.25*BETA - 0.5*GAMMA)
      IF( PHI .GT. (.210/EPS/(0.5*ALPHA - 0.5*GAMMA)) ) RETURN
      IER = 0
```

```
C
C     DECIDE IF AN INTIAL ESTIMATE TO THE COMPOSITION IS
C     REQUIRED OR IF T < 1000. IN WHICH CASE FARG WILL SUFFICE
C
C     Y(1)=0.0825
C     Y(2)=0.165
C     Y(3)=0.725
C     Y(4)=0.0277
C     Y(5)=0.005
C     Y(6)=0.0001
C     Y(7)=0.0001
C     Y(8)=0.0001
C     Y(9)=0.0005
C     Y(10)=0.005
C
      SUM = 0.
      DO 10 I = 1,10
10    SUM = SUM + Y(I)
C
C     USE AFRES IF THETA IS THEVO LESS 2 DEGREES
C
      THEVO=157.
      IF(THEVO-THETA.LE.2.)GO TO 21
      IF( T .GT. 1000..AND. SUM .GT. 0.998 ) GO TO 20
21    CALL AFRES(P,T,PHI,1.0D00,H,U,V,S,YO,CP,DLVLT,DLVLP)
      DO 30 I = 1,10
30    Y(I) = 0.
      DO 40 I = 1,6
      Y(I) = YO(I)
C     Y(7)=0.0001
C     Y(8)=0.0001
C     Y(9)=0.0001
C     Y(10)=0.002
40    CONTINUE
C     Y(4)=0.0277
C     Y(5)=0.005
C     Y(6)=0.001
      IF( T .LE. 1000. ) RETURN
      IF(THEVO-THETA.LE.2.)RETURN
20    CONTINUE
C
C     EVALUATE THE REQUISITE CONSTANTS
C
      PATM = .9869233*P
      DO 50 I = 1,6
      K(I) = 10.**(KP(1,I)*DLOG(T/1000.) + KP(2,I)/T + KP(3,I) +
     &       KP(4,I)*T + KP(5,I)*T*T)
50    CONTINUE
      DO 777 I=1,10
777   CONTINUE
      C(1) = K(1)/DSQRT(PATM)
      C(2) = K(2)/DSQRT(PATM)
      C(3) = K(3)
      C(4) = K(4)
```

```
      C(5) = K(5)*DSQRT(PATM)
      C(6) = K(6)*DSQRT(PATM)
      D(1) = BETA/ALPHA
      D(2) = (GAMMA + .42/EPS/PHI)/ALPHA
      D(3) = (DELTA + 1.58/EPS/PHI)/ALPHA
C
C     SET UP ITERATION LOOP FOR NEWTON-RAPHSON ITERATION AND
C     INTRODUCE TRICK TO PREVENT INSTABILITIES NEAR PHI = 1.0
C     AT LOW TEMPERATURES ON 24 BIT MACHINES (VAX). SET
C     TRICK = 1.0 ON 48 BIT MACHINES (CDC)
C
      TRICK = 10.
      CHECK = DABS(PHI - 1.0) .LT. TOL
      IF(CHECK) PHI = PHI*(1.0 + DSIGN(TOL,PHI - 1.0))
      ICHECK = 0
      DO 5 J = 1,MAXITS
      DO 4 JJ = 1,10
       IF(Y(JJ).GT.1.0D-25)THEN
       YTEMP=Y(JJ)
       ELSE
       YTEMP=1.0D-25
       ENDIF
       IF(YTEMP.LT.1.0)THEN
       Y(JJ)=YTEMP
       ELSE
       Y(JJ)=1.0
       ENDIF
4      CONTINUE
      D76 = 0.5*C(1)/DSQRT(Y(6))
      D84 = 0.5*C(1)/DSQRT(Y(4))
      D94 = 0.5*C(3)*DSQRT(Y(6)/Y(4))
      D96 = 0.5*C(3)*DSQRT(Y(4)/Y(6))
      D103 = 0.5*C(4)*DSQRT(Y(4)/Y(3))
      D104 = 0.5*C(4)*DSQRT(Y(3)/Y(4))
      D24 = 0.5*C(5)*Y(6)/DSQRT(Y(4))
      D26 = C(5)*DSQRT(Y(4))
      D14 = 0.5*C(6)*Y(5)/DSQRT(Y(4))
      D15 = C(6)*DSQRT(Y(4))
      A(1,1) = 1. + D103
      A(1,2) = D14 + D24 + 1. + D84 + D104 + D94
      A(1,3) = D15 + 1.0
      A(1,4) = D26 + 1.0 + D76 + D96
      A(2,1) = 0.0
      A(2,2) = 2.0*D24 + D94 - D(1)*D14
      A(2,3) = -D(1)*D15 - D(1)
      A(2,4) = 2.0*D26 + 2.0 + D76 + D96
      A(3,1) = D103
      A(3,2) = 2.0*D14 + D24 + 2.0 + D84 + D94+ D104 - D(2)*D14
      A(3,3) = 2.0*D15 + 1.0 - D(2)*D15 - D(2)
      A(3,4) = D26 + D96
      A(4,1) = 2.0 + D103
      A(4,2) = D104 - D(3)*D14
      A(4,3) = -D(3)*D15 - D(3)
      A(4,4) = 0.
```

```
C
C     SOLVE THE MATRIX EQUATIONS 3.81 FOR COMPOSITION CORRECTIONS
C
      SUM = 0.
      DO 55 I = 1,10
55    SUM = SUM + Y(I)
      B(1) = -(SUM - 1.0)
      B(2) = -(2.0*Y(2) + 2.0*Y(6) + Y(7) + Y(9) - D(1)*Y(1) -
     &         D(1)*Y(5))
      B(3) = -(2.0*Y(1) + Y(2) + 2.0*Y(4) + Y(5) + Y(8) + Y(9)
     &     +   Y(10) -   D(2)*Y(1) - D(2)*Y(5))
      B(4) = -(2.0*Y(3) + Y(10) - D(3)*Y(1) - D(3)*Y(5))
      IFAIL=0
      DO 9988 IIIZ=1,4
9988  CONTINUE
      IFAIL=0
      CALL F04ATF(A, 4,B, 4,BS,AA,4,WK1,WK2,IFAIL)
C     CALL F04ARF(A,4,B,4,BS,WK1,IFAIL)
C     CALL GAUSS(A,B,4,4,BS)
      ERROR = 0.
      DO 56 L = 3,6
      LL = L - 2
      Y(L) = Y(L) + BS(LL)/TRICK
      ERROR = DMAX1(ERROR,ABS(BS(LL)))
      IF(Y(L).GT.1.0D-25)THEN
      YTEMP=Y(L)
      ELSE
      YTEMP=1.0D-25
      ENDIF
      IF(YTEMP.LT.1.0)THEN
      Y(L)=YTEMP
      ELSE
      Y(L)=1.0
      ENDIF
56    CONTINUE
      Y(7) = C(1)*DSQRT(Y(6))
      Y(8) = C(2)*DSQRT(Y(4))
      Y(9) = C(3)*DSQRT(Y(4)*Y(6))
      Y(10)= C(4)*DSQRT(Y(4)*Y(3))
      Y(2) = C(5)*DSQRT(Y(4))*Y(6)
      Y(1) = C(6)*DSQRT(Y(4))*Y(5)
      IF(ERROR .LT. TOL)  ICHECK = ICHECK + 1
      IF(ERROR .LT. TOL .AND. ICHECK .GE. 2) GO TO 57
5     CONTINUE
      IER = 1
C
C     COMPUTE THE REQUISITE CONSTANTS TO FIND PARTIAL DERIVATIVES
C
57    DO 60 I = 1,6
60    DKDT(I) = 2.302585*K(I)*(KP(1,I)/T - KP(2,I)/T/T + KP(4,I)
     &        + 2.0*KP(5,I)*T)
      DCDT(1) = DKDT(1)/DSQRT(PATM)
      DCDT(2) = DKDT(2)/DSQRT(PATM)
      DCDT(3) = DKDT(3)
```

```
      DCDT(4) = DKDT(4)
      DCDT(5) = DKDT(5)*DSQRT(PATM)
      DCDT(6) = DKDT(6)*DSQRT(PATM)
      DCDP(1) = -0.5*C(1)/P
      DCDP(2) = -0.5*C(2)/P
      DCDP(5) =  0.5*C(5)/P
      DCDP(6) =  0.5*C(6)/P
      X1 = Y(1)/C(6)
      X2 = Y(2)/C(5)
      X7 = Y(7)/C(1)
      X8 = Y(8)/C(2)
      X9 = Y(9)/C(3)
      X10= Y(10)/C(4)
      DFDT(1) = DCDT(6)*X1 + DCDT(5)*X2 + DCDT(1)*X7 + DCDT(2)*X8
     &        + DCDT(3)*X9 + DCDT(4)*X10
      DFDT(2) = 2.0*DCDT(5)*X2 + DCDT(1)*X7 + DCDT(3)*X9 -
     &          D(1)*DCDT(6)*X1
      DFDT(3) = 2.0*DCDT(6)*X1 + DCDT(5)*X2 + DCDT(2)*X8
     &        + DCDT(3)*X9 + DCDT(4)*X10 - D(2)*DCDT(6)*X1
      DFDT(4) = DCDT(4)*X10 - D(3)*DCDT(6)*X1
      DFDP(1) = DCDP(6)*X1 + DCDP(5)*X2 + DCDP(1)*X7 + DCDP(2)*X8
      DFDP(2) = 2.0*DCDP(5)*X2 + DCDP(1)*X7 - D(1)*DCDP(6)*X1
      DFDP(3) = 2.0*DCDP(6)*X1 + DCDP (5)*X2 + DCDP(2)*X8 -
     &          D(2)*DCDP(6)*X1
      DFDP(4) = -D(3)*DCDP(6)*X1
C
C     SOLVE THE MATRIX EQUATIONS 3.91 FOR THE INDEPENDENT DERIVATIVES
C     AND THEN DETERMINE THE DEPENDENT DERIVATIVES
C
      DO 70 I = 1,4
70    B(I) = -DFDT(I)
      IFAIL=0
      IFAIL=0
      CALL F04ATF(A, 4,B,4,BS,AA,4,WK1,WK2,IFAIL)
C     CALL F04ARF(A,4,B,4,BS,WK1,IFAIL)
C     CALL GAUSS(A,B,4,4,BS)
      DYDT(3) = BS(1)
      DYDT(4) = BS(2)
      DYDT(5) = BS(3)
      DYDT(6) = BS(4)
      DYDT(1) = DSQRT(Y(4))*Y(5)*DCDT(6) + D14*DYDT(4) + D15*DYDT(5)
      DYDT(2) = DSQRT(Y(4))*Y(6)*DCDT(5) + D24*DYDT(4) + D26*DYDT(6)
      DYDT(7) = DSQRT(Y(6))*DCDT(1) + D76*DYDT(6)
      DYDT(8) = DSQRT(Y(4))*DCDT(2) + D84*DYDT(4)
      DYDT(9) = DSQRT(Y(4)*Y(6))*DCDT(3) + D94*DYDT(4) + D96*DYDT(6)
      DYDT(10)= DSQRT(Y(4)*Y(3))*DCDT(4) + D104*DYDT(4) + D103*DYDT(3)
C
      DO 80 I = 1,4
80    B(I) = -DFDP(I)
      IFAIL=0
      CALL F04ATF(A, 4,B,4,BS,AA,4,WK1,WK2,IFAIL)
C     CALL F04ARF(A,4,B,4,BS,WK1,IFAIL)
C     CALL GAUSS(A,B,4,4,BS)
      DYDP(3) = BS(1)
```

```
      DYDP(4) = BS(2)
      DYDP(5) = BS(3)
      DYDP(6) = BS(4)
      DYDP(1) = DSQRT(Y(4))*Y(5)*DCDP(6) + D14*DYDP(4) + D15*DYDP(5)
      DYDP(2) = DSQRT(Y(4))*Y(6)*DCDP(5) + D24*DYDP(4) + D26*DYDP(6)
      DYDP(7) = DSQRT(Y(6))*DCDP(1) + D76*DYDP(6)
      DYDP(8) = DSQRT(Y(4))*DCDP(2) + D84*DYDP(4)
      DYDP(9) = D94*DYDP(4) + D96*DYDP(6)
      DYDP(10)= D104*DYDP(4) + D103*DYDP(3)
C
C
C     COMPUTE THE THERMODYNAMIC PROPERTIES
C
      DO 90 I = 1,10
      CPO(I) = AO(1,I) + AO(2,I)*T + AO(3,I)*T*T + AO(4,I)*T**3
     &       + AO(5,I)*T**4
      HO(I) = AO(1,I) +AO(2,I)/2*T+ AO(3,I)/3.*T*T + AO(4,I)/4.*
     &        T**3 +AO(5,I)/5*T**4+ AO(6,I)/T
90    SO(I) = AO(1,I)*DLOG(T) + AO(2,1)*T + AO(3,1)/2.*T**2
     &      + AO(4,I)/3.*T**3 + AO(5,1)/4.*T**4 + AO(7,I)
C
C     Y(1),Y(2) ARE REEVALUTED TO CLEAN UP ANY ROUND-OFF ERRORS WHICH
C     CAN OCCUR FOR THE LOW TEMPERATURE STOICHIOMETRIC SOLUTIONS
C
      Y(1) = (2.*Y(3) + Y(10))/D(3) - Y(5)
      Y(2) = (D(1)/D(3)*(2.*Y(3) + Y(10)) - 2.*Y(6) - Y(7) - Y(9))/2.
C
      MW = 0.
      CP = 0.
      H = 0.
      S = 0.
      MT = 0.
      MP = 0.
      DO 100 I = 1,10
      IF( Y(I) .LE. 1.0D-25 ) GO TO 100
      H = H + HO(I)*Y(I)
      MW = MW + M(I)*Y(I)
      MT = MT + M(I)*DYDT(I)
      MP = MP + M(I)*DYDP(I)
      CP = CP + Y(I)*CPO(I) + HO(I)*T*DYDT(I)
      S = S + Y(I)*(SO(I) - DLOG(Y(I)))
100   CONTINUE
C
      R = RO/MW
      V = 10.*R*T/P
      CP = R*(CP - H*T*MT/MW)
      DLVLT =  1.0 + DMAX1(-T*MT/MW,0.0D0)
      DLVLP = -1.0 - DMAX1( P*MP/MW,0.0D0)
      H = H*R*T
      S = R*(-DLOG(PATM) +S)
      U = H - R*T
C     DIF=THEVO-THETA
C     IF(DIF.LT.3..AND.DIF.GT.1.)THEN
C     DO 111 KK=1,10
```

```
C     PRINT*,Y(KK),THETA
C111  CONTINUE
C     ENDIF
      RETURN
      END
C
C
C
C     ************** TRANSPORT PROPERTIES ********************
C
C
C
      SUBROUTINE TRANSP(T,Y,CP,MU,LAMBDA)
C
C     COMPUTES THE TRANSPORT PROPERTIES OF EQUILIBRIUM
C     COMBUSTION PRODUCTS
C
C     GIVEN:
C           T   TEMPERATURE (K)
C           Y   a TEN DIMENSIONAL COMPOSITION VECTOR OF MOLE
C               FRACTIONS
C               1 - CO2, 2 - H2O, 3 - N2, 4 - O2, 5 - CO, 6 - H2,
C               7 - H,   8 - O,   9 - OH, 10 - NO
C           CP  SPECIFIC HEAT AT CONSTANT PRESSURE (J/G/K)
C
C     RETURNS:
C           MU  VISCOSITY (G/CM/S OR POISE)
C           LAMDA  THERMAL CONDUCTIVITY (W/CM/K)
C
C     NOTES:
C          1. VALID FOR 300 < T < 4000
C          2. TREATS WATER (A POLAR MOLECULE) THE SAME AS NON-POLAR
C             MOLECULES; (DANON AND ADMUR (1969)
C          3. FUEL AIR RESIDUAL GAS TRANSPORT PROPERTIES CAN BE
C             COMPUTED BY MODELLING THE FUEL AS CARBON DIOXIDE
C             IN THIS CASE INPUT FOR Y(1) : Y(1)+YFUEL
C          4. IF A FROZEN THERMAL CONDUCTIVITY IS THE DESIRED
C             OUTPUT, THEN INPUT CP = 0
C
C
C
      IMPLICIT REAL*8(A-H,O-Z)
       REAL*8 LAMBDA,LMMIX1,LMMIX2,LMBDA1,LMBDA2,M,MJ,MI,MU,
     / MU1,MU1I,MU1J,MW
       DIMENSION AO(7,10),A(7,6),M(10),SIGMA(10),EPS(10),
     /MU1(10),CPO(10),Y(10),LMBDA1(10),LMBDA2(10)
C
C     SPECIFIC HEAT DATA
C
C     HIGH TEMPERATURE SET
C
      DATA AO/
     1  .44608041D+01, .30981719D-02, -.12392571D-05, .22741325D-09,
     1 -.15525954D-13,-.48961442D+05, -.98635982D+00,
```

```
     2  .27167633D+01, .29451374D-02, -.80224374D-06, .10226682D-09,
     2 -.48472145D-14,-.29905826D+05,  .66305671D+01,
     3  .28963194D+01, .15154866D-02, -.57235277D-06, .99807393D-10,
     3 -.65223555D-14,-.90586184D+03,  .61615148D+01,
     4  .36219535D+01, .73618264D-03, -.19652228D-06, .36201558D-10,
     4 -.28945627D-14,-.12019825D+04,  .36150960D+01,
     5  .29840696D+01, .14891390D-02, -.57899684D-06, .10364577D-09,
     5 -.69353550D-14,-.14245228D+05,  .63479156D+01,
     6  .31001901D+01, .51119464D-03,  .52644210D-07,-.34909973D-10,
     6  .36945345D-14,-.87738042D+03, -.19629421D+01,
     7  .25000000D+01,0., 0., 0., 0.,  .25471627D05, -.46011763D+00,
     8  .55420596D+01,-.27550619D-04, -.31028033D-08, .45510674D-11,
     8 -.43680515D-15, .29230803D+05,  .49203080D+01,
     9  .29106427D+01, .95931650D-03, -.19441702D-06, .13756646D-10,
     9  .14224542D-15, .39353815D+04,  .54423445D+01,
     £  .31890000D+01, .13382281D-02, -.52899318D-06, .95919332D-10,
     £ -.64847932D-14, .98283290D+04,  .67458126D+01/
C
C
C     LOW TEMPERATURE SET
C
C
      DATA A/
     1.24007797D+01,.87350957D-02,-.6607878D-05,.20021861D-08,
     1.63274039D-15,-.48377527D+05,.96951457D+01,
     2.40701275D+01,-.11084499D-02,.41521180D-05,-.29637404D-08,
     2.80702103D-12,-.30279722D+05,-.32270046D+00,
     3.36748261D+01,-.12081500D-02,.23240102D-05,-.63217559D-09,
     3-.22577253D-12,-.10611588D+04,.23580424D+01,
     4.36255985D+01,-.18782184D-02,.70554544D-05,-.67635137D-08,
     4.21555993D-11,-.10475226D+04,.43052778D+01,
     5.37100928D+01,-.16190964D-02,.36923594D-05,-.20319674D-08,
     5.23953344D-12,-.14356310D+05,.2955535D+01,
     6.30574451D+01,.26765200D-02,-.58099162D-05,.5521039D-08,
     6-.18122739D-11,-.98890474D+03,-.22997056D+01/
C
C
C     MOLECULAR COLLISION PARAMETERS FROM SVHELA (1962)
C     LENNARD JONES  6 - 12
C
      DATA SIGMA/3.941,2.641,3.798,3.467,3.690,2.827,2.708,
     /3.050,3.147,3.492/
      DATA EPS/195.2,809.1,71.4,106.7,91.7,59.7,37.0,106.7,
     /79.8,116.7/
C
C     MOLECULAR WEIGHTS
C
      DATA M/44.01,18.02,28.008,32.000,28.01,2.018,1.009,16.,
     /17.009,30.004/
C
C     GAS CONSTANT
C
      DATA RO/8.3143/
C
```

```
C      STATEMENT FUNCTION FOR COLLISION INTEGRAL, HATTIKUDUR AND
C      THODOS (1970)
C
       OMEGA(TSTAR)=1.155*TSTAR**(-.1462)+.3945*EXP(-.6672*TSTAR)
      /+2.05*EXP(-2.168*TSTAR)
C
C
C      STATEMENT FUNCTIONS FOR AUXILLIARY COEFFICIENTS, BROKAW (1961)
C
       PHI(MU1I,MU1J,MI,MJ)=(1+(MU1I/MU1J)**0.5*(MJ/MI)**0.25)**2/
      &(2*DSQRT(2.*(1.+MI/MJ)))
       PSI(PHIIJ,MI,MJ)=PHIIJ*(1.+2.41*(MI-MJ)*(MI-0.142*MJ)/
      &(MI+MJ)**2)
C
C      COMPUTE THE NORMALISED CP OF INDIVIDUAL COMPONENTS
C
       IF(T.GT.1000.)GOTO10
       N=6
       DO 20 I=1,6
20     CPO(I)=A(1,I)+A(2,I)*T+A(3,I)*T*T+A(4,I)*T*T*T+A(5,I)*T**4
       GOTO25
10     N=10
       DO 30 I=1,10
       CPO(I)=AO(1,I)+AO(2,I)*T+AO(3,I)*T*T+AO(4,I)*T*T*T+
      &AO(5,I)*T**4
30     CONTINUE
C
C      COMPUTE THE VISCOSITY AND THERMAL CONDUCTIVITY OF THE
C      INDIVIDUAL COMPONENTS
C
25     DO 40 I=1,N
       TSTAR=T/EPS(I)
       MU1(I)=26.693D-06*DSQRT(M(I)*T)/SIGMA(I)**2/OMEGA(TSTAR)
       LMBDA1(I)=3.75*RO*MU1(I)/M(I)
       LMBDA2(I)=0.88*(0.4*CPO(I)-1.)*LMBDA1(I)
40     CONTINUE
C
C      COMPUTE THE VISCOSITY, FROZEN SPECIFIC HEAT AND FROZEN THERMAL
C      CONDUCTIVITY OF THE MIXTURE; BROKAW (1961)
C
       CPFROZ=0
       MW=0
       MU=0
       LMMIX1=0
       LMMIX2=0
       DO 50 I=1,N
         IF(Y(I).LE.0)GOTO50
         DEN1=1.
         DEN2=1.
         DO 60 J=1,N
         IF(J.EQ.I.OR.Y(J).LE.0)GOTO60
         DUMMY=PHI(MU1(I),MU1(J),M(I),M(J))
         DEN1=DEN1+DUMMY*Y(J)/Y(I)
         DEN2=DEN2+PSI(DUMMY,M(I),M(J))*Y(J)/Y(I)
```

```
60    CONTINUE
      CPFROZ=CPFROZ+CPO(I)*Y(I)
      MW=MW+Y(I)*M(I)
      MU=MU+MU1(I)/DEN1
      LMMIX1=LMMIX1+LMBDA1(I)/DEN2
      LMMIX2=LMMIX2+LMBDA2(I)/DEN1
50    CONTINUE
C
      LAMBDA=LMMIX1+LMMIX2
C
C     COMPUTE EQUILIBRIUM THERMAL CONDUCTIVITY ASSUMING UNITY
C     REACTION LEWIS NUMBER AS DEFINED BY SVHELA & MCBRIDE (1973)
C
      CPFROZ=CPFROZ*RO/MW
      IF(CP.GT.CPFROZ)THEN
      CP=CP
      ELSE
      CP=CPFROZ
      ENDIF
      LAMBDA=LAMBDA*CP/CPFROZ
      RETURN
      END
C
C
      SUBROUTINE WOCHNI(V,P,SPV,MU,LAMBDA,HEAT,THETA)
C
C     Predicts engine heat transfer coefficients using the
C     correlations due to Woschni (1967)
C
C     Requires:
C              SPV - gas specific volume (cm**3/g)
C              P - instantaneous cylinder pressure (bar)
C              V - instantaneous cylinder volume (cm**3)
C              MU - viscosity (g/cm/s or Poise)
C              LAMBDA - thermal conductivity (W/cm/K)
C     Returns:
C             HEAT - heat transfer coefficient (W/m**2 K)
C
C
C             UP - mean piston speed (cm/s)
C             UMG - mean gas velocity (m/s)
C             T1 - temperature at inlet valve closing (K)
C             P1 - pressure at inlet valve closing (bar)
C             V1 - cylinder volume at inlet valve closing (cm**3)
C             PMOT - motoring cylinder pressure estimated from
C                    isentropic p-v relationship
C
C
C             RE & NU - Reynolds and Nusselt numbers based on bore
C
      IMPLICIT REAL*8(A-H,O-Z)
      REAL*8 MU,LAMBDA,NU,MNOT
      COMMON/ENGINE/R,B,S,EPS,RPM,C,THETAB,THETAS,
     &PHI,F,P1,T1,TW,MNOT,OMEGA,UNOT,UFINAL,ACOMB,THEVO,THIVC
```

```
C
C
      PI=3.141593
      UP=2*S*RPM/60
      RIVC=THIVC*PI/180.
      VTDC = PI/4.*B**2*S/(R - 1.)
      V1 = VTDC*(1. + (R - 1.)/2.*(1. - DCOS(RIVC) + 1./EPS*(1. -
     &    DSQRT(1. - (EPS*DSIN(RIVC))**2))))
      VS = PI/4.*B**2.*S
      PMOT=P1*(V1/V)**1.4
      DPC=P-PMOT
      IF(THETA.LT.THETAS)THEN
      UMG=2.28*UP*1E-2
      ELSE
      UMG=2.28*UP*1E-2+0.00324*T1*VS/V1/P1*DPC
      ENDIF
C
      RE=UMG*1E2/SPV/MU*B
      NU=0.035*RE**0.8
C
      HEAT=LAMBDA*NU/B*1E4
      RETURN
      END
C
C
C
C
      SUBROUTINE EICH(P,T,HEAT)
C
C     Predicts engine heat transfer coefficient using the correlation
C     of Eichelberg
C
C     Requires instantaneous cylinder pressure, (P) unburnt and burnt
C     gas temperatures (T). Engine speed and stroke.
C
C     Returns HEAT - heat transfer coefficient (W/m**2)
C
      IMPLICIT REAL*8(A-H,O-Z)
      REAL*8 MNOT
      COMMON/ENGINE/R,B,S,EPS,RPM,C,THETAB,THETAS,
     &PHI,F,P1,T1,TW,MNOT,OMEGA,UNOT,UFINAL,ACOMB,THEVO,THIVC
C
      HEAT=523*(S*RPM/30.)**0.3333*(SQRT(P*T))
      RETURN
      END
C
C     ************************************ Output ************
C
      SUBROUTINE WRIT1
C
C     Subroutine to write results to output file
C
C     $INSERT SYSCOM>A$KEYS.INS.FTN
      IMPLICIT REAL*8(A-H,O-Z)
```

```
      REAL*8 MNOT,MG,IMEP
      CHARACTER*12 FUELN
      COMMON/ENGINE/R,B,S,EPS,RPM,C,THETAB,THETAS,PHI,F,
     &P1,T1,TW,MNOT,OMEGA,UNOT,UFINAL,ACOMB,THEVO,THIVC
      COMMON/FUEL/AO,FS
      COMMON/FUEN/FUELN
      COMMON/RESULT/THETAG(361),YG(6,361),VOLG(361),XG(361),MG(361)
     &,CO2G,H2OG,GN2,O2G,COG,H2G,HG,OG,OHG,GNO,Y2MAXG
     &,QEN,PMAXE,TPMAXE,PMAXT,TPMAXT,PMAX1,TPMAX1,PMAX,TPMAX
     &,TBMAX,TTBMAX,TEVO
      OPEN(UNIT=6,FILE='EMODR.LIST')
      WRITE(6,1)
1     FORMAT(80(1H-))
      WRITE(6,2)
2     FORMAT(20X,'OXFORD POLYTECHNIC ENGINEERING DEPARTMENT')
      WRITE(6,3)
3     FORMAT(20X,'FUEL INDUCTED SPARK IGNITION ENGINE MODEL')
      WRITE(6,4)
4     FORMAT(35X,'FOUR STROKE')
      WRITE(6,30)
30    FORMAT(80(1H-))
C     CALL DATE$A(DATE)
C     CALL TIME$A(TIME)
C     WRITE(6,5)DATE
C5     FORMAT(1H0,5X,'Date  ',A8)
      WRITE(6,6)
6     FORMAT(5X,14(1H-))
C     WRITE(6,7)TIME
C7     FORMAT(1H0,5X,'Time  ',A8)
      WRITE(6,6)
      WRITE(6,8)
8     FORMAT(' ')
      WRITE(6,9)
9     FORMAT(5X,'Engine physical and operational data')
      WRITE(6,99)
99    FORMAT(5X,36(1H-))
      BMM=B*10
      SMM=S*10
      WRITE(6,10)BMM,SMM,R
10    FORMAT(5X,'Bore   ',F5.2,'  mm',9X,'Stroke   ',F5.2,'  mm',
     &7X,'Compression ratio   ',F4.1)
      WRITE(6,11)EPS
11    FORMAT(5X,'Crank radius to con-rod length ratio   ',F5.3)
      WRITE(6,12)ACOMB
12    FORMAT(5X,'Surface area of combustion chamber (less top of
     &piston)   ',F5.2,'  cm**2')
      WRITE(6,13)RPM
13    FORMAT(5X,'Engine speed   ',F6.1,'  rev/min')
      WRITE(6,14)PHI,F
14    FORMAT(5X,'Fuel-air equivalence ratio   ',F4.2,5X,'Residual
     &exhaust gas fraction   ',F4.2)
      WRITE(6,15)P1,T1
15    FORMAT(5X,'Pressure at IVC   ',F4.2,'  bar',13X,'Temperature at
     &IVC   ',F5.1,'  K')
```

```
      WRITE(6,161)
      WRITE(6,16)TW
161   FORMAT(5X,'Surface temperature of cylinder walls and
     X combustion')
1 6   FORMAT(5X,'chamber (assumed uniform)   ',15X,F5.1,' K')
      WRITE(6,17)C
17    FORMAT(5X,'Blowby coefficient   ',F4.2)
      WRITE(6,50)
50    FORMAT(5X,'Fuel')
      WRITE(6,51)
51    FORMAT(5X,'----')
      WRITE(6,52)FUELN
52    FORMAT(5X,A12)
      SAFR=1/FS
      WRITE(6,53)AO,SAFR
53    FORMAT(5X,'Calorific value   ',F7.1,'  kJ/kg',5X,'Stoichiometric
     &air fuel ratio   ',F5.2)
      WRITE(6,18)
18    FORMAT(5X,'Heat release')
      WRITE(6,19)
19    FORMAT(5X,12(1H-))
      WRITE(6,20)
20    FORMAT(5X,'Heat release modelled by prescribed weibe function ')
      WRITE(6,201)
201   FORMAT(5X,'of crank angle for mass fraction burned')
      WRITE(6,21)THETAS,THETAB
21    FORMAT(5X,'Start of heat release   ',F5.1,11X,'Burn duration
     & ',F5.1)
      WRITE(6,30)
      WRITE(6,31)
31    FORMAT(5X,'Notes')
      WRITE(6,32)
32    FORMAT(5X,5(1H-))
      WRITE(6,33)
33    FORMAT(5X,'1.  Surface heat transfer coefficient estimated using
     &Woschni correlation')
      WRITE(6,1)
      PI=3.14159
      KVCLOS=THEVO-THIVC+1.
      ETA = YG(4,KVCLOS)/MNOT*(1. + PHI*FS*(1. - F))/PHI/FS/(1. -F)/AO
      IMEP = YG(4,KVCLOS)/(PI/4.*B**2*S)*10.
      POWER=YG(4,KVCLOS)*RPM/120*1E-3
      FMEP=2104.*RPM/60.+64109.
      FPWR=FMEP*PI/4.*B**2.*S*RPM/60./2.*1E-9
      BPWR=POWER-FPWR
      QCOOL=YG(5,KVCLOS)*RPM/120*1E-3
      QRATIO=QCOOL/QEN*100.
      WRITE(6,299)
299   FORMAT(20X,'PREDICTED PERFORMANCE')
      WRITE(6,30)
      WRITE(6,298)
298   FORMAT(5X,'Indicated performance')
      WRITE(6,280)
280   FORMAT(5X,'--------------------')
```

```
      WRITE(6,300)ETA,IMEP
300   FORMAT(5X,'Thermal efficiency   ',F5.3,2X,'Indicated mean
     X effective pressure   ',F5.2,' bar')
      WRITE(6,297)POWER
297   FORMAT(5X,'Indicated power   ',F6.3,'  kW')
      WRITE(6,281)BPWR
281   FORMAT(5X,'Brake performance ',F6.3,'  kW')
      WRITE(6,282)
282   FORMAT(5X,'-----------------')
      WRITE(6,283)
283   FORMAT(5X,'Heat transfers')
      WRITE(6,284)
284   FORMAT(5X,'--------------')
      WRITE(6,285)QCOOL
285   FORMAT(5X,'Rate of heat loss to coolant   ',F6.3,'  kW')
      WRITE(6,286)QRATIO
  286 FORMAT(5X,'Ratio of predicted to experimental heat loss to'
     &' coolant  ',F4.1,' (%)')
      WRITE(6,287)PMAXT,TPMAXT
  287 FORMAT(5X,'Predicted maximum rate of pressure rise  ',F5.3,
     &'   bar/deg at ',F5.1,'  deg')
      WRITE(6,288)PMAXE,TPMAXE
  288 FORMAT(5X,'Predicted maximum rate of pressure rise  ',F5.3,
     &'   bar/deg at ',F5.1,'  deg')
      WRITE(6,1)
      WRITE(6,101)
      WRITE(6,102)
 101  FORMAT('   CO2    H2O     N2     O2   CO     H2       H      O
     & OH     NO   NOMAX')
102   FORMAT('   (%)    (%)    (%)    (%)  (PPM)  (PPM)   (PPM)  (PPM)
     &(PPM)  (PPM)  (PPM)')
      WRITE(6,34)CO2G,H2OG,GN2,O2G,COG,H2G,HG,OG,OHG,GNO,Y2MAXG
  34  FORMAT(10F7.2,1X,F7.2)
      WRITE(6,1)
      WRITE(6,100)
100   FORMAT(' THETA   VOLUME  BRN FRA  PRESS    BRN T  T UBRN   WORK
     &         MASS   H-LEAK')
      WRITE(6,105)
105   FORMAT('          CM**3            BAR       K       K       J
     &    J       G       J')
      WRITE(6,30)
      WRITE(6,110)THETAG(1),VOLG(1),XG(1),(YG(J,1),J=1,5),
     XMG(1),YG(6,1)
110   FORMAT(10F8.3)
      DO 200 I=2,THEVO-THIVC+1
      WRITE(6,110)THETAG(I),VOLG(I),XG(I),(YG(J,I),J=1,5),
     XMG(I),YG(6,I)
200   CONTINUE
      WRITE(6,30)
      CLOSE(UNIT=6)
      RETURN
      END
C
C
```

```
C
      SUBROUTINE WRIT2(BLBYT)
C
C     Subroutine to write results to data file
C
      IMPLICIT REAL*8(A-H,O-Z)
      REAL*8 MNOT,MG,IMEP
      COMMON/ENGINE/R,B,S,EPS,RPM,C,THETAB,THETAS,PHI,F,
     &P1,T1,TW,MNOT,OMEGA,UNOT,UFINAL,ACOMB,THEVO,THIVC
      COMMON/RESULT/THETAG(361),YG(6,361),VOLG(361),XG(361),MG(361)
     &,CO2G,H2OG,GN2,O2G,COG,H2G,HG,OG,OHG,GNO,Y2MAXG
     &,QEN,PMAXE,TPMAXE,PMAXT,TPMAXT,PMAX1,TPMAX1,PMAX,TPMAX
     &,TBMAX,TTBMAX,TEVO
      COMMON/FUEL/AO,FS
      OPEN(UNIT=6,FILE='DATA')
      PI=3.14159
      KVCLOS=THEVO-THIVC+1.
      ETA = YG(4,KVCLOS)/MNOT*(1. + PHI*FS*(1. - F))/PHI/FS/(1. -F)/AO
      IMEP = YG(4,KVCLOS)/(PI/4.*B**2*S)*10.
      POWER=YG(4,KVCLOS)*RPM/120*1E-3
      FMEP=2104.*RPM/60.+64109.
      FPWR=FMEP*PI/4.*B**2.*S*RPM/60./2.*1E-9
      PWR1=POWER-FPWR
      QCOOL=YG(5,KVCLOS)*RPM/120*1E-3
      QRATIO=QCOOL/QEN*100.
      WRITE(6,300)ETA,IMEP,POWER,FPWR,PWR1,QCOOL,QRATIO
     &,PMAXT,TPMAXT,PMAXE,TPMAXE
      WRITE(6,301)PMAX,TPMAX,PMAX1,TPMAX1,TBMAX,TTBMAX,TEVO,C,BLBYT
  301 FORMAT(9F8.2)
  300 FORMAT(11F7.3)
      WRITE(6,34)CO2G,H2OG,GN2,O2G,COG,H2G,HG,OG,OHG,GNO,Y2MAXG
   34 FORMAT(10F7.2,1X,F7.2)
      WRITE(6,110)THETAG(1),VOLG(1),XG(1),(YG(J,1),J=1,5),
     XMG(1),YG(6,1)
110   FORMAT(10F8.2)
      DO 200 I=2,THEVO-THIVC+1
      WRITE(6,110)THETAG(I),VOLG(I),XG(I),(YG(J,I),J=1,5),
     XMG(I),YG(6,I)
200   CONTINUE
      CLOSE(UNIT=6)
      RETURN
      END
C
C     ************************************ Graphics *************
C
      SUBROUTINE PICTUR(PMEAN,TMEAN)
C
C     Subroutine to provide graphical output
C
      IMPLICIT REAL*8(A-H,O-Z)
      REAL*4 YP,TGRA,TMEAN,PMEAN
      REAL*8 MNOT,MG,IMEP
      CHARACTER*12 FUELN
      DIMENSION YP(361),TGRA(361),PMEAN(361),TMEAN(361)
```

```
      COMMON/ENGINE/R,B,S,EPS,RPM,C,THETAB,THETAS,PHI,F,
     &P1,T1,TW,MNOT,OMEGA,UNOT,UFINAL,ACOMB,THEVO,THIVC
      COMMON/FUEL/AO,FS
      COMMON/FUEN/FUELN
      COMMON/RESULT/THETAG(361),YG(6,361),VOLG(361),XG(361),MG(361)
     &,CO2G,H2OG,GN2,O2G,COG,H2G,HG,OG,OHG,GNO,Y2MAXG
     &,QEN,PMAXE,TPMAXE,PMAXT,TPMAXT,PMAX1,TPMAX1,PMAX,TPMAX
     &,TBMAX,TTBMAX,TEVO
      CALL PAPER(1)
      CALL PSPACE(0.1,1.33,0.1,1.0)
      CALL MAP(-180.0,180.0,0.0,80.0)
      CALL BORDER
      CALL SCALSI(30,10)
      CALL GRATSI(30.0,10.0)
      DO 10 I=1,THEVO-THIVC
      TGRA(I)=THETAG(I)
10    YP(I)=YG(1,I)
      CALL POSITN(TGRA(1),YP(1))
      DO 22 I=2,THEVO-THIVC
22    CALL JOIN(TGRA(I),YP(I))
      CALL POSITN(TMEAN(1),PMEAN(1))
      DO 23 I=2,360
23    CALL JOIN(TMEAN(I),PMEAN(I))
      CALL GREND
      RETURN
      END
```

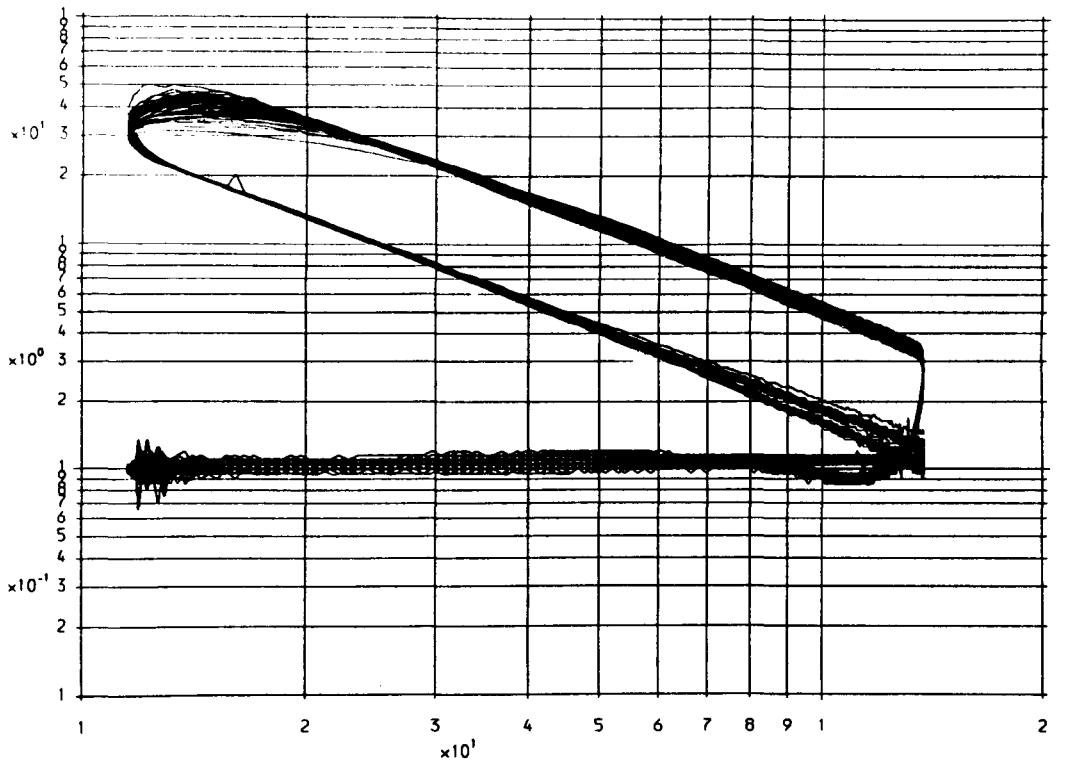

Analysis of engine pressure data

Test carried out on 17/02/89

Reference number for test and engine configuration T34H3CH2

Engine speed (rev/min) 1516.0 Ignition timing 20

Excess air 1.09

Statistical data

Mean work = 91.50 Standard deviation work 2.45
%age dispersion of work = 2.7

Mean power = 1.156 Standard deviation power = 0.031
%age dispersion of power = 2.7

Mean peak pressure = 40.810 Standard deviation of peak pressure = 4.1
%age dispersion of peak pressures = 10.2

Mean crank angle for peak pressure = 15.9 Standard deviation of crank angle = 2.1
%age dispersion of crank angle for peak pressure = 13.3

Specimen output: single cycle analysis, log p/log v plot and statistical data.

APPENDIX IV - CALIBRATION PROCEDURES

Introduction

In addition to the following procedures, calibration was further supported by calculating and comparing the values of important parameters or quantities, such as air-to-fuel ratio and heat transfers, from experimentally derived data obtained simultaneously from different measuring systems. The validity of the measurements was also confirmed by conducting energy balances at numerous operating points; the results from this procedure are discussed further in Section 7.6.

Combustion pressure

Preparation and calibration of the piezoelectric pressure transducer and calibration of the measuring system as a whole - to ensure accurate phasing of pressure data with the appropriate crankangle - was achieved using the rigorous technique described by Lancaster et al., (2.3). This procedure was conducted with each change in design variable and the results analysed prior to testing.

In the absence of an absolute pressure reference it was assumed that atmospheric pressure less 0.1 bar applied to the cylinder contents at the beginning of the induction stroke. It was concluded that any possible error arising from this assumption would be small because an inspection of the pumping loop on log P/log V diagrams (see Figures I.2 - I.57) indicated only a moderate difference in the spread between exhaust and induction pressures of around 0.1 to 0.2 bar as a consequence of operation at wot conditions. Furthermore, this assumption had the effect of adjusting the pressure at the end of the induction stroke to approximately atmospheric - a procedure previously employed in the absence of an absolute pressure reference, (2.3).

To satisfy the stringent restrictions on space within the combustion chamber it was found necessary to mount the pressure transducer remote from the chamber, connected by a small passageway. Whilst advantageous from the perspective of reduced thermal loading, this type of arrangement has been reported, (2.1, 2.2), to be disadvantaged by

pressure oscillations in the passageway under some conditions, which may lead to errors in pressure measurements. It was concluded in Reference 2.1 that such errors diminish with slower engine speeds and as the clearance volume below the transducer diaphragm reduces. Additionally, they are influenced by the length and bore of the connecting passageway. In firing tests, References 2.1 and 2.2 report satisfactory results from aperture ratios (passageway diameter-to-length ratio) varying from 0.02 to 0.04.

To establish the significance of these possible sources of error, tests were undertaken on the Ricardo E6 engine which allowed easy access to the combustion space through an additional spark plug orifice. Pressure-crankangle data were obtained using the two independent measuring systems appropriate to each engine. In the case of the system utilised on the Task engine, an identical remote transducer mounting was simulated by an adapter designed for this purpose. The data obtained were compared at a similar operating point, under motoring and firing operation, with the system normally used on the Ricardo engine which features a flush mounted transducer. The derived fractional mass parameters are presented in Table IV.5 for both systems. The effect of the connecting passageway is noted to be negligible.

Pressures

Instrumentation for the measurement of gas pressure, the air flow meter pressure drop and the manifold pressure was supplied calibrated by Furness Controls, a typical calibration and test certificate is shown in Figure IV.6. At the end of the test programme the calibration was confirmed by connecting all pressure measuring instruments to a variable pressure source, and recording the output from each instrument as the pressure was varied incrementally over the range encountered during the experiments. The difference in the output between the instruments was found to be negligible.

Gas analysis

These instruments were set to zero and subsequently calibrated to gases of certified purity supplied by BOC special gases. This procedure was

followed prior to each experiment and repeated after the experiment to account for any drift.

Temperatures

With the exception of the gas and air temperatures at the manifold and other temperatures used for monitoring purposes only, such as the oil and gas sample, the temperature data are used almost exclusively for heat transfer calculations where it is necessary only that instruments register equal output for equal input since the various transfers are evaluated from differences in temperatures.

The thermocouples and platinum resistance thermometers were immersed together in boiling water and subsequently in melting ice. The output of the measuring systems was then compared with the known temperatures of water in these conditions. During the warm-up period preceding each experimental run, a further check on these instruments was conducted by noting the output as the engine coolant circulated through the system under thermostatic control at constant temperature.

Gas flow

A Wright saturator and wet meter interfaced with Gemini were supplied calibrated by British Gas. The calibration was referenced to laboratory standards whose values are traceable to United Kingdom national standards.

Air flow

The Alcock viscous flow meter was calibrated by an orifice plate to BS 848:1:1980/BS 1042:section 1.1:1980. The calibration details are presented in Figure IV.7.

Coolant flow

Both the hot and cold water flow meters were calibrated by measuring the volume of fluid passed in a given time interval over the range of operational flow rates and temperatures.

Engine load

The load cell was calibrated to Cussons specifications prior to each experiment. Calibration involves loading the cell with a known weight and comparing this with the indicated reading, zero and span control are provided for adjustment.

Engine speed

The test facility incorporated two independent speed measuring systems. The output of both these instruments was compared over the range of speed with that of a portable digital tachometer, the details of which are presented in Figure IV.8.

Gas quality

Gas quality data applicable to the local area on the dates of testing were kindly supplied by R.J. Wadsworth of British Gas. A sample analysis is presented in Figure IV.9 and includes gas composition, density and calorific values.

Ignition timing

Since the pressure-crankangle calibration procedure requires the angular displacement of the engine crankshaft to be referenced precisely to bdc, the setting and function of the stepper motor-controlled spark-ignition system were conveniently checked following each calibration.

Effect of two pressure transducers.

		Mass burned (degrees after spark)				
Transducer	Mounting	1%	10%	50%	90%	100%
Kistler 7055B	Flush	16	25	39	53	68
Kistler 6123A1	Remote	16	25	38	52	68

Operating condition:

Engine : Ricardo E6
Cr : 12:1
Speed : 1800 (rpm)
A/F ratio: Stoichiometric
Ignition : 28 (Degrees btdc)

Remote mounting, dimensions of connecting passageway:

Length: 13.5 mm
Bore : 1.0 mm

CALIBRATION CHART
AND
TEST CERTIFICATE
FOR
FCO11, FCO12, FCO14, FCO15 MICROMANOMETERS

THIS IS TO CERTIFY THAT the following instrument has been tested in accordance with the standards laid down and adhered to by Furness Controls Ltd., Bexhill, England.

All instruments are calibrated using precision water column manometers or equivalent standards to an in-house accuracy of .002% or .2% or .3% depending on range of pressure. They are checked for linearity using the same standard and adjusted to give the optimum accuracy of reading. Calibration devices are not approved nor maintained to any national standard.

Instrument type FCO....12.....
Description...DIGITAL..MODEL.3.....
Serial number...FCB..6649.....
Customer name..OXFORD.:.POLY.TECHNIC.....
Our SO Ref....SB..3323.....
Transducer size 20mm *Serial* FCB 6649... *Tuning* ...2.:5....
Supply voltage....240.V.AC..CHARGER.INPUT.....
Meter scale.....±19.99.mm.H₂O.....
.....±199.9.mm.H₂O.....
.....0.-.56..m/s.....
Temperature coefficient: ≤0.004% per 1 °C
Output signal....±5.V.DC.....
Time constant...0.-.10.secs.....
Leak tight.....✓.....

LINEARITY

	20%	40%	60%	80%	100%
		of selected range			
~~Range 1% +~~					
~~Range 1% —~~					
Range 10% +	-0·6 %	-0·45%	-0·45%	-0·25%	-0·05%
Range 10% —	-0·5%	-0·3%	-0·15%	±0%	+0·2%
Range 100% +	+0·1%	±0%	±0%	+0·05%	+0·15%
Range 100% —	+0·2%	+0·05%	+0·05%	+0·1%	+0·2%
Range Flow	-0·5%	-0·2%	-0·1%	-0·05%	±0%

Signal output noise level.....<1mV.....

Signed .....JRC..... Date 17.-.10.-.86

Chief Test Engineer

P.N

1

AIRFLOW

SPECIALISTS IN AIR MOVEMENT TECHNOLOGY

CERTIFICATE OF CALIBRATION

AIRFLOW DEVELOPMENTS LIMITED
Lancaster Road, High Wycombe
Buckinghamshire HP12 3QP England
Telephone (0494) 25252/443821
Telex 83288

Germany Airflow Lufttechnik GmbH 5308
Rheinbach
West Germany

COMPANY

DEPARTMENT OF ENGINEERING.
OXFORD POLYTECHNIC
GYPSY LANE
HEADINGTON
OXFORD

CERTIFICATE NUMBER I/87/219.

DATE CERTIFIED

INSTRUMENT TYPE ALCOCK VISCOUS FLOW AIR METER

INSTRUMENT SERIAL NUMBER 471V.

This Certificate is issued in accordance with the "Standard Conditions of Acceptance for Calibration" as currently published by Airflow Developments Limited.

The measurements were correct at the time of calibration.

G.J. Matthews

Authorised Signatory ENGINEERING LABORATORY MANAGER.
For and on behalf of
Airflow Developments Limited

PROPERTY OF

SPECIFICATION VOLUME FLOW RATE BY ORIFICE PLATE TO BS 848:1:1980/BS-1042:SECTION 1:1 1980 BETTER THAN ±2%.

DATE OF CALIBRATION 28.7.87.

This is to certify that the above item has been calibrated in accordance with our Specification.

All measured parameters are traceable to the National Maritime Institute or to National Standards where applicable.

This Instrument should be re-calibrated at least ONCE annually.

G.J. Matthews

CALIBRATION ENGINEER

BS 5750 Registration No FM 152 FM 152/1

nevac

Ranges	
"Non Contact"	60 to 19,999 rpm
"Contact"	60 to 19,999 rpm } Using optional
Surface Speed	6.0 to 1,999.9 m/min } Contact Adaptor Kit
Accuracy	±1 rpm (60 to 4,000 rpm) ±2 rpm (4,000 to 12,000 rpm) ±3 rpm (over 12,000 rpm)
"Non Contact" Sensing Distance	50 to 300 mm between photo head and 10 x 10 mm reflective tape target with light projection angle within ±30°
Sample Time	0.5 to 1 second
Display Hold Time	Approximately 2 minutes from release of push button. Auto switch-off.
Overrange Indicator	" - - - - " display
On Target Indicator	" ⬅ " symbol
Low Battery Indicator	" - " on left of display
Temperature Range	+5 to +10°C operating -25 to +70°C storage
Batteries	4 x 1.5 V. Type UM3, R6, HP7 or AA
Supplied Accessories	Reflective tape (pack of 10 strips) Carrying Case
Optional Accessory	Contact Adaptor Kit Comprises: Adaptor, Rubber tips (quantity 3), and Surface Speed Wheel

Specifications of the tachometer.

ANALYSIS	1989 (Continued)					
	6 Mar	13 Mar	20 Mar	28 Mar	2 May	15 May
Nitrogen % v/v:	1.54	1.58	1.51	1.72	1.40	1.85
Methane % v/v:	94.20	94.00	94.23	93.96	94.45	93.65
Ethane % v/v:	3.07	3.19	3.10	3.15	3.02	3.25
Carbon Dioxide % v/v:	0.24	0.23	0.24	0.25	0.23	0.36
Propane % v/v:	0.69	0.71	0.66	0.67	0.66	0.62
iso-Butane % v/v:	0.11	0.10	0.08	0.08	0.08	0.09
n-Butane % v/v:	0.11	0.13	0.13	0.12	0.10	0.12
Pentanes % v/v:	0.04	0.06	0.05	0.05	0.06	0.06
Total:	100.0	100.0	100.0	100.0	100.0	100.0
C.V. Real-Gross MJ/m3:	38.60	38.66	38.60	38.53	38.61	38.46
Wobbe Real-Gross MJ/m3:	50.28	50.31	50.30	50.16	50.36	49.98
S.G. Real Gas:	0.589	0.591	0.589	0.590	0.588	0.592
Stoichiometric Air/Fuel Ratio:	9.8	9.8	9.8	9.8	9.8	9.7

Sample fuel gas analysis.

APPENDIX V - GAS CHROMATOGRAPH ANALYSIS OF EXHAUST HYDROCARBONS

Introduction

Figures V.2 - V.3 detail the composition of exhaust hydrocarbons determined by gas chromatography at a typical operating condition. The analysis was kindly undertaken by Watson House Research Station at British Gas plc.